THE GENESIS OF THE SANGDONG TUNGSTEN DEPOSIT, THE REPUBLIC OF KOREA.

by

K. J. MOON, M.Sc.

Submitted in partial fulfilment of the requirements for the Degree of Doctor of Philosophy.

UNIVERSITY OF TASMANIA

HOBART

1983

(to be conferred Dec. 1983)

This thesis contains no material which has been accepted for the award of any other degree or diploma in any University and, to the best of my knowledge and belief, contains no copy or paraphrase of material previously published or written by another person, except where due reference is made in the text of this thesis.

K. J. MOON

University of Tasmania

June, 1983

ABSTRACT

Scheelite mineralization at Sangdong is probably related to a late Cretaceous episode of igneous activity following the Daebo Orogeny in the Korean peninsula. It occurs in stratabound skarns that replace Cambrian limestones of the Myobong Slate or the overlying Pungchon Limestone, and also in a number of associated quartz veins.

These sediments in the Sangdong area overlie the Jangsan Quartzite and Precambrian schists and lie in the southern limb of the Hambaeg Syncline, striking N 70-80°E and dipping 25-35°NW. The M1(6 m thick) and F.(0.3 to 0.8 m thick) orebodies are stratiform, extend about 1.2 km along strike and down dip, and grade laterally to interbedded limestones in the Myobong Formation. H1 orebody has an irregular shape, bounded on the bottom by the Myobong slate and on top by Pungchon limestone, with thickness varying from 10 to 100 m. The M1 and F. orebodies show a generalized zonal distribution of the major component minerals: a central quartz-mica zone is surrounded by an amphibole-rich zone, which in turn is enveloped by a pyroxene-garnet zone. Scheelite is highly concentrated in the quartz-mica zone where the grades average 6 % WO_3. No zonation and little mica is observed in the H1 orebody.

Relics of pyroxene-garnet skarn in the quartz-mica zone, relict blocks of limestone in the pyroxene-garnet skarn zone, and small-scale veins and fractures with quartz-mica skarns rimmed by amphibole and the pyroxene-garnet skarn, demonstrate the sequential metasomatic replacement of limestone. Early garnet-pyroxene±wollastonite skarns are replaced by late pyroxene-garnet skarns, then amphibole skarn, and finally, mica skarn.

Geochemical analyses, fluid inclusion and stable isotope data assist in defining fluid composition and source, and P - T conditions. $\delta^{18}O$, $\delta^{34}S$ and $\delta^{13}C$ of ore minerals indicate a derivation from magmatic fluids, and the high temperatures indicated by the mineralogy and fluid inclusions

(up to 600°C) strongly suggest a magmatic heat source. Though drilling has not encountered granite to a depth of 500 m below the mine, a granitoid pluton is inferred within a kilometre of the deposit.

Tectonic fracturing may have caused a change from lithostatic to hydrostatic pressure(from 800 to 300-400 bars), while precipitating pyroxene-garnet at 350-500°C, and the fluid boiled. Later in pyroxene-garnet growth, lithostatic pressure was restored, possibly because of fracture sealing by mineral precipitation. In the M1 and F. ore zones, hydrous skarns formed mainly during the non-boiling phase, growing outwards from a central feeder zone marked by a concentration of footwall veins. The skarn assemblages appear to approach equilibrium with the hydrothermal fluid, justifying the use of phase equilibria. Fluid inclusion evidence indicates that the major solution species were NaCl, KCl, $CaCl_2$ and $MgCl_2$, with an average salinity of about 1 m NaCl. There was also localized development of CO_2-rich and more saline fluids.

The f_{O_2}- f_{S_2} conditions were close to the pyrrhotite-magnetite-pyrite point with f_{O_2} increasing slightly towards the central core, and $\Sigma S = 2.5 \times 10^{-3}$ m. Part of the mica zone is muscovite-rich and probably lower temperature(350°C); the pH range estimated for this assemblage, assuming $m_{K^+} = 0.1$, is between 4.2 and 5.9. Under these conditions, tungsten was transported mainly as HWO_4^- and at pH = 4, the maximum $a_{Ca^{++}}$ in the fluid to maintain 2 ppm W in solution in equilibrium with scheelite is 10^{-7} at 350°C.

Double diffusive mechanisms may have maintained steep temperature and chemical gradients at the margins of the skarn zones, with the central, hot, dilute magmatic plume in contact with an outer envelope of hot, saline groundwater. Local and occasional mixing, or influx, of groundwater may have given rise to the saline fluids identified locally in fluid inclusions.

The quartz veins appear to have formed in similar P-T-X conditions, with wolframite- and molybdenite-bearing veins forming at higher temperatures than sulphide-bearing veins.

Late fluid circulation involved formation of calcite and local hematite, with $\delta^{13}C$ values indicating non-magmatic fluid.

CONTENTS

ABSTRACT	i
CONTENTS	iv
LIST OF FIGURES	vii
LIST OF TABLES	xiii
LIST OF APPENDICES	xv
ACKNOWLEDGEMENTS	xviii
1. INTRODUCTION	1
1.1 Location and Topography	2
1.2 Production and Ore Reserves	4
2. REGIONAL GEOLOGY	7
3. GEOLOGY OF THE SANGDONG MINE AREA	10
3.1 Stratigraphy	10
3.2 Intrusive Rocks and Mineral Deposits	16
3.3 Dyke Rocks	17
3.4 Geochronology of Intrusive Rocks and Mineral Deposits	18
4. THE SANGDONG ORE DEPOSIT	20
4.1 Structure	23
4.2 Zonal Distribution of Minerals	25
4.3 The Quartz-Mica Zone	29
4.4 The Amphibole-rich Zone	31
4.5 The Pyroxene-Garnet Zone	32
4.6 Marble and Limestone	35
4.7 Cherty Rocks	35
4.8 Quartz Veins	39
4.9 The Discovery of A New Molybdenite Deposit and A New Reserves of Tungsten Skarn	44
5. PETROGRAPHY OF THE SKARN	46
5.1 Early or Marginal Skarns	46
5.1.1 Wollastonite-Garnet Skarn	46
5.1.2 Garnet Skarn	47
5.2 Late Pyroxene-Garnet Skarns	56
5.2.1 Pyroxene-Garnet Skarn	56
5.2.2 Pyroxene-Quartz Skarn	58
5.2.3 Pyroxene-Plagioclase	58
5.3 Amphibole-rich Skarn	67
5.3.1 Amphibole-Pyroxene-Quartz Skarn	67
5.3.2 Amphibole-Quartz-Chlorite Skarn	68

page

5.3.3 Amphibole-Plagioclase-Quartz-Sphene Skarn 69

5.4 Mica-rich Skarns 75

5.4.1 Quartz-Mica-Chlorite 75

5.4.2 Quartz-Mica Skarn in the F. Orebody 77

6. MINERAL CHEMISTRY 83

6.1 Garnet 83

6.2 Pyroxene 90

6.3 Compositional Relationship Between Garnet and Pyroxene 98

6.4 Amphibole 103

6.5 Biotite 109

6.6 Muscovite 114

6.7 Chlorite 116

6.8 Newly Identified Minerals 122

6.8.1 Scapolite 122

6.8.2 Zeolite 122

6.8.3 K-feldspar 122

6.8.4 Rutile 122

6.8.5 Apophyllite 123

6.8.6 Illite 123

6.8.7 Other Minerals 123

6.9 Sulphide Minerals 127

6.9.1 Bismuthinite 127

6.9.2 Pyrrhotite and Pyrite 127

6.9.3 Arsenopyrite 128

6.9.4 Sphalerite 135

6.10 Wolframite 135

6.11 Scheelite 135

7. GEOCHEMISTRY OF THE MAIN OREBODY 140

7.1 Chemical Composition of the Unmineralized Early Skarn and the Late Pyroxene-Garnet Skarn 140

7.2 Composition of the Amphibole Skarn 142

7.3 Composition of the Quartz-Mica Skarn 142

7.4 Summary of Variation in Chemical Composition between Skarn Zones of the M1 Orebody 143

8. A DETAILED STUDY OF SMALL SCALE ZONING 158

8.1 Petrography and Mineral Chemistry 158

8.2 Chemical Changes 159

page

9. ALTERATION OF THE SLATE HOST 170

9.1 Mineralogy of the Slate in Mineralized and Unmineralized Zones 170

9.2 Geochemical Studies 172

9.3 Formation of Cherty Rocks 174

10. FLUID INCLUSIONS 181

10.1 Types of Fluid Inclusions and Their Distribution 182

10.2 Homogenization of Type A Inclusions in the Quartz Veins 191

10.3 Homogenization of Type A Inclusions in the M1 Skarn 196

10.3.1 Quartz of the M1 Skarn Orebody 196

10.3.2 Fluorite of the M1 Skarn Orebody 199

10.3.3 Pyroxene of the M1 Orebody 199

10.3.4 Scheelite of the M1 Orebody

10.3.5 Fluid Inclusions in Other Minerals of the M1 Orebody 206

10.4 Homogenization of Type B Inclusions 209

10.5 Homogenization of Type C Inclusions 213

10.6 Determination of Pressure and Pressure Corrections 216

10.7 Composition of The Fluid Inclusions 219

10.8 Summary 226

11. STABLE ISOTOPES 228

11.1 Sulphur Isotope Study 228

11.2 Carbon and Oxygen Isotopes in Carbonates 232

11.3 Oxygen Isotopes in Quartz 233a

12. CONDITIONS OF SKARN FORMATION 237

12.1 General Statement 237

12.2 Formation of Early Skarns 240

12.3 Formation of Later Pyroxene-Garnet Skarns 241

12.4 Formation of the Biotite and Amphibole Skarns 247

12.5 Formation of the Quartz-Muscovite-Chlorite Skarn 251

12.6 Formation of Chlorite 257

12.7 Formation of Scheelite 259

12.8 Formation of the Quartz Veins 268

13. THE EVOLUTION OF THE SANDONG SKARNS 270

REFERENCES 276

APPENDICES 285

LIST OF FIGURES

Figure		page
0.0	A view of the Sangdong mine.	0
1.1	Location map of the Sangdong mine.	3
2.1	Simplified geological map of the Korean peninsula.	8
3.1	Geological map of the Sangdong area.	11
3.2	An outcrop of the interbedded limestone stratigraphically equivalent to F2 orebody.	15
3.3	Typical microscopic appearance of the interbedded limestone equivalent to the M1 orebody.	15
4.1	Vertical cross section through the Sangdong orebodies.	21
4.2	A schematic view of the zonation in skarn orebodies.	22
4.3	Horizontal projection of the main underground structures.	24
4.4	A photograph of typical wollastonite skarn.	26
4.5	Horizontal projections showing zonal distribution of skarn zones in M1 and F2 orebodies.	27
4.5a	Illustration of difference in usage between zone and skarn.	28
4.6	A small scale quartz-mica skarn rimmed by amphibole skarn.	30
4.7	Quartz-mica skarn in direct contact with pyroxene skarn.	30
4.8	Longitudinal sections of the M1 orebody.	33
4.9	Sections of the Hangingwall Orebody(H1).	34
4.10	Photomicrograph of the interbedded limestone equivalent to the M1 orebody.	37
4.11	Photomicrograph of the limestone at the margin of skarn.	37
4.12	A cherty rock.	38
4.13	Generalized classification of "cherty rock" related to adjacent rocks.	38
4.14a	Mode of occurrence of molybdenite in quartz veins.	42
4.14b	Common association of molybdenite and sericite at the margins of quartz veins.	42
4.15	Wolframite-scheelite-quartz vein.	43
4.16	Occurrence of scheelite locally replacing wolframite.	43
4.17a	Location of a new discovery of skarn outside of the eastern margin of the M1 skarn.	45
4.17b	A new discovery of molybdenite deposit in the Jangsan Quartzite.	45
5.	Generalized spatial and paragenetic relations of zoned skarns at the Sangdong M1 orebody.	50
5.1	Typical wollastonite skarn close to the pyroxene-garnet skarn.	51
5.2	Photomicrograph of wollastonite-garnet skarn.	52
5.3	Photomicrograph of an andradite-diopside-calcite assemblage.	52

Figure		page
5.4a	Photomicrograph of wollastonite-garnet skarn replaced by late hydrated mineral.	53
5.4b	Apophyllite.	53
5.5	Wollastonite-garnet vein in the Pungchon Limestone above the H1 orebody.	54
5.6	Remnants of wollastonite-garnet skarn being replaced by pyroxene-garnet skarn.	54
5.7	Change of mineral composition in the pyroxene-rich zone with depth.	55
5.8	Two generations of garnet.	61
5.9	Vesuvianite associated with quartz and scheelite.	61
5.10a	Pyroxene-garnet skarn.	62
5.10b	Pyroxene-garnet skarn, crossed polars.	62
5.11	Epidote associated with quartz and scheelite.	63
5.12	Vein of magnetite replacing pyroxene skarn.	63
5.13a	Localization of magnetite, sphene and epidote in the pyroxene-garnet-rich zone.	64
5.13b	A schematic diagram showing distribution of the plagioclase-pyroxene skarn in deeper levels.	64
5.14a	Photomicrograph of the pyroxene-garnet skarn.	65
5.14b	A typical rock specimen of the pyroxene-garnet skarn.	65
5.15a	Photomicrograph of the pyroxene-plagioclase skarn.	66
5.15b	Same as above, crossed polars.	66
5.16a	Photomicrograph of pyroxene-quartz skarn.	71
5.16b	Replacement of pyroxene by amphibole at the boundary between the pyroxene-garnet and the amphibole zones.	71
5.17a	Replacement of the pyroxene-garnet skarn by amphibole and hedenbergite.	72
5.17b	A minor feature showing formation of amphibole-pyroxene skarn by replacement of the garnet dominant skarn.	72
5.18	A polished thin section showing the formation of the amphibole skarn by replacing the pyroxene skarn.	73
5.19	Typical microscopic appearance of amphibole-quartz-chlorite skarn.	73
5.20	Typical microscopic appearance of amphibole-quartz skarn	74
5.21	Formation of amphibole-plagioclase-quartz-sphene skarn by replacement of pyroxene-plagioclase skarn.	74
5.22	Photomicrograph of the quartz-mica(muscovite) skarn.	79
5.23	Photomicrograph of the quartz-mica(muscovite) skarn.	79
5.24	A specimen showing an ovoid of biotite, quartz and calcite formed within the quartz-mica zone.	80
5.25	A specimen showing the formation of quartz-biotite in the amphibole skarn.	80

Figure		page
5.26	Photomicrograph of amphibole and biotite at the the boundary of amphibole skarn and biotite skarn.	81
5.27	Green biotite-quartz-scheelite-apatite assemblage.	81
5.28	Quartz-mica skarn snowing abundant apatite and little scheelite.	82
5.29	Silicified quartz-mica skarn.	82
6.1	Chemical compositions of garnets plotted in terms of mole % of grossularite, andradite and others.	87
6.2	Variation in chemical compositions of zoned garnets.	88
6.3	Variation in chemical composition of zoned garnet plotted in terms of mole % of andradite, grossularite and others.	89
6.4	Pyroxene compositions plotted in terms of mole % of hedenbergite, johannsenite and diopside.	93
6.5	A polished thin section showing replacement of early formed garnet-pyroxene by late formed pyroxene.	96
6.6	A polished thin section showing replacement of the garnet-pyroxene skarn by late pyroxene.	96
6.7a	A typical specimen showing the formation of late pyroxene by replacing the pyroxene-garnet skarn along the rim of a quartz vein.	97
6.7b	Photomicrograph of late pyroxene in quartz associated with pyrite.	97
6.8a	Compositional zonation within the pyroxene.	99
6.8b	Comparative variation in the ratio of Mg/Mg + Fe between the early pyroxene in the skarn and the late pyroxene in the quartz vein.	99
6.9	Plotted K' values from Table 6.6.	100
6.10	Plotted K' values from Table 6.7.	101
6.11	Plotted K' values from Table 6.8.	102
6.12	Amphibole plotted in the diagram from Leake(1978).	108
6.13	Biotite locations.	112
6.14	Variation in chemical compositions of biotites in different zones(based on Table 6.12).	113
6.15	Ratios of Mg/Mg+Fe in biotite and coexisting chlorite.	118
6.16	Variation in Al_2O_3 contents of chlorites related to Al_2O_3 contents of coexisting minerals.	119
6.17	Correlation of the Ratio of Mg/Mg+Fe in coexisting chlorite and muscovite.	119
6.18	Nomenclature of chlorites.	120
6.19	Spatial variation in the Mg/Mg+Fe ratio of chlorites.	121
6.20	Generalized distribution of pyrite, pyrrhotite and bismuthinite.	131
6.21	Common appearance of bismuthinite in the quartz-mica skarn.	132

Figure		page
6.22	Native bismuth associated with chalcopyrite and pyrrhotite in the quartz-mica skarn.	132
6.23	Replacement of pyrrhotite by native bismuth.	133
6.24	Euhedral pyrite in the pyroxene-garnet skarn.	133
6.25	Coexisting magnetite, pyrite and pyrrhotite in the pyroxene-garnet skarn.	134
6.26	Pyrrhotite veins in magnetite.	134
6.27	Diagram showing change of colour of fluorescent scheelite with molybdenite content.	137
6.28	Diagram showing proportions of abundance of Mo-bearing scheelite in three different orebodies related to content of tungsten.	137
6.29a	Scheelite crystals showing zonation of molybdenum content.	138
6.29b	Enlarged picture of zoned scheelite crystals.	138
6.30	Zonal distribution of molybdenum-bearing scheelite in the Sangdong M1 orebody.	139
7.1	The chemical compositions of the early skarn and the pyroxene-garnet skarn plotted on an ACF diagram.	147
7.2	Variation in some elements in the amphibole skarn.	151
7.3	Variation in chemical composition of the quartz-mica skarn.	153
7.4	Variation in chemical compositions of different skarns in the M1 skarn orebody.	156
7.5	Variation in chemical compositions of three different skarns within the M1 orebody plotted on ACF & A'KF.	157
8.1a	A sketch showing mineralogical zonation in a relict block of the pyroxene-garnet skarn within the quartz-mica zone.	162
8.1b	Location of small scale zoning.	162
8.2	A sketch showing small-scale mineralogical zoning in the pyroxene-garnet skarn zone at the 7th level.	163
8.3	Variations of major elements across the 6 zones.	165
8.4	Element changes from part A to part F.	168
8.5	A schematic diagram showing formation of small scale and major zones at the Sangdong deposit.	169
9.1	Outline of skarn and scheelite mineralization.	175
9.2	Typical slate.	176
9.3	Scheelite in quartz veinlets in slate.	176
9.4	W versus SiO_2 contents in the mineralized slate.	178
9.5	Cherty rock facies cutting through bedding plane of Myobong slate.	180

Figure		page
9.6	A sketch showing an occurrence of cherty rock facies alteration in the Myobong slate between H1 and M1.	180
10.1a	Type A inclusions in a scheelite crystal.	186
10.1b	Type A inclusions in an apatite crystal.	186
10.2a	Typical type A inclusions in pyroxene crystal.	187
10.2b	Typical type A inclusions in fluorite.	187
10.3a	Type B inclusion in fluorite.	188
10.3b	Coexisting type A and type B inclusions in quartz.	188
10.4a	Type C inclusions showing halite and opaque daughter minerals in scheelite.	189
10.4b	Type C inclusions showing halite daughter mineral.	189
10.5a	Type C inclusion showing accidentally trapped solid crystals.	190
10.5b	Type D inclusions with type A inclusions in a scheelite crystal.	190
10.6a	Variation in the range of T_h shown by different groups of quartz veins.	192
10.6b	Variation of T_h in type A inclusions in a quartz vein.	192
10.7	Frequency distribution of T_h for vein quartz.	193
10.8	Variation in the range of T_h of vein quartz with depth.	194
10.9	Comparative histograms of T_h of fluid inclusions within quartz from three different skarns.	197
10.10	Plan showing distribution of T_h in fluid inclusions in quartz in the M1 skarn orebody.	198
10.11	Histograms plotting frequency versus T_h of fluid inclusions in pyroxenes and garnets from the M1 skarn.	201
10.12	Variation of T_h of fluid inclusions at the marginal part of the M1 skarn orebody.	203
10.13	Plan showing distribution of the highest T_h values in pyroxene crystals.	204
10.14	Plan showing distribution of the lowest T_h values in pyroxene crystals.	205
10.15a	Histogram showing a comparative range of T_h between Mo-rich and Mo-poor scheelites.	207
10.15b	T_h values in scheelite of the M1 orebody.	207
10.16	Distribution of T_h values in scheelite crystals.	208
10.17a	Fluid inclusion(type A) in garnet enclosing scheelite.	210
10.17b	Fluid inclusions in amphibole.	210
10.18	Two liquids in one single inclusion.	211
10.19	Extrapolated solubility curve along the Sangdong halite trapping.	214
10.20a	Type C inclusion showing halite and sylvite.	215

Figure		page
10.20b	Type C inclusion showing two daughter minerals, halite and sylvite, in pyroxene.	215
10.21	Phase diagram for part of the system NaCl-KCl-H_2O.	222
10.22	Variation in salinities of fluid inclusions in quartz with depth.	223
10.23	T_h versus salinities from quartz, scheelite, fluorite and pyroxene.	224
10.24	A possible range of P-T-X estimated by plotting critical temperatures in the system NaCl-H_2O.	225
11.1	Comparison of $\delta^{13}C$ versus $\delta^{18}O$ values of calcite from the interbedded limestone and the skarn orebody.	234
11.2	A schematic diagram showing variation of $\delta^{13}C$ values for non-mineralized limestone and mineralized zone in the Sangdong area.	234
12.1	Trends in the change of bulk chemistry and mineral assemblages st Sangdong skarns.	239
12.2	Stability fields of the Sangdong skarns.	242
12.3	Stability fields for pyrite, pyrrhotite, hedenbergite and andradite.	245
12.4	Estimate of conditions during late pyroxene-garnet skarn and amphibole skarn formation in terms of f_{O_2}- f_{S_2} at 400°C.	246
12.5	Estimate of conditions of muscovite-rich skarn formation in the system Fe-O-S on an f_{S_2}- f_{O_2} diagram at 350°C.	250
12.6	Estimate of formation temperature from atomic % As in arsenopyrite.	252
12.7	Comparison of conditions of formation between pyroxene-garnet skarn and quartz-muscovite skarn in which ferberite, magnetite, calcite and scheelite occurs.	254
12.8a	Log$\Sigma SO_4/\Sigma H_2S$ versus T diagram displaying the possible fields of formation of sulphide minerals in the hydrous skarns.	256
12.8b	Log$\Sigma SO_4/\Sigma H_2S$ versus pH (at 350°C) diagram.	256
12.9	Log f_{O_2}- f_{S_2} diagram indicating the stability field of scheelite.	263
12.10	Scheelite stability field dependent on $^aCa^{++}$, pH, f_{S_2} and f_{O_2} at 350°C.	264
12.11	Dependence of K_2 on ionic strength.	265
12.12	Control of pH and $^aCa^{++}$ at 350°C, I = 1.0, on the stability of W in equilibrium with scheelite.	266
12.13	Solubility of W_t in equilibrium with scheelite at I = 1.0 for $^aCa^{++}$= 10^{-7}, 10^{-6}, & 10^{-5}.	267
13.1	Diagrammatic vertical section of Sangdong skarns showing fluid circulation.	274
13.2	Generalized conditions of evolution of the Sangdong deposit.	275

LIST OF TABLES

Table		page
1.	Production of tungsten from the Sangdong Mine.	5
3.1	Geological column at the Sangdong Mine.	12
3.2	Geochronology of plutons and mineral deposits near the Sangdong Mine.	19
4.1	Mineral assemblages in quartz veins.	41
5.1	Outline of mineralogical compositions of different zones in the M1 orebody.	48
5.2	A summary of paragenesis of minerals in wollastonite-garnet skarn and garnet skarn.	49
5.3	A summary of paragenesis of minerals in late anhydrous skarns.	60
5.4	A summary of paragenesis of minerals in amphibole skarn.	70
5.5	A summary of paragenesis of minerals in mica-rich skarn.	78
6.1	Chemical compositions of typical garnets occurring in the main rock types.	85
6.2	Chemical compositions of garnets occurring in the pyroxene-garnet skarn at the 7th level.	86
6.3	Chemical compositions of representative pyroxenes.	91
6.4	Chemical compositions of pyroxene and garnet separated from the M1 orebody.	94
6.5	Comparison of chemical composition between early and late formed pyroxenes.	95
6.6	Comparison of average ratios of X_{hd}/X_{ad} between garnet and pyroxene from the 7th level.	100
6.7	Ratios of $X_{hd}/1-X_{hd}/X_{ad}/1-X_{ad}$ in garnet and pyroxene pairs.	
6.8	The ratios of $X_{hd}/1-X_{ad}$ versus $X_{ad}/1-X_{ad}$ of coexisting garnet(rim) and pyroxene pairs.	102
6.9	Representative chemical compositions of amphiboles analysed by electron microprobe.	105
6.10	Chemical compositions by XRF of amphiboles separated from the M1 orebody.	106
6.11	Chemical zonation within single amphibole crystals.	107
6.12	Mean of chemical compositions of biotites.	111
6.13	Chemical compositions of muscovites.	115
6.14	Chemical composition of biotite coexisting with muscovite.	117
6.15	Chemical compositions of chlorites.	117
6.16	Chemical compositions of zeolite minerals in the pyroxene-plagioclase skarn.	124
6.17	Microprobe analyses of K-feldspar, rutile, scapolite, illite and apophyllite.	125
6.18	Microprobe analyses of epidote, plagioclase, vesuvianite, sphene and wollastonite.	126

Table		page
6.19	Microprobe analyses of pyrite, pyrrhotite and arsenopyrite.	129
6.20	Microprobe anlyses of sphalerite in a quartz-mica skarn and quartz veins.	130
7.1	Chemical composition of typical anhydrous skarns.	148
7.2	Calculated chemical losses and gains of elements during formation of the wollastonite skarn from limestone and for the formation of pyroxene-garnet skarn from the wollastonite skarn.	149
7.3	Chemical gains and losses in the formation of the late pyroxene-garnet skarn.	150
7.4	Chemical compositions of amphibole skarn.	152
7.5	Chemical compositions of typical quartz-mica skarn.	154
7.6	Chemical gains and losses in the formation of the amphibole and mica skarns from pyroxene-garnet skarn.	155
8.1	Summary of mineralogical variation in different zones of the small scale zoning on the 7th level.	164
8.2	Chemical compositions of different zones in the small scale zoning.	166
8.3	Chemical gains and losses in the formation of a small scale zoning.	167
9.1	Chemical compositions of mineralized and unmineralized Myobong slate.	177
9.2	The analytical data of Kim(1976) for the Myobong Formation.	178
9.3	Comparison of chemical compositions between slate, the cherty facies, and the horizontal rock.	179
10.1	Comparison of the T_h in fluorite and quartz in quartz veins.	195
10.2	Comparison of T_h of fluid inclusions in fluorites from the quartz veins and the M1 orebody.	195
10.3	Comparison of T_h of fluid inclusions for different styles of homogenization in pyroxenes.	202
10.4	Calculated values of bulk density of CO_2-bearing inclusions.	217
10.5	Critical temperatures applied to estimate pressures of of trapping inclusions.	217
10.6	Range of possible correction to the homogenization temperatures of type A inclusions at different pressures and salinities at the Sangdong tungsten skarn deposit.	218
11.1	$\delta^{34}S$ values of sulphide minerals.	230
11.2	$\delta^{34}S$ values of coexisting pairs.	231
11.3	Carbon and oxygen isotope analyses of calcite.	235
11.4	Calculated $\delta^{18}O_{fluid}$ and $\delta^{13}C_{fluid}$ from $\delta^{18}O$ and $\delta^{13}C$ values of calcite and T_h values.	236
11.5	Calculated $\delta^{18}O_{fluid}$ from $\delta^{18}O$ values of quartz.	236

LIST OF APPENDICES

Appendix		page
1.	List of specimens.	285
2.	Location of samples from the interbedded limestone equivalent to the M1 orebody.	293
3.	Chemical compositions of the interbedded limestone.	294
4.	Chemical compositions of granitic rocks near Sangdong mine.	295
5.	Chemical compositions of dykes in the mineralized zone and unmineralized zone.	296
6.1	Chemical compositions of different zones in garnet crystals between different coloured crystals.	297
6.2	Variation in chemical compositions of three garnets.	298
6.3	Variation in chemical compositions of garnets.	299
6.4	Comparison of chemical compositions of pyroxenes between early and late ones in specimen 103148.	300
6.5	Chemical compositions of coexisting pyroxene and garnet rims, specimen 103104.	301
6.6	Microprobe analyses of amphiboles.	302
6.7	Classification of calcic amphiboles.	303
6.8	Comparison of chemical compositions of biotites occurring in different host rocks.	304
6.9	Comparison of chemical compositions of biotites in the quartz-mica skarn at the 7th level.	305
6.10	Chemical compositions of chlorites closely associated with biotite, amphibole, muscovite and illite.	306
6.11	Microprobe analyses of amphiboles from the minor zonal structure.	307
6.12	Analytic results of amphibole-pyroxene skarn occurring along a quartz vein in the garnet-dominant skarn.	308
6.13	Comparison of chemical compositions of pyroxenes in part A and in part B from 103084.	309
6.14	Chemical composition of chlorite occurring in a quartz vein.	310
7.	A spectrometric method for the determination of FeO in rock.	311
7.1	Semi-quantitative analyses of the pyroxene-garnet skarn to show variation in the chemical composition with depth.	312
7.2	Average chemical compositions of different skarns and original limestone.	313
8.1	Petrography of the small scale zoning.	314
8.2	Chemical compositions of pyroxenes in Parts F and E.	316

Appendix		page
8.3	Chemical compositions of garnet from parts F and E.	317
8.4	K' values of garnet and pyroxene in parts E and F.	318
8.5	Variation in chemical compositions of pyroxenes and amphiboles.	319
8.6	Variation in contents of major elements of amphiboles.	320
8.7	Variation in chemical composition of amphibole from part C to part F.	321
8.8	Variation in chemical composition of a single crystal of amphibole from part F.	322
8.9	Comparison of chemical compositions of biotites. between part C and part B.	323
8.10	Comparative chemical compositions of biotites in different localities.	324
8.11	Composition of muscovite in part A.	325
8.12	Comparison of chemical composition of chlorites in part A and part B.	326
9.1	Difference in FeO/Fe_2O_3 in mineralized and unmineralized Myobong slate.	327
9.2	Difference in mineralogical compositions between mineralized and unmineralized slate.	327
10	Fluid inclusion studies.	328
10.1	Microthermometry apparatus.	328
10.2	Data from fluid inclusions of quartz in the quartz veins.	329
10.3	Data from fluid inclusions of quartz in the M1 skarn.	333
10.4	Data of fluid inclusions from pyroxene.	338
10.5	Data from fluid inclusions in fluorite.	342
10.6	Data from type A inclusions in scheelite.	343
10.7	Comparison of T_h values between Mo-rich part and Mo-poor part in the zonation of a scheelite, and between two different single crystals.	345
10.8	T_h of fluid inclusions in apatite, amphibole, and biotite from the M1 orebody.	346
10.9	Data for fluid inclusions in garnets of the M1 orebody.	347
10.10	Data for type B inclusions.	348
10.11	Data from type C inclusions.	349
10.12	Examples of significant differences in T_h.	351
10.13	Description of phase changes in fluid inclusions on cooling and heating runs.	352
10.14	$NaCl-CaCl_2-H_2O$ system, compositions in weight percent.	359
10.15	$NaCl-CaCl_2-MgCl_2-H_2O$ system.	360

Appendix		page
11	SO_2 extraction for sulphur isotope analyses.	361
11.1	CO_2 extraction for carbon & oxygen isotope analyses.	362
11.2	Carbon and oxygen isotope values.	363
11.3	Detection limits of trace elements analysed by XRF.	363
12.1	Calculated free energy data(G_f,KJ/mol).	364
12.2	Miscellaneous thermodynamic data.	365
12.3	Calculation of $G^{\ominus}_{f,T}$ values from C_p data, $S^{\ominus}_{298}$ and $H^{\ominus}_{f,298}$ data.	366

ACKNOWLEDGEMENT

First of all, I am a great deal indebted and grateful to my supervisor, Dr. M. Solomon, who, with unfailing patience, guided my research during the course of the work at the University of Tasmania and assisted me with my English expression to complete this work. I would also like to express thanks to Prof. D.H. Green and Dr. R. Varne for their help in solving some financial problems for me.

I am grateful to Dr. N.C. Higgins who used his precious time to improve the final manuscript. Dr. C.J. Eastoe, whose advice and help were invaluable, supervised the first half of my research and to him I extend my thanks. I am also indebted to Dr. J.L. Walshe and my colleague Wayne Taylor, who contributed to my understanding of thermodynamic problems. All other members of academic staff at the University - particularly Mr. R.J. Ford, Drs. J.C. van Moort, D.V. Ellis, R.F. Berry and B.A. Stait - are thanked for their kind assistance.

Mr. P. Robinson's assistance enabled me to complete the analyses using XRF and spectrometric method, and Dr. D.C. Green and Mr. P. Robinson aided me in carrying out isotopic analyses. I am grateful to them for their assistance. I would also like to thank Mr. W. Jablonski in the Central Science Lab. for his kind instruction in the use of the electron microprobe.

I have to thank my fellow students, W. Taylor, E. Reid, G. Dixon, N. Ortez and J. Hajitaheri, for their assistance.

My thanks are extended to other University staff who helped me in various ways: Dr. T.A.P. Kwak at La Trobe University for up-to-date information on the study of fluid inclusions; Dr. G. Morrison at James Cook University for inviting me to a skarn workshop and showing me useful specimens of tungsten deposits in northern America; Prof. P. Ypma at the Adelaide University for his kind help with on fluid inclusion studies.

I would like to thank Dr. P. Blattner at the Geological Survey of New Zealand, for analysing oxygen isotopes in quartz from Sangdong. I would also express my thanks to Dr. A. Clark at Queen's University for his data on K-Ar ages of vein-type tungsten deposit near Sangdong Mine. I am also indebted to one of my previous colleagues at the mine, Mr. Hangjai Lee, who provided recent information on drilling.

I am very happy to express my thanks to Dr. D. Evans and Mrs. Topsy Evans, and Mr & Mrs. A. Eastgate, for their hospitality and friendship which helped maintain in comfortable circumstances during my study.

Financial assistance was received under the Colombo Plan and from a University of Tasmania research award, and also from the K.T.M.C.

Finally, for her support, encouragement and patience, I express my gratitude to my wife, So Yun.

Fig. 0.0. A view of the Sangdong mine(looking south).

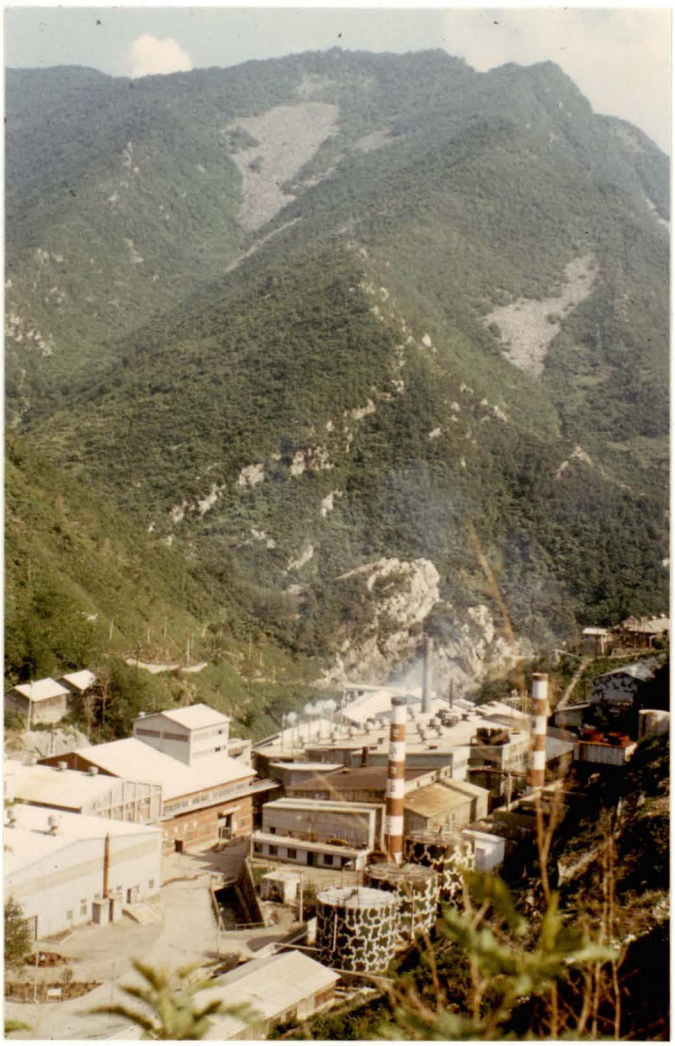

1. INTRODUCTION

They say in Korean that the Sangdong Tungsten Deposit is one of the miracles of the Republic of Korea, one of the poorest countries of the world in terms of natural resources.

Since the deposit was discovered by Soon Won Hwang in 1916, this mine has operated for more than fifty years, maintaining an annual production of scheelite concentrates between several hundred and about 5,000 metric tons. The Korea Tungsten Mining Company(K.T.M.C), established in 1952, has ore reserves to last several more decades and has expanded its mining interest to metallurgical extraction and manufacture of tungsten products. Besides, tungsten, substantial amounts of molybdenum, bismuth and gold are produced from this deposit. Recent exploration has disclosed a new molybdenite deposit lying mainly in the Jangsan Quartzite underneath the present orebodies.

The deposit was first described by Gallagher(1947) and Klepper(1947). Their investigations were limited to the upper part of the Main Orebody. Gabert and Vinken(1962) undertook the first microscopic study of the Main Orebody and they classified those mineral assemblages closely associated with scheelite. John(1963) undertook a microscopic examination of the Main Orebody and Jeong(1963) first suggested the zonal distribution of mineral assemblages. Yun(1966), Kim and Park(1970), and Hong et al.(1970) investigated and described the underground geology of the Sangdong mine as well as the regional geology. A detailed mineralogical description was carried out by So(1968), and Lee and Kim(1969), and a study of the geology and zoning of several orebodies such as the Main Orebody(called M1), Hanging-wall Orebody(called H1), and Footwall Orebody(called F1, F2 and F3) was performed by this author(Moon, 1972 & 1974). Kim(1976) approached the problem of the source of the tungsten by a geochemical study of the host slate. Finally, Farrar et al.(1978) and Clark(1981) carried out potassium-

argon age dating on Sangdong intrusive rocks and ore material.

There is considerable difference of opinion about the origin of this ore deposit with ideas varying from magmatic metasomatic to sedimentary. Though most early authors favoured a magmatic origin, several recent papers have postulated a syngenetic sedimentary origin for the tungsten(So, 1968; Maucher, 1976; Kim, 1976). This thesis is an attempt to resolve this problem by geological, mineralogical, and geochemical studies.

1.1. Location and Topography

The Sangdong Tungsten Mine is situated at Guraeri, Sangdongeup, Youngwolgun, Gangwondo(Gangwon province), in the middle of the eastern part of the Korean peninsula(Fig. 1.1). This area is approximately located by latitude 37°08'45" and longitude 128°50'10", and is about 200 km east-south-east of Seoul, the capital city of the Republic of Korea. The most convenient way of approaching the mine from Seoul is by taking an express train to Seokhang station, and using a local regular bus or the mine's travel service.

The Sangdong area is in the central portion of the highest and the most rugged part of the Taebaegsan Range in one of the deep valleys running north-south on the southern slopes of Baegun Mountain(Baegunsan, 1428 m). The highest outcrop of the Sangdong orebodies is about 800 metres above sea level, the main adit(called Sangdonghang) is at about 650 metres, and the mine office is located on the floor of the valley at about 550 metres. Many peaks in the Sangdong area, e.g. Sunkyeongsan(1,152 m), Maebongsan (1,282 m) to the southeast, and Jangsan(1,408 m) to the southeast, consist of the Jangsan Quartzite and form long narrow ridges paralleling the axis of the Baegunsan Syncline(Kim, 1976). These peaks are separated by V-shaped valleys in general, forming a dendritic pattern. However, north-south trends of valleys are dominant in the Sangdong mine area.

Fig. 1.1. Location map of the Sangdong mine.

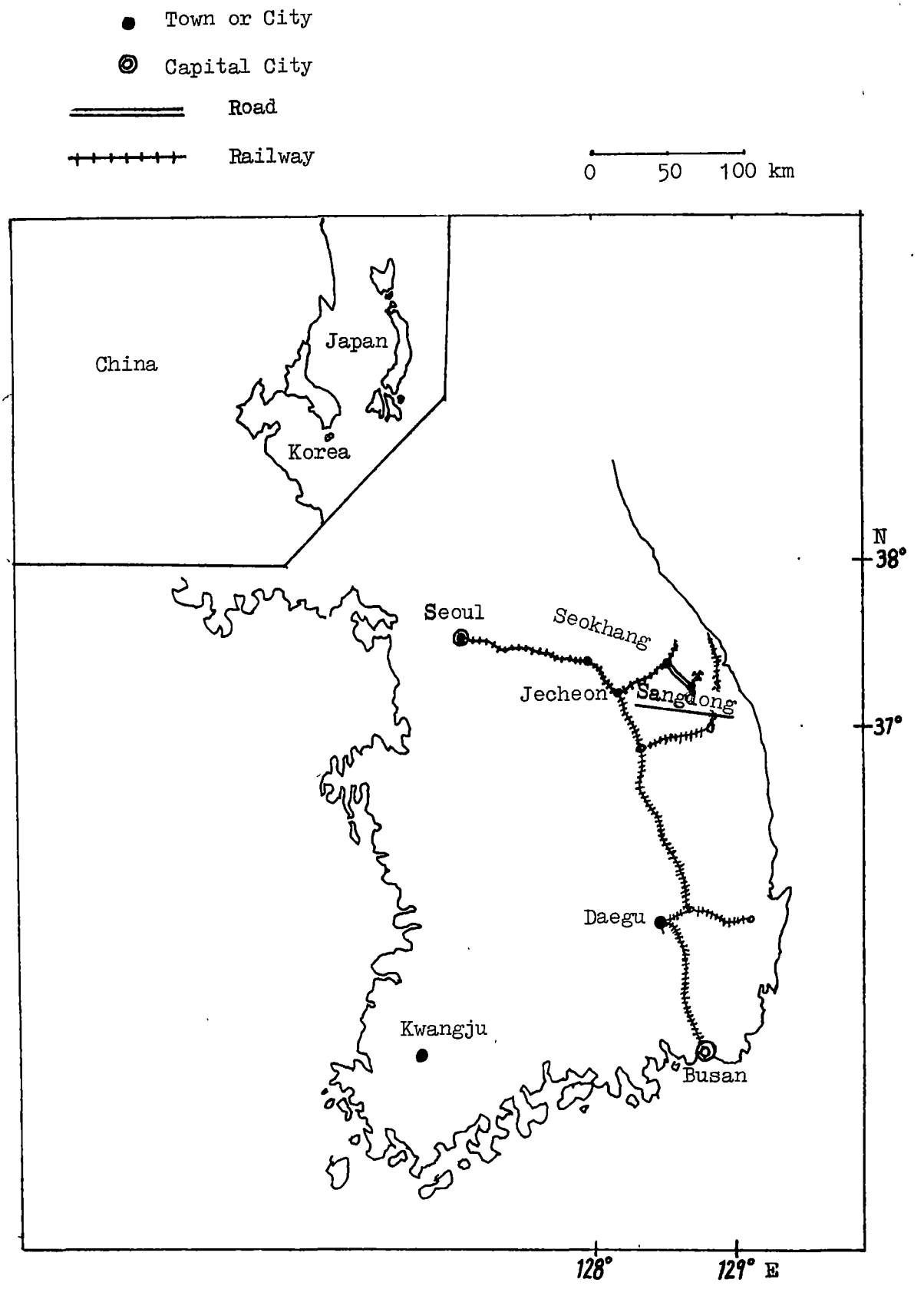

1.2. Production and Ore Reserves

No reliable data about the output of tungsten concentrates from the Sangdong Mine before 1951 are available althnough Gallagher(1947) and Klepper(1947) described the mining history and production in the Sangdong Mine. Until 1939 the surface portion of the Main Ore Body(M1) was exploited at or near the Sunkyeong level(top level in the mine) and from 1938 to 1946, 7,500 tons of scheelite concentrates(about 70 % WO_3) are estimated to have been produced. Since the K.T.M.C began operating this mine in 1952, the annual production of scheelite concentrates has been maintained at about 4,000 tons. The recovery of scheelite from the crude ores was improved by chemical processes in 1960. Ammonium paratungstate (APT) has been produced at the mine since 1973, as the first step in the production of tungsten metal. The mine has produced(Table 1) approximately 160,000 metric tons of scheelite concentrates(74 % WO_3), equivalent to 118,400 metric tons of metallic tungsten. The total reserves plus production are estimated at about 591,000 tons of scheelite concentrates. The relative proportion of scheelite in the three ore bodies, the Main Ore Body(M1), Footwall Ore Body(F.) and Hangingwall Ore Body(H1), is 6 : 1 : 3.

Ore reserves have been increased as economic cut-off grades have become lower. For instance, before 1945, mining was concentrated in the highest grade tungsten ore from the quartz-mica-rich zone above the Sangdong level(present main adit). Old data before 1945 describing the thickness of the ore body as three or four metres indicate that only the quartz-mica zone was considered to be minable ore. After the geological department was established at the mine in 1964, the ore reserves have been changed through the inclusion of about 0.5 to 1.0 metres of the cherty rock below the central part of the M1 orebody, which has an average grade of 0.5 to 0.8 % WO_3.

Table 1. Production of tungsten(74 % WO_3 concentrates) from the Sangdong mine/(metric tons).

	scheelite concentrate	synthetic scheelite conc.	APT (89 % WO_3)
1938 - 1946	7,500		
1948 - 1949	10,000		
1950 - 1959	56,000		
1960 -	3,797	768	
1961	4,587	1,734	
1962	4,100	1,736	
1963	3,305	1,224	
1964	3,354	1,325	
1965	2,607	1,257	
1966	2,318	1,269	
1967	2,030	1,223	
1968	1,948	1,465	
1969	1,901	1,450	
1970	1,733	1,377	
1971	1,192	1,972	
1972	1,017	1,921	
1973	1,630	1,070	560
1974	1,835	797	928
1975	1,820	1,270	640
1976	880	1,370	1,467
1977	1,040	512	2,016
1978	1,070	477	1,950
1979	790	685	2,063
1980	720	800	2,160

Secondly, the No.1 Footwall Ore Body(F1) lying about two metres below the Main Ore Body(M1), and the slate between, were added to the ore reserves. This new ore reserve is limited to the area below the quartz-mica-rich zone and the amphibole rich zone, in which quartz veinlets bearing scheelite occur in the slate.

Molybdenite in quartz veins was mined by a separate mining method until 1967, but no data on the output of molybdenite are available. Nowadays, the mine recovers molybdenum by a chemical process and the proportion of molybdenum concentrate that comes from molybdenite in quartz veins is not known. The average contents of Mo and Bi are each about 0.03 %.

The Sangdong mine has a master plan to develop the Hangingwall Ore Body(H1) from 1984 with a new mining method. Cavities of the mine have been filled with sandy slimes pumped from the dressing plant since 1965, and the rest of the tailings is retained in two dams. Minor contents of scheelite, about 0.19 % WO_3, in the tailings of two dams also will be a significant ore reserve in the future.

2. REGIONAL GEOLOGY

The Korean peninsula is located in the south-eastern margin of the North China-Korean Platform. The southern half of the Korean peninsula, the Republic of Korea, has been classified into four geological provinces by*Kim(1975), viz. the Gyeonggi Massif, the Ryeongnam Massif, the Ogcheon geosynclinal zone, and the Gyeongsang sedimentary basin(Fig. 2.1).

The Gyeonggi Massif province occupies the north-eastern region of South Korea and is mainly composed of granite gneiss and schist of Precambrian age, while Jurassic granites occur widely along a NE-SW trend known as the Sinian direction(Reedman and Um, 1976). The Ryeongnam Massif province covers the south-western part of the Republic. It consists mainly of granite gneiss and schists of the Yulri Group of Precambrian age, and in addition, large intrusions of anorthosite, gabbro and diorite are found in the southern part of the massif.

The Ogcheon geosynclinal zone lies between the Gyeonggi Massif and the Ryeongnam Massif along the Sinian direction. This province comprises two different basins, the Ogcheon and Taebagsan basins. This division is also evident on metamorphic grade. The Ogcheon Group within the Ogcheon basin consists of metamorphosed pelitic rocks, pebbly mudstone and thin limestone layers with some mafic volcanics. The Taebaegsan basin contains the Joseon Group of Cambro-Ordovician age and the Pyeongan Group of late Carboniferous to early Triassic age. Both are unmetamorphosed. Jurassic and late Cretaceous granites occur widely in this province.

The Gyeongsang sedimentary basin comprises a thick sequence of post-orogenic molasse-type sediments intercalated with lavas and volcanic rocks of Cretaceous age(Reedman and Um, 1976). Late Cretaceous and Paleogene granite stocks crop out in the basin.

Four distinct phases of granitic activity are recognized in the Korean

*Kim(1975) : O.J. Kim

Figure 2.1. Simplified geological map of the Korean peninsula.
(after Reedman & Um 1976)

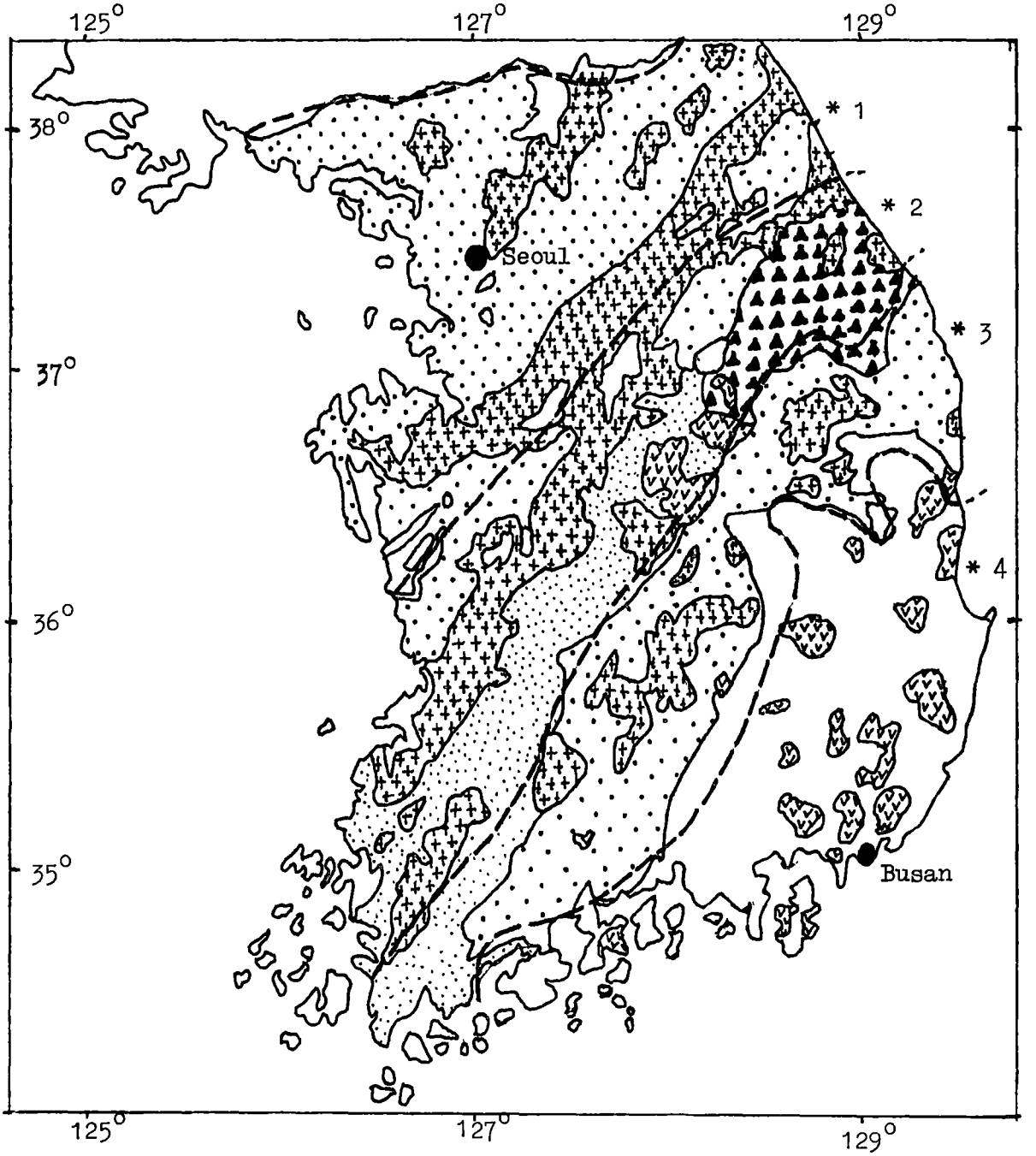

peninsula: Precambrian, Triassic, Jurassic and Cretaceous. The Triassic granitoids are distributed only in the northern half of the peninsula. The Jurassic granites, related to the Daebo Orogeny, crop out mainly in the central part of the peninsula and have a NE-SW elongation: The Cretaceous Bulgugsa granites occur mainly in the southeast corner of the peninsula. These spatial and temporal distributions of the granitoids are apparantly associated with a northwest to southeast progression with time of a subduction system(Reedman and Um, 1976).

The Daebo Orogeny, of Jurassic age, was the main metamorphic and tectonic episode in the geological history in the Korean peninsula. It formed the Ogcheon Fold Belt, the Daebo granite series, and caused the destruction of the Ogcheon Basin as well as of the marginal parts of the Gyeonggi Massif and Ryeongnam Massif.

The Sangdong area occupies the southeastern most part of the non-metamorphic zone in the Ogcheon Fold Belt. It is situated in the southern limb of the Baegunsan Syncline which is one of the major folds of the non-metamorphic zone in the belt. The axis of the Baegunsan Syncline lies transverse to the main northeasterly trend of the Ogcheon Belt(Reedman and Um, 1976).

3. GEOLOGY OF THE SANGDONG MINE AREA

3.1. Stratigraphy

Detailed descriptions of the geology of the Sangdong area have been presented by mining geologists from the Sangdong mine. These are summarized in the geological map of Fig. 3.1 and details of the stratigraphy are summarized in Table 3.1.

Sangdong is on the southern limb of the Baegunsan Syncline. Precambrian schists of the Yulri Group occupying most of the area to the south are overlain unconformably by Paleozoic meta-sediments and early Mesozoic sediments.

The Yulri Group, commonly also known as the Taebaegsan Group, comprises micaceous quartzites, chlorite schists, biotite-sillimanite schists, muscovite-biotite-cordierite schists, biotite-quartz-andalusite schists, phyllites and lime-silicate rocks(Reedman and Um, 1976). The strike of the units ranges from N 30°W to N 60°W, and the dip varies from a general 10 or 20 to 50° to the east.

Paleozoic Metasediments.

* Joseon Supergroup (Yangdeok Series);-

The Jangsan Quartzite and the Myobong Slate(Formation) constitute the Joseon Supergroup. They strike generally N 70 to 80°E and dip 25 to 35°NW. The Jangsan Quartzite, the basal unit of the Joseon Supergroup, crops out at the entrance of the mine. It consists of compact, white, grey or pink quartzite. Reedman and Um(1976) have suggested that the presence of scattered pebbles and thin pebbly lenses, together with small-scale cross-bedding at many localities, is indicative of deposition in a shallow water, near-shore environment. Its thickness varies from 50 to 200 m and it is at its thickest in the Sangdong area.

The Myobong Slate, 150 m thick, consists of brown, dark grey and black slate or micaceous phyllite intercalated with several thin limestone beds and locally a few impersistent, thin beds. It overlies the Jangsan

Fig. 3.1. Geological map of the Sangdong area.

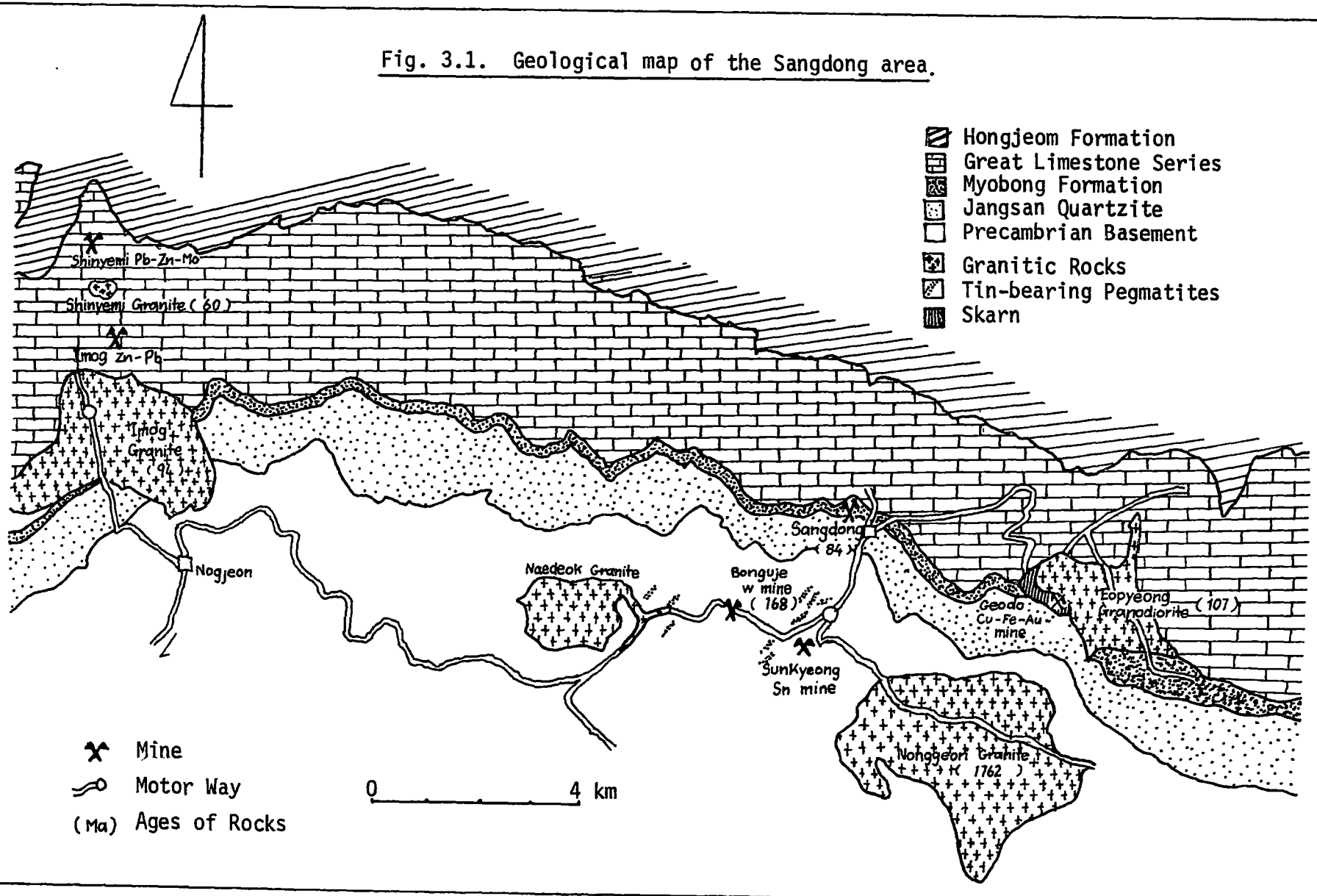

Table 3.1. Geological column at the Sangdong mine.

Geologic Age	System	Series	Formation name and description	Thickness (metre)
Upper Carboniferous	Pyeongan	Hongjeom	sandstone, shale, hornstone conglomerate and limestone; sandstone and shale are reddish.	250-350
	**********	Unconformity	**********	
Ordovician	Chosun	Great Limestone	Maggol Limestone Grey and dark grey limestone and dolomitic limestone	250-300
			Dumugol Formation Vermicular limestone and greenish grey sandy shale and marl	200-250
			Dongjeom Quartzite Dark grey and pale brown quartzite	20 - 30
Cambrian			Hwajeol Formation Vermicular limestone and sandy shale (Sesong Slate)	100 - 150
			Pungchon Limestone Milky white limestone(H1)	350—400
		Yangdeok (Joseon Supergroup)	Myobong Slate Shale, clay slate and thin beds(M1 & F.) or lenses of limestone	80 - 150
			Jangsan Quartzite White to dark grey quartzite	150 - 200
**********		Unconformity	**********	
Pre-cambrian		Taebaek (Yulri Group)	Mica Schist Spotted micaceous schist, Argillaceous slate or phyllite	

Quartzite conformably. The thin interbedded limestones in this formation were a prelude to deposition of the Great Limestone Series(Fig. 3.2). They range in thickness from 0.3 m in the lower horizon to 7 m in the highest horizon, about 20 m below the top of the Myobong Slate. This limestone horizon has been identified at other deposits, e.g. the Imog, Geodo, and Yeonhwa deposits, thus it extends for more than 40 km. Relics of fossils are observed in a specimen from these interbedded limestones near the mine (Fig. 3.3). Kobayashi(1966) has recognized trilobites such as Redlichia Obelella, and these indicate an early Cambrian age for the Myobong Slate (Formation).

* The Great Limestone Series

The Great Limestone Series, which consist dominantly of calcareous sediments, overlies the Myobong Slate conformably. The Pungchon Limestone (described as the Daegi Formation by Reedman and Um, 1976) is the basal unit of the Great Limestone Series. It consists of massive white and grey limestone with a thin intercalation of shale and marl in the lower part. It has a uniform thickness of about 280 m with no distinct bedding planes. Three trilobites, Megaraulos, Solenoparia and Olenoides, have been described thin intraformational limestone conglomerate beds at several localities. These are occasionally observed where cross-cuts intersect the Pungchon Limestone in the mine.

The Sesong Slate overlying the Pungchon Limestone consists of black slate, dark red and brown marl, and some thin limestone beds, with a thickness of 20 to 50 m. This unit is overlain by the Hwajeol Formation which is the youngest member of Cambrian sediments in this mine area,

The Hwajeol Formation has a characteristic vermicular texture formed by selective weathering of the surface. This peculiar appearance has led to the name 'worm-eaten-limestone'. The Hwajeol Formation is overlain conformably by the Dongjeom Quartzite which is the lowest Ordovician unit.

The Dongjeom Quartzite, with a thickness of 10 to 50 m, a widespread and distinctive marker horizon, consists of dark grey hematite-bearing quartzite, brown quartzite, thin shale beds and rare limestone lenses.

The Dumugol Formation overlies the Dongjeom Quartzite. It is composed of calcareous shale and grey limestone which contains a rich conodont fauna correlated with the Arenigian of Europe by Lee and Lee(1971). It displays the same peculiar vermicular texture as the Hwajeol Formation. Above the Dumugol Formation lies the top unit of the Great Limestone Series, the Maggol Limestone. This formation, about 300 m thick, is mainly composed of blue grey, massive to tabular limestone units containing a few thin shale bands(Reedman and Um, 1976). Lee and Lee(1971) suggested conodonts from this formation correlate with the Llanvirnian of Europe.

* Pyeongan Group;-

This group crops out between the middle part of the southern slope of Baegunsan(Mt. Baegun) and the summit.

The Hongjeom Group is Carboniferous to Triassic in age and contains the most important coal fields of Korea. The basal beds of the Pyeongan Group rest disconformably upon limestone of the Great Limestone Series of Ordovician age.

Fig. 3.2
An outcrop of the interbedded limestone stratigraphically equivalent to the F2 orebody.
Lenses of calcareous rock in the shale are converted to skarn while the thick limestone layer is altered to marble. Location; 500 m east of the M1 skarn orebody in Danyangchon creek.

Fig. 3.3. Typical microscopic appearance of the interbedded limestone stratigraphically equivalent to the M1 orebody. There appears to be a relict fossil in the middle. 103146, ═══ indicates 0.2 mm.

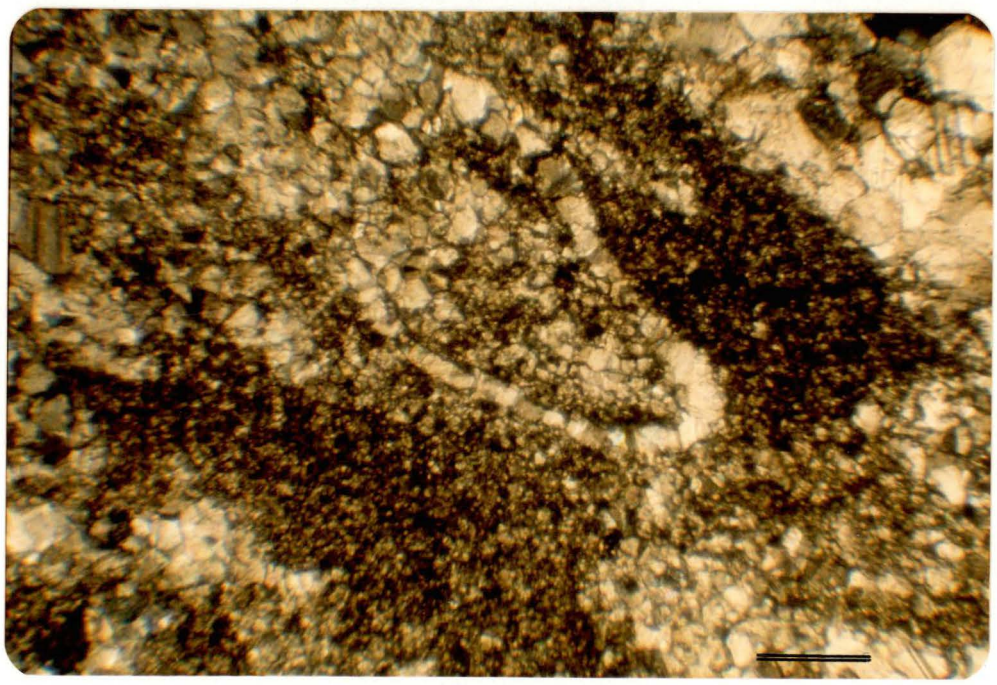

3.2. Intrusive Rocks and Mineral Deposits

There are few plutonic intrusions in the Sangdong mine area(Fig. 3.1). Two Mesozoic plutons, the Imog Granite and the Eopyeong Granodiorite, intrude the same sequences of rocks as occur in the Sangdong mine; the former is about 15 km to the west of the mine, the latter is about 4 km to the east. Two Precambrian granites intrude the Yulri Group(Taebaegsan metasediments) to the south of the mine.

Apart from the Sangdong mine, the mineral deposits of the area are spatially associated with intrusive rocks at the present erosional level.

The Eopyeong Cu-Fe-Au deposit(Geodo mine) is localized in a skarn found at the contact between the Eopyeong Granodiorite and the Myobong Slate and the Pungchon Limestone. Gold, chalcopyrite and magnetite have also been worked at the Geodo mine; no scheelite is associated with this deposit.

The Imog Granite intrudes both Yangdeok Series and the Great Limestone Series. Zinc and lead ores in skarn have been worked at the Imog mine on the northern boundary of this pluton; the Imog mine was closed recently.

The Shinyemi Granite is exposed about 1.5 km north of the Imog Granite, and the Shinyemi Zn-Pb-Mo deposit is located to the north of this pluton. This deposit has yielded sphalerite, galena and molybdenite from skarn, formed in lower Paleozoic limestone, mainly in the Maggol limestone. The skarn is associated with felsic intrusive dykes which have a north-south strike(Kim & Kim , 1978). An occurrence of scheelite was recently reported and confirmed by the author in a skarn orebody at the Shinyemi mine.

One of the Precambrian granites, Naedeok Granite, crops out about 5 km to the south-west of the Sangdong mine. The other one, the Nonggeori Granite, is exposed about 3 km to the south-east of the Sangdong mine. Contact metamorphic zones around these two granites are characterized by staurolites spotting of Precambrian schists. A number of tin-bearing pegmatites are thought to be derived from the two Precambrian granites on spatial evidence. The Sunkyeong mine, once the largest tin producers in

Korea, is occasionally worked. Scheelite is found rarely in the pegmatites. The Bongujae deposit, which is located between Naedeok Granite and the Sunkyeong mine (Fig. 3.1), was mined before 1940 and it consists of scheelite- and wolframite-bearing quartz veins which cut Precambrian schist. Quartz veins with thicknesses of a few centimetres to ten centimetres have silicified the schist and locally have sericite along their rims. The Sangdong mine(K.T.M.C) has a license to develop the mine in future.

3.3. Dyke Rocks

Extrusive rocks are not known in the mine area though Gabert and Vinken (1962) described a keratophyre. Recently a number of intrusive dykes have been found in and outside of the mine. They include altered felsic rocks (keratophyre), dolerite and basaltic dykes. The felsic dykes locally contain Cu, Fe and Mo sulphides, and apparently formed after the tungsten mineralization. The mafic dykes are older and have been metamorphosed during skarn formation. Chemical compositions of dykes in the Sangdong area are given in Appendix 5.

3.4. Geochronology of Intrusive Rocks and Mineral Deposits

Kim(1971) reported a K-Ar age for the Eopyeong Granodiorite of 107 Ma, which was confirmed by Farrar et al.(1978) who reported an age of 105 Ma. However, Ueda(1969) reported a K-Ar age of 169 Ma for the granite porphyry at the Geodo mine(Eopyeong deposit). Three different types of granitoids were recognized in the Eopyeong Granodiorite during a short visit to the pluton by the author and thus these conflicting results may reflect sampling of these different phases.

Kim and Kim(1978) reported two different ages, 94 and 193 Ma, for biotites in the Imog Granite, but the discrepancy was not clearly explained. They dated the age of the Shinyemi stock at 60 Ma. Sato et al.(1981) obtained a K-Ar age from phlogopite occurring in the Pb-Zn-Mo Shinyemi deposit of 75 Ma. They interpreted the age of the Shinyemi deposit as very close to that of the No.2 Yeonhwa Zn-Pb deposit(Yun and Einaudi, 1982) which is located 24 km to the east of the Sangdong mine.

Farrar et al.(1978) gave an age of 81 to 84 Ma for various minerals from the Sangdong mine, and Clark(personal communication, 1981) obtained 85.1 Ma by $^{40}Ar/^{39}Ar$ from the same sample of amphibole skarn used by Farrar et al. (1978). Clark(1981) gave an age of 168.7±0.8 Ma for sericite from scheelite -wolframite bearing quartz veins at the Bongujae deposit.

The Nonggeori Granite was dated at 1762 Ma by Farrar et al.(1978) and by Ueda(1969) at 1530 Ma, using muscovite(John, 1978).

The geochronological data are summarized in Table 3.2.

Table 3.2. Geochronology of plutons and mineral deposits near the Sangdong mine.

Pluton	Age(Ma)	Reference
Shinyemi stock	60	Kim and Kim(1978)
Imog Granite	94, 193	Kim and Kim(1978)
Nonggeori Granite	1762	Farrar et al.(1978)
	1530	Ueda(1969)
Eopyeong Granodiorite	107	Kim(1971)
	105	Farrar et al.(1978)
Eopyeong Granite porphyry	169	Ueda(1969)
Mineral Deposit		
Shinyemi Zn-Pb-Mo mine	75	Sato et al.(1981)
Bonguje W deposit	168	Clark(1981)
Sangdong mine (amphibole)	81 - 85	Farrar et al.(1978) Clark(1981)
Yeonhwa Zn-Pb mine	73	Sato et al.(1981)
Sangdong Skarn Orebody(in detail)		
Footwall slate (whole rock)	84.0 ± 2.6	Farrar et al.(1978)
Amphibole skarn (hornblende)	83.9 ± 2.8	Farrar et al.(1978)
(hornblende)	85.1	Clark(1981)
Quartz-Mica skarn (biotite)	83.6 ± 2.6	Farrar et al.(1978)
Quartz-Mica skarn (muscovite)	81.2 ± 2.4	Farrar et al.(1978)

4. THE SANGDONG ORE DEPOSIT

The orebodies are generally divided into two different types, viz. massive skarns and quartz veins. The skarn orebodies(Figs. 4.1 & 4.2) are classified as the Main Orebody(M1), the Footwall Orebody(F1, F2, .) and the Hangingwall Orebody(H1), while quartz veins are divided into two groups depending on the predominant ore minerals, generally either wolframite or molybdenite.

M1 is located in the upper horizon of the Myobong Formation, about 20 m below the top of the formation. It extends 1.5 km along strike and 1.2 km down dip, with a thickness of about 6 metres. Along strike, it passes into unmineralized limestones.

H1 is located at the boundary between the Myobong Formation and the Pungchon limestone. It is generally 10 to 30 m thick, but reaches over 100 m where mineralization extends into the Pungchon limestone along a vertical extension of the high grade core of the M1 orebody(Fig. 4.2). This extension of H1 in the Pungchon limestone is known as 'Expanded H1 in Pungchon limestone' at the mine(Fig. 4.9). H1 extends more than 1 km along strike, and 400 m down dip. This orebody was not regarded as economic one until 1964, however, the main output from the mine will be from H1 after 1984.

F. orebody consists of several thin stratiform lenses with thicknesses of 0.3 to 0.8 m. F1 lies only 2 m below the M1, so ore reserves of this orebody have been included in the reserves of M1. The F2 lies about 40 m below the M1 with an average thickness of 0.5 km. The F3 appears about 5 m below the F2, comprising two or four separate lenses, with an average thickness of 0.3 m. A few thin Footwall Ore Beds have been confirmed by drilling in lower horizons of the Myobong Formation, about 10 m above the Jangsan Quartzite.

Fig. 4.1. Vertical cross section through the Sangdong scheelite orebodies(looking east).
(after Moon, 1974)

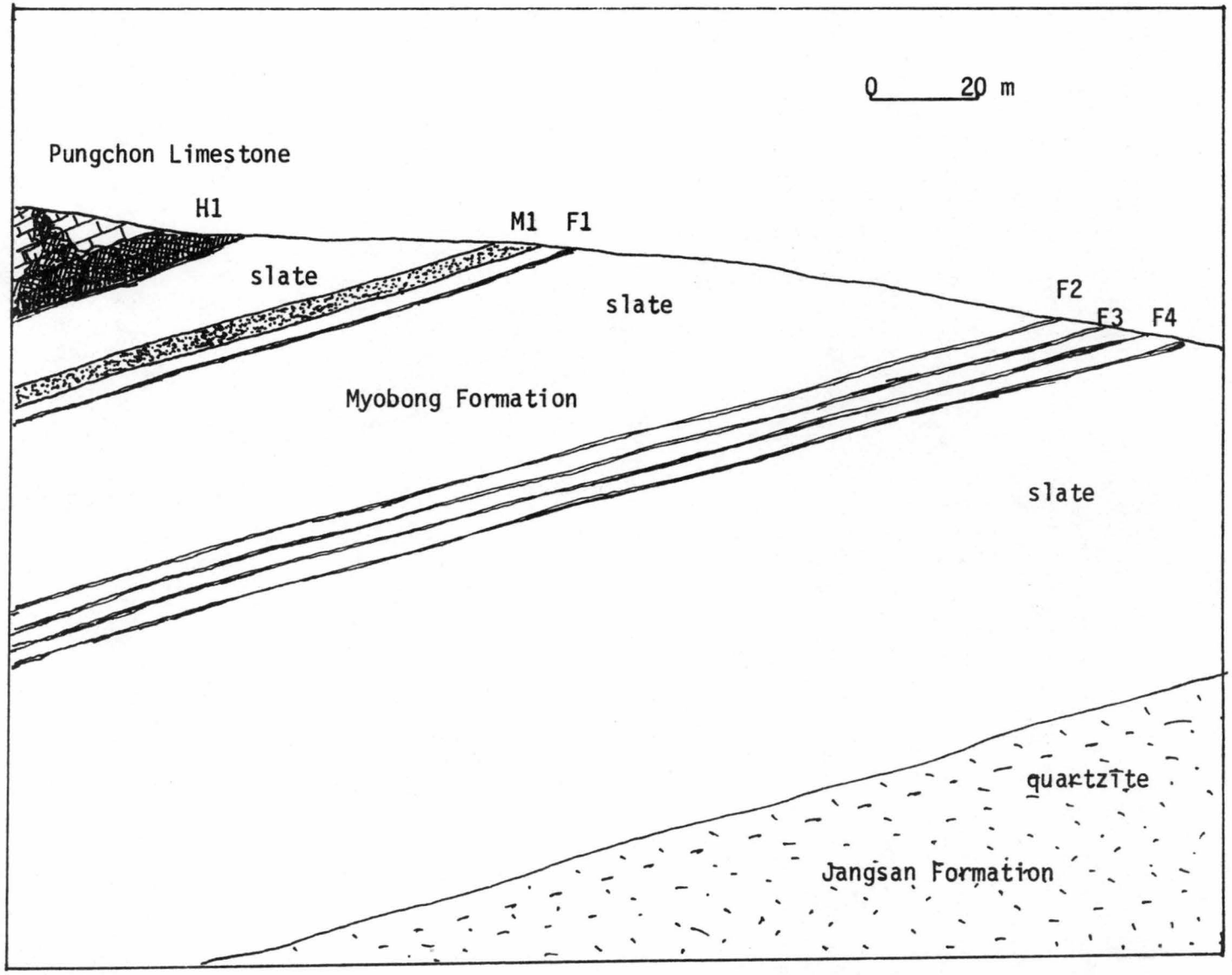

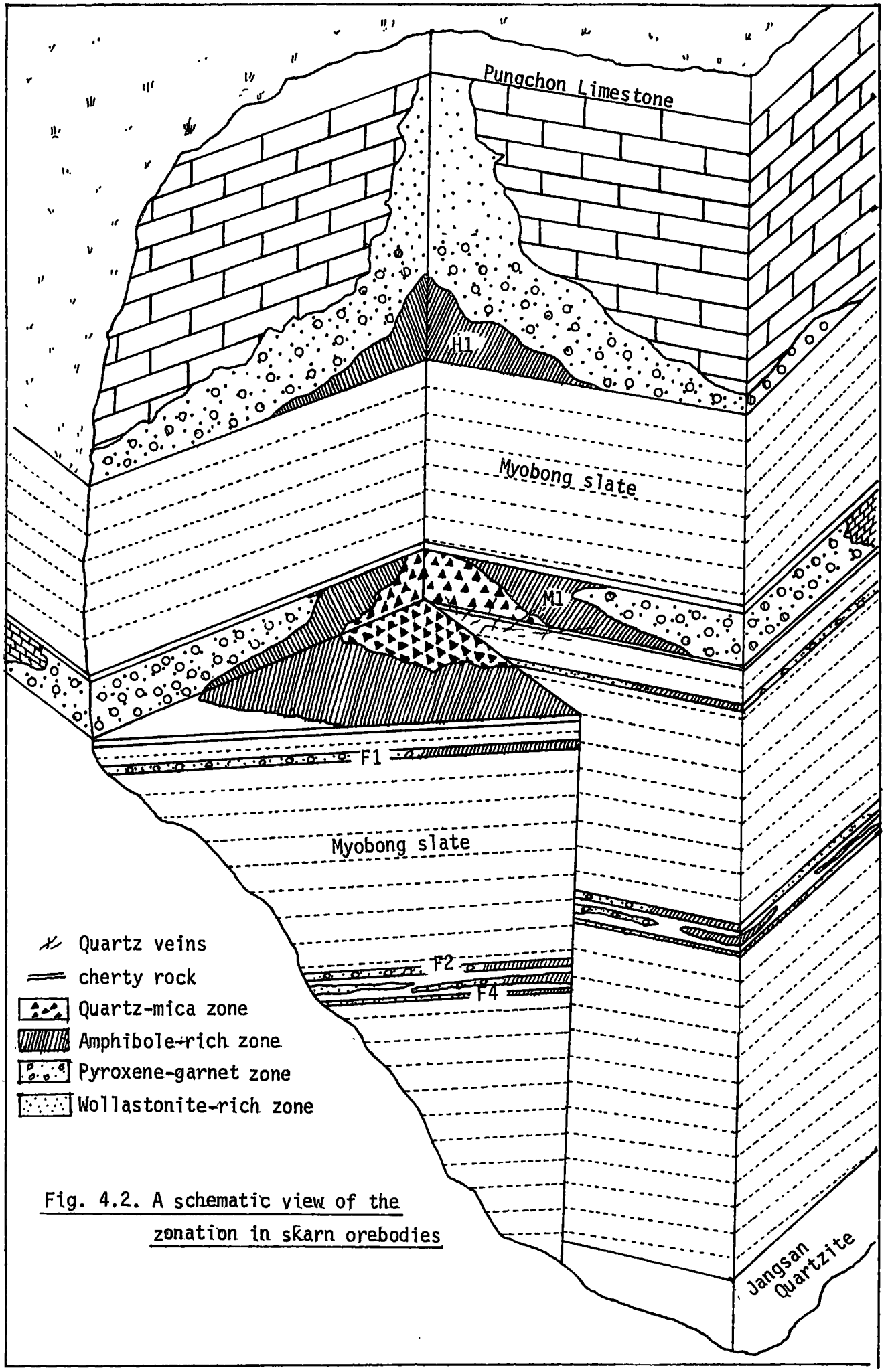

Fig. 4.2. A schematic view of the zonation in skarn orebodies

4.1. Structure

The form of the M1 & F. orebodies in the Myobong slate are primarily controlled by the bedding(Fig. 4.1), but the distribution of H1 in the Pungchon limestone and the late stage mineralization in M1 and F. orebodies are controlled by other structures.

In the upper mine levels, bedding-plane thrusts are developed along the boundary between M1 and the hangingwall slate, mainly in the middle part of the M1 orebody. These thrusts may have been formed at the time of formation of the Baegunsan Syncline. Clay along these faults causes collapse of the hangingwall during mining.

There are also shear zones that cause sharp changes in strike of the M1, and these strike parallel to the pitch of the orebody. These two dominant fault types,which are premineralization structures,caused local upwarping or anticlinal folding of the Myobong slate and the Pungchon limestone. Quartz veins beneath the M1 orebody are generally concordant with the bedding plane, however, discordant quartz veins occupy transverse tension fractures.

The dominant post-mineralization structures in the mine trend NE-SW and are near vertical. The Daegog, Shindaegog and Mungog deep valleys probably developed along such structures. About 30 m of horizontal displacement is observed in the Daegog valley creek.

An outline map of the underground structures at the Sangdong mine is shown in Fig. 4.3.

Fig. 4. 3. Horizontal projection of the main underground structures at the Sangdong mine.

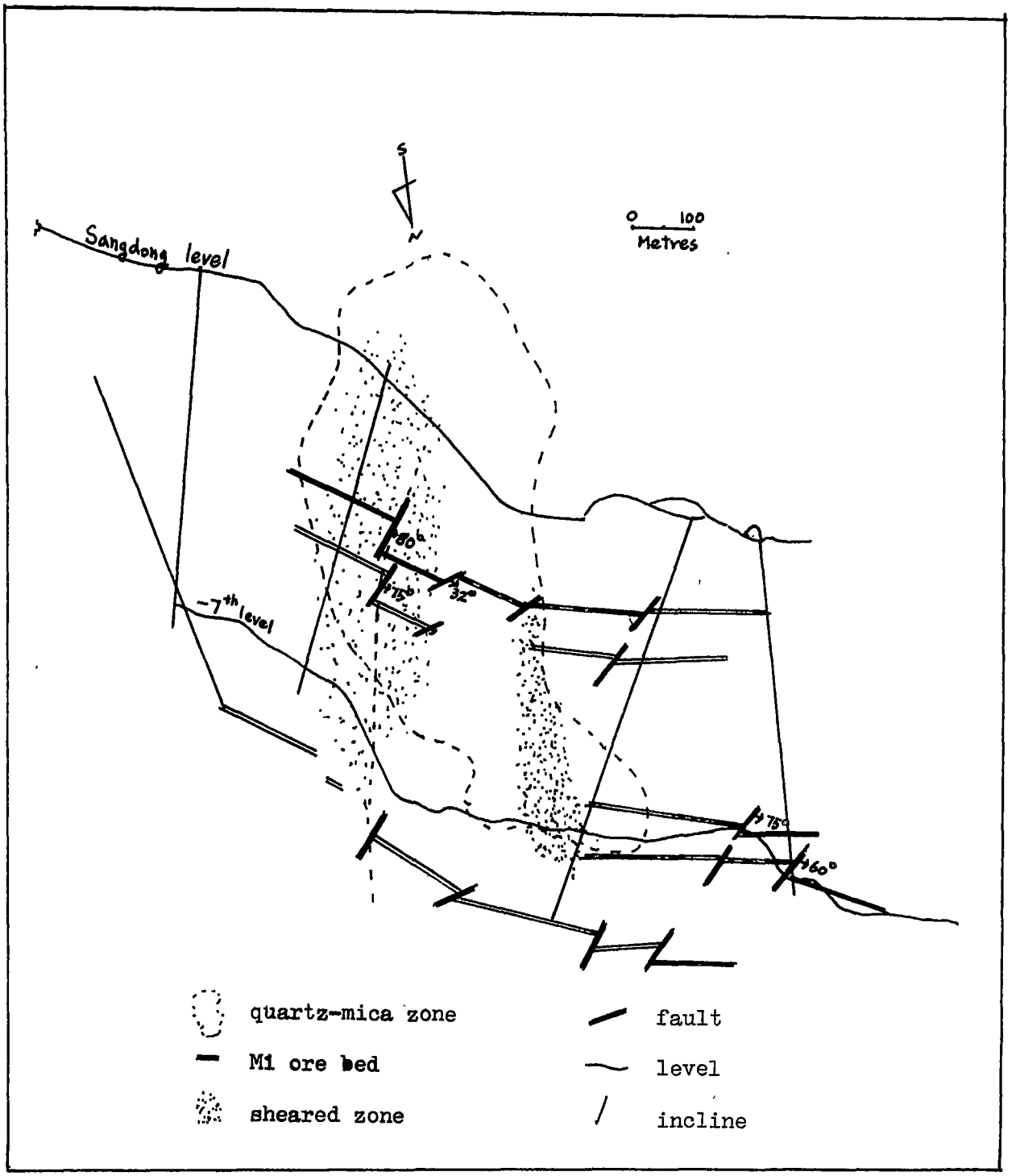

4.2. Zonal Distribution of Minerals

The skarn orebodies in the Sangdong deposit are chiefly composed of four minerals: quartz, mica, amphibole and pyroxene, and the colours of the ore correspond to the relative proportions of these four minerals. These may be grouped as zones depending on their dominant mineralogy. There are three main zones, quartz-mica, amphibole-rich and pyroxene-garnet. It is important to realize that a zone defines a spatial distribution of a dominant assemblage and that all assemblages(e.g. mica-rich and pyroxene-rich) can be found in each zone(see Fig. 4.5a). Where reference is made solely to a rock type, then terms like skarn, rock or assemblage are used. Projections of zone distribution(e.g. Fig. 4.5) are very generalized because in places the zones are arranged vertically(Figs. 4.5a & 4.8).

Megascopic and microscopic observations reveal that the pyroxene is replaced by amphibole but the relationship between amphibole and mica is obscure. The M1 and F. orebodies show a systematic zonal distribution, but the H1 appears to have no systematic zonal distribution and lacks mica.

Mica is localized in the central part of the skarn orebodies(M1 and F.). An amphibole-rich zone surrounds the mica-rich zone, and the amphibole-rich zone is surrounded in turn by the pyroxene-rich zone which grades into unmineralized limestone. Frequently a rock consisting chiefly of wollastonite is found in the transitional zone between unmineralized and pyroxene-rich skarn(Fig. 4.4).

Scheelite with quartz and mica is abundant in the central zone where the WO_3 content commonly exceed 6 %. The scheelite content then gradually decreases in the amphibole-rich zone, averaging about 1.5 % WO_3, and in the pyroxene zone, scheelite is sparsely distributed, averaging 0.3 % WO_3.

Generally pyroxene is rarely associated with scheelite, but scheelite is frequently observed in those parts in which quartz replaces the pyroxene

Fig. 4.5. Horizontal projections showing zonal distribution of skarn zones in M1 and F2 orebodies.

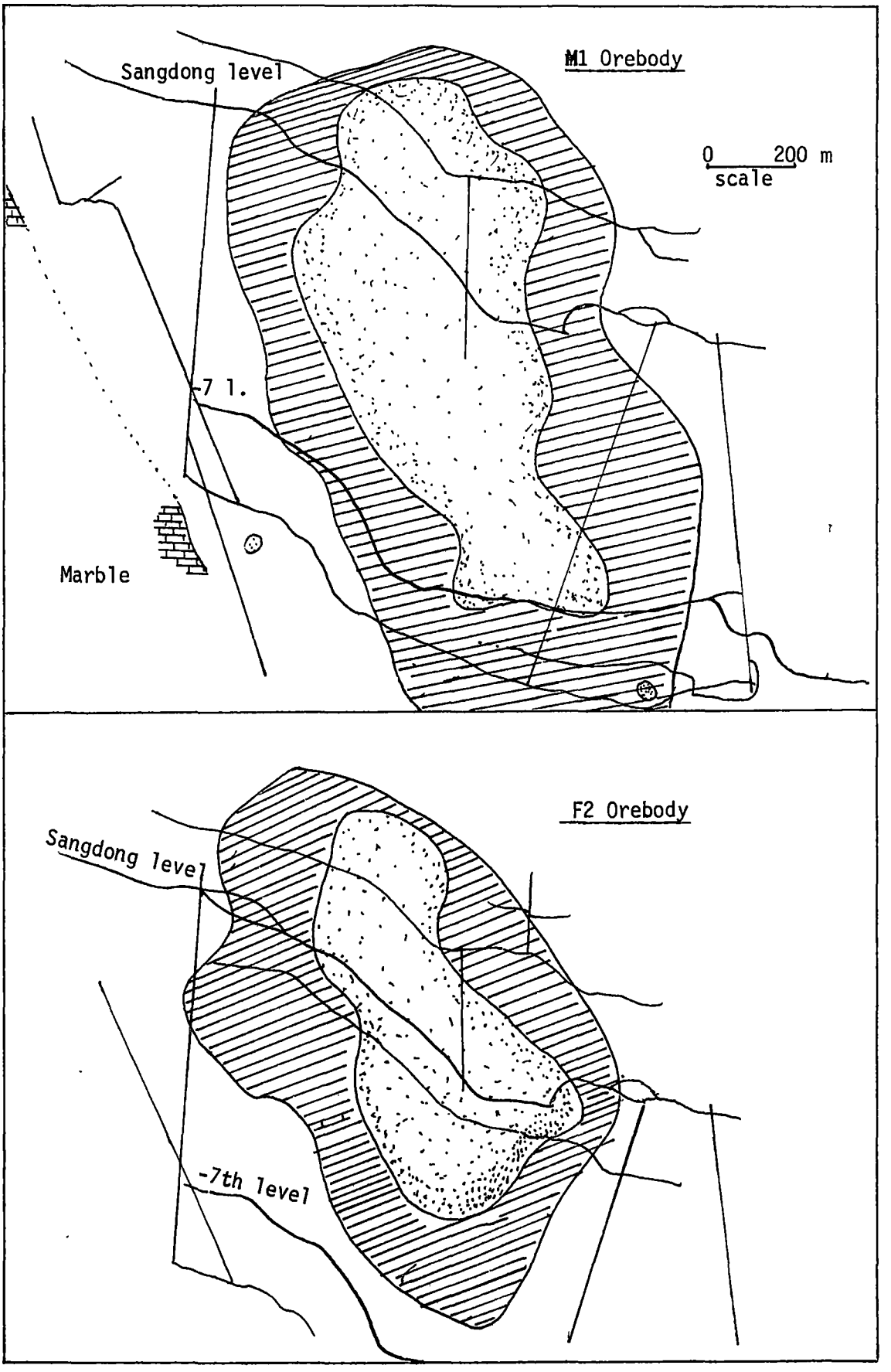

Fig. 4.5a. Illustration of difference in usage between zone and skarn at the Sangdong mine.

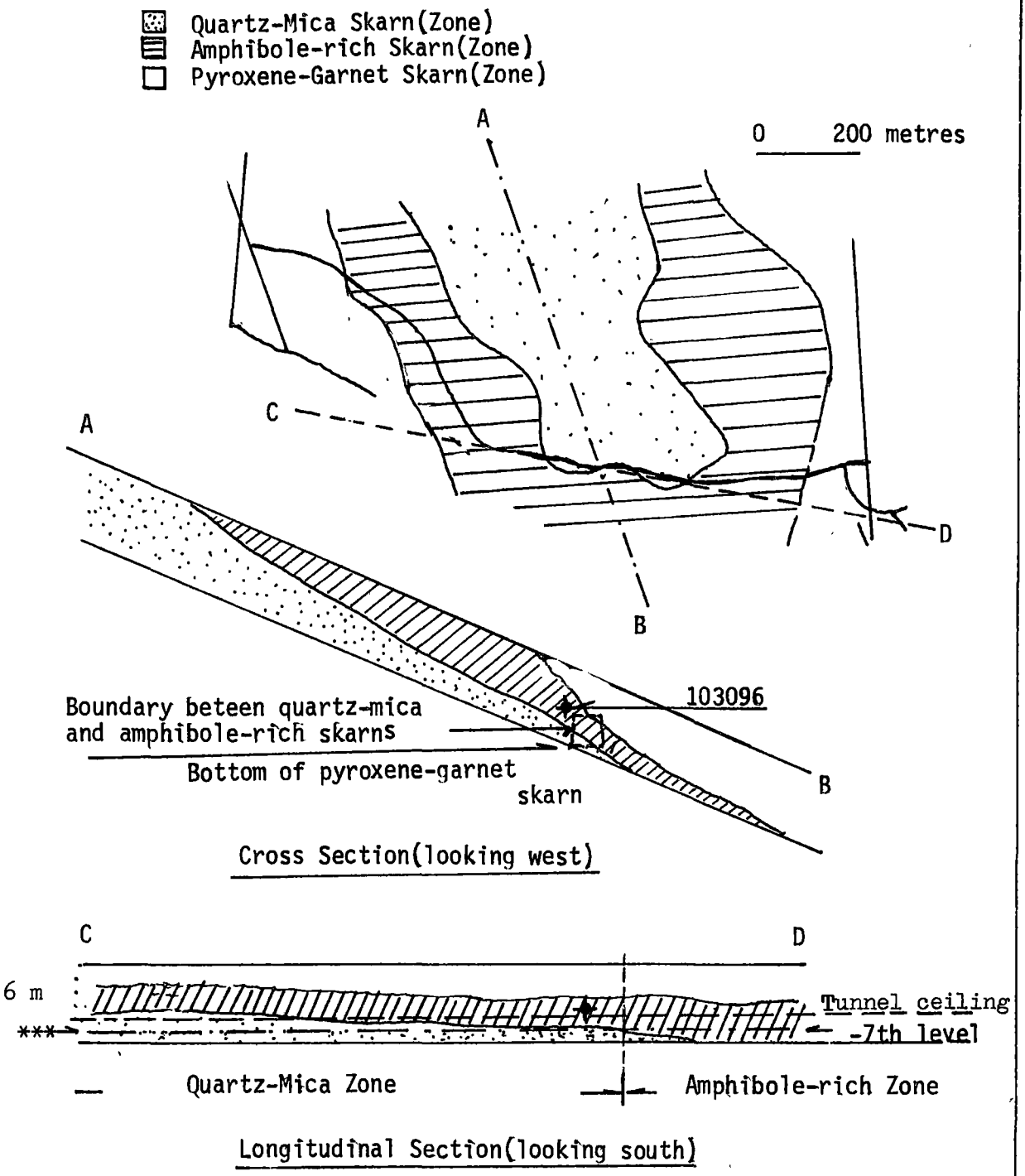

Sampling Description : e.g. Specimen 103096

Spatial term - Quartz-Mica Zone

Assemblage - Amphibole skarn

*** a standard mapping line plotted on the underground map at the Sangdong mine

zone or intersects this zone in veinlets, or where the pyroxene is recrystallized. Most of the pyroxene closely associated with scheelite is classified as late green skarn, in contrast with the primary green skarn which is more or less barren and generally associated with garnet.

Quartz occurs in all three zones, its abundance varying in direct proportion to the abundance of scheelite. Sphene has a characteristic distribution occurring only at the bottom and top of the M1 skarn orebody close to the country rock slate.

4.3. The Quartz-Mica Zone

The quartz-mica-rich zone in the central part of the M1(Fig. 4.5) extends along strike about 100 m in the top level(805 m above sea level), 250 m in the Baegun level(730 m a.s.l), 200 m in the Sangdong level(658 m a.s.l), 200 m in the 3rd level(594 m a.s.l), 70 m in the 5th level(536 m a.s.l), and about 50 m in two separated parts of the 7th level(482 m a.s.l). This zone is observed in few areas below the 8th level(457 m a.s.l). Small patches of quartz-mica assemblages occur along joints or faults outside the central part of the M1 orebody in the pyroxene-rich zone. These small scale quartz-mica skarns are generally separated from pyroxene-rich skarn by amphibole-rich skarn(Fig. 4.6), however, mica skarn has been observed in direct contact with pyroxene-rich skarn(Fig. 4.7). Other occurrences of small scale quartz-mica skarn have been found in the 12 and 15th levels (270 m a.s.l).

The outline of the quartz-mica zone in the M1 orebody appears to form a part of a truncated ellipsoid with downdip axis of about 900 m and a strike axis of about 250 m. It is about 6 m thick in the thickest part of the centre, lying with its long axis in NS to N 10°W direction with about 20° plunge. The quartz-mica zone in the F. orebody has almost the same outline as the quartz-mica zone in the M1 orebody(Fig. 4.5), but extends more widely in the central part and terminates more rapidly downwards than in

Fig. 4.6
A small scale quartz-mica skarn rimmed separated by amphibole skarn from pyroxene-garnet skarn(location ; see Fig. 8.1a & b)

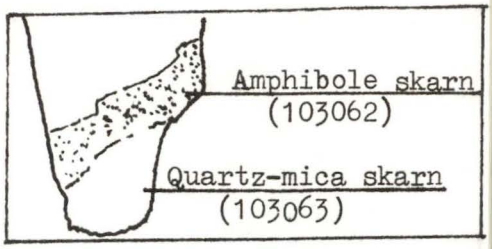

Fig. 4.7. Quartz-mica skarn in direct contact with pyroxene skarn at the Jangsan level in M1 orebody.

the M1 orebody.

The mineralogy of the quartz-mica zone includes quartz, muscovite, biotite, chlorite, scheelite, apatite, fluorite, bismuthinite, native bismuth, pyrrhotite, pyrite, chalcopyrite, magnetite and arsenopyrite. Sphalerite, rutile, wolframite and molybdenite have been found for the first time in this skarn. Phlogopite was reported by Lee and Kim(1969) but has not been confirmed in this study. The major assemblages within the quartz-mica zone are quartz-muscovite-scheelite, quartz-biotite-scheelite, and amphibole-biotite-quartz-scheelite(Gabert & Vinken, 1962; Lee and Kim, 1969; Moon, 1974; Hahn, 1978).

4.4. The Amphibole-rich Zone

The boundary between the quartz-mica zone and the amphibole-rich zone is not distinguishable without careful observation, because both assemblages are black and the change is transitional. The zone extends about 100 to 200 metres outward from the quartz-mica zone, and below the 7th level it extends out for more than 500 m(Fig. 4.8).

In the F. orebody, this zone extends about 200 m outward as in the M1 orebody. According to drilling, it seems to terminate at the 8th level.

Hornblende, quartz, chlorite, hendenbergite, tremolite, scheelite, apatite, fluorite, calcite, sphene, plagioclase and opaque minerals have been described from this zone. Scheelite appears to be closely associated with the opaque minerals which include pyrrhotite, pyrite, magnetite, bismuthinite, native bismuth and chalcopyrite in order of decreasing abundance(Moon, 1974).

Hornblende-quartz, hornblende-quartz-scheelite, tremolite-quartz-scheelite(Lee & Kim , 1969), hornblende-pyroxene-quartz, and hornblende-quartz-chlorite (skarns) are the main mineral assemblages (rocks or skarns) within the amphibole-rich zone.

4.5. The Pyroxene-Garnet Zone

The pyroxene-garnet zone forms a discus-shaped shell about 1.5 km in diameter and 0.3 to 6 m thick within the Myobong Formation. The central part of this zone is replaced by the quartz-mica and the amphibole-rich zones in which remnant blocks of the pyroxene-garnet skarn are occasionally observed. At the margins of the pyroxene-garnet zone, its thickness decreases markedly and it passes into unmineralized limestone. In many localities, garnet-dominant skarn or wollastonite-garnet skarn appears between the pyroxene-garnet zone and the limestone. The marginal garnet-dominant skarn occurs mainly at the top of the pyroxene-garnet skarn zone in the M1 and the F. orebodies. Wollastonite is particularly well developed at the top of the H1 orebody(Fig. 4.9).

Hedenbergite, diopside, andradite, grossularite, amphibole, quartz, epidote, calcite, fluorite, chlorite, scheelite, pyrrhotite, pyrite, native bismuth, bismuthinite, locally sphalerite, and very minor sulphide minerals such as arsenopyrite and galena make up the bulk of this skarn. Magnetite occurs locally in veinlets. Plagioclase(anorthite) is localized in the deep levels below the 10th level and is associated with sphene. An unusual occurrence of a vesuvianite-scheelite-quartz-plagioclase assemblage is found in this skarn zone between 12 and 14th levels.

Generally scheelite is observed in quartz or hornblende-quartz veinlets. Andradite-hedenbergite, hedenbergite-quartz, and hedenbergite-plagioclase-grossularite are the dominant mineral assemblages. Wollastonite-andradite-diopside-calcite assemblages are confined to the marginal part of this pyroxene-garnet zone.

Fig. 4.8. Longitudinal sections of the Main Orebody(M1), showing the change of mineral zonation with depth.

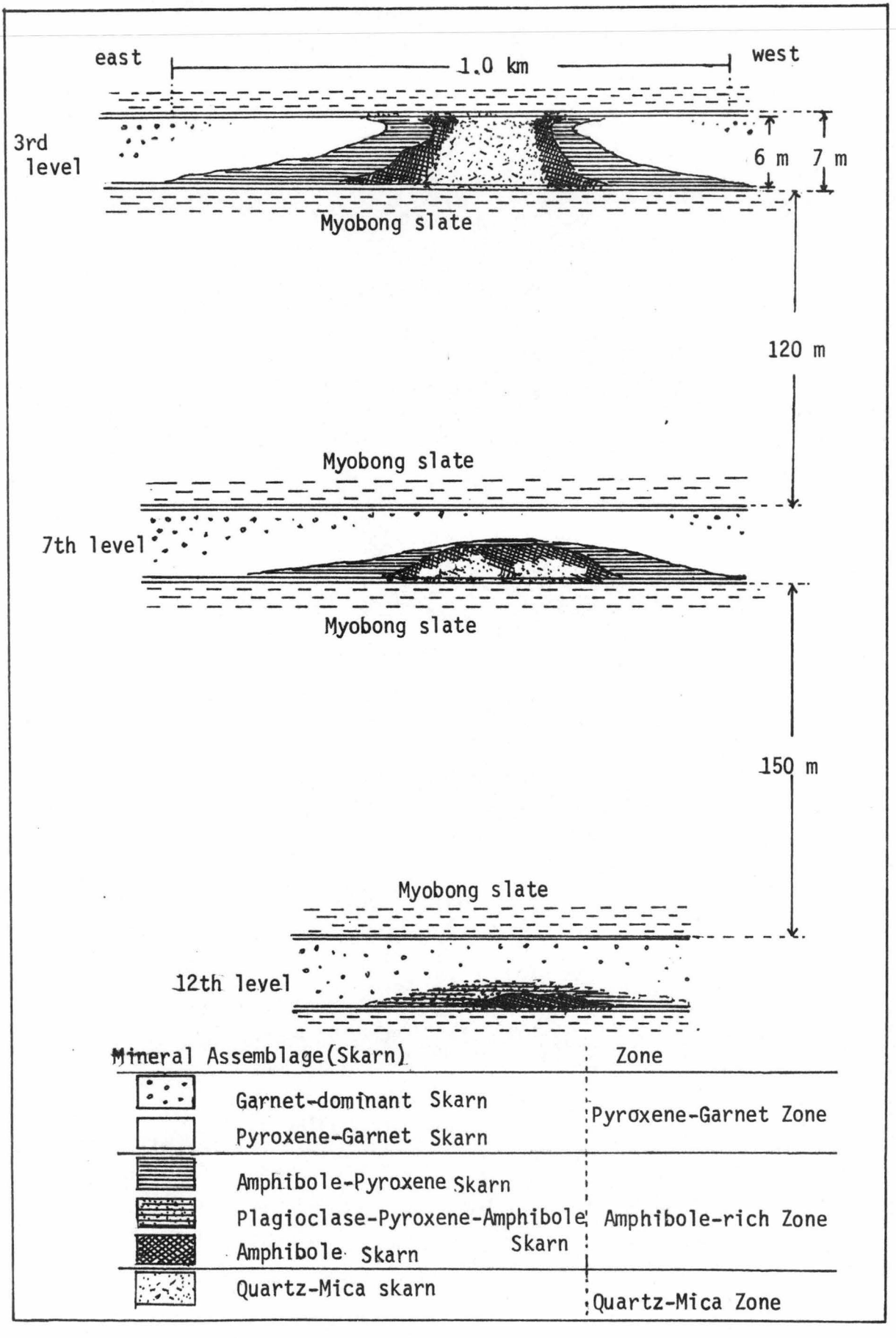

Fig. 4.9. Sections of the Hangingwall Orebody(H1).

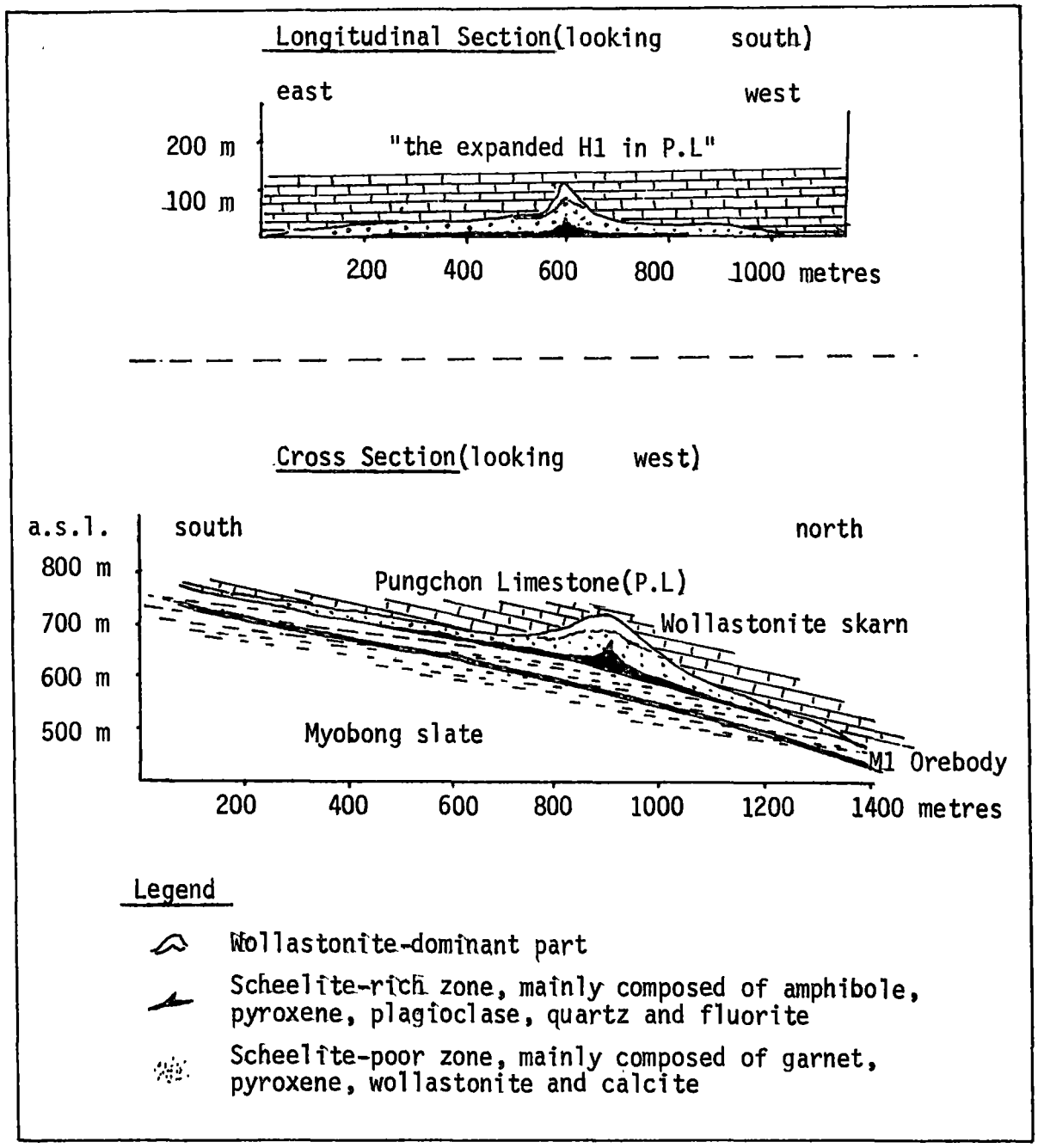

4.6. Marble and Limestone

Blocks of marble are found at the margins of the pyroxene-garnet zone in a few localities, mainly on the 17th level(212 m a.s.l). The thickness of the marble on the 17th level is about 6 m, about the same as the interbedded limestone at the surface outcrop. This marble is silicified along joints and fractures near the skarn orebodies.

A few interbedded thin limestone units can be traced on the surface outside the mineralized area and are 0.5 to 0.8 m thick. Some of the thin layers are lenticular, but the thicker ones are continuous. They are stratigraphically equivalent to the F. orebody. Outside of the mineralized zone, the limestones are very fine grained and contain organic material(Fig. 3.3 & Fig. 4.10) with larger, partly recrystallized grains of calcite. Marble near the skarn is recrystallized to an equigranular fabric(Fig. 4.11). On the 17th level of the M1 orebody it contains very fine garnet veinlets, which are also common at the outcrop of the limestone near the eastern margin of the M1 orebody.

4.7. Cherty Rocks

At the boundaries between the M1 orebody and the host slate, there are rocks known locally as 'cherty rocks', which occur only in the mine area. These are easily distinguished from the skarn orebody and country rocks by their greyish white or pale green colour and their hornfelsic fabric (Fig. 4.12). Typical cherty rock forms regular layers at the bottom and top of the M1 orebody with a thickness of about 0.5 to 1.0 m. In the F. orebody, cherty rock is observed within the orebody or occurs in the adjacent slate as lenticular thin beds, up to 10 cm thick. In the H1 orebody, it shows no regular layering but appears irregularly in the lower part of the orebody which is composed of alternating slate, skarn and cherty rocks.

The cherty rock adjacent to the strongly mineralized portions of the M1 orebody has been replaced by amphibole-quartz and is locally obliterated. However, even in this replaced part, remnants of unaltered white-grey cherty rock are occasionally observed.

Cherty rock is mainly composed of quartz, plagioclase, epidote, chlorite, pyroxene and sphene. It is commonly laced with fractures that are filled with quartz, amphibole and scheelite. Such amphibole-quartz veinlets are more common in the footwall of the cherty rock than the hangingwall. Scheelite occurs in the amphibole-quartz veinlets, but not in the cherty rock itself.

The cherty rocks can be classified into three facies as follows(Fig. 4.13): (1) Close to the slate, it has a similar texture to the slate, mainly consisting of quartz, plagioclase, sphene and grossularite. (2) Close to the skarn ore, it has mesh texture, mainly composed of plagioclase, quartz, diopside and epidote with minor sphene. (3) Close to the limestone at the marginal part of the skarn, it is composed of quartz and plagioclase with minor sphene.

The cherty rocks were probably originally sedimentary units in the shale-limestone succession. Alternating layers of cherty rocks, slate and skarn in the F2 and F3 orebodies and lower parts of the H1 orebody demonstrate that the composition of the cherty rock was originally different from that of the limestone and shale.

An unusual cherty rock appears along the cross-cutting structure linking the M1 and H1 orebodies in the Myobong slate in the outcrop near the adit of the Baegun level. This type of cherty phase alteration in the Myobong slate is occasionally observed elsewhere on a small scale(Figs. 9.5 & 9.6)

Fig. 4.10. Photomicrograph of the interbedded limestone stratigraphically equivalent to the M1 orebody. Sedimentary quartz grains are observed locally. The inequigranular grains of calcite are characteristic of the limestone away from the mineralized zone. 103145, Sesong area(outside of mineralized zone), ═══ represent 0.1 mm.

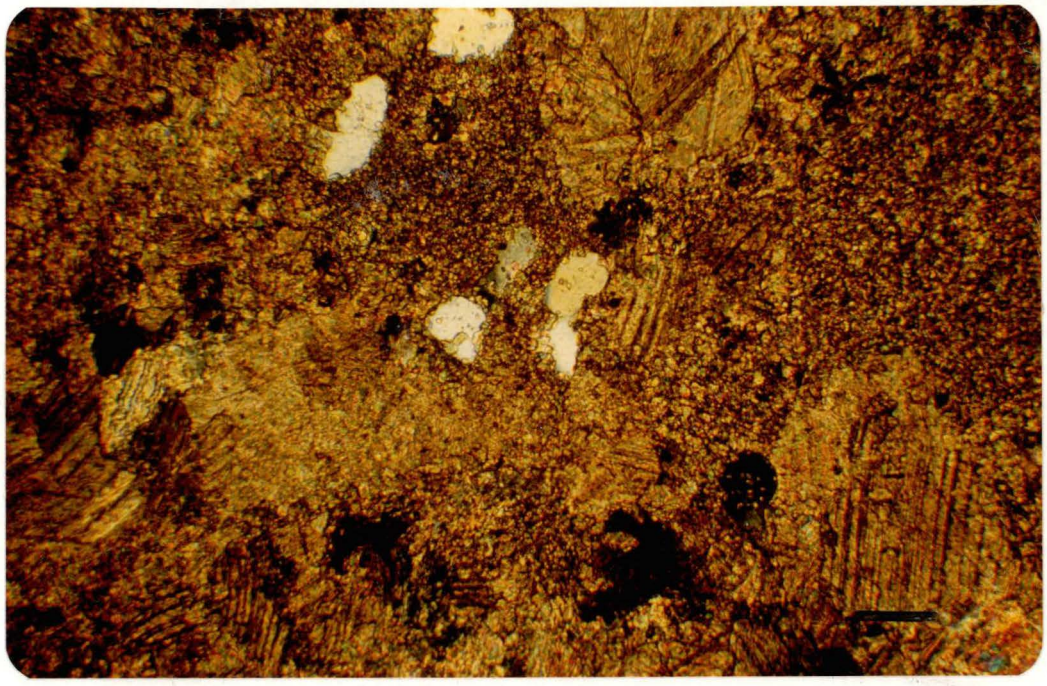

Fig. 4.11. Photomicrograph of the limestone(marble) at the margins of the skarn. The equigranular texture is characteristic of the limestone near the skarn and the occurrence of garnet(black) in veinlets increases towards the skarn.
103053, -16th level, ═══ represents 0.1 mm.

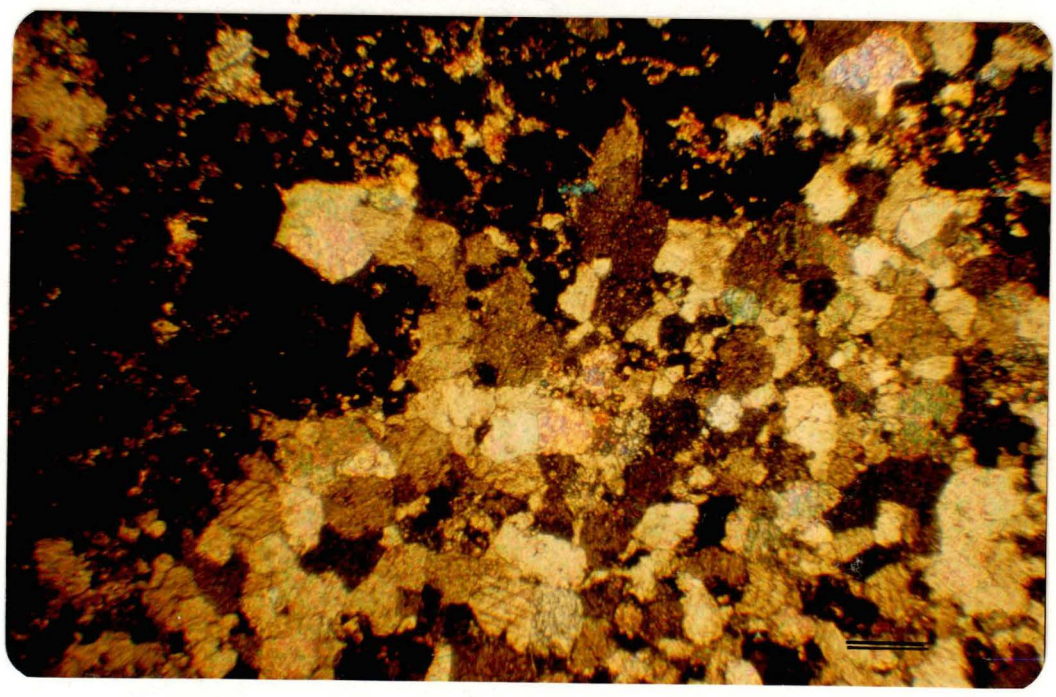

Fig. 4.12.
A "cherty rock" showing an unusually irregular boundary with slate at the hangingwall of the M1 orebody.
103075(cherty)/103076(slate)
-16th level, X 2.1

Fig. 4.13. Generalized classification of "cherty rock" related to adjacent rocks.

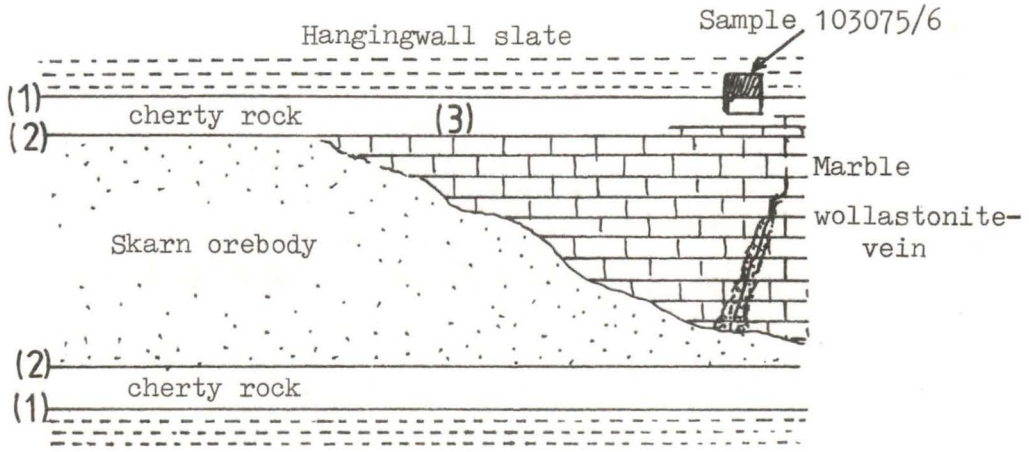

(1) cherty rock close to slate
(2) cherty rock close to the skarn
(3) cherty rock close to the marble

4.8. Quartz Veins

Quartz veins trending parallel to the strike of the skarn orebodies are developed mainly in the footwall of the skarn orebodies. Other quartz veins intersect the skarn orebodies obliquely. In the Myobong slate between the M1 orebody and the Jangsan Quartzite, the veins are particularly common beneath the quartz-mica zone. Very few quartz veins occur in the upper horizon of the Myobong slate between the M1 and H1 orebodies, but quartz veins occur in the lower part of the H1 orebody.

The thickness of the quartz veins ranges from a fraction of a centimetre to about 50 cm in general. One continuous group of quartz veins containing wolframite and scheelite extends about 250 m along strike and 150 m down dip, and is 30 to 50 cm wide. The density of quartz veining decreases with increasing distance from the centre of the skarn orebodies.

Scheelite, molybdenite, wolframite, chalcopyrite, pyrite, arsenopyrite, pyrrhotite, sphalerite, galena, bismuthinite, calcite, fluorite and sericite occur in the quartz veins. Frequently apatite, showing a bright chrome yellow fluorescent colour under the ultraviolet lamp, is seen in barren quartz veins.

Typical assemblages are listed in Table 4.1. The most significant difference in ore mineral assemblages between the skarn orebodies and the quartz veins is the occurrence of wolframite and molybdenite and the virtual absence of amphibole, pyroxene, garnet and magnetite in the quartz veins. Arsenopyrite is much more common and pyrrhotite much less common in the quartz veins than in the skarn orebodies. Molybdenite-bearing quartz veins are confined to a zone from the surface to the 7th level, whereas wolframite-bearing quartz veins are observed from the outcrop to the 16th level. The molybdenite-bearing types are the most common quartz veins in the Sangdong Mine. Molybdenite also occurs in calcite veins.

Wolframite and scheelite are very closely associated in wolframite-bearing quartz veins, but scheelite is uncommon in quartz veins bearing molybdenite. Quartz veins bearing mainly polymetallic sulphides characteristically lack tungsten minerals. The bismuthinite-bearing quartz veins are so rare that it is difficult to find one in many localities.

The two dominant types of veins are wolframite-scheelite quartz veins and the molybdenite-sericite quartz veins.

Their major features include :

(a) molybdenite-sericite-quartz veins

Molybdenite is generally close to the margins of the veins(Fig. 4.14a) where there is generally abundant sericite(Fig. 4.14b). Molybdenite and sericite commonly show a systematic banding(John, 1963). Scheelite, where present, is free of molybdenum, showing blue fluorescent colour under the ultraviolet-lamp. Rare calcite veinlets cut the quartz grains in the veins.

(b) wolframite-scheelite-quartz veins

These contain wolframite, scheelite, bismuthinite, chalcopyrite, pyrite, native bismuth, galenobismuth and galena. Needle or blades(about 1 cm long) of wolframite occur randomly or sporadically, cutting quartz grains. Scheelite occurs in association with muscovite in many places where there is no wolframite. If there is abundant wolframite, scheelite occurs surrounding and apparently replacing wolframite(Fig. 4.15 & Fig. 4.16). Pyrite occurs as subhedral grains, locally enclosing scheelite. Tiny acicular bismuthinite crystals are mainly enclosed in quartz and they are common also in drusy cavities. Where quartz veins intersect the M1 orebody, wolframite is closely associated with chalcopyrite. If wolframite occurs in a fluorite-bearing quartz vein, it is accompanied by sphalerite, pyrrhotite, arsenopyrite, galena and sericite. The proportion of wolframite to scheelite in this group of quartz veins is generally 1 : 1.3 in the whole vein(Moon, 1974). Locally fractures are filled with calcite and barren quartz veinlets cut all the minerals.

Table 4.1. Mineral assemblages in quartz veins at the Sangdong mine.
(in order of abundance)

(1) Molybdenite-quartz veins

molybdenite-sericite-scheelite
molybdenite-pyrite
molybdenite-chalcopyrite
molybdenite-fluorite-calcite-sericite
molybdenite-calcite-fluorite-galena
molybdenite-chalcopyrite-bismuthinite-fluorite
calcite-molybdenite(calcite vein)

(2) Wolframite-scheelite-quartz veins

wolframite-scheelite-chalcopyrite-pyrite
wolframite-chalcopyrite-scheelite
wolframite-pyrite-chalcopyrite-scheelite
wolframite-pyrite-chalcopyrite-arsenopyrite-scheelite
wolframite-sphalerite-galena-arsenopyrite-fluorite-sericite-scheelite
wolframite-scheelite-pyrrhotite

(3) Chalcopyrite-quartz veins

chalcopyrite-pyrite-galena-sphalerite-sericite
chalcopyrite-sphalerite-sericite
chalcopyrite-sphalerite-pyrite-arsenopyrite

(4) Bismuthinite-quartz veins

bismuthinite-galena
bismuthinite-chalcopyrite-pyrite-calcite-sericite

Fig. 4.14(a).
Mode of occurrence of molybdenite in quartz veins, in footwall Myobong slate. Baegun level, X 0.3.

Fig. 4. 14(b)
Common association of molybdenite and sericite at the margins of quartz veins.
103202, -4th level, X 1.8

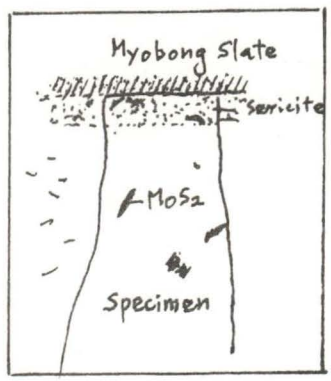

Fig. 4.15
Wolframite-scheelite-quartz vein. Later quartz-scheelite (brown) veinlets cut wolframite crystals. 103126, Sangdong level, X 0.78

Fig. 4.16 Occurrence of scheelite locally replacing wolframite (scheelite shows blue fluorescent colour under ultra-violet lamp). 103126, Sangdong level, —— represents 5 mm.

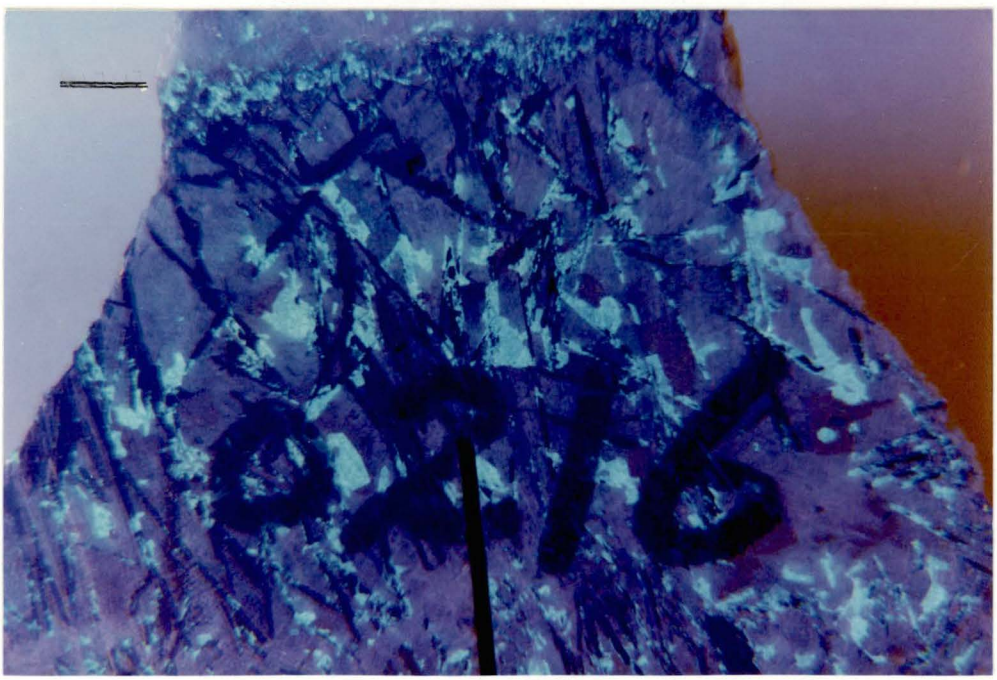

4.9. The Discovery of A New Molybdenite Deposit and A New Reserve of Tungsten Skarn

4.9.1. Molybdenite deposit

Two 500 m drill holes from the 3rd level discovered molybdenite in fine quartz veinlets in fractured Jangsan Quartzite and disseminated in partly recrystallized quartzite. The veins extend down into Precambrian schist and analyses indicate that the whole thickness of the Jangsan Quartzite underneath the quartz mica zone of the M1 orebody, might be economic(Fig. 4.17b). Very few sulphides are associated with molybdenite and no tungsten-bearing mineral was detected in this mineralization (personal communication, Lee, 1983).

4.9.2. A new scheelite-bearing skarn

The occurrence of molybdenite-bearing quartz veins is primarily confined to middle and upper levels above the 7th level. However, one molybdenite-bearing quartz vein was recently discovered in the Myobong slate at the 14th level(298 m a.s.l) cross-cut near the eatern margin of the M1 orebody (Fig. 4.17a). Subsequent drillings led to the discovery of a new reserve of tungsten skarn ore in a horizon lower than any previously known(Fig. 4.17a). Drilling results showed that scheelite occurs in pyroxene skarn containing little hydrous skarn minerals.

Fig. 4.17a. Location of a new discovery of skarn outside of the eastern margin of the M1 skarn.

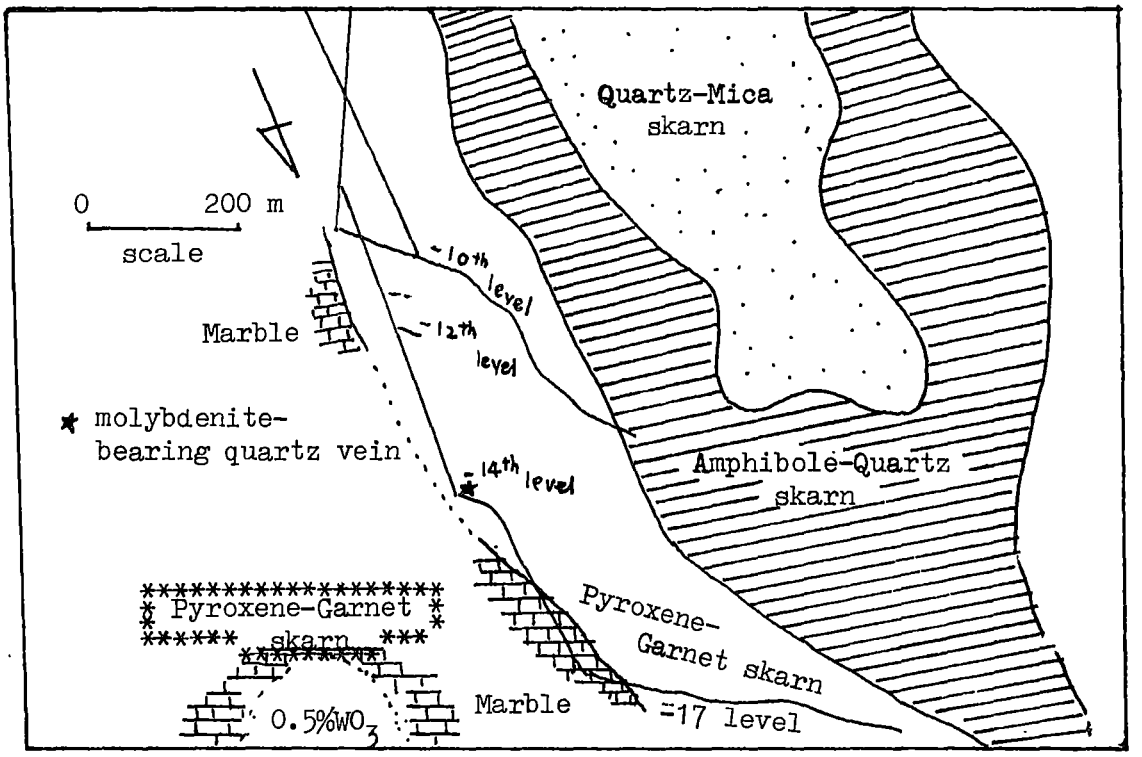

Fig. 4.17b. A New discovery of molybdenite deposit in the Jangsan Quartzite.

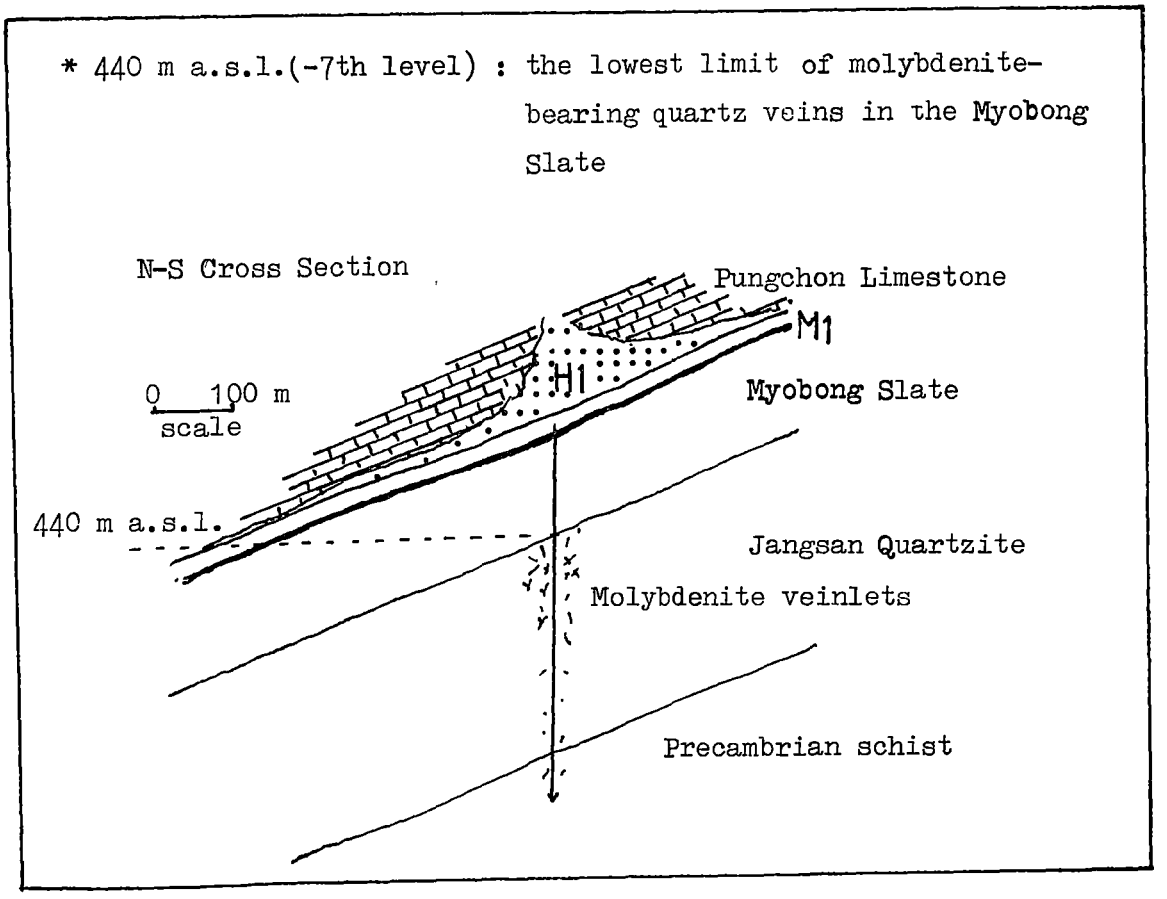

5. PETROGRAPHY OF THE SKARN

This chapter is a summary of a previous work(Moon, 1974) together with new observations on typical specimens from each zone of the M1 orebody at the 7th level.

Reviewing the previous chapters, there are three main orebodies, viz. the M1, H1 and F. orebodies, and the M1 and the F. orebodies are mineralogically zoned(Fig. 4.2). The three major zonal or skarn types are easily distinguished by colour. The pyroxene-garnet skarn is pale to dark green(pyroxene-rich) or brown(garnet-rich), the amphibole-rich skarn is dark green to black, and the mica-rich skarn is pale grey to white, except in marginal areas of the mica skarn where it becomes dark due to the dominance of biotite. Microscopic and field observations show that the pyroxene-garnet is commonly replaced by amphibole-rich skarn, but the relationship of the mica-rich skarn to the amphibole-rich skarn is less obvious because the boundaries are transitional. At the margins of these skarns there are wollastonite and garnet-bearing assemblages(white skarn) that are replaced by the pyroxene-garnet skarn(green skarn). Generalized spatial and paragenetic relations of skarns are presented in Fig. 5. and a summary of mineral distribution is given in Table 5.1.

5.1. Early or Marginal Skarns

Early or marginal skarn considered to have formed by metasomatic alteration of limestone include the following types.

5.1.1. Wollastonite-Garnet Skarn

This rock is mainly composed of wollastonite, pyroxene, garnet and calcite, locally associated with minor quartz and apophyllite. It is characterized by the absence of sulphide or iron oxide minerals(Fig. 5.1), although a sphalerite grain has been found in the apophyllite(Fig. 5.4a,b). At the top of the H1 orebody, this skarn contains greenish garnet occurring

as spots in a matrix of wollastonite crystals(Fig. 5.2). The garnet grains (about 0.5 mm in diameter) are commonly replaced or surrounded by pyroxene. Most of the garnets are andradites and the pyroxenes are diopsides(Fig. 5.3). Apophyllite is frequently observed replacing wollastonite(Figs. 5.4a & b). Scheelite has only been observed in late veinlets of quartz, pyroxene (hedenbergite) or amphibole. Locally large patches of calcite are observed under the microscope(Fig. 5.3) and quartz veinlets cut earlier garnet, pyroxene and wollastonite(Fig. 5.2). A relic of this skarn has been recently found in the quartz-mica zone of the M1 orebody(sample 103054).

In a drive intersecting the Pungchon limestone above the H1 orebody, a 5 cm vein of wollastonite and garnet occurs along a vertical joint in the limestone(Fig. 5.5). The garnet is brown and it occurs mainly in the middle of the vein. Microprobe analysis reveals no difference in chemical composition between the greenish garnet of the skarn described above and the brown garnet in this vein type wollastonite-garnet skarn. In many places, this skarn appears as remnant patches within the margins of the pyroxene-garnet zone(Fig. 5.6). As shown in Fig. 5.6, early skarn(white skarn) is commonly replaced by late pyroxene-garnet skarn(green skarn). Cassiterite inclusions up to several microns diameter within the andradite have been identified by microprobe analysis(specimen 103054). A summary of paragenesis of minerals in the wollastonite-garnet skarn is given in Table 5.2.

5.1.2. Garnet Skarn

This is mainly composed of garnet with minor pyroxene and calcite, and forms much of the upper horizon of the H1 orebody and most of the marginal parts of the M1 and F. orebodies. It is frequently observed as remnant blocks close to the hangingwall in the M1 orebody(Fig. 5.7). The garnet in this skarn commonly occurs as euhedral or anhedral crystals corroded by pyroxene and calcite. There are no occurrences of sulphide minerals or scheelite except in association with later replacement(Fig. 5.17b).

Table 5.1. Outline of mineralogical compositions of different zones in the M1 orebody.

	Pyroxene Zone white skarn	Pyroxene Zone green skarn	Amphibole Zone	Mica Zone	Cherty Rock	Quartz Veins
Andradite	@@@@@	@@@@@	*			
Grossularite		**			**	
Diopside	* * *	**			**	
Hedenbergite	*	@@@@@	*			
Wollastonite	@@@@@					
Calcite	* * *	*	*	*		*
Plagioclase		**			@@@@@	
Fluorite		*	**	**		*
Epidote		*	*		*	
Quartz		*	@@@@@	@@@@@	@@@@@	@@@@@
Amphibole		*	@@@@@	*	*	
Mica				@@@@@		
Chlorite		*	***	@@@@@		
Apatite			*****	*****		*
Scheelite		*	*****	@@@@@	*	* * *
Sphene		*	*		**	
Magnetite		*	* * *	*		
Wolframite				*		** **
Molybdenite				*		** **
Pyrite		*	**	**		**
Pyrrhotite		** **	**	*		*
Bismuthinite		**	**	* * *		*
Native Bismuth		*	*	*		
Sphalerite	*	*		*		**
Chalcopyrite			**	**		**
Arsenopyrite				*		**

Key; @@@@@ major components *** minor components

@@@@@ second major component *** > ** > *

Table 5.2. A Summary of paragenesis of minerals in wollastonite-garnet skarn and garnet skarn.

Wollastonite-Garnet Skarn	Early	Late		Remarks
Wollastonite	xxxxxxxxxx			increasing toward limestone
Calcite	xxxxxxxxxxxxxx			remnant marble
Garnet (andradite)	xxxxxxxxxx			decreasing toward limestone
(grossular)		x x		
Pyroxene (diopside)	xxxxxxxxxx			
(hedenbergite)		xxxxx		vein type
Quartz			xxxxxxx	veinlet
Apophyllite			xxxxx	
Scheelite			xx	occurring in qtz,px or amp veinlet
Amphibole			xx	veinlet, rare
Sphalerite			x	very few
Cassiterite	x			inclusions in garnet
Garnet Skarn				
Andradite	xxxxxxxxxxx	x x ?		dominant
Grossularite		xxxxx ?		
Hedenbergite			xxx	interstitial fillings
Amphibole			xxx	or vein type " "
Quartz			x	very few
Scheelite			x	negligible
Calcite	xxxxx			marble

xxxx continuous & major

x x continuous & minor

x minor

Fig. 5. Generalized spatial and paragenetic relations of zoned skarns at the Sangdong M1 orebody.

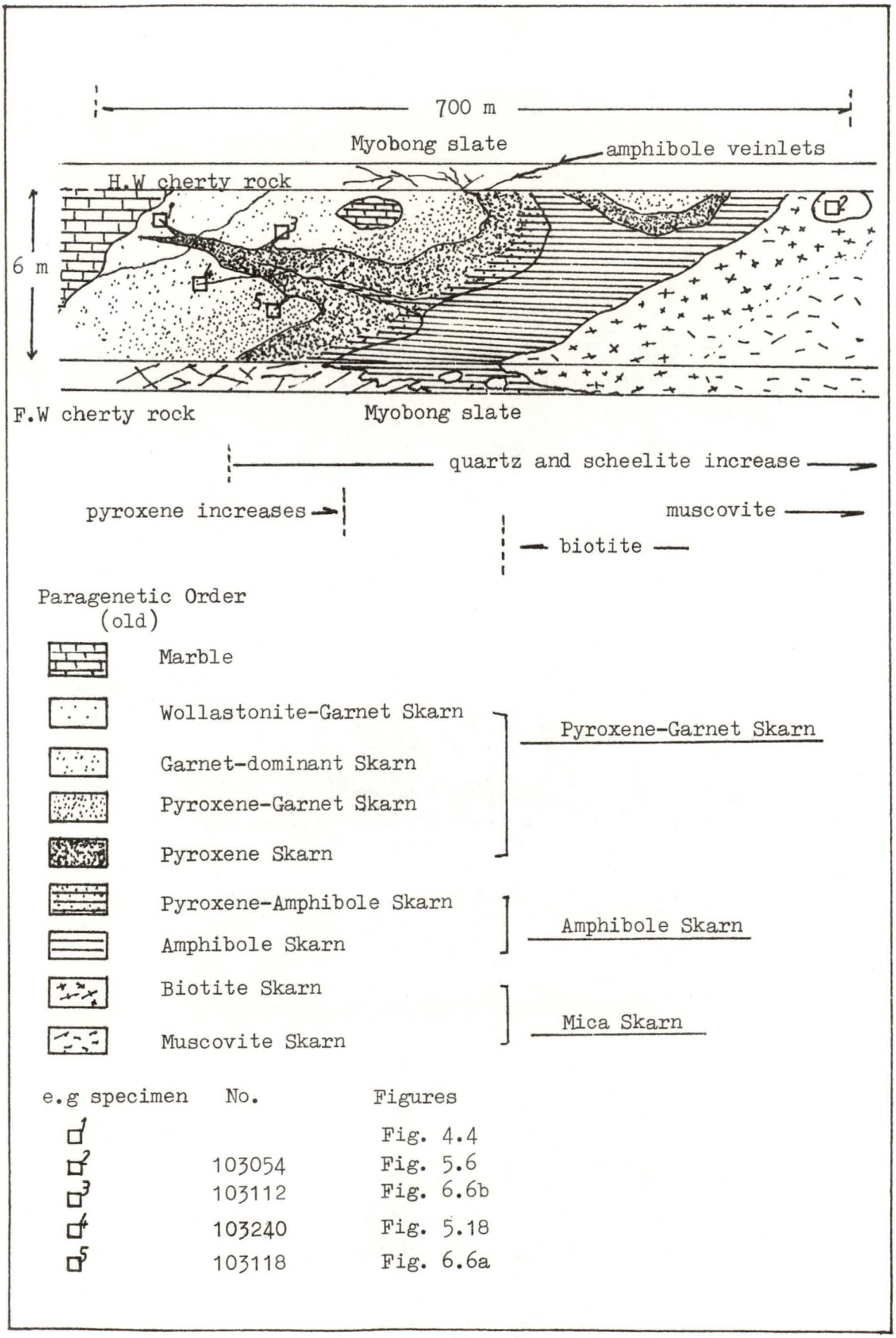

Fig. 5.1. Typical wollastonite-garnet skarn close to the pyroxene-garnet skarn. White skarn(mainly wollastonite, andradite, and diopside) is replaced by green skarn(mainly hedenbergite). Quartz occurs in places in hedenbergite veinlets(green) which cut garnet veinlets(pale brown). Scheelite occurs only in quartz veinlets.
This specimen was taken from 19 block of -5th level, quartz-mica-rich zone.

103054, X 0.24.

Fig. 5.2. Photomicrograph of wollastonite-garnet skarn occurring within the quartz-mica-rich zone. Wollastonite and euhedral garnet are cut by quartz veinlet.
103054, -5th level, cross polars. ═══ represents 0.1 mm.

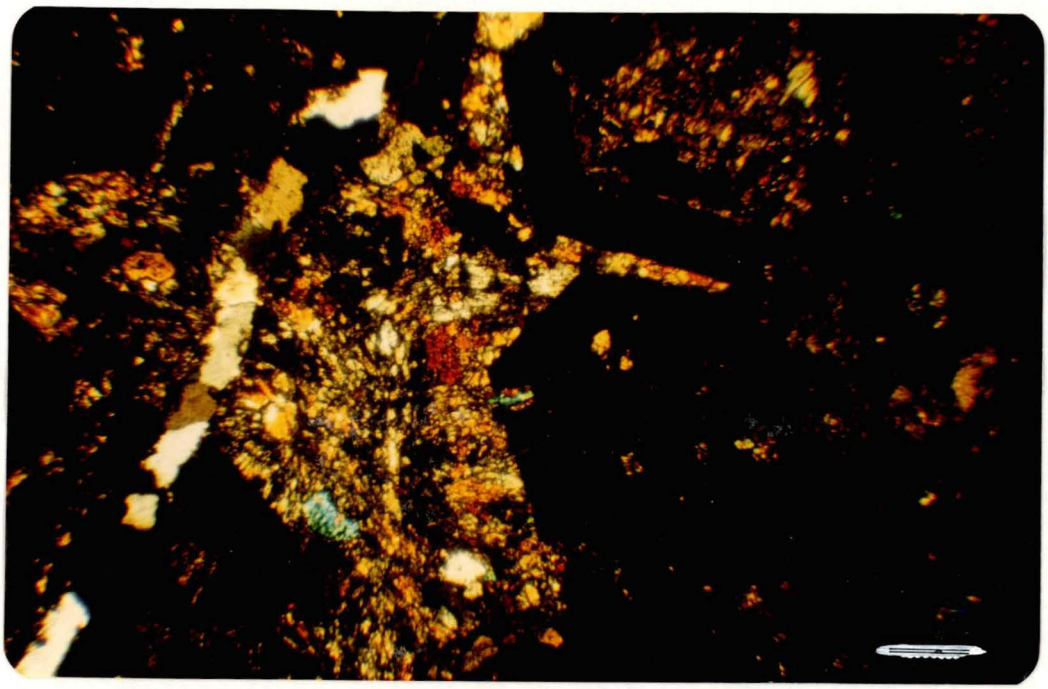

Fig. 5.3. Photomicrograph of an andradite-diopside-calcite assemblage in the wollastonite-garnet skarn. Black = andradite, blue = diopside, yellow = calcite.
103136, -5th level, cross polars. ═══ represents 0.1 mm.

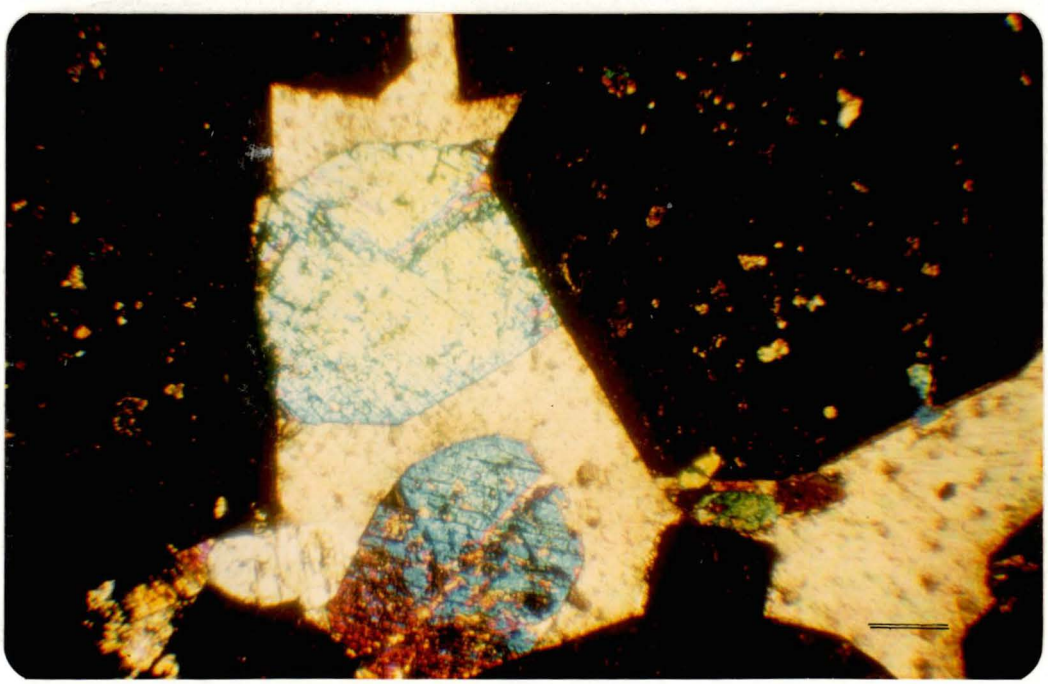

Fig. 5.4(a). Photomicrograph of wollastonite-garnet skarn replaced by late hydrated mineral, apophyllite(?). A sphalerite crystal (reddish brown) is observed in the apophyllite(?). 103136, -6th level. ═══ represents 0.1 mm.

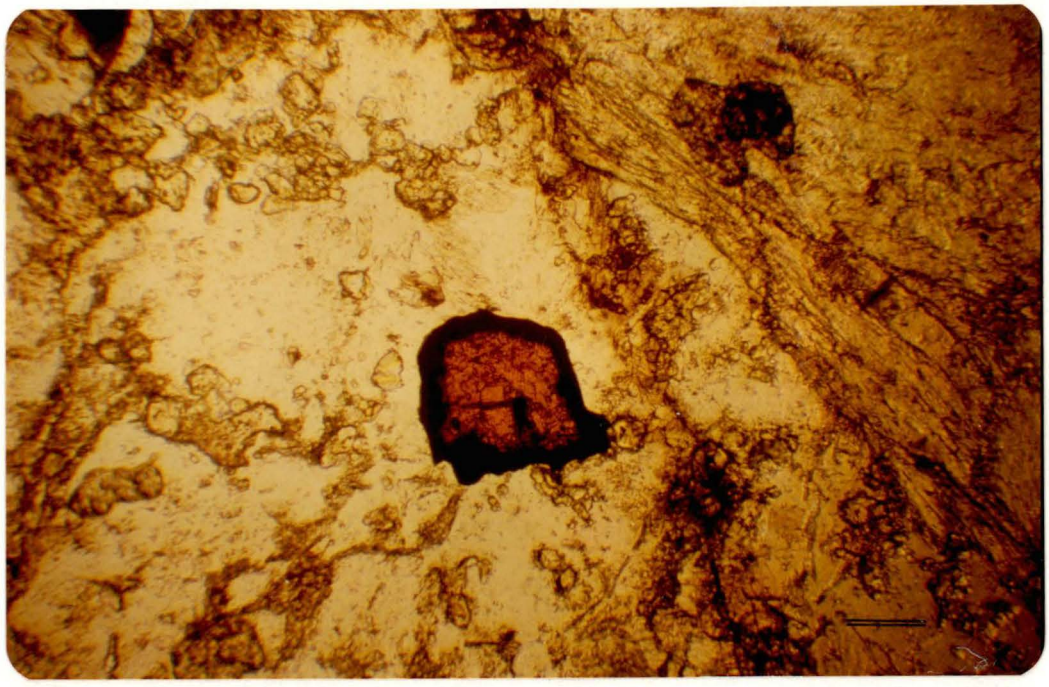

Fig. 5.4(b). Same as above.
Apophyllite(?) is characterized by by very low birefringence (pale brown to dark brown). Wollastonite = right middle corner, elongate.
-6th level, cross polars. ═══ represents 0.1 mm.

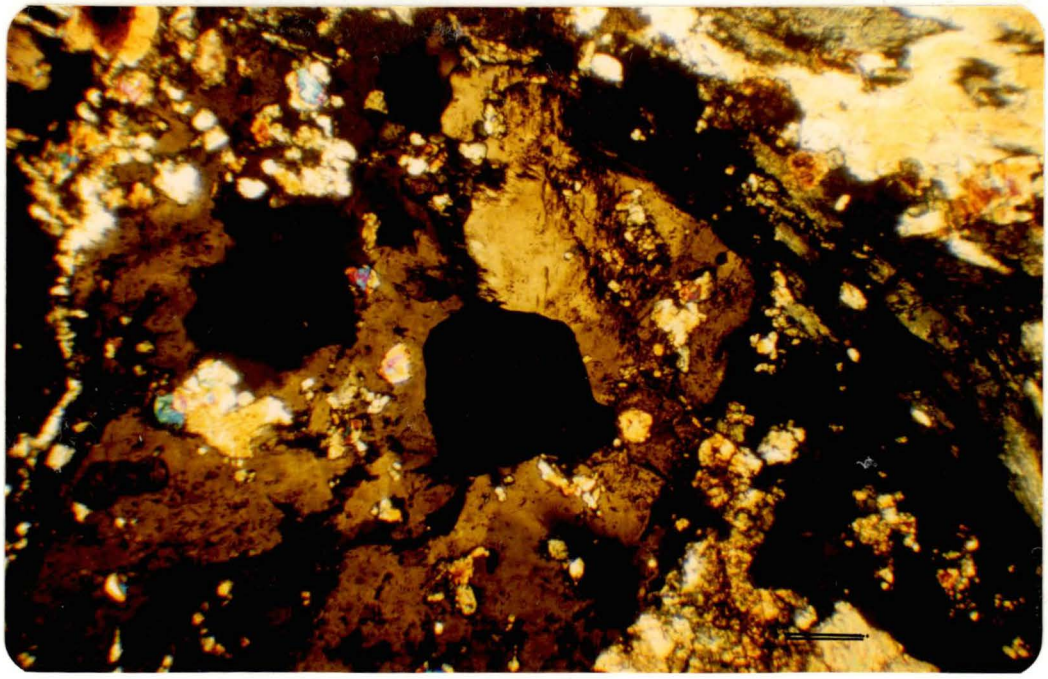

Fig. 5.5. Wollastonite-garnet vein in the Pungchon Limestone above the H1 orebody.

103136(field no. 0192), -6th level, X 0.65

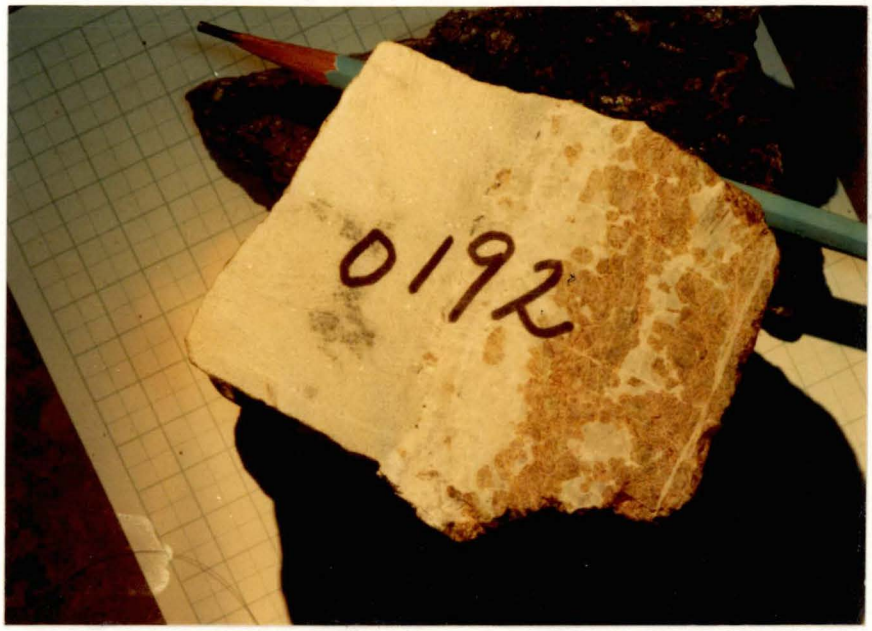

Fig. 5.6. Remnants of wollastonite-garnet skarn(white skarn) being replaced by pyroxene-garnet skarn(green skarn). White skarn (103054) and green skarn(103055) were separately analysed by XRF and microprobe. Photomicrographs of these are shown in Figs.5.2 and 5.3.

103054/5, -5th level M1, ═══ represents 1.0 cm.

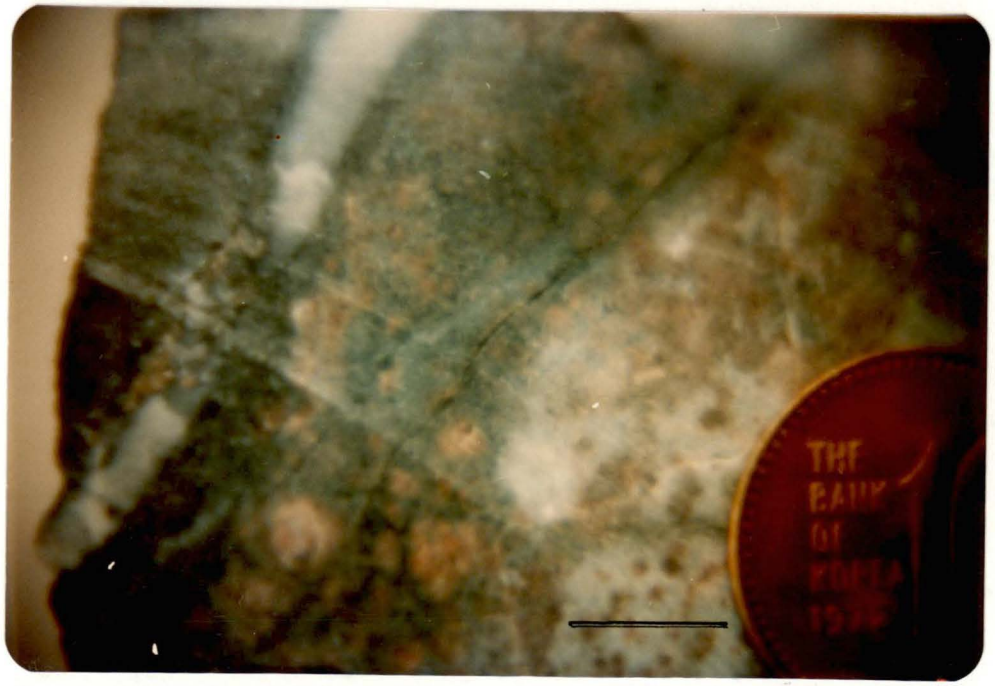

Fig. 5.7. Change of mineral composition in the M1 pyroxene-rich zone with depth(longitudinal section, looking south).

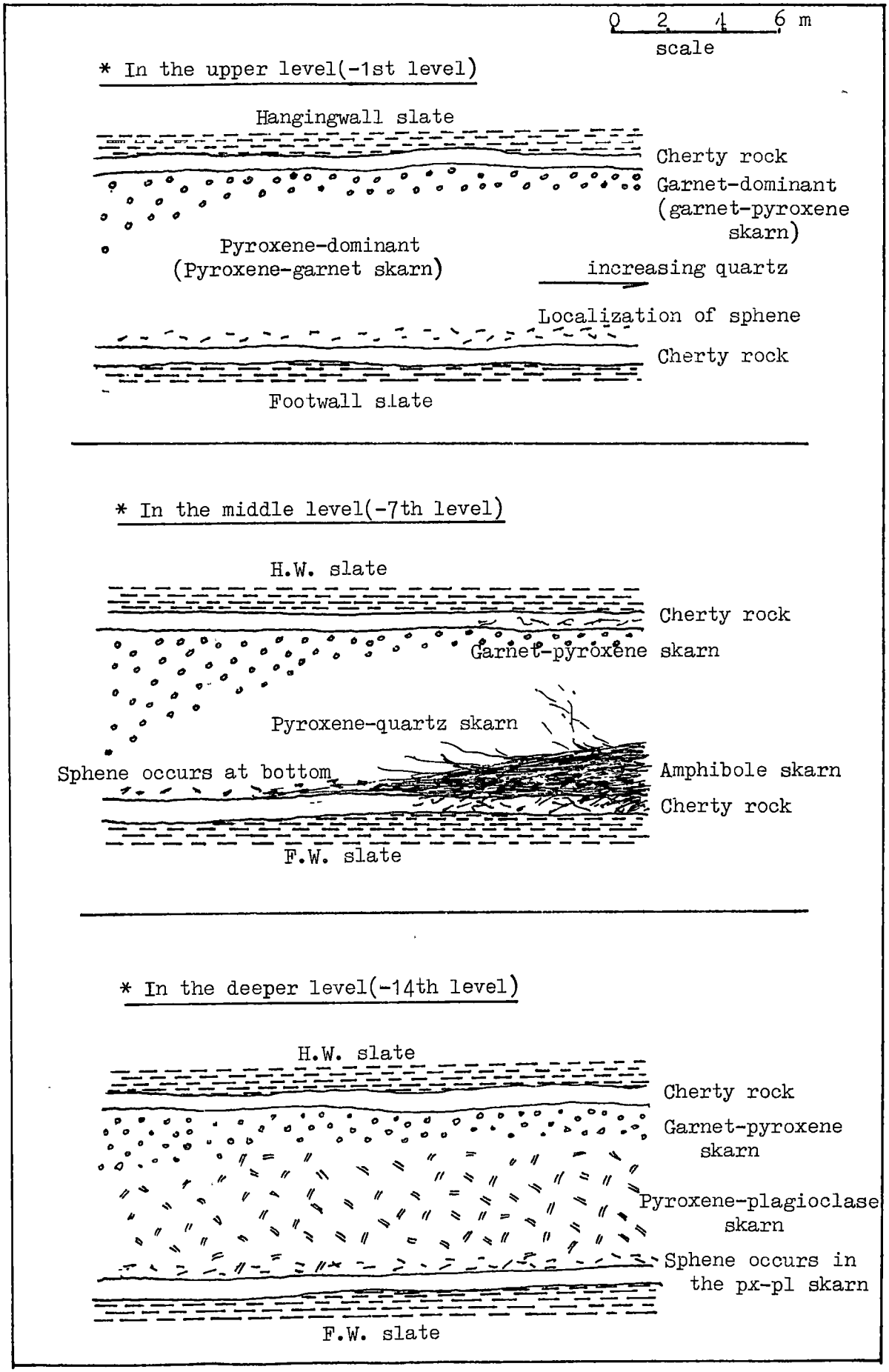

5.2. Late Pyroxene-Garnet Skarns

This skarn is characterized by the presence of hedenbergite, plus variable garnet and minor epidote. The varieties are as follows:-

5.2.1. Pyroxene-Garnet Skarn

Pyroxene(hedenbergite), garnet(andradite-grossularite), fluorite, chlorite, quartz, vesuvianite, calcite, amphibole, pyrrhotite, pyrite, native bismuth, bismuthinite, sphalerite and scheelite have been described from this skarn. Sphene is also frequently observed in this skarn within the H1 orebody. There appear to be two generations of garnet (Fig. 5.8, Fig. 5.14b). Garnet which is thought to have formed at an earlier stage than hedenbergite is dominant in the upper part of the M1 orebody. The garnet crystals usually occur in massive aggregates as anhedral brown and isotropic grains. Later garnet which is coeval with hedenbergite is clear brown or colourless and rarely anisotropic. Microprobe analyses have identified the early generation as mainly andradite, and the later tends to be grossularite-rich. There are not necessarily two garnet phases. The changes in composition may be more or less continuous over the whole deposit so that "early" and "late" can not necessarily be correlated from place to place.

Vesuvianite, which was originally described as grossularite(Moon, 1974), is observed mainly in the deeper part of the M1 orebody, particularly in the eastern part of the 12th & 14th levels(Fig. 5.9). It occurs as euhedral grains with quartz and scheelite.

Approaching the amphibole-rich zone, garnet decreases in abundance and pyroxene locally makes up most of this skarn. Quartz increases, replaces pyroxene and is associated with scheelite, and amphiboles appear randomly or as veinlets replacing pyroxenes.

The pyroxene-dominant part has a granoblastic, equigranular and interlobate fabric, but larger grains commonly occur in a matrix of finer

grains, showing a seriate, polygonal fabric. The pyroxene in this skarn is hedenbergite, and replaces most garnets (Figs. 5.10a & b). Recrystallized pyroxene crystals form elongate large grains, and exhibit lower birefringence, a darker green colour and more fluid inclusions.

Epidote occurs in some places closely associated with quartz and scheelite(Fig. 5.11). Fluorite appears at the edges of the grains of pyroxene or garnet, or replacing pyroxene and garnet(Figs. 5.10a & b). It is more common in the H1 orebody than in the M1 orebody. Near the margin of the M1 orebody, calcite is common in the interstices between garnet and pyroxene, but is rare close to the amphibole-rich skarn. Calcite appears to be replaced by fluorite during later hydrothermal mineralization. Chlorite is rare and occurs only in veinlets. The apophyllite occurs in some places as a late-stage veinlet that cuts all other minerals.

Pyrrhotite, pyrite, bismuthinite, native bismuth, sphalerite occur generally in the fractures in pyroxene or in interstices between garnet or pyroxene grains. Each phase occurs separately in silicates except for a few intergrowths of bismuth and bismuthinite. Paragenetic relationships are not clear but all the sulphides appear to be later than the early silicate skarn. For example, pyrite in Fig. 6.24 occurs intergrown with late hedenbergite pyroxene. Pyrrhotite is the dominant sulphide and occurs locally in massive bands accompanying amphibole and a little scheelite. Fine grained patches of bismuthinite about 0.02 mm across are sufficiently common to make this rock an economic bismuth ore. Most specimens have no iron oxide minerals but a few contain a little magnetite in discrete grains as well as sulphide minerals. Sphalerite appears to have replaced the magnetite. Magnetite veins are occasionally observed(Fig. 5.12) near the contact with amphibole-rich skarn(Fig. 5.13a).

5.2.2. Pyroxene-Quartz Skarn

This is composed of pyroxene(hedenbergite), quartz, epidote(clinozoisite), amphibole, chlorite, garnet(grossularite-andradite), scheelite and sulphide minerals. Garnet is observed as fresh unaltered grains, showing a translucent pale brown colour, generally partly replaced by hedenbergite(Fig. 5.14). Hedenbergite is commonly replaced by quartz, but hedenbergite and epidote also occur associated with quartz without obvious replacement texture. Scheelite is generally closely associated with the quartz, but it occurs rarely in pyroxene assemblages(hedenbergite) without quartz. Amphibole occurs frequently in veinlets(fig. 5.16a). Fluorite is also generally associated with quartz. Pyrite, pyrrhotite and bismuthinite occur separately mainly associated with quartz, or filling interstices between amphibole, chlorite, pyroxene and quartz.

Hedenbergite and quartz make up most of the pyroxene-quartz skarn. It is richer in scheelite than the other variants of the pyroxene skarn (about 1.5 % WO_3); it is characteristically friable compared with other types of skarn.

5.2.3. Pyroxene-Plagioclase Skarn

Pyroxene(hedenbergite), plagioclase, quartz, sphene, amphibole, apatite, garnet(grossularite), epidote and scheelite are the usual minerals in this skarn. Zircon is rare. Pyrrhotite, magnetite and molybdenite occur associated with amphibole veinlets(e.g. 103113). Microprobe analysis has identified scapolite and zeolite, previously unreported: these phases appear as alteration products of the skarn, replacing all other minerals.

This skarn is generally observed in the transitional zone between the pyroxene-garnet rich skarn and the cherty rock; it makes up the main part of the skarn orebody at deeper levels(Fig. 5.7, Fig. 5.13b).

Early euhedral or subhedral hedenbergite crystals occur in a matrix of later quartz or plagioclase, and may be replaced by it. Sphene and plagioclase occur together as in the cherty rock. This skarn is different from the cherty rock in having scheelite associated with plagioclase and sphene without amphibole(Fig. 5.15). The ratio of plagioclase to quartz increases with depth in the M1 orebody(Fig. 5.7, Fig. 5.13b). Quartz-amphibole veins along fractures or joints are common. (e.g. sample 103113).

A summary of paragenesis of minerals in this skarn, including pyroxene-garnet skarn and pyroxene-quartz skarn is given in Table 5.3.

Table 5.3. A Summary of paragenesis of minerals in late anhydrous skarns (Pyroxene-Garnet, Pyroxene-Plagioclase and Pyroxene-Quartz Skarns).

	Pyroxene-Garnet Skarn		Pyroxene-Plagioclase Skarn		Pyroxene-Quartz Skarn	
	early	late	early	late	early	late
Hedenbergite	xxxxx		xxxxx		xxxxxxxx	
Garnet (grossular)	xx		xx		xx	
Epidote	xxx		xxx		xxxx	
Fluorite	x x x x				x x x x x	
Quartz	x x x x		x x		x x xxxxxxx	
Amphibole	x		x	x	xxx	
Calcite	xxxx					
Plagioclase			xxxx			
Scheelite	x x x		x x		x x x x x	
Vesuvianite	x					
Apatite			x			
Sphene			xxxx			
Zircon			x			
Chlorite		x				x
Apophyllite		x				
Scapolite				x		
Zeolite				x		
Pyrrhotite	x x x		x	x	xxx	
Pyrite	x				x	
Chalcopyrite						
Bismuth	x x x					
Bismuthinite		xxx			xxx	
Sphalerite		x				
Molybdenite				x		
Magnetite	xx			x		

xxxx continuous & major

x x continuous & minor

x minor

Fig. 5.8. Two generations of garnet: Euhedral garnet(grossularite-clear ones) occurs in a matrix of anhedral garnet(andradite-dark brown).
103083, Baegun(+ 2) level. ═══ represent 0.2 mm.

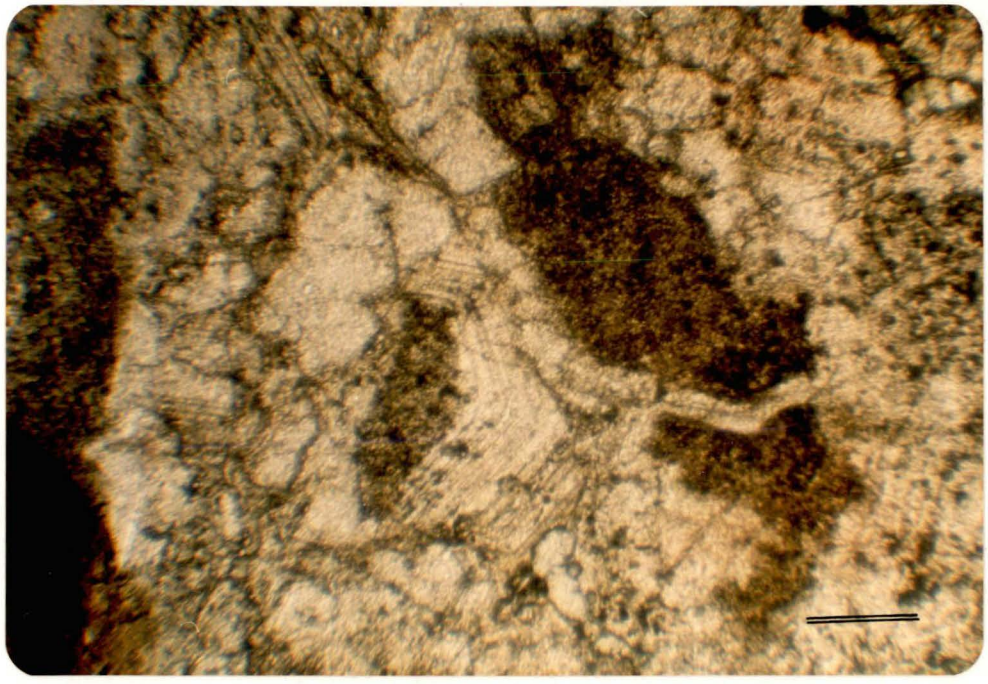

Fig. 5.9. Vesuvianite associated with quartz and scheelite replacing pyroxene skarn at the eastern margin of the M1 orebody. Hexagonal = vesuvianite, high relief fine grain = scheelite, white matrix = quartz
103139, -14th level. ═══ represent 0.1 mm.

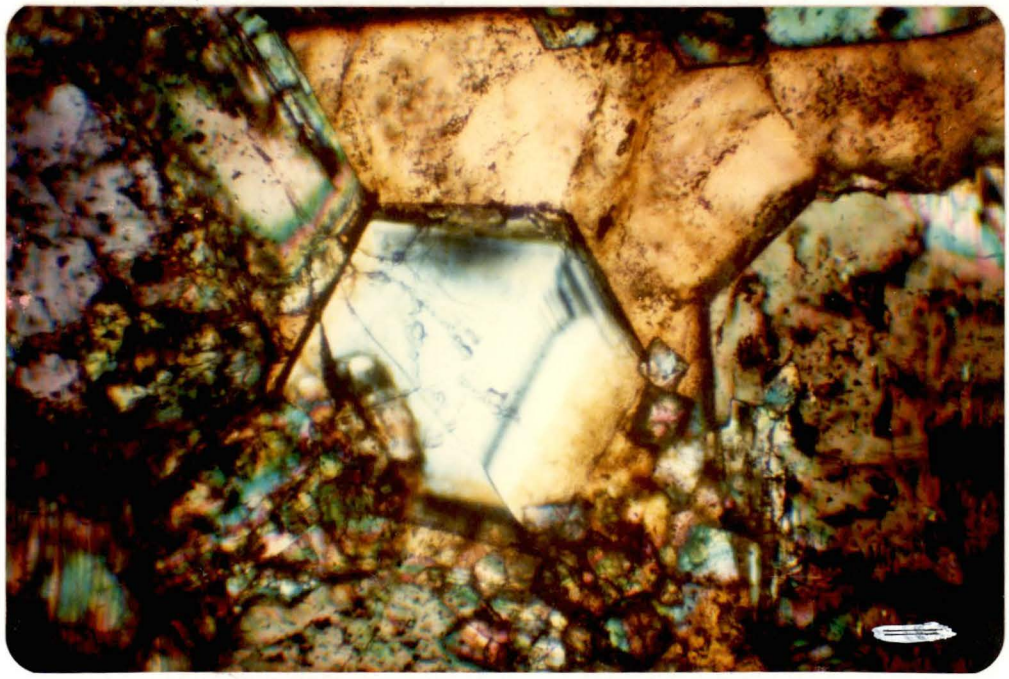

Fig. 5.10a. Pyroxene-garnet skarn. Most garnets are replaced by pyroxenes(hedenbergites).
103065, H1. ——— represent 0.2 mm.

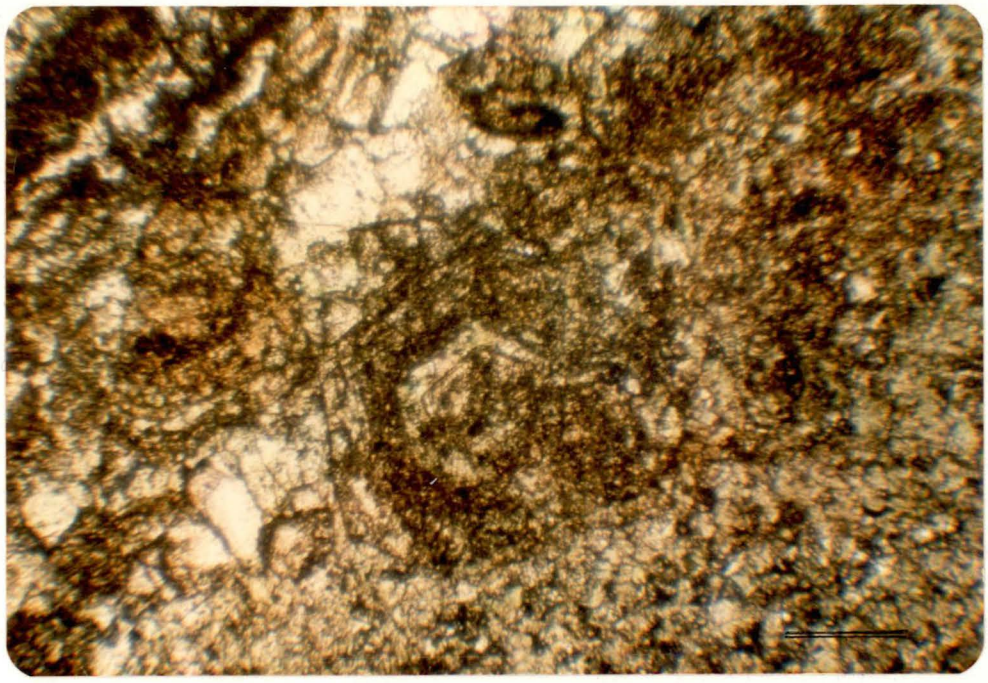

Fig. 5.10b. Same as above, crossed polars.
Black(isotropic) one is garnet and coloured one is pyroxene.
——— represent 0.2 mm.

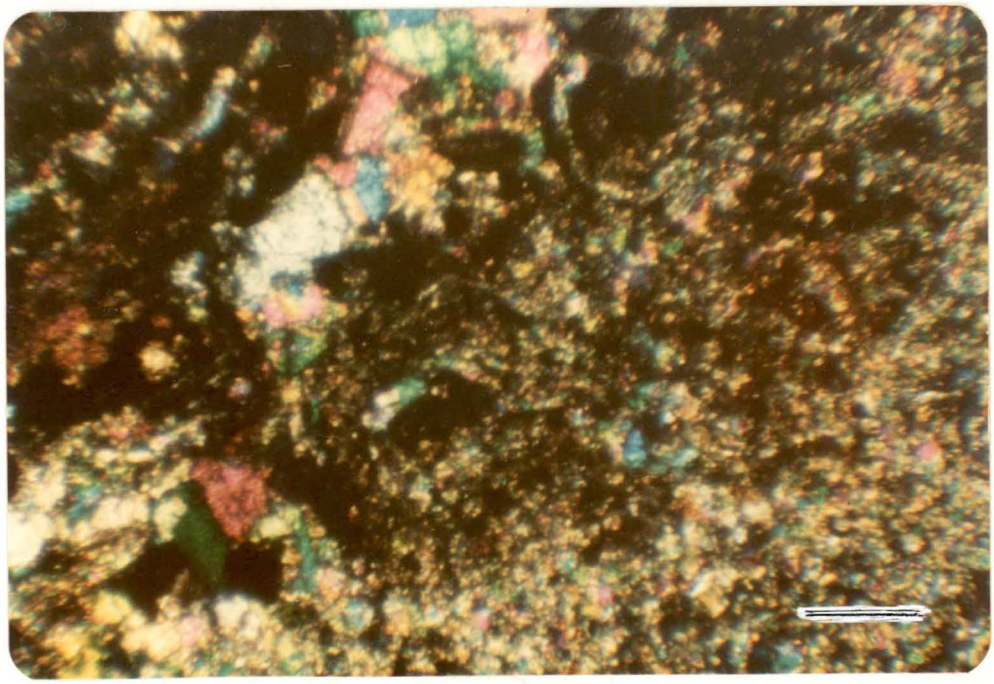

Fig. 5.11. Epidote associated with quartz and scheelite, replacing pyroxene. Ep=epidote, Sch=scheelite, Q=quartz, Px=pyroxene.
103180, -10th level, X 70, crossed polars.

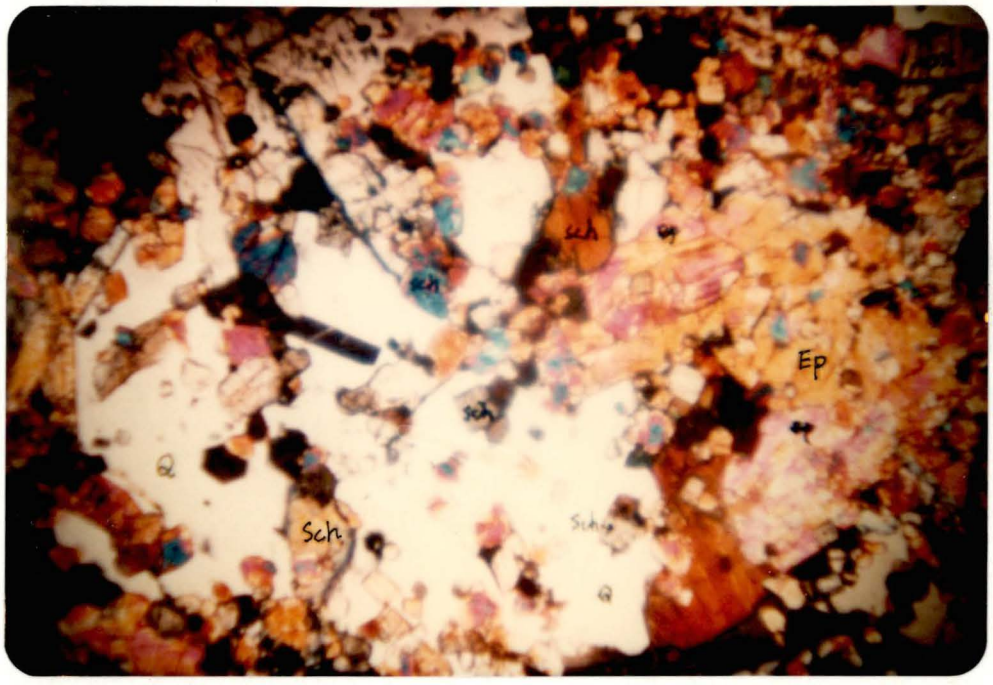

Fig. 5.12. Vein of magnetite replacing pyroxene skarn.
103175(field no. 0137), Sangdong level, X 0.7.

Fig.5.13a. Localization of sphene, epidote and magnetite in the pyroxene-garnet skarn (based on empirical observation).

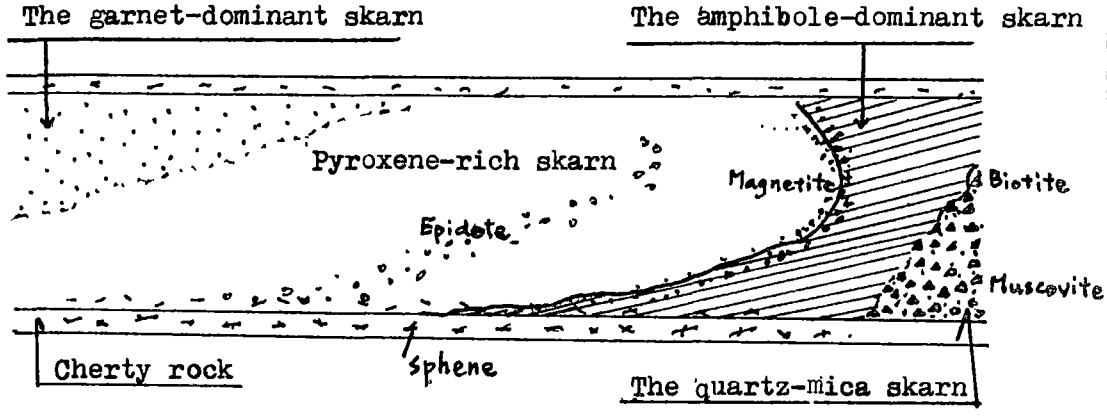

Fig. 5.13b. A schematic diagram showing distribution of the plagioclase-pyroxene skarn in deeper levels (cross section looking to west, based on empirical observation).

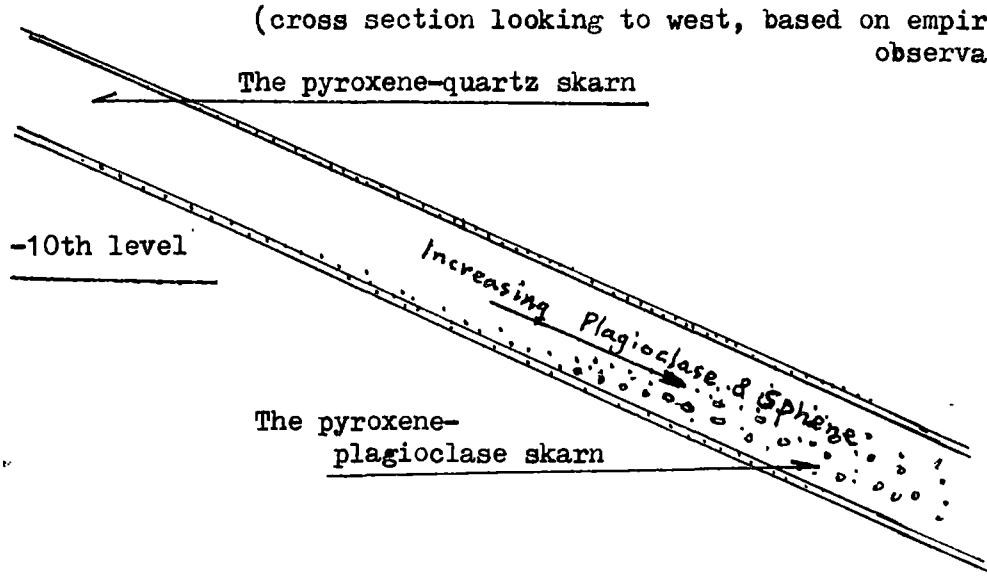

Fig. 5.14(a). Photomicrograph of the pyroxene-garnet skarn. Garnet is replaced by fine pyroxene grains (hedenbergite).
103141, -7th level. ═══ represent 0.1 mm.

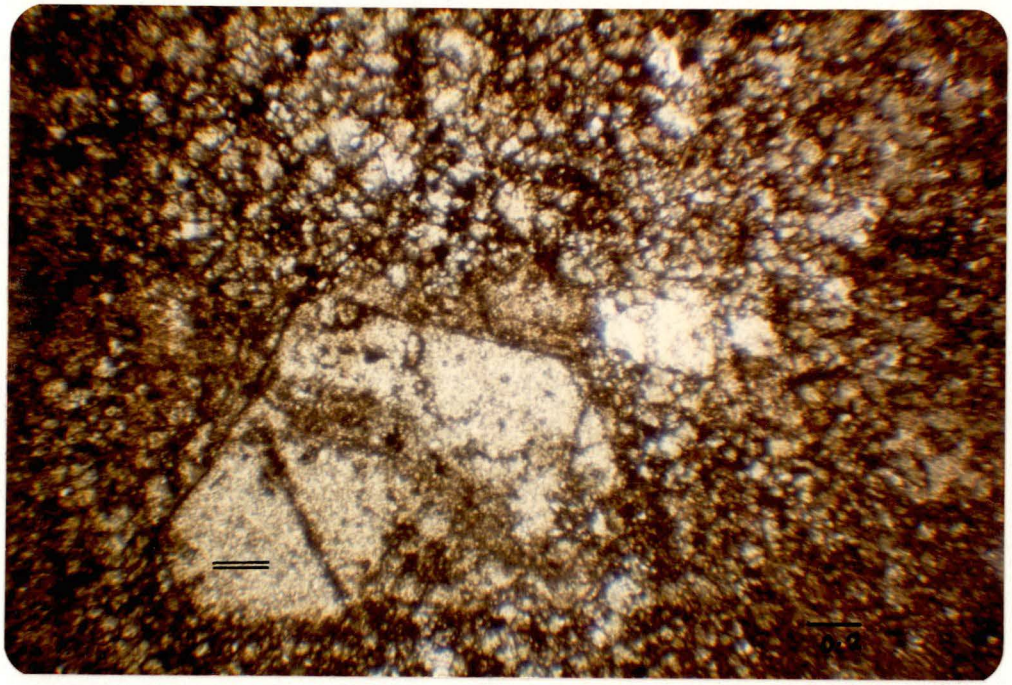

Fig. 5.14(b). A typical rock specimen of the pyroxene-garnet skarn. It consists mainly of hedenbergite replacing garnet as shown in Fig. 5.14(a). Secondary garnet(forming a vein) is observed. Square mark represents Fig. 5.14(a).
103141, -7th level, X 0.73.

Fig. 5.15(a). Photomicrograph of the pyroxene-plagioclase skarn consisting of plagioclase(pl), hedenbergite(hd), quartz(Q), scheelite(sch), sphene(sph) and apatite(ap). 103144, -14th level. ═══ represent 0.1 mm.

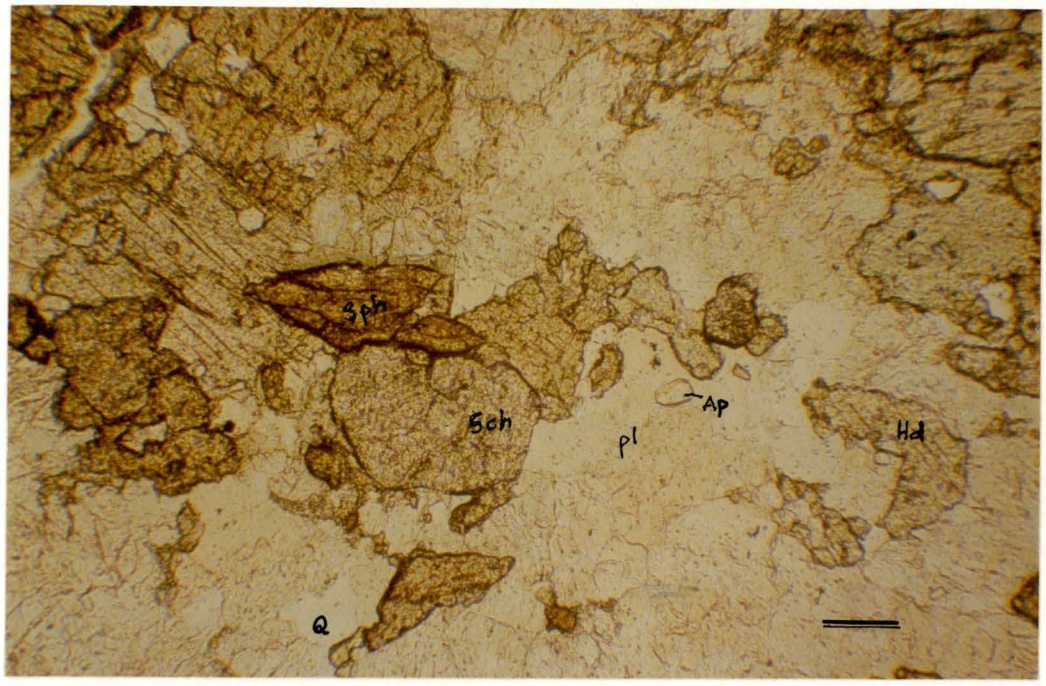

Fig. 5.15(b). Same as above, crossed polars.
The plagioclase is anorthite, locally showing twinning.
103144, -14th level, cross polars. ═══represent 0.1 mm.

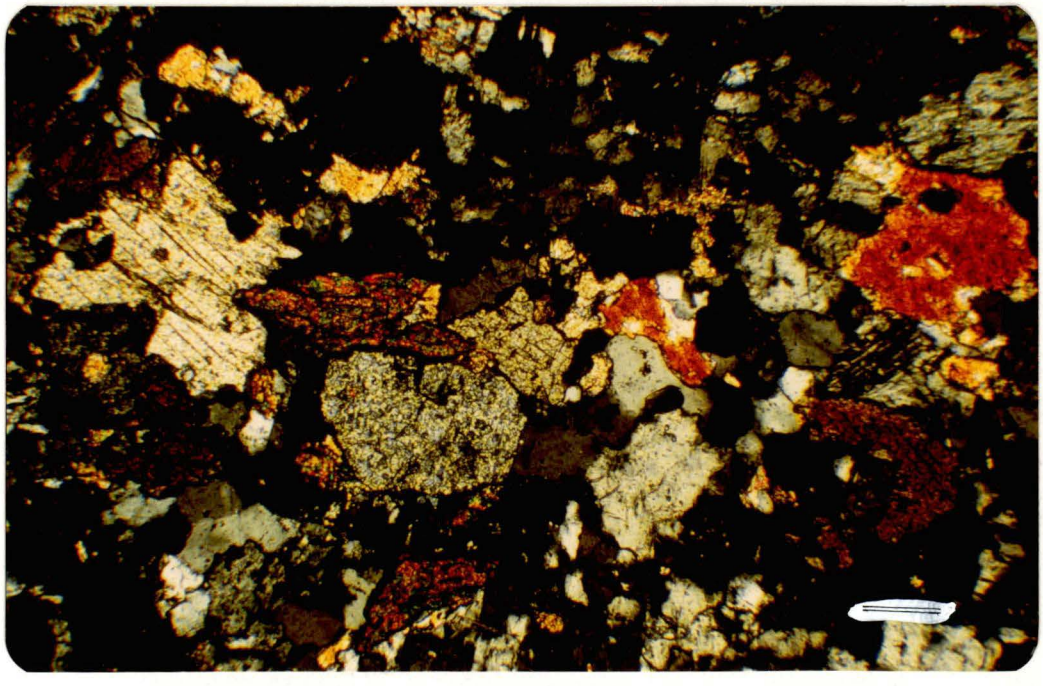

5.3. The Amphibole-rich Skarn

This assemblage replaces the pyroxene-garnet skarn(Figs. 5.16a,b and 5.17). The amphibole is mainly hastingsitic hornblende and amphibole content increases towards the central part of the skarn orebody. A summary of paragenesis of minerals in this skarn is given in Table 5.4, and mineralogical varieties include :

5.3.1. Amphibole-Pyroxene-Quartz Skarn

This variety occurs at the transition between the pyroxene-rich skarn and the amphibole-rich skarn. Pyroxene(hedenbergite) is the dominant constituent, but it is commonly replaced by amphibole and quartz. In some parts, isolated equigranular pyroxene crystals are surrounded and irregularly replaced by quartz. Amphibole occurs generally as euhedral or subhedral ferroedenitic hornblende replacing pyroxene(Fig. 5.16b). Some of the amphibole is tremolite and is not associated with scheelite.

Chlorite replaces amphibole and also occurs between partly replaced amphibole grains. Fluorite with quartz replaces pyroxene and amphibole. Calcite is observed in complex veinlets developed along fractures and cleavages in other minerals. Two generations of hedenbergite are observed in this skarn. Scheelite is closely associated with late hedenbergite which is darker green than the earlier hedenbergite. The late hedenbergite and amphibole occur along fracture systems or at the rim of quartz veins, replacing the earlier pale green pyroxene which is commonly associated with garnet(Figs. 5.17a & b). The difference in chemical composition between the primary and secondary pyroxene will be described in a following chapter.

Bismuthinite and native bismuth occur sporadically, separately or together, and magnetite and pyrrhotite are locally enriched at the margins (eg. specimen 103122) of the amphibole-rich zone. Magnetite and pyrrhotite generally accompany amphibole and secondary pyroxene. This skarn appears in all three orebodies, although there is more fluorite and less scheelite in the H1 orebody than in the M1 and F. orebodies.

5.3.2. Amphibole-Quartz-Chlorite Skarn

This assemblage makes up most of the amphibole-rich zone. Amphibole (mostly hastingsitic hornblende), chlorite and quartz are the major constituents of this skarn, with minor scheelite, apatite, fluorite, calcite, pyroxene, pyrrhotite, magnetite, pyrite, bismuth, bismuthinite and chalcopyrite(sulphides in order of abundance). Figures 5.17b and 5.18 show the formation of amphibole-rich skarn through replacement of pyroxene-garnet skarn. Sulphides occur dispersed or along cleavages in amphibole and chlorite and apparently in close association with scheelite.

The average grade of ore is reported as about 1.5 % WO_3. Sphene and plagioclase are occasionally found close to the footwall side of the skarn orebodies. The hastingsitic hornblende aggregates show decussate texture or meshed texture(Figs. 5.18 and 5.20) where replaced by quartz. Locally tremolite or actinolite takes the place of hastingsitic hornblende. Ripidiolite and brunsvigite are the common forms of chlorite, forming hemispherical radial aggregates in some cases. It occurs with, and locally replaces amphibole(Fig. 5.19). Garnet is rarely observed and appears to be a relict of pyroxene-garnet skarn and largely replaced by amphibole and quartz. Apatite is generally associated with scheelite. It occurs as fine aggregates in a matrix of quartz, looking like bubbles in water. The ratio of apatite to scheelite varies a great deal but if there is abnormally abundant apatite, there is little scheelite. Scheelite occurs most commonly in quartz and amphibole, and also along the cracks or cleavages of amphibole or chlorite. Fluorite is very common with quartz mainly developed in between amphibole or quartz grains, or locally associated with calcite. Quartz is a major constituent of this assemblage and most of the scheelite and the sulphide minerals are closely associated with it. Both the H1 and the M1 orebodies show this assemblage but sphene and plagioclase are encountered in the F. ore body, and there are fewer sulphide minerals.

5.3.3. Amphibole-Plagioclase-Quartz-Sphene Skarn

This mineral assemblage is restricted to the footwall side of the skarn orebodies, and appears to have formed by replacement of pyroxene-plagioclase (Fig. 5.21) or cherty rock.

The individual minerals are generally similar to those occurring in the amphibole-quartz-chlorite skarn described previously except that sphene and plagioclase are common in this skarn. It shows a similar mineralogy and texture to some amphibolite except that this skarn has non-oriented amphiboles. Hastingsitic hornblende, chlorite and scheelite have a more irregular outline to their crystals than those in other skarns. Zircon is rarely associated with scheelite and sphene.

Table 5.4. A Summary of paragenesis of minerals in the amphibole-rich skarn.

	Amphibole-Pyroxene-Quartz Skarn		Amphibole-Plagioclase-Quartz Skarn		Amphibole-Quartz Chlorite Skarn	
	early	late	early	late	early	late
Hedenbergite	xxxx				xx	
Garnet	x				x	
Amphibole	xxxxxxxx		xxxxxxxx		xxxxxxxxxx	
Chlorite	xxxx		xxxxxx		xxxxxx	
Quartz	xxxxxxxxxxxx		xxxxx		xxxxxxxxxxxxx	
Fluorite	x x x x x		x x x x		x x x x x x	
Plagioclase			xxxxxx			
Scheelite	x x x x x		x x x x		x x x x x x x	
Apatite	x x x		x x x		x x x x x	
Sphene			xxxx			
Calcite	x x x		x		x x x x	
Zircon			x			
Pyrrhotite	x x x x		x		x x x x	
Pyrite	x x		x		x x	
Chalcopyrite					x x	
Bismuth	x x x		x		x x x	
Bismuthinite	x x x		x		x x x	
Sphalerite	x					
Magnetite	x x				x	

xxxx continuous & major

x x continuous & minor

x minor

Fig. 5.16(a). Photomicrograph of pyroxene-quartz skarn near the amphibole-rich zone. It consists mainly of quartz and hedenbergite, and amphibole veinlets are frequently observed.
103089, -7th level. ═══ represent 0.2 mm.

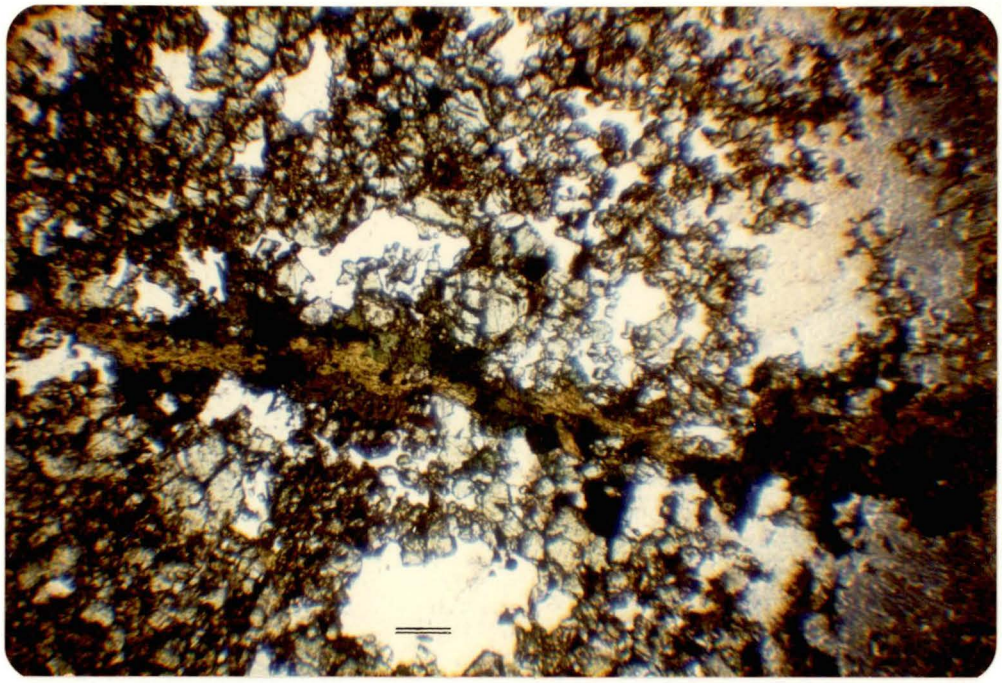

Fig. 5.16(b). Replacement of pyroxene by amphibole at the boundary between the pyroxene-garnet zone and the amphibole zone.
103147, Taebag level. ═══ represent 0.1 mm.

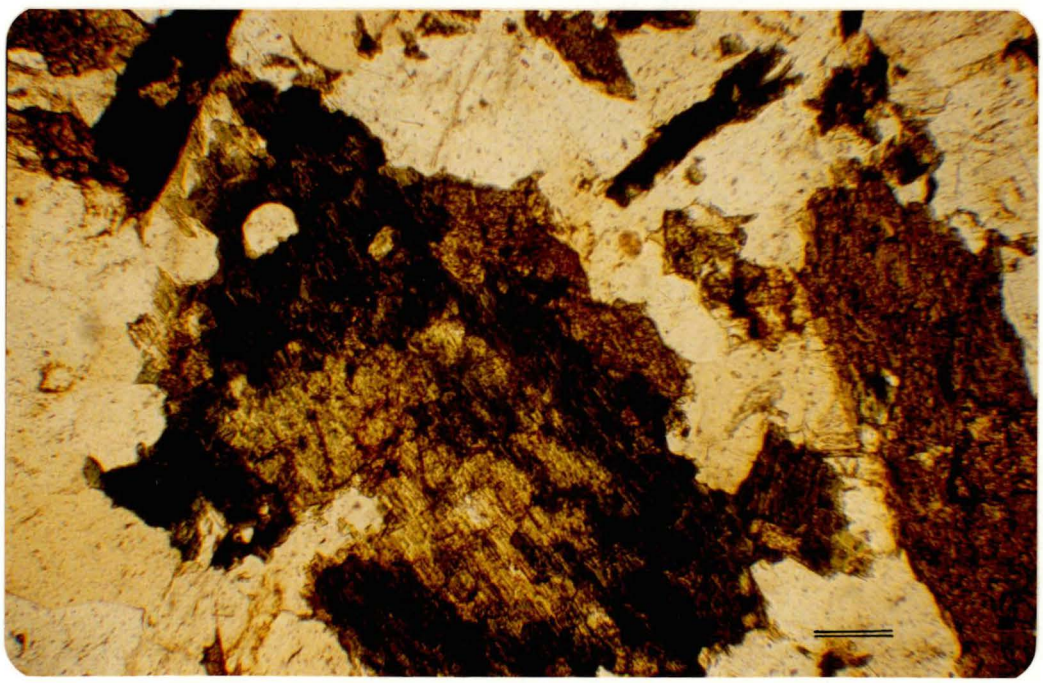

Fig. 5.17(a). Replacement of the pyroxene-garnet skarn by amphibole and hedenbergite. The dark band is mainly composed of amphibole and secondary dark green hedenbergite with scheelite and quartz at the middle of the band. 103148, -1st level. ═══ represent 1.0 cm.

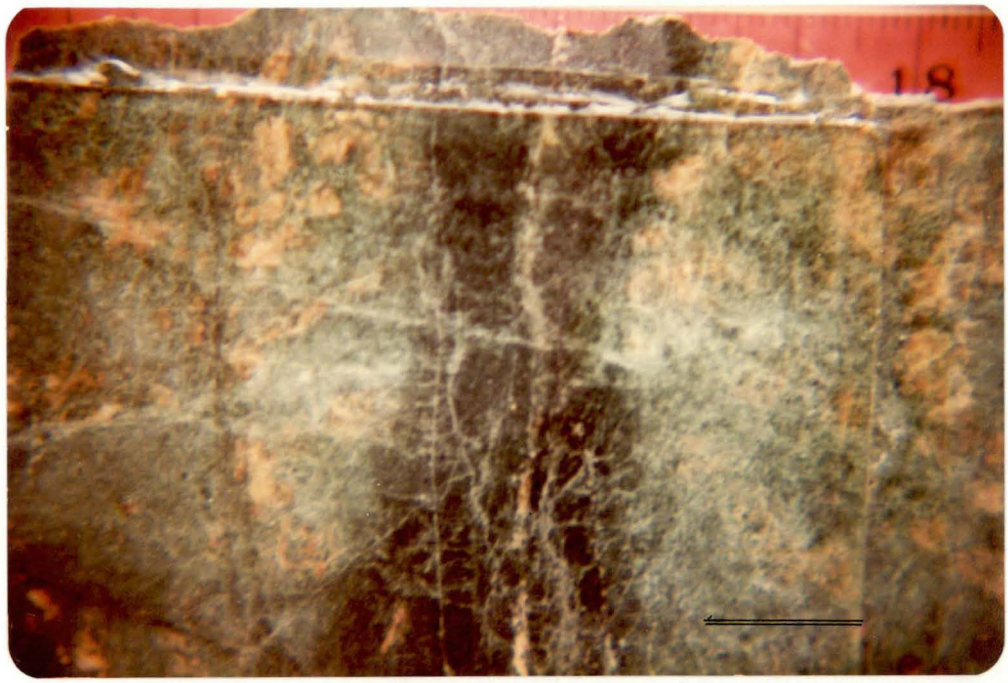

Fig. 5.17(b). A minor feature showing formation of amphibole-pyroxene skarn by replacement of the garnet-dominant skarn along a quartz vein.
103084(field no. 0162), Baegun level.
═══ represent 1.0 cm.

Fig. 5.18.

A polished thin section showing the formation of the amphibole skarn by replacing the pyroxene skarn.
103240, -7th level.
═══ represent 5 mm.

Fig. 5.19. Typical microscopic appearance of amphibole-quartz-chlorite skarn. Amp = amphibole, Sch = scheelite, Ch = chlorite, Q = quartz.
103149, Sangdong level. ═══ represent 0.1 mm.

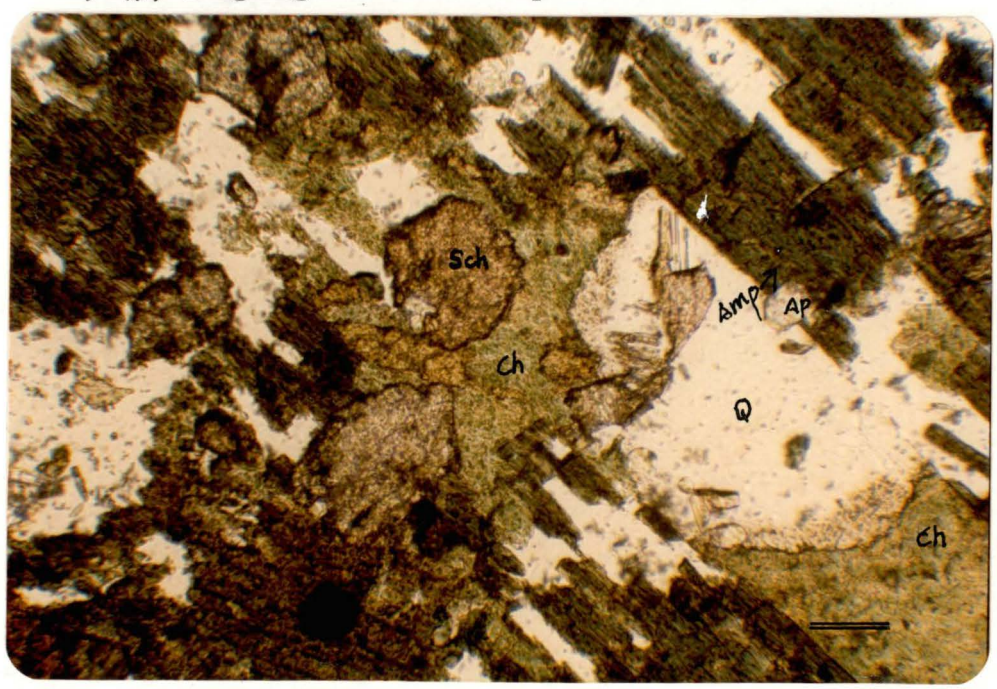

Fig. 5.20. Typical microscopic appearance of amphibole-quartz skarn, showing meshed texture.
Amp = amphibole, Sch = scheelite, Q = quartz.
103149, Sangdong level. ═ represent 0.1 mm.

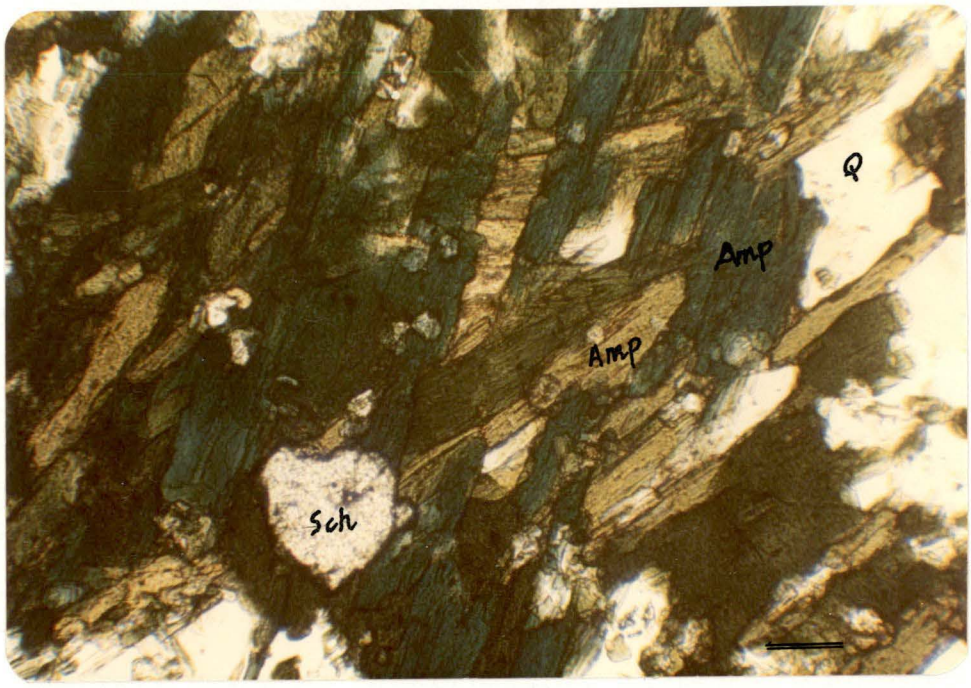

Fig. 5.21. Formation of amphibole-plagioclase-quartz-sphene skarn by replacement of pyroxene-plagioclase skarn.
Pl = plagioclase, Px = pyroxene, Sch = scheelite, Q = quartz.
103144, -14th level. ═ represent 0.1 mm.

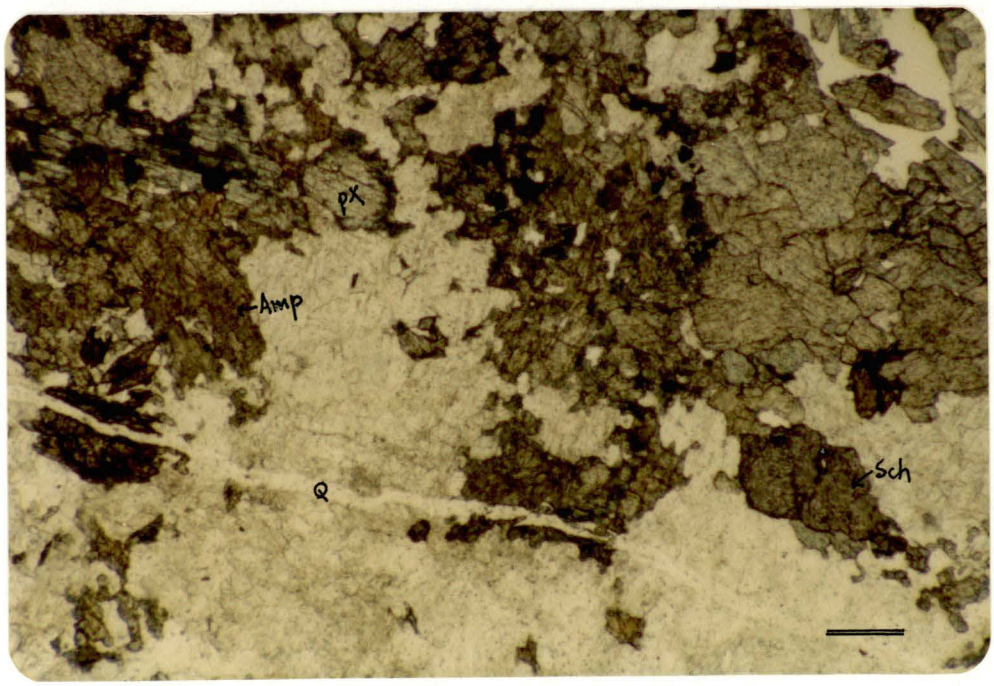

5.4. Mica-rich Skarns

This skarn forms the central part of the M1 and F. orebodies, and is the richest in scheelite, ranging in grade from about 6 to 15 % WO_3. This skarn can be sub-divided into two types, one generally confined to the central part of this skarn zone and characterized by a pale greyish or brownish colour because of dominant muscovite(sericite) and brown chlorite; the other characterized by dark brown or black colour due to dominant biotite. The biotite-rich part surrounds the muscovite-rich part. A summary of paragenesis of minerals in this skarn is given in Table 5.5.

5.4.1. Quartz-Mica-Chlorite Skarn

Muscovite, biotite, quartz, chlorite and scheelite are the most common minerals. This zone in the M1 orebody is accessible only over a limited area and the following description is based on observations of specimens taken from the 3rd and 7th levels. Muscovite and biotite decrease along strike and down dip from the centre of the M1 orebody, and are replaced by chlorite or locally by calcite(Fig. 5.22, 5.23). Muscovite is enriched in the central part of this zone and is altered to illite near fractures. Muscovite is closely associated with scheelite and shows an abrupt decrease with depth in contrast to the gradual decrease of the biotite; it is not observed in the mica-rich skarn on the 7th level. Muscovite occurs commonly as radiating clusters of large crystals closely intergrown with scheelite and it is locally replaced by calcite. Biotite is predominant close to the boundary between this assemblage and the amphibole-rich skarn. At the boundary between these two zones, it is not clear which phase is replacing the other(Fig. 5.25). In specimen 103093(Fig. 5.26), the biotite seems to have been replaced by amphibole. Generally biotite is observed as fine grained euhedral crystals in the higher level(from the 3rd to top level), while anhedral ones predominate in lower levels(from the 4th to 8th level).

Biotite close to the amphibole-rich zone tends to show a green colour(Fig. 5.27), while a brownish colour is dominant close to muscovite-rich areas. Ovoids of biotite-quartz-calcite assemblage were observed replacing biotite-rich skarn(Fig. 5.24). Most biotites are altered to chlorite in the muscovite zone. Quartz is subordinate in muscovite-dominated parts and in places it is intergrown with muscovite in which scheelite has developed along the cleavage, or it occurs as isolated round or elongate grains in the muscovite. Apatite is observed commonly as euhedral grains or as aggregates (Fig. 5.28). Scheelite occurs in the same manner as apatite and fine scheelite grains are generally enclosed in larger grains. As shown in the amphibole-rich skarn, the frequency of occurrence of scheelite and apatite are inversely related. Fluorite is closely associated with quartz, calcite and chlorite and locally occurs in aggregates. A fragment of andradite was detected by microprobe analysis and is assumed to be a relic of early skarn. Late silicification occurs locally(Fig. 5.29).

Opaque minerals are mainly found in biotite, chlorite and muscovite, forming irregular shapes or elongate grains along the cleavages. Locally bismuthinite is abundant enough to be seen in hand specimen. Pyrrhotite, chalcopyrite, native bismuth, sphalerite and magnetite also occur but separately. Molybdenite, wolframite, arsenopyrite and hematite have not been described previously but the author has found few grains of molybdenite 1 to 2 mm in diameter(e.g. 103125) and a wolframite-arsenopyrite-hematite-magnetite-pyrite assembalge(specimen 106174).

Sphene is encountered only in the footwall of this skarn close to the Myobong slate. Rutile, reported here for the first time, occurs in this skarn(e.g. 103125) especially where muscovite is largely replaced by calcite.

5.4.2. Quartz-Mica Skarn in the F. Orebody

In the F. orebody, the quartz-mica skarn is classified into the following varieties(Moon, 1974);

Quartz-biotite-scheelite assemblage:

This skarn has similar mineralogy to the M1 orebody, except for an occurrence of garnet associated with quartz.

Quartz-muscovite-chlorite-scheelite assemblage:

This skarn is also similar to the M1 skarn, except for the occurrence of sphene and close association of pyrrhotite, native bismuth and bismuthinite.

Quartz-muscovite-biotite assemblage:

This skarn is characterized by abundant apatite and occurrence of siderite, while scheelite is rarely observed.

Table 5.5. A Summary of paragenesis of minerals in mica-rich skarns.

	Quartz-Mica Skarn	
	early	late
Amphibole	xx	
Biotite	xxxxxxxxxx	
Muscovite	xxxxxxxxxx	
Quartz	xxxxxxxxxxxxxxxxxxxxx	
Calcite	x x x x xxxx	
Scheelite	xxxxxxxxxxxxxxxxxxxx x x	
Apatite	x x x x x x x	
Fluorite	x x x x x x x	
Chlorite	x x x x xxxxxxx	
Rutile	x	
Illite		x
Pyrrhotite	x x	
Pyrite	x x xxx x x	
Chalcopyrite	x x x	
Bismuth	x x x x x x x x x	
Bismuthinite	x xxx xxx xxx xxx x	
Sphalerite	x	
Arsenopyrite		x
Molybdenite		x
Magnetite	x x x x	
Hematite		x
Wolframite		x

xxxxxx continuous & major

x x continuous & minor

x minor

Fig. 5.22. Photomicrograph of the quartz-mica(muscovite) skarn. The muscovite is commonly replaced by calcite. Sch=scheelite, Ms = altered muscovite(to calcite), Ca = calcite, Q=quartz. 103150, -7th level. represent 0.1 mm.

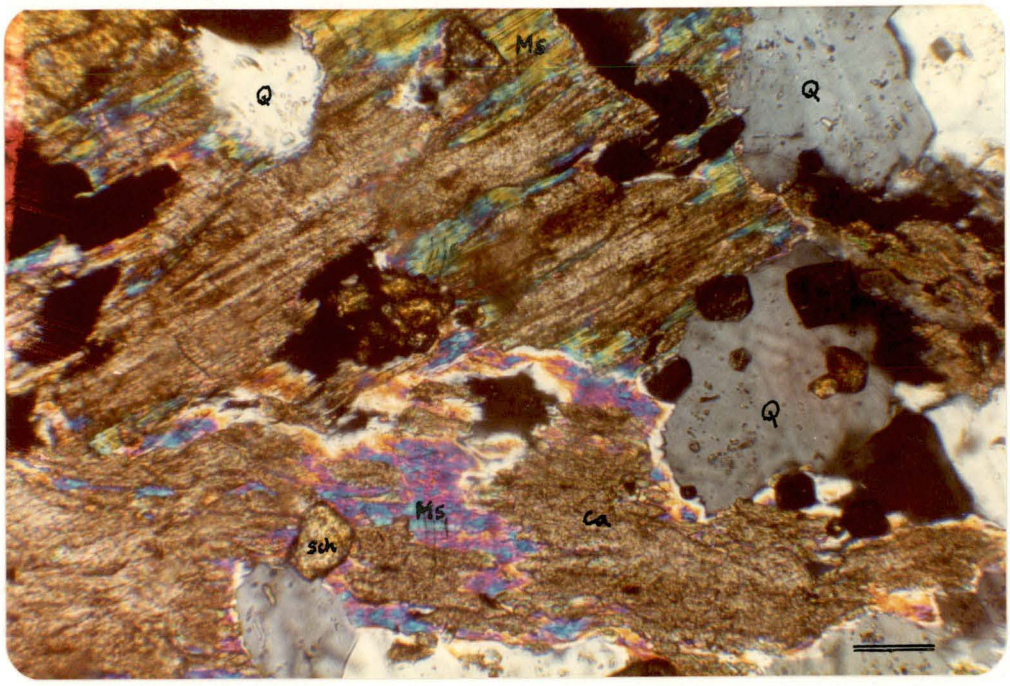

Fig. 5.23. Photomicrograph of the quartz-mica(muscovite) skarn. It consists of quartz, muscovite, brown chlorite, scheelite and opaque minerals. Ms = muscovite, Q = quartz, Sch = scheelite, Ch = chlorite. 103107, -7th level. represent 0.1 mm.

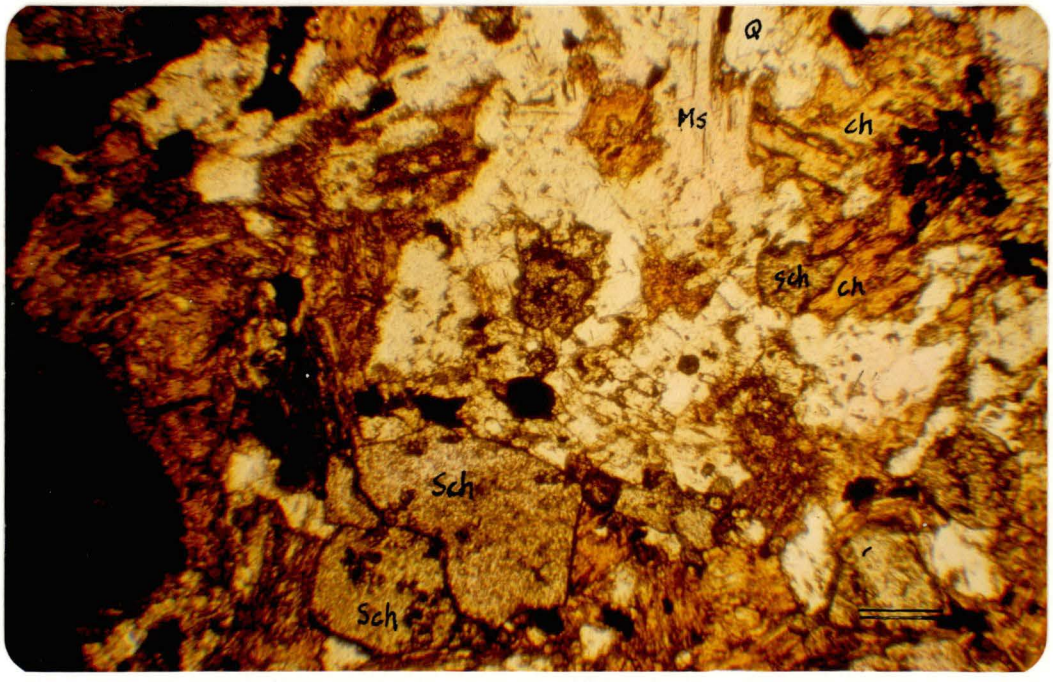

Fig. 5.24. A specimen showing an ovoid of biotite, quartz and calcite formed within the quartz-mica zone. This ovoid replaced the early quartz-biotite skarn. The core of ovoid is mainly composed of calcite, quartz, fluorite, chlorite, scheelite and biotite and its rim is mainly composed of green biotite.
103120, Sangdong level, X 0.83

Fig. 5.25. A specimen showing the formation of quartz-biotite in the amphibole skarn.
103093, -7th level,
═══ represent 5 mm.

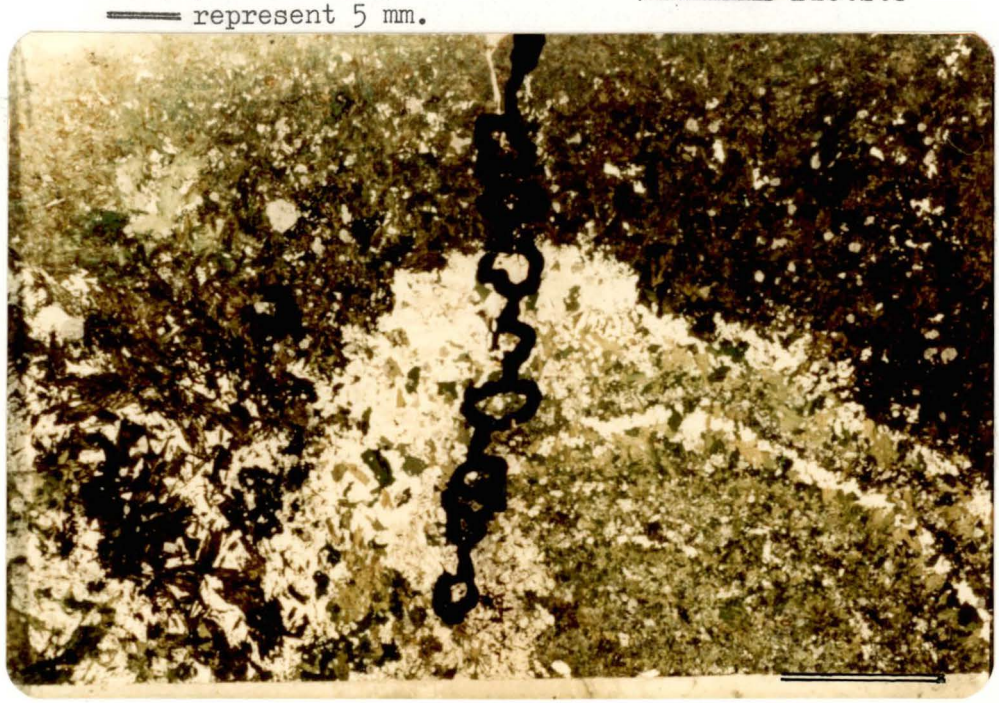

Fig. 5.26. Photomicrograph showing occurrence of amphibole and biotite at the boundary of amphibole skarn and biotite skarn. Dark green = amphibole, Pale green = biotite, sch = scheelite, Q = quartz.
103093, -7th level. ═══ represent 0.1 mm.

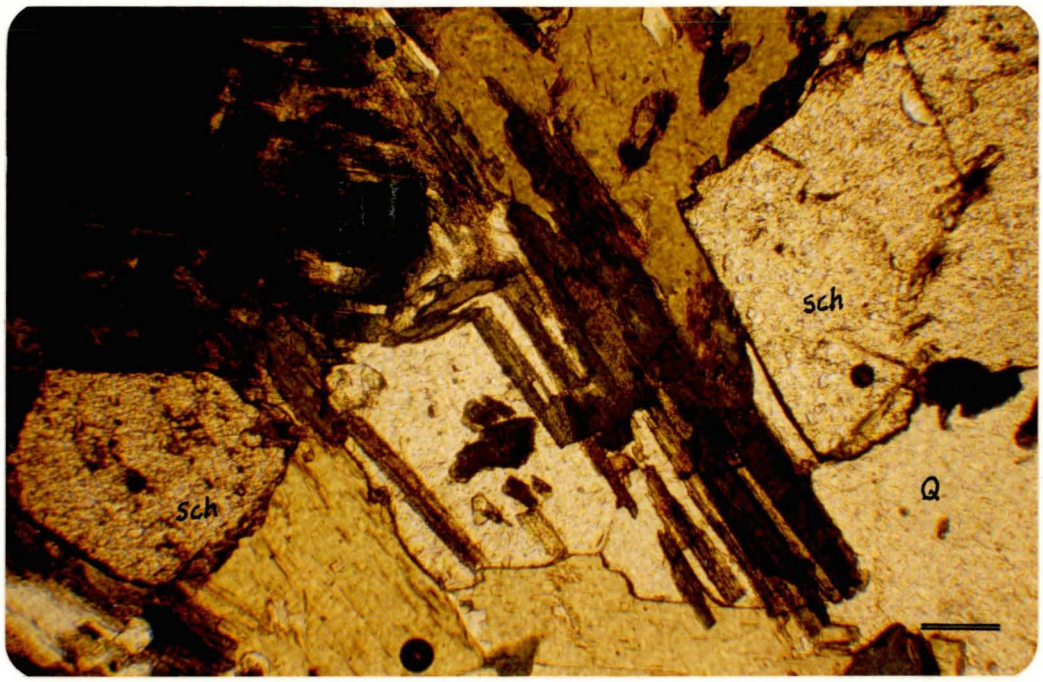

Fig. 5.27. Green biotite-quartz-scheelite-apatite assemblage. Sch = scheelite, Q = quartz, Ap = apatite, Bt = biotite.
103093, -7th level. ═══ represent 0.1 mm.

Fig. 5.28. Quartz-mica skarn showing abundant apatite and little scheelite. Ap = apatite, Sch = scheelite, Bt = biotite. 103067, Sangdong level. ═══ represent 0.1 mm.

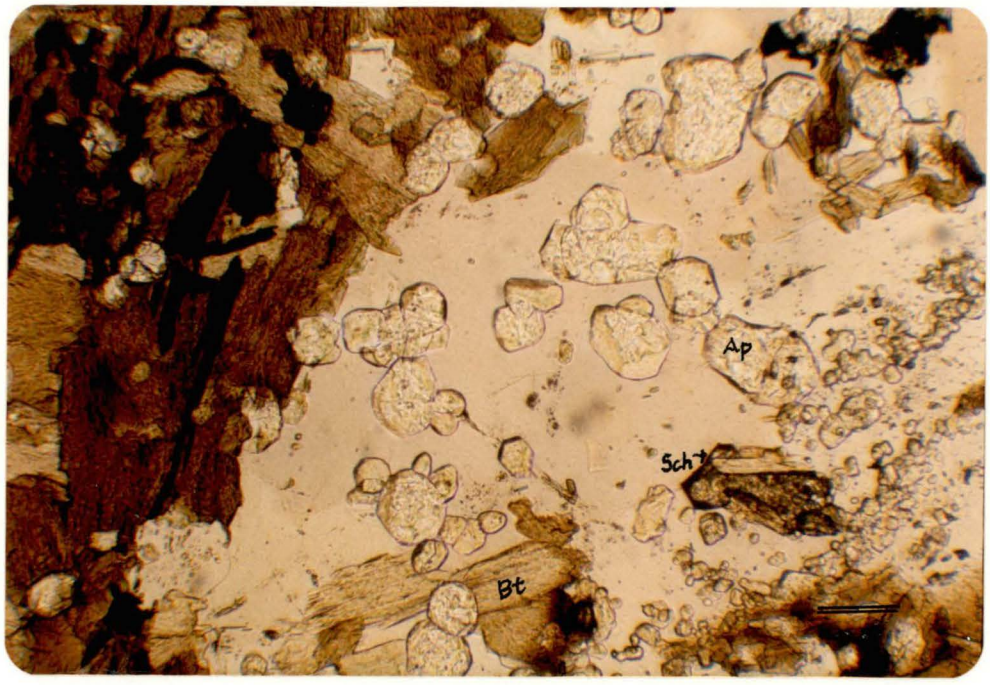

Fig. 5.29. Silicified quartz-mica skarn.
Muscovite, fluorite and scheelite occur in interstices of quartz crystals.
103134, Sangdong level. ═══ represent 0.1 mm.

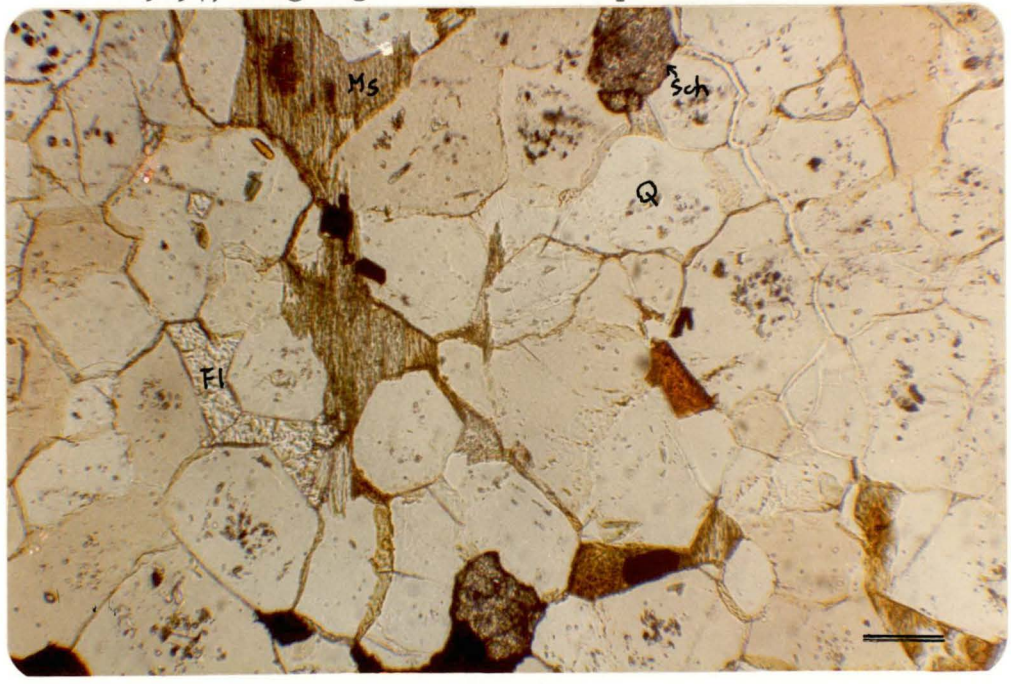

6. MINERAL CHEMISTRY

Samples were taken systematically at the 7th level which is the only level on which there is access to all three major skarn zones within the M1 orebody. Some of the specimens representing the quartz-mica skarn were taken from the 1st and 3rd levels. Microprobe analyses have been normalized to 100 % total compositions for garnet and pyroxene, 97 % for amphibole, 96 % for mica, and 88 % for chlorite. More detailed results of microprobe analyses are given in Appendix 6 and details of analytical techiniques for FeO are given in Appendix 7.1.

6.1. Garnet

Garnet is generally restricted to anhydrous skarns(ie. wollastonite-, garnet-, and pyroxene-garnet skarns) although two residual grains of garnet were identified in both the quartz-mica skarn and the amphibole-rich skarn. Garnet compositions from each skarn type are presented in Tables 6.1 and 6.2. The garnets are plotted in terms of their end members andradite-grossularite-(pyrope + spessartine + almandine + uvarovite) compositions in Fig. 6.1.

In general early formed garnet from wollastonite and garnet-dominated skarns is andradite-rich while later garnet of the pyroxene-garnet skarn tend to be grossularite-rich(Fig. 6.1). However, in fact, garnets from the pyroxene-garnet skarn on the 7th level show a wide range of variation in compositions between andradite and grossularite; the most andradite-rich garnet shows 87 mole % andradite and 10 mole % grossularite compositions(e.g. 103087), while the highest grossularite composition is represented by 87 mole % grossularite with 11 mole % andradite compositions (e.g. 103091). Chemically the two types(early and late garnets) are distinguished by MnO(and TiO_2)contents with the later grossularite-rich garnets, having 0.26 to 1.74 % MnO compared to the andradite-rich garnets which contain negligible MnO.

The two analyses of residual garnets from the anhydrous skarns show a marked variation in composition from a high Mg - low Ca garnet(103096) to a pure end member andradite garnet(103134). There is no obvious explanation for the dramatic difference in composition between these two residual garnets.

Colours of garnet in hand specimen range from dark brown to pale brown (colourless under the microscope), to greenish. In specimen 103098 brown andradite contains detectable TiO_2 and Cr_2O_3 distinguishing it chemically from a colourless part, which contains negligible TiO_2 and Cr_2O_3(see Appendix 6.1). Grossularite-rich garnet becomes brown due to an increase of Fe_2O_3 content(e.g. 103102). A green garnet(103135) containing significant Cr_2O_3 is thus chemically distinguished from brown garnets(103136 & 103054) which contain no Cr_2O_3(Table 6.1). It cannot be stated that those elements mentioned above are responsible for a certain colour, but it is obvious that variations in these elements occur between different coloured grains or zoned portions of the garnet.

The variation in chemical composition within a single crystal spans a similar range in composition to that existing between different grains(Figs. 6.1 and 6.3). There is an increase in TiO_2 and CaO from core to the margin in the grossularite of sample(103089 & 103101) and an inverse correlation with SiO_2, but in the andradite of sample(103087) there is no TiO_2 and CaO decreases from the core to the rim(Fig. 6.2). Al_2O_3 and Fe_2O_3 contents in both types(andradite-rich and grossularite-rich) show inverse correlation and irregular variation from the core to the rim. MgO content, which is generally negligible in the Sangdong garnet, is occasionally detected in the rim of grains coexisting with pyroxene(103083, Appendix 6.3). This suggests that the pyroxene and the garnet may have partially equilibrated. Zonation of the garnets is generally displayed by colour, weak birefringence or extinction angle variations(Appendices. 6.1 & 6.2).

Table 6.1. Chemical compositions of typical garnets occurring in the main rock types.

	wollastonite skarn			garnet skarn		amphibole skarn	mica skarn	cherty rock	**
	M1 brown	H1 brown	H1 green	M1	M1	M1	M1		
	103054	103136	103135	103118	103083	103096	103134	103137	
SiO_2	37.28	37.15	37.38	37.01	37.39	43.15	44.56	39.50	
TiO_2	n.d	n.d	n.d	n.d	n.d	n.d	0.12	n.d	
Al_2O_3	3.75	n.d	2.89	2.12	0.87	5.33	n.d	20.5	
*Fe_2O_3	24.39	28.80	24.99	26.44	28.78	35.52	29.15	3.57	
Cr_2O_3	n.d	n.d	0.23	n.d	n.d	n.d	0.45	n.d	
MnO	n.d	n.d	n.d	n.d	0.77	2.75	1.89	n.d	
MgO	n.d	n.d	n.d	0.25	0.31	11.36	n.d	n.d	
CaO	34.58	34.05	34.51	34.19	31.88	1.09	23.84	36.43	
K_2O	n.d	n.d	n.d	n.d	n.d	n.d	n.d	n.d	
	Numbers of ions on the basis of 12 oxygens								
Si	3.227	3.031	3.087	3.244	3.307	3.000	3.568	3.014	
Ti	0.000	0.000	0.000	0.000	0.000	0.000	0.007	0.000	
Al	0.382	0.000	0.282	0.219	0.091	0.436	0.000	1.843	
Fe	1.766	1.768	1.553	1.939	2.129	1.564	1.757	0.228	
Cr	0.000	0.000	0.014	0.000	0.000	0.000	0.026	0.000	
Mn	0.000	0.000	0.000	0.000	0.058	1.819	0.128	0.000	
Mg	0.000	0.000	0.000	0.032	0.041	1.384	0.000	0.000	
Ca	3.208	2.977	3.053	3.212	3.021	0.166	2.046	2.979	
Total	8.583	7.776	7.989	8.646	8.647	8.315	7.532	8.064	
X_{ad}	0.822	1.000	0.843	0.887	0.928	0.301	0.927	0.110	
X_{gr}	0.178	0.000	0.153	0.100	0.050	0.084	0.000	0.890	
X_{oth}	0.000	0.000	0.004	0.003	0.032	0.615	0.073	0.000	

ad = andradite, gr = grossularite, oth = pyrope + almandine + uvarovite + spessartine

* Total Fe as Fe_2O_3

** pyroxene-garnet skarn(see Table 6.2)

*** Unusually high total Fe (e.g. 103096) probably indi-ates high ferrous content. Two independent spectrometric analyses of garnet from wollastonite and garnet skarns had very low ferrous iron contents.

Table 6.2. Chemical compositions of garnets occurring in the pyroxene-garnet skarn at the 7th level.

	103086	103087	103089	103091	103100	103101	103102
SiO_2	39.24	36.3	37.19	39.25	37.32	38.05	39.06
TiO_2	n.d	n.d	0.52	0.27	n.d	n.d	n.d
Al_2O_3	26.15	1.89	11.95	20.34	3.69	13.76	16.17
$Fe_2O_3^*$	9.99	26.13	15.07	3.7	24.77	13.19	9.6
Cr_2O_3	n.d	n.d	0.17	n.d	n.d	n.d	n.d
MnO	0.44	0.28	1.74	0.63	0.26	1.23	0.48
MgO	n.d	0.53	0.08	n.d	n.d	n.d	n.d
CaO	24.18	34.60	33.28	35.81	33.96	33.78	34.70
K_2O	n.d	0.27	n.d	n.d	n.d	n.d	n.d
Total	98.93	99.50	99.93	101.02	100.04	100.45	100.01
			Numbers of ions on the basis of 12 (O)				
Si	2.955	3.031	3.050	3.003	3.234	3.071	3.020
Ti	0.000	0.000	0.032	0.016	0.000	0.000	0.000
Al	2.321	0.187	1.152	1.834	0.376	1.309	1.476
Fe	0.629	1.641	1.037	0.236	1.794	0.890	0.559
Cr	0.000	0.000	0.011	0.000	0.000	0.000	0.000
Mn	0.028	0.020	0.121	0.041	0.018	0.084	0.032
Mg	0.000	0.066	0.007	0.000	0.000	0.000	0.000
Ca	1.951	3.095	2.924	2.935	3.152	2.921	2.875
K	0.000	0.029	0.000	0.000	0.000	0.000	0.000
Total	7.884	8.069	8.334	8.065	8.574	8.275	7.962
X_{ad}	0.210	0.873	0.451	0.112	0.822	0.393	0.272
X_{gr}	0.776	0.100	0.502	0.874	0.172	0.579	0.717
X_{other}	0.014	0.027	0.047	0.014	0.006	0.028	0.021

* Total Fe as Fe_2O_3 ** Total before normalized

Fig. 6.1. Chemical compositions of garnets plotted in terms of mole % of grossularite, andradite and others.

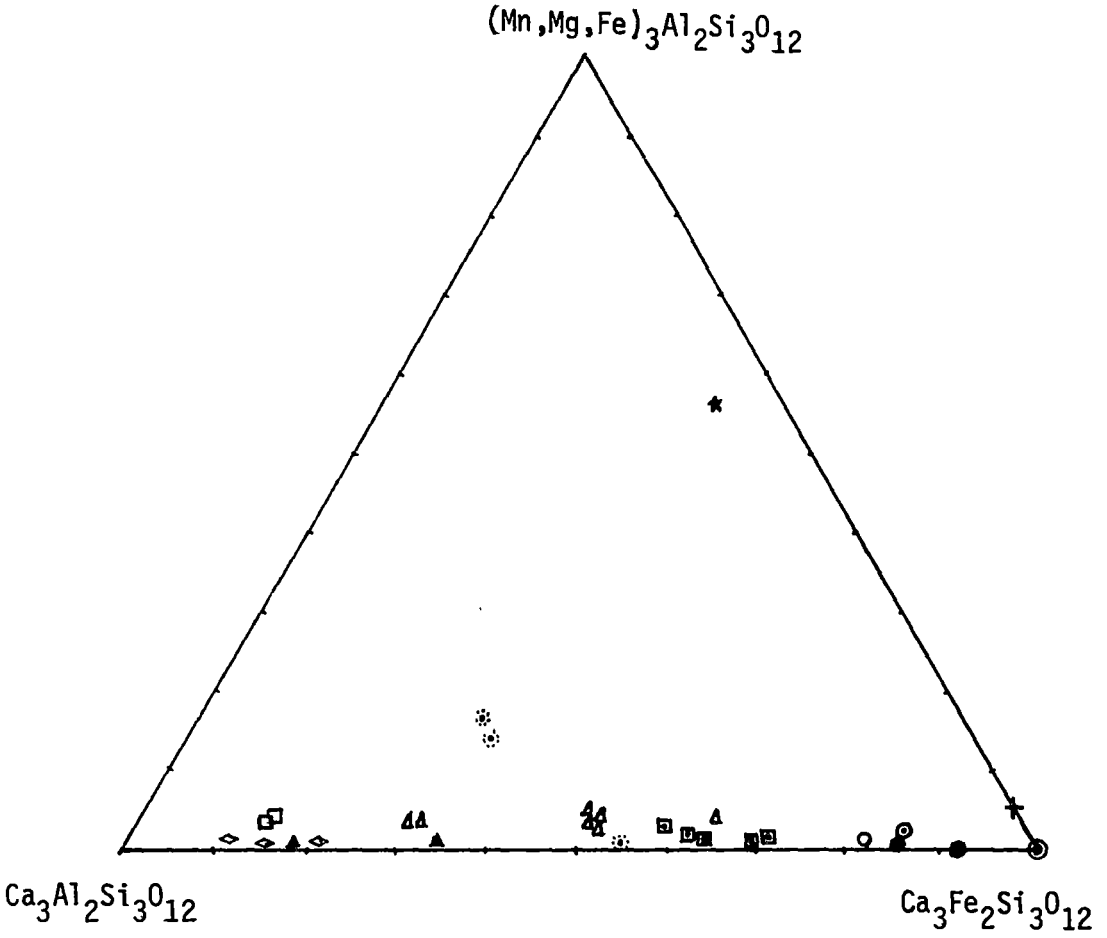

Location of Samples

⊙ 103118 = a residual block of the wollastonite skarn at -1st level
+ 103134 = a residual particle of garnet in the QM zone at -3 level
⊙ 103136 = wollastonite-garnet vein in the Pungchon limestone at -6 level

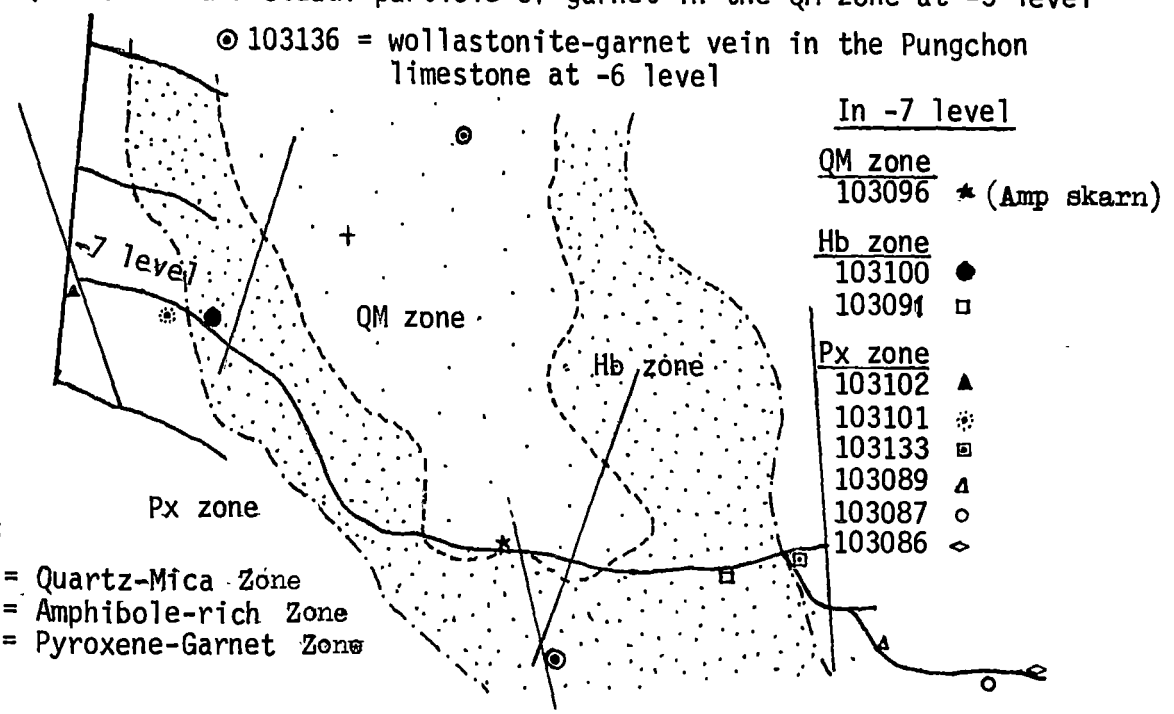

Fig. 6.2. Variation in chemical compositions of zoned garnets.

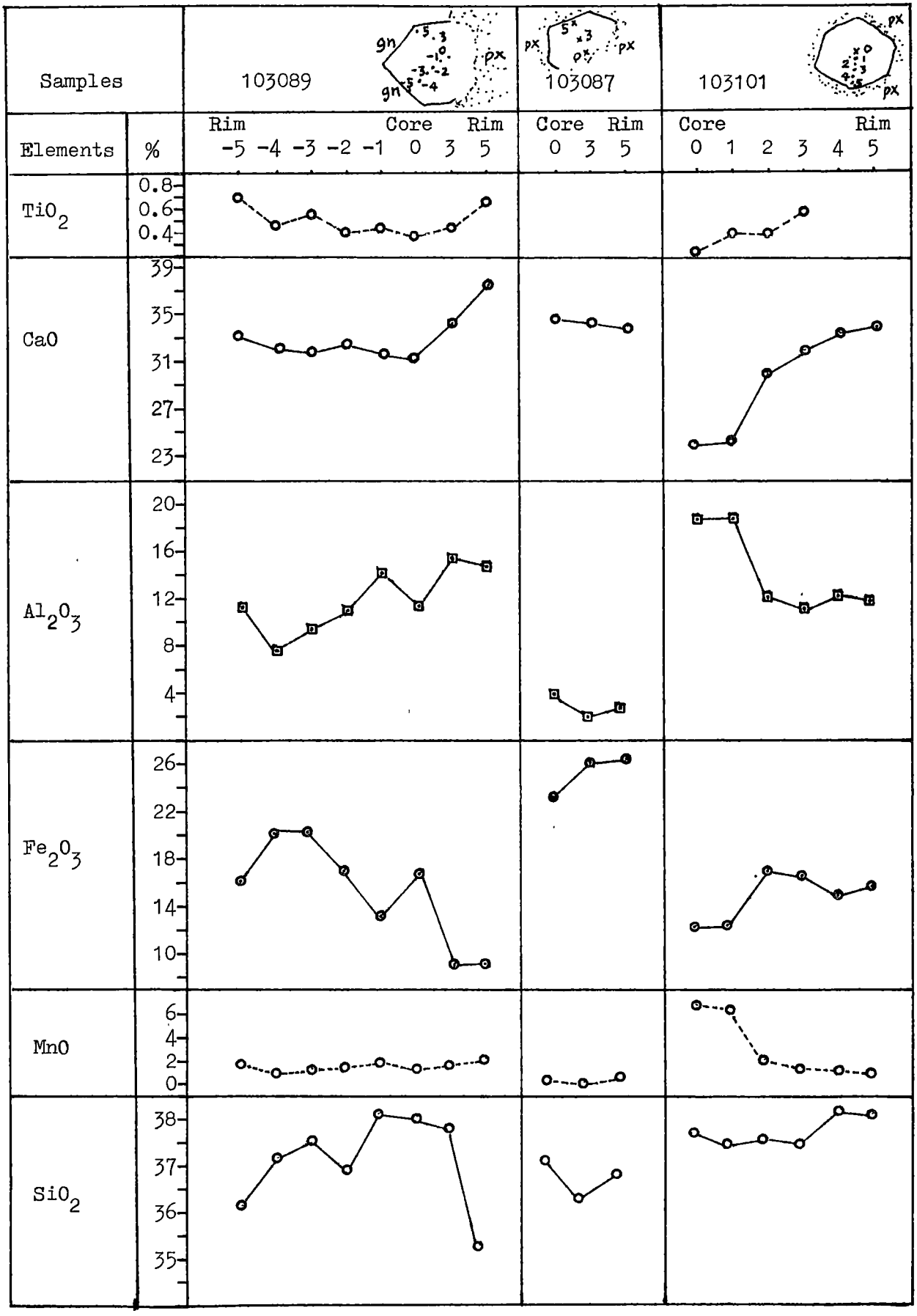

Fig. 6.3. Variation in chemical compositions of the zoned garnets plotted in terms of mole % of andradite, grossularite, and spessartine + pyrope

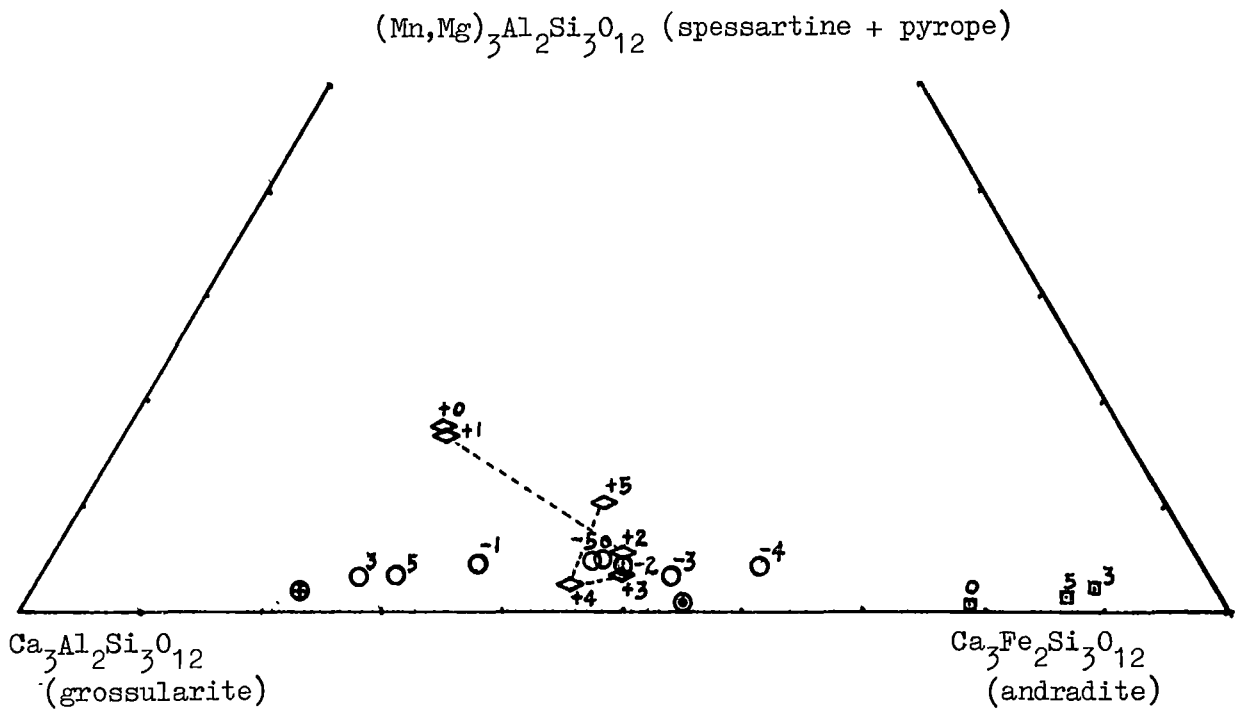

	Sample No.	rim			core			rim	
○	103089	-5,	-4,	-3, -2, -1,	0,		3,		5,
◇	103101				+0,	+1, +2,	+3,	+4,	+5
□	103087				0		3		5
⊕	103101(anisotropic garnet)								
◉	103101(isotropic garnet)								

6.2. Pyroxene

Chemical compositions of representative pyroxenes from the skarns are given in Table 6.3. Most pyroxenes are members of the hedenbergite-johannsenite-diopside solid solution series and chemical compositions range from 95 to 3 mole % of hedenbergite(hd), 13 to 0 mole % of johannsenite, and 97 to 3 mole % of diopside(dp). Fig. 6.4 shows that early formed pyroxenes from wollastonite skarn and the H1 orebody are diopsidic while later pyroxenes replacing the wollastonite skarn(103118) and most of pyroxenes from the M1 pyroxene-garnet skarn tend to be hedenbergitic.

Pyroxene separates were analysed by XRF(Kim, 1976) and results are shown in Table 6.4. These results show a higher content of Al_2O_3 and lower content of CaO compared to any of the microprobe analyses of this study; TiO_2 and K_2O present in Kim's(1976) results were not detected by microprobe analysis. The presence of potassium is probably due to impurites such as fine veinlets of apophyllite or K-feldspar inclusions, which present a difficulty in the interpretation of chemical analysis of separates from the Sangdong skarns.

In some places it is possible to distinguish texturally the early and the late pyroxene in the pyroxene-garnet skarn as illustrated in Figs. 6.5, 6.6 and 6.7(a). Table 6.5 presents the results of microprobe analyses on the two different pyroxenes(early and late), and the early pyroxene may be distinguished by its lack of aluminium. Such pyroxene normally coexists with garnet(Al-rich). The late pyroxene, which generally makes up a monomineral assemblage and is darker green in colour, contains appreciable Al contents apparently through replacement of garnet.

In specimen, 103104, late pyroxene replaces early pyroxene and is associated with quartz(Fig. 6.7a,b). These two pyroxenes show different compositional zonation within the crystals, as shown in Figs. 6.8a & 6.8b. The late pyroxene in the quartz vein has a more hedenbergitic composition

Table 6.3. Chemical compositions of representative pyroxenes occurring at the Sangdong ore deposit.

	103064	*103112	103118	103104	*103087	*103091	*103087	*103090	*103094
grain no.	1d	b5	g2	c2	a4	a3	a3	c1	c5
SiO_2	48.02	48.48	48.31	48.49	48.72	48.82	48.60	48.69	48.71
Al_2O_3	0.36	n.d	n.d	n.d	n.d	0.53	1.00	0.49	0.93
Cr_2O_3	0.32	n.d	n.d	n.d	0.22	n.d	n.d	n.d	n.d
FeO	27.58	26.91	26.71	25.46	24.96	23.94	23.11	23.63	24.42
MnO	1.48	1.92	1.47	3.09	2.00	1.89	3.03	2.23	1.55
MgO	n.d	0.42	0.68	0.56	1.62	2.19	1.53	2.22	3.00
CaO	22.23	22.28	22.31	22.40	22.48	22.63	22.72	22.72	21.41
Total	99.99	100.01	99.48	100.0	100.0	100.0	99.99	99.98	100.02
				Numbers of ions on the basis of 6 oxygens					
Si	1.984	1.998	1.990	1.997	1.992	1.982	1.977	1.979	1.972
Al	0.018	0.000	0.000	0.000	0.000	0.025	0.048	0.023	0.044
Cr	0.010	0.000	0.000	0.000	0.007	0.000	0.000	0.000	0.000
Fe	0.953	0.928	0.920	0.877	0.853	0.813	0.786	0.803	0.827
Mn	0.052	0.067	0.052	0.108	0.069	0.064	0.105	0.076	0.053
Mg	0.000	0.026	0.041	0.041	0.034	0.099	0.092	0.134	0.181
Ca	0.985	0.984	0.985	0.988	0.984	0.984	0.990	0.989	0.929
Total	4.002	4.003	3.988	4.004	4.004	4.000	3.998	4.004	4.006
X_{hd}	0.948	0.909	0.907	0.861	0.835	0.806	0.800	0.793	0.779
X_{jh}	0.052	0.104	0.051	0.106	0.068	0.063	0.107	0.075	0.050
X_{dp}	0	0.025	0.041	0.033	0.097	0.013	0.094	0.132	0.171

* = Samples from the 7th level, pyroxene-garnet skarn.

103064 = Pyroxene coeval with amphibole and magnetite (the 6th level).

103118 = Pyroxene coexisting with garnet in the garnet skarn(1st level)

103104 = Pyroxene in the pyroxene-garnet skarn(Sangdong level)

Table 6.3 continued

	*103096	*103102	*103095	*103089	*103087	*103096	*103102	103138	103169	103169
grain no.	f1	d3	c1	h1	a4	b1	d4	2	1a	2a
SiO_2	48.80	49.61	48.80	49.22	49.80	49.84	50.63	53.55	53.84	54.78
Al_2O_3	1.06	0.55	0.66	0.36	0.59	0.83	0.49	n.d	n.d	n.d
Cr_2O_3	n.d	n.d	n.d	n.d	n.d	n.d	n.d	0.28	0.26	0.23
FeO	23.58	22.05	23.56	21.81	18.83	18.86	18.01	6.68	4.75	0.94
MnO	1.56	0.72	1.94	3.89	2.89	1.68	0.61	1.29	1.25	n.d
MgO	3.17	3.86	3.48	2.66	4.71	6.12	6.60	13.71	15.11	18.62
CaO	23.58	23.20	21.56	22.10	23.18	22.65	23.67	24.54	24.78	25.31
Total	101.7	99.99	100.0	100.0	100.0	99.98	100.0	100.05	99.99	99.88
Numbers of ions on the basis of 6 oxygens										
Si	1.969	1.986	1.972	1.992	1.982	1.970	1.986	1.997	1.993	1.986
Al	0.050	0.055	0.033	0.017	0.027	0.038	0.022	0.000	0.000	0.000
Cr	0.000	0.000	0.000	0.000	0.000	0.000	0.000	0.208	0.147	0.029
Fe	0.796	0.738	0.796	0.738	0.627	0.623	0.591	0.008	0.008	0.007
Mn	0.053	0.024	0.066	0.132	0.097	0.056	0.020	0.041	0.039	0.000
Mg	0.190	0.230	0.209	0.161	0.279	0.360	0.386	0.762	0.834	1.006
Ca	0.944	0.995	0.934	0.958	0.987	0.959	0.995	0.981	0.983	0.983
Total	4.002	3.998	4.010	3.998	3.999	4.006	4.000	3.997	4.004	4.011
X_{hd}	0.766	0.744	0.743	0.716	0.625	0.600	0.593	0.206	0.144	0.028
X_{jh}	0.051	0.024	0.062	0.128	0.097	0.054	0.020	0.041	0.038	0.000
X_{dp}	0.183	0.232	0.195	0.129	0.278	0.346	0.387	0.754	0.818	0.972

* = Pyroxene in the pyroxene-garnet skarn(M1) from the 7th level

103138 = Pyroxene in the H1 ore body at the 6th level

103169 = Pyroxene in the pyroxene-garnet skarn(M1) from the 10th level

Fig. 6.4. Pyroxene compositions plotted in terms of mole % of hedenbergite, johannsenite and diopside.

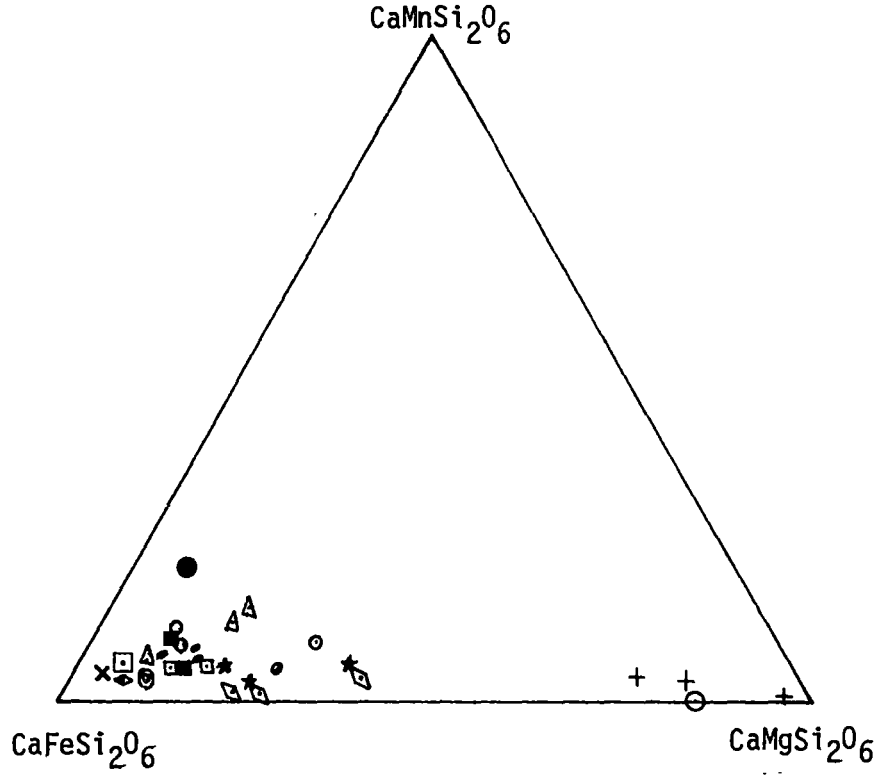

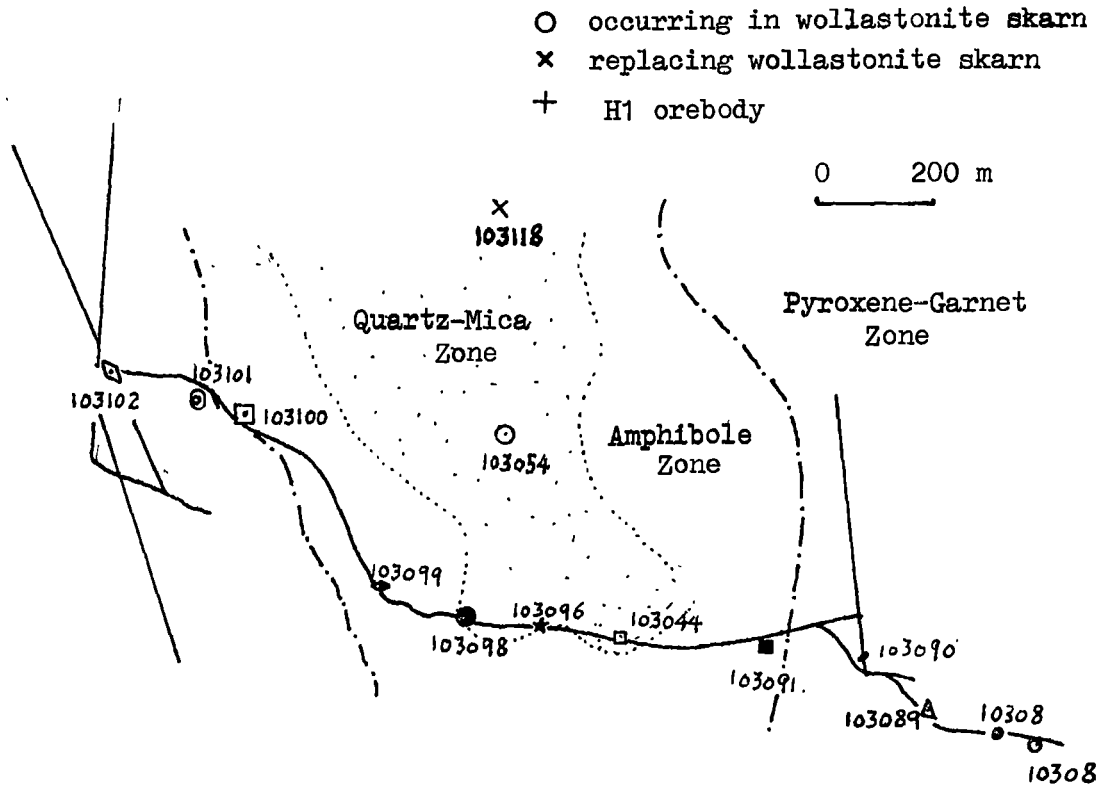

Table 6.4. Chemical composition of pyroxene(Px) and garnet(Gn) separated from the M1 orebody, pyroxene-garnet skarn (from Kim, 1976).

	Pyroxene			Garnet	
	6034	1015	1466	10036	14481
SiO_2	48.12	49.01	50.23	39.61	38.96
TiO_2	0.02	0.32	0.18	n.d	0.35
Al_2O_3	3.33	2.87	3.69	12.89	14.26
FeO	24.18	23.06	18.94	16.51	11.48
MnO	1.33	2.24	2.05	0.75	0.64
MgO	1.10	3.46	3.86	0.36	0.76
CaO	18.24	16.78	20.30	29.18	30.87
K_2O	0.08	0.06	0.03	n.d	n.d
Na_2O	0.01	0.03	0.14	n.d	n.d
P_2O_5	0.16	0.14	0.11	0.07	0.06
H_2O	1.75	1.43	1.07	0.59	1.16
Total	98.34	99.40	100.60	99.96	98.54
			Trace Elements(ppm)		
W	208	248	105	56	62
Bi	101	30	0	49	30
Mo	0	16	0	0	0
Cu	57	78	81	55	38
Zn	0	69	90	46	139
Sn	28	24	24	0	90
Sr	0	0	0	19	21
Rb	0	0	0	0	0
Ni	14	24	23	11	25

Table 6.5. Comparison of chemical composition between early and late formed pyroxenes.

	Late Pyroxene			Early Pyroxene			Average	
	103118	103104	103083	103118	103104	103083		
	b	e1	px4	a	a2	c1	late	early
SiO_2	47.65	49.20	49.55	48.56	48.90	49.29	48.80	48.92
Al_2O_3	0.63	0.22	0.23	n.d	n.d	n.d	0.36	n.d
FeO	27.00	25.10	20.62	26.62	24.84	21.91	24.24	24.46
Cr_2O_3	n.d	n.d	n.d	n.d	n.d	n.d	n.d	n.d
MnO	1.97	2.50	3.18	1.51	2.43	4.22	2.55	2.72
MgO	1.26	0.71	3.56	0.74	1.32	1.67	1.84	1.24
CaO	21.17	22.27	22.87	22.57	22.52	22.90	22.10	22.66
Na_2O	0.32	n.d	n.d	n.d	n.d	n.d	0.11	n.d
* Total	100.00	100.00	100.01	100.01	99.99	99.99	100.0	100.0
	Numbers of ions on the basis of 6 oxygens							
Si	1.964	2.011	1.992	1.996	2.000	2.005		
Al	0.031	0.010	0.011	0.000	0.000	0.000		
Fe	0.931	0.858	0.693	0.915	0.850	0.745		
Mn	0.069	0.087	0.108	0.053	0.084	0.146		
Mg	0.078	0.043	0.213	0.046	0.080	0.101		
Ca	0.935	0.975	0.985	0.994	0.987	0.998		
Na	0.026	0.000	0.000	0.000	0.000	0.000		
Total	4.034	3.984	4.002	4.004	4.001	3.995		
X_{hd}	0.864	0.868	0.683	0.902	0.838	0.751		
X_{jh}	0.064	0.088	0.107	0.052	0.083	0.147		
X_{dp}	0.072	0.044	0.210	0.045	0.079	0.102		

Fig. 6.5. A polished thin section showing replacement of early formed garnet-pyroxene(A) by late formed pyroxene(B).
103118, -1st level. ═══ represent 3 mm.

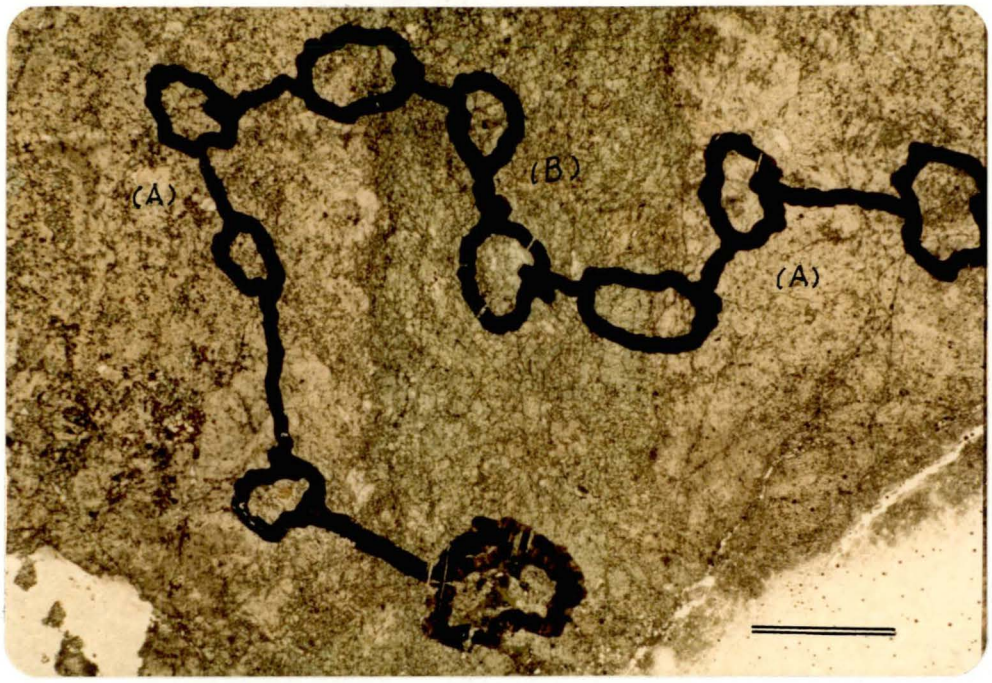

Fig. 6.6. A polished thin section showing replacement of the garnet-pyroxene skarn by late pyroxene(dark green band) along with an amphibole veinlet(Amp).
103112, -7th level, ═══ represent 3 mm.

Fig. 6.7(a). A typical specimen showing the formation of late pyroxene(dark green) by replacing the pyroxene-garnet skarn along the rim of a quartz vein. Due to its dark green colour it is hardly distinguishable from amphibole without microscopic observations.
103104, Sangdong level, X 2.

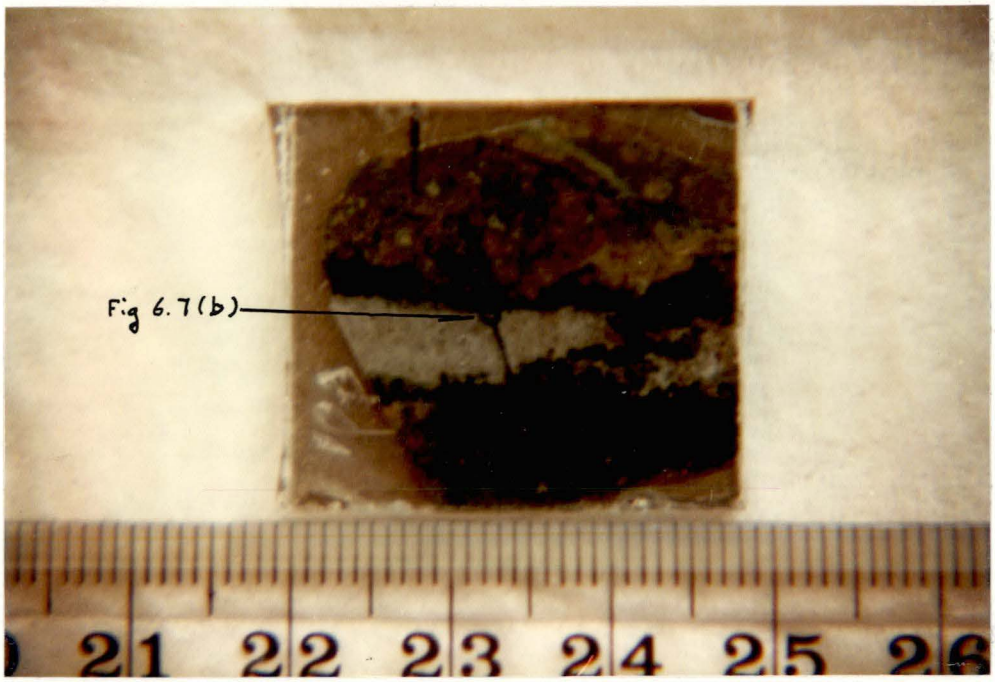

Fig. 6.7(b). Photomicrograph of late pyroxene(hedenbergite) in quartz associated with pyrite, taken from the same specimen as above(as marked on Fig. 6.7a) 103104, Sangdong level. represent 0.1 mm.

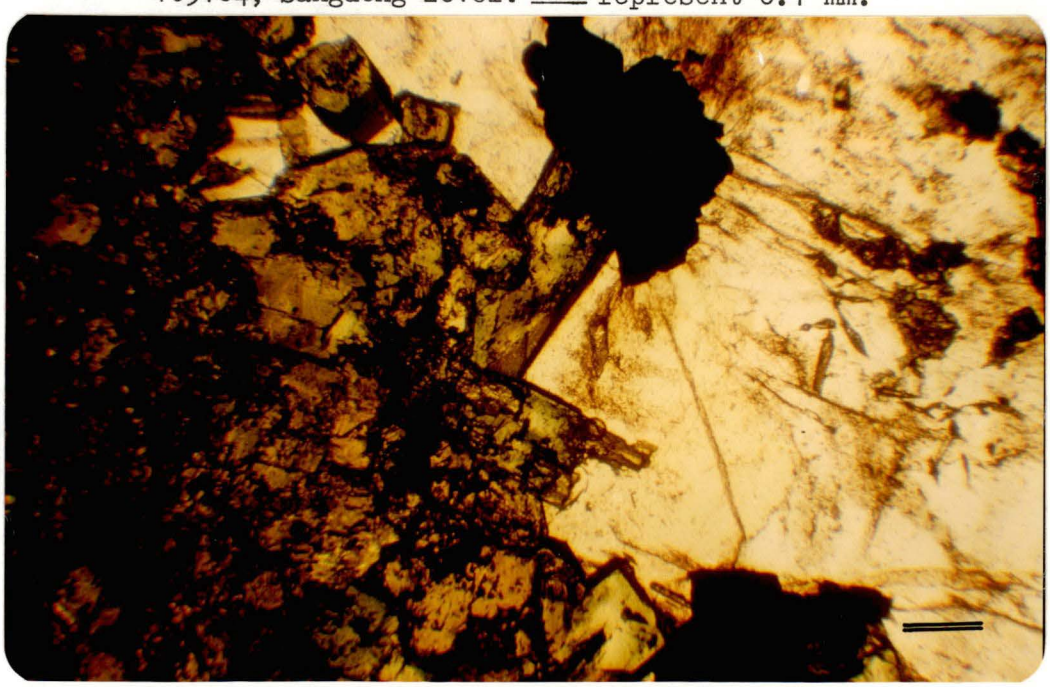

(i.e. lower Mg/Mg+Fe) at the edge than in the interior of the grain, whilst the late pyroxene in the skarn shows a more hedenbergitic composition at the core than the rim of the grains. These compositional variations may represent incomplete examples of a compositional evolutionary trend of equilibration with a fluid of changing Mg/Fe ratio.

6.3. Compositional Relationship Between Garnet and Pyroxene

Zharikov(1970) has defined the ratio of hedenbergite in pyroxene to andradite in garnet as follows:

$$K' = X_{hd}/1 - X_{hd} \Big/ X_{ad}/1 - X_{ad}$$

where X_{hd} is the molefraction of hedenbergite and X_{ad} is the mo fraction of andradite. He showed that W-Mo skarn deposits have high values of K' and Cu-Pb-Zn-Fe skarns have low values. The ferruginous correlation ratio of Burton(1978) is equal to the K' value of Zharikov(1970). Einaudi(1977) and Burton(1978) demonstrated that W-Mo skarns have higher K' values than 1.0 and relate this to oxidation state.

K' values were calculated, using average analyses of grains of andradite and hedenbergite, assuming total Fe as Fe^{+3} in the garnet and Fe^{+2} in the pyroxene. In general, the values are not constant(Fig. 6.9 and Table 6.6), but are mainly higher than 1.0, as anticipitated. A series of contiguous pyroxene-garnet pairs was studied, using average whole-grain analyses(Table 6.7, Fig. 6.10). These show good consistency over a wide area of the deposit and indicate an approach to large-scale equilibrium during growth of the main garnet-pyroxene skarn.

In another study, rims of andradites adjacent to pyroxenes were analysed(Table 6.8, Fig. 6.11). One sample was from the amphibole-rich zone (103100), one from pyroxene skarn(103104), and one from garnet skarn(103118). In this study the K' values showed some variation, with the pair in the amphibole zone having $K' < 1$. This grain boundary readjustment may have

Fig. 6.8a. **Compositional zonation within** the pyroxenes, and differences **between the early** and late pyroxenes in specimen 103104.

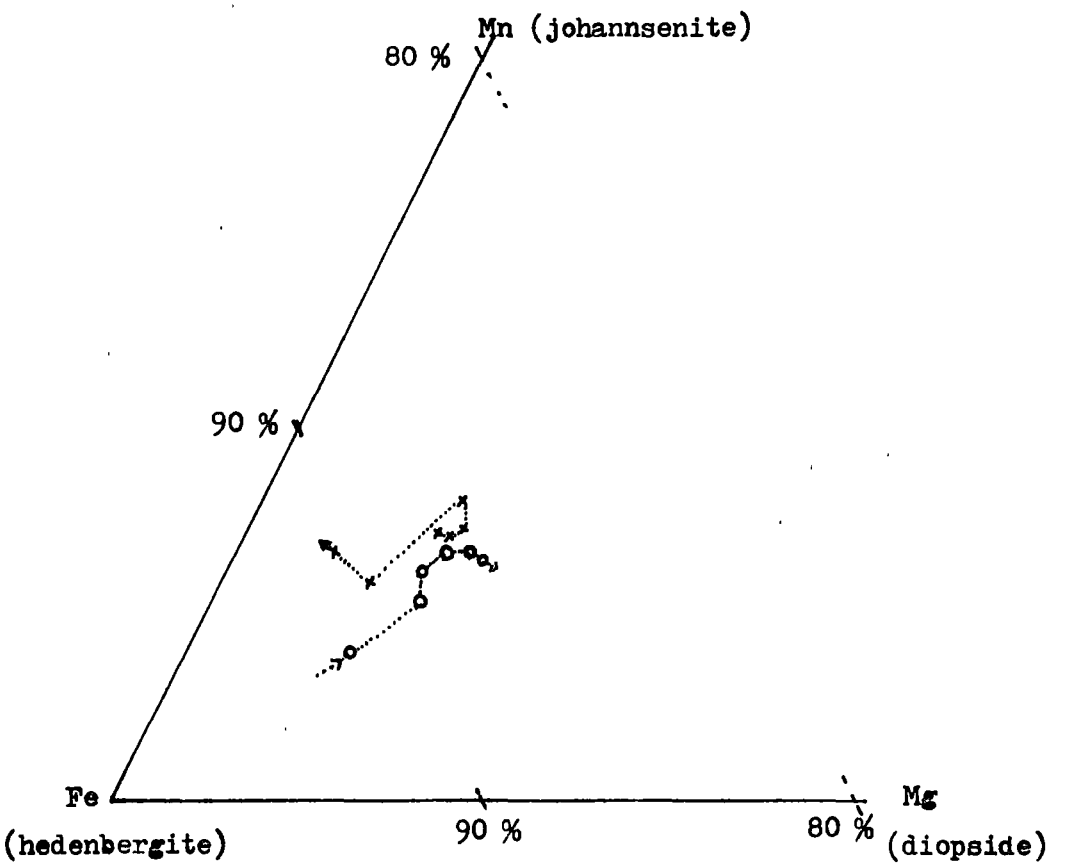

Fig. 6.8b. **Comparative variation in the ratio of Mg/Mg + Fe between** the early pyroxene in the skarn and the late pyroxene **in the quartz vein.**

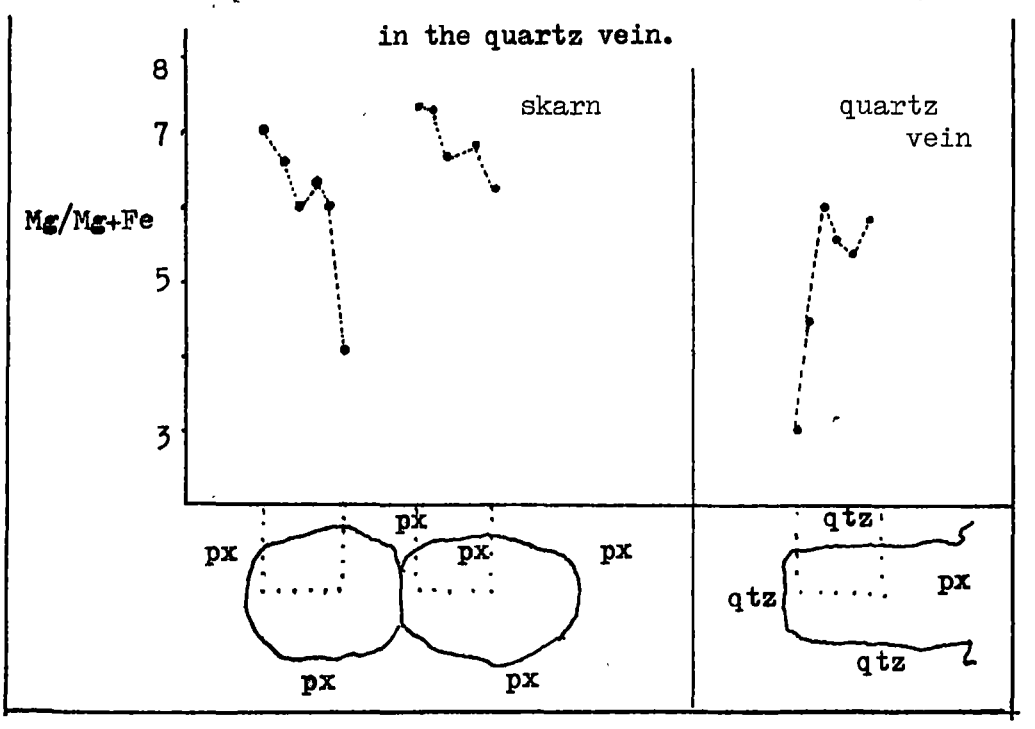

Table 6.6. Comparison of average ratios of X_{hd}/X_{ad} between garnet and pyroxene from the 7th level at the Sangdong mine.

Sample No(Zone)		Average values of grains					Mean	K'
103087(Px)	X_{hd}	0.625	0.796	0.799			0.74	0.46
	X_{ad}	0.801	0.902	0.877			0.86	
103089(Px)	X_{hd}	0.836	0.716	0.832	0.683	0.854	0.784	3.59
	Xad	0.483	0.622	0.508	0.510	0.389	0.502	
103091(Hb)	X_{hd}	0.806					0.806	1.35
	X_{ad}	0.755					0.755	
103096(QM)	X_{hd}	0.723	0.599	0.766			0.723	4.66
	X_{ad}	0.361					0.361	
103102(Px)	X_{hd}	0.636	0.595				0.410	1.97
	X_{ad}	0.171	0.346				0.259	
103104(Px)	X_{hd}	0.898	0.903	0.861			0.887	1.28
	X_{ad}	0.885	0.835				0.860	
103132(Px)	X_{hd}	0.865	0.862				0.864	6.4
	X_{ad}	0.516	0.477				0.497	
103133(Px)	X_{hd}	0.908	0.846	0.721			0.825	4.49
	X_{ad}	0.317	0.630	0.592			0.513	

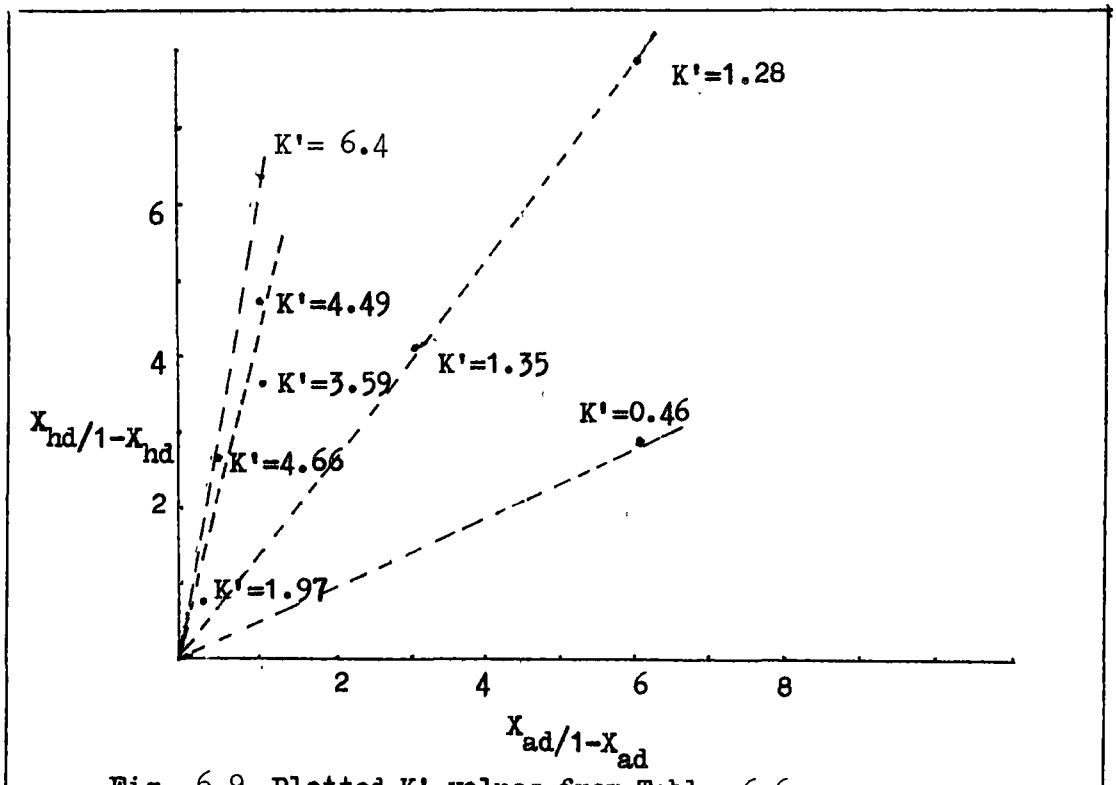

Fig. 6.9 Plotted K' values from Table 6.6.

Table 6.7. Ratios of $X_{hd}/1-X_{hd}/X_{ad}/1-X_{ad}$ in garnet and pyroxene pairs.

	Garnet			Pyroxene		Ratios		
Sample	Zone	Grains No.	X_{ad}	Grains No.	X_{hd}	$X_{hd}/1-X_{hd}$	$X_{ad}/1-X_{ad}$	K'
103089	Px	G-1a	0.483	G-4	0.854	5.85	0.93	6.3
103096	QM	B-2	0.361	F-4	0.766	3.27	0.56	5.8
103102	Px	D-1	0.171	D-4	0.636	1.75	0.21	8.3
103111	Px	A-1	0.477	A-1	0.862	6.25	0.91	6.9
103111'	Px	B-1	0.516	B-2	0.865	6.41	1.06	6.0
103112	Px	D-4	0.630	D-1	0.909	9.99	1.70	5.9

Fig. 6.10. Plotted K' values using data in Table 6.7.

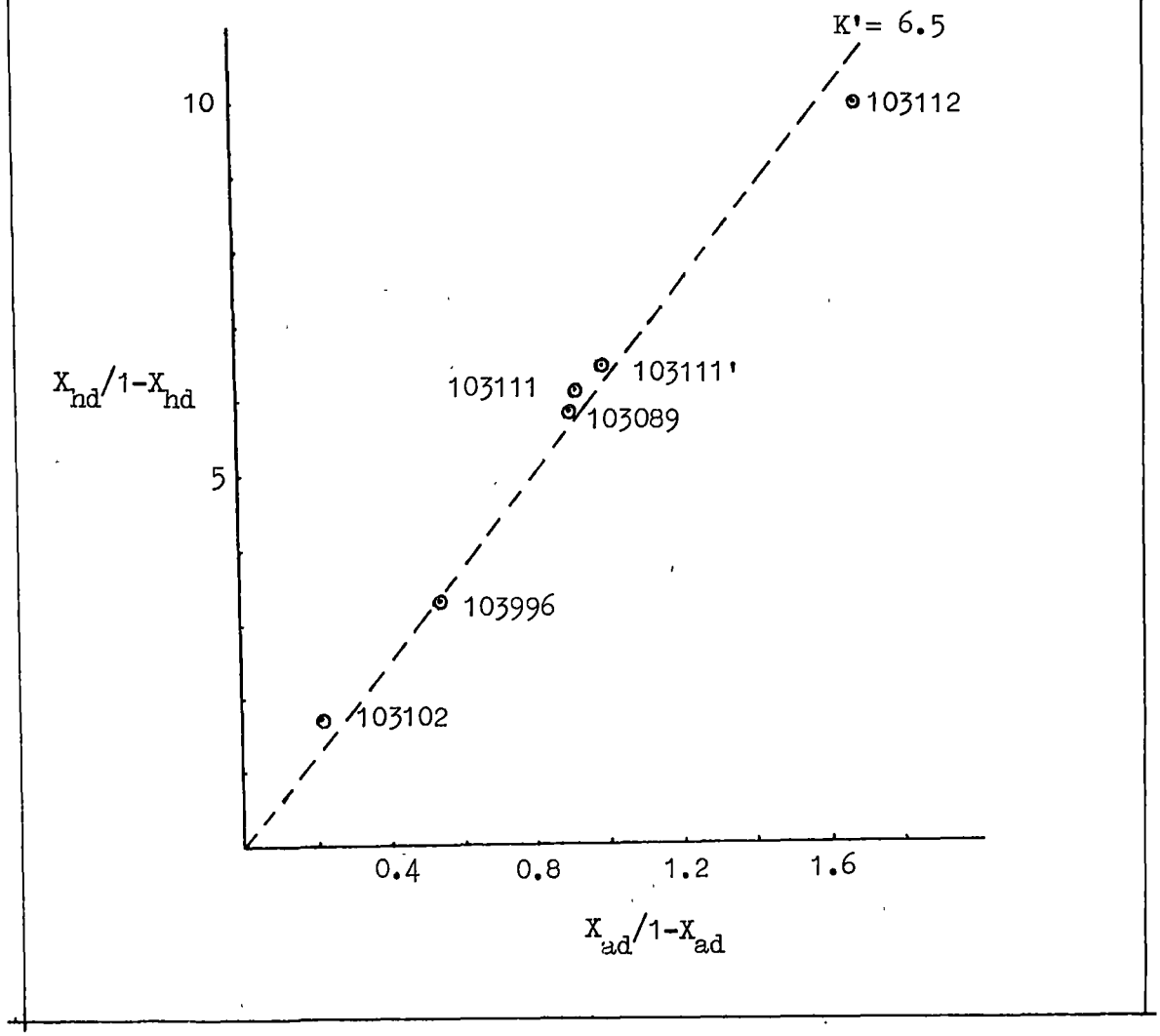

Table 6.8. The ratios of $X_{hd}/1-X_{hd}$ versus $X_{ad}/1-X_{ad}$ of coexisting garnet(rim) and pyroxene pairs.

Sample No. (Zone)	Garnet grains no.	X_{ad}	Pyroxene grains	X_{hd}	Ratios $X_{hd}/1-X_{hd}$	$X_{ad}/1-X_{ad}$	K'
103100 (Amp)	gn-14	0.902	px-9	0.884	7.62	9.2	0.83
	gn-11	0.887	px-8	0.838	5.17	7.85	0.66
	gn-12	0.898	px-7	0.856	5.94	8.80	0.68
103104 (Px)	a	0.793	a'	0.888	7.93	3.83	2.07
	b	0.918	b'	0.880	7.33	11.2	0.65
	c	0.773	c'	0.872	6.81	3.41	2.0
	d	0.769	d'	0.876	7.1	3.35	2.13
103118 (Gn)	c	0.879	i	0.9	9.0	7.26	1.24
	h	0.850	d	0.86	6.14	5.67	1.08
	h'	0.78	g'	0.69	2.23	3.55	0.63

Fig. 6.11. Plotted K' values using data in Table 6.8.

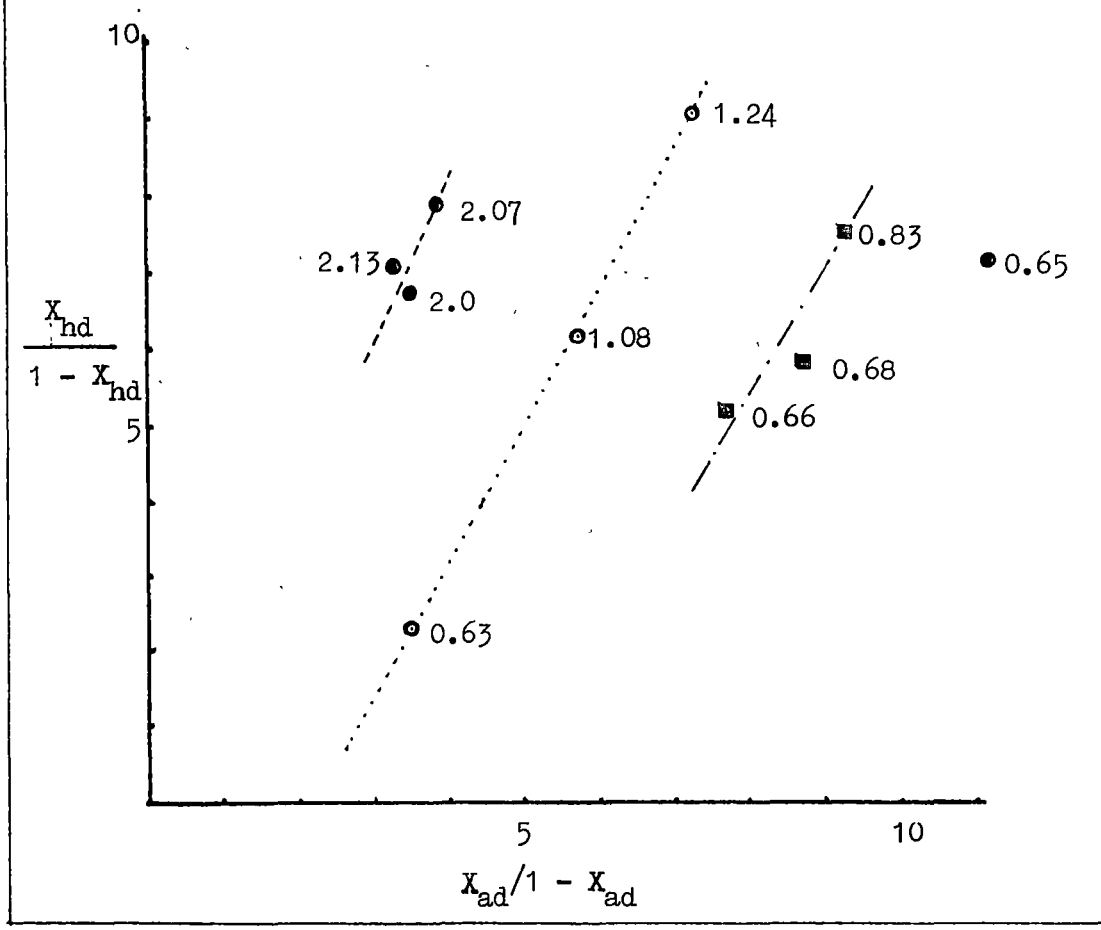

taken place late in the growth of the hydrous skarns, at which time there may have been an increase in f_{O_2} and/or X_{CO_2} of the hydrothermal fluid (see Chapter 12).

6.4. Amphibole

The separation of pure amphibole for wet chemical analyses was attempted with the help of ore dressing engineers at the mine, but it was found that the amphibole could not be freed of contamination by tiny inclusions of scheelite. Thus usually high values of tungsten in the separated amphiboles are due to scheelite contamination. This also applies to XRF analyses of amphibole separated from the cherty rock by Kim(1976, Table 6.10).
An average Fe_2O_3/FeO was obtained from amphibole separates analysed by the Geological Survey in Korea, and the ratio was confirmed by FeO analyses of amphiboles by colorimetry(see methods in Appendix 7.1).

Microprobe analyses of amphiboles are presented in Table 6.9. Amphiboles of the Sangdong deposit have previously been described as hornblende, tremolite and actinolite(Gabert and Vinken, 1962; So, 1967; Lee and Kim, 1969; Moon, 1974; Kim, 1976). On the basis of microprobe analyses the amphiboles are more correctly classified in terms of three mineral end-members of the calcic amphibole group. The standard amphibole formula is taken to contain 8 tetrahedral sites and to have the general form(Leake, 1978):

$$A_{0-1}\ B_2\ C_5\ T_8^{vi}\ O_{22}^{iv}\ (OH,\ F,\ Cl)_2$$

where A = Na, K, B = Ca, Na, C = Mg, Fe, Al, T = Si, Al.
The amphiboles occurring in the quartz-mica zone close to the amphibole-rich zone are ferroedenitic hornblende(Fig. 6.12).

The amphiboles forming the main component of the amphibole-rich zone are higher in total iron, Al_2O_3 and K_2O and lower in SiO_2 and MgO than

those in other zones. This amphibole is a hastingsitic hornblende.

Amphiboles occurring as veinlets in the cherty rock and the slate show lower contents of Al_2O_3, Fe_2O_3(total Fe), Na_2O and K_2O, and higher contents of SiO_2 and MgO than those in the amphibole-rich zone. The amphibole in the cherty rock and the slate is a magnesio-hornblende(Fig. 6.12).

Amphibole occurring in the pyroxene-garnet zone shows a wide range of SiO_2 contents varying from 41 to 48 % and tend to be depleted in K_2O as it occurs further away from the amphibole-rich zone(Table 6.9 & Appendix 6.6). Amphiboles replacing garnet are ferro-actinolite or ferro-actinolitic hornblende, while amphiboles replacing pyroxene are ferro-actinolitic hornblende or ferro-hornblende(Fig. 6.12).

This variation in amphibole composition may reflect variation in earlier pyroxene-garnet skarn composition as well as changes in the composition of the amphibole-forming fluids.

Table 6.11 illustrates the variation in the chemical composition within a single amphibole crystal. Some of the amphiboles are altered at the rim to chlorite. Variation in the chemical composition from the core to the rim of amphiboles are different from crystal to crystal and from place to place. However, in one specimen(103140), there is a systematic variation in several grains as shown by the ratio of $K_2O + Al_2O_3/SiO_2 + FeO + MnO$, which decreases from the core to the margin. Al_2O_3 content decreases and K_2O tend to increase systematically from the core to the rim within single crystals, whilst FeO, SiO_2 and MnO contents show irregular variation.

Table 6. 9. Representative chemical compositions of amphiboles analysed by electron microprobe(ratio of Fe_2O_3/FeO based on colorimetric analyses).

(Zone)	(QM-Hb) 103093	(Hb) 103094	(Hb) 103095	(Px-Hb) 103096	(Cherty) 103115	(Slate) 103115
SiO_2	41.70	39.73	39.85	41.08	46.88	44.9
TiO_2	0.11	0.12	0.11	0.39	0.45	0.18
Al_2O_3	9.21	9.82	9.53	8.77	6.05	8.30
Fe_2O_3	9.31	9.97	9.96	9.77	7.60	7.68
FeO	18.90	20.28	20.21	19.84	15.44	15.59
Cr_2O_3	0.18	0.20	0.18	0.16	0.16	0.15
MnO	1.05	1.07	0.93	0.98	0.98	0.44
MgO	3.76	2.33	2.54	2.91	7.39	7.35
CaO	10.80	11.03	11.08	10.88	11.06	11.39
Na_2O	1.33	1.36	1.37	1.34	0.52	0.98
K_2O	0.97	1.31	1.53	1.08	0.50	0.74
Total	97.32	97.22	97.29	97.2	97.03	97.7
		Numbers of ions on the basis of 23 (O)				
Si	6.742	6.363	6.399	6.520	7.124	6.812
Al^{iv}	1.177	1.637	1.601	1.480	0.876	1.188
Al^{vi}	-	0.219	0.205	0.163	0.209	0.298
Cr	0.023	0.025	0.023	0.021	0.020	0.018
Ti	0.014	0.015	0.014	0.047	0.051	0.021
Fe^{+3}	1.133	1.201	1.152	1.167	0.869	0.877
Mg	0.906	0.556	0.608	0.689	1.674	1.662
Fe^{+2}	2.556	2.717	2.717	2.634	1.962	1.978
Mn	0.144	0.145	0.126	0.132	0.126	0.057
Ca	1.871	1.893	1.907	1.850	1.802	1.851
Na	0.129	0.107	0.093	0.150	0.154	0.149
Na	0.707	0.315	0.333	0.056	-	0.139
K	0.200	0.198	0.268	0.220	0.096	0.144
Total	15.602	15.391	15.446	15.129	14.963	15.194
Mg/(Mg+Fe)	0.25	0.14	0.16	0.18	0.59	0.58

Table 6.10. Chemical compositions by XRF of amphiboles separated from the M1 ore body(from Kim, 1976).

	6033	1010	1025	Mean
SiO_2	46.51	49.84	46.08	47.48
TiO_2	0.04	0.20	0.15	0.13
Al_2O_3	8.28	12.09	8.79	9.72
Fe_2O_3	16.56	19.86	17.68	18.03
MnO	1.41	0.69	0.18	0.76
MgO	10.26	2.48	9.63	7.46
CaO	11.43	7.95	12.39	10.59
K_2O	1.06	0.78	0.89	0.91
Na_2O	1.48	2.17	2.06	1.90
P_2O_5	-	-	-	-
LOI	1.58	2.34	1.97	1.96
Total	98.61	99.40	97.85	98.94
Trace elements(ppm)				
W	408	4756	671	1945
Bi	17	18	19	18
Mo	-	29	24	18
Cu	63	66	76	68
Zn	88	130	118	112
Sn	41	58	41	47
Pb	-	33	-	11
Sr	18	38	40	32
Rb	-	20	-	7
Ni	-	38	72	37

* Average F content = 0.28 %(from Mine lab. report, 1982)

Average ratio of Fe_2O_3/FeO = 0.48(Geological Survey Analyses)

Table 6.11. Chemical zonation within single amphibole crystals, specimen 103112.

	(A)		(B)		(C)		
	2d interior	2h margin	1b interior	2a margin	g5 interior	g6	g7 margin
SiO_2	42.30	42.16	42.43	44.84	37.67	39.75	47.79
TiO_2	0.15	0.12	0.10	0.15	n.d	n.d	n.d
Al_2O_3	8.26	6.00	8.57	6.32	11.05	9.57	1.45
FeO	30.72	32.51	29.75	29.92	33.66	33.48	34.32
Cr_2O_3	0.18	0.11	0.19	0.21	n.d	n.d	n.d
MnO	1.12	0.88	0.93	1.03	0.84	0.98	1.22
MgO	2.93	2.41	2.92	3.17	n.d	0.22	n.d
CaO	10.79	0.25	10.86	10.81	11.28	11.09	11.28
Na_2O	0.83	n.d	0.64	0.58	0.78	0.88	0.91
K_2O	1.00	1.81	0.78	0.53	1.73	1.03	n.d
Total	98.27	86.25	97.18	97.54	97.0	97.0	97.0
$\frac{K_2O+Al_2O_3}{SiO_2+FeO+MnO}$	0.12	0.10	0.13	0.09	0.18	0.14	0.02

Fig. 6.12. Amphiboles plotted in the diagram from Leake(1978).

Calcic Amphibole: $(Ca+Na)_B > 1.34$, $Na_B < 0.67$

$(Na+K)_A < 0.50$, $Ti < 0.50$ | $(Na+K)_A > 0.50$, $Ti < 0.50$, $Fe^{3+} > Al^{vi}$

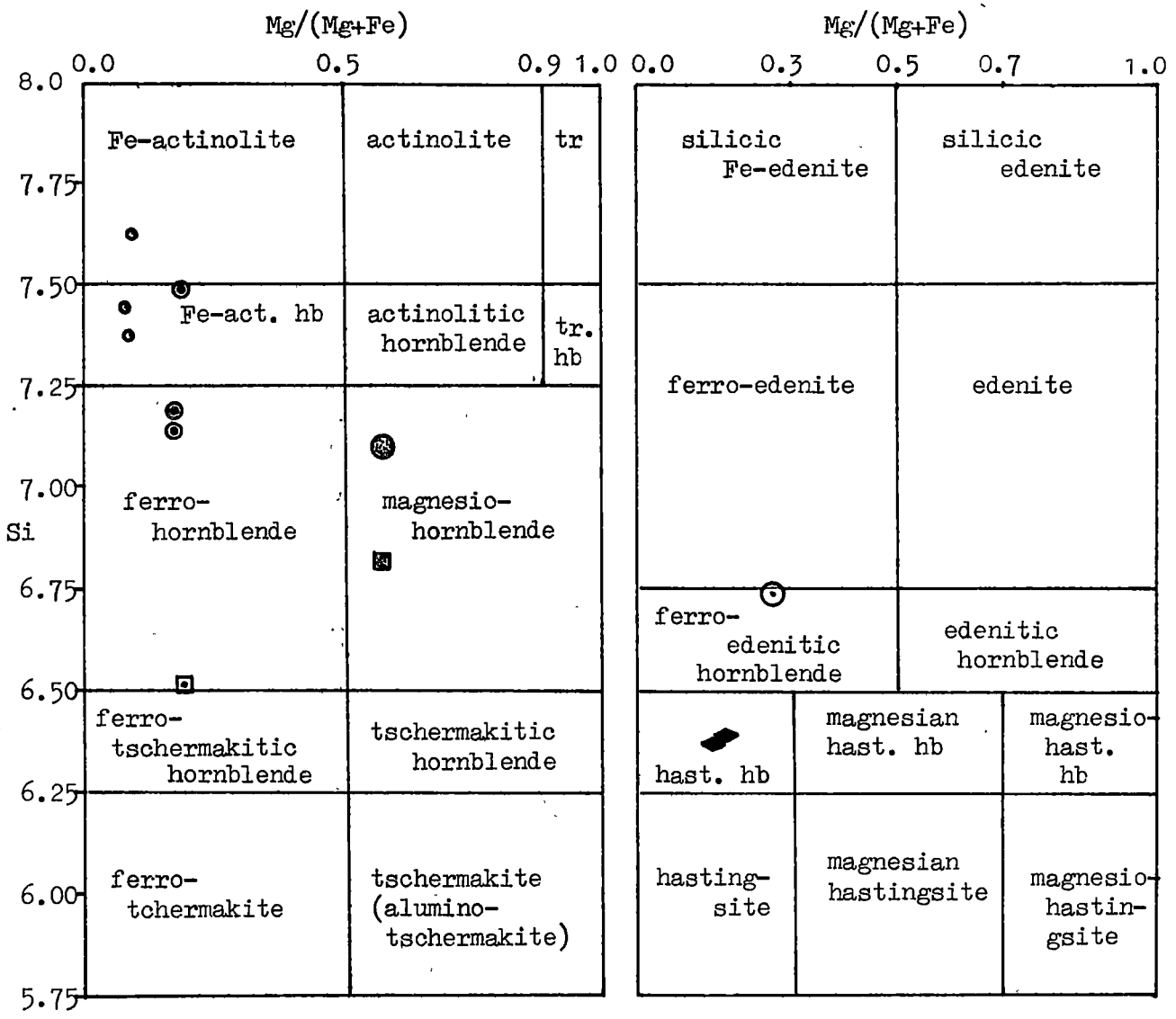

Average chemical composition of amphibole

- ⊙ in the quartz-mica zone
- ◆ in the middle of the amphibole-rich zone
- ⊡ in the pyroxene-garnet zone
- ▪ in slate
- ◉ in the cherty rock
- ◎ Amphibole replacing garnet
- ○ Amphibole replacing pyroxene

Fe = ferro, tr = tremolite, tr. = tremolitic, hast.= hastingsitic
hb = hornblende.

6.5. Biotite

Biotite occurs mainly in the quartz-mica zone of the M1 and F. orebodies and also locally in the amphibole and the pyroxene-garnet zones, forming globular aggregates with internal radial clusters in the former and replacing pyroxene along minor structures in the latter.
Sample locations for this study are shown in Fig. 6.13. Microprobe analyses of biotites are given in Appendices 6.8 and 6.9 and are summarized as mean values in Table 6.12.

Analysis 103120 represents biotite grains taken from a globular shaped occurrence(Fig. 5.24) in the amphibole-rich zone, in which biotite and chlorite occur mainly at the margins of a globule composed of quartz, calcite and scheelite.

Analysis 103119 represents biotite grains from the pyroxene-garnet skarn where it is cut by a vein of biotite-quartz-scheelite. Direct contact between quartz-mica skarn and pyroxene-garnet skarn is rarely observed(e.g. Fig. 4.7).

Appendix 6.9 presents the compositions of biotites occurring within and at the margin of the mica zone. Most biotites show high iron contents and are lepidomelanes(Deer et al., 1972). The biotite in the quartz-mica skarn(103092, 103093, 103097) has higher contents of MgO, MnO and CaO than those in the amphibole and pyroxene-garnet skarns(103120, 103119). The TiO_2 content varies inversely with the total iron content. The content of Al_2O_3 in the biotite tends to increase from the central zone to the outer skarn zone and MnO content shows a reverse trend. The composition of biotite in the pyroxene-garnet skarn(remnant block of the pyroxene-garnet skarn in the quartz-mica zone) is characterized by absence of CaO and a higher content of TiO_2 than in other zones(Fig. 6.14).

Comparison between a biotite replacing an amphibole(103120) and a

biotite replacing pyroxene(103119) shows that MgO and TiO_2 in the latter are higher. This correlates inversely with the higher contents of MgO and TiO_2 in amphiboles than in pyroxenes(early pyroxene).

Analyses for biotite occurring with amphibole(103093) at the marginal part of the quartz-mica zone are only slightly different from biotite occurring with chlorite within the quartz-mica zone(103097, 103092). The latter have similar compositions, even though they occur 250 metres apart (Fig. 6.13). Biotite from the marginal zone shows generally higher content of FeO and lower MgO content than biotite within the quartz-mica skarn.

The biotite of Sangdong exhibits strong pleochroism, but varying colour. Biotites from specimens 103119 & 103097 are brownish while biotites from 103120, 103092 and 103093 are greenish(Appendices 6.8 and 6.9). As Deer et al(1963, 1972) showed the colour of biotites varies with composition(i.e. (TiO_2/MgO) : (Fe as FeO)), the brownish biotites of Sangdong differ from the greenish biotites in having a higher TiO_2 content.

The average ratios of Mg/(Mg + Fe) in coexisting biotite and chlorite are plotted in Fig. 6.15 and the linear correlation between these indicates chemical equilibrium was obtained between the two phases.

Table 6.12. Average chemical compositions of biotites.

	Small-scale quartz-mica skarn		Quartz-mica skarn from the 7th level		
	103120	103119	103092	103093	103097
Numbers of analyses	(5)	(10)	(3)	(13)	(6)
SiO_2	35.11	35.11	36.12	34.89	36.25
TiO_2	0.14	1.46	0.45	0.18	0.65
Al_2O_3	14.94	15.04	13.86	14.81	14.66
FeO	31.38	29.68	28.55	30.67	27.33
MnO	0.34	0.28	0.72	0.57	0.72
MgO	4.68	5.96	7.95	6.02	6.99
CaO	0.26	n.d	0.53	0.70	0.51
Na_2O	0.58	0.42	n.d	n.d	n.d
K_2O	8.46	8.00	7.71	8.13	8.91
Total	95.89	95.95	95.89	95.97	96.02
100 x TiO_2/MgO	2.99	24.50	5.66	2.99	9.3
TiO_2/MgO : FeO	9.53	82.55	19.82	9.75	34.03
Colour	Green	Brown	Green	Green	Brown

Fig. 6.13. Biotite location.

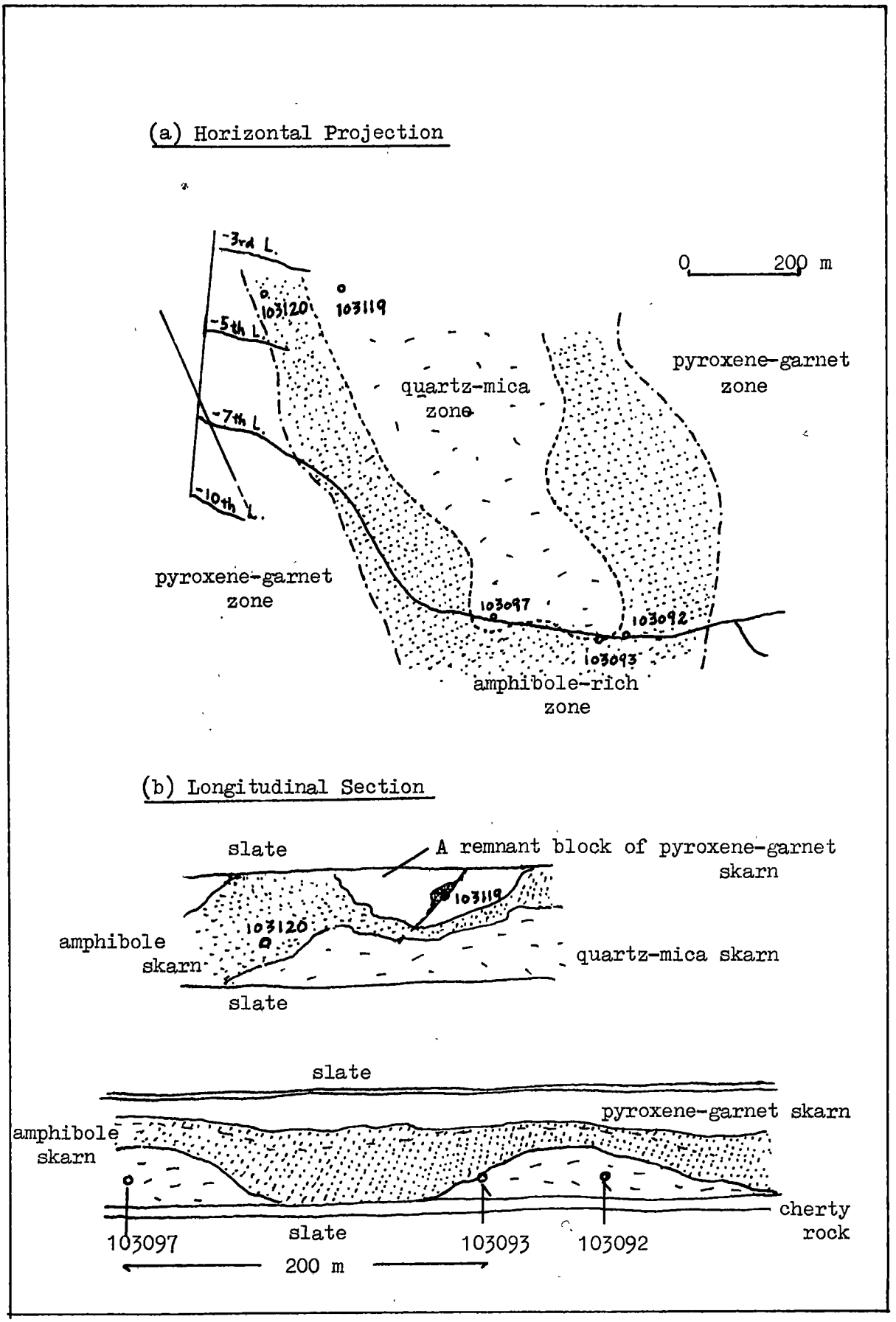

Fig. 6.14. Variation in chemical compositions of biotites occurring in different zones(based on Table 6.12)

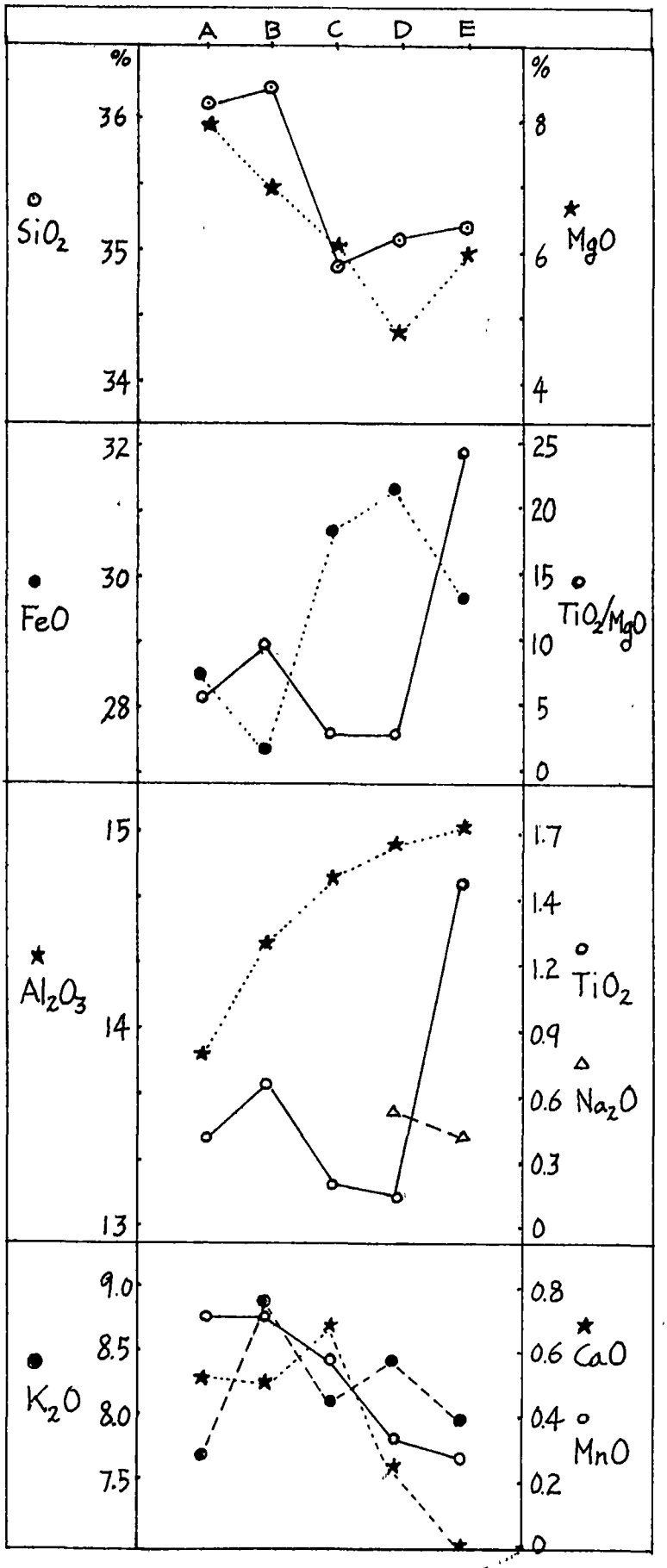

Quartz-Mica Skarn

A = sample 103092
B = 103097
C = 103093

Amphibole Skarn

D = 103120

Pyroxene-Garnet Skarn

E = sample 103119

6.6. Muscovite

Table 6.13 includes representative microprobe analyses of muscovite from the quartz-mica skarn ore; muscovite is generally confined to the central part of this zone and appears to have replaced biotite.

Specimen 103127 was taken from a quartz-mica vein, replacing the pyroxene-garnet skarn at the 15th level. Specimen 103116 and 103117 were taken from the quartz-mica zone at the Sangdong level and the 3rd level respectively.

MgO and K_2O contents in muscovite tend to increase with depth. The Al_2O_3 content in the muscovite from the vein type quartz mica skarn (103127) is lower than that from the main part of the quartz-mica skarn (103116 & 103117). CaO was detected only in the upper level and this muscovite contained no Na_2O.

Muscovite 103116 and 103117 are associated with Mo-rich scheelite and Mo-free scheelite, respectively and they have significantly different Mg/(Mg + Fe) ratios (35 : 61).

There are few muscovites associated with biotites and most of the biotites described by previous workers as associated with muscovite are actually chlorites. The biotite that is associated with muscovite(103116, Table 6.14) shows different contents of Al_2O_3 and FeO compared to other biotites. As demonstrated elsewhere by Wones(1981), the biotite associated (in equilibrium) with muscovite has the highest Al content.

The Mg/(Mg + Fe) ratios of coexisting muscovite and chlorite show a linear correlation(Fig. 6.17), indicating that these minerals are in equilibrium.

Table 6.13. Chemical compositions of muscovites.

	103116		103117			103127		
	a-1	b-1	a-3	c-1	e-1	b-1	c-1	d-2
SiO_2	48.35	48.10	48.53	47.83	48.37	48.39	48.37	47.37
TiO_2	n.d	n.d	n.d	0.42	n.d	n.d	n.d	n.d
Al_2O_3	32.0	32.36	32.49	32.96	32.35	29.14	28.37	30.25
FeO	3.36	3.73	1.81	1.76	2.14	3.68	3.73	3.77
MnO	n.d	n.d	n.d	n.d	n.d	n.d	n.d	n.d
MgO	0.99	1.18	1.7	1.57	1.68	3.39	4.06	3.00
CaO	0.63	0.61	n.d	n.d	n.d	n.d	n.d	n.d
Na_2O	n.d	n.d	0.55	0.64	0.50	0.31	0.34	0.30
K_2O	10.66	10.02	10.9	10.93	10.95	11.11	11.04	11.21
Total	95.99	96.0	95.98	96.11	95.99	96.02	95.91	96.0
	Numbers of ions on the basis of 22 oxygens							
Si	6.443	6.4	6.429	6.347	6.422	6.498	6.504	6.376
Al	1.557	1.6	1.571	1.653	1.578	1.502	1.496	1.624
Al	3.470	3.475	3.503	3.487	3.484	2.812	3.488	3.190
Ti	0.000	0.000	0.000	0.042	0.000	0.000	0.000	0.000
Fe	0.374	0.415	0.201	0.196	0.237	0.412	0.420	0.424
Mn	0.000	0.000	0.000	0.000	0.000	0.000	0.000	0.000
Mg	0.196	0.233	0.337	0.310	0.333	0.678	0.814	0.604
Ca	0.090	0.088	0.000	0.000	0.000	0.000	0.000	0.000
Na	0.000	0.000	0.142	0.165	0.130	0.082	0.088	0.078
K	1.813	1.702	1.843	1.849	1.855	1.904	1.894	1.924
Total	13.943	13.913	14.026	14.049	14.039	13.888	14.704	14.22
Mg/(Mg+Fe)	0.344	0.360	0.626	0.613	0.584	0.622	0.660	0.588

* Location of Samples

103116 = Sangdong level(650 m above sea level)

103117 = -3rd level(about 90 m below the Sangdong level)

103127 = -15th level(about 450 m below the Sangdong level)

6.7. Chlorite

Chlorite occurs mainly in the quartz-mica zone, associated with biotite or muscovite, and less commonly in the amphibole zone. Table 6.16 presents the chemical compositions of chlorite associated with biotite, muscovite and illite. These compositions are plotted in Fig. 6.18, which is a classification diagram for chlorites according to the ratio Mg/(Mg + Fe) and numbers of Si atoms per formula unit(Deer et al., 1963, 1972).

As shown previously, chlorite associated with biotite or muscovite appears to be in chemical equilibrium(Figs. 6.15 and 6.17) with respect to their Mg/(Mg + Fe) ratios. The highest Mg/(Mg + Fe) values in chlorites occur in the central spine of the deposit(Fig. 6.19). The Mg/(Mg + Fe) ratios of chlorites occurring in the pyroxene-garnet skarn zone are the lowest(5), whilst the chlorite occurring in the deepest level, associated with muscovite at the marginal part of the amphibole zone, shows the highest of Mg/(Mg + Fe) (44 to 47). In the 7th level and 3rd level, the Mg/(Mg + Fe) ratio decreases from the central part of the M1 orebody outward.

Most of the analyses of chlorites show a small content of calcium or alkali ions, and Deer et al.(1963) has suggested that these are likely to be due to impurities adsorbed on the surface or as interlayer cations.

The aluminium content of chlorite is a function of the activity of Al in the coexisting mineral(Fig. 6.16); the chlorite coexisting with muscovite having the highest Al content, while chlorite associated with biotite have the lowest.

Table 6.14. Chemical composition of biotite coexisting with muscovite.

	Specimen 103116		103120, 103119 103092, 103093, 103097
	Muscovite	Biotite	Average of biotites without muscovite
SiO_2	48.23	35.53 35.26	35.5
TiO_2	n.d	0.51 n.d	0.6
Al_2O_3	32.18	18.38 19.41	14.7
FeO	3.55	24.95 27.55	29.5
MnO	n.d	n.d n.d	0.5
MgO	1.09	6.61 9.38	6.3
CaO	0.62	0.63 0.28	0.4
Na_2O	n.d	n.d n.d	0.2
K_2O	10.34	9.40 4.14	8.2
Total	96.01	96.01 96.02	95.9

****

Table 6.15. Chemical compositions of chlorites.
(based on Appendix 6.10)

	Closely associated with biotite					muscovite		illite
	103120	103119	103092	103090	103096	103116	103127	103124
SiO_2	23.46	23.66	25.92	23.28	34.19	25.70	24.64	27.67
TiO_2	n.d	n.d	0.08	n.d	n.d	n.d	n.d	n.d
Al_2O_3	18.76	18.43	17.62	19.37	10.92	21.36	21.80	20.81
FeO	40.22	37.0	34.53	43.45	30.50	35.31	25.77	33.22
MnO	0.36	0.68	0.61	0.81	1.34	0.59	2.18	0.76
MgO	4.91	6.09	8.77	1.20	10.16	8.39	11.86	5.84
CaO	n.d	n.d	n.d	n.d	0.9	n.d	n.d	0.04
Na_2O	0.17	0.18	n.d	n.d	n.d	n.d	0.10	0.32
K_2O	0.10	n.d	0.07	n.d	n.d	0.36	n.d	0.07
Total	87.98	86.04	87.6	88.11	88.01	91.71	86.35	88.73
$\frac{Mg}{(Mg+Fe)}$	0.179	0.227	0.305	0.470	0.372	0.303	0.450	0.235

Fig. 6.15 Ratios of Mg/Mg+Fe in biotites and coexisting chlorites.

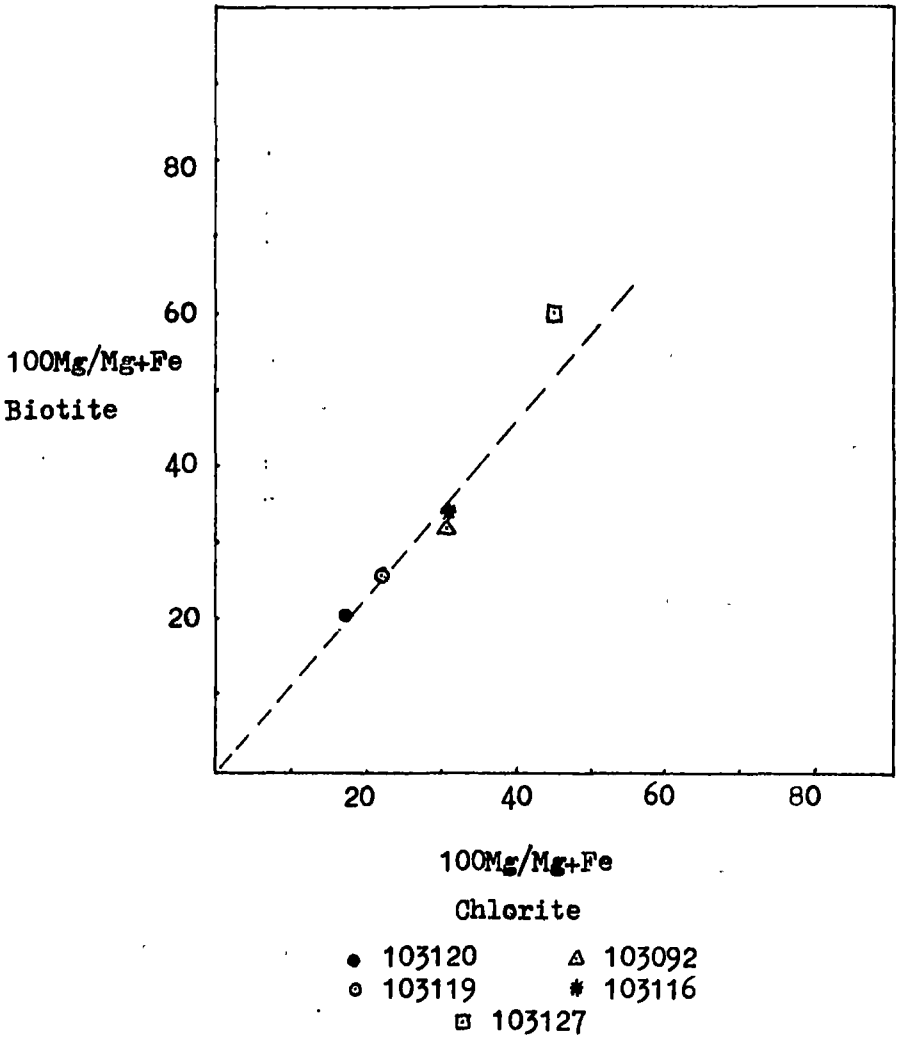

Fig. 6.16. Variation in Al_2O_3 content of chlorites related to the Al_2O_3 content of coexisting minerals.

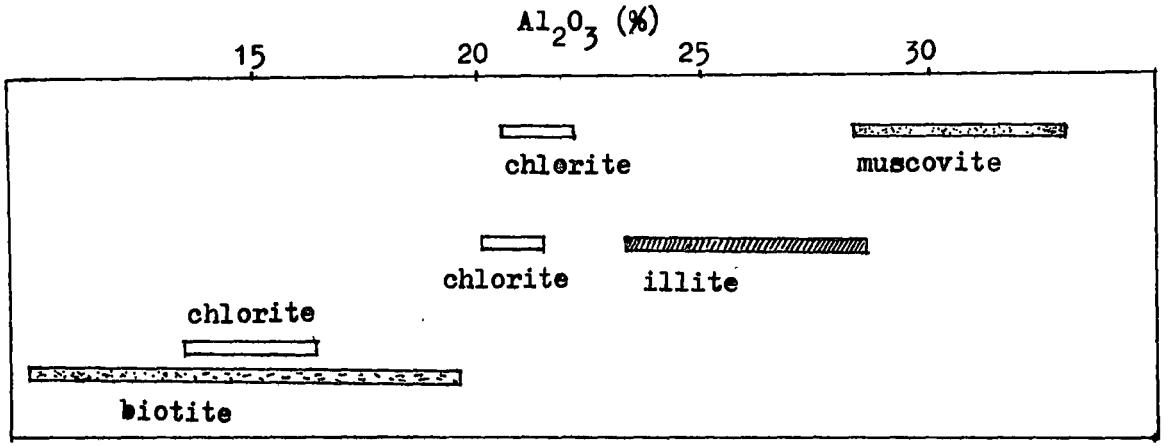

Fig. 6.17. Correlation of the ratios of Mg/(Mg+Fe) in coexisting chlorite and muscovite.

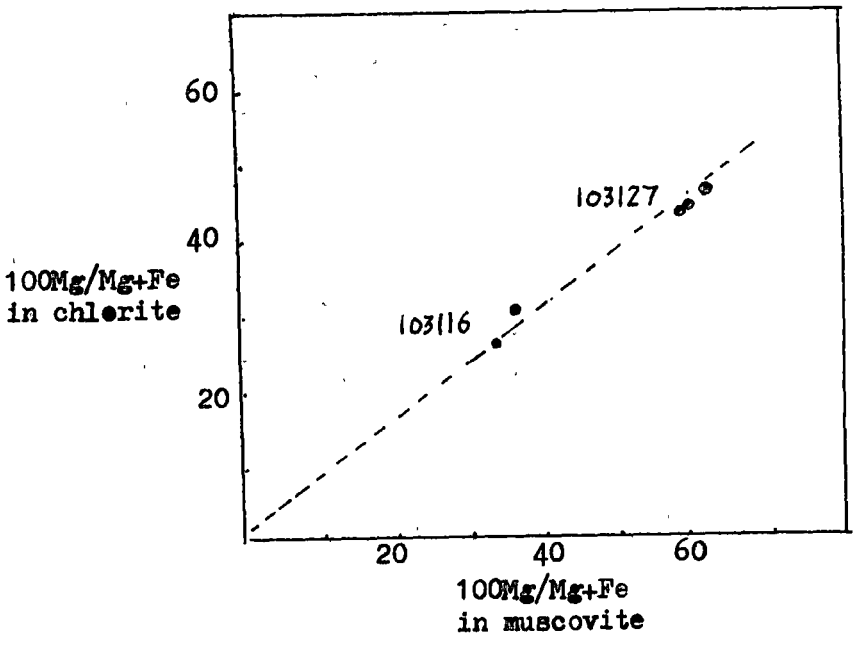

Fig. 6.18. Nomenclature of chlorites.
(after Deer et al.,1972)

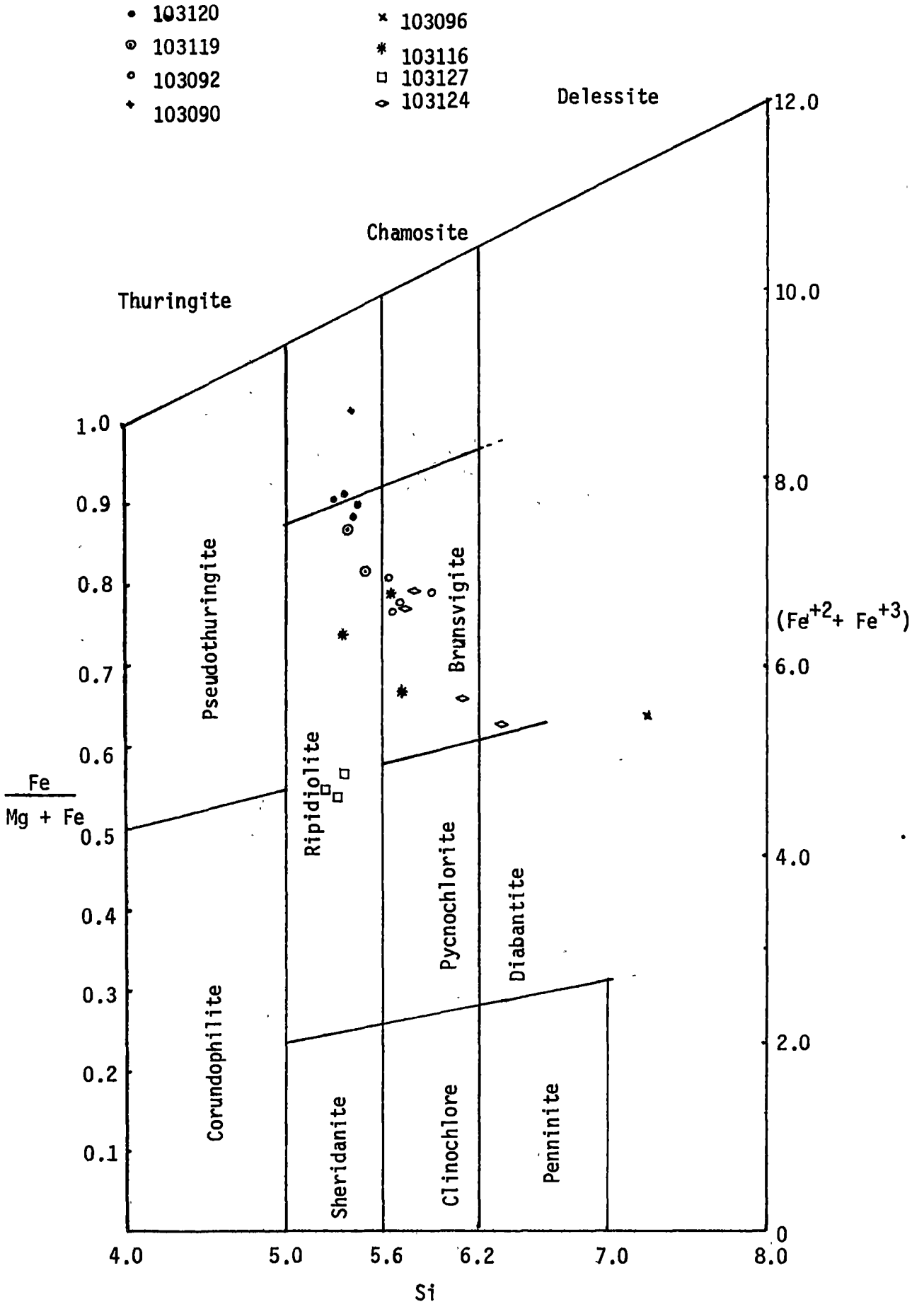

Fig. 6.19. Spatial variation in the Mg/(Mg + Fe) ratio of chlorites.

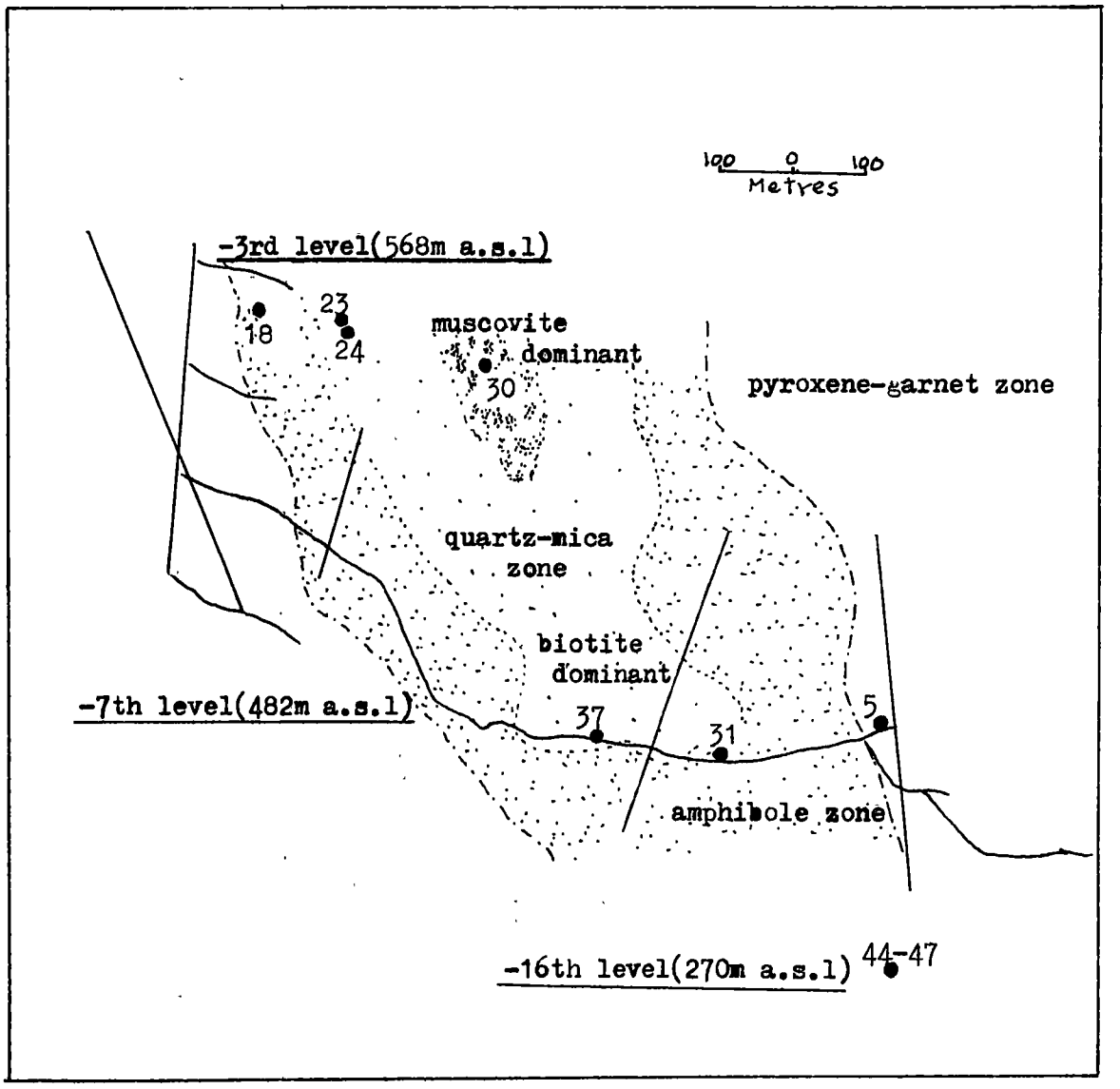

6.8. Newly Identified Minerals

The microprobe study has identified several minerals which were previously unrecorded from the deposit. They are scapolite, zeolite, K-feldspar, rutile, illite and apophyllite.

6.8.1. Scapolite

Scapolite is closely associated with zeolite. It occurs as an alteration product of amphibole and plagioclase and is frequently replaced by fine veinlets of scolecite(zeolite). Microprobe analysis of scapolite is given in Table 6.18.

6.8.2. Zeolite

Zeolites occur in the pyroxene-plagioclase skarn and may be either scolecite, thomsonite or stilbite(Table 6.16).

Scolecite and thomsonite are closely associated and both replace pyroxene. Thomsonite shows a generally brownish tint and is commonly replaced by scolecite. Stilbite and scolecite generally replace pyroxene and plagioclase. These zeolite are locally associated with scheelite. Thomsonite is associated with molybdenite, Mo-free scheelite and amphibole, while stilbite is associated with Mo-rich scheelite(sample 103113 A & B). Scolecite may occur with either type of scheelite.

6.8.3. K-feldspar

K-feldspar has not been recognized in the field or under the microscope, but it is frequently observed in products of the ore dressing procedure and is one of the obstacle to the satisfactory recovery of scheelite by floatation. It appears to occur in the pyroxene-plagioclase skarn. It has a brownish colour, is closely associated with plagioclase, and partly replaces pyroxene(hedenbergite). Chemical analyses are given in Table 6.17.

6.8.4. Rutile

Rutile occurs associated with sphene in a vein of the quartz-mica skarn cutting the pyroxene-garnet skarn(sample 103127, Table 6.17)

6.8.5. Apophyllite

Apophyllite has been observed in a few samples as veinlets replacing all other minerals in the pyroxene-garnet skarn and as an alteration product of wollastonite in the wollastonite skarn(Fig. 5.4a,b). Optically it is very similar to quartz except for its low birefringence and optic figure, showing a diluted black inky colur and a biaxial optic figure. It has a chemical composition as follows:

	103055	103055	103136	103136	103139	103139
SiO_2	61.79	51.49	53.48	52.76	51.66	52.48
K_2O	3.67	4.60	5.05	4.99	4.63	4.35
CaO	20.37	24.12	24.94	24.68	24.50	24.86
Cr_2O_3	0.23	0.33	0.24	0.26	n.d	n.d
FeO	0.22	0.18	0.21	n.d	n.d	n.d
Total	86.28	80.72	83.92	82.69	80.79	81.69
			Numbers of ions on the basis of 20(O)			
Si	8.340	7.787	7.787	7.787	7.795	7.810
K	0.633	0.887	0.940	0.940	0.890	0.825
Ca	2.947	3.907	3.893	3.907	3.960	3.963
Cr	0.027	0.040	0.027	0.027	0.000	0.000
Fe	0.027	0.020	0.027	0.000	0.000	0.000
Total	11.974	12.621	12.674	12.661	12.645	12.598

6.8.6. Illite

Illite is restricted to quartz-muscovite skarn and occurs as an alteration product of muscovite. It is characteristically fine grained occurring as submicroscopic aggregates of flakes and its chemical composition is given in Table 6.17.

6.8.7. Other Minerals

Plagioclase(anorthite), epidote, vesuvianite, wollastonite and sphene have been confirmed by microprobe analyses(Table 6.18).

Table 6.16. Chemical compositions of zeolite minerals in the pyroxene-plagioclase skarn.

Specimen 103113

	Thomsonite	Scolecite				Stilbite		
SiO_2	39.26	46.86	46.04	46.66	46.62	52.67	55.46	54.12
TiO_2	n.d	n.d	n.d	n.d	n.d	n.d	n.d	n.d
Al_2O_3	29.46	25.80	25.89	25.86	26.03	15.22	16.9	18.15
Fe_2O_3	n.d	n.d	n.d	n.d	0.21	n.d	n.d	n.d
Cr_2O_3	n.d	n.d	0.2	0.22	n.d	0.19	n.d	n.d
MnO	n.d	n.d	n.d	n.d	n.d	n.d	n.d	n.d
MgO	n.d	n.d	n.d	n.d	n.d	n.d	n.d	n.d
CaO	12.87	13.60	14.32	13.59	13.09	8.49	8.67	11.42
Na_2O	2.81	n.d	n.d	0.26	0.73	n.d	0.45	0.29
K_2O	n.d	n.d	0.19	n.d	0.18	0.36	0.19	0.21
Total	84.39	86.25	86.63	86.6	86.87	79.94	81.68	84.44
	Numbers of ions on the basis of 80 (thomsonite, scolecite) and 72 (stilbite) oxygens.							
Si	21.35	24.36	23.99	24.22	24.17	26.73	26.51	25.43
Al	18.88	15.81	15.9	15.82	15.91	9.108	9.52	10.05
Cr	-	-	0.08	0.09	-	0.081	-	-
Ca	7.5	7.57	7.99	7.56	7.27	4.617	4.44	5.75
Na	2.96	-	-	0.26	0.73	-	0.42	0.26
K	_	_	0.13	-	0.12	0.234	0.12	0.13
Fe	-	-	-	-	0.09	-	-	-
Total	50.69	47.74	48.09	47.95	48.29	40.77	41.01	41.62

Table 6.17. Microprobe analyses of k-feldspar, rutile, scapolite(dipyre), illite and apophyllite.

	K-feldspar (103088)			Rutile (103127)	Scapolite (103113)	Illite (103124)		
SiO_2	65.07	65.27	65.23	0.25	52.78	55.73	54.47	55.67
TiO_2	n.d	n.d	n.d	98.43	n.d	n.d	n.d	n.d
Al_2O_3	17.70	17.83	18.18	n.d	23.34	28.78	27.47	27.01
FeO	0.88	0.63	0.54	1.00	0.22	3.27	2.91	3.01
Cr_2O_3	n.d	n.d	n.d	0.33	0.20	n.d	n.d	n.d
MnO	n.d	n.d	n.d	n.d	n.d	n.d	n.d	n.d
MgO	n.d	n.d	n.d	n.d	n.d	1.74	1.95	1.89
CaO	0.92	0.50	0.35	n.d	10.73	0.62	0.50	0.50
Na_2O	n.d	n.d	n.d	n.d	1.83	0.21	0.44	0.31
K_2O	15.44	15.76	15.71	n.d	n.d	3.53	4.22	4.62
Total	98.75	99.12	98.76	100.01	89.10	93.88	91.96	93.01
	Numbers of ions							
Si	3.009	3.0152	3.009	0.003	7.89	7.178	7.197	7.281
Al	0.965	0.970	0.988	0.000	4.113	4.302	4.279	4.164
Ti	0.000	0.000	0.000	0.989	0.000	0.000	0.000	0.000
Fe	0.034	0.0248	0.021	0.011	0.027	0.352	0.321	0.329
Mg	0.000	0.000	0.000	0.000	0.000	0.334	0.384	0.370
Ca	0.045	0.0248	0.017	0.000	1.719	0.086	0.071	0.069
Na	0.000	0.0000	0.000	0.000	0.531	0.052	0.112	0.079
K	0.911	0.9288	0.924	0.000	0.000	0.581	0.712	0.771
Cr	0.000	0.0000	0.000	0.011	0.024	0.000	0.000	0.000
Total	4.964	4.9636	4.959	1.014	14.304	12.885	13.076	13.063

	Apophyllite					
	103055	103055	103136	103136	103139	103139
SiO_2	71.62	63.80	63.71	63.80	63.94	64.24
K_2O	4.25	5.70	6.02	6.04	5.73	5.32
CaO	23.61	29.88	29.73	29.85	30.32	30.43
Cr_2O_3	0.27	0.41	0.29	0.31	n.d	n.d
FeO	0.26	0.22	0.25	n.d	n.d	n.d
Total	(86.28)	(80.71)	83.92)	(82.69)	(80.8)	(81.7)

Table 6.18. Microprobe analyses of epidote, plagioclase, vesuvianite, sphene and wollastonite.

	Plagioclase				Vesuvianite	Sphene		Wollastonite
	103088	103113	103137	103137	103139	103141	103090	103142
SiO_2	47.78	44.23	44.13	44.34	37.86	31.90	31.45	51.75
TiO_2	n.d	n.d	n.d	n.d	1.05	30.33	31.24	n.d
Al_2O_3	33.34	34.67	35.86	36.0	14.46	6.58	6.10	n.d
FeO	0.35	0.77	n.d	n.d	10.34	n.d	n.d	0.63
Cr_2O_3	n.d	n.d	n.d	n.d	0.22	n.d	n.d	0.32
MnO	n.d	n.d	n.d	n.d	4.18	n.d	n.d	n.d
MgO	n.d	n.d	n.d	n.d	n.d	n.d	n.d	n.d
CaO	17.58	19.96	19.57	19.65	31.89	30.19	29.69	47.31
Na_2O	0.95	n.d	0.45	n.d	n.d	n.d	n.d	n.d
K_2O	n.d	0.37	n.d	n.d	n.d	n.d	n.d	n.d
Total	97.77	100.0	99.55	99.4	100.00	99.1	98.2	100.43

	Epidote				
	103141(a)	103141(b)	103141(c)	103090(a)	103090(b)
SiO_2	39.72	40.49	39.66	39.34	39.10
Al_2O_3	28.59	28.65	25.79	24.47	24.47
FeO	6.23	5.58	10.54	11.44	11.86
MnO	n.d	n.d	n.d	0.27	0.75
CaO	25.47	25.28	24.01	24.47	24.47
Total	(94.2)	(91.7)	(93.7)	(97.5)	(97.5)
	Numbers of ions on the basis of 13 oxygens				
Si	3.056	3.098	3.109	3.113	3.102
Al	2.592	2.583	2.383	2.273	2.288
Fe	0.401	0.357	0.691	0.757	0.787
Mn	0.000	0.000	0.000	0.018	0.050
Ca	2.099	2.073	2.017	2.075	2.024
Total	8.148	8,111	8.200	8.236	8.251

6.9. Sulphide Minerals

The three major sulphide minerals in the skarn orebodies are pyrrhotite, pyrite and bismuthinite. Pyrite and bismuthinite decrease in abundance from the centre of the quartz-mica zone outwards to the other zones whilst pyrrhotite increases(Fig. 6.20).

6.9.1. Bismuthinite

Bismuthinite occurs as interstitial fillings between quartz or pyroxene grains and commonly replaces mica(Fig. 6.21) or amphibole along cleavage. Microprobe analyses have also identified micron-size inclusions of bismuthinite in late hedenbergite crystals(e.g. 103054) which replaces wollastonite-garnet skarn. In contrast with the quartz veins, the skarns commonly contain both bismuthinite and native bismuth, both separately or together. The ratio of native bismuth/bismuthinite tends to increase from the central zone outward in the M1 orebody and is higher in the H1 orebody(Moon, 1972). Intergrowths of bismuthinite and native bismuth are common although native bismuth may be rimmed by bismuthinite. The frequency of occurrence of coexisting native bismuth and bismuthinite decreases from the central zone outward. Bismuthinite coexists in a few samples with chalcopyrite and/or pyrrhotite as does native bismuth(Fig. 6.22). Textures indicate that native bismuth replaces pyrrhotite(Fig. 6.23).

Native bismuth occurs more commonly with other sulphide minerals than does bismuthinite, particularly in the quartz-mica skarn. In one specimen (103125) from a quartz-mica(muscovite) skarn, bismuthinite and molybdenite occur together. An inclusion of native bismuth was also observed in a scheelite crystal from a quartz-mica zone sample(103125).

6.9.2. Pyrrhotite and Pyrite

The pyrite/pyrrhotite ratio at Sangdong tends to increase towards the central quartz-mica zone and is correlated with an increase of quartz. Within quartz veins, pyrite is dominant and pyrrhotite is relatively rare.

Pyrrhotite occurs generally as interstitial fillings between pyroxene grains or as bands of massive pyrrhotite replacing the pyroxene-garnet skarn and is associated with amphibole and late pyroxene(characterized by a dark green colour not unlike amphibole). Scheelite associated with pyrrhotite is Mo-poor(blue under the ultra-violet lamp). Magnetite and pyrrhotite occur together at the contact between the amphibole and pyroxene skarns. One specimen(103166) from the pyroxene-garnet skarn showed coexisting pyrite, magnetite and amphibole(Fig. 6.25) while pyrrhotite veining magnetite is also observed(Fig. 6.26). Coexisting pyrrhotite and pyrite occur locally in the amphibole and the quartz-mica skarns, however, these two minerals occur separately.

Pyrite is more frequently observed in the quartz-mica zone than in the pyroxene-garnet zone. In contrast to pyrrhotite, pyrite commonly shows euhedral or semi-euhedral crystal form(Fig. 6.24). There are also local concentrations of pyrite in amphibole-rich zones(Table 8.1). Late pyroxene (hedenbergite) is associated with pyrite in a quartz vein intersecting earlier pyroxene(specimen 103104, Fig. 6.7b).

6.9.3. Arsenopyrite

In contrast with quartz veins, skarns contain very few arsenopyrites. The arsenopyrite was observed from the quartz-mica skarn where it coexists with pyrite. Microprobe analyses reveal little zonation in As content within arsenopyrite grains as follows(Table 6.19):

	atomic % As		
	core	middle	rim
grain 1.	31.46	31.36	30.27
grain 2.	31.59		30.52

Kretschmar and Scott(1976) suggest that marked zoning in the arsenopyrite reflect changing conditions during formation and the lack of variation in the Sangdong arsenopyrite attests to their strong resistence to reequilibration characteristic of other minerals in this deposit.

Table 6.19. Microprobe analyses of pyrite, pyrrhotite and arsenopyrite.

Pyrite

element %	103067	103067	103067	103110	103110	103125	103125
S	52.88	52.92	53.47	53.79	52.37	52.89	52.70
Fe	46.80	46.57	46.79	46.03	47.42	47.68	48.38
Cu	0.27	0.24	0.23	n.d	n.d	0.22	n.d
Zn	0.51	0.41	0.41	0.59	0.54	0.46	0.43
atomic %							
S	65.99	66.17	66.30	66.82	65.58	65.81	65.32
Fe	33.52	33.43	33.31	32.82	34.09	33.77	34.42
Cu	0.17	0.15	0.15	n.d	n.d	0.14	n.d
Zn	0.31	0.25	0.25	0.36	0.33	0.28	0.26

Pyrrhotite

element %	103067	103067	103067	103110	103110	103108	103067
S	38.99	39.68	40.20	39.14	39.45	39.45	39.31
Fe	60.24	60.75	59.64	59.67	60.58	60.30	60.65
Cu	n.d	0.25	0.31	0.22	n.d	n.d	0.27
Zn	0.21	0.27	n.d	0.47	0.27	n.d	0.37
atomic %							
S	52.92	53.04	53.89	53.08	53.05	53.58	52.80
Fe	46.94	46.62	45.90	46.45	46.77	46.42	46.77
Cu	n.d	0.17	0.21	0.15	n.d	n.d	0.18
Zn	0.14	0.18	n.d	0.31	0.18	n.d	0.25

Arsenopyrite

element %	106144(grain 1)			106174(grain 2)	
	core		rim	core	rim
S	21.42	21.36	22.04	21.33	21.86
Fe	34.37	34.30	34.57	34.11	34.34
Cu	0.31	0.36	n.d	0.39	0.35
As	44.3	44.01	42.49	44.35	42.85
atomic %					
S	35.54	35.57	36.70	35.55	36.38
Fe	32.75	32.78	33.03	32.60	32.81
Cu	0.25	0.29	n.d	0.32	0.28
As	31.46	31.36	30.27	31.59	30.52

Table 6.20. Microprobe analyses of sphalerite in a quartz-mica skarn and quartz veins.

*Skarn(103121)

element %	a	b	c	d	e	f	Mean
S	36.41	36.74	36.69	37.74	36.56	36.98	36.85
Fe	11.61	10.02	11.16	11.06	10.98	10.77	10.93
Cu	3.34	n.d	n.d	n.d	n.d	n.d	n.d
Zn	47.77	53.24	51.80	52.70	52.1	52.50	51.67
Total	99.13	100.0	99.65	101.5	99.64	100.25	99.45
atomic %							
S	53.40	53.56	53.56	53.55	53.44	53.67	53.53
Fe	9.77	8.38	9.35	9.16	9.21	8.97	9.14
Cu	2.47	n.d	n.d	n.d	n.d	n.d	0.41
Zn	34.36	38.06	37.07	37.29	37.35	37.36	36.92
Total			100				
FeS mole %	20.96	18.04	20.13	19.72	19.78	19.36	19.67

* Sphalerite coexists with pyrite and pyrrhotite

@ Quartz Veins

element %	103171	103172a	103172c	103173a	103173c
S	31.74	31.36	31.65	32.71	32.90
Mn	0.42	0.97	0.47	5.96	0.05
Fe	8.78	9.43	6.75	5.04	4.44
Cu	0.40	0.13	2.40	0.52	1.17
Zn	55.29	59.38	55.79	59.12	59.19
Cd	3.65	2.73	2.93	2.57	2.25
FeS mole %	16.2	15.99	11.6	10.01	7.77

@ Sphalerite is closely associated with arsenopyrite, pyrite and chalcopyrite in the quartz veins.

Fig. 6.20. Generalized distribution of pyrite, pyrrhotite and bismuthinite.

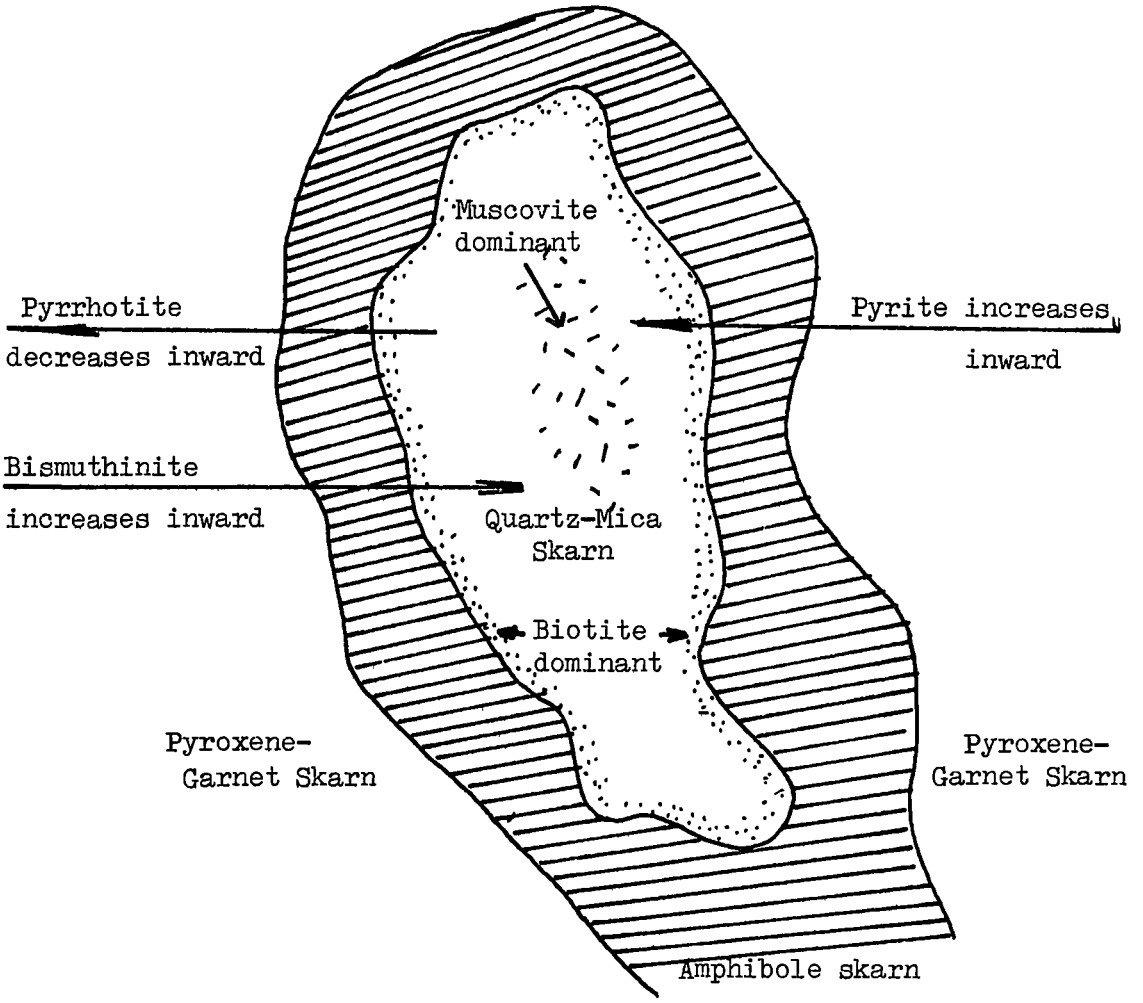

Distribution of bismuth minerals is based on chemical assays; distribution of pyrite(py) and pyrrhotite(po) is qualitatively based on visual estimation.

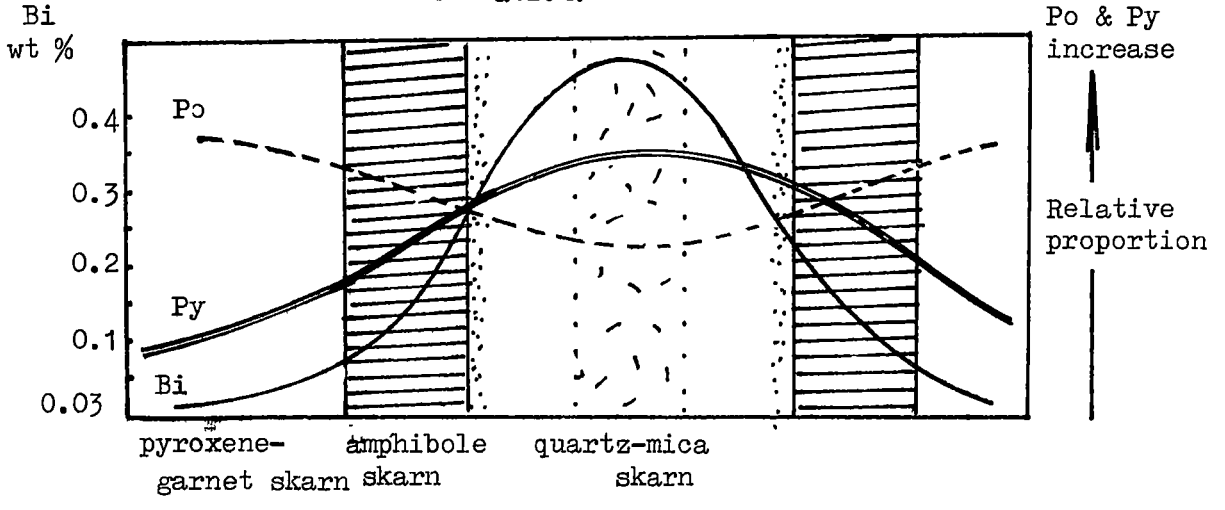

Fig. 6.21. Common appearance of bismuthinite in the quartz-mica skarn. Bt = biotite, Q = quartz, sch = scheelite, white(Bi_2S_3) = bismuthinite.
103167, -7th level. ═══ represent 0.2 mm.

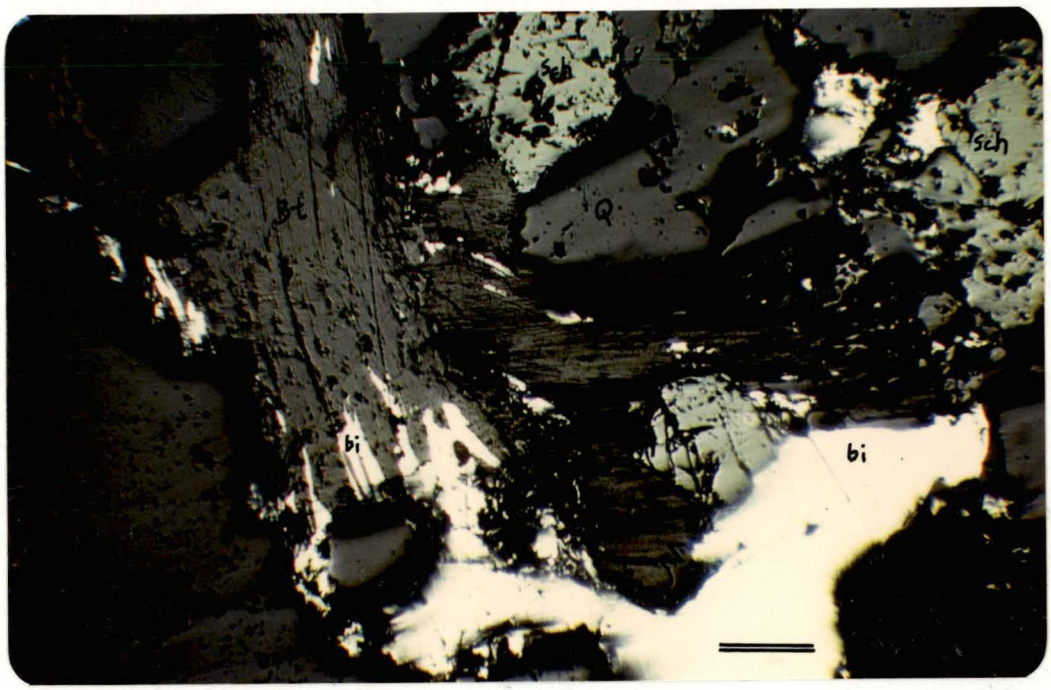

Fig. 6.22. Native bismuth associated with chalcopyrite and pyrrhotite in tne quartz-mica skarn.
ccp = chalcopyrite, po = pyrrhotite, Bi = native bismuth.
103163, Sangdong level. ═══ represent 0.05 mm.

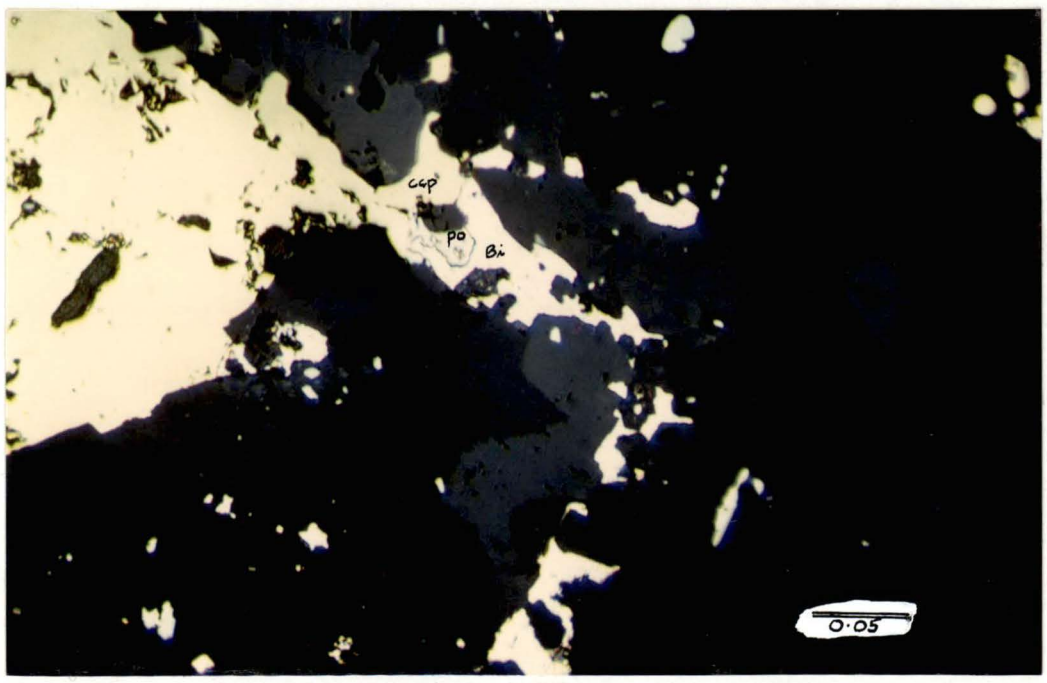

Fig. 6.23. Replacement of pyrrhotite(po) by native bismuth in the quartz-mica skarn.
103163, Sangdong level. ═══ represent 0.05 mm.

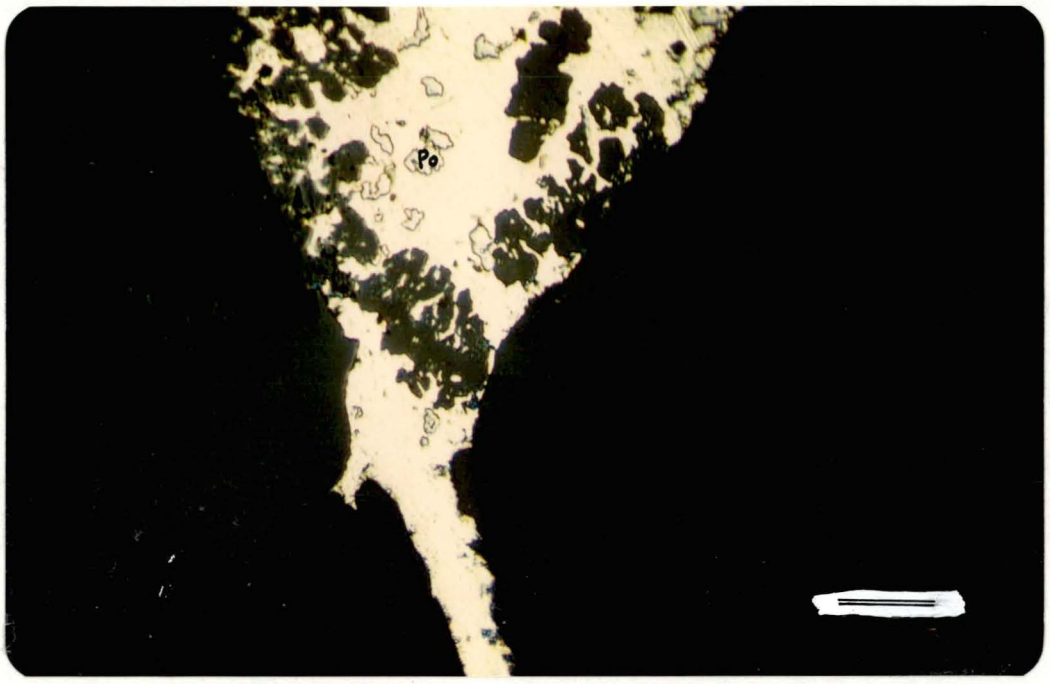

Fig. 6.24. Euhedral pyrite in the pyroxene-garnet skarn.
103166, -3rd level. ═══ represent 0.05 mm.

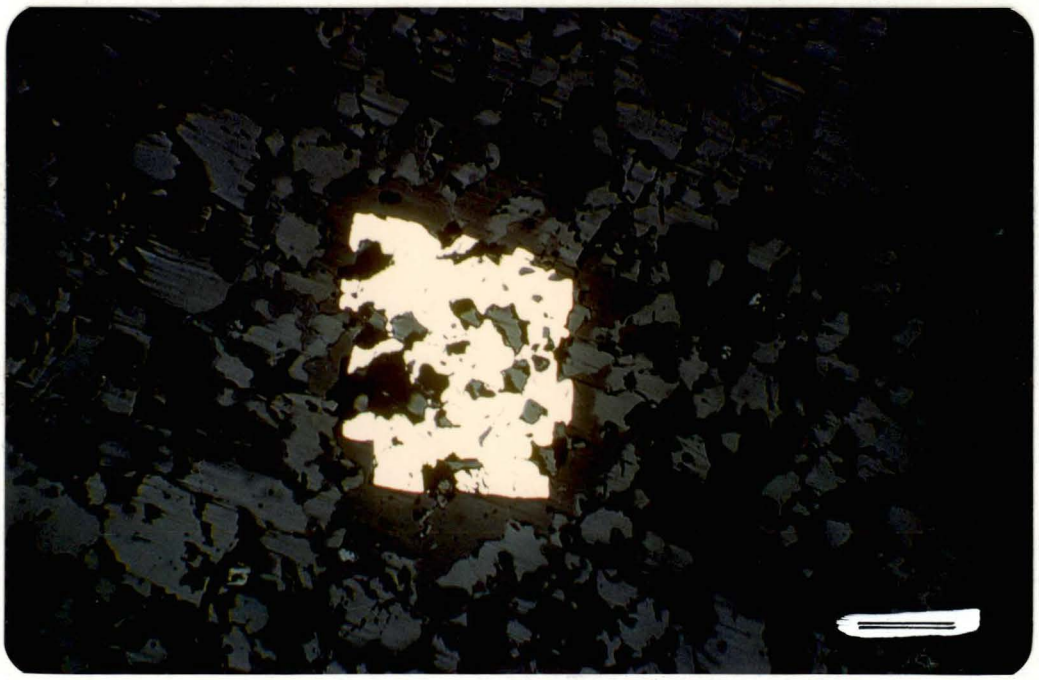

Fig. 6.25. Coexisting magnetite(Mt), pyrite(Py) and Pyrrhotite(Po) in the pyroxene-garnet skarn.
103166, -3rd level, ═══ represent 0.2 mm.

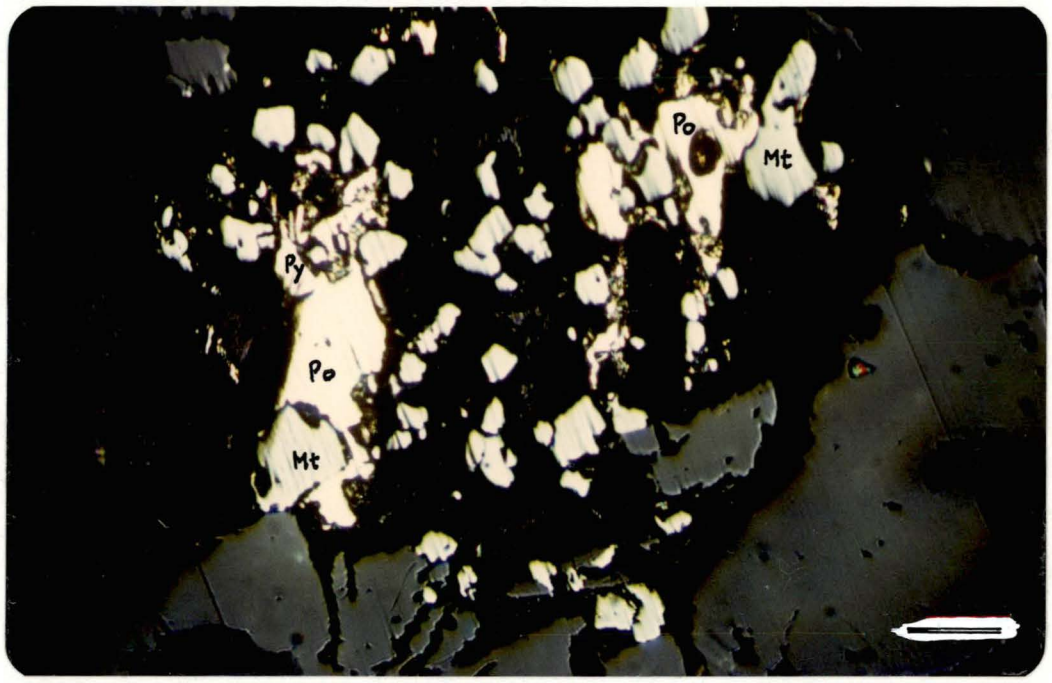

Fig. 6.26. Pyrrhotite veins in magnetite(from the M1 orebody near the boundary between the pyroxene zone and the amphibole zone)
103178, -5th level. ═══ represent 2 cm.

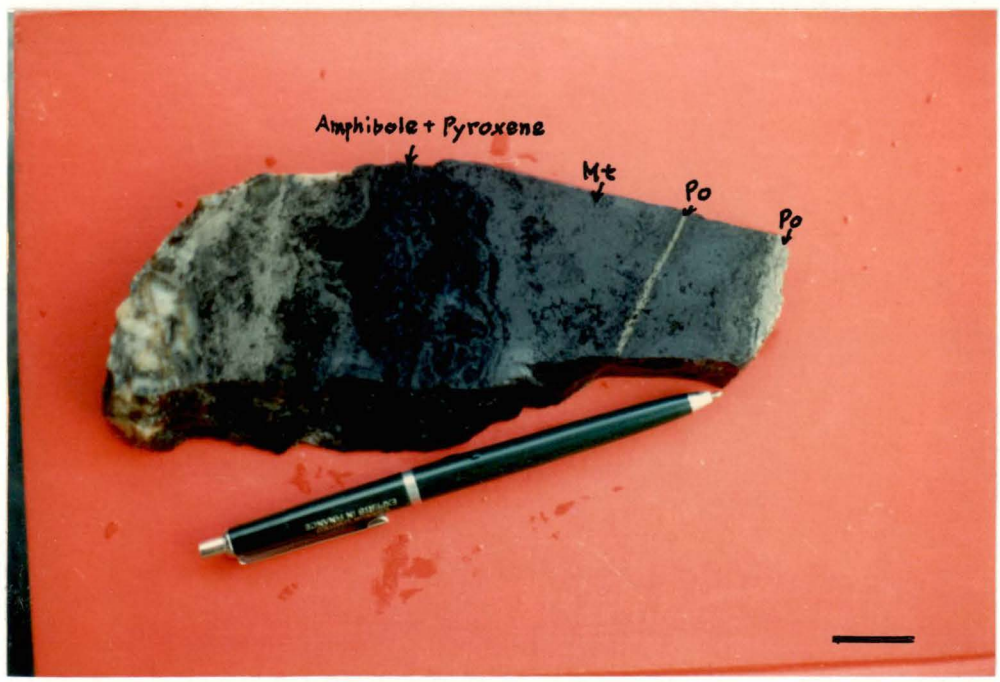

6.9.4. Sphalerite

Sphalerite is also rare in the Sangdong skarn orebodies although a few grains of sphalerite were reported from a wollastonite skarn(Fig. 5.4) and also from the quartz-mica skarn. In the latter, sphalerite is associated with pyrrhotite and pyrite. Sphalerite analyses from the quartz-mica skarn are presented in Table 6.20 and are compared to sphalerite occurring in quartz veins. Sphalerite is more common in quartz veins and exhibits a wide range of composition(Table 6.20).

6.10. Wolframite

Wolframite occurs rarely in the skarn orebodies and is recorded from the quartz-mica zone(106174). There it is associated predominantly with magnetite but is also with scheelite, quartz, fluorite, muscovite, calcite (which replaces muscovite), pyrite, arsenopyrite and hematite.

Wolframite is more common in quartz veins as bladed crystals and has a huebnerite to ferberite ratio of 11.37 : 10.66. Wolframite from the quartz-mica skarn irregular shapes and is Fe-rich(ferberite).

6.11. Scheelite

A recent study of the molybdenum content of scheelite in the Sangdong deposit has shown that both Mo-rich and Mo-poor scheelite occur within the orebody(Moon and Lee, 1980).

The effect of the molybdenum content on fluorescent colour of the Sangdong scheelite has been studied by Hwang(1972). According to Hwang (1970) and Kim(1976) the Sangdong scheelite contains variable amounts of molybdenum ranging from a trace amounts to about 4 wt % Mo, the fluorescent colour changing from pale blue through white to yellow with an increasing molybdenum content(Fig. 6.27).

The fluorescent colour of scheelite in the skarn orebodies varies with location and with carful observation under ultra-violet lamp, it is possible to distinguish a dominant colour(blue or yellow) and zoning(Fig. 6.29b). Mo-bearing scheelite is concentrated in the central zone of the M1 orebody and decreases outwards as the scheelite content decreases(Fig. 6.30).

Compared to the F. orebody, Mo-bearing scheelite is more common in the H1 orebody(Fig. 6.28). Mo-free scheelite is more abundant than Mo-bearing scheelite in quartz veins and commonly large scheelite crystals are zoned in terms of molybdenum content(Figs. 6.29a,b).

Zoning on a crystal scale matches the zonal distribution of Mo-rich, Mo-poor scheelite on the deposit scale.

Fig. 6.27. Diagram showing change of colour of fluorescent scheelite with molybdenum content.
(from Hwang, 1970)

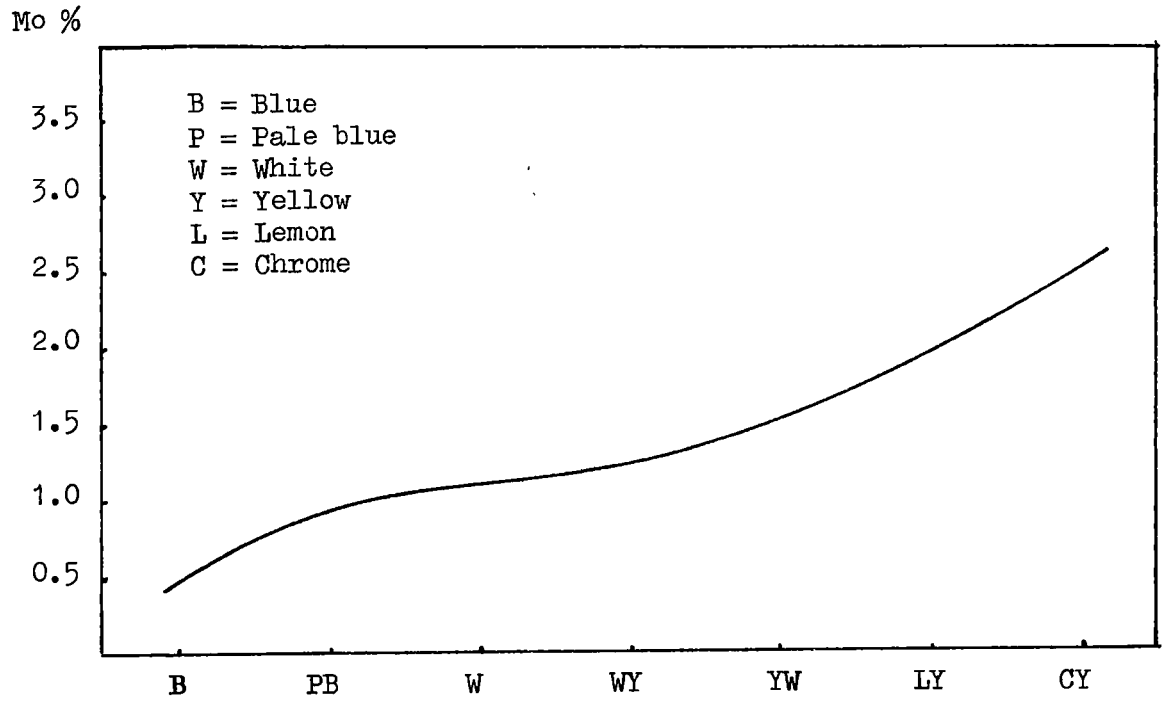

Fig. 6.28. Diagram showing proportions of abundance of Mo-bearing scheelite in three different orebodies related to content of tungsten(from Moon and Lee, 1980).

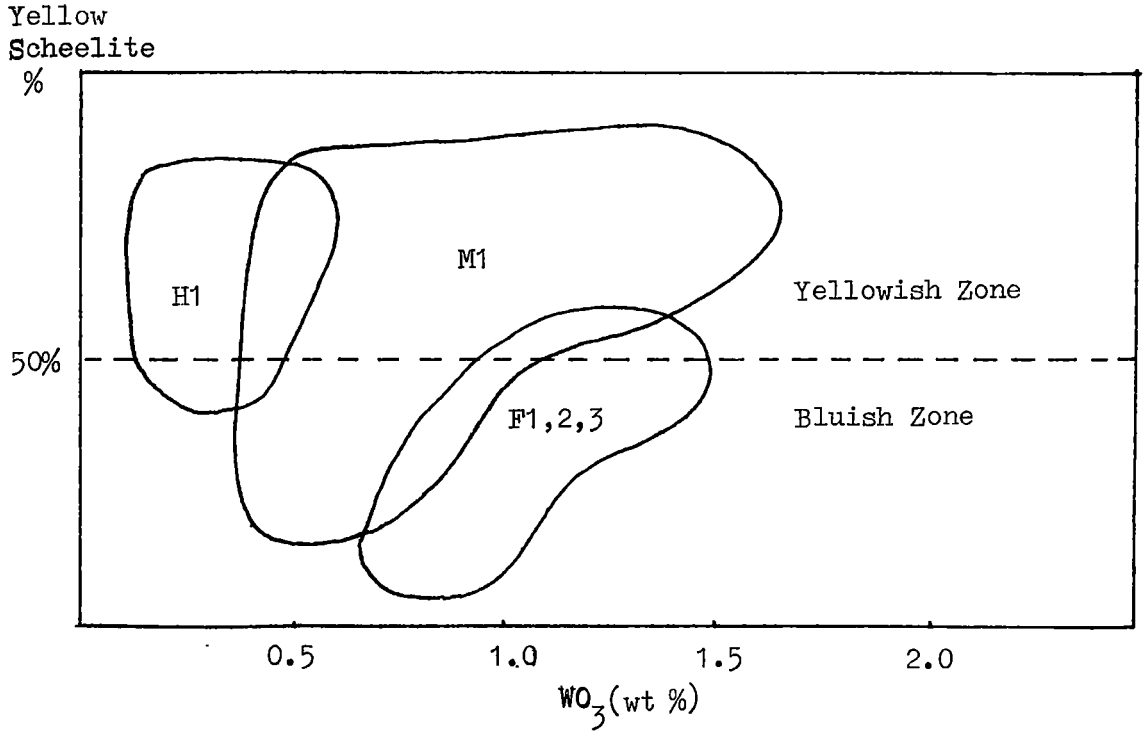

Fig. 6.29(a). Scheelite crystals showing zonation of molybdenum content. Mo-rich scheelite core fluoresces yellow while Mo-poor scheelite rims exhibit a blue fluorescent colour.
103170, Sangdong level. ═══ represent 1.0 cm.

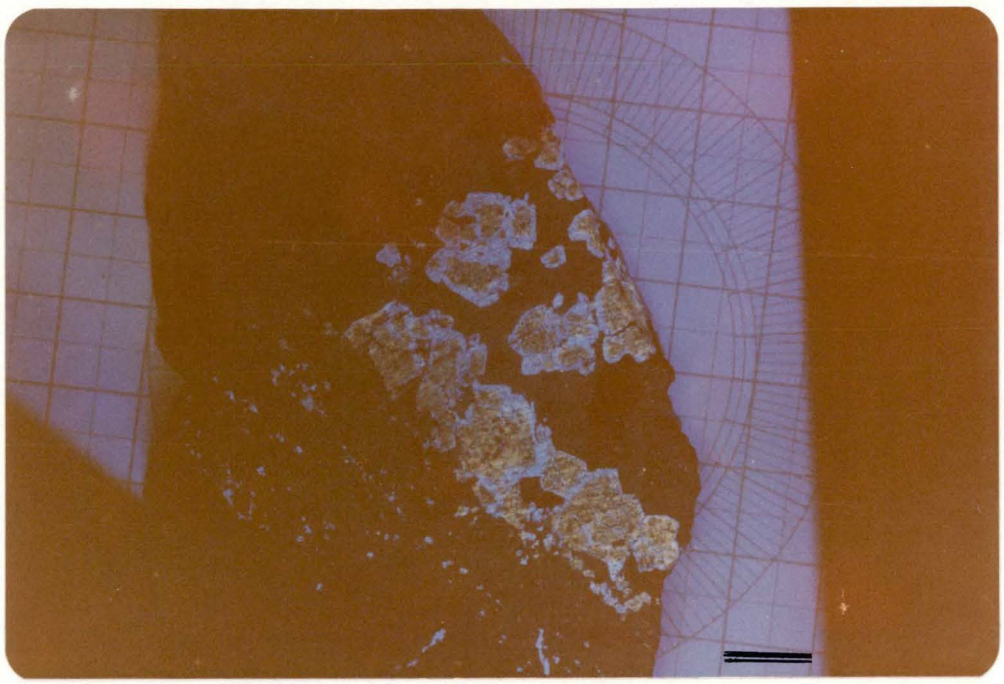

Fig. 6.29(b). Enlarged picture of zoned scheelite crystals. Matrix is mainly quartz. (This zoned crystal was used for fluid inclusion study)
103170, Sangdong level. ═══ represent 3 mm.

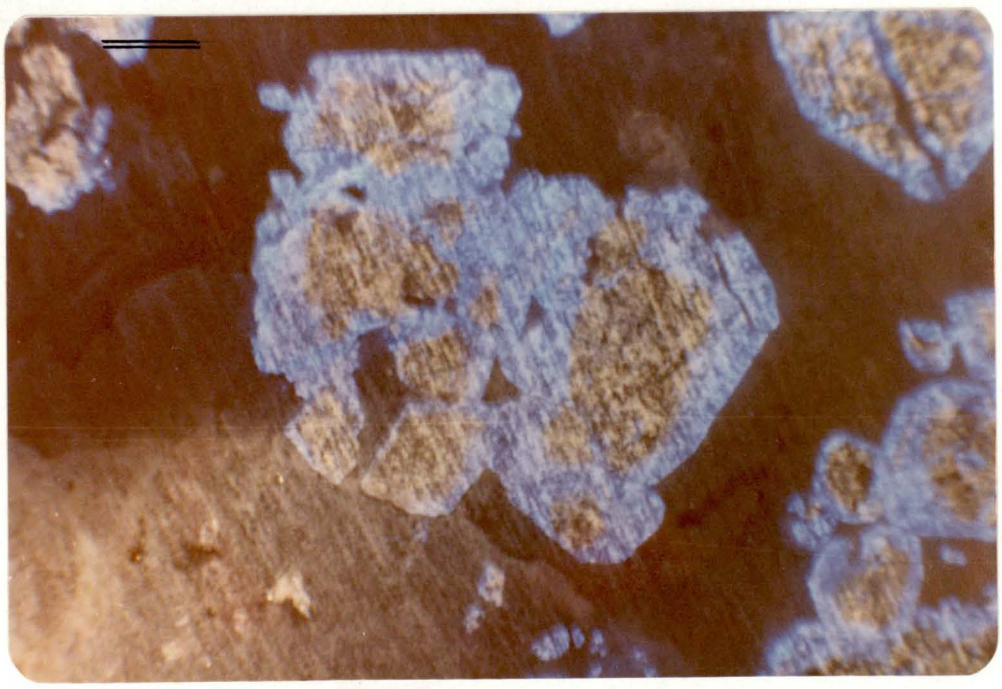

Fig. 6.30. Zonal distribution of molybdenum-bearing scheelite in the Sangdong M1 orebody(from Moon and Lee, 1980).

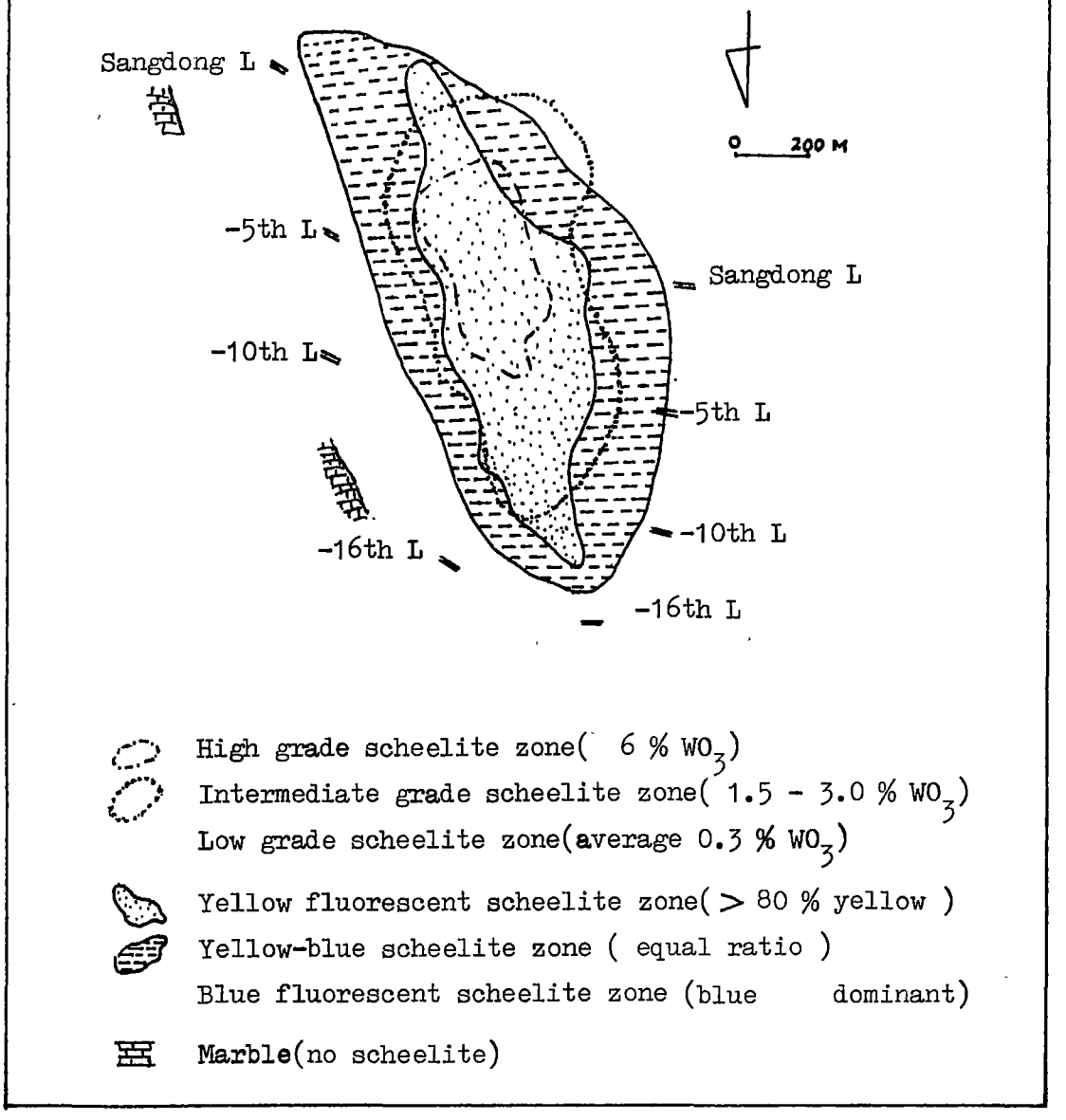

7. GEOCHEMISTRY OF THE MAIN OREBODY

A previous geochemical study of this orebody by Kim(1976) was limited to the 6th and 10th levels and a significant part of the quartz-mica zone was excluded from his study. Recent mining operation have brought new information by reopening old levels in the central part of the M1 orebody and the marginal part of the skarn at the 17th and 18th levels.

In the present study, major and trace element compositions were determined by XRF. Spectrometric methods were used to analyse ferrous iron from a number of representative samples. The analytical methods are described in Appendix 7.

ACF and AKF triangular diagrams are used, the apices being determined as follows:

(a) ACF diagram

$$A = (Al_2O_3) + (Fe_2O_3) - (K_2O) - (Na_2O)$$

$$C = (CaO) - 3.3(P_2O_5)$$

$$F = (FeO) + (MnO) + (MgO)$$

(b) AKF diagram

$$A' = (Al_2O_3) + (Fe_2O_3) + ((Na_2O) + (K_2O) + (CaO))^2$$

$$K = K_2O$$

$$F = FeO + MnO + MgO$$

7.1. Chemical Composition of the Unmineralized Early Skarn and the Late Pyroxene-Garnet Skarn

An ACF diagram displays the variation in composition from the wollastonite skarn, via the garnet skarn, to the pyroxene skarn(Table 7.1; Fig. 7.1). It suggests that in a broad sense the contact metamorphic and metasomatic replacement of the original limestone involves a loss of CaO and gain of FeO + MnO + MgO, and that Na, K and Al_2O_3 appear to be only moderately affected.

Appendix 7.1 lists semi-quantitative analyses determined in the mine laboratory to test for variation in chemistry of pyroxene-garnet skarn with depth, there does not appear to be any significant changes.

In order to quantitatively evaluate the transfer of elements during formation of the skarns, losses and gains are calculated(Table 7.2) assuming that the volume of the rock remained unchanged during formation of skarn formation and that the composition of the original limestone was the same as that of the interbedded limestone on the eastern side of the zone. The specific gravity of the limestone was taken as 2.8 and that of the skarn as 3.1, these being values used at the mine for ore reserve calculations. Table 7.2 shows the chemical changes which occur in the formation of wollastonite skarn(103054) from an average limestone and of pyroxene-garnet skarn(103055) from the wollastonite skarn.

The calculated losses in the formation of the wollastonite skarn are CaO, CO_2(expressed as the ignition loss) and MgO, whilst the principal calculated gains are SiO_2, Fe_2O_3, FeO, K_2O and MnO. Al_2O_3, P_2O_5, TiO_2 and Na_2O are substantially unchanged. Sn, W, Bi and Rb are significant trace elements added during formation of this skarn. In the formation of the pyroxene-garnet skarn from the wollastonite skarn, only FeO, MnO and Al_2O_3 were added. In changing from the limestone to the pyroxene-garnet skarn, the principal gains are SiO_2, FeO, Fe_2O_3, MnO and Al_2O_3, whilst losses are CaO, CO_2 and MgO. The late pyroxene-garnet skarns(103056, 103057, 103058) show much greater addition of FeO and depletion of Al_2O_3 than sample 103055(Tables 7.2 and 7.3), but otherwise the general trend in replacing average limestone by these skarns is the same. The depletion of Al_2O_3 is compatible with a decrease of garnet and a concomitant increase of hedenbergite in the late formed pyroxene-garnet zone.

7.2. Composition of the Amphibole Skarn

Table 7.4 presents chemical compositions of characteristic amphibole skarns from the M1 orebody. The amphibole skarn generally exhibits a small range of variation in SiO_2, however, an usually low SiO_2 content in specimen 103060 is attributed to relicts of the garnet skarn. SiO_2 and CaO, and FeO and Fe_2O_3 contents vary inversely(Fig. 7.2). The Sn content of amphibole skarn is much higher than that in the quartz-mica skarn(see Tables 7.4 and 7.5), but generally lower than Sn contents in early wollastonite and pyroxene-garnet skarns. The Bi content of amphibole skarn tend to vary inversely with Sn content. Enrichment of Mo in sample 103064 is attributed to the occurrence of Mo-rich scheelite.

The composition of the amphibole skarn associated with Mo-rich scheelite (103064) is in striking contrast to that associated with Mo-poor scheelite (103065). The lower ratio of FeO/Fe_2O_3 in 103064 indicates a more oxidized environment for the Mo-rich scheelite(Fig. 7.2).

Assuming the amphibole skarn is derived from the pyroxene-garnet skarn and using average rock compositions suggests that SiO_2, MgO, FeO, Fe_2O_3, Na_2O, K_2O, P_2O_5, H_2O and WO_3 were added and TiO_2, Al_2O_3, MnO and CaO were depleted during formation of the amphibole skarn(Table 7.6).

7.3. Composition of the Quartz-Mica Skarn

Table 7.5 presents chemical composition of typical quartz-mica skarn. In general, this quartz-mica skarn has higher contents of Si, Al, K and W and contents of Fe and Ca than the amphibole skarn(cf. Table 7.5 to Table 7.4). For most samples, the WO_3 content in the skarn orebody is directly proportional to the K_2O and SiO_2 contents, but the quartz-mica skarn does not follow this trend internally. Al_2O_3 and SiO_2 contents vary proportionally and they are inversely proportional to FeO content.

The ratio of SiO_2/Al_2O_3 is directly proportional to the content of WO_3. Higher than average contents of Al_2O_3 and SiO_2 can be attributed to an increase in sericite, chlorite and quartz in the central part of this zone, probably developed during post-ore alteration. In contrast with the high content of Sn in the pyroxene-garnet skarn, this skarn has a very low Sn content, which is generally inversely proportional to that of WO_3. Zn and (Mo + Bi) contents increase with W content, similar to the pyroxene-garnet skarn.

As shown in Fig. 7.3, this skarn shows systematic chemical variations from the central part to the margin of the zone. SiO_2, Al_2O_3, CaO, Sn and Sr contents increase and FeO, MgO and WO_3 contents decrease from the margin to the centre. The ratio of FeO/Fe_2O_3 is much higher in the margin than in the central part, continuing the trend noticed in the amphibole zone. The higher content of CaO in the central part is due to carbonatization, mica commonly being replaced by calcite.

On a broad scale, it seems that this quartz-mica skarn was derived from replacement of the amphibole skarn, each of the hydrous skarn zones moving outward with time. Such considerations are reinforced by the small scale zoning of 103063(Fig. 7.3 and Fig. 8.2).

In forming the quartz-mica skarn from the amphibole skarn, mass balance calculations suggest K_2O, Al_2O_3, H_2O, P_2O_5 and TiO_2 were added, and Fe_2O_3, FeO, MnO, MgO, CaO and Na_2O were removed(Table 7.6).

7.4. Summary of Variation in Chemical Composition between Skarn Zones of the M1 Orebody

General geochemical trends between skarn zones of the M1 orebody are presented in Figs. 7.4 and 7.5.

7.4.1. Major Elements

SiO_2 :- Silica shows the same distinctive distribution as tungsten,

molybdenum, aluminium and potassium, enriched in the mica skarn and depleted in others. The silica content is normally between 40 and 47 % SiO_2 in the pyroxene-garnet skarn. A higher content of SiO_2 than 47 % in the skarn indicates the presence of quartz veinlets or replacement of skarn minerals by quartz associated with scheelite. However, the ratio of W/Si in the pyroxene-garnet skarn does not vary systematically.

In the amphibole skarn, silica ranges from 53 to 58 %, but some of the samples show a lower SiO_2 content especially at the margin with the pyroxene-garnet zone because of relict garnet and lack of quartz.

Silica is enriched in most specimens from the quartz-mica skarn relative to the other skarn. Even though the ratio of W/Si shows a broadly systematic variation in the whole M1 orebody, the ratio within the quartz-mica skarn is inversely related to SiO_2 content, suggesting that late quartz mineralization might remobilize scheelite.

TiO_2:- Titanium is one of the insignificant elements in the skarn, but is relatively enriched in the hydrous skarns(amphibole and quartz-mica skarns).

Al_2O_3:- Alumina shows a similar trend to silica, i.e. an increase from pyroxene-garnet skarn to quartz-mica skarn.

FeO and Fe_2O_3:- Ferric iron shows a fluctuating variation in the whole M1 orebody. The ferric iron content is always below ferrous iron content except in the wollastonite-garnet skarn(Table 7.1).

MnO :- Manganese decreases from the pyroxene-garnet skarn inward, indicating that MnO was depleted during formation of hydrous skarns from the pyroxene-garnet(anhydrous) skarn.

MgO :- Magnesium is a little more enriched in the hydrous skarn than in the anhydrous skarn, whilst MgO was depleted during formation of the pyroxene-garnet skarn from the limestone.

CaO :- Calcium decreases from the pyroxene-rich skarn to the mica-rich skarn.

Na_2O :- Sodium is insignificant in the quartz-mica and the pyroxene-garnet skarns but reaches 1 % in the amphibole skarn.

K_2O :- Potassium exhibits a distinctive zonal distribution the same as tungsten, molybdenum, bismuth, aluminium and silica, with a decrease from the mica skarn, except that potassium in the wollastonite skarn is significantly higher than in the pyroxene-garnet skarn.

P_2O_5:- Phosphorus shows a gradual decrease from the mica skarn to the pyroxene skarn. Phosphorus occurs in apatite which is mainly concentrated in the quartz-mica skarn.

7.4.2. Trace Elements

Sn :- Tin is considerably enriched in the wollastonite skarn, in which andradite contains inclusions of cassiterite, and it decreases to the central quartz-mica skarn, ranging from 1340 ppm to 20 ppm. Tin varies inversely with tungsten in anhydrous skarns(Table 7.1).

Zn :- Zinc is a little more enriched in the pyroxene-garnet skarn than hydrous skarns. Only in the quartz-mica skarn are contents of tungsten and zinc directly proportional to each other.

Cu :- Copper is enriched in the mica skarn and decreases towards pyroxene skarn.

Ni :- Nickel shows insignificant variation, but its average content in the pyroxene-garnet skarn is lower than in the quartz-mica and the amphibole skarns.

Sr :- The strontium content in the M1 skarn orebody is very low compared to the content of strontium in the original rock, but it shows a gradual increase from the outer skarn to the central skarns.

Rb :- Rubidium is considerably enriched in the quartz-mica skarn. The content of rubidium in the pyroxene-garnet skarn is very low compared to that in the quartz-mica and the amphibole skarns. The wollastonite

skarn has higher rubidium content(103 ppm) than the pyroxene-garnet skarn (less 4 ppm). The content of rubidium varies in direct proportion to that potassium.

Pb :- Lead is localized in the quartz-mica skarn and drops of markedly in other skarns.

Mo, Bi, W :- These elements are concentrated mainly in the mica and the amphibole skarns. The molybdenum content is generally directly proportional to the tungsten content, but it does not always follow, since this content is dependent on the Mo content of scheelite, or molybdenite occurring in quartz veinlets.

Fig. 7.1 The chemical composition of the early skarn and the pyroxene-garnet skarn plotted on an A C F diagram (see Table 7.1. for analyses).

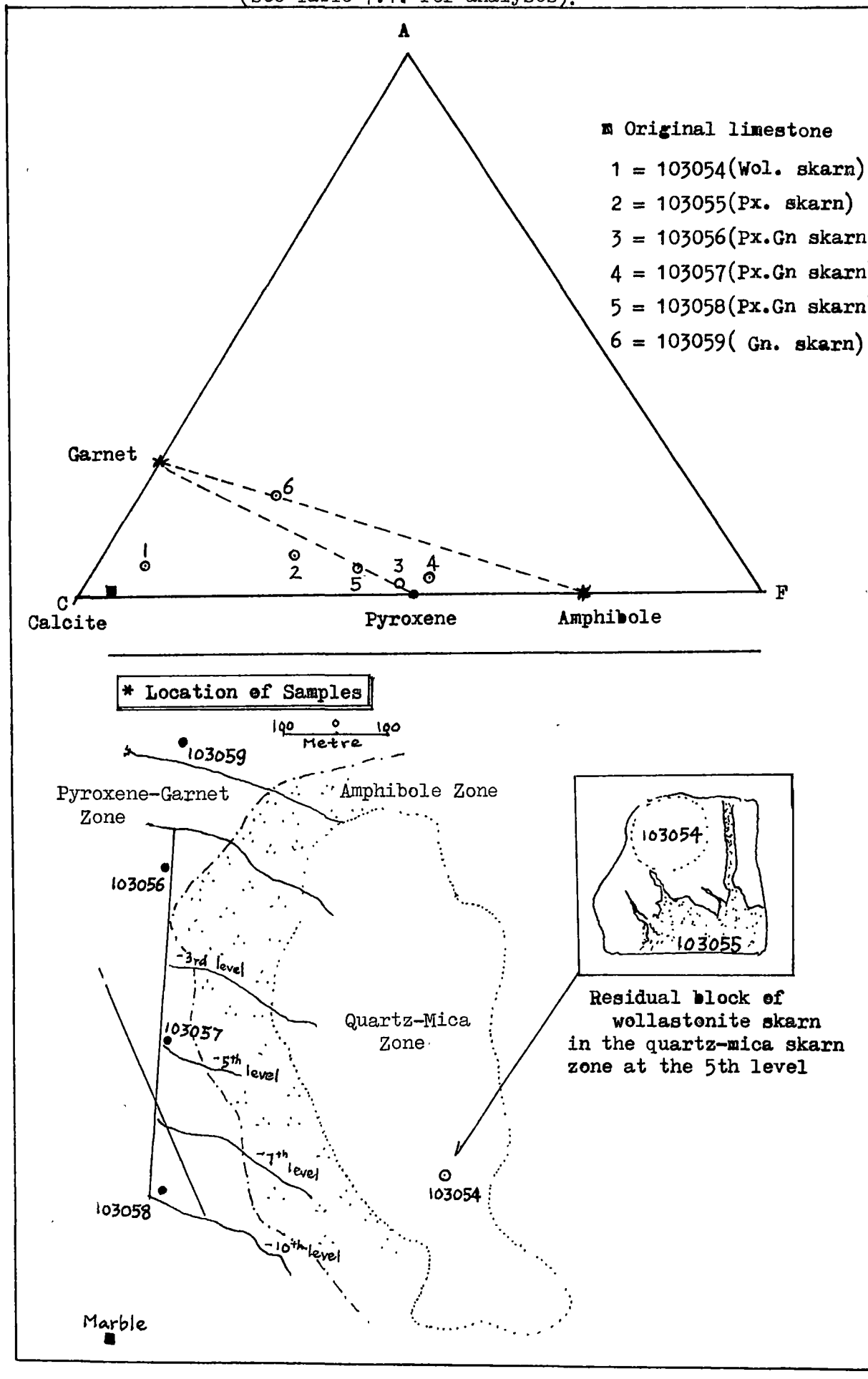

Table 7.1. Chemical compositions of typical anhydrous skarns from the Sangdong tungsten deposit(analysed by XRF, Fe_2O_3/FeO is based on colorimetric FeO analyses).

	wollastonite skarn 103054	pyroxene skarn 103055	garnet skarn 103059	pyroxene-garnet skarn -1st level 103056	-5th level 103057	-10th level 103058
SiO_2	42.98	40.49	46.2	46.88	54.22	45.25
TiO_2	n.d	n.d	1.01	0.02	0.03	0.01
Al_2O_3	1.3	1.7	9.29	0.87	0.68	1.05
Fe_2O_3	6.75	5.96	6.19	1.04	2.24	5.07
FeO	1.70	13.62	5.54	23.83	21.99	19.04
MnO	0.56	2.57	1.88	1.64	1.17	1.71
MgO	0.93	0.59	1.44	0.72	1.39	0.65
CaO	32.24	29.12	23.24	23.89	19.02	25.23
Na_2O	n.d	n.d	n.d	n.d	n.d	n.d
K_2O	1.68*	0.03	0.05	0.03	0.01	0 03
P_2O_5	0.05	0.05	0.04	0.07	0.09	0.06
LOI	11.62**	2.7	2.33	1.09	2.44	2.11
Total	99.81	99.83	97.58	100.07	101.04	100.23
Trace elements(ppm)						
Sn	1338.7	1212.5	412.5	78.3	6.5	152.2
Zn	48.9	430.7	185.9	287.2	204.6	237.3
Cu	12.2	17	77.8	26.1	20.4	13.4
Ni	5.7	8.2	19.2	8.0	26.2	5.5
Sr	21.6	9.0	27.6	4.1	5.9	0.6
Rb	103.3	1.6	3.4	0.0	1.9	1.1
Th	1.5	0	32.4	0.0	5.5	14.0
Pb	10.4	1.0	5.4	16.1	4.0	9.8
Bi	206.8	187.9	6.0	199.6	13.5	170.1
Mo	0	4.0	0	5.0	27.5	7.0
W	79.3	104.5	224.3	866.2	1278.0	1004.0

* High content of potassium due to occurrence of apophyllite

103055(pyroxene skarn) replaces 103050(wollastonite skarn) at the 5th level in mica zone.

103059(garnet skarn) is a residual block being replaced by amphibole at the Baegun(+2) level.

**#103054 → LOI (Loss on Ignition) may be mainly CO_2.

Table 7.2. Calculated chemical losses and gains of elements during formation of the wollastonite skarn from limestone and for the formation of pyroxene-garnet skarn from the wollastonite skarn.

	limestone(mean) 103145 103146 103151		wollastonite skarn 103054		gain or loss(-) mg/cc	pyroxene-garnet skarn 103055		gain or loss(-) mg/cc
	wt%	mg/cc	wt%	mg/cc		wt%	mg/cc	
SiO_2	4.22	118.2	42.98	1332.4	1214.2	40.49	1255.2	-77.2
TiO_2	0.03	0.8	0	0	-0.8	0	0	0
Al_2O_3	1.34	37.5	1.3	40.3	2.8	1.7	52.7	12.4
Fe_2O_3	0.14	3.9	6.75	209.3	205.4	5.96	184.8	-24.5
FeO	0.59	16.5	1.70	52.7	36.2	13.62	422.2	369.5
MnO	0.16	4.5	0.56	17.4	12.9	2.57	79.7	62.3
MgO	1.73	48.4	0.93	28.8	-19.6	0.59	18.3	-10.5
CaO	49.33	1381.2	32.24	999.4	-381.8	29.12	902.7	-96.7
Na_2O	0	0	0	0	0	0	0	0
K_2O	0.35	9.8	1.68	52	42.2	0.03	0.9	-51.1
P_2O_5	0.04	1.12	0.05	1.55	0.43	0.05	1.55	0
LOI	40.96	1146.9	11.62	360.2	-786.7	5.7	176.7	-183.5
Trace elements(ppm)								
Sn	0		1339		1339	1213		-126
Zn	5		49		44	431		387
Cu	8		12		4	17		5
Ni	5		6		1	8		2
Sr	350		22		-328	9		-13
Rb	10		103		93	2		-101
Th	0		2		2	0		-2
Pb	9		10		1	1		-9
Bi	4		207		203	188		-19
Mo	4		0		-4	4		4
W	2		79		77	1045		966

Table 7.3. Chemical gains and losses in the formation of the late pyroxene-garnet skarn(103056,103057,103058).

	limestone		pyroxene-garnet skarn		gain or loss (+)	(-)
	wt %	mg/cc	wt %	mg/cc		
SiO_2	4.22	118.2	48.78	1512.18	+1393.98	
TiO_2	0.03	0.8	0.02	0.62		-0.18
Al_2O_3	1.34	37.5	0.87	26.97		-10.53
Fe_2O_3	0.14	3.9	2.78	86.18	+82.28	
FeO	0.59	16.5	21.62	670.22	+653.72	
MnO	0.16	4.5	1.51	46.81	+42.31	
MgO	1.73	48.4	0.92	28.52		-19.88
CaO	49.33	1381.2	22.71	704.01		-677.19
Na_2O	0	0	0	0	0	
K_2O	0.35	9.8	0.02	0.62		-9.18
P_2O_5	0.04	1.12	0.07	2.17	+1.05	-
LOI (CO_2)	40.96	1146.96	1.88	58.28		-1088.62
Trace element(ppm)						
Sn		0		79	+79	
Zn		5		243	+238	
Cu		8		20	+12	
Ni		5		13	+8	
Sr		350		4		-346
Rb		10		1		-9
Th		8		7		-1
Pb		9		10	+1	
Bi		0		128	+128	
Mo		3*		13	+10	
W		2*		1049	+1047	

* below detection limit by XRF analyses

Fig. 7.2. Variation in some elements in the amphibole skarn.

(based on Table 7.4)

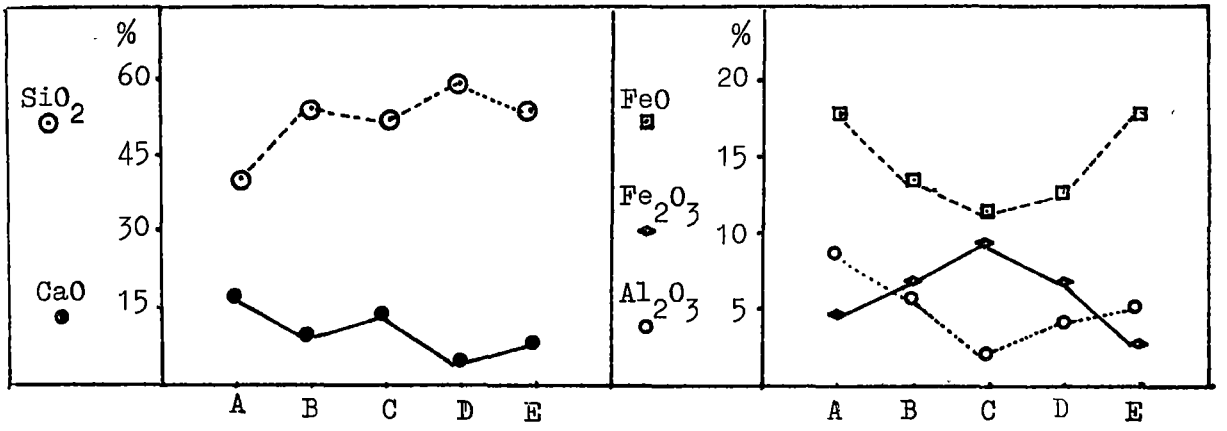

A = 103060 (replacing garnet skarn)

B = 103061 (replacing pyroxene-garnet skarn)

C = 103062 (as rim of small scale quartz-mica skarn)

D = 103064 (associated with Mo-rich scheelite)

E = 103065 (associated with Mo-free scheelite)

Table 7.4. Chemical compositions of amphibole skarn.

	103060	103061	103062	103064	103065	Mean
SiO_2	41.17	55.06	53.48	58.33	54.39	52.49
TiO_2	1.0	0.06	0.03	0.09	0.07	0.25
Al_2O_3	9.05	6.08	2.27	4.65	5.27	5.46
Fe_2O_3	4.68	6.43	9.2	6.96	2.86	6.03
FeO	17.6	13.45	11.38	12.56	17.62	14.52
MnO	1.05	0.8	0.59	0.59	0.69	0.74
MgO	1.79	1.52	1.03	1.47	2.32	1.63
CaO	17.13	11.58	14.8	5.45	8.8	11.55
Na_2O	0.38	0.99	n.d	0.35	0.58	0.46
K_2O	1.33	0.57	0.44	1.22	0.6	0.83
P_2O_5	0.31	0.12	0.07	0.15	0.18	0.17
WO_3	0.2	0.2	0.31	5.9	5.9	2.50
LOI	4.72	3.33	5.32	3.9	2.43	3.94
Total	100.41	100.19	98.91	101.62	101.71	100.57
Trace elements(ppm)						
Sn	389.3	336.3	113.7	104	59	200
Zn	231	250	184.2	162.1	180.5	202
Cu	21.1	78.2	28.1	82.3	13.8	45
Ni	22.9	5	18.7	16.1	87.4	30
Sr	48.1	6	26.2	17.5	10.7	22
Rb	52.8	14.8	115.9	337.1	25.8	109
Th	45.1	1358.1	0	0	0	281
Pb	0	21.9	25.5	0	68.6	23
Bi	203.6	0	223.9	502	4997.9	1185
Mo	0.8	23.5	117.3	1297.9	112.1	310

103060(replacing garnet skarn) 103061(replacing pyroxene-garnet skarn)
103062(rim of a small scale quartz-mica skarn)
103064(associated with Mo-rich scheelite)
103065(associated with Mo-poor scheelite)

Fig. 7.3. Variation in chemical compositions of the quartz-mica skarn.

Samples : (A) = 103066 (C) = 103068
(B) = 103067 (D) = 103063

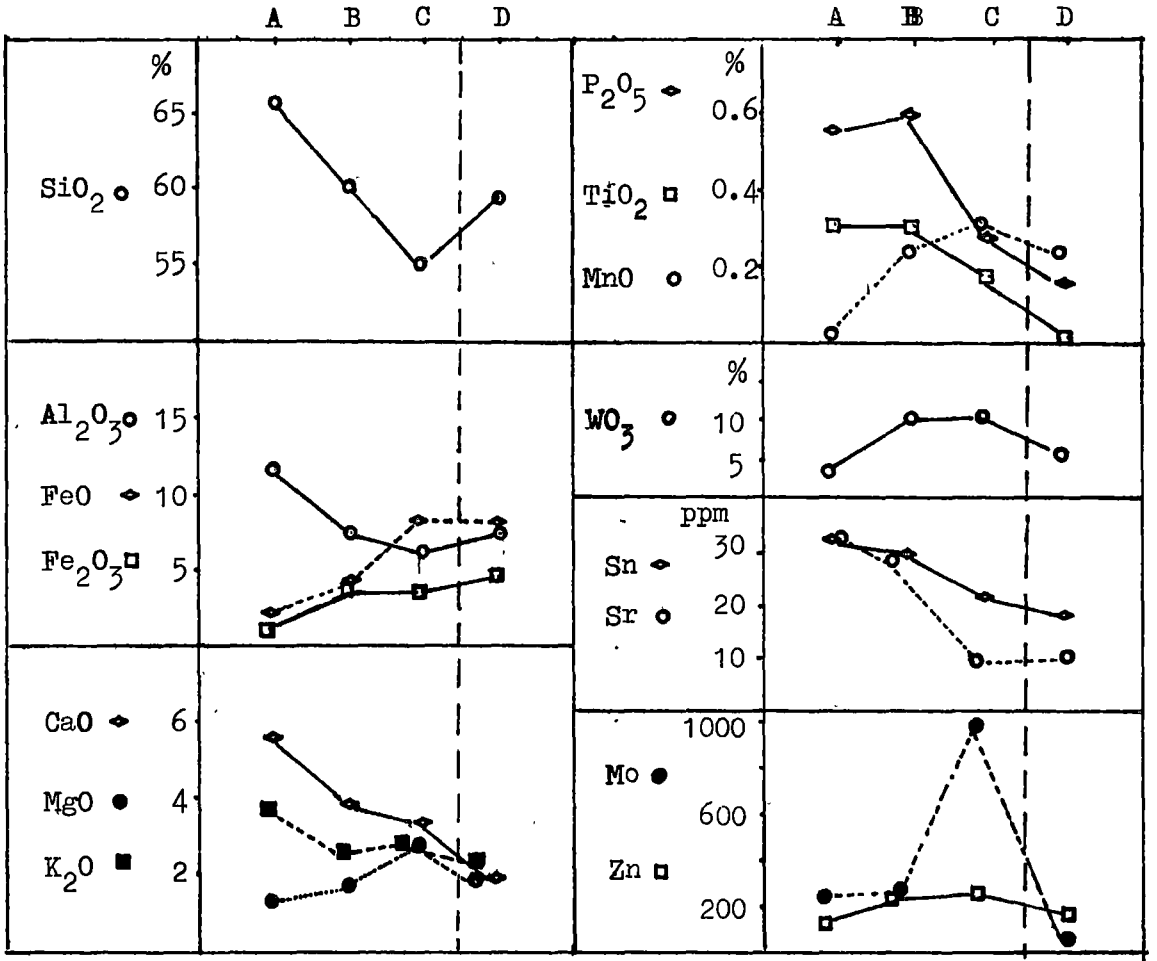

Location of samples and major changes in mineral assemblage

(A) 103066 = quartz-sericite-calcite(central core to quartz-mica zone)

(B) 103067 = quartz-muscovite-chlorite(intermediate part to ")

(C) 103068 = quartz-biotite-chlorite(outer rim of quartz-mica zone)

(D) 103063 = a small scale of the quartz-mica skarn in pyroxene-garnet skarn

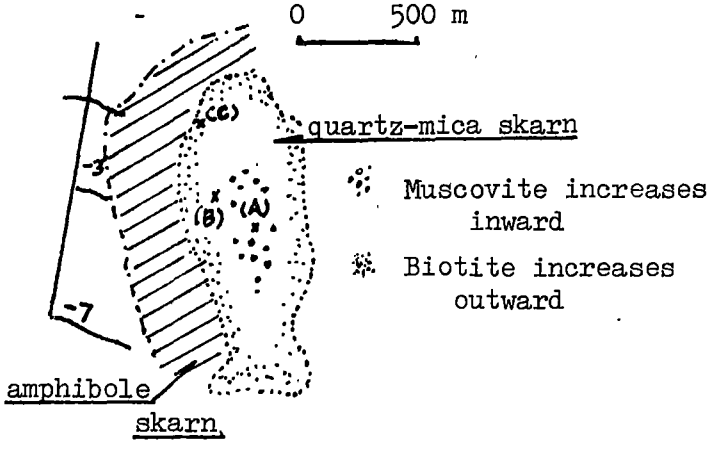

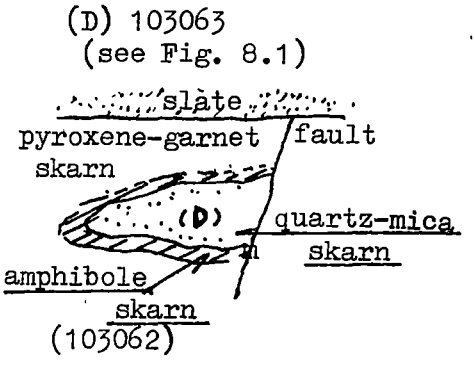

Table 7.5. Chemical compositions of typical quartz-mica skarn.

	103066	103067	103068	103063	Mean
SiO_2	65.68	59.55	54.99	58.37	59.65
TiO_2	0.31	0.31	0.18	0.09	0.22
Al_2O_3	11.56	7.36	6.35	7.39	8.17
Fe_2O_3	1.29	4.05	3.85	4.73	3.48
FeO	2.10	4.36	8.55	8.09	5.78
MnO	0.1	0.24	0.33	0.25	0.23
MgO	1.3	1.85	2.89	1.98	2.01
CaO	5.65	3.94	3.35	1.96	3.73
Na_2O	0	0.14	0	0	0.04
K_2O	3.8	2.53	2.73	2.6	2.92
P_2O_5	0.56	0.6	0.26	0.16	0.40
WO_3	4.1	10.1	10.88	6.9	8.0
LOI	4.92	4.3	4.5	8.42	5.54
Total	101.39	99.32	98.87	100.94	100.17
Trace elements(ppm)					
Sn	33.6	30.3	21.3	18.9	104
Zn	132.9	213.6	218.6	202.7	192
Cu	59.2	218.2	92.8	249.9	155
Ni	24.9	26.6	25.1	16.8	23
Sr	33.7	29	9.1	11	21
Rb	534.6	481.3	627.4	476.1	530
Th	0	0	0	0	0
Pb	11.7	391.9	23.5	58.8	121
Bi	362.8	8078.2	900.3	2415	2939
Mo	236.4	262.5	1416.1	79	498

Assemblage — Location(in quartz-mica zone)

103066 = quartz-sericite-calcite-chlorite-scheelite(cenral core)
103067 = quartz-muscovite-chlorite-scheelite(intermediate part)
103068 = quartz-biotite-chlorite-scheelite(outer rim)
103063 = small scale quartz-mica skarn(occurring in pyroxene-garnet skarn)

Table 7.6. Chemical gains and losses in the formation of the amphibole and mica skarns from pyroxene-garnet skarn.

	Anhydrous skarn	Hydrous skarn				
	pyroxene-garnet skarn mg/cc	amphibole skarn mg/cc	gain(+) loss(-)	quartz-mica skarn mg/cc	gain(+) loss(-)	*gain *loss
SiO_2	1426	1627	+201	1862.2	+436.2	+235
TiO_2	0.6	7.8	+7.2	8.4	+7.8	+0.6
Al_2O_3	76.9	169.3	+92.4	261	+184.1	+91.7
Fe_2O_3	140.7	186.9	+46.2	94.9	-45.8	-92
FeO	448.6	450.1	+1.5	155	-293.6	-295.1
MnO	49.3	22.9	-26.4	6.8	-42.5	-16.1
MgO	26.4	50.5	+24.1	62.3	+35.9	-11.8
CaO	789.3	357.1	+432.3	133.6	-655.7	-223.5
Na_2O	0	14.9	+14.9	1.6	+1.6	-13.3
K_2O	9.6	25.7	+16.1	93.6	+84	+67.9
P_2O_5	1.9	5.3	+3.4	14.6	+12.7	+9.3
WO_3	3.1	77.5	+74.4	260.4	+257.3	+82.9
LOI(H_2O,CO_2)	109.4	122.1	+12.7	141.7	+32.3	+19.6

* On assumption that the quartz-mica skarn replaced the amphibole skarn, and amphibole skarn replaced the pyroxene-garnet skarn; values for each rock are averages from Tables 7.5 and 7.6.

Fig. 7.4 Variation in chemical compositions of different skarn in the M1 skarn orebody (based on Appendix 7.2).

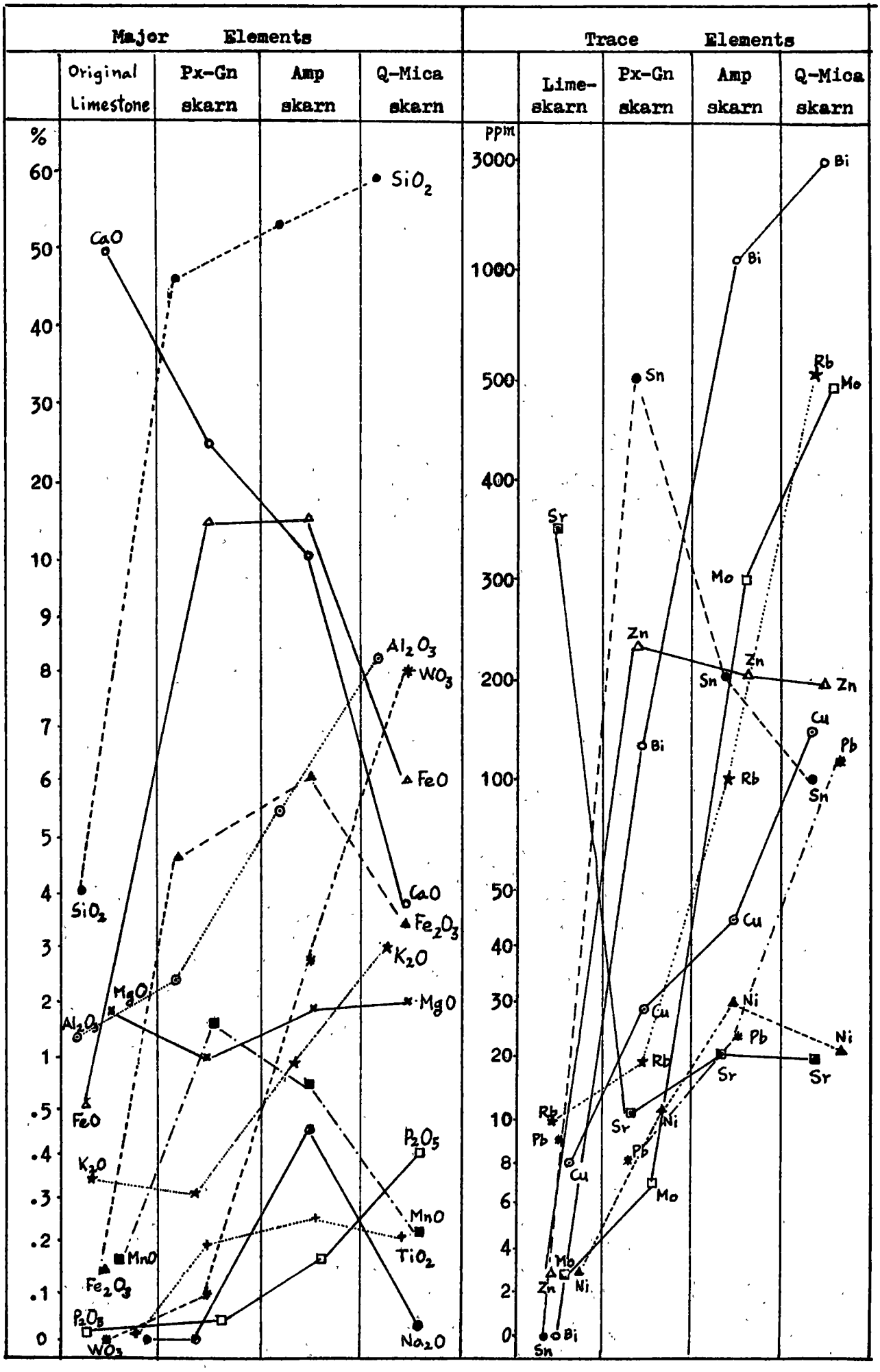

Fig. 7.5 Variation in chemical compositions of three different skarns within the M1 ore body plotted on A C F & A'K F diagrams.

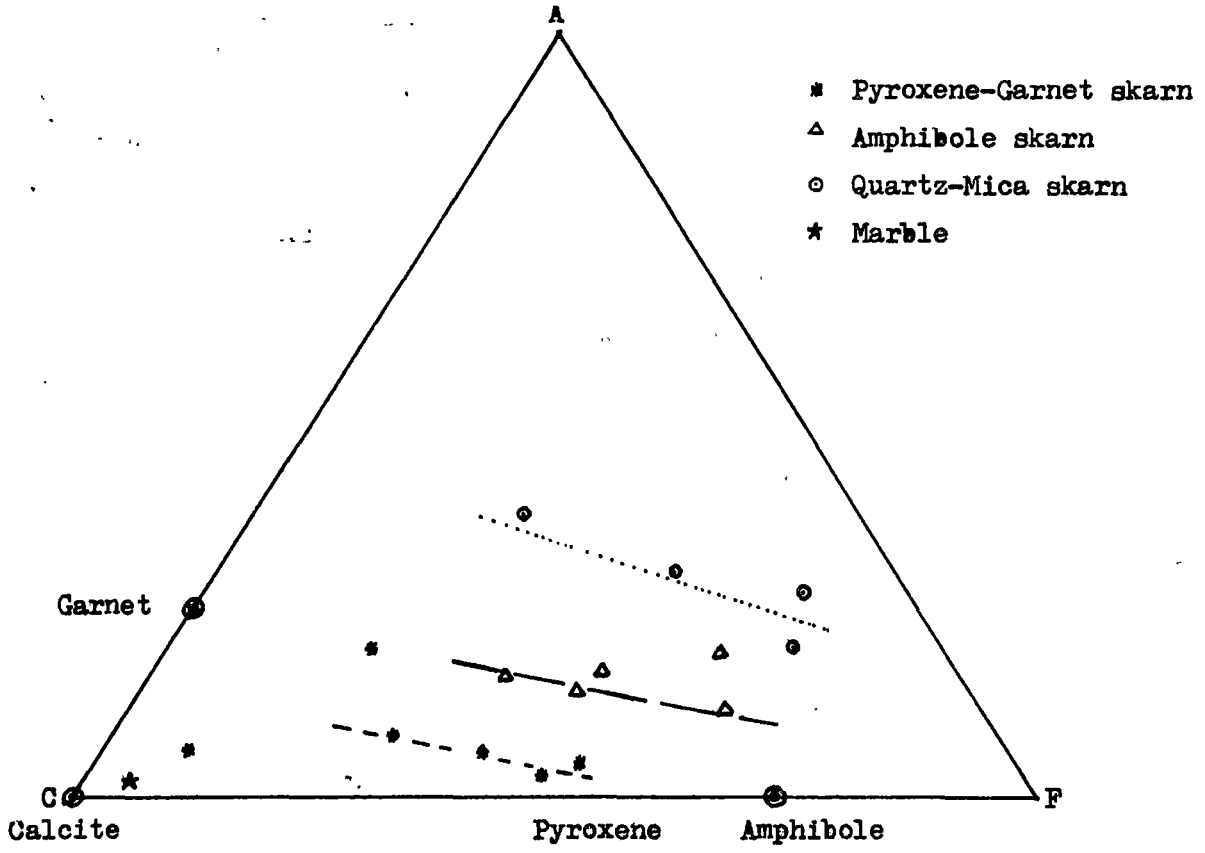

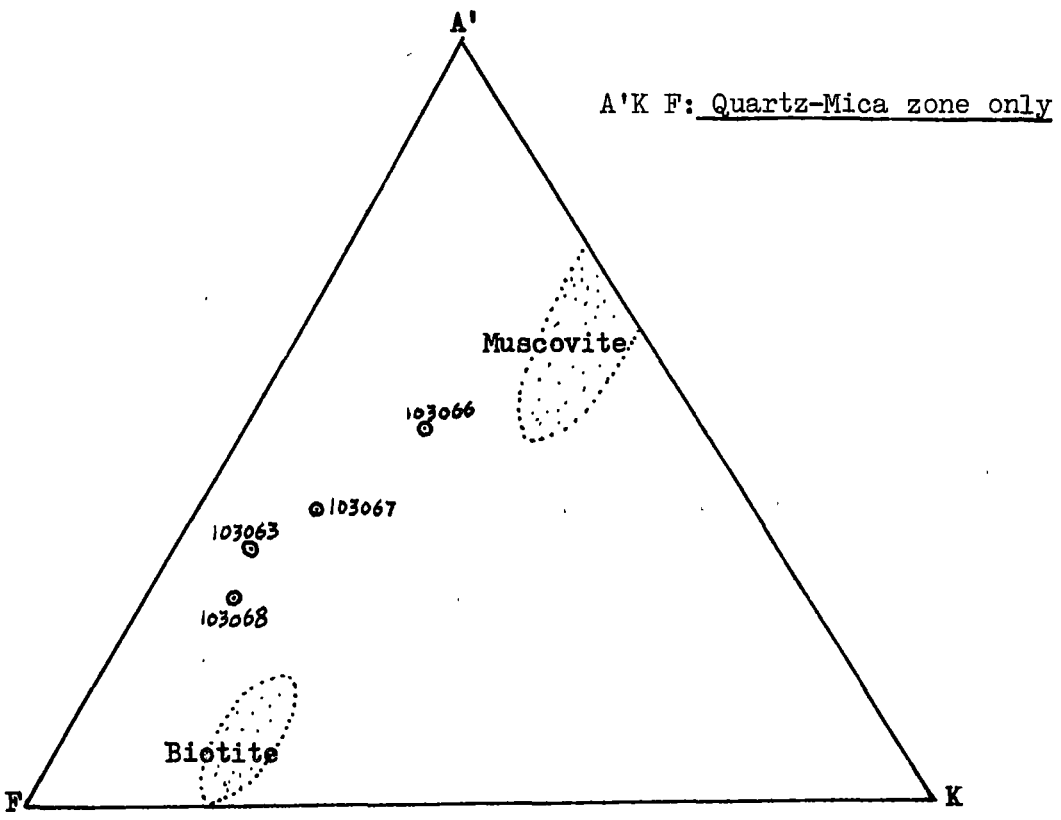

8. A DETAILED STUDY OF SMALL SCALE ZONING

Small (centimetric) scale mineralogical zoning is observed in two places. One(Fig. 8.1a) occurs in a relict block of the pyroxene-garnet skarn within the quartz-mica zone on the 1st level, the other(Fig. 8.2) occurs in the pyroxene-garnet zone near the amphibole zone on the 7th level. The former one was used for comparing chemical compositions of the amphibole and the quartz-mica skarns in the small scale zoning(103062) to the whole M1 skarn(Tables 7.4 & 7.5). The latter was studied more systematically, since the small scale mineralogical zoning mirrors the zoning of the whole of the M1 orebody. This zoning is described in detail to understand the possible mechanism by which the whole orebody formed.

The small scale zoning shows almost the same mineralogical changes and chemical changes as does the whole of the M1 orebody. Samples were taken from 6 different zones, which can be classified by different colours, as shown in Fig. 8.2.

The small scale mineral zonation is parallel to a fracture(a minor joint filled with fine quartz veinlets) which was obviously a solution channel from which the zones developed. By analogy, the quartz-muscovite zone of the M1 orebody may have been the main feeder zone to the whole M1 skarn system.

8.1. Petrography and Mineral Chemistry

The major mineralogy of the samples and the zones is represented in Table 8.1. The detailed petrography of the samples can be found in Appendix 8.1. Significant differences in the occurrences of minerals within each zone between the small scale zoning and the whole of the M1 orebody are as follow:

	Small scale	M1
Chlorite	in quartz-mica zone	both in quartz-mica and amphibole zones
Epidote	in quartz-mica zone (muscovite-rich)	mainly in pyroxene-garnet skarn within the pyroxene-garnet zone
Pyrite & Native Bismuth	localized in amphibole skarn	in all zones

These differences may be attributed to repeated or more extensive overprinting by late fluids in the M1 orebody. Some features of the mineralogy of the small scale zones are as follows.

The late pyroxenes of Part E tend to contain Al_2O_3 while those of Part F do not(Appendix 8.2). This is in keeping with observations from the M1 skarn study(section 6.2). The late pyroxenes also show a narrow range of Mg content(Appendix 8.5).

The garnet of Part E is partly replaced by late pyroxene. The few grains of Part E garnet differ from these in Part F in having no titanium (Appendix 8.3). The garnets and coexisting pyroxenes of Part F have $K' > 1$ and show a wide variation, indicating lack of equilibrium. However, the Part E garnets, even though few in number, apparently show a linear distribution of the K' values, indicating an approach to grain-to-grain chemical equilibrium during growth of the late skarns(Appendix 8.4).

Amphiboles from Part C to Part F show a range of chemical composition (Appendix 8.7). Sodium, magnesium and calcium vary most in Part D which is the main portion of the amphibole-rich zone. Silica and aluminium contents have the widest range in Part C which is a transitional zone between amphibole-rich and biotite-rich rocks. The Mg and Fe contents vary inversely and continuously from Part C through D and E to Part F. Dramatic changes in pressure and temperature are most unlikely over such a short distance, indicating that the reacting fluid had a declining Mg/Fe ratio

from the fracture outward. SiO_2 and Al_2O_3 also vary inversely but not systematically. The variation in a single amphibole crystal from core to rim in Part F(Appendix 8.8) shows that silica and aluminium again vary inversely and the crystal is silica-enriched and aluminium-depleted at the rim. There is no systematic behaviour of the Mg/Fe ratio, indicating that the Mg/Fe ratio across the zonal system is not a time sequence.

The compositions of biotites in Parts B and C are slightly different, those of Part C having more CaO and lower Mg/Fe ratios than these in Part B(Appendix 8.9). Biotites of Part C are more like these of the M1 quartz-mica skarn than these of Part B. Most of the biotites from small scale quartz-mica skarn have Na_2O, unlike the M1 biotites(Appendix 8.10).

The compositions of muscovites in Part A have slightly lower SiO_2 and higher TiO_2 and CaO contents(Appendix 8.11) than those in the M1 orebody.

Chlorite appears to be an alteration product of biotite. It does not extend into Part C where fresh biotite can be observed. The Mg/Fe ratio is considerably higher in Part A than in Part B, in sympathy with the trend established in biotites of Part B and Part C, and the amphiboles of Parts C to F.

8.2. Chemical Changes

The mineralogical zones and their spatial arrangement suggest that Part E is derived from Part F, Part D is derived from Part E, Part B is derived from Part D(Part C being an interim stage), and Part A from Part B. The resulting changes, calculated assuming constant volume, are shown in Table 8.3.

Alteration of that section of Part E that is close to Part D appears to involve addition of Si, Al, Fe, K, P and W, and depletion of Mg and Ca. For the formation of the amphibole skarn(Part D), Al, Fe, Mg, K and W were added, and Si, Mn and Ca were removed. Elements added to derive the

quartz-biotite skarn(Part B) from the amphibole skarn(Part D) were Si, Ti, Al, Fe, Mg, K, P and W, whereas elements lost were Fe, Mn and Ca. Alteration of Part B to Part A was achieved by addition of Si.

The steady changes in certain trace elements, e.g. Sn, Mo and Zn, tend to confirm the chemical continuum(Fig. 8.4). Higher contents of Zn in the Parts E and F, which have no Zn minerals, than these in Parts B and D, which have sphalerite, indicates the high contents of Zn in pyroxene and garnet crystals. Rb is fixed in mica, and is probably depleted in the central zones by mica alteration. The depletion of Sn follows the pattern of the M1 orebody.

As shown in Fig. 8.3 and Table 8.2, the changes across the 6 zones are variable, but if the average compositions of the major mineralogical zones are compared(Fig. 7.4), the trends of increase and decrease of elements from the mica skarn to pyroxene skarn are more or less the same as shown in the M1 orebody. Thus the small scale zoning provides clear information on the evolution of the zoned skarns in the M1 orebody, and the chemical changes taking place during formation of the different skarns, as shown in Fig. 8.5.

Fig. 8.1a. A sketch showing mineralogical zonation in a relict block of the pyroxene-garnet skarn within the quartz-mica zone on the 14th block of the Sangdong level.

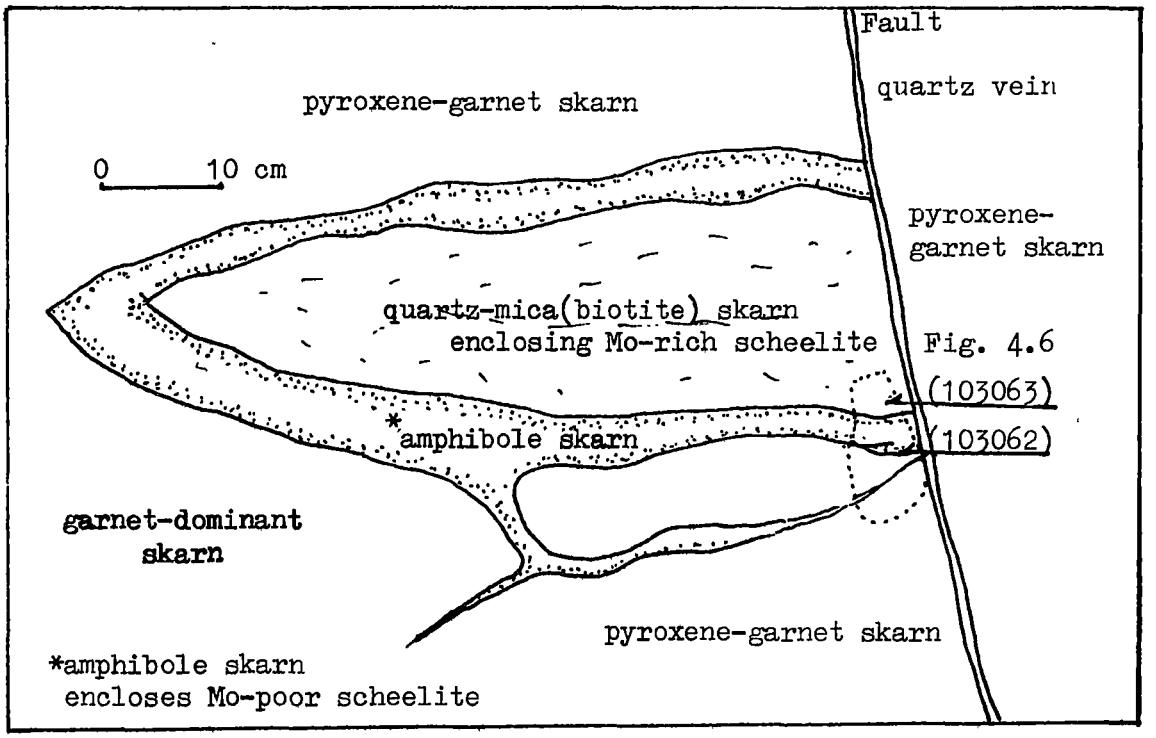

Fig. 8.1b. Location of small scale zoning.

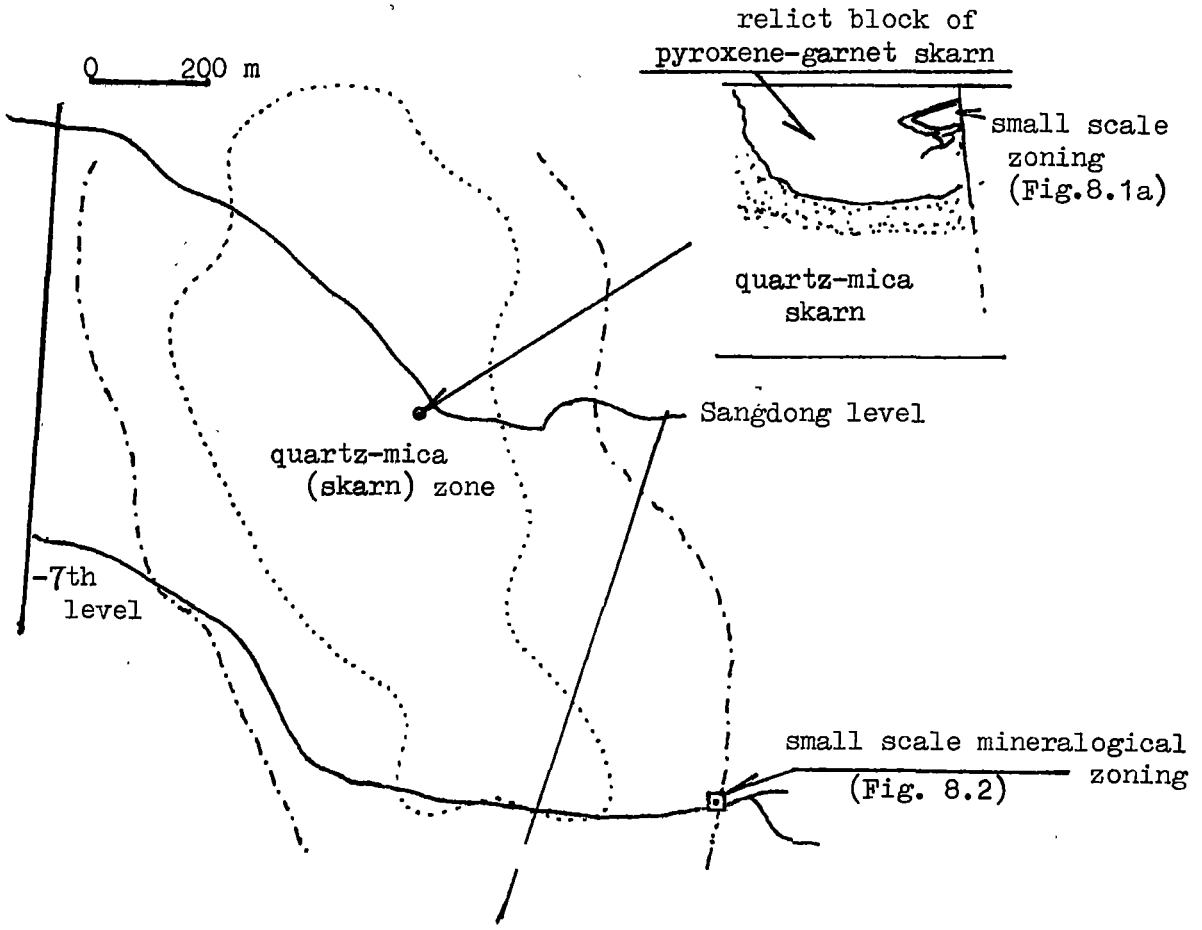

Fig. 8.2. A sketch showing small-scale mineralogical zoning in the pyroxene-garnet skarn zone at the 7th level.

Square(□) indicates approximate size and location of samples.

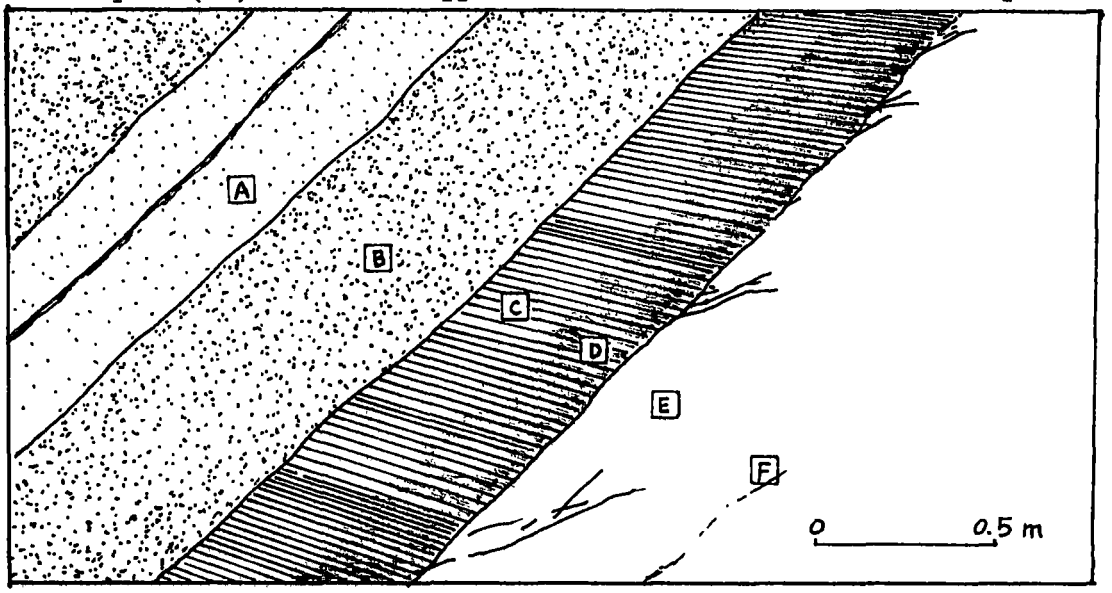

A = 103107 (**quartz-muscovite skarn**) : pale grey with brown tint

B = 103108 (**quartz-biotite skarn**) : brownish grey colour

C = 103109 (**quartz-amphibole-biotite skarn**) : brownish black

D = 103110 (**amphibole-quartz skarn**) : dark black

E = 103111 (**pyroxene-garnet skarn**) : dark green

F = 103112 (**pyroxene-garnet skarn**) : pale green and brown

Fine quartz veinlets along a joint

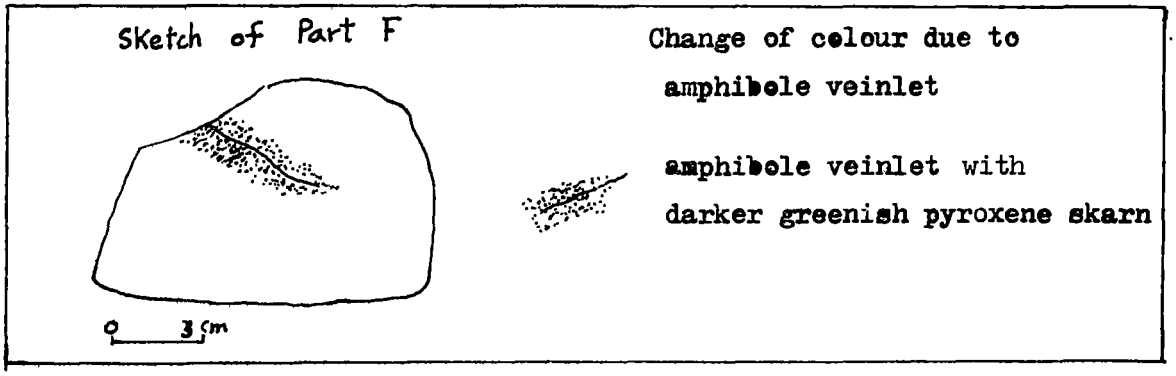

Table 8.1. Summary of mineralogical variation in different zones of the small scale zoning on the 7th level.

	F	E	D	C	B	A
Pyroxene	@@@@@@@@	@@@@@@@@				
Garnet	@@@@@@@@	@@@				
Amphibole			@@@@@@@@	@@@		
Biotite				@@@@@	@@@@@@@@	
Muscovite						@@@@@@@@
Chlorite					@@@@@@@@	@@@@@@@@
Fluorite	*	* * *	* * * *	* * * *	********	********
Calcite		* *	***	***	***	***
Scheelite	*	* *	***	****@**@@	**@*@*@*@	@@@@@@@@
Apatite			***	* * * *	********	********
Quartz			*******	**@*@*@**	@@@@@@@@	@@@@@@@@
Epidote						* * * *
Magnetite			****			
Pyrrhotite	*	*	********	* * * *	* * * *	* * * *
Pyrite			* * * *			
Bismuthinite	* *	* *	*******	*		********
Sphalerite			***			
Galena			*			
Native Bismuth			* *			

Major component: @@@@ > @@@@ > @*@* > @@@@

Minor component: ***** > * * * > *

Fig. 8.3. Variations of major elements across the 6 zones.

-•- represents chemical compositions in the 6 zones.

o represents average composition in terms of major 3 mineralogical zones, i.e. A + B = quartz-mica zone, C + D = amphibole-rich zone, E + F = pyroxene-garnet zone.

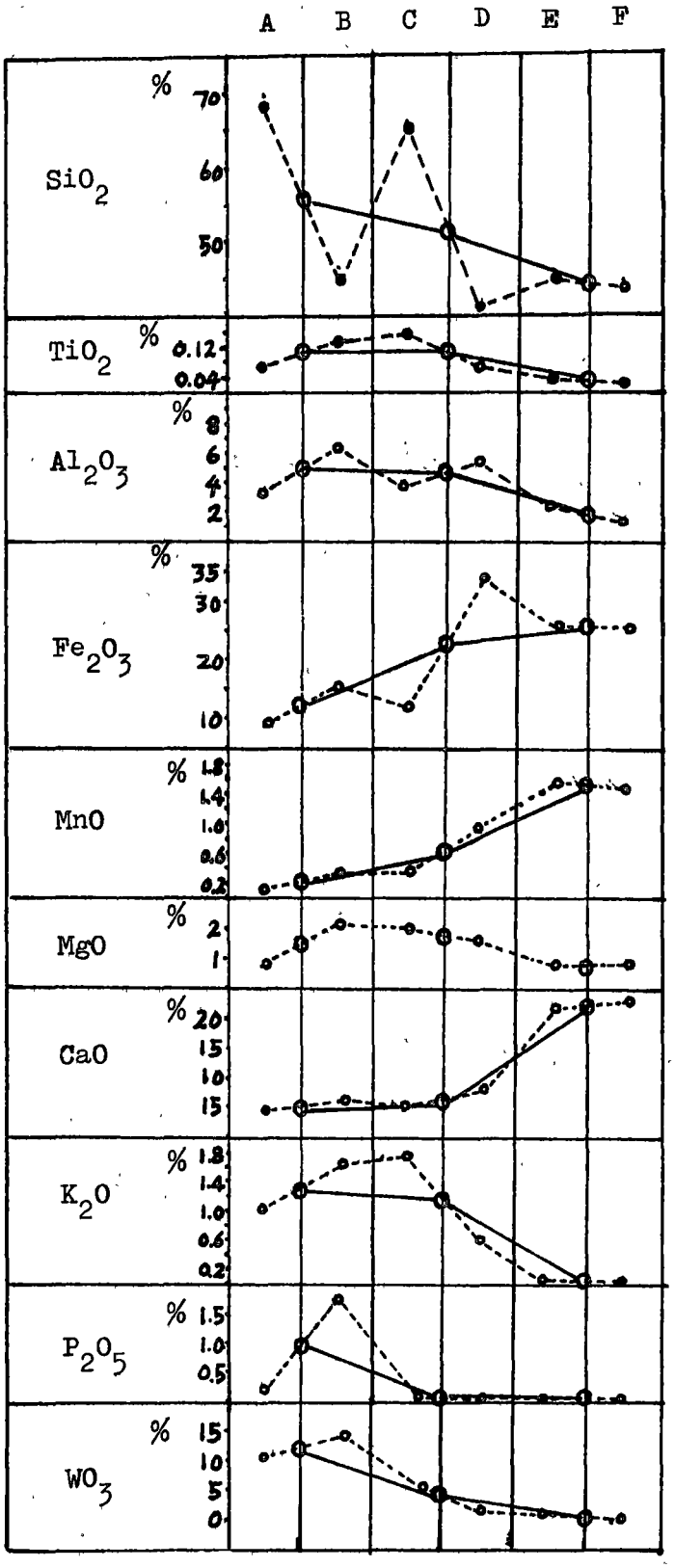

Table 8.2. Chemical compositions of different zones in the small-scale zoning.

	103107 (A)	103108 (B)	103109 (C)	103110 (D)	103111 (E)	103112 (F)
SiO_2	68.71	45.14	64.85	41.27	44.66	43.96
TiO_2	0.06	0.14	0.16	0.07	0.04	0.03
Al_2O_3	3.06	6.16	3.95	5.16	2.26	1.16
Fe_2O_3	7.71	15.59	12.11	34.92	26.72	25.75
MnO	0.16	0.35	0.36	0.98	1.58	1.55
MgO	0.81	2.21	2.02	1.73	0.91	0.97
CaO	4.55	6.06	5.26	8.3	21.71	24.92
Na_2O	n.d	n.d	n.d	n.d	n.d	n.d
K_2O	1.03	1.65	1.73	0.64	0.09	0.01
P_2O_5	0.26	1.93	0.13	0.05	0.1	0.06
WO_3	10.42	14.87	5.37	1.38	1.23	tr
LOI	1.62	3.08	2.63	5.49	1.02	1.32
Total	98.39	99.78	98.57	99.99	100.03	99.73
Trace elements(ppm)						
Rb	236.18	331.7	428.2	99.3	2.1	1.3
Sr	17.04	15.8	24.3	16.6	9.2	6.8
Th	0	85.7	0	0	20.2	0
Zn	34.6	132.3	138	264.5	230.9	284
Cu	318.7	211.6	64.8	299.5	61.7	16.2
Pb	379.3	23.0	24.7	26.8	0.3	19.6
Ni	11.3	32.1	31.1	28.1	12	4.8
Sn	36	42.3	44.2	123.5	185.3	260.7
Bi	3798.5	0	6.28	1457.6	58.5	185.2
Mo	699.5	683.6	323.2	141.1	36.1	1.5
W	%	%	%	%	%	236.2

Table 8.3. Chemical gains and losses in the formation of a small zoning. Gain(+) and Loss(-)

	Part E derived from Part F	Part D derived from Part E	Part B derived from Part D	Part A derived from Part B
SiO_2	+23	-239	+120	+731
TiO_2	0	+1	+2	-2
Al_2O_3	+38	+83	+31	-96
Fe_2O_3	+32	+175	-600	-263
MnO	+1	-24		-6
MgO	-2	+23	+15	-44
CaO	-109	-451	-69	-47
K_2O	+3	+17	+31	-19
P_2O_5	+1	-1	+58	-52
WO_3	+35	+1	+418	-138

wt % x specific gravity
(calculated based on Table 8.2)

	Part A	Part B	Part C	Part D	Part E	Part F
SiO_2	2130	1399	2010	1279	1518	1495
TiO_2	2	4	5	2	1	1
Al_2O_3	95	191	122	160	77	39
Fe_2O_3	220	483	375	1083	908	876
MnO	5	11	11	30	54	54
MgO	25	69	63	54	31	33
CaO	141	188	163	257	708	847
K_2O	32	51	54	20	3	0.3
P_2O_5	8	60	4	2	3	2
WO_3	323	461	166	43	42	7

Fig. 8.4. Element changes from part A to part F.

- Tin
- Molybdenum
- Rubidium
- Zinc

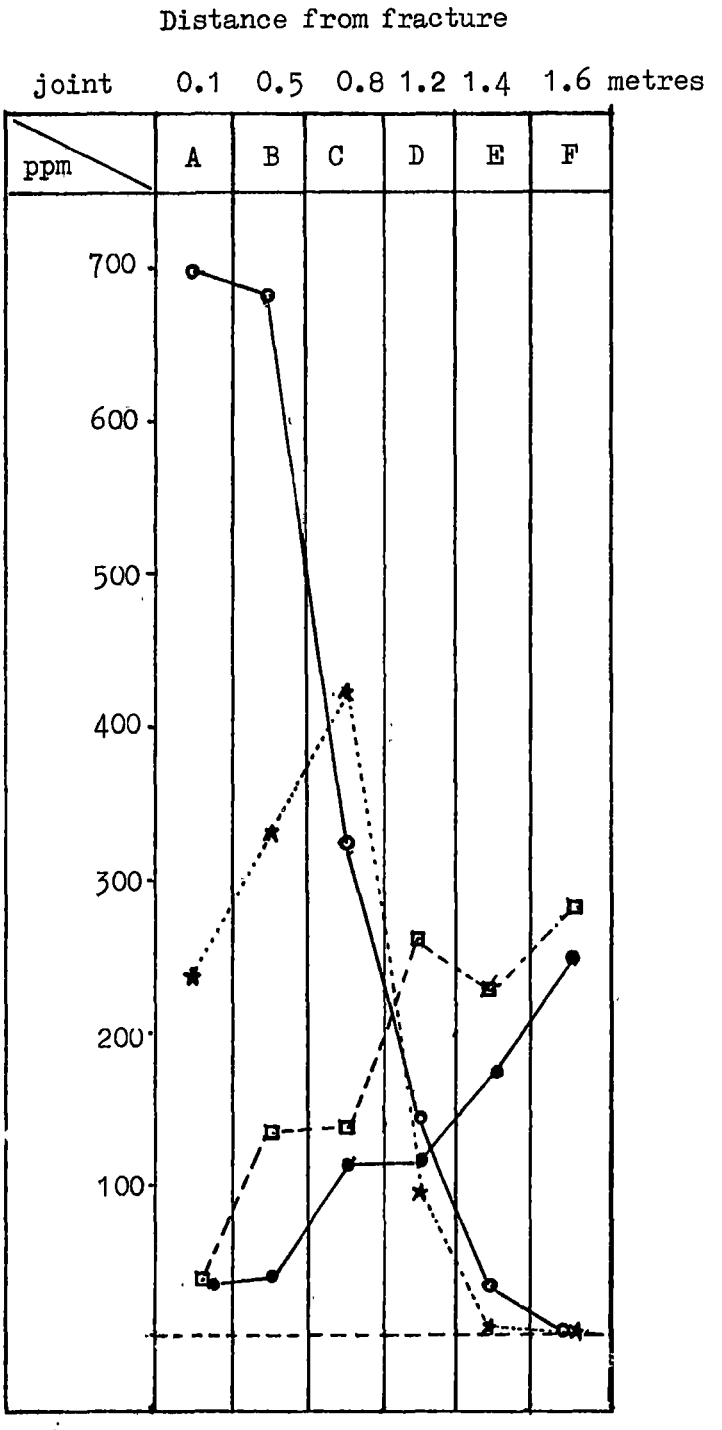

Fig. 8.5. A Schematic diagram showing formation of small-scale and major zones at the Sangdong deposit.

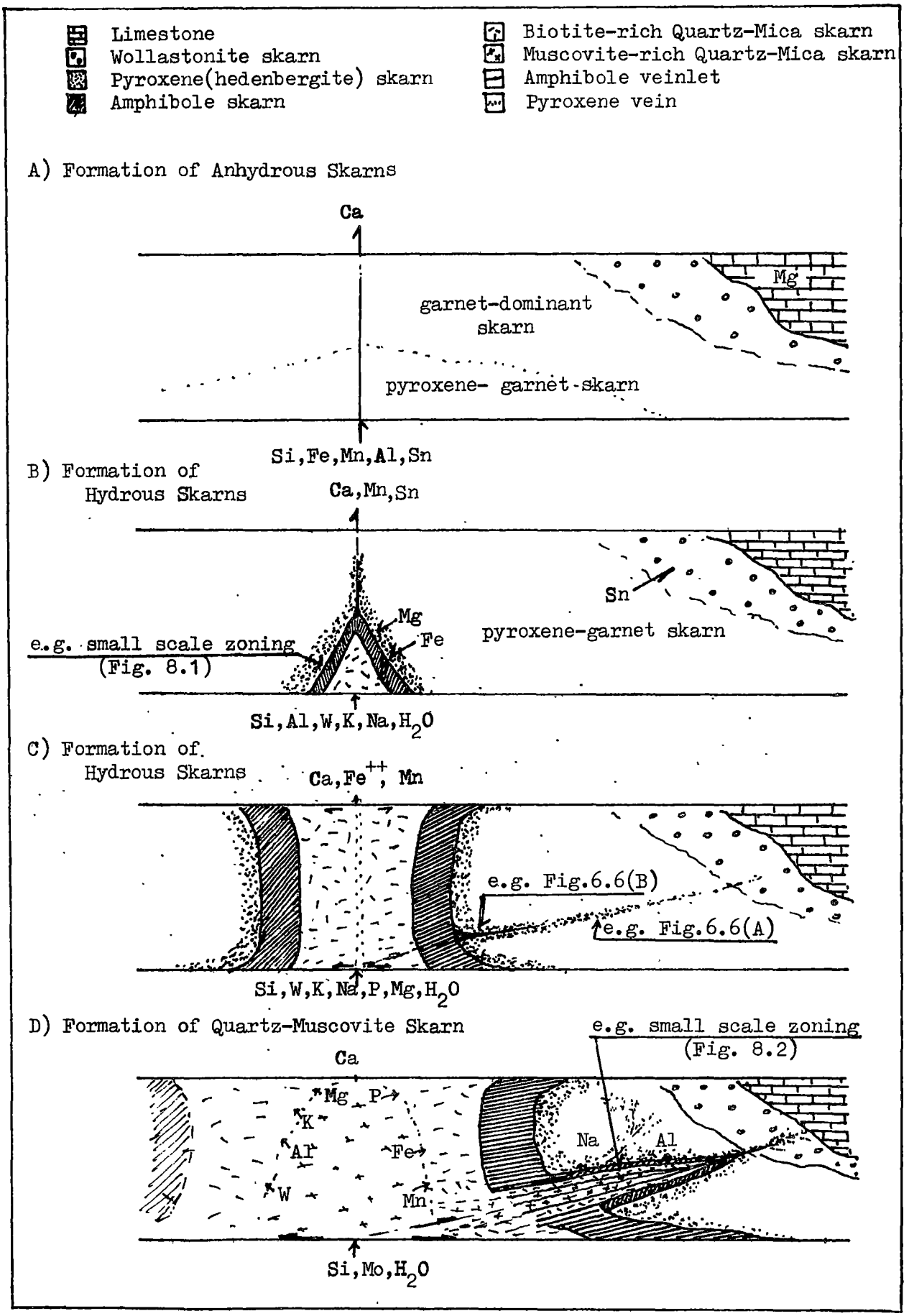

9. ALTERATION OF THE SLATE HOST

Economic tungsten mineralization is confined to an ellipsoid with a minor axis of about 1.2 km wide. However, thermal metamorphism, which is well represented by skarn alteration in the Hwajeol Formation, extends up to 4 km west of the mine(Fig. 9.1).

Within the thermally metamorphosed area, the Pungchon Limestone is recrystallized, and the interbedded limestone layers in the Myobong Slate are almost changed to marble. In this study, mineralized slate is defined as biotite hornfels in which interbedded limestone layers are altered to skarn and related to tungsten mineralization.

The discussion of elemental changes has centered on the limestone units but the slates in and near the ore zones are also altered.

The slate in the mineralized ellipsoid(Fig. 9.1) is characterized by a chocolate colour, easily distinguishable from the pale bluish grey of the slate away from tungsten mineralization. Many samples of the Myobong slate were analysed by Kim(1976). In the present study, a limited number of samples were taken from a level about 20 m below the uppermost interbedded limestone outside of tungsten mineralization as well as within the ore zone.

9.1. Mineralogy of The Slate in Mineralized and Unmineralized Zones

The Myobong Formation has been described as shales or mudstones intercalated with a few impersistent, thin sandy beds in the middle, and thin limestone beds in the upper parts of the formation(Reedman and Um, 1976). A quartzitic horizon called 'silicified slate' by mine geologists lies about 6 m below the M1 orebody and may have originally been sandstone. White-grey cherty layers occur at both the top and bottom boundaries of the skarn orebodies and may have been calcareous shale or mudstone. Apart from these rock types, the Myobong Formation is mainly composed of slate.

Fresh surfaces of unmineralized slate displaying a sheen resulting from the parallel orientation of mica. In thin section, the slate is composed of microcrystalline porphyroblasts in an oriented micaceous matrix. The main mineral components identified by electron-microprobe are as follows:

Hematite of irregular forms the largest grains(about 0.1 mm radius). Chlorite is flaky, green, pleochroic and of similar composition to ripidolite. Rutile is frequently observed as oval grains with a radius of about 0.05 mm. Apatite occurs as subhedral, colourless crystals showing very low birefringence, and with a radius of about 0.03 mm. Muscovite occurs as single flakes out of alignment with the oriented micas. Ilmenite is irregular in form.

All the above minerals occur, in general, as single porphyroblasts in a matrix of biotite, plagioclase and quartz. The biotite occurs as small fascicular aggregates, parallel to sub-parallel, with plagioclase(mainly albite) and quartz. Quartz also occurs rarely as veinlets replacing all other minerals.

All these components in the unmineralized slate are assumed to have formed during regional metamorphism.

The regular alignment of minerals observed in the unmineralized slate does not occur in the mineralized slate which shows a hornfelsic texture. Mineralized slate has quartz, biotite, chlorite, plagioclase, zircon, tourmaline, orthoclase, apatite, calcite, ilmenite and pyrite.

Quartz is closely associated with biotite, and both are major components of this rock. The biotite is reddish-brown in colour, irregularly shaped and has a reticulate texture with quartz. The biotite is responsible for the chocolate colour of the slate in the mineralized zone. Euhedral apatite occurs locally in the matrix of biotite-plagioclase aggregates.
The chlorite is compositionally a ripidolite. The plagioclase varies from

anorthite to oligoclase. Zircon(up to 0.06 to 0.07 mm in grain size), tabular tourmaline, calcite and orthoclase are absent in the unmineralized slate but found in mineralized slate. Rutile and ilmenite occur in the same way as in the unmineralized zone. Pyrite is locally abundant and chalcopyrite is occasionally observed while sulphides were not observed in the unmineralized zone. Differences in mineralogical compositions between mineralized and unmineralized slates are given in Appendix 9.2.

9.2. Geochemical Studies

Kim(1976) has classified the Myobong Formation in the mineralized zone into four groups according to chemical composition, as follows:

Group I : magnesian-pelitic rocks

Group II : hornblende-quartz-feldspathic rocks

Group III : calc-silicate rocks

Group IV : calcareous rocks

The classification may be acceptable, but the distribution of these four groups in the Myobong Formation was not clearly described.

Most of the Myobong Formation is generally composed of group I and group IV, however, group II and group III are distributed in small areas confined to the mineralized zone. Group I consists of biotite hornfels in the mineralized zone at the mine and is called slate by local mining geologists. Group IV corresponds to several interbedded limestone layers which have locally become tungsten orebodies, that is the M1 and F. orebodies; the chemical changes and alteration of these rocks have already been discussed. Group II and III appear to correspond to the cherty rock, including the'silicified slate', and local occurrence of thin lenticular layer or nodules of amphibole in the mine slate. Because of the difficulty in finding the equivalent horizon as group II and III in the unmineralized zone, a chemical comparison between unmineralized and mineralized slate

is restricted to group I rocks. The chemical data of Kim(1976) indicate that group I and group II in the mineralized zone are very similar to each other(Table 9.2).

Comparing the mineralized and unmineralized rocks of group I(Table 9.1) it can be seen that there are significant differences in K, Na, Ca, Al, Si, Rb and Cu contents between two zones. The average chemical composition of the mineralized slate is much lower in SiO_2, Fe_2O_3 and Cu, and higher in FeO, CaO, K_2O, Al_2O_3, Na_2O and Rb than unmineralized slate. Ratios of FeO/Fe_2O_3 suggest a more reduced environment in the mineralized zone(Appendix 9.1). The higher content of Cu in the unmineralized zone may be due to the effects of copper mineralization related to the Eopyeong Granodiorite, since specimens of the unmineralized slate were located close to the Eopyeong copper deposit. Depletion of silica content in the mineralized slate may indicate that sustantial amounts of silica were removed to form skarn minerals.

The tungsten content of the mineralized slate tends to be higher than that of unmineralized slate, as described by Kim(1976). Scheelite grains are frequently observed along fine quartz veinlets in the mineralized slate(Fig. 9.3), and this could explain the unusually high content of tungsten in the slate. Hundreds of samples have been studied while the author worked in this mine, and it was concluded that the high tungsten values can be attributed to microstructures containing scheelite or skarn lenses, or very thin veinlets, or analytical contamination. Kim(1976)'s data for tungsten and SiO_2 contents of the mineralized slate(Fig. 9.4) could be explained by either addition of quartz-scheelite veinlets(high SiO_2) or development of skarn lenses(low SiO_2).

9.3. Formation of Cherty Rocks

A cherty rock commonly lies on the boundary between slate and skarn, but it also occurs alongside minor cross-cutting structures(Figs. 9.5 and 9.6). Samples from one of these exposures show that they have similar chemical compositions except for iron and calcium(Table 9.3). This difference might be due to a difference in original rock compositions(e.g. the cherty rock cross-cutting slate was derived from slate only, while the cherty rock lying on the boundary of slate was derived from the mixture of slate and calcareous beds). The sample(103129) of the cross-cutting structure shows significant differences in Fe, Ca and K compared to the slate. The removal of K and Fe from the slate in forming the cherty rock may be significant processes in providing a source of these elements for the mica-rich zone, and addition of Ca suggests that substantial transport of Ca took place.

Fig. 9.1. Outline of skarn and scheelite mineralization in the Sangdong mine area(based on exploration drilling).

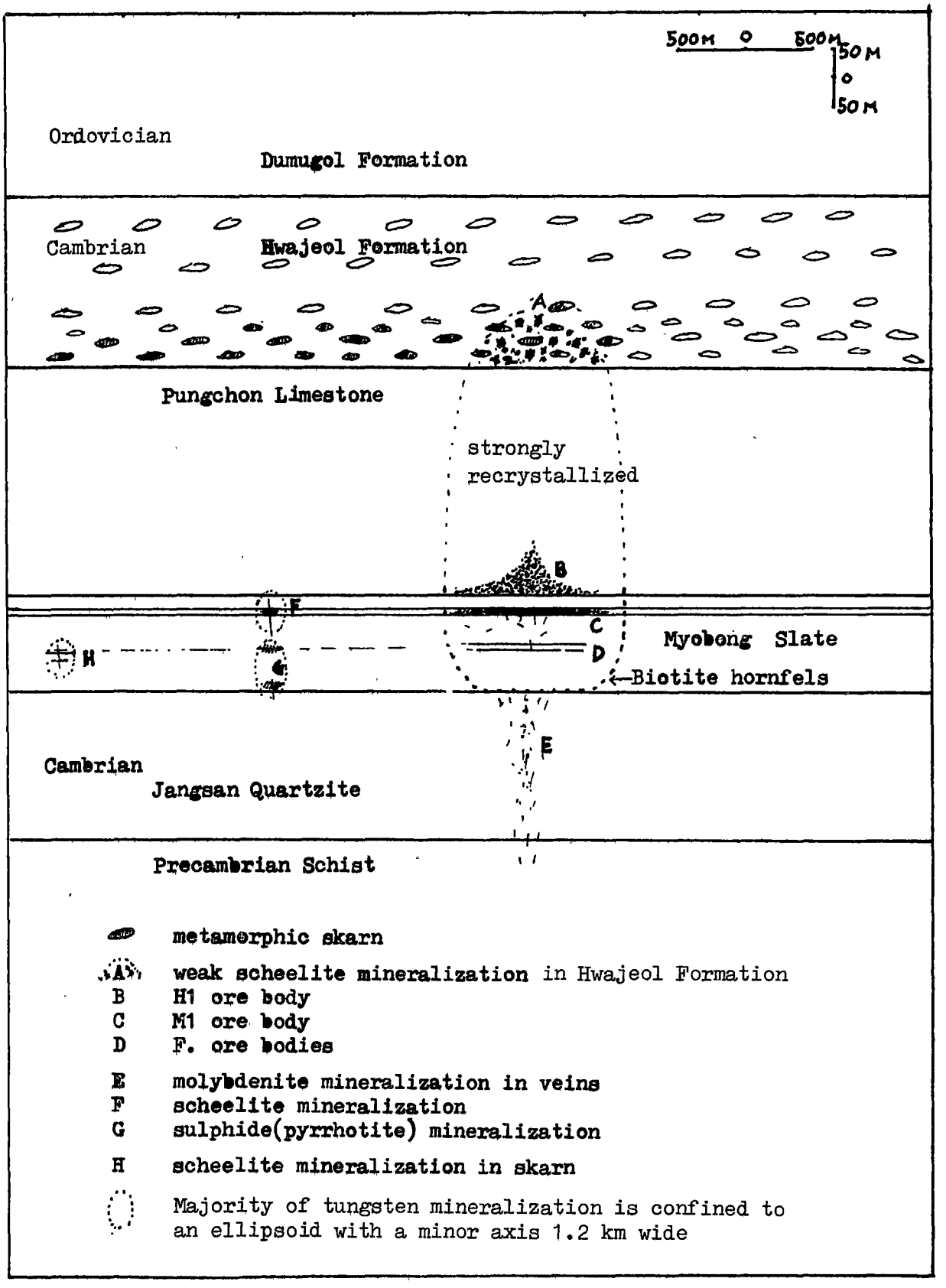

Fig. 9.2. Typical slate.
103114, -7th level, crossed polars.
represent 0.1 mm.

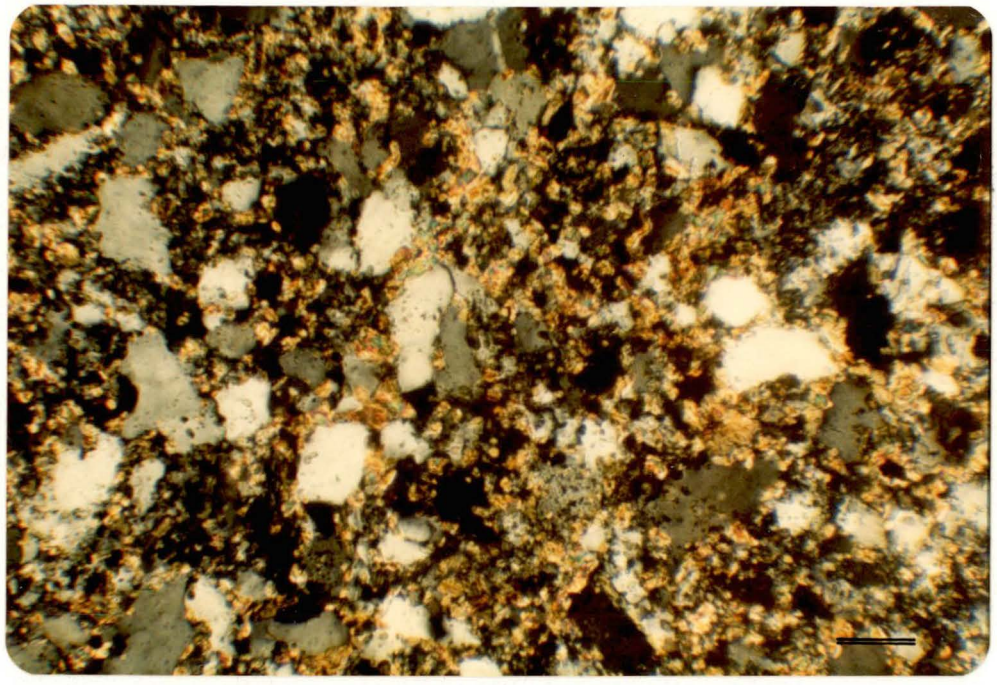

Fig. 9.3. Scheelite in quartz veinlets in slate.
103114, -7th level, crossed polars.
represent 0.1 mm. Scheelite is in

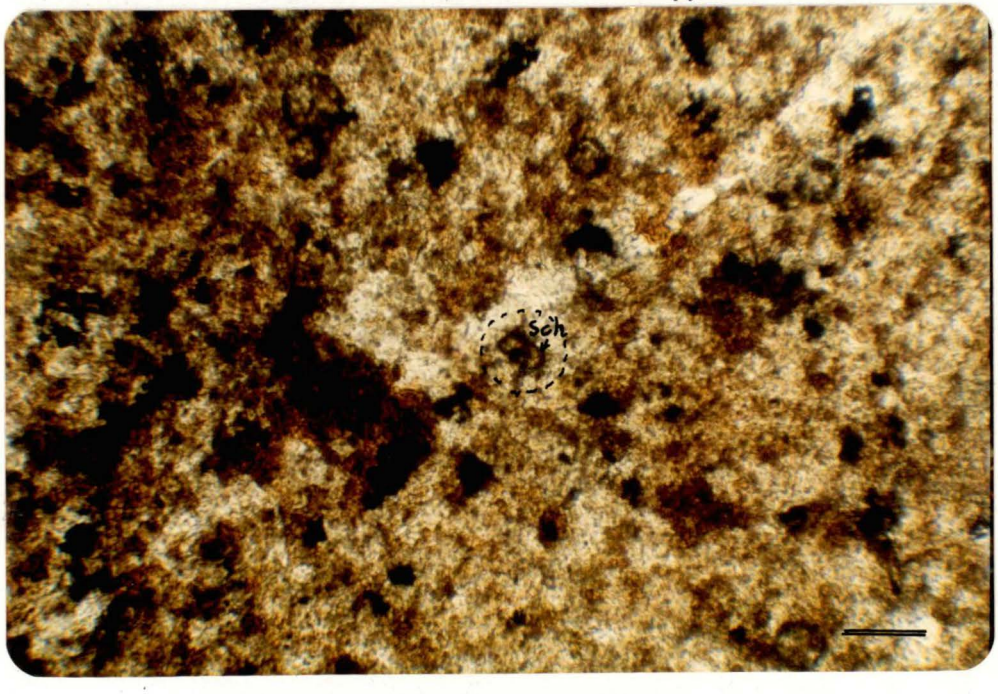

Table 9.1. Chemical compositions of mineralized and unmineralized Myobong slate(analysed by XRF).

	Unmineralized zone				Mineralized zone				
	103070	103071	103143	Mean	103076	103072	103073	103074	Mean
SiO_2	60.44	71.57	61.99	64.67	54.76	51.71	63.37	57.56	56.85
TiO_2	1.04	0.85	1.09	0.99	0.82	1.38	1.07	1.69	1.24
Al_2O_3	16.64	11.39	15.0	14.34	18.64	18.26	15.85	15.01	16.94
Fe_2O_3	3.12	2.83	10.13	2.98	1.44	0.49	1.27	1.69	1.22
FeO	0.32	4.65		4.99	4.98	12.43	5.61	8.98	8.0
MnO	0.09	0.04	0.10	0.08	0.09	0.16	0.11	0.16	0.13
MgO	4.57	1.79	4.68	3.68	3.31	3.40	4.16	5.5	4.09
CaO	0.24	1.25	0.55	0.68	3.22	2.26	1.04	0.36	1.72
K_2O	4.0	2.84	3.93	3.59	4.5	7.7	5.09	5.82	5.78
Na_2O	n.d	0.49	0.45	0.31	3.13	1.19	0.88	n.d	1.3
P_2O_5	0.13	0.24	0.13	0.17	0.25	0.2	0.15	0.11	0.18
LOI	4.49	3.81	3.46	3.92	2.99	2.99	2.31	3.78	2.84
Total	100.08	101.75	101.53	100.9	98.14	101.46	100.91	100.09	100.65
Trace elements(ppm)									
Rb	161.5	127.6			788.4	367.2	809.6		
Sr	21.9	35.8			166.9	45.8	19.0		
Th	14.7	12.6			3.1	22.1	n.d		
Zn	63.7	102.2			94.7	113.0	94.3		
Cu	131.8	106.5			18.4	17.5	24.4		
Pb	8.5	13.3			13.7	2.5	5.9		
Ni	26.7	35.7			42.3	40.6	45.7		
Sn	29.1	1.7			18.4	5.8	17.8		
Bi	2.4	6.8			0.4	0	0.4		
Mo	0	0			0	10.3	0		
W	18.0	4.9			7.6	12.8	28.5		

Table 9.2. The analytical data of Kim(1976) for the Myobong Formation.

	Unmineralized slate		Mineralized slate			
			-6 cross cut		-10 cross cut	
*Group	I	II	I	II	I	II
SiO_2	59.14	64.87	54.97	54.48	56.49	59.57
TiO_2	1.21	0.99	1.08	1.18	1.32	0.92
Al_2O_3	18.11	13.72	15.66	17.09	15.58	16.99
Fe_2O_3	9.17	9.61	14.62	9.84	12.70	9.82
MnO	0.08	0.10	0.33	0.07	0.22	0.11
MgO	3.40	2.38	4.78	2.86	4.67	2.57
CaO	0.61	0.96	0.87	1.08	0.98	1.21
K_2O	4.59	5.46	4.26	6.52	4.36	6.16
Na_2O	0.13	0.37	0.38	0.41	0.68	0.54
P_2O_5	0.19	0.22	0.15	0.17	0.16	0.15
LOI	2.46	1.86	2.54	2.98	2.25	2.44
Total	99.09	100.54	99.64	100.58	99.81	100.48

* Chemical grouping after Kim(1976)

****

Fig. 9.4. W versus SiO_2 contents in the mineralized slate, from data of Kim(1976)

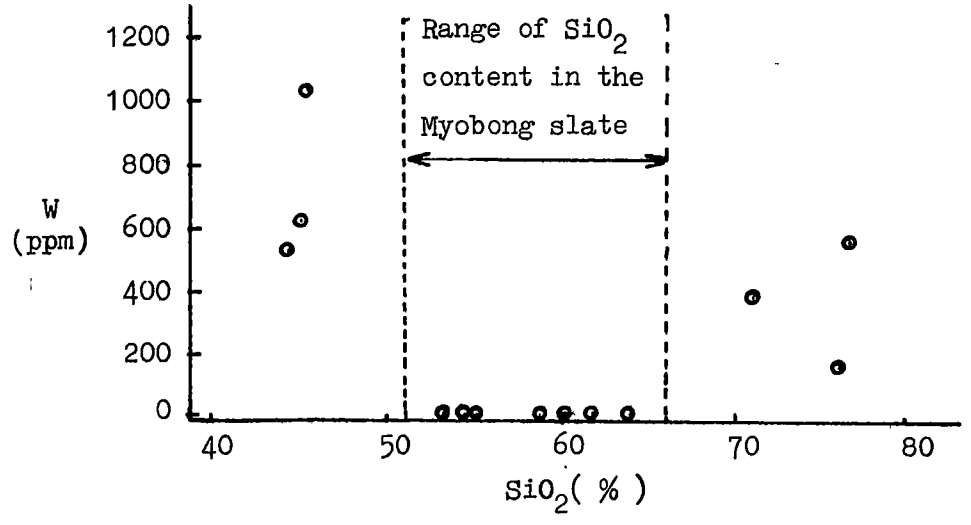

Table 9.3. Comparison of chemical compositions between slate, the cherty facies, and the horizontal rock.

*103129 = the cross-cutting cherty rock(outcrop, Baegun-Jangsan levels)
*103069 = the horizontal cherty rock(beneath M1 skarn)
*103075 = cherty part(Fig. 4.12)
*103076 = slate part(Fig. 4.12)

	103129	103069	103075	103076
SiO_2	53.89	53.14	46.68	54.76
TiO_2	1.18	1.57	1.0	0.82
Al_2O_3	18.76	14.0	23.29	18.64
Fe_2O_3	0.95	1.12	0.74	1.44
FeO	3.19	6.69	2.38	4.98
MnO	0.16	0.34	0.14	0.09
MgO	3.62	2.84	3.68	3.31
CaO	15.68	17.77	17.62	3.22
K_2O	0.21	0.09	0.54	4.5
Na_2O	n.d	n.d	0.71	3.13
P_2O_5	0.19	0.66	0.38	0.25
LOI	1.45	0.8	2.49	2.99
Total	99.28	99.02	99.65	98.14
Trace elements(ppm)				
Rb	23.3	10.2	51.3	318.8
Sr	185	162.5	367.9	485.1
Th	4.9	0	34.5	11.2
Zn	61.6	92.7	116.9	103.4
Cu	8.3	7.6	3.2	15.5
Pb	4.9	22.1	0	14.1
Ni	24.6	33.0	29.4	41.0
Sn	39.2	8	7.9	6.1
Bi	1.3	727.0	0	0
Mo	3.7	2.3	130.4	0
W	63.9	2810	47.1	6.9

Fig. 9.5. Cherty rock facies cutting through bedding plane of Myobong slate at the 1st level.
x 0.6

Fig. 9.6. A sketch showing an occurrence of cherty rock facies alteration in the Myobong slate between H1 and M1 orebodies.

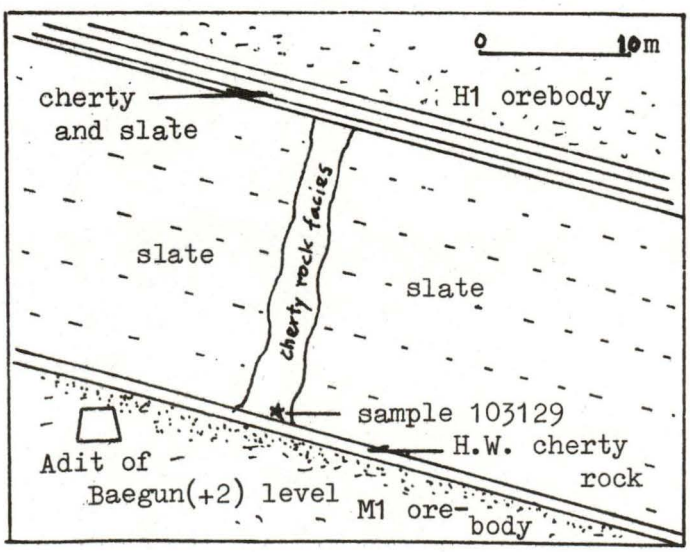

10. FLUID INCLUSIONS

The only previous fluid inclusion study of Sangdong material was made by John(1978) who investigated inclusions in quartz veins and found that molybdenite-bearing quartz veins were formed at relatively lower temperatures(average T_h = 170°C) than scheelite-bearing quartz veins(average T_h = 217°C).

In the present study, inclusions were studied in quartz from various zones of the M1 skarn orebody and from quartz veins. Other minerals which contained inclusions include pyroxene, garnet, scheelite, apatite, fluorite, biotite, amphibole and vesuvianite.

A description of the heating and freezing stage, and methods used, is given in Appendix 10.1. Fluid inclusions which were not clearly of secondary origin according to the criteria of Roedder(1979) were treated as primary or pseudosecondary inclusions.

The following symbols are used:

T_h temperature of homogenization of two fluid phases(during heating).

$T_h(L)$ temperature of homogenization into the liquid phase.

$T_h(V)$ temperature of homogenization into the vapour phase.

T_hCO_2 temperature(measured during heating) of homogenization of CO_2phases.

T_d temperature of decrepitation.

T_m temperature of melting (or dissolving).

T_mNaCl temperature (measured during heating) of disappearance of halite.

T_mKCl temperature (measured during heating) of disappearance of sylvite.

T_f temperature (measured during warming) of fusion of ice.

T_e temperature of eutectic, i.e., first recognized formation of liquid on warming a completely crystalline inclusion.

C.P critical temperature.

% NaCl equivalent weight percentage of NaCl(corresponding to a $T_m$ice or C.P. reading).

T_n temperature of nucleation in fluid on cooling.

10.1. Types of Fluid Inclusions and Their Distributions

Inclusions in the quartz from quartz veins and from the M1 skarn orebody have various shapes, i.e. oval, round, longish, tabular, negative forms or irregular shapes. However, there are differences in the frequency of sizes and types in the quartz from quartz veins and that from the M1 skarn orebody. Inclusions in the veins are generally larger (average 0.02 mm diameter against 0.01 mm in the skarn), and more abundant than in the skarn.

Fluid inclusions in scheelite and apatite are similar, being spherical or ovoid in shape(Figs. 10.1a & b) but fluid inclusions in fluorite exhibit many different shapes, e.g. circular, oval, tabular or irregular.

Fluid inclusions in pyroxene and garnet are relatively uniform in shape, being mainly ovoid, but some are round, semi-square or have negative forms.

The major types of inclusions are classified into four types as follows:

Type A = liquid + vapour inclusions with variable size of vapour bubble.

Type B = liquid + vapour inclusions containing liquid CO_2 at room temperature.

Type C = liquid + vapour inclusions with less than 50 volume percent vapour and with solid crystals.

Type D = monophase inclusions.

Type A inclusions(Figs. 10.2a & b)

These inclusions are by far the most abundant in all minerals. Most type A inclusions in the growth zones of host minerals are than 0.025 mm, but some are larger, commonly associated with secondary inclusions in process of necking down. In terms of volume % of vapour bubble at room temperature, type A inclusions with more than 50 volume % vapour are much less common than type-A inclusions with 1 to 7 volume % vapour.

High temperature type A inclusions occur mainly in pyroxene and garnet within the M1 skarn orebody, and in quartz from the central zone(-3rd and -4th levels) of the M1 skarn. All type A inclusions in quartz homogenized into the liquid phase, but some type A inclusions in pyroxene and garnet homogenized into the vapour phase, and some of these inclusions show near-critical behaviour(Roedder, 1967). Some inclusions did not homogenize even when heated to 580°C.

Vapour bubbles in the inclusions show different relief and colour(i.e. clear or dark); dark bubbles with strong relief are commonly found in fluid inclusions that are associated with high temperature type A inclusions in quartz and more commonly in pyroxene.

The population of fluid inclusions in quartz associated with abundant scheelite, particularly in the quartz-muscovite skarn, is remarkably reduced, although scheelite shows a few inclusions. This may result from recrystallization and removal of inclusions during scheelite growth.

Many type A inclusions with relatively small vapour bubbles(less than 5 area %) have a moving bubble at room temperature. Generally, these inclusions show low T_h values. Many inclusions also exhibit Brownian motion at elevated temperatures. The vigorous motion of the bubble as a dark spot just before homogenization makes it possible to measure accurately the homogenization temperature, even in tiny inclusions.

Type B inclusions(Figs. 10.3a & b)

These inclusions consist of three phases at room temperature, viz. an aqueous liquid and a vapour bubble ringed by liquid CO_2. The shapes and sizes of most type B inclusions are indicated in Appendix 10.10. They are always found in company with type A inclusions, but their distribution is confined to quartz and fluorite crystals and they are found only in small numbers of specimens, as indicated in the following table:

Host Rock	Host Mineral: quartz — quartz vein	Host Mineral: quartz — quartz-mica skarn	Host Mineral: fluorite — quartz vein
Numbers of observed specimens showing type B inclusions	5	1	2
Total observed specimens	46	102	16

Pyroxene and scheelite did not show type B inclusions.

More inclusions of this type were seen in quartz veins in the Jangsan Quartzite than anywhere else.

Type C inclusions(Figs. 10.4a & b)

These inclusions are polyphase containing liquid, vapour and solid crystals. Most of them have a small bubble with one or two solid phases, which may be isotropic, anisotropic or opaque. Opaque minerals may be hematite(specimen 103125) or magnetite(specimen 103170) and as they occur in only a few cases, may be due to accidental trapping(Fig. 10.5a). Most of anisotropic solid inclusions did not dissolve even when heated to 580°C and also may not be daughter minerals. One anisotropic crystal in a type C inclusion from the Jangsan Quartzite has been identified as a calcite because of its rhombohedral crystal form(Fig. 10.5a).

A cubic daughter mineral is most common and has been tentatively identified as halite. T_mNaCl may greater or smaller than T_h. Halite occurs in inclusions of quartz, pyroxene, fluorite and scheelite in each zone of the M1 skarn orebody.

The occurrence of halite-bearing inclusions in quartz veins is confined to the molybdenite-bearing quartz veins at the 4th and 5th levels. No halite-bearing inclusions were observed in specimens from the M1 skarn orebody at the 4th and 5th levels.

Only a few inclusions from scheelite, quartz and pyroxene were identified as sylvite-bearing. The sylvite is associated with the halite

and was identified by its lower melting temperature. The shapes and sizes of these type C inclusions are presented in Appendix 10.12.

Type D inclusions(Fig. 10.5b)

Monophase inclusions are common in all minerals. Large monophase inclusions in fluorite formed bubbles after heating and cooling runs. Scheelite and fluorite commonly enclose many irregular monophase inclusions with a pale pink colour, which result in spotty surfaces in these minerals under low magnification microscopy.

Dark monophase inclusions were occasionally observed in scheelite crystals(Fig. 10.5b). They are so dark they hardly showed any change on heating and are believed to be gas phase or gas-rich inclusions. Rarely they formed two phases on cooling runs.

Fig. 10.1,a. Type A inclusions in a scheelite crystal.
103237(quartz-mica skarn), Sangdong level.
═══ represent 0.025 mm.

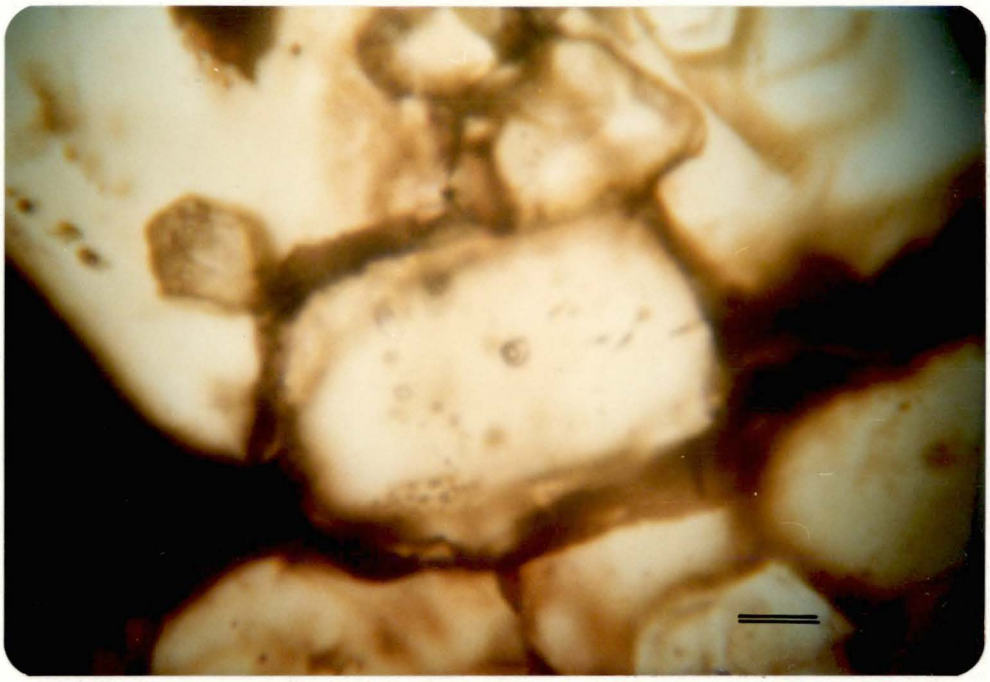

Fig. 10.1,b. Type A inclusions in an apatite crystal.
103239(amphibole skarn), -5th level.
═══ represent 0.02 mm.

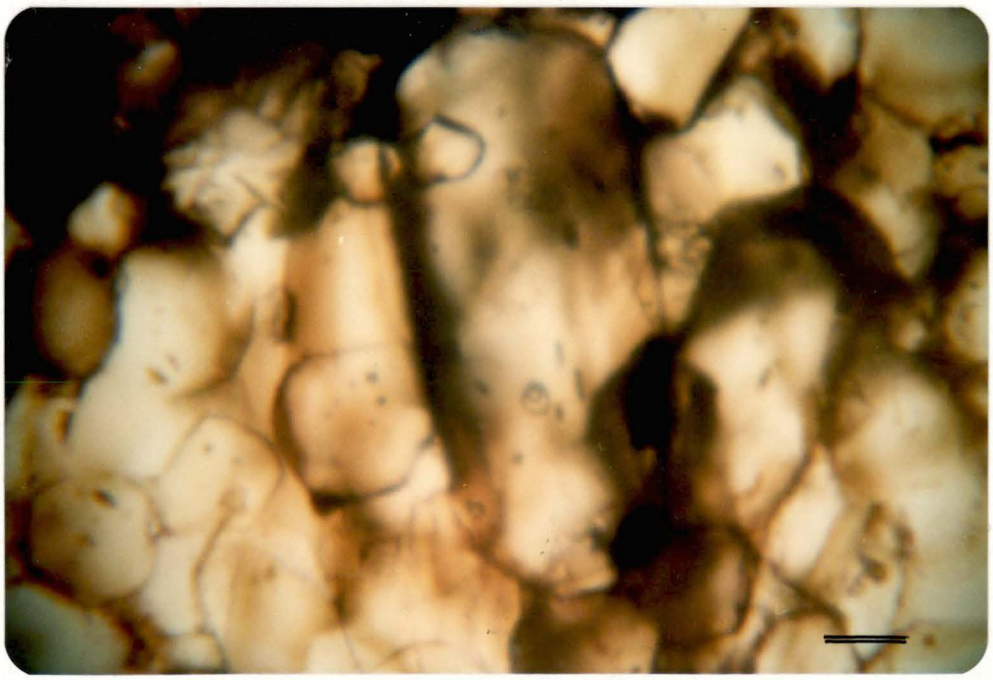

Fig.10.2(a).Typical type A inclusions in pyroxene crystal
106039(px-gn skarn), -7th level. ═══ represent 0.025 mm.

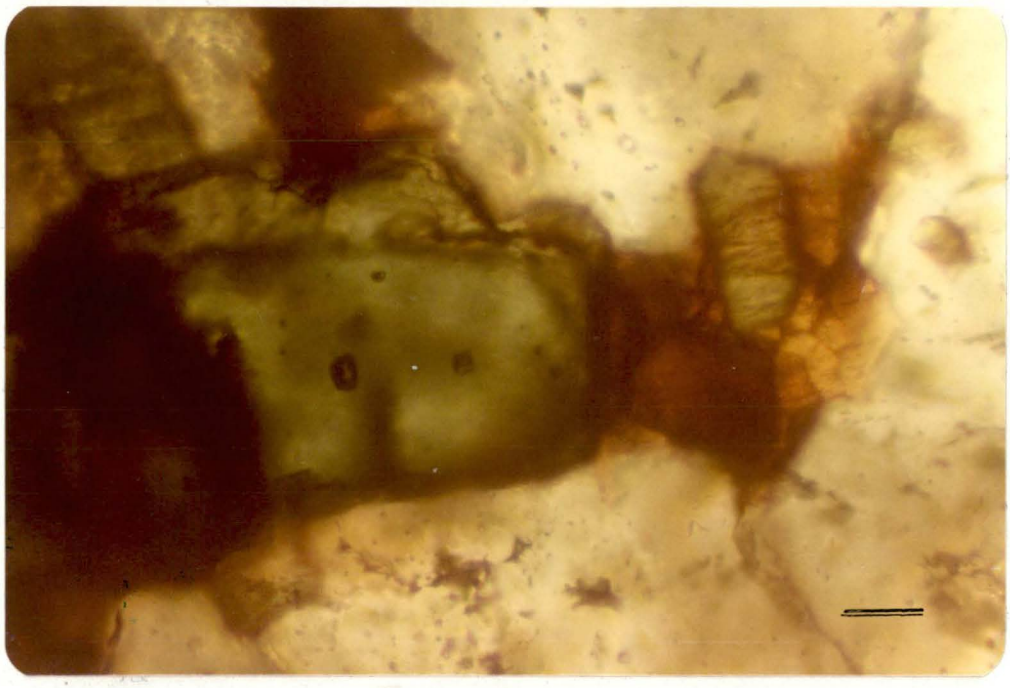

Fig. 10.2(b). Typical type A inclusions in fluorite
103158(quartz vein), -5th level. ═══ represent 0.025 mm.

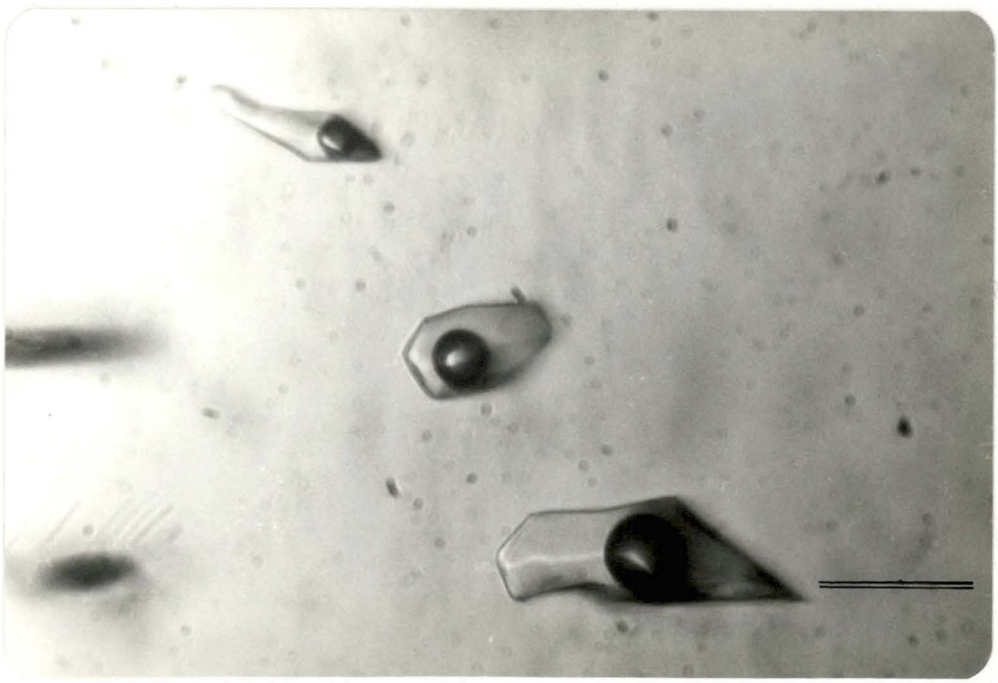

Fig. 10.3(a). Type B(liquid CO_2-bearing) inclusion in fluorite.
103238(quartz vein), Sangdong level. ═══ represent 0.02 mm.

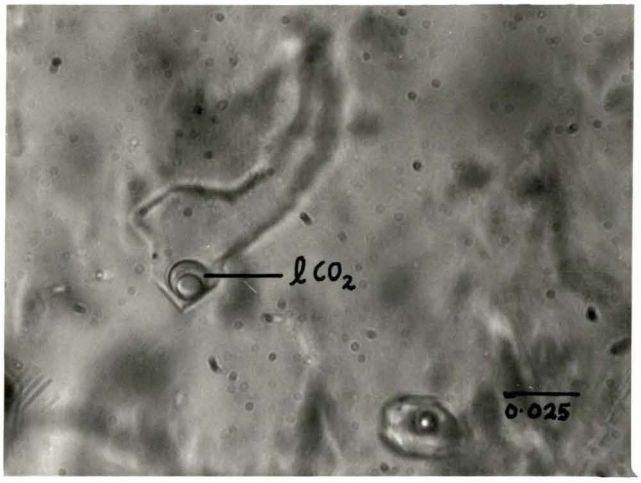

Fig. 10.3(b). Coexisting type A and type B inclusions in quartz.
103156(calcite vein). ═══ represent 0.02 mm.

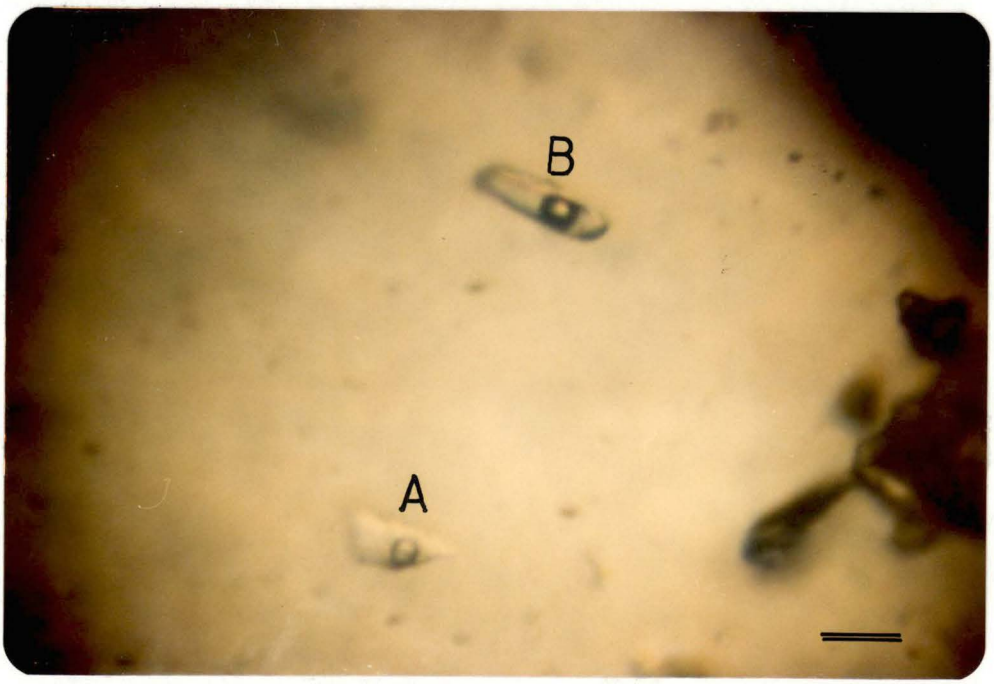

Fig. 10.4(a). Type C inclusions showing halite and opaque daughter minerals in scheelite.
103170(scheelite in quartz-mica skarn), 15 block - Sangdong level. —— represent 0.025 mm.

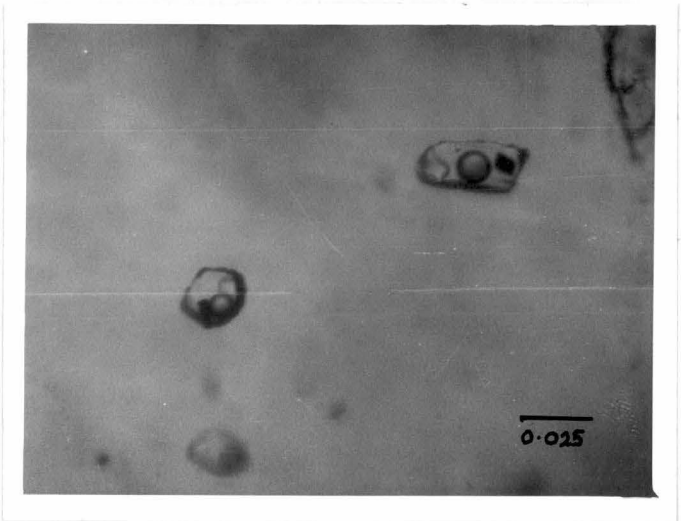

Fig. 10. 4(b) Type C inclusions showing halite daughter mineral.
103154(clear quartz in quartz vein), 15 block -5th level.
—— represent 0.025 mm.

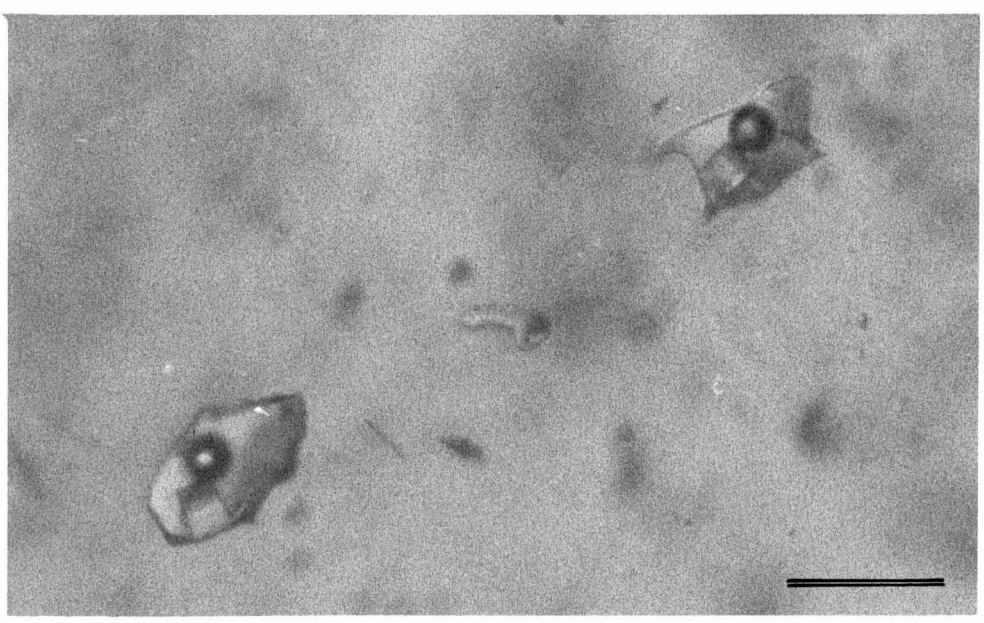

Fig. 10.5(a). Type C inclusion showing accidently trapped solid crystals(a rhombic crystal may be a calcite). 103160. Jangsan Quartzite. ═══ represent 0.02 mm.

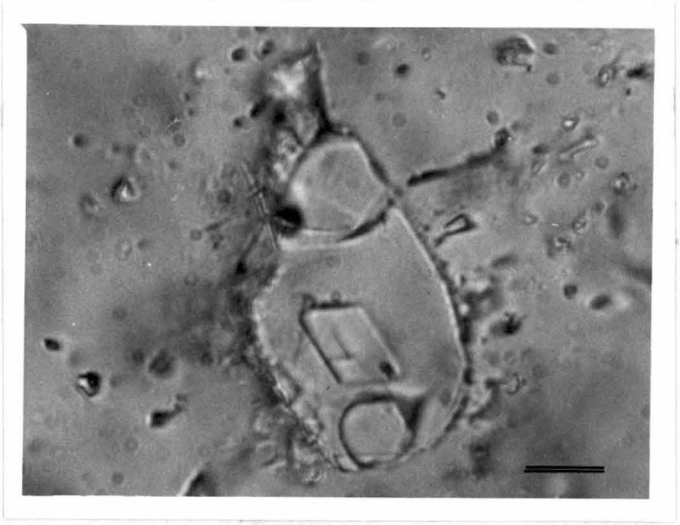

Fig. 10.5(b). Type D inclusions with type A inclusions in a scheelite crystal. O = monophase inclusion 103239(scheelite in amphibole skarn), Sangdong level. ═══ represent 0.025 mm.

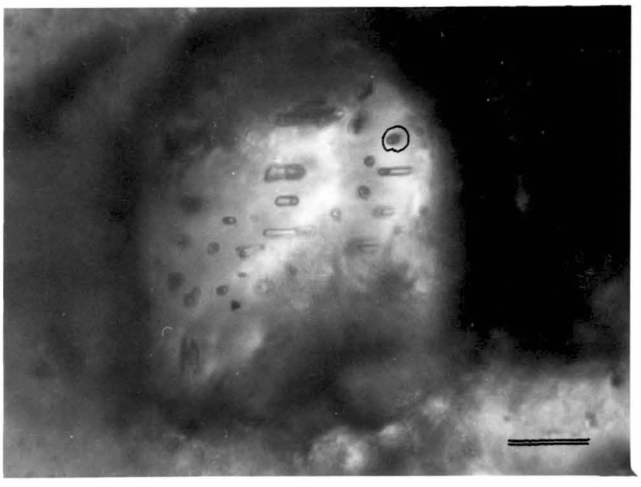

10.2. Homogenization of Type A Inclusions in the Quartz Veins

10.2.1. Quartz

As previously described in Table 4.1, quartz veins can be subdivided according to mineralogy into five vein types, e.g.

(1) Molybdenite-bearing(Mo q.v)

(2) Wolframite-bearing(Wlf q.v)

(3) Chalcopyrite-bearing(Ccp q.v)

(4) Bismuthinite-bearing(Bi q.v)

(5) Barren(Brn q.v)

T_h data of fluid inclusions from quartz veins are presented in Appendix 10.2. T_h ranges from 138°C to 405°C and the average and range for each the five vein types are shown in Fig. 10.6a. Quartz-wolframite and quartz-molybdenite veins were apparently deposited at higher temperature than chalcopyrite-, bismuthinite- and barren quartz veins.

Part of the considerable range of T_h in the individual vein types may reflect local variation of temperature of crystallization with time, and possibly overprinting of earlier fluids by later fluids. Specimen 103203 (Fig. 10.6b) is an admirable example of local time-space-temperature variation at the centimetre scale. The highest T_h values are confined to the central portion of the vein.

Average T_h values from vein quartz show a gradual decrease from $292° \pm 50°C$ in the upper levels through $264° \pm 66°C$ in the middle levels to $233° \pm 54°C$ in the lower levels(Fig. 10.7). However, the highest T_h values occur in the middle levels and it can be seen from Fig. 10.8 that is difficult to identify a vertical temperature gradient.

10.2.2. Fluorite in Quartz Veins

Fluorite occurring in the quartz veins is generally pale violet, pale blue or white in colour. Blue coloured fluorite has few fluid inclusions compared to the other fluorites. There is a narrow range of T_h in fluorite

Fig. 10.6a. Variation in the range of T_h shown by different groups of quartz veins(based on Appendix 10.2).

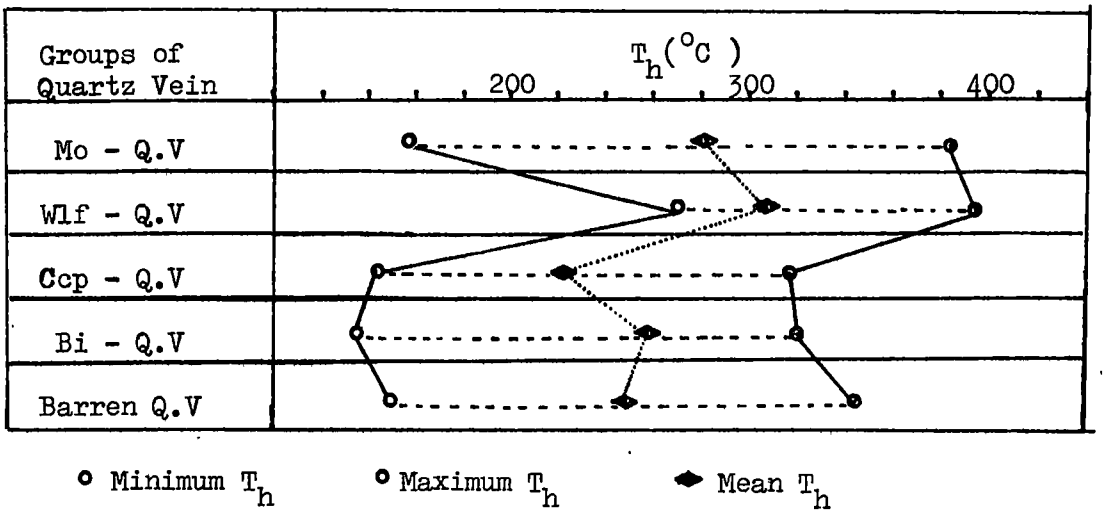

Fig. 10.6b. Variation of T_h in type A inclusions in a quartz vein. (Specimen 103203).

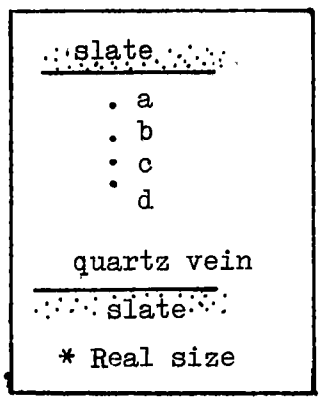

	T_h(°C)
(a)	158, 178, 215
(b)	229, 270
(c)	282, 333
(d)	262, 333, 344

Fig. 10.7. Frequency distribution of T_h for vein quartz.

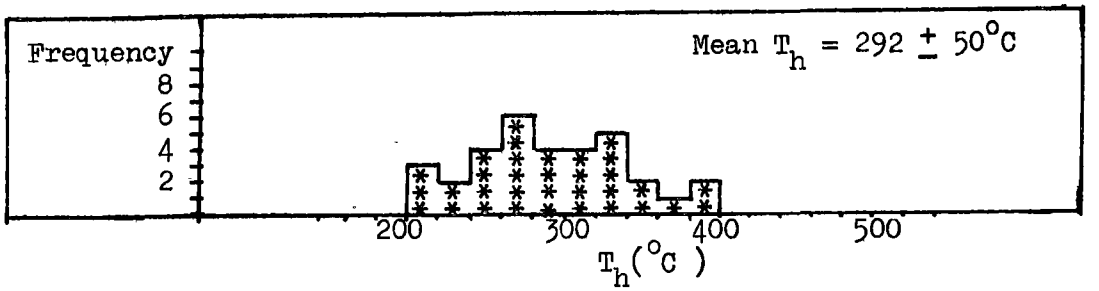

Upper levels(650 m above sea level)

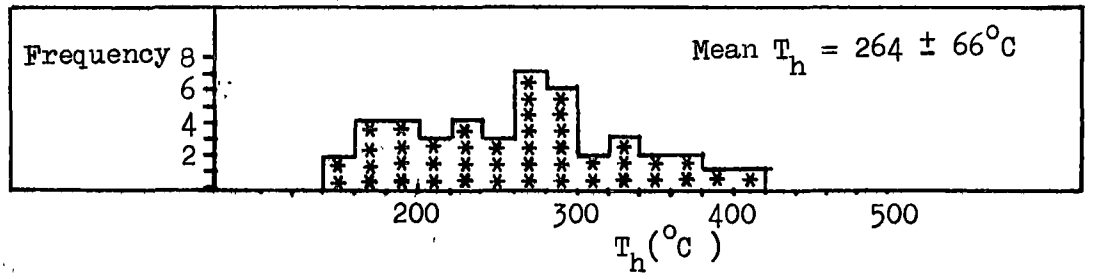

Middle levels(650 - 430 m a.s.l.)

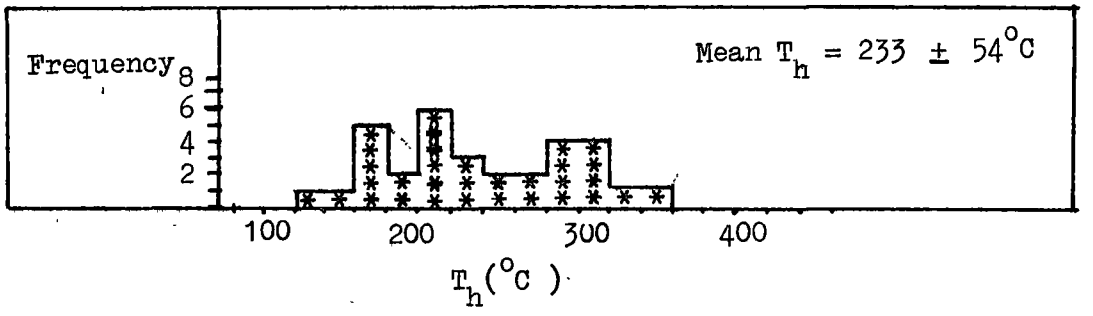

Lower levels(below 430 m a.s.l.)

Fig. 10.8. Variation in the range of T_h of vein quartz with depth.

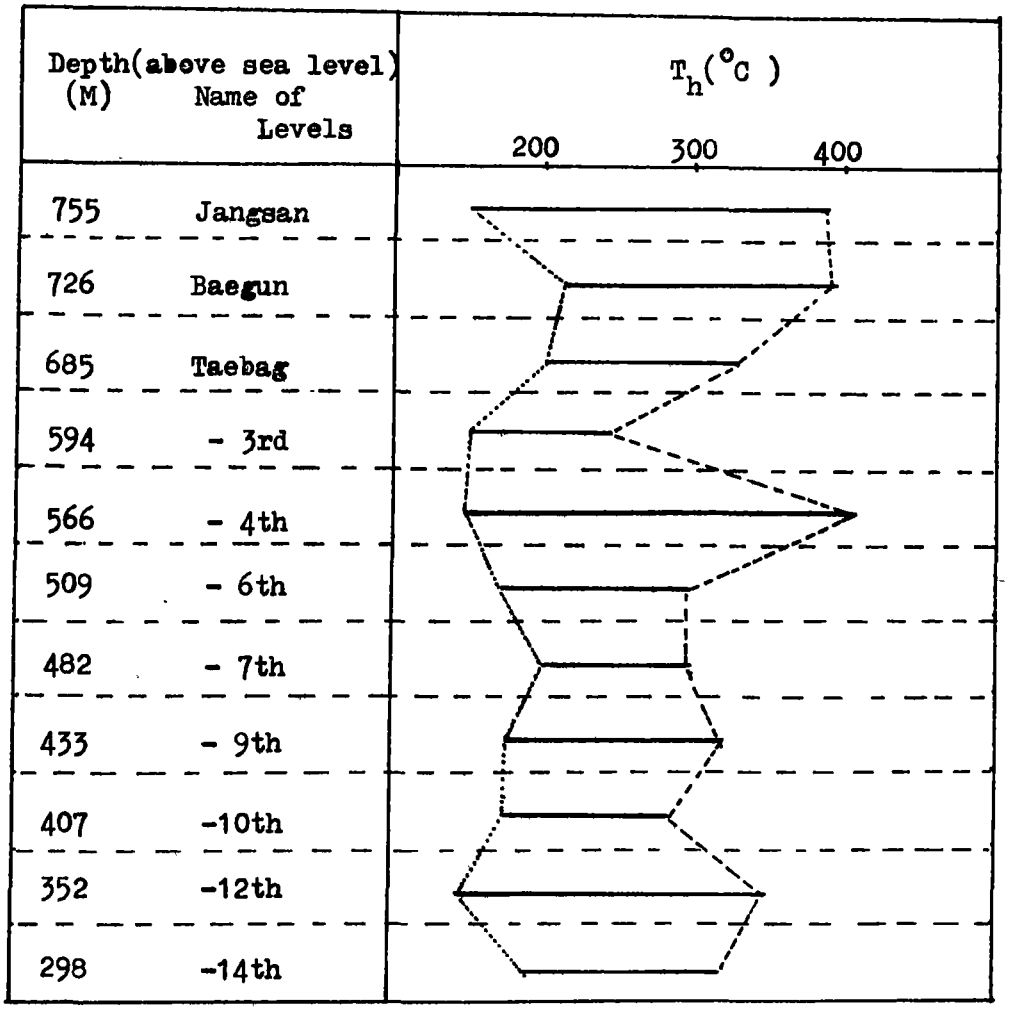

Table 10.1. Comparison of the T_h in fluorite and quartz in quartz veins.

Sample No.	Major Associated Ore Minerals	Range of $T_h(C^o)$	
		Fluorite	Quartz
103214	Wolframite	146 - 201	214 - 280
103158	Barren	220 - 225	226 - 239
103142	Scheelite	162 - 361	233 - 280
103221	Chalcopyrite	127 - 262	283 - 317

Table 10.2. Comparison of T_h of fluid inclusions in fluorites from the quartz veins and the M1 orebody(based on Appendix 10.5).

	$T_h(^oC)$ in the Quartz Vein	$T_h(^oC)$ in the M1 Skarn
Maximum	361	394
Minimum	127	161
Mean	218 ± 66	218 ± 58

and the values are generally lower than those in quartz(Table 10.1). However, fluid inclusions in fluorite closely associated with scheelite show a wide range of T_h(e.g. 103142) and some are higher than the T_h measured in quartz in contact with fluorite(Appendix 10.5). Similar T_h values were found in fluorite associated with scheelite in the M1 orebody.

10.3. Homogenization of Type A Inclusions in the M1 Skarn

10.3.1. Quartz of the M1 Skarn Orebody

Homogenization temperatures increase from the pyroxene-garnet skarn zone through the amphibole zone to the quartz-mica zone in maxima and average values(Fig. 10.9).

In plan(Fig. 10.10), the highest T_h values form an irregular zone down the centre of the M1 ore shoot, more or less coincident with the highest grade ore. As shown in this diagram, the contour for $T_h = 270^{\circ}C$ forms a "+" shape in the middle levels and the intersection has the highest grade ore(8 % WO_3). Yet nearby is a zone of relatively low T_h values that coincides with the quartz-muscovite zone, indicating the centre of the "+" acted as a major channel for very late ore solutions.

Considerable variation in T_h occurs within quartz crystals, these in the core generally having higher values than those near the margin(e.g. Appendix 10.12. ex.4). Within a sample(chip), inclusions enclosed in different quartz grains more or less in contact with each other generally have different T_h values. There is a positive correlation between the maximum difference and the maximum T_h. The greatest differences occur within samples formed in the "+" area, indicating this area was a solution channel for a protracted period involving substantial temperature changes.

Unusually high T_h values(273° to $319^{\circ}C$) were found at an early stage of this study on the 12th and 14th levels(Fig. 10.10). This zone corresponded with a mineralogical anomaly in which vesuvianite occurs with abundant scheelite. This information led to further exploration from

Fig. 10.9. Comparative histograms of homogenization temperatures of fluid inclusions within quartz from three different skarns at the Sangdong deposit.

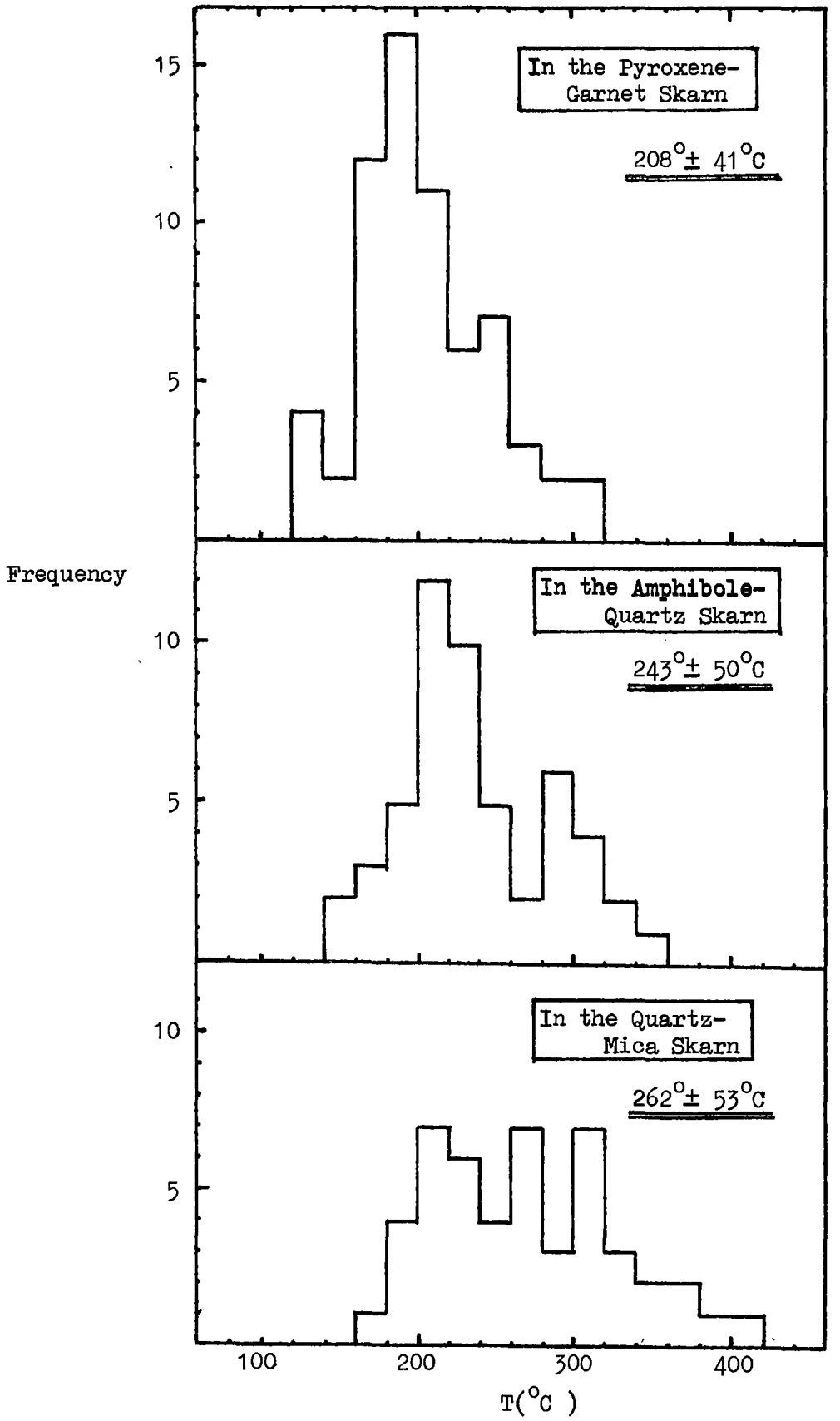

Fig. 10.10. Plan showing distrbution of T_h in fluid inclusions in quartz in the M1 skarn orebody.

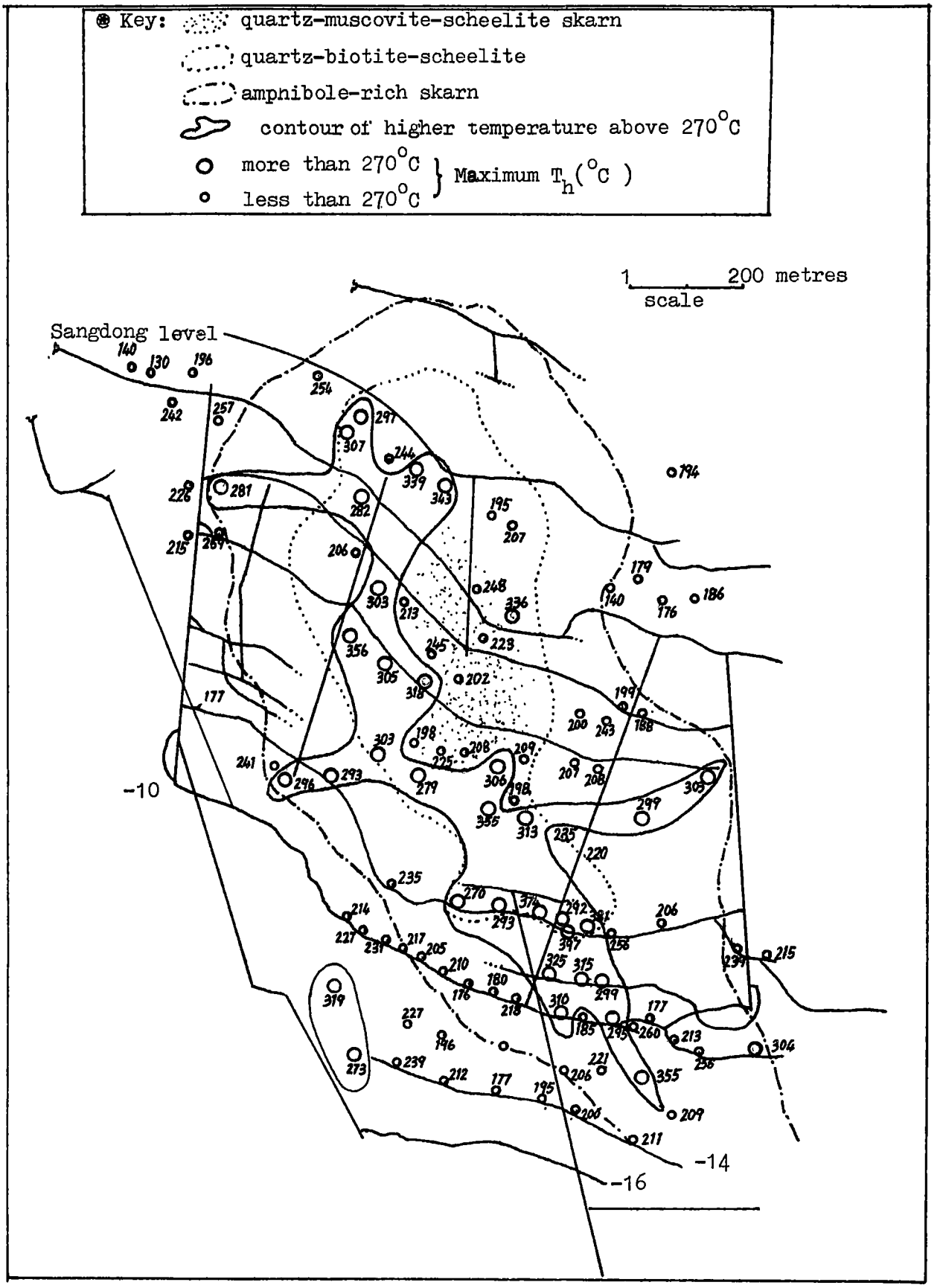

the lower levels and the discovery of a new zone of scheelite-bearing pyroxene-garnet skarn(about 0.5 % WO_3) outside the present skarn zone at about 215 metres above sea level(equivalent to the 17th level of the mine); details are shown in Fig. 4.17a.

10.3.2. Fluorite of the M1 Skarn Orebody

Fluorite in the M1 skarn has fewer inclusions than that in the quartz veins, but T_h values show a wider range and higher maxima(Appendix 10.5). Fluorite and contiguous quartz in the ore give similar T_h readings, as already shown in Table 10.2.

In specimen 103120 (Appendix 10.5) two different inclusions, one characterized by a round bubble, the other showing a long elliptic bubble, yielded the same T_h. The former homogenized by the meniscus fading at 376°C, and latter homogenized by normal homogenization at the same temperature. The first one probably formed at or near the critical surface. If so, then the T_h value may be a true temperature. There are many type D inclusions(liquid phase) associated with type A inclusions which show a T_h ranging from 160° to 200°C. Many of the one phase inclusion became -two-phase inclusions after heating, presumably due to leakage.

10.3.3. Pyroxene of the M1 Orebody

Inclusions in pyroxene are extremely small from vanishing size to 32 microns in diameter. They are round, longish, oval, square and negative forms and contain relatively large dark bubbles. Occasionally transparent bubbles were observed. In general, elongate pyroxene grains enclosed more fluid inclusions than rounded pyroxene grains, approximately unrelated to fractures. These fluid inclusions homogenized in three different ways, (a) by expansion of the vapour phase, (b) expansion of the liquid phase (the majority), or (c) fading of the meniscus, as in near-critical behaviour. Transparent fluid inclusions tended to homogenize into the vapour phase.

T_h data from fluid inclusions in pyroxenes are given in Fig. 10.11 and Appendix 10.4. High values may be due to leaking or necking and the lowest values to reworking by later fluids. T_h values range from 313°C to over 600°C with a mean of 418° ± 42°C(calculated with $T_h$max. = 600°C).

Most vapour-homogenizing inclusions gave similar temperatures to adjacent liquid-homogenizing inclusions(Table 10.3), indicating they were derived from a two-phase system. Near-critical inclusions in the same samples gave similar T_h values. The lowest coexisting gas-rich and liquid-rich T_h values was 366°C and it is assumed that the T_h values below 366°C require pressure correction for 500 to 800 bars(see section 10.6).

At the eastern margin of the M1 orebody, the garnet-pyroxene skarn thins along strike over about 500 metres and T_h values decrease as shown in Fig. 10.12. The apparent gradient is considerably modified if $T_h > 366°C$ requires little or no correction for pressure and these with $T_h < 366°C$ do (see section 10.6).

Maxima and minima T_h measured in each sample were plotted on the underground plan as shown in Figs. 10.13 and 10.14. In each figure, the lowest values tend to be near the main ore channel, possibly indicating reworking of pyroxene by later tungsten-bearing solutions. Other evidence of a temperature decline with time is apparent in sample 106114, which shows a decline in T_h from early pyroxene skarn to late pyroxene skarn(Fig. 10.13).

Several pyroxene samples contain type C fluid inclusions(Appendix 10.11). In each case $T_h > T_m$, indicating the presence of undersaturated solution at the time of trapping. These saline solutions could have coexisted with gas-rich inclusions in a two phase, NaCl-rich, aqueous system.

Fig. 10.11. Histograms plotting frequency versus T_h of fluid inclusions in pyroxenes and garnets from the M1 skarn ore body.

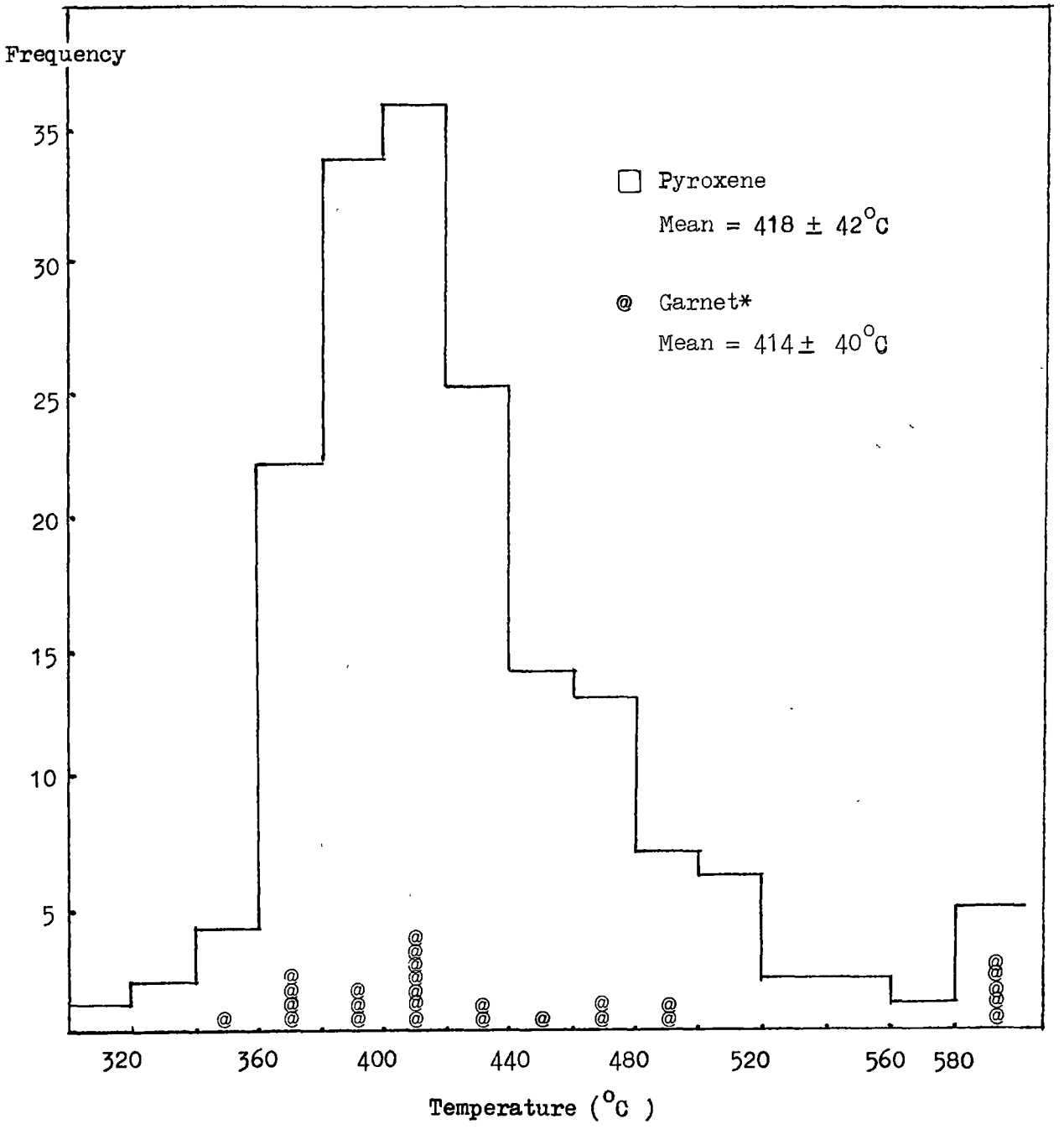

* The number of @ indicates the frequency of fluid inclusions in garnets.

Table 10.3. Comparison of T_h of fluid inclusions for different styles of homogenization in pyroxenes.

Sample No.	Phase of Homogenization(°C) T_h(V) Vapour	T_h(L) Liquid	Critical Point (°C)
106084(B-4)		423	425
106086(T-2)	404	380	
106106(5-0A)		396	403
106113(7-24)	418	418	
106119(9-5)	405	418	
106131(N-25-2)	462	424	
106135(N-34-1)		409	
106133(N-29-2)	411	439	
106140(12-29)	420 465	373	
106144(12-33)	456	432	
106137(12-23)	462	414 476	
106130(N-23-2)		444	422
106089(T-5)	397	413	
106103(3-2)	380	422	
106116(9-1)	384	384	
106121(9-9)	366 383	366 371	
106039(K-10)			416

Fig. 10.12. Variation of T_h of fluid inclusions at the marginal part of the M1 skarn orebody.

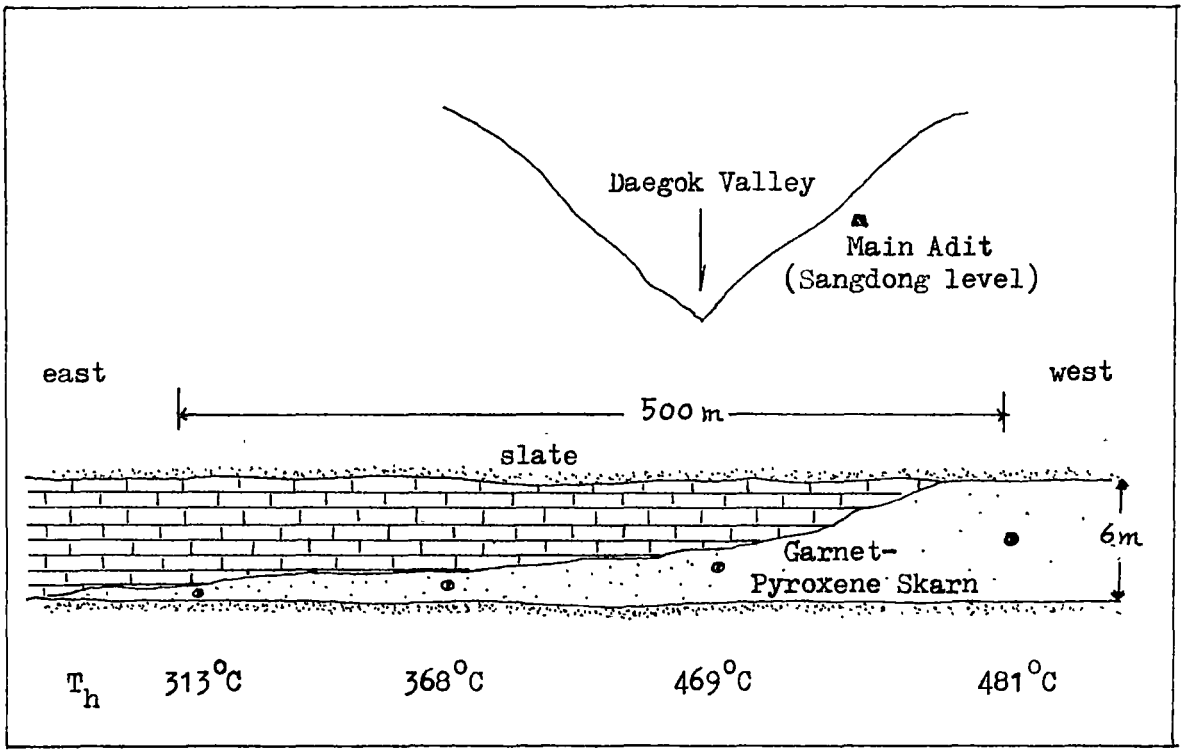

Fig. 10.13. Plan showing distribution of the highest T_h values in pyroxene(hedenbergite) crystals.

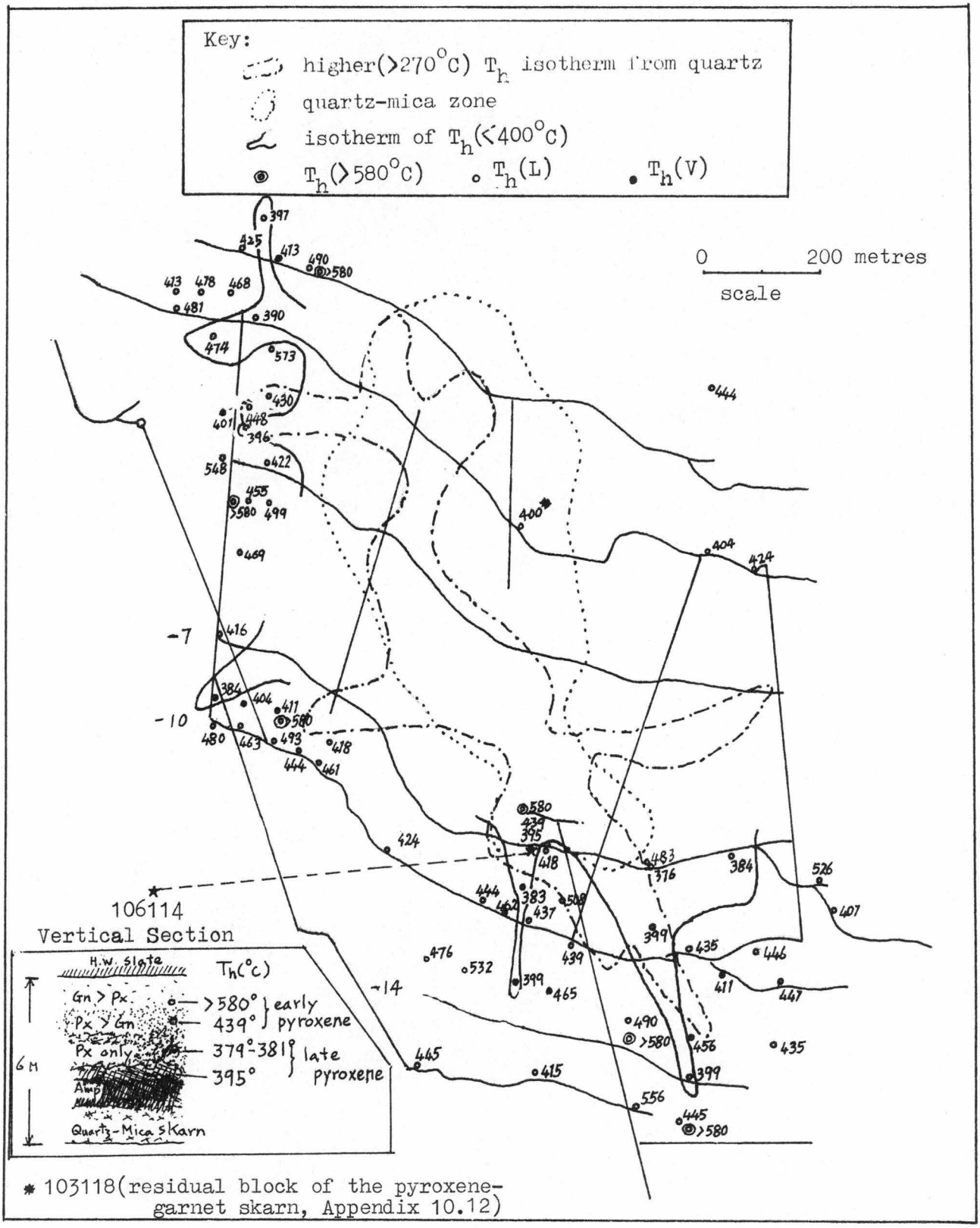

Fig. 10.14. Plan showing distribution of the lowest T_h values in pyroxene(hedenbergite) crystals.

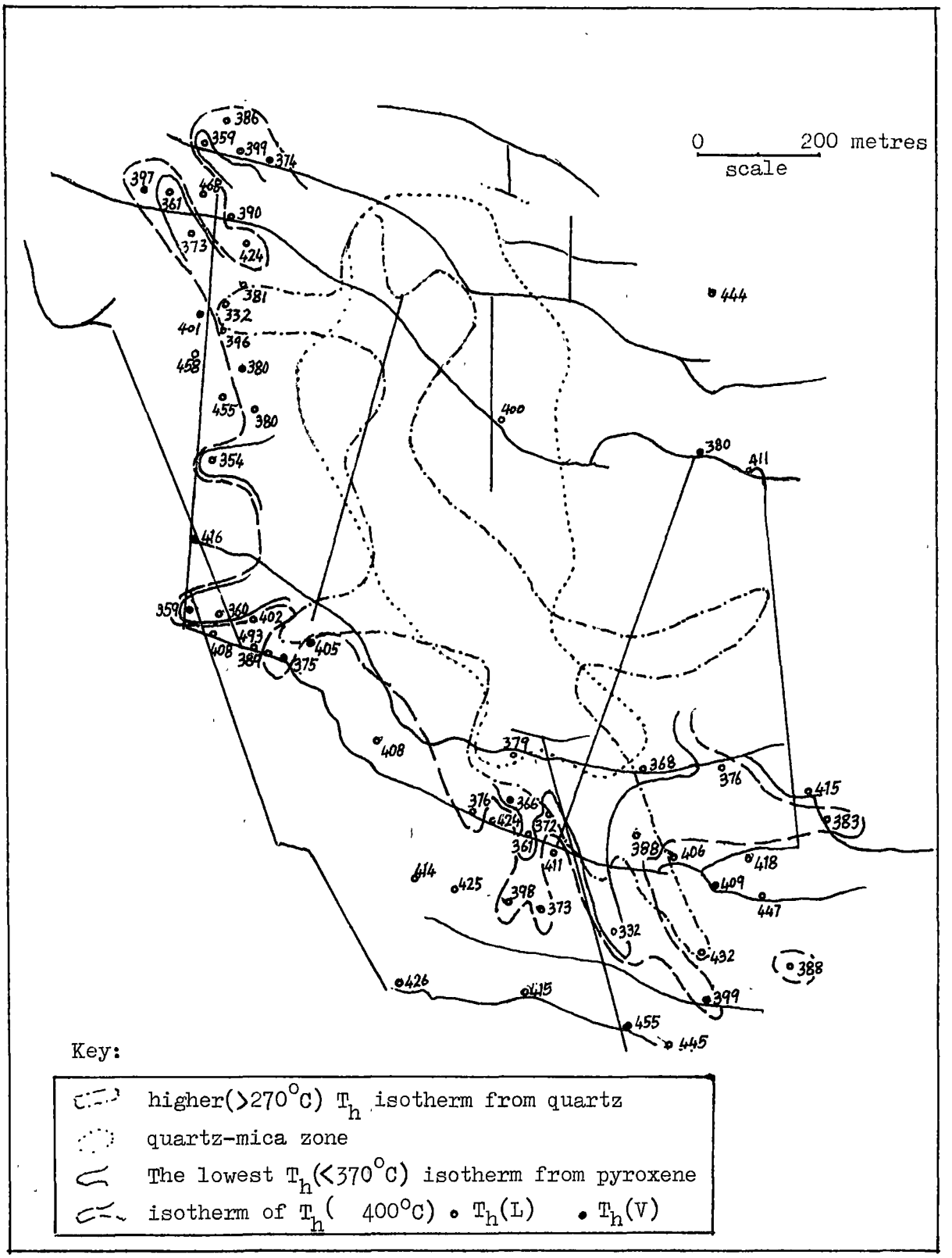

10.3.4. Scheelite of the M1 Orebody

Fluid inclusions in scheelite are up to 0.05 mm in diameter, but most of them are too small to study. Type A inclusions and type C inclusions containing halite, sylvite and opaque minerals as daughter minerals, are restricted to one sample(103170).

T_h values of types A and C inclusions range from 207° to 498°C with a mean of 302°C(Figs. 10.15a & b) and are plotted on the plan of the mine (Fig. 10.16). An exceptionally high T_h was measured in a scheelite crystal associated with pyroxene(and without quartz). That temperature of 498°C (specimen 106039) is as high as the highest observed in coexisting pyroxene(Appendix 10.6) indicating that this scheelite crystallized at an early stage of skarn formation.

As already mentioned, one specimen(103170) of scheelite has a Mo-rich core and Mo-poor rim, and T_h data therein have been compared with data obtained from individual single crystals showing the yellow colour(Mo-rich) or the blue(Mo-poor) scheelite(Fig. 10.15a).

10.3.5. Fluid Inclusions in Other Minerals of the M1 Orebody

In Apatite

As shown in Appendix 10.8, fluid inclusions in apatite have a narrow range of T_h from 250° to 320°C, with a mean of 280°C. Apatite is closely associated with scheelite and quartz. T_h values in the apatites are almost the same as those of coexisting scheelite but higher than those in adjacent quartz.

In Garnet

In general, most garnets do not show fluid inclusions, but a few that appear to have formed at the later stage of skarn formation contain a few type A inclusions(Fig. 10.17a). These inclusions homogenized

Fig. 10.15a. Histograms showing a comparative range of T_h between Mo-rich scheelite and Mo-poor scheelite.

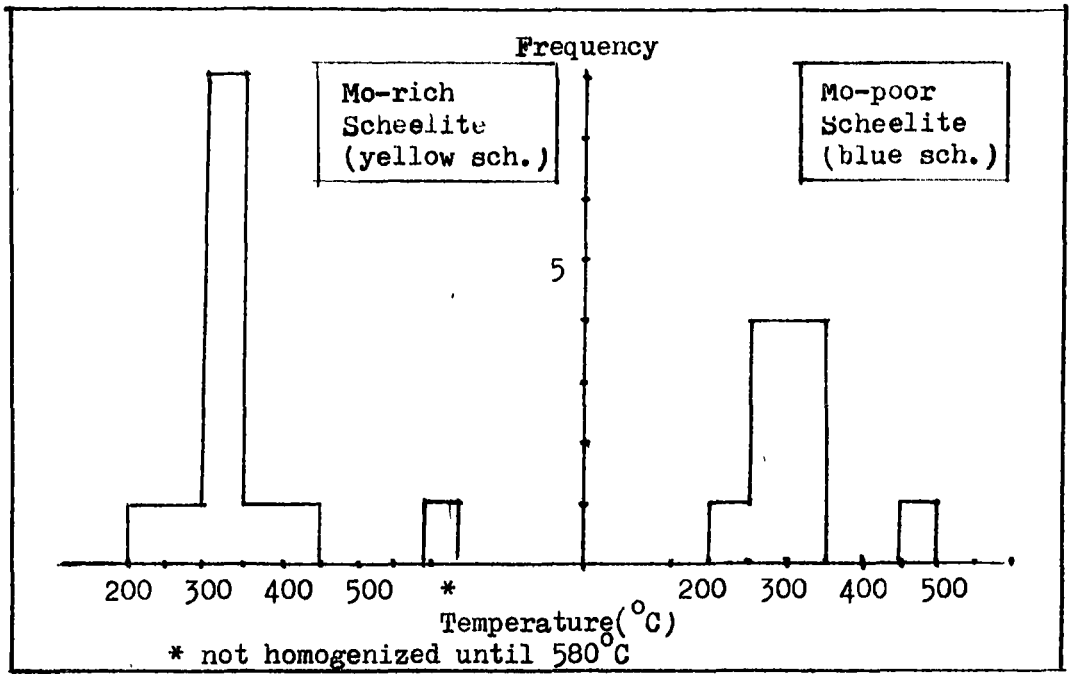

Fig. 10.15b. Histograms of T_h values in scheelites of the M1 Orebody.

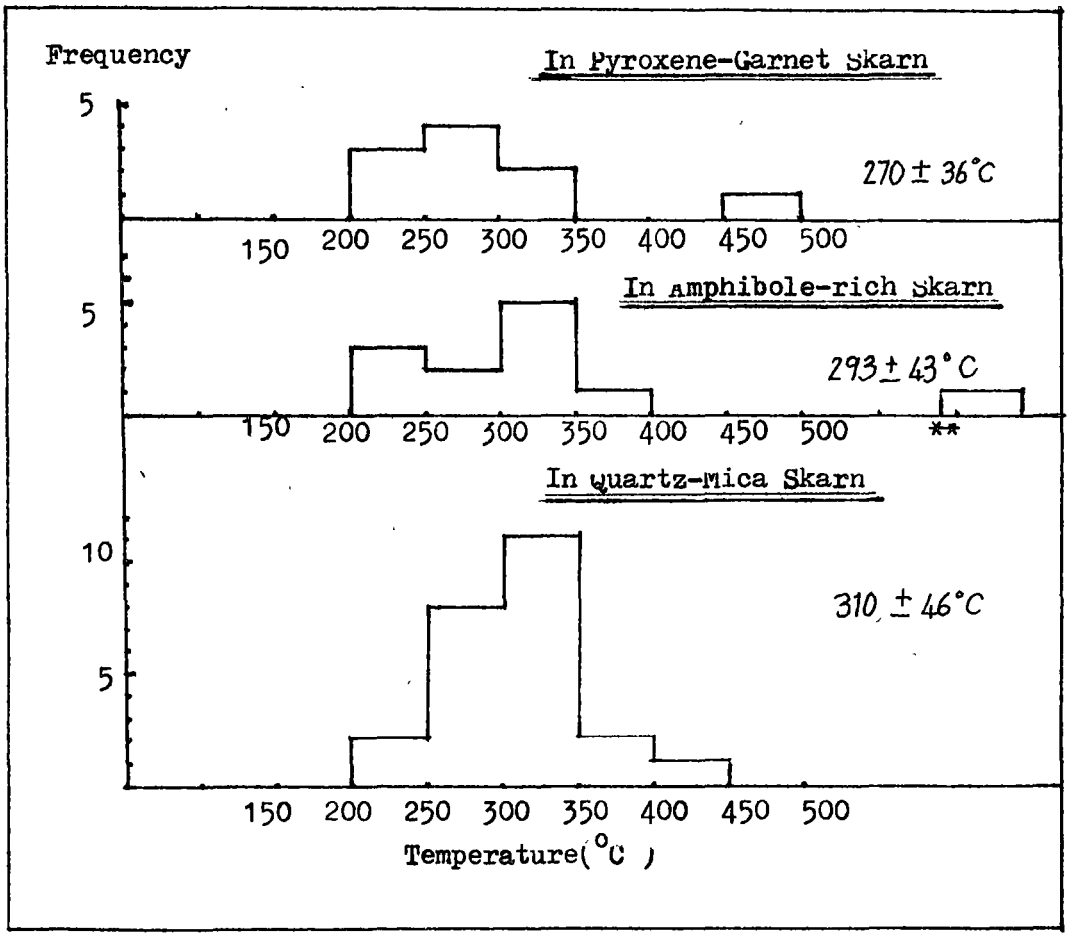

Fig. 10.16. Distribution of T_h values in scheelite crystals.

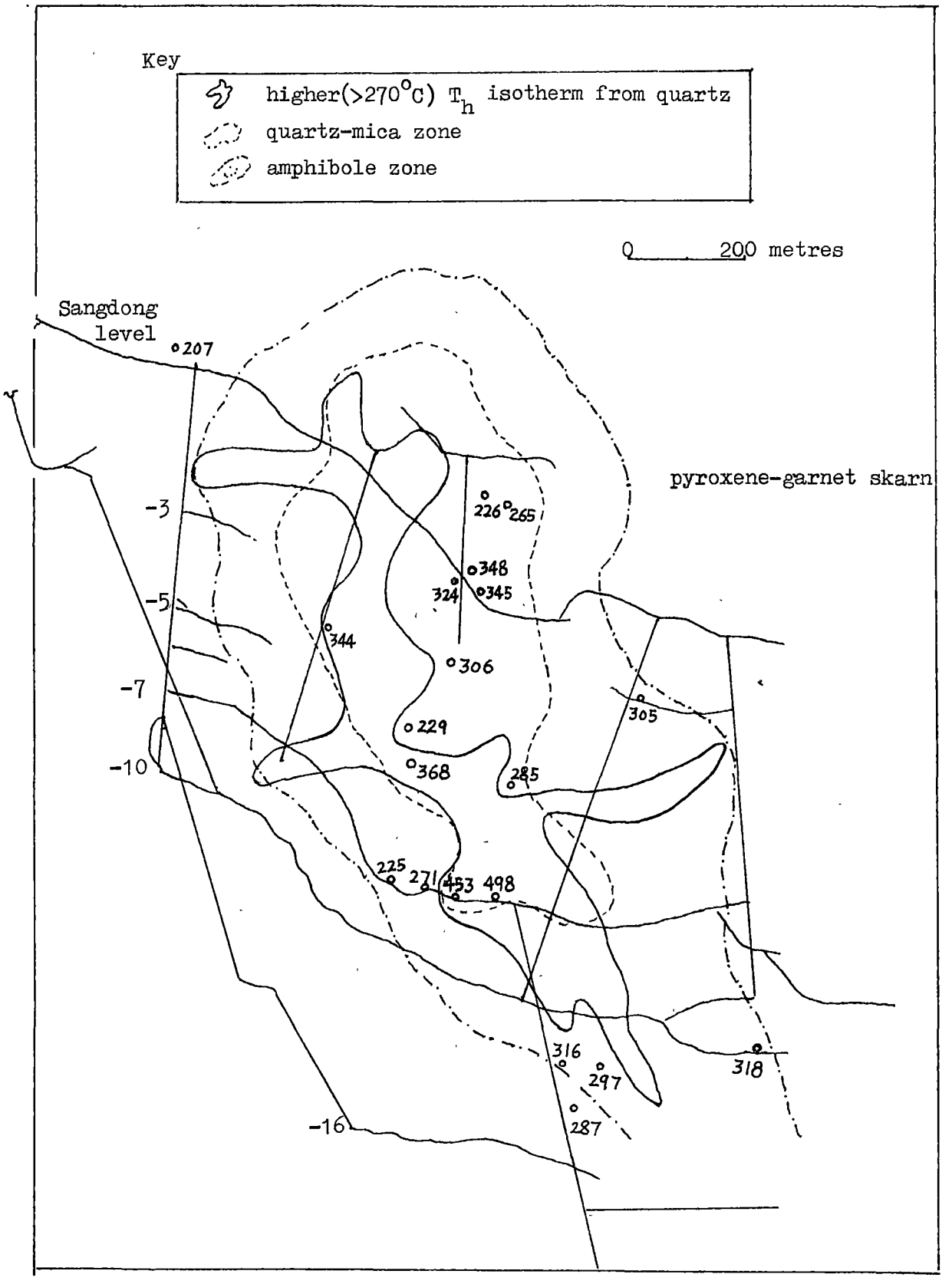

at almost the same temperature as the coexisting pyroxene, ranging from 340° to 500°C with a mean of 411°± 54°C. However, some of these inclusions did not homogenize even above 580°C. As in pyroxene, some homogenized in the vapour phase. One(e.g. 106047) showed near-critical behaviour with a T_h = 433°C. All data from fluid inclusions in garnets are presented in Appendix 10.9.

In Amphibole(Fig. 10.17)

Observation of inclusions in amphibole requires extra thin slices. It was possible to measure filling temperatures in only two specimens. Inclusions in specimen(106126) homogenized between 292° and 307°C, and in specimen(106048) between 287° and 293°C, whilst inclusions in coexisting quartz homogenized at 207°C(Appendix 10.8).

In Biotite

Only two(103093, 106173) T_h values were obtained, one at 381°C and the other at 286°C. A nearby amphibole gave 293°C and coexisting quartz 194°C.

In Vesuvianite

Sample(106171) from an altered dyke yielded three T_h measurements, 365°, 397° and 454°C. The highest T_h was measured from an inclusion homogenizing in the vapour phase. As shown in Fig. 10.18, one inclusion exhibited two immiscible liquids, the nature of which are unknown. One is clear, the other darker, and both are present on disappearance of the vapour bubble.

10.4. Homogenization of Type B Inclusions

Data from the CO_2-rich inclusions are given in Appendix 10.10. Two phases of CO_2 at room temperature(15°to 17°C) were observed, the liquid CO_2 forming a thin layer around the gas bubbles. Only quartz and fluorite have this type of inclusions. In most inclusions, the CO_2 homogenized to the liquid(between 23.7° and 29.1°C), but two, one from

Fig. 10.17(a). Fluid inclusion (type A) in garnet enclosing scheelite (see Table 10.8).
103118, -1st level. ═══ represent 0.025 mm.

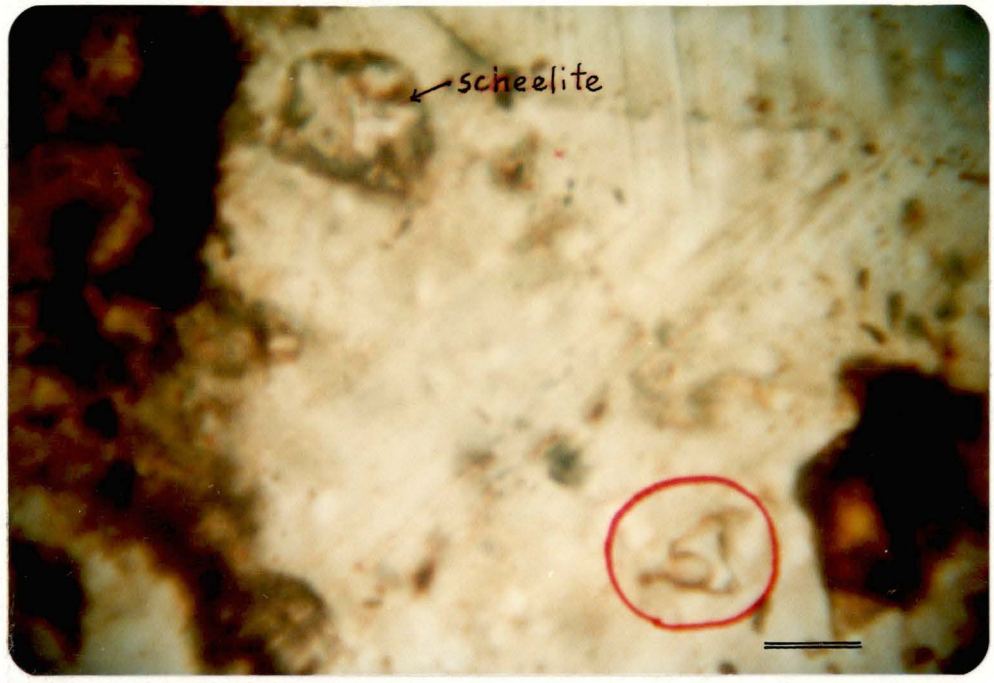

Fig. 10.17(b). Fluid inclusions in amphibole.
T_h = 287° to 293°C.
106048(amphibole skarn), -7th level. ═══ 0.025 mm.

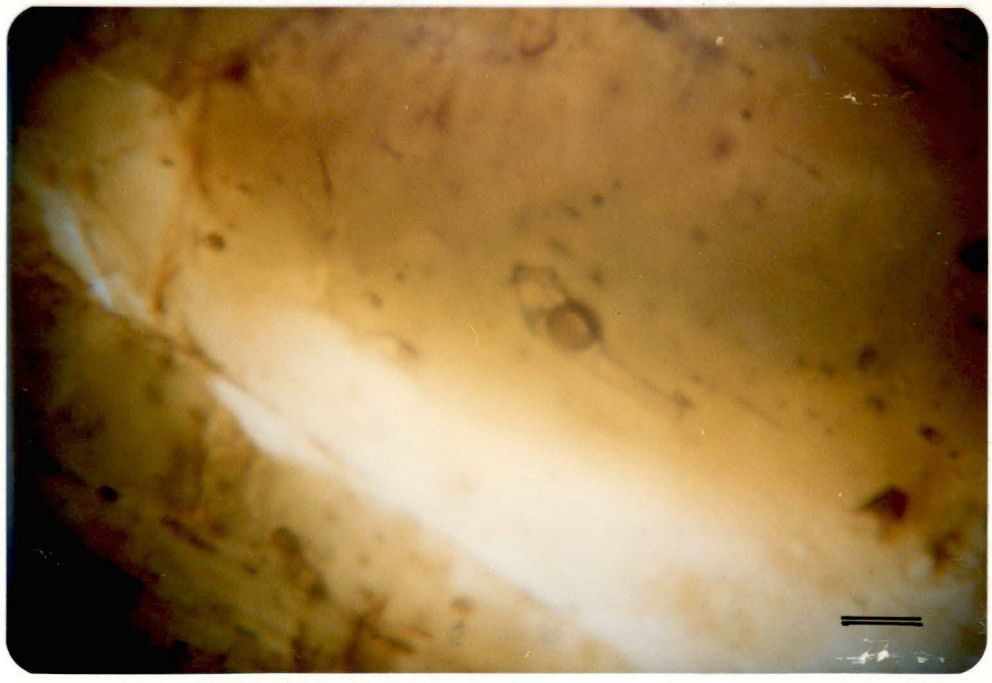

Fig. 10.18. Two liquids in one single inclusion

Specimen 106171(vesuvianite).

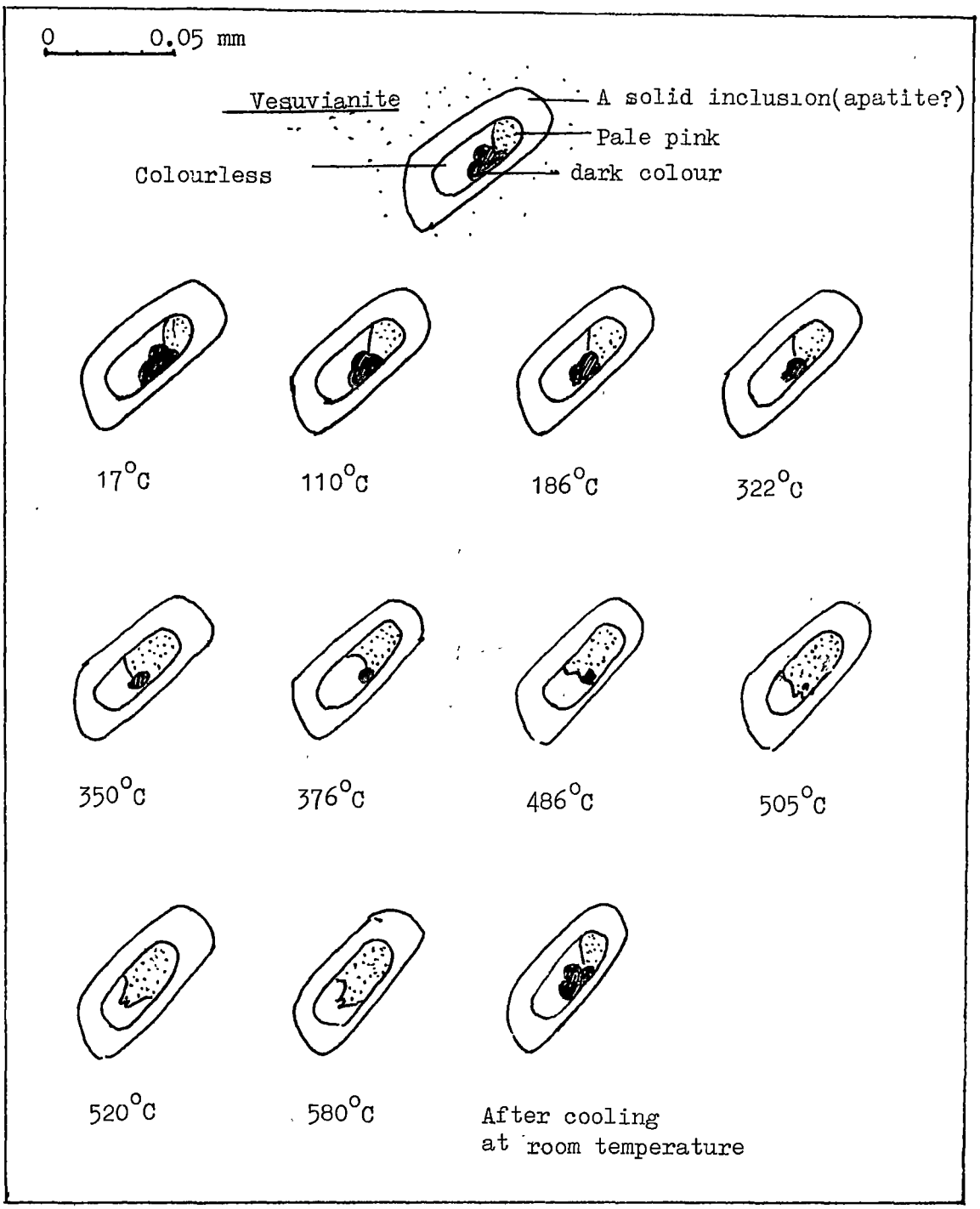

the Jangsan Quartzite(specimen 103160) and one from a quartz vein(specimen 103214), homogenized into the gas phase. CO_2 in the former homogenized at 23.7°C and in the latter at 30.5°C.

The CO_2-rich inclusions generally coexist with type A inclusions and a few of them show similar T_h values(e.g. 103156, Appendix 10.10). However, most type A inclusions are thought to have been derived from different fluids because the CO_2-rich inclusions are only few in number, there generally being only one or two inclusions among a number of type A inclusions in one specimen, and some of them occur separately(e.g. 103214, Appendix 10.10).

The presence of CO_2 in fluids in veins and particularly quartz veins in the Jangsan Quartzite indicate that CO_2 was a component of the ore solutions. However, T_h values are relatively low and it is possible that the CO_2-bearing fluids were formed by reaction with limestone during secondary fluid circulation in the ore zone.

CO_2 was found in only one specimen in the M1 skarn, but CO_2 may have been eliminated from other inclusions during fluid reworking or it may have formed only locally during relatively late secondary circulation.

In CO_2-bearing inclusions, clathrate formation during freezing runs was rarely observed because of the small size of the inclusions. Although clathrate was observed in a few larger inclusions, the T_m clathrate could not be determined accurately.

Using the methods outlined by Burruss(1981), it is possible to calculate the mole fraction of CO_2 in the CO_2-bearing inclusions(Table 10.4). Most range between 0.1 and 0.2, the lowest value(0.05) being in the one sample from the M1 skarn(106020). For most Sangdong inclusions, the absence of visible liquid-CO_2 indicates CO_2 contents less than 2-3 mole % CO_2(Collins, 1979) and the scarcity of clathrate observation probably indicates less than 0.2 mole % CO_2.

10.5. Homogenization of Type C Inclusions

The T_h and T_m data from these salt-bearing inclusions are given in Appendix 10.11. Most contain only halite(recognized by its perfect cubic form), but a few inclusions, one from scheelite(specimen 103170), one from pyroxene(Fig. 10.20b, specimen 103063), and others from clear quartz (specimen 103154), contained a sylvite crystal in addition to a halite crystal. Specimen 103154, a clear transparent quartz crystal in milky white quartz, showed a number of halite-bearing inclusions and several inclusions with both halite and sylvite(Fig. 10.20a).

Using data of Ravich & Borovaya(1949) and Roedder(1971) for salt melts K/Na ratios for sylvite inclusions were determined as varying from 0.29 to 0.73(Fig. 10.21; Appendix 10.11). The variation is considerable but the data are too few to indicate trends.

In some type C inclusions $T_m NaCl > T_h$, a situation possibly explained by the halite trend of Cloke and Kesler(1979) as illustrated in Fig. 10.19. The results for sample 103154 are shown and cooling paths shown to illustrate precipitation of halite before(in some cases) or after(in other) the fluid intersects the vapour curve.

It has already been noted that the type C inclusions in pyroxenes of the pyroxene-garnet skarn could be the saline component of a two-phase system, coexisting with the gas-rich inclusions. This remains a possibility but type C inclusions exist in the quartz-mica skarn and the quartz veins where there is no other evidence of boiling.

A second, perhaps more likely, hypothesis is that the high salinities represent groundwater incorporated into the hydrothermal system more or less continuously through its life. They are present from the highest skarn temperatures down to the relatively low temperatures of the late quartz veins.

Fig. 10.19. Extrapolated solubility curve along the Sangdong halite trapping(e.g. specimen 103154).

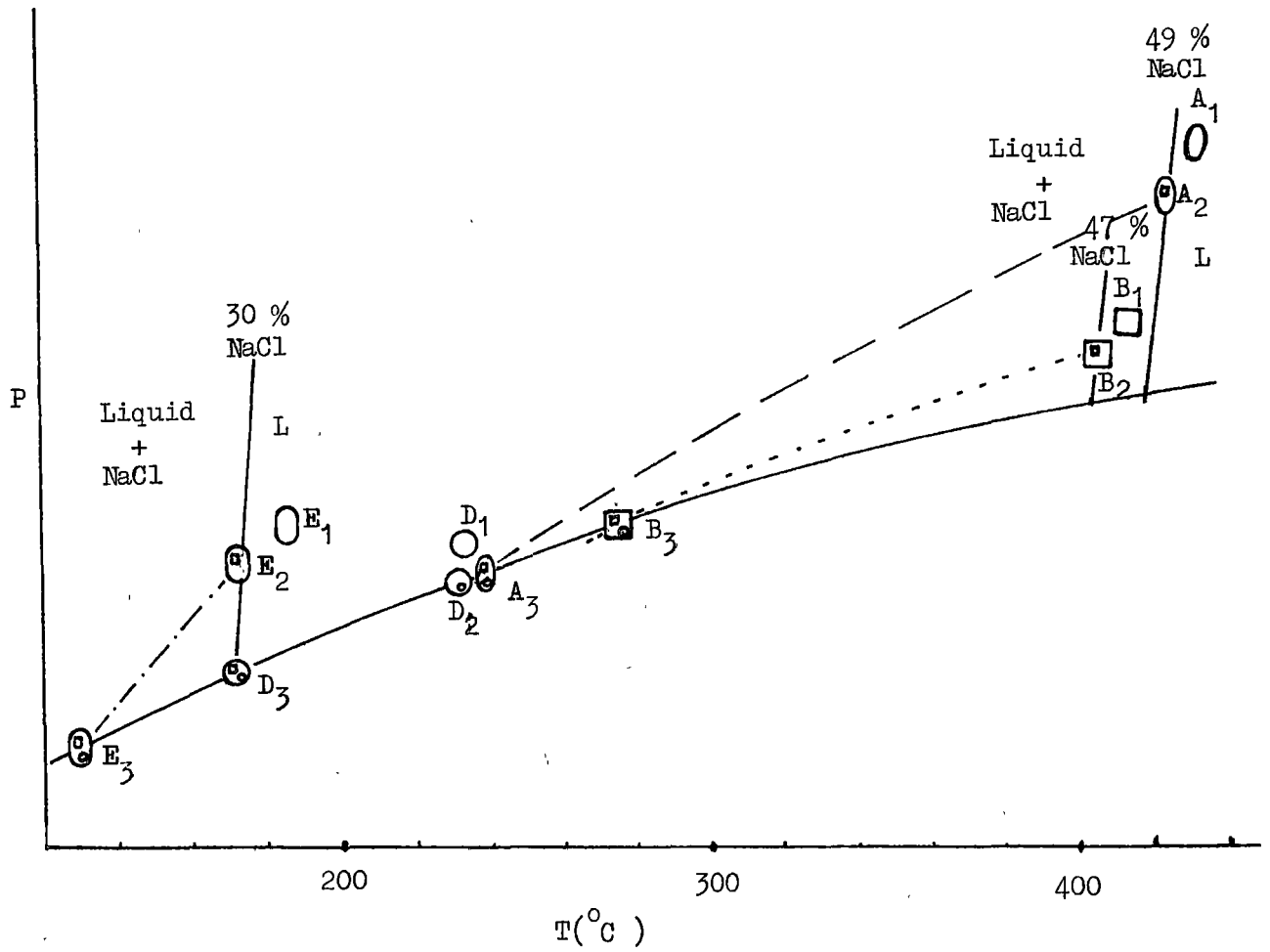

Changes of salinity in the fluids by crystallization of halite

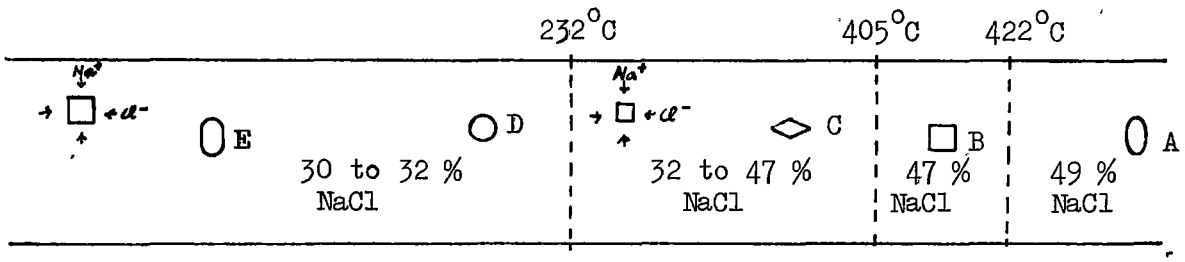

Homogenization Temperatures

	E	D	C	B	A
T_h	128	233	277	275	238
T_m(NaCl)	170	172	232	405	422

Fig. 10.20(a). Type C inclusion showing two solid inclusions, halite and sylvite. S=sylvite, H=halite. 103154(clear quartz in quartz vein), 15 block, -5th level. ——— represent 0.01 mm.

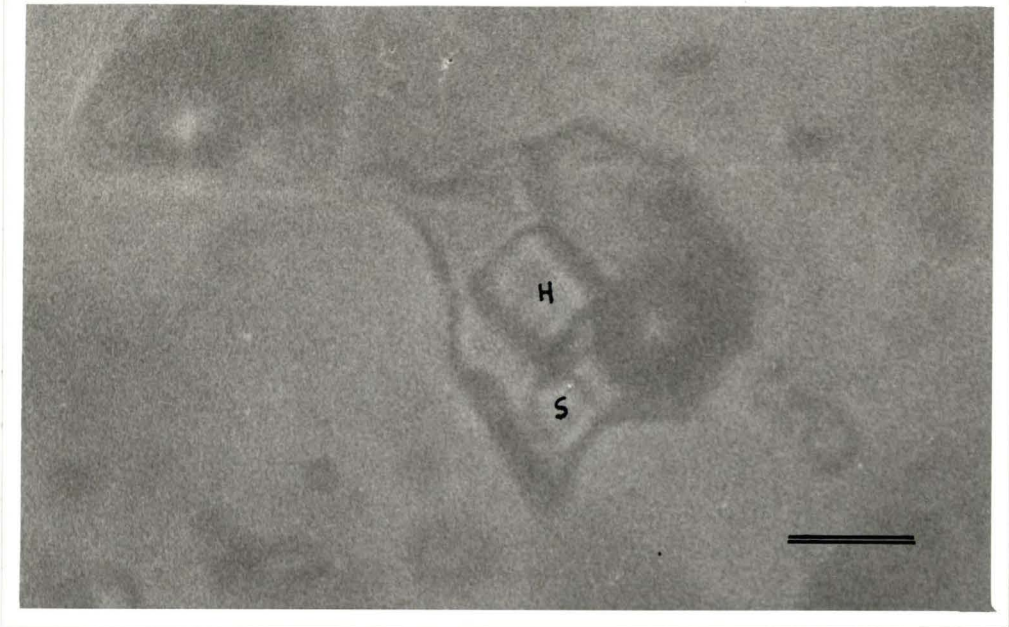

Fig. 10.20(b). Type C inclusion showing two daughter minerals, halite and sylvite, in pyroxene. 103063(pyroxene skarn), Jangsan(+ 3) level. ——— represent 0.02 mm.

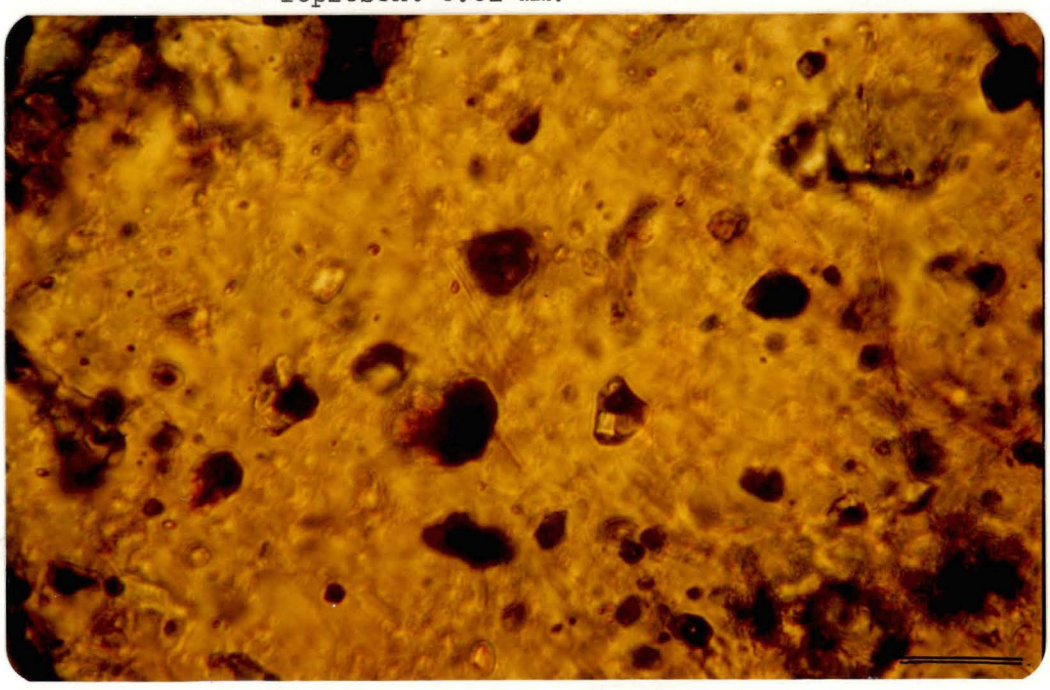

10.6. Determination of Pressure and Pressure Corrections

The evidence of boiling during pyroxene growth indicates that T_h values above 366°C do not require pressure corrections.

Fluids showing near-critical behaviour on homogenization give T_h values equal to or less than the true trapping temperatures. Assuming the inclusions are represented by a simple NaCl-H_2O system(Fig. 10.24), minimum pressure estimates between 225 and 375 bars are indicated(Table 10.5). These values are only qualitative as the fluids are clearly more complex. The near-critical T_h values in pyroxenes have values similar to T_h values associated with gas-dominated inclusions, indicating they are realistic trapping temperatures. Near critical inclusions in quartz and fluorite are not associated with gas-rich inclusions but probably also require minor corrections for pressure as they have T_h values compatible with corrected trapping temperatures of coexisting type A inclusions which did not exhibit critical phenomena.

An independent estimate of pressure is possible using the composition of sphalerite coexisting with pyrite and pyrrhotite in the mica skarn (specimen 103121, Table 6.26). This allows an estimate of the total pressure for skarn formation, using an equation recently determined by Shimizu and Shimazaki(1981), based on Scott and Barnes(1971), as follows:

$$P(kb) = 42.30 - 32.10 \log M_{FeS}^{sph}$$

where M_{FeS}^{sph} is mole % FeS in sphalerite. In specimen 103121 the mole % FeS has a range of 19.36 to 20.96 % yielding average pressure of 800 bars.

According to K-Ar age dating(Farrar et al., 1978), tungsten mineralization followd the formation of the Hambaeg Syncline, suggesting that at least Triassic sedimentary rocks had been accumulated when mineralization occurred in the Sangdong area. The thickness of the cover of Carboniferous to Triassic age over the present mine would appear to have been more than 2.5 km. This suggests a lithostatic pressure of approximately 625 bars.

Table 10.4. Calculated values of bulk density of CO_2-bearing inclusions (using data from Burruss, 1981).

Sample No.	$T_h CO_2$ (°C)	Dco_2 g/cc	Pco_2 at 40°C (bars)	Bulk D mole/l	Bulk Molar V cm^3/mole	H_2O Mol%	H_2O V %	X_{CO_2}	T_h (°C)
103161	28.8	0.70	120	46	21.7	83.9	65	0.16	254
103161	23.7	0.78	135	42.6	23.5	88.0	68	0.12	236
103155	29.1	0.55	98	36.4	27.5	81.6	52.3	0.19	243
103156	25.1	0.6	100	48.6	20.6	90	82.5	0.1	223
103106	28.1	0.67	113	43	23.3	88.6	68.3	0.11	220
106020	28.9	0.65	110	50.1	19.9	95	87.5	0.05	308
103198	28.9	0.65	199	42.5	23.5	89	69	0.11	199
103215	30.7	0.5	90	47.5	21.1	94	81.4	0.06	394

D = density, V = volume

Table 10.5 . Critical temperatures applied to estimate minimum pressure of trapping inclusions.

(from Sourirajan and Kennedy,(1962))

Sample No.	Host Mineral	Critical Temperature (°C)	NaCl content (%)	Pressure (bars)
103200	quartz	405	3.0	380
106044	quartz	397	2.2	275
106084	pyroxene	425	5.0	340
106039	pyroxene	416	4.2	330
106130	pyroxene	422	4.8	340
106106	pyroxene	403	3.7	280
103120	fluorite	376	0.2	225

Table 10. 6. Range of possible corrections to the homogenization temperatures of type A inclusions at different pressures and salinities at the Sangdong tungsten skarn deposit.

300 bars

Salinity NaCl(%)	T_h(°C) 150	200	250	300	350	400
1	30	24	15	15		
5	32	25	21	19	20	
10			25	20	20	20
15			30	22	18	15
20			35	25	20	18
25			27	20	17	15

500 bars

Salinity NaCl(%)	T_h(°C) 150	200	250	300	350	400
1	45	40	40	47	60	80
5	45	40	38	38	45	48
10			43	39	40	42
15			45	40	38	38
20			50	45	45	48
25			40	48	60	80

800 bars

Salinity NaCl(%)	T_h(°C) 150	200	250	300	350	400
1	66	62	64	75	90	108
5	66	63	62	66	78	100
10			70	69	72	78
15			71	70	70	104
20			80	74	70	72
25			70	70	71	78

At pressures of 300 bars, 500 bars and 800 bars the pressure corrections for fluids of the salinities encountered in type A inclusion from quartz using Potter(1977)'s diagrams are presented in Table 10.6.

Applying corrections for fluids in type A inclusions except those with near-critical behaviour and evidence of boiling(in pyroxene only), it is found that most trapping temperatures lie in a broad band between 300°- 500° C throughout the skarn and in veins. Variation within minerals, across veins, etc., occur within this spectrum but there was no obvious temperature gradient across the skarn zones during the main growth period. However the early skarns(e.g. wollastonite-bearing) formed at relatively high temperature and the muscovite-rich at a relatively low temperature, indicating an overall decline in temperature with time.

10.7. Composition of The Fluid Inclusions

The most common species detected in fluid inclusions are Na^+, K^+, Ca^{++}, Mg^{++}, Cl^-, SO_4^{-2}, CO_3^{-2}, HCO_3^-, CO_2, CH_4 and N_2(Roedder, 1972). The phase diagrams for the systems containing these ions have made possible the estimation of the composition and density of individual inclusions. Crawford(1981) pointed out that bulk analysis of extracted fluid from many inclusions is generally not satisfactory for the study of aqueous inclusions, due to the variety of fluid compositions which may occur. It is also very difficult to avoid surface contamination(Patterson et al., 1981).

On the assumption that fluid inclusions observed are constant in volume and composition, cooling and heating observations have been made on inclusions that were large enough to observe clearly. Phase changes during freezing studies allow identification of the composition of the fluids in inclusions. In type A inclusions T_e, T_m and T_f measurements provide information of the solute species(e.g. $CaCl_2$, $MgCl_2$, NaCl) and the total

solute concentration. Melting temperatures of solid daughter minerals (NaCl, KCl) in type C inclusions allow reasonably accurate determinations of solute concentration of NaCl and KCl in fluids of the inclusions and K/Na ratios(Fig. 10.21). Salinities determined from melting temperature of ice(T_f) in type B inclusions are likely to be erroneous because of clathrate formation during cooling(Collins, 1979).

Records of typical phase changes are summarized in Appendix 10.13.

Most type A inclusions showed hydrohalites on warming from $-50^{\circ}C$ though these are very difficult to observe and distinguish from ice. Type C inclusions exhibited hydrohalite until the halite started to crystallize at about $0.1^{\circ}C$(e.g. specimen 103154 showed final T_m of hydrohalite was $-0.6^{\circ}C$ and first appearance of halite was at $+0.5^{\circ}C$, Appendix 10.13, ex.3).

Only a few specimen showed type C inclusions with sylvite + halite(Fig 10.20a & b). Although sylvite has not been observed in most type C inclusions, the abundance of micas in the scheelite-rich zone and evidence of K-metasomatism show that potassium must have been an important element in the ore solution. It would appear that the KCl/NaCl ratio is relatively high(in Appendix 10.11, e.g. KCl/NaCl in scheelite = 0.9; KCl/NaCl in quartz = 0.4 - 0.9).

A number of inclusions showed eutectic points(T_e) somewhat lower than for the NaCl-H_2O system, i.e. lower than $-20.8^{\circ}C$(Potter et al., 1978; Crawford, 1981). T_e varied between -20° and $-30^{\circ}C$, and some of this eutectic depression could be due to the presence of KCl. A possible cause of the eutectic depression to $-30^{\circ}C$ is the existence of a metastable eutectic in the NaCl-H_2O system at $-28^{\circ}C$(Crawford, 1981).

Kwak and Tan(1982) have stressed the likely importance of $CaCl_2$ in fluids of the King Island skarn deposit. A number of inclusions showed first melting temperatures(T_e) of -50° to $-55^{\circ}C$, presumably due to melting of $CaCl_2 \cdot 6H_2O$ and/or $MgCl_2 \cdot 12H_2O$. Freezing data given by Linke(1965), Ypma(1979) and Crawford(1981) indicate that the eutectic point of the

$CaCl_2$-H_2O is depressed below -55°C by the addition of NaCl, KCl and $MgCl_2$. Roedder(1963) quoted Seidell's data that the eutectic temperature in the $CaCl_2$-NaCl-$MgCl_2$-H_2O system is -58°C, whereas that of $CaCl_2$-H_2O is -51°C and of $CaCl_2$-NaCl-H_2O is -52°C. In specimen 103154(Ex. 3 & 4 in Appendix 10.13), the first melting temperatures of -56°C to -61°C may indicate the presence of $MgCl_2$, KCl and $CaCl_2$. A few daughter minerals thought to be NaCl may in fact be $FeCl_2$ or $FeCl_3$, species which are hard to detect by freezing and heating observations but which are likely to be present.

Liquid CO_2-bearing(type B) inclusions are rare and mostly in quartz veins. However, a small amount of CO_2 may well be present in much of the system, the presence of clathrates on cooling being very hard to detect in such small inclusions(12-18 microns). Similar T_h values occur in coexisting type B and type A inclusions but there are no CO_2-rich inclusions such as would be expected in an immiscible system. Inclusions with low T_h values have anomalously high CO_2 contents for fluids of about 5 wt % NaCl equivalent and those with high T_h values have anomalously low CO_2 contents, if they are considered as the part of an immiscible CO_2-NaCl-H_2O system(see Table 10.4, & Gehrig et al.,1979). Thus the inclusions appear to have been trapped from one phase system and may be relics of an earlier fluid now largely removed by reworking by later fluids.

The total salinities of type B inclusions measured by T_f probably include the effects of CO_2 and therefore too high when expressed in terms of equivalent weight % NaCl. The range of salinity obtained from limited numbers of type A and B inclusions in various minerals lies between nearly fresh water and about 22 wt % NaCl equivalent concentration. Halite-bearing type C inclusions show a wide range of salinities, from 28 to 51 wt % NaCl. There is no obvious variation of salinity with depth(Fig. 10.22). Fig. 10.23 plots salinity versus T_h according to host mineral and type of occurrence. There is a slight indication of a bimodal distribution which tends to confirm previous suggestions of there being two(or more) fluids involved.

Fig. 10.21. Phase diagram for part of the system NaCl-KCl-H_2O. Data from Roedder(1971).

Sample No.	Host Mineral	KCl	NaCl	H_2O
103170(b)	scheelite *	20	22	58
103154	quartz ★	29	31	40
	quartz ⊙	14.5	38.6	46.9
	quartz ●	16.6	28.3	55.1

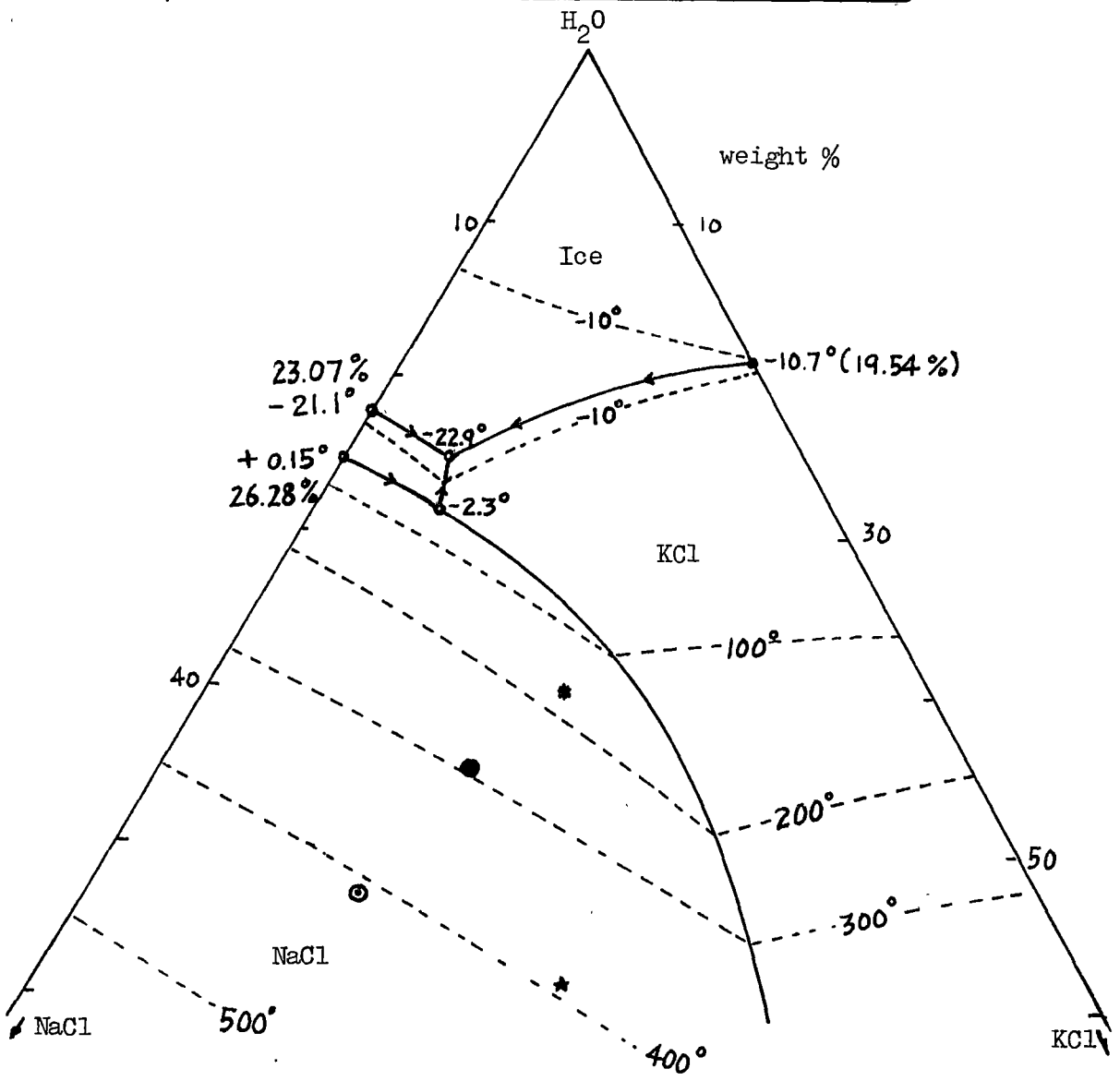

Fig. 10. 22. Variation in salinities of fluid inclusions in quartz with depth.

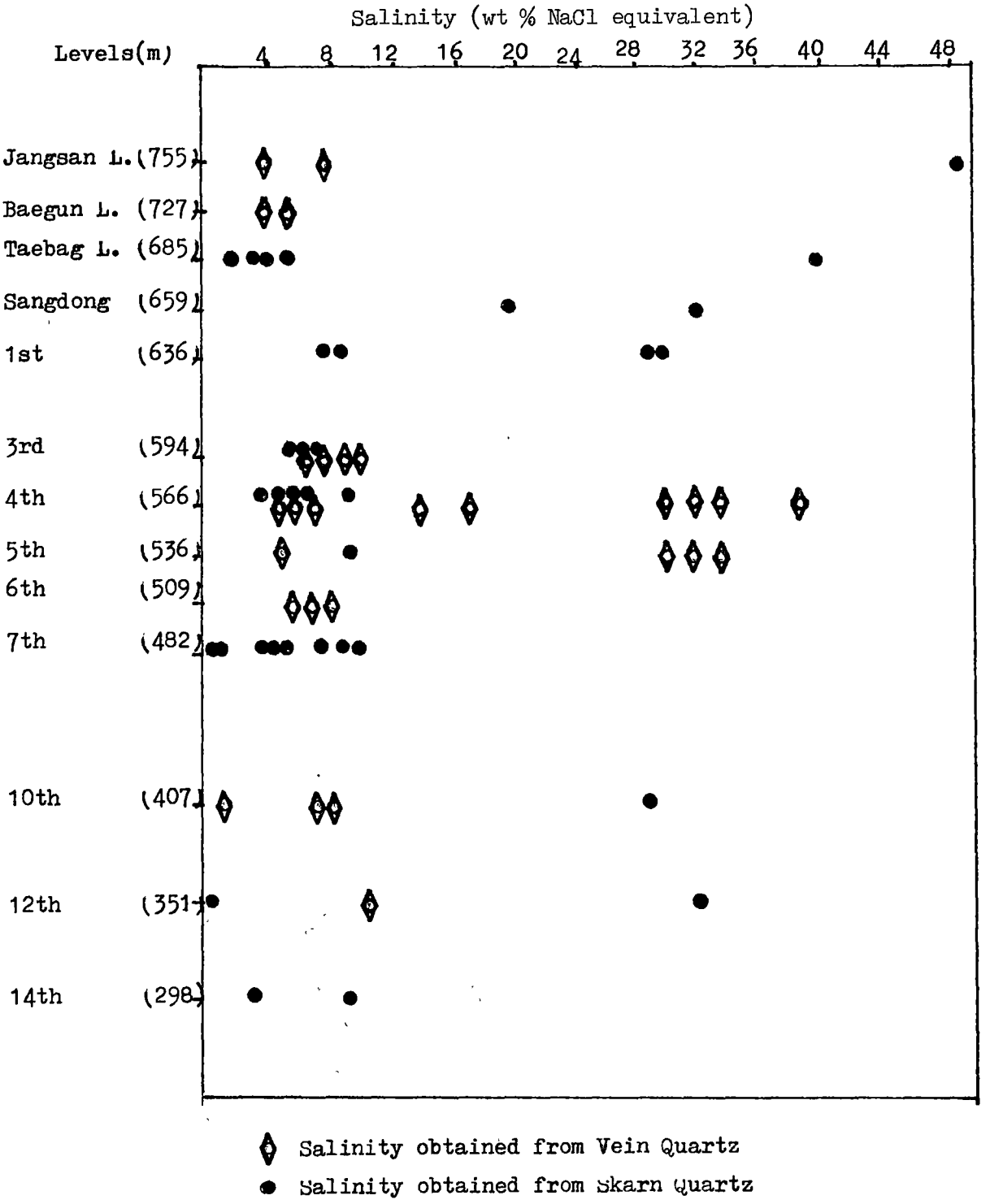

Fig. 10.23. T_h versus salinities from quartz, scheelite, fluorite and pyroxene.

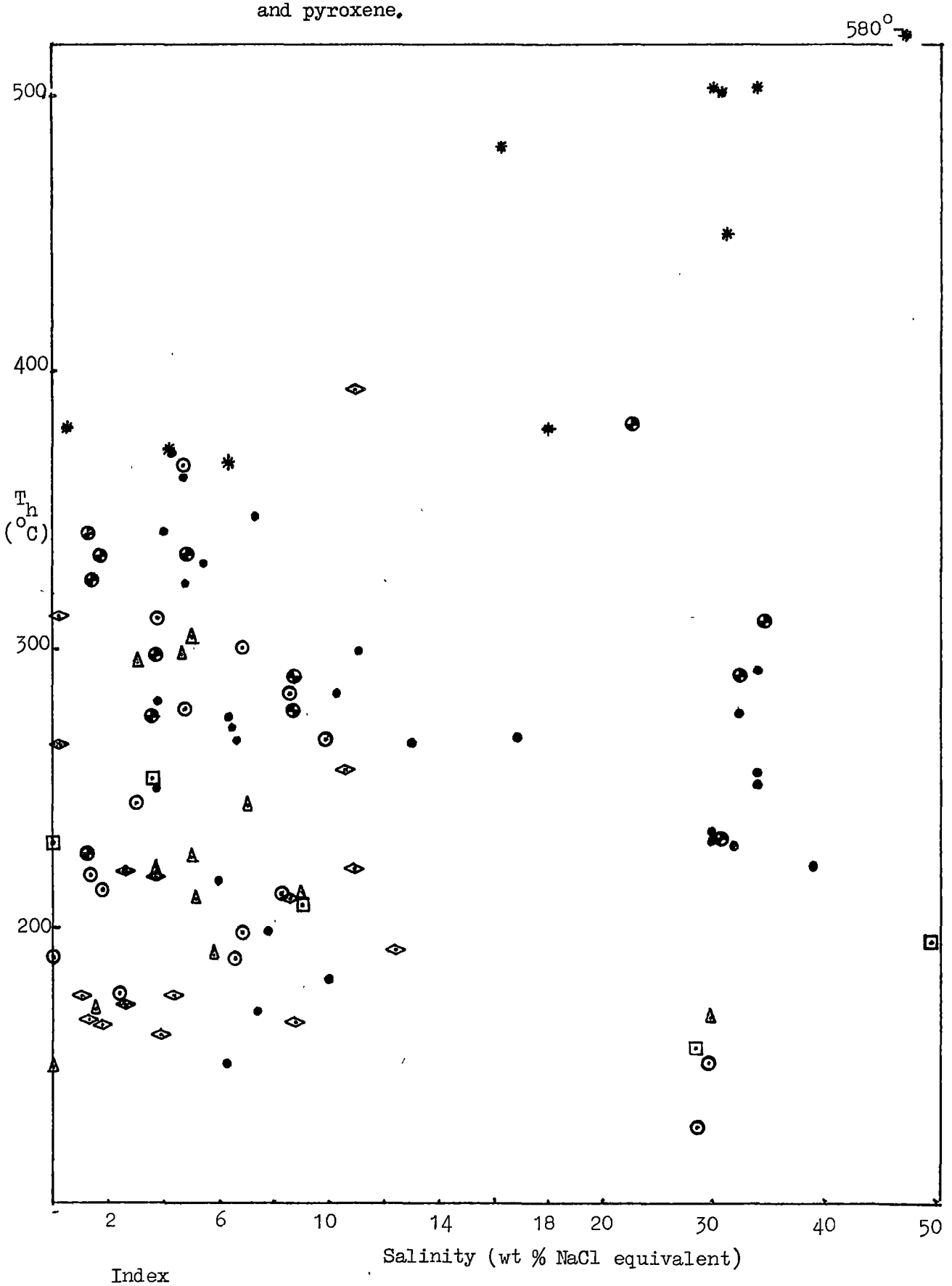

Fig. 10.24. A possible range of P-T-X estimated by plotting critical temperatures in the system NaCl-H_2O, from Sourirajan and Kennedy(1962).

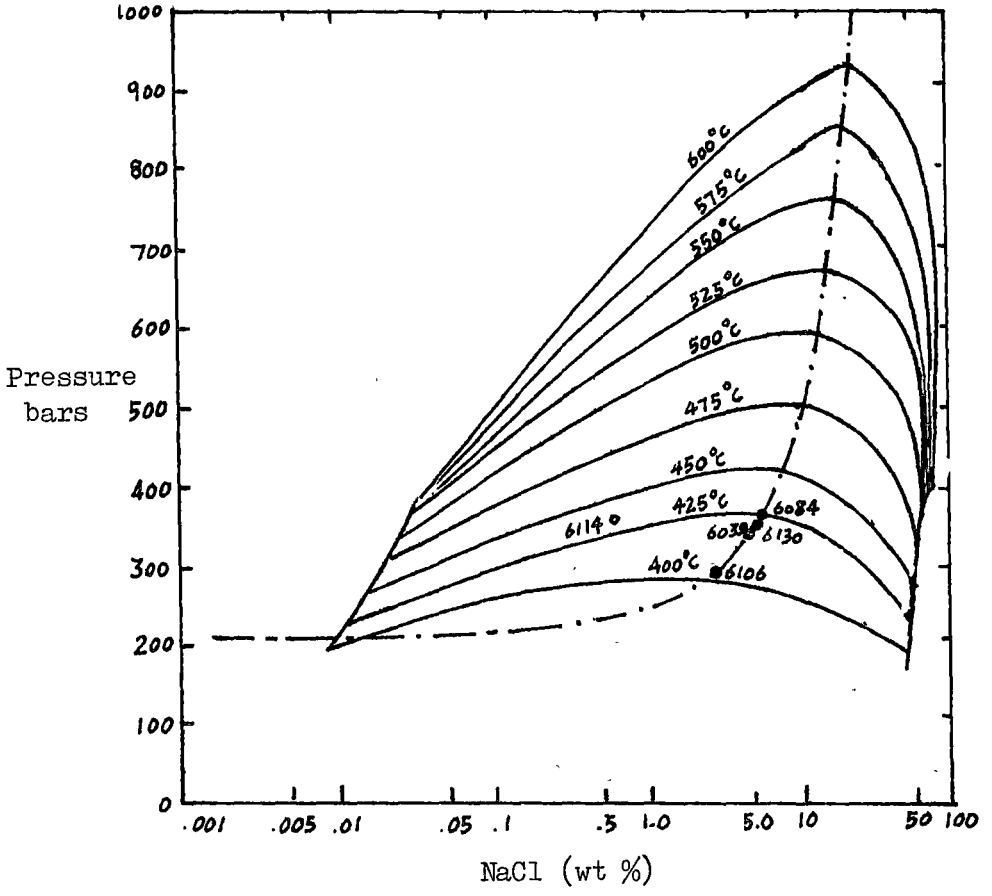

Data plotted are based on Table 10.5.

Sample No.s ; 6106 = 106106; 6084 = 106084 . . . .

10.8. Summary

Coexisting vapour and liquid type A inclusions with similar T_h values in the pyroxene skarn indicate boiling, and a few in this group show near-critical behaviour. As there are no experimental data available for the $KCl-NaCl-MgCl_2-CaCl_2-H_2O$ system, it is not possible to plot the position of the gas-liquid cone analogous to that of Sourirajan and Kennedy(1962) for the $NaCl-H_2O$ system. Nevertheless, the available data are plotted on in this system to indicate in general terms the probable P - T conditions (Fig. 10.24). The $NaCl-H_2O$ system would indicate pressures of 225-380 bars for the near critical fluids but the two-phase cone probably shrinks with addition for other salts(see, for example, the $NaCl-KCl-H_2O$ system, Linke, 1965), indicating even lower pressures.

Type C inclusions in the pyroxene with relatively high salinities may represent the salt-rich member of the two phase system but a more likely explanation is that they represent groundwaters that have penetrated the system and mixed with the ore solutions. The presence of two fluids of contrasting salinity is indicated by the bimodal distribution of salinities in quartz from other skarn zones and quartz veins(Fig. 10.23). Type C inclusions with $T_m NaCl > T_h$ and $T_h > T_m NaCl$ probably reflect slightly different cooling paths from a supercritical fluid.

The highest T_h values occur in pyroxenes of the pyroxene-garnet skarn (Fig. 10.11, Appendix 10.4). Quartz coexisting with the pyroxene generally has a lower T_h and no vapour-rich inclusions. T_h in quartz increases progressively from this skarn through the amphibole skarn to the quartz-mica skarn(Fig.10.9), though these T_h values are not as high as in the pyroxene. Relatively low T_h values(Fig.10.10) occur near the centre of the quartz-mica zone, Scheelite shows a similar trend to quartz(Fig. 10.15b, Appendix 10.6). These data are interpreted as follows:

(1) Pyroxene-garnet skarn formed by replacement of limestone from two-phase fluids of temperature 350°- 550°C. The lower T_h values may result from later reworking. Because all but the coolest of these the fluids lay on the gas-liquid surface, no pressure correction to the T_h values is required above 366°C. This skarn formed mainly at lower temperatures than the earlier wollastonite-bearing skarn.

(2) The pyroxene-garnet skarn was partly replaced by pyroxene, amphibole and mica skarns from non-boiling fluids at a temperature probably ranging from 300° to 500°C(pressure corrected T_h values).

The temperature decreased outward from the central mica zone during deposition of part of the quartz, fluorite and scheelite(and probably chlorite).

(3) Late fluids associated with the formation of muscovite, quartz in the core of the mica skarn were relatively dilute and lower temperature, probably about 350°C.

Quartz veins may have formed at the same time as the muscovite-rich skarn as inclusions have similar homogenization characteristics. There is no evidence of a temperature gradient in the veins but wolframite- and molybdenite-bearing veins appear to have formed at a higher temperature than other types.

(4) Quartz and fluorite deposition continued to even lower temperature ($\sim$250°C).

11. STABLE ISOTOPES

11.1. Sulphur Isotope Study

Representative sulphide samples were taken from the skarn orebody and from the quartz veins, including five pairs of coexisting sulphide minerals for geothermometry. Analyses were made on pyrrhotite, pyrite, chalcopyrite, molybdenite, bismuthinite, galena and sphalerite. The analytical procedures in use at the University of Tasmania laboratory are described in Appendix 11. The $\delta^{34}S$ permil values are standardized to Canon Diablo troilite, and the precision is approximately $\pm$ 0.1 permil.

The sulphur isotope values range from +3.5 to +6.7 permil and average +5.0 permil with a standard deviation of 0.77 permil(Table 11.1). The order of decreasing average $\delta^{34}S$ of molybdenite, pyrite, pyrrhotite, sphalerite, chalcopyrite, bismuthinite and galena is in agreement with the observations of Bachinski(1969). For both pyrite and pyrrhotite, there is an apparent increase in $\delta^{34}S$ values with depth(e.g. for pyrite, upper levels have $\delta^{34}S$ below +5.4 permil while at deep levels(-10 & -12th) $\delta^{34}S$ is greater than +6.6 permil; for pyrrhotite, upper levels have $\delta^{34}S$ below +5.0 permil while deep levels(-15 & -17th) have greater than +5.8 permil; Table 11.1).

Five pairs of sulphides were used for geothermometry(Table 11.2), the members of each pair occurring in contact.
However, lack of consistency in fractionation of mineral pairs containing pyrite indicates a lack of equilibrium, a common occurrence for any relationships involving pyrite(Ohmoto et al.,1979). The temperatures for the pyrite-galena pairs range from 471° to 686°C (based on the equation of Ohmoto and Rye, 1979) and for the sphalerite-galena pair from 547° to 607°C. These isotopic temperatures are higher than the corrected T_h values of fluid inclusions in quartz associated with these sulphide minerals(Fig. 10.6a). It must be assumed therefore that even minerals in

contact did not form together in isotopic equilibrium.

Although most of the sulphide minerals used for isotopic analyses were taken from quartz veins, the $\delta^{34}S$ of sulphides from the skarn orebody and from quartz veins are similar, for example, molybdenite and pyrrhotite (Table 11.1).

The skarns and quartz veins formed from acid($pH \approx 4$), reduced(magnetite-pyrrhotite-pyrite) solutions. $H_2S_{(aq)}$ is likely to be the dominant sulphur species in such conditions and hence the $\delta^{34}S$ value of the solution sulphur was probably similar to that of sphalerite and slightly less than that of pyrite(Ohmoto et al.,1979).

The fluid sulphide composition has been calculated using the data of Ohmoto and Rye(1979), assuming a temperature of 350° or $400^{\circ}C$ for the relatively late-stage pyrrhotite of the pyroxene-garnet skarn and the sulphides of the quartz-mica skarn, and a temperature of $350^{\circ}C$ for the quartz veins. For the skarn and the quartz veins, $\delta^{34}S_{H_2S}$ ranges from +4.5 to +5.3 permil, suggesting a magmatic origin for the sulphur.

The upward decrease in $\delta^{34}S_{po}$ & $\delta^{34}S_{py}$ may be due to a gradual depletion in ^{34}S during deposition of pyrite and pyrrhotite in a closed system.

Table 11.1 $\delta^{34}S$ values of sulphide minerals from the Sangdong deposit.

Sulphides	Sample No.(field no.)	Host Rock	$\delta^{34}S$ (per mil)	Mean	Standard Deviation
Pyrite				+ 5.4	0.74
	106154 (B-1-2)	quartz vein	+ 4.9		
	106155 (B-1-6)	quartz vein	+ 5.0		
	106157 (Sang)	quartz vein	+ 4.6		
	106158 (3-21)	quartz vein	+ 5.3		
	103208 (G-1-4)	quartz vein	+ 5.4		
	103214 (M-2-4)	quartz vein	+ 4.9		
	103216 (N-1-7)	quartz vein	+ 6.7		
	103222 (p-1-5)	quartz vein	+ 6.6		
Molydenite				+ 5.5	0.68
	103125 (0217)	quartz-mica skarn	+ 5.8		
	103156 (0138)	calcite vein	+ 6.2		
	103203 (F-3-2)	quartz vein	+ 6.3		
	103200 (F-2-2)	quartz vein	+ 5.4		
	103151 (0185)	quartz vein	+ 4.9		
	103152 (0208)	Jangsan Quartzite	+ 4.4		
Pyrrhotite				+ 4.9	0.66
	103153 (0168)	quartz vein	+ 4.9		
	106159 (0128)	quartz vein	+ 4.4		
	106160 (Po-0)	pyroxene skarn -0	+ 4.6		
	106161 (Po-5)	pyroxene skarn -5	+ 4.2		
	106162 (Po-7)	pyroxene skarn -7	+ 5.0		
	103150 (Bt-1)	quartz-mica skarn	+ 4.3		
	106163 (Po-15)	pyroxene skarn-15	+ 6.1		
	106164 (Po-17)	pyroxene skarn-17	+ 5.8		
Sphalerite				+ 4.9	0.4
	103208 (G-1-4)	quartz vein	+ 5.3		
	103216 (N-1-6)	quartz vein	+ 4.5		
Chalcopyrite				+ 4.8	0.24
	106157 (Sang)	quartz vein	+ 4.8		
	106158 (3-21)	quartz vein	+ 5.1		
	106165 (005)	quartz vein	+ 4.7		
	106166 (0056)	quartz vein	+ 4.4		
	106167 (0035)	quartz vein	+ 5.0		
Bismuthinite				+ 4.3	0.4
	106168 (0119)	quartz vein	+ 4.7		
	106169 (SK)	total skarn	+ 3.9		
Galena				+ 3.6	0.1
	103208 (G-1-4)	quartz vein	+ 3.7		
	103214 (M-2-4)	quartz vein	+ 3.7		
	103216 (N-1-6)	quartz vein	+ 3.5		

**Key: field no. indicates levels; B=Baegun lv. Sang=0 lv. 3=3rd lv. G=5th lv. M=9th lv. N=10th lv. P=12th lv. Po-5=5th lv. Po-17=17th lv.

Table 11.2 $\delta^{34}S$ values of coexisting pairs.

Sample No.	$\delta^{34}S_{py}$	$\delta^{34}S_{cp}$	$\delta^{34}S_{sp}$	$\delta^{34}S_{gn}$	Δ	Temperature(T_h) ^{o}C
106157	4.6	4.8			-0.2	
106158	5.3	5.1			+0.2	
103208	5.4		5.3		+0.1	
				3.7	+1.7	471 - 502 (*280)
103214	4.9			3.7	+1.2	612 - 686 (*350)
103216			4.5	3.5	+1.0	547 - 607 (*300)

(*) Corrected T_h values, from T_h data of coexisting quartz

11.2. Carbon and Oxygen Isotopes in Carbonates

A carbon and oxygen isotope study was undertaken on the samples from (a) the unmineralized interbedded limestone layers equivalent to the M1 orebody, (b) the relict limestone in the skarn ores, (c) a calcite occurring in the quartz-mica(biotite) skarn, and (d) calcite veins mainly associated with molybdenite. No graphite has been identified in the Sangdong deposit. Carbon isotopes($^{13}C/^{12}C$) are quoted relative to PDB and oxygen($^{18}O/^{16}O$) to SMOW(Ohmoto and Rye, 1979), with precisions of ± 0.1 permil. The method is as described in Appendix 11.1.

The limestone samples include six samples from outcrops in the unmineralized zone, two samples of limestone relics in the M1 skarn from the 7th level, and one sample from unmineralized limestone outside the skarn on the 17th level. Calcites were separated from two different calcite veins, one containing molybdenite(samples 103200 & 103105), the others(samples 103182 & 103157) containing fluorite, quartz, muscovite and pyrite. Coarse grained patches of calcite occurs associated with fluorite, scheelite, biotite and quartz in skarn ore(sample 103120).

As shown in Table 11.3 and Figs. 11.1 and 11.2, the $\delta^{13}C$ values of the interbedded limestones range from +1.25 to -1.64 permil and the $\delta^{18}O$ values range from +10.9 to +15.4 permil. Kim(1980) reported similar $\delta^{13}C$ values of the Pungchon Limestone ranging from -1.2 to +1.3 permil and $\delta^{18}O$ values from +10.6 to +18.7 permil; these results are typical of of marine limestones(Ohmoto and Rye, 1979). However, some of the spread reflects a trend of increasing $\delta^{13}C$ values of the interbedded limestones with distance from the central zone of the Sangdong mineralization. This may reflect recrystallization effects but is more likely the result of metasomatism by a fluid rich in $\delta^{12}C$.

Using T_h values of quartz or fluorite coexisting with calcite(Table 11.3), it is possible to determine the carbon and oxygen isotopic

composition of the fluids from the carbonate determinations. The fractionation factors used were from Bottinga(1968) for $\delta^{13}C$ and O'Neil et al.(1964) for $\delta^{18}O$ (Table 11.4). Some of the variation in calculated $\delta^{18}O_{H_2O}$ may reflect the use of inappropriate temperatures.

The $\delta^{18}O$ results suggest that the water in the fluids was probably of magmatic origin, since the calculated $\delta^{18}O$ values of the water are in the range of primary magmatic water($\delta^{18}O_{H_2O}$ = +5.5 to +9.0 permil, Taylor, 1979). The $\delta^{13}C$ values indicate reaction with fluids having varying negative values for $\delta^{13}C_{CO_3^{=}2}$. Absence of graphite as mineral in the ore-bodies, the apparent lack of CH_4 in the fluids(though small amounts could be present), and knowledge of solution conditions indicate that H_2CO_3 (apparent) was the dominant solution species of carbon.

For conditions of log f_{O_2} = about -32 at 350°C, the $\delta^{13}C$ value of the fluid can be represented by the $\delta^{13}C$ value of the calcites. Under this assumption, the $\delta^{13}C_{\Sigma C}$ in the fluid derived from the magma was about -8 permil. Negative values of $\delta^{13}C$ fluids appear to be typical of many ore deposits including those of magmatic origin(Patterson et al., 1981; Collins, 1981). The vein values, less negative, and cannot be different solely due to the use of inappropriate temperatures and may reflect more oxidizing conditions.

11.3. Oxygen Isotope in Quartz

$\delta^{18}O$ values have been determined for 7 samples of quartz by Peter Blattner of the DSIR, New Zealand, using methods described by Blattner (1975). The results show only a small range in $\delta^{18}O$(Table 11.5). Using T_h values, both corrected and uncorrected, the $\delta^{18}O_{H_2O}$ can be calculated using the fractionation factors of Clayton et al.(1972). Four results show good agreement, throwing suspicion in the low T_h value of sample 103156. However, this calculated $\delta^{18}O_{H_2O}$ may be valid indicating the

quartz crystal occurring in the calcite vein was derived from a cooler fluid of different isotopic character.

The calculated $\delta^{18}O$ values of the fluids are typical of those derived from magmatic sources, except 103156(Table 11.4).

Fig. 11.1. Comparison of $\delta^{13}C$ versus $\delta^{18}O$ values of calcite from the interbedded limestone and the skarn ore body at the Sangdong mine.

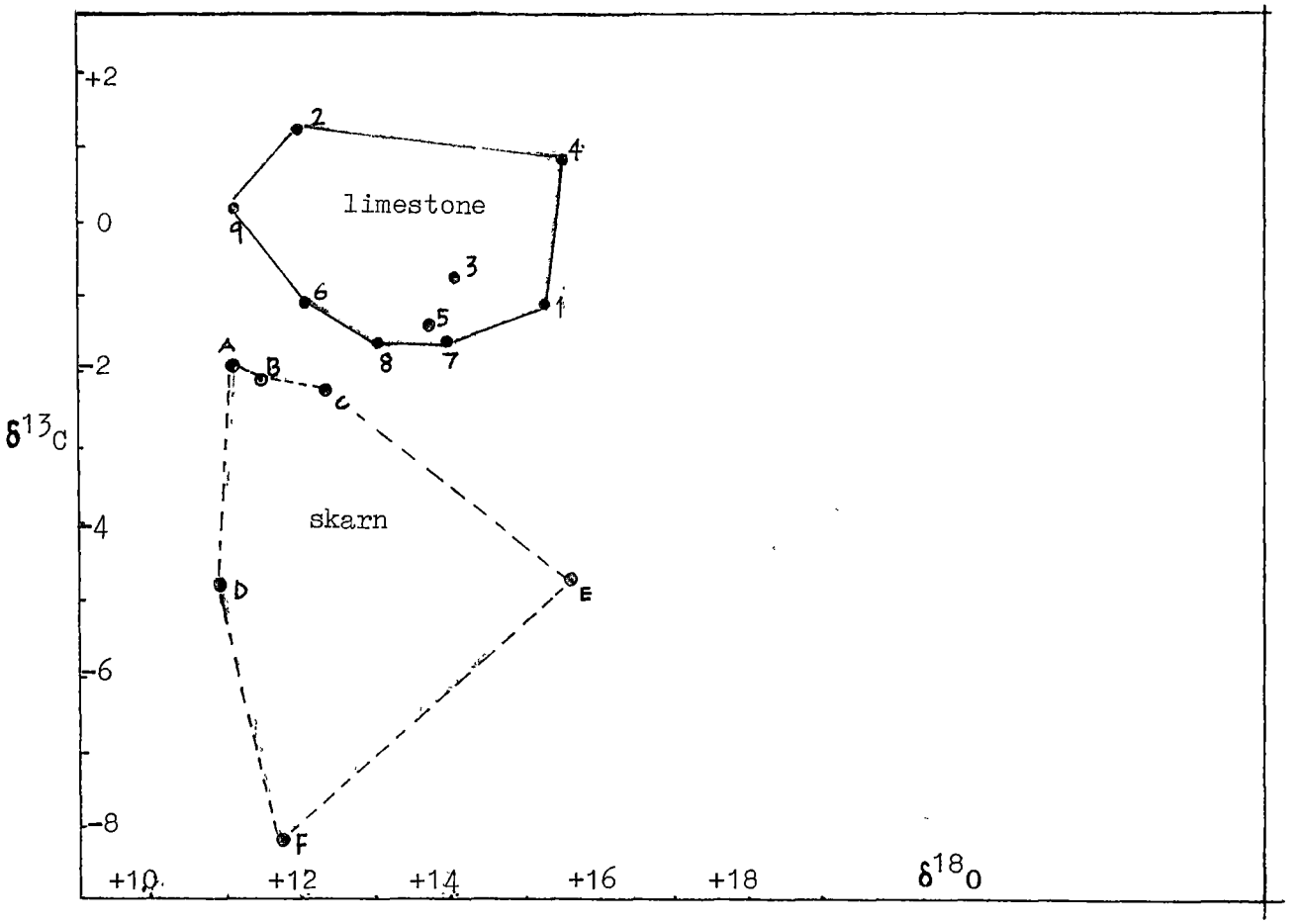

Fig. 11.2. A schematic diagram showing variation of $\delta^{13}C$ values for non-mineralized limestone and mineralized zone at the Sangdong Area

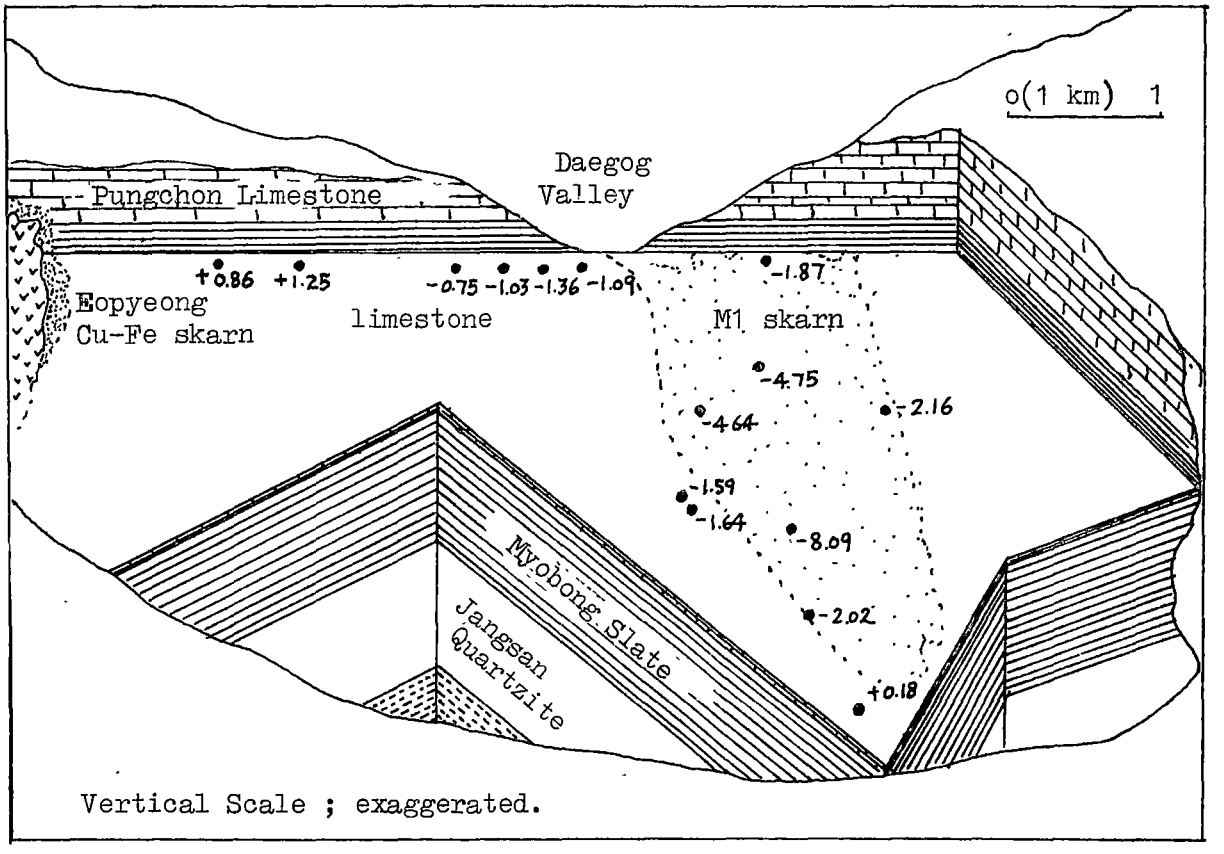

Table 11.3 Carbon and Oxygen isotope analyses of calcite from the Sangdong deposit.

Sample (field) No.	Host Rock	$\delta^{13}C$	$\delta^{18}O_{PDB}$	$\delta^{18}O_{SMOW}$	T_h(°C)
106075 (ls-5)	limestone at Eopyeong	+ 0.86	-14.97	15.43	
103145 (ls-7)	limestone	+ 1.25	-18.4	11.89	
106076 (ls-11)	limestone	- 0.75	-16.34	+ 14.01	
106077 (ls-12)	limestone	- 1.03	-15.17	+ 15.22	
106078 (ls-13)	limestone	- 1.36	-16.87	+ 13.47	
106079 (ls-14)	limestone	- 1.09	-18.29	+ 12.01	
106080 (ls-17)	limestone at -17th lv.	+ 0.18	-19.33	+ 10.93	
106181(K-38-1)	relict of limestone at -7th lv.	- 1.59	-16.56	+ 13.79	
106182(K-38-2)	same as above	- 1.64	-17.52	+ 12.80	
103182(J-1-3)	MoS_2-bearing calcite vein	- 1.87	-19.21	+ 11.05	281 375-385
103200(F-2-2)	MoS_2-bearing calcite vein	- 4.64	-14.97	+ 15.61	302 378
103157(0049)	Barren calcite vein	- 2.16	-18.03	+ 12.27	
103105 (007)	calcite vein	- 2.02	-18.88	+ 11.39	
103156 (0138)	MoS_2 calcite vein	- 4.75	-19.35	+ 10.91	243
103120 (0212)	quartz-mica (biotite) skarn	- 8.09	-18.49	+ 11.80	376(fluo) 342(sch)
Average value of limestone		- 0.57 ± 1.7		+ 13.3 ± 1.4	
Average value of calcite in the skarn orebody		- 3.92 ± 2.2		+ 12.2 ± 1.6	

Table 11.4. Calculated $\delta^{18}O_{fluid}$ and $\delta^{13}C_{fluid}$ from $\delta^{18}O$ and $\delta^{13}C$ values of calcite and T_h values.

Sample No.	Types of Occurrence	$\delta^{18}O_{H_2O}$	$\delta^{13}C_{CO_2}$	T_h(°C) approx.	T_h(°C) (corrected)
103182	MoS_2-calcite vein	7.6(9.3)*	0.83(0.93)*	380	470
103200	MoS_2-calcite vein	12.1(13.4)*	-1.94(-1.84)*	380	470
103156	MoS_2-calcite vein	3.1(3.2)*	-3.12(-2.75)*	240	300
103120	calcite in skarn	8.3(10.2)*	-5.39(-5.29)*	380	480

* Values in bracket are calculated using corrected T_h for pressure.

Table 11.5. Calculated $\delta^{18}O_{fluid}$ from $\delta^{18}O$ values of quartz.

Sample No.	Types of Occurrence	$\delta^{18}O$ of quartz	T_h(°C)	1000 ln	$\delta^{18}O_{H_2O}$
103068	quartz in skarn	10.8 ± 0.3	374 @(464)	4.67 *(3.7)	6.13 *(7.1)
103190	quartz vein	10.8 ± 0.3			
103154	quartz vein	11.56 ± 0.2	350 @(428)	5.31 *(4.25)	6.25 *(7.31)
103156	quartz in calcite vein	11.14 ± 0.2	243 @(305)	9.29 *(7.05)	1.85 *(4.1)
103159	quartz vein in Jangsan Formation	10.59 ±	371 @(461)	4.79 *(4.0)	5.84 *(6.59)
106156	wolframite-scheelite quartz vein	11.53			
103209	MoS_2-quartz vein	11.5 ± 0.5	380 @(470)	4.53 *(3.65)	6.97 *(7.85)

@( ) : Corrected T_h for pressure

* Values in bracket are calculated o$^{18}O_{H_2O}$ using the corrected T_h.

12. CONDITIONS OF SKARN FORMATION

12.1. General Statement

The skarn assemblages at Sangdong are broadly similar to those in other tungsten deposits(e.g. King Island in Australia, Salau in France, Pine Creek in U.S.A., MacTung in Canada). However, in detail there are important differences, particularly in mineral proportions, e.g. some of the Sangdong samples are almost monomineralic. As in other skarns(see, for example, Kwak, 1978a,b; Guy, 1979; Newberry, 1982; Dick and Hodgson, 1982), there is clear overprinting, indicating a protracted fluid evolution, perhaps with changing fluid composition and temperature. The major mineralogical zoning pattern: mica-amphibole-pyroxene, results from intergranular fluid flow outward from a central fluid column. Though diffusion must have taken place, the scale of the zones demands "infiltration metasomatism"(Korzhinski, 1968, 1970) as the dominant mechanism. As the hydrous skarns migrate from the feeder column, earlier pyroxene-garnet±wollastonite skarn is replaced successively by late-stage pyroxene±garnet, and then amphibole- and mica-rich assemblages. Petrographic evidence indicates that the amphibole- and mica-rich zones migrate together, more or less at "equilibrium", and with only minor relics of earlier assemblages within them. However, the amphibole "front" against the late pyroxene-garnet zone is clearly one of replacement and the pyroxene-garnet zone itself is in process of patchy recrystallization with growth of secondary garnets and pyroxenes and localized alteration to amphibole. The dramatic chemical changes and the tendency for metasomatic rocks to become almost monomineralic(e.g. hedenbergite in the late pyroxene-garnet skarn) further supports infiltration processes and an abundance of "mobile" components(see review of Rose and Burt, 1979).

The system was "open" in a chemical sense and resulted from interaction between waves of hot fluid and original or metamorphosed rock. Though the fluids penetrating the lower part of the mine succession were initially

largely of magmatic origin(see stable isotope data), secondary circulation of these fluids as they became modified by rock interaction and the likely incorporation of ground water, probably resulted in the presence of fluids of complex origin.

In this chapter, evaluation is made of the P - T - X conditions responsible for some of the major assemblages. All the thermodynamic data were obtained from Robie et al.(1978) and Helgeson(1969) or calculated from data in Helgeson et al(1978) and Barin et al.(1977), as shown in the Appendix 12.1 & 12.2. Some general trends in condition and composition are shown in Fig. 12.1.

There are obvious difficulties and inaccuracies inherent in the application of experimental and theoretical data which deal largely with pure compounds when the Sangdong phases are clearly otherwise. However, the total salinity of much of the fluid is low and there is some experimental data on the effect on phase equilibria of changing phase composition(e.g. Burton et al., 1982; Gamble, 1982). A more important question is whether any of the assemblages can be regarded as in equilibrium. The occurrence of near-monomineralic rocks and of consistent partition of elements between adjacent grains(e.g. Mg/Fe in hedenbergite and andradite) indicates a system at least near equilibrium. It is suggested that the gross mineralogical zones represent successive mineral assemblages formed in equilibrium with a fluid that is changing in composition as it migrates outwards from the feedr zone. As the fluid at any point changes composition, overprinting results in coexistence of of assemblages themselves more or less in equilibrium but in disequilibrium with their hosts, and in this respect, considerable difficulties have been experienced in unravelling the paragenetic sequence at Sangdong, particularly in the pyroxene-garnet skarns. Overprinting by later fluids of different initial composition results in further complication.

Fig. 12.1. Trends in the change of bulk chemistry and mineral assemblages at Sangdong skarns.

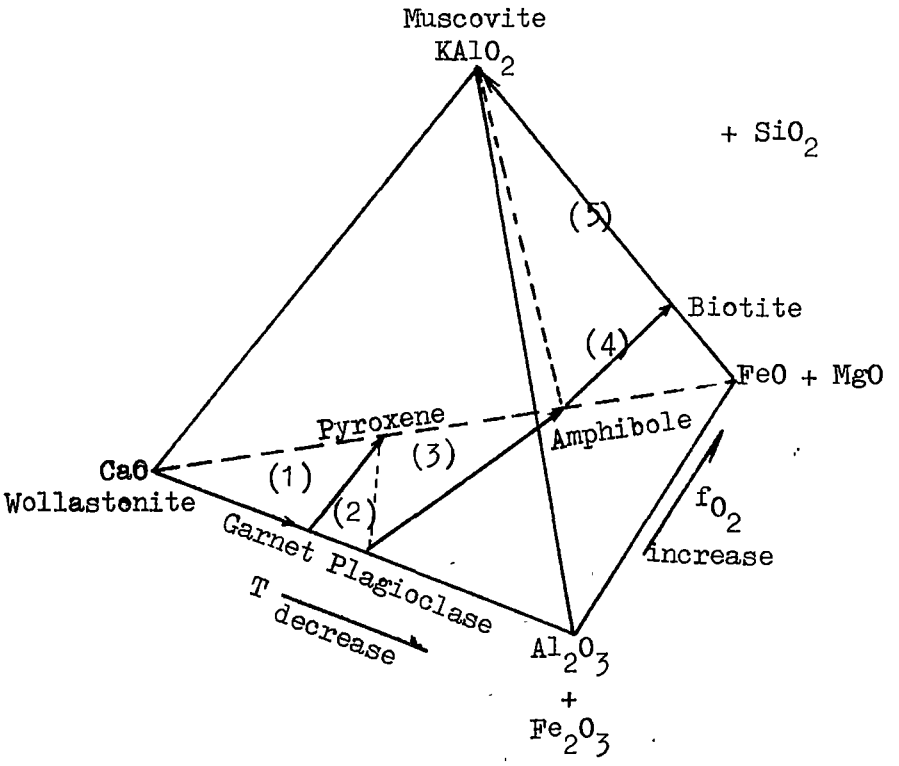

(1) Wollastonite-Andradite-Diopside

(2) Hedenbergite-Plagioclase-Garnet(grossularite-andradite)

(3) Hedenbergite-Plagioclase-Amphibole-Quartz
Amphibole-Quartz

(4) Amphibole-Biotite-Quartz
Quartz-Biotite

(5) Muscovite-Biotite-Quartz
Quartz-Muscovite-Chlorite

12.2. Formation of Early Skarns

These are mainly garnet-pyroxene-calcite rocks with or without wollastonite. The formation of wollastonite is explained by the well known reaction(Greenwood, 1967; Gustafson, 1974; Liou, 1974; Taylor & Liou,1978):

$$CaCO_3 + SiO_2 = CaSiO_3 + CO_2 \qquad (1)$$

No fluid inclusions were found in this skarn, but the temperature of the formation of the wollastonite skarn can be estimated from P-T-X_{CO_2} data of Greenwood(1967), where X_{CO_2} is the mole fraction of CO_2. The limited fluid inclusion data(Table 10.11) indicate that the CO_2 mole fraction in the Sangdong skarns and in the veins was between 0.05 and 0.19. At P_{total}= 1000 bars and X_{CO_2}= 0.1, the equilibrium temperature is about 510°C, for X_{CO_2} = 0.2 the temperature is about 560°C(Shimazaki et al.,1973; Kerrick & Slaughter, 1976; Uchida & Iiyama, 1982). The T_h values (uncorrected) in the pyroxene-garnet skarn near wollastonite-bearing skarn are 556°- 580°C(specimens 106143 & 106149. Appendix 10.4).

To derive wollastonite skarn from limestone requires addition of silicon and other elements(Table 7.3). These components were probably in part added to the circulatory fluid as a result of reaction between fluid and local shales. Wollastonite is most abundant in the Pungchon Limestone above the H1 skarn(Fig. 4.9), where the primary fluids must have been considerably modified by circulation in the shales beneath the limestone. Where the activity of iron is high enough, andradite and hedenbergite are stable and where Mg becomes significant, diopside is stable. Potential reactions are:

$$3CaCO_3 + 3SiO_2 + 2FeCl_2 + 2H_2O + \tfrac{1}{2}O_2 = Ca_3Fe_2Si_3O_{12} + 3CO_2 + 4HCl \qquad (2)$$

$$CaCO_3 + 2SiO_2 + FeCl_2 + H_2O = CaFeSi_2O_6 + CO_2 + 2HCl \qquad (3)$$

$$CaSiO_3 + FeCl_2 + SiO_2 + H_2O = CaFeSi_2O_6 + 2HCl \qquad (4)$$

$$CaCO_3 + 2SiO_2 + MgCl_2 + H_2O = CaMgSi_2O_6 + CO_2 + 2HCl \qquad (5)$$

The assemblage andradite-hedenbergite-calcite-wollastonite can be accomodated by the following reactions:

$$2CaFeSi_2O_6 + 2CaCO_3 + \tfrac{1}{2}O_2 = CaSiO_3 + Ca_3Fe_2Si_3O_{12} + 2CO_2 \quad (6)$$

$$2Ca(Mg,Fe)Si_2O_6 + 2CaCO_3 + \tfrac{1}{2}O_2 = CaSiO_3 + Ca_3Fe_2Si_3O_{12} + 2Mg^{+2} + 2CO_2 \quad (6a)$$

For a given f_{CO_2}, the reaction is dependent on f_{O_2} and T(Fig.12.2). The early garnet(andradite)-pyroxene skarn contains calcite but little or no quartz and no wollastonite(see section 5.1.2). This is compatible with the following reaction, with $^{a}SiO_2 < 1$:

$$Ca_3Fe_2Si_3O_{12} + SiO_2 + CO_2 = 2CaFeSi_2O_6 + CaCO_3 + \tfrac{1}{2}O_2 \quad (7)$$

This reaction is thus dependent on both f_{O_2} and $^{a}SiO_2$ for a given temperature and f_{CO_2}.

12.3. Formation of Later Pyroxene-Garnet Skarns

In contrast to the wollastonite-bearing early pyroxene skarns, the minerals of the later skarns, particularly hedenbergite, have abundant fluid inclusions. T_h values range from 580°C to 320°C, and average 418°C (Fig. 10.11). In chapter 10, it was concluded that T_h values >366°C required no correction but those below 366°C should be corrected for pressure, presumably of 800 bars. This yields a trapping temperature range of 390° to 600°C(?) for the late pyroxenes.

There is evidence in specimen 103118(Fig. 10.13) of a temperature decline from early pyroxenes to later pyroxenes adjacent to amphibole-rich rock, T_h varying from >580°C to 395°C. T_h values also decrease away from the apparent fluid source near the margin of the skarn(Fig. 10.12).

Reactions forming hedenbergite are important, as this is the dominant mineral. Apart from equation(4), in which wollastonite is replaced, hedenbergite may form by replacement of andradite:

$$Ca_3Fe_2Si_3O_{12} + SiO_2 \longrightarrow 2CaFeSi_2O_6 + O_2 + Ca^{++} \quad (8)$$

or, where with calcite, as per equation (7). Reaction (8) is dependent on $^{a}Ca^{++}$ for which there is no definitive information. The equilibrium assemblage hedenbergite-andradite-quartz-calcite is represented by equation (7) and plotted with respect to temperature and f_{O_2} for X_{CO_2}

Fig. 12.2. Stability fields of the Sangdong skarns.

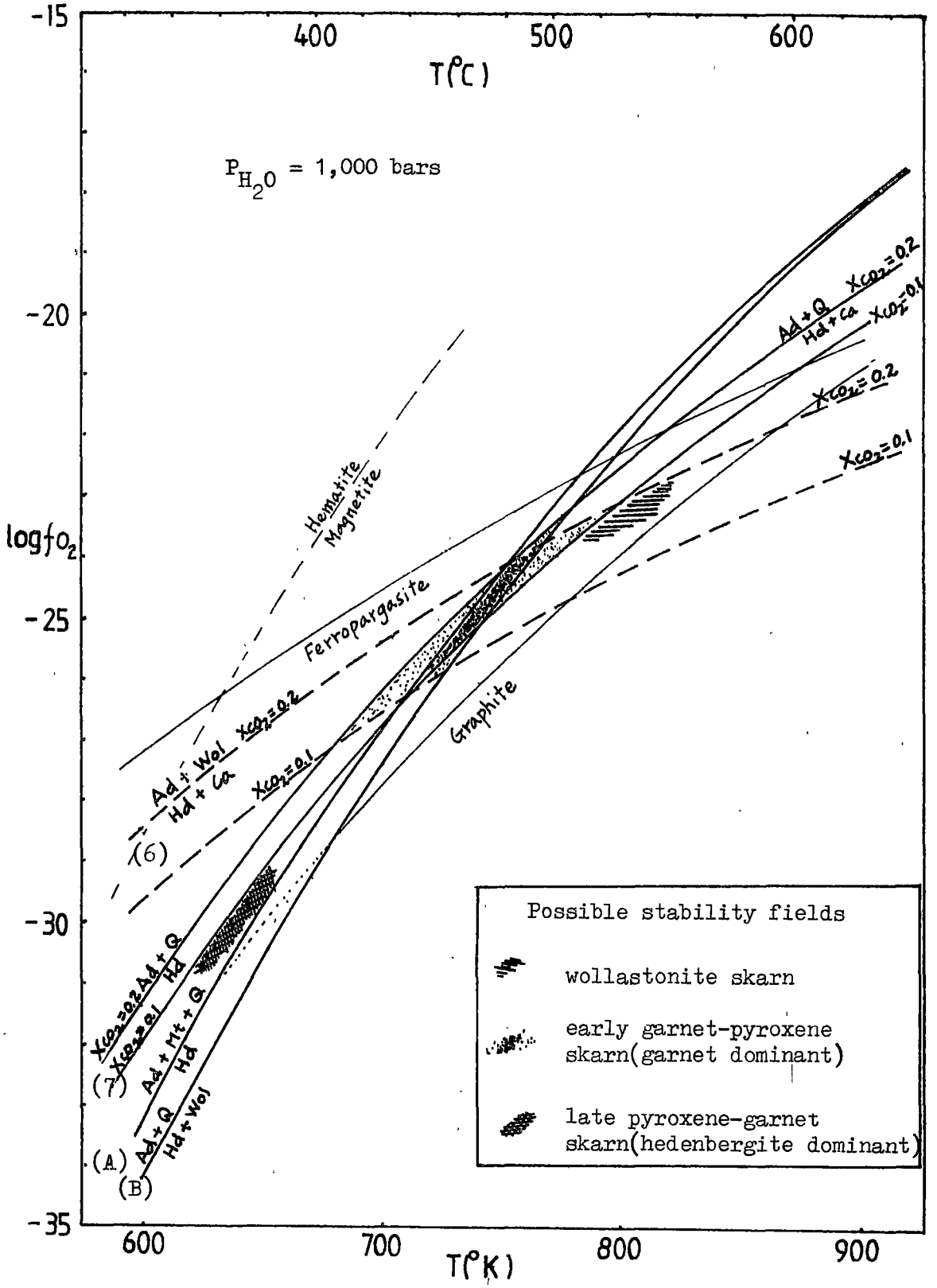

$2CaFeSi_2O_6 + 2CaCO_3 + \frac{1}{2}O_2 = CaSiO_3 + Ca_3Fe_2Si_3O_{12} + 2CO_2$ (6)

$Ca_3Fe_2Si_3O_{12} + SiO_2 + CO_2 = 2CaFeSi_2O_6 + CaCO_3 + \frac{1}{2}O_2$ (7)

Curve (A) from Burton et al.(1979); Curve (B) from Gustafson(1974);
Curve for ferropargasite from Gilbert(1966)
Curve for graphite from French(1966)

values of 0.1 and 0.2 in Fig. 12.2. The low value of $X_{CO_2}(0.05)$ in the one skarn inclusion carrying CO_2 suggests 0.1 as the most likely value.

The tendency to develop monomineralic hedenbergite assemblages could result from decreases in f_{O_2} and $^{a}Ca^{++}$ and/or an increase in $^{a}SiO_2$.

In deeper levels of the M1 pyroxene-garnet zone, an assemblage of anorthite, grossular, quartz, clinozoisite and hedenbergite is present, with hedenbergite undergoing replacement. A possible equilibrium is :

$$Ca_3Al_2Si_3O_{12} + 5CaAl_2Si_2O_8 + 2H_2O = 4Ca_2Al_3Si_3O_{12}(OH) + SiO_2 \quad (9)$$

The plagioclase is about 90 mole % anothite. Using Bird and Helgeson's (1981) phase relations for the $CaO-FeO-Fe_2O_3-Al_2O_3-SiO_2-HCl-H_2O$ system at 400°C, 1 kb and $^{a}H_2O = 1$, and the composition of two epidote samples of $X_{Ca_2Fe_3Si_3O_{12}(OH)} = 0.13$ and 0.26(Table 6.22), the calcium content of the fluid can be loosely constrained as follows:

$$\log {}^{a}Ca^{++}/({}^{a}H^{+})^2 = 5.7 \text{ to } 6.6$$

The sulphides in the pyroxene-garnet skarns appear to be later than the early silicates and later than much of the later silicates. Some sulphides have formed at the same time as pyroxene as seen in specimen 103166(Fig. 6.24), where pyrite, hedenbergite and quartz appear to have grown together. It thus seems likely that quartz, scheelite, sulphides and some pyroxenes formed together fairly late in the evolution of the skarn. The low T_h values of some quartz in the skarn(Fig. 10.9) indicate quartz deposition continued to very late stages.

Pyrrhotite is the most abundant sulphide and replaces pyroxenes but pyrite is locally present(without pyrrhotite) and in a few specimens magnetite is present(no sulphides in contact). Possible sulphidation reactions are:

$$2CaFeSi_2O_6 + S_2 + 2CO_2 = 2FeS + 4SiO_2 + 2CaCO_3 + O_2 \quad (10)$$

$$CaFeSi_2O_6 + S_2 = FeS_2 + 2SiO_2 + Ca^{++} \quad (11)$$

$$Ca_3Fe_2Si_3O_{12} + S_2 = 2FeS + 3SiO_2 + 3O_2 + 3Ca^{++} \quad (12)$$

The experiments of Gamble(1982) and Burton et al.(1982) provide useful data on the influence of varying silicate composition. Taking Sangdong hedenbergite as having a mole fraction of diopside of 0.26 and of johannsenite of 0.06(average values based on Table 6.5) indicates that pyrite could only form in equilibrium with the silicates below 376°C at 1 kb pressure(Fig. 12.3). If the application of the pressure correction to the lower T_h values in pyroxenes is correct then pyrite must be later (at lower temperature) than most of the silicates. Combining this with the bulk of the petrographic evidence indicates that the sulphides probably formed at a very late stage in pyroxene-garnet skarn evolution and to some extent, later than the silicates. The abundance of pyrrhotite and relatively scarce non-coexisting, pyrite and magnetite, indicate f_{O_2} - f_{S_2} conditions mainly in the pyrrhotite field at 400°C but not far removed from pyrite and magnetite stability(Fig. 12.4). Coexisting bismuth and bismuthinite provide a useful constraint on f_{S_2}.

Fig. 12.3. Stability fields for pyrite, pyrrhotite, hedenbergite and andradite.

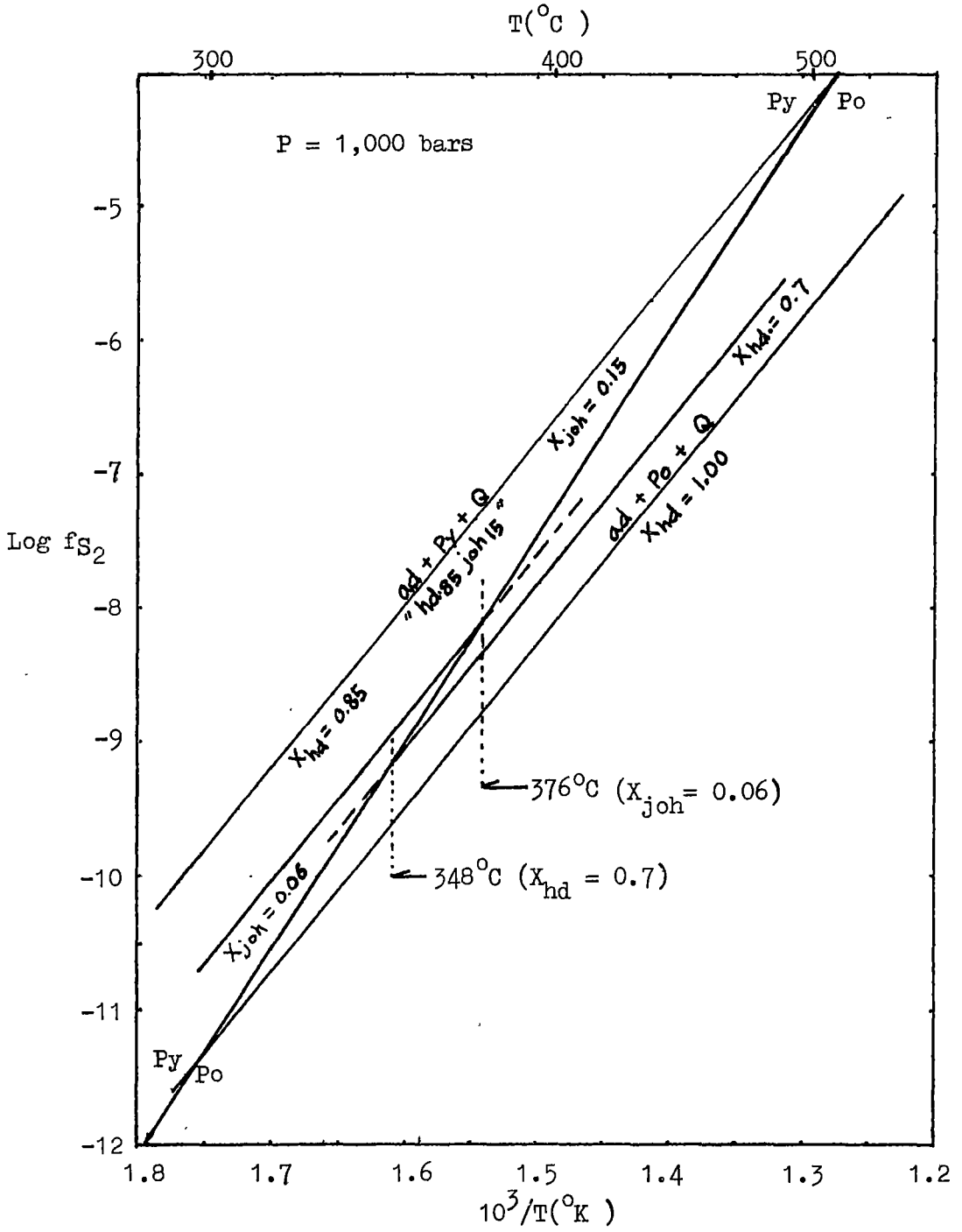

Stability of hedenbergite(hd) and andradite(ad) is based on Burton et al.(1982) and Gamble(1982).

Average X_{hd} = 0.7, X_{dip} = 0.26 and X_{joh} = 0.06 are based on Table 6.3. dip = diopside joh = johannsenite

py = pyrite po = pyrrhotite Q = quartz

Fig. 12.4. Estimate of conditions during late pyroxene-garnet skarn and amphibole skarn formation in terms of fO_2- fS_2 at 400°C.

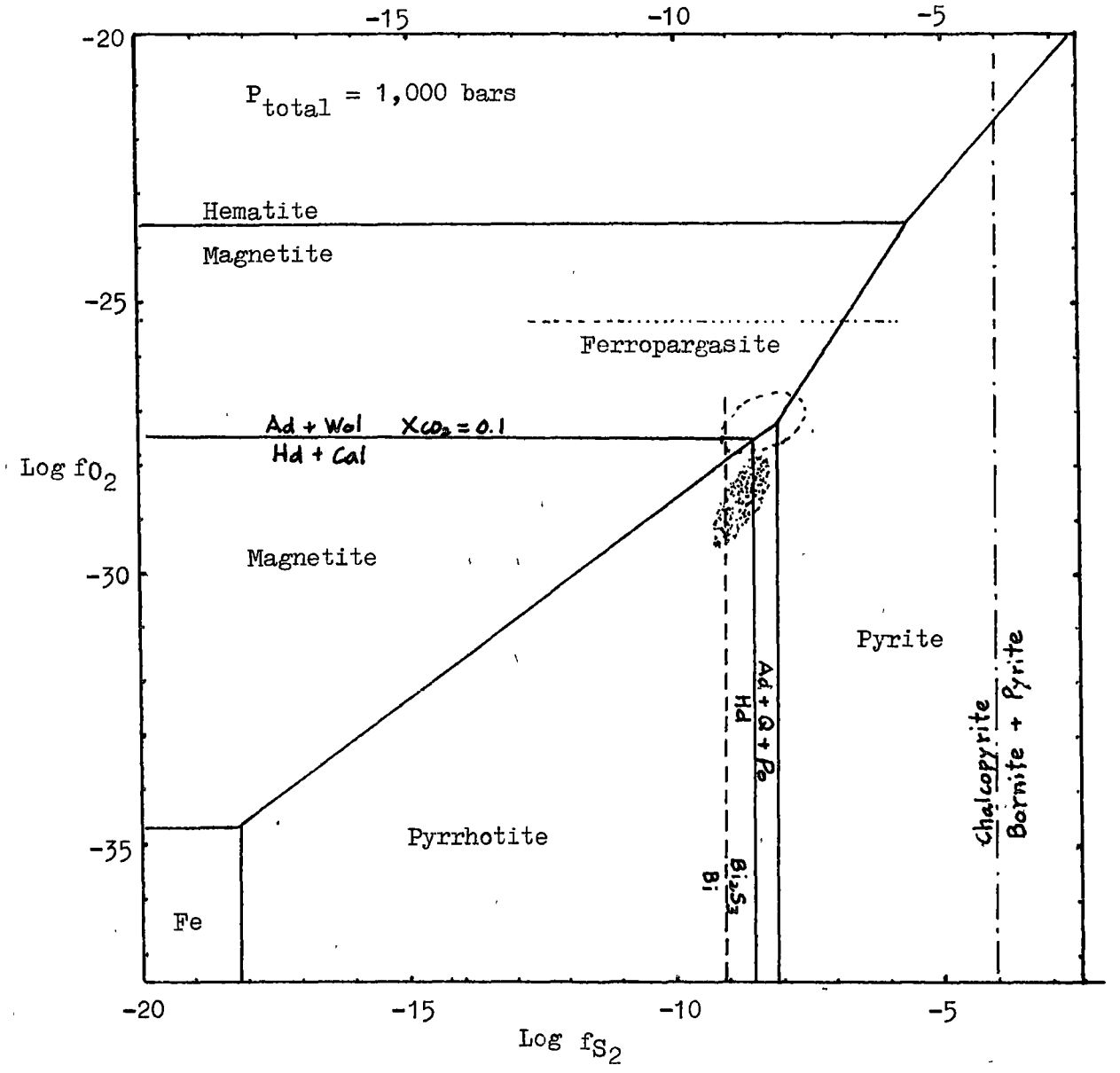

The stippled area indicates the environment of late pyroxene-garnet skarn mineralization.

The stability field of hedenbergite is from eq.(6) and Burton et al. (1979). The equilibria are calculated from data of Robie et al.(1978)

- stability fields of amphibole and mica skarns formation.

The stability field of ferropargasite is from Gilbert(1966).

12.4. Formation of the Biotite and Amphibole Skarns

These skarns appear to exist in chemical and textural equilibrium. At the "front" of the amphibole zone, however, there is clear evidence of replacement, and amphibole occurs in veins, veinlets and patches anastomosing the pyroxene-garnet rock. Three possible reactions producing tremolite, hastingsitic hornblende, ferroedenitic hornblende and ferro-hornblende are shown here:

$$7Ca_3(Al,Fe)_2Si_3O_{12} + 2(Na,K)Cl + 32HCl = 17CaCl_2 + 9SiO_2 + 2(Na,K)Ca_2Fe_2(Al,Fe)_5Al_2Si_6O_{22}(OH)_2 + 14H_2O + 2O_2 \quad (13)$$

$$5Ca(Mg,Fe)Si_2O_6 + 3CO_2 + H_2O = Ca_2(Mg,Fe)_5Si_8O_{22}(OH)_2 + 3CaCO_3 + 2SiO_2 \quad \text{(Kwak, 1978a)} \quad (14)$$

$$8Ca(Mg, Fe)Si_2O_6 + 2CaAl_2Si_2O_8 + 4H^+ = 2Ca_2(Mg,Fe)_4Al_2Si_7O_{22}(OH)_2 + 6SiO_2 + 6Ca^{++} + 2O_2 \quad (15)$$

These reactions release calcium to the fluid, causing precipitation of calcite and scheelite. The production of oxygen may explain the abundance of magnetite(with pyrrhotite and pyrite), particularly at the amphibole "front".

Chlorite is abundant in much of this skarn(section 5.3.2), replacing amphibole. Both the chlorite and amphibole appear to accompany fluorite, quartz, and scheelite. The replacement of amphibole by chlorite can be represented by the following reaction:

$$3Ca_2(Mg,Fe)_4Al_2Si_7O_{22}(OH)_2 + \tfrac{1}{2}O_2 = 2(Mg,Fe)_6Al_2Si_3O_{10}(OH)_8 + 13SiO_2 + CaAl_2Si_2O_8 + 5Ca^{++} + 3H_2O \quad (16)$$

Again, calcium is released to the fluid, allowing precipitation of calcite, scheelite and fluorite.

Only two specimens of amphibole have yielded fluid inclusions and these have T_h values ranging from 287 to 307°C(Append.10.8) and indicate somewhat lower temperatures than in the pyroxene-garnet skarn. Uncorrected T_h values in coexisting scheelite have a similar range to these in the pyroxene-

garnet skarn zone(Fig. 10.15b), suggesting a fairly constant temperature across the boundary in later stages. There is no evidence of boiling within the amphibole association so a range of trapping temperatures for the assemblage is from a maximum of 500°C for scheelite down to about 250°C for quartz.

Pyrrhotite and magnetite, native bismuth and bismuthinite occur as coexisting pairs in the amphibole skarn, associated with amphibole and/or chlorite. These assemblages provide a fairly tight constraint on the range of fO_2 and fS_2 in these rocks(Fig. 12.4), and suggest the sulphides(with scheelite, chlorite?) formed in slightly higher oxidation conditions compared to these of the late pyroxene-garnet skarn.

The fO_2 value is consistent with the upper stability limit of ferropargasite determined by Gilbert(1966),as shown in Fig. 12.2 and 12.4.

The biotite-amphibole equilibrium can be expressed by the following reaction:

$$Ca_2(Mg,Fe)_4Al_2Si_7O_{22}(OH)_2 + 2KCl + 2H_2O + 2(Mg,Fe)Cl_2 = \quad (17)$$
$$2K(Mg,Fe)_3AlSi_3O_{10}(OH)_2 + 2CaCl_2 + SiO_2 + 2HCl \text{ (Eastoe, 1979)}$$

Two inclusions in biotite have T_h values of 381°C and 286°C(Appendix 10.8) which pressure correct to 480°C and 365°C approximately. Scheelite trapping temperatures for this skarn range from 600°C to 300°C and quartz from 460°C to 220°C. The high T_h value of scheelite inclusions(specimen 106044) coincides with a T_h in adjacent pyroxene of 580°C(Appendix 10.6).

Purtscheller and Rammlmair(1982) have empirically and qualitatively correlated the partition of Mg and Fe between amphibole and biotite in a metamorphic terrain. Comparable data from specimen 103109 (Appendix 8.7) indicates a minimum equilibration temperature a little below 400°C.

Bismuthinite and bismuth, pyrrhotite and magnetite occurring with biotite again loosely constrain fO_2 and fS_2 conditions(Fig. 12.4).

The volume % native bismuth/bismuthinite ratio increases outward from the mica skarn(section 6.13.1), roughly confirming with a trend to lower f_{O_2} and f_{S_2} in that direction.

Although the arrangement biotite-amphibole-pyroxene+garnet is the usual one at all scales, biotite in contact with pyroxene-garnet has been observed(Fig. 4.7) as a quartz-mica skarn veining the pyroxene-garnet skarn and surrounding a dyke in the pyroxene-garnet skarn (at -12th level). The reactions involved can be expressed as:

$$3Ca(Mg,Fe)Si_2O_6 + Ca_3(Al,Fe)_2Si_3O_{12} + K^+ + 2H^+ = K(Mg,Fe)_3AlSi_3O_{10}(OH)_2 + 6SiO_2 + 6Ca^{++} + 3O_2 + Fe^{3+} \quad (18)$$

$$6Ca(Mg,Fe)Si_2O_6 + CaAl_2Si_2O_8 + 2K^+ + 12H^+ = 2K(Mg,Fe)_3AlSi_3O_{10}(OH)_2 + 8SiO_2 + 7Ca^{++} + 4H_2O \quad (19)$$

Fig. 12.5. Estimate of conditions of muscovite-rich skarn formation in the system Fe-O-S on an fS_2- fO_2 diagram at 350°C.

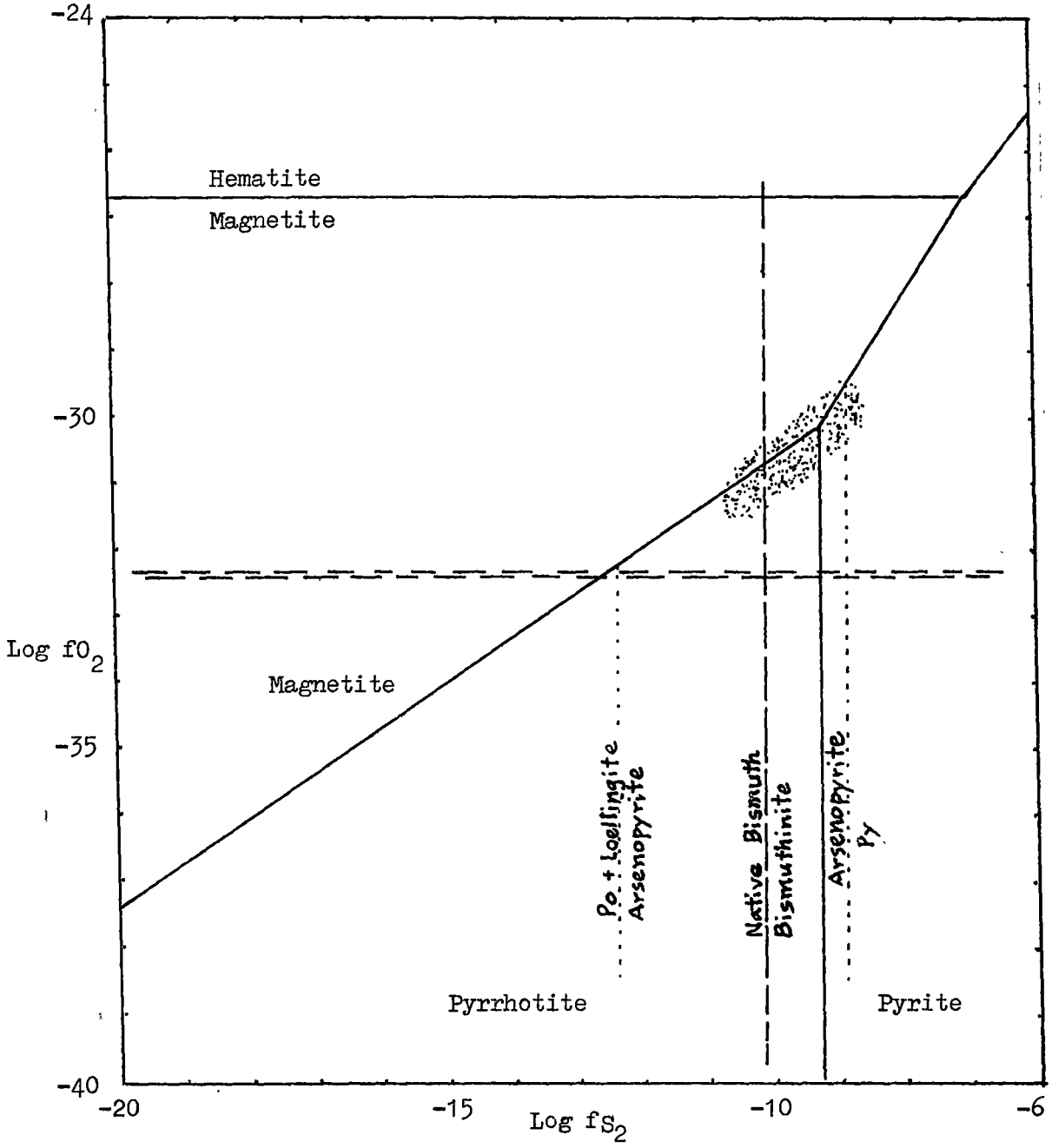

Oxygen fugacity of chlorite formation

Stability field of muscovite-rich skarn

Py = pyrite, Po = pyrrhotite

12.5. Formation of the Quartz-Muscovite-Chlorite Skarn

This skarn appears to have been derived from the biotite skarn by alteration. It is unusual in containing small amounts of wolframite, hematite and arsenopyrite. The arsenopyrite occurs with pyrite. The composition of the arsenopyrite(Table 6.19) indicates a temperature range of 370° to 425°C from rim to core(Fig. 12.6) and log f_{S_2} of -6 to -7.4 (using data of Kretschmar and Scott, 1976).

The presence of hematite in one specimen(106174) with magnetite and pyrite indicates an oxidation state too high to be compatible with the presence of bismuthinite, pyrrhotite and arsenopyrite, and it may be a very late phase. Possible chemical reactions to form this skarn are as follows:

$$5K(Mg,Fe)_3AlSi_3O_{10}(OH)_2 + 22HCl = KAl_3Si_3O_{10}(OH)_2 + (Mg,Fe)_6Al_2Si_3O_{10}(OH)_8 + 4KCl + 6FeCl_2 + 3MgCl_2 + 9SiO_2 + 11H_2O + \tfrac{1}{2}O_2 \quad (20)$$

$$3CaAl_2Si_2O_8 + 4H^+ + 2K^+ = 2KAl_2AlSi_3O_{10}(OH)_2 + 3Ca^{++} \quad (21)$$

$$3Ca_3Al_2Si_3O_{12} + 4H^+ + 2K^+ = 2KAl_3Si_3O_{10}(OH)_2 + 3SiO_2 + 9Ca^{++} + 3O_2 \quad (22)$$

Equation (21) represents replacement of plagioclase in the footwall-side-cherty rock by muscovite skarn in the quartz-mica zone, and equation (22) represents the formation of the quartz-muscovite skarn in parts of the F. orebody. All result in decrease of acidity in the fluid.

Development of muscovite is associated with precipitation of scheelite and quartz. Corrected temperatures of homogenization of scheelite inclusions range from values compatible with the arsenopyrite temperature down to about 300°C while quartz precipitation apparently continues to even lower temperatures(Fig. 10.9 & 10.10).

The highest T_h values in scheelite occur in the mica skarn in the lower mine levels and T_h values of quartz show a pronounced high in the core of the mica skarn and a low coinciding with the late muscovite-chlorite skarn. The muscovite skarn thus appears to be a lower temperature, late stage assemblage. Later activity appears to involve hematite and quartz;

Fig. 12.6. Estimate of formation temperature from atomic % As in arsenopyrite (from Kretschmar and Scott, 1976).

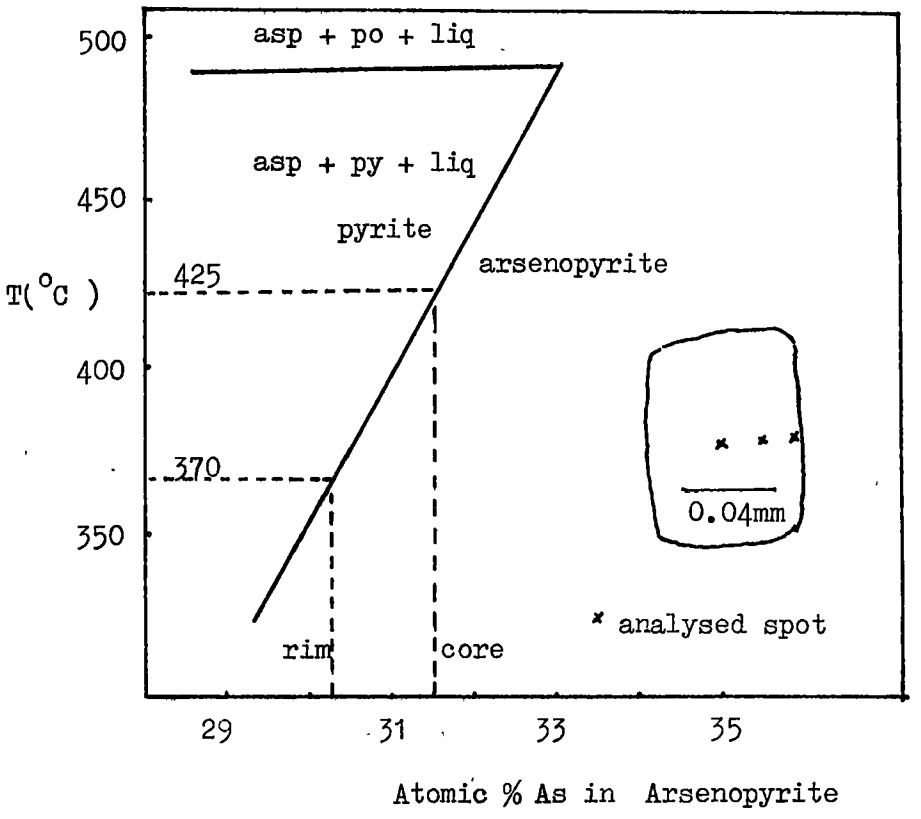

(Based on results of microprobe analyses of arsenopyrite, see Table 6.19)

in addition, calcite is seen replacing muscovite and T_h values of fluorite inclusions indicate low temperature, hence late precipitation.

The wolframite in specimen(106174) has a very low manganese content, and unlike wolframite in quartz veins(see section 6.14), occurs with calcite and magnetite. Possible reactions are as follows:

$$3CaWO_4 + Fe_3O_4 + 3CO_2 = 3FeWO_4 + 3CaCO_3 + \tfrac{1}{2}O_2 \qquad (23)$$

Rose and Burt(1979) explained the presence of scheelite and ferberite by a reaction involving fluorine:

$$Fe_3O_4 + 3CaWO_4 + 3F_2O_{-1} = 3CaF_2 + 3FeWO_4 + \tfrac{1}{2}O_2 \qquad (24)$$

The common occurrence of fluorite and scheelite in the Sangdong skarns, the close association in the veins of wolframite and scheelite commonly without fluorite, and the replacement of muscovite by calcite indicate the first reaction seems to be more pertinent at Sangdong and that f_{CO_2} is critical. The $T - f_{O_2} - X_{CO_2}$ dependence of these reactions are plotted in Fig. 12.7, using scheelite data from Robie et al.(1978). The f_{O_2} values for the likely mole % CO_2 in solution are too clearly too high, indicating problems with the thermodynamic data.

The presence of muscovite allows a crude estimate of pH in the fluids. Leachate analyses of fluid inclusions in tin-tungsten deposits apparently derived from granitoid magmas indicate $^mK^+$ of about 0.1 at temperatures of 300-400°C, e.g.

	$^mK^+$	T(°C)
Cligga Head(Charoy, 1979)	0.1 - 0.17	300 - 450
Renison(Patterson et al., 1981)	0.2	350

Using, say, $^mK^+ = 0.1$ at 350°C indicates that the pH was between 4.2 and 5.9 because there is little or no kaolinite or K-felspar in this skarn. The appropriate reactions are:

$$3KAlSi_3O_8 + 2H^+ = KAl_3Si_3O_{10}(OH)_2 + 6SiO_2 + 2K^+ \qquad (25)$$

$$2KAl_3Si_3O_{10}(OH)_2 + 2H^+ + 3H_2O = 3Al_2Si_2O_5(OH)_4 + 2K^+ \qquad (26)$$

Fig. 12.7. Comparison of conditions of formation between pyroxene-garnet skarn and quartz-muscovite skarn in which ferberite, magnetite, calcite and scheelite occur.

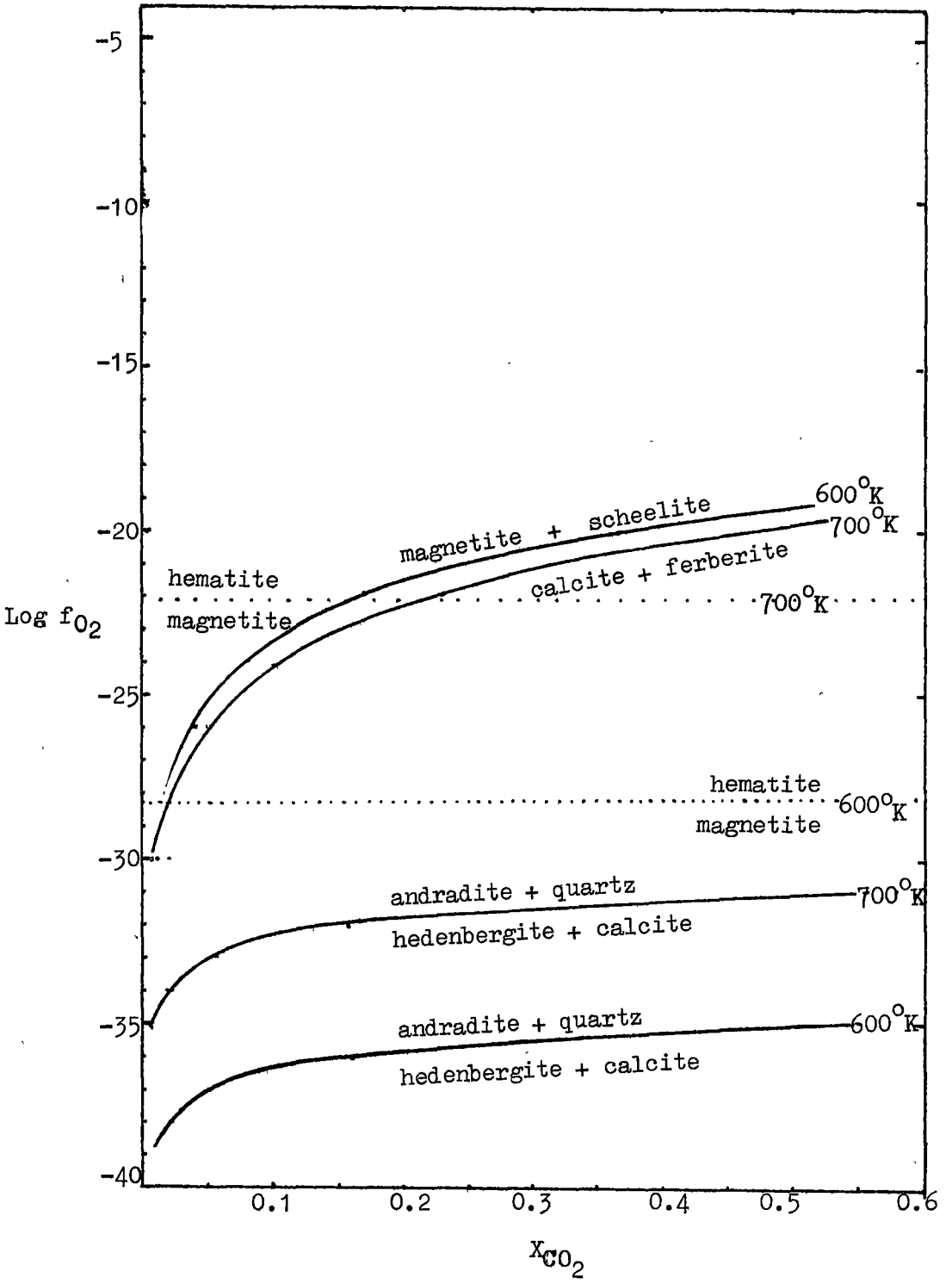

At 350°C, neutral pH is 5.7 so the solutions are neutral to acid.

The mineralogy and other constraints can be used to indicate a likely value for the molality of total sulphur. In Fig. 12.8a, the oxidation state is shown as $\Sigma SO_4/\Sigma H_2S$ where

$$\Sigma SO_4 = SO_4^{2-} + HSO_4^- + NaSO_4^- + KSO_4^- + MgSO_4^- + CaSO_4^-$$

$$\Sigma H_2S = H_2S + HS^- + S^{2-}$$

The diagram is calculated using a programme prepared by Ripley & Ohmoto (1980) and modified by J.L. Walshe, D.J. Patterson and G.R. Green at the University of Tasmania.

The fluid is assumed to have the following characteristics:

pH = 4, $^mK^+ = 0.1$, $^mNa^+ = 0.85$, $^mMg^{++} = 0.014$, $^mCl^- = 1.00$, $^mCa = 0.00$

$^mCu = 10^{-9.99}$, $^mMn = 10^{-7}$, $^m\Sigma C = 0.10$.

Manipulating values of $^m\Sigma S$ gives a reasonable fit at $^m\Sigma S = 2.5 \times 10^{-3}$.

in Fig. 12.8b, the temperature is fixed at 350°C and conditions other than pH are as for 12.8a.

Fig. 12.8a. $\text{Log}\Sigma SO_4/\Sigma H_2S$ versus T diagram displaying the possible fields of formation of sulphide minerals in the hydrous (amphibole-rich and mica rich) skarns. $\overset{m}{\Sigma}S = 2.5 \times 10^{-3}$.

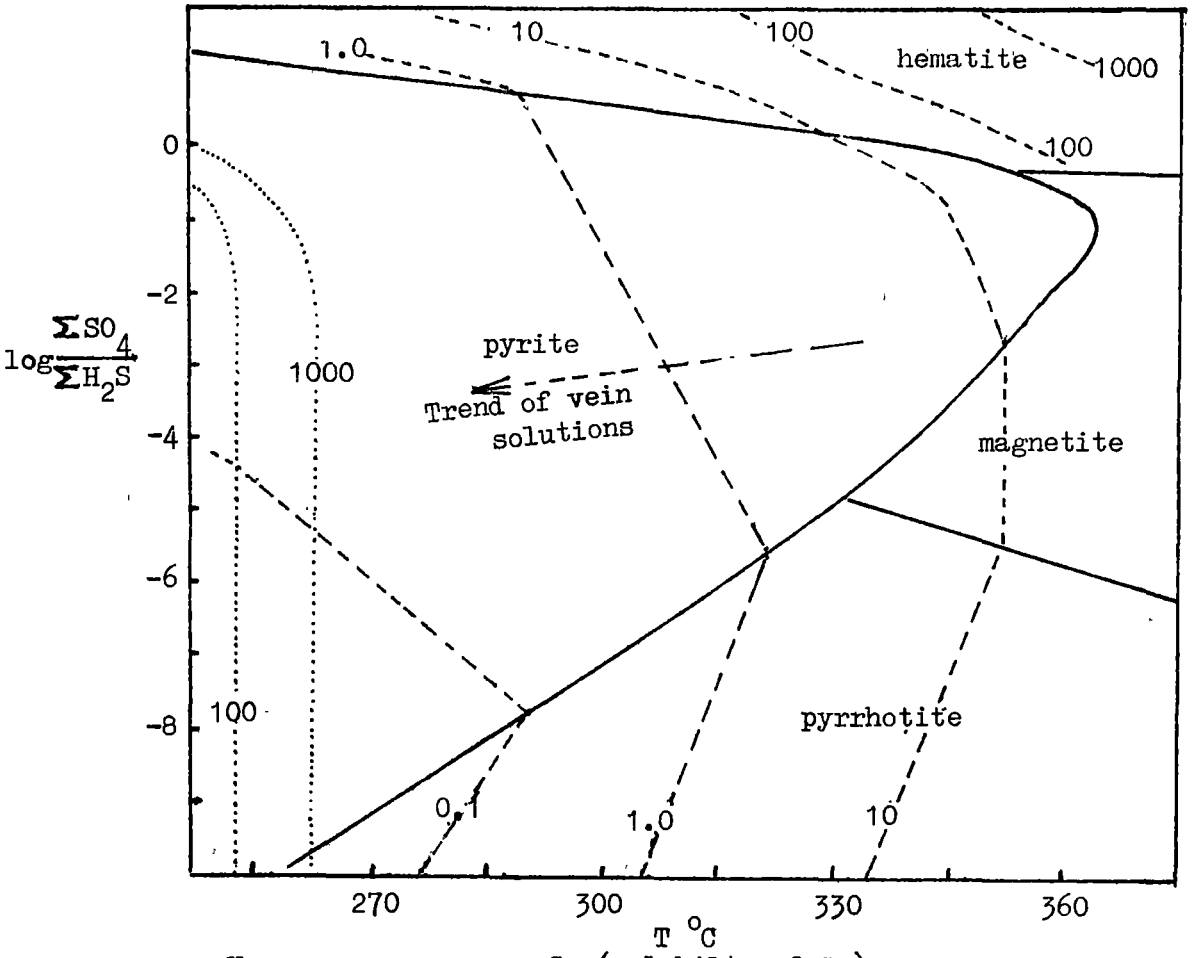

Key: ----- , ppm Cu (solubilty of Cu)

····· , ppm Zn (solubilty of Zn)

Fig. 12.8b. $\text{Log}\Sigma SO_4/\Sigma H_2S$ versus pH (at 350°C) diagram. $\overset{m}{\Sigma}S = 2.5 \times 10^{-3}$.

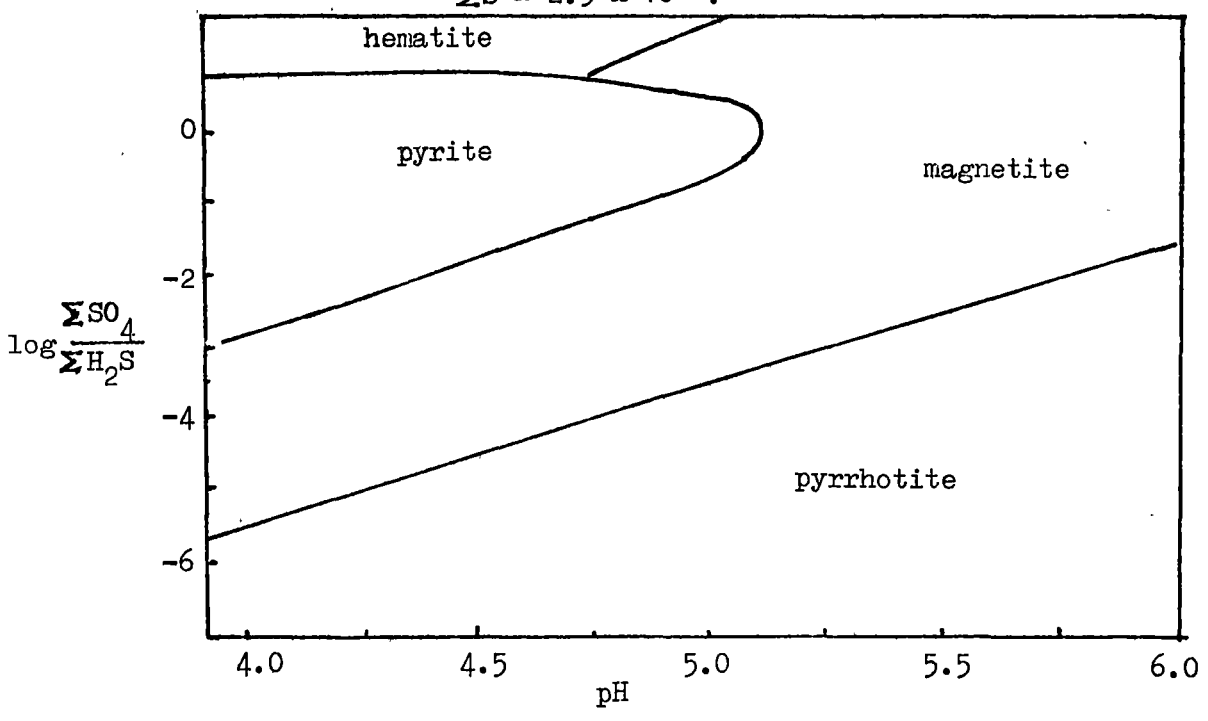

12.6. Formation of Chlorite

Walshe and Solomon(1981) have developed a model involving substitutions in chlorite to obtain estimates of the temperature and fO_2 at which the chlorite assemblages equilibrate.

Among the common six end-members of the chlorites, only four could be used to represent Sangdong chlorites, viz.

$$Mg_5AlSi_3AlO_{10}(OH)_8 + 5/3\ Fe_3O_4 + 10/3\ SiO_2 + 10/3\ H_2O =$$
$$Fe^{++}_5AlSi_3AlO_{10}(OH)_8 + 5/6\ Mg_6Si_4O_{10}(OH)_8 + 5/6\ O_2 \qquad (27)$$

for which $\log K = \log a_3 + 5/6 \log a_1 + 5/6 \log(fO_2) - \log a_2$

where a_i is the activity of ith thermodynamic component. Chlorites analyzed by microprobe are given in Table 12.1 for two samples(103120 and 103119) from the quartz-mica skarn. The chlorite and magnetite occur in a specimen from the quartz-muscovite-chlorite rock but tney are not quite in contact.

The fO_2 values obtained from the above equation are as follows;

Temperature (^oC)	specimen 103120	specimen 103119
250	-38.72	-38.84
300	-35.31	-35.42
350	-32.37	-32.48

These results indicate that the formation of chlorite may take place at fO_2 condition slightly lower than the mica assemblage at 350^oC.

Table 12.1. Chlorite Structural Formulae.

	Specimen 103120	Specimen 103119
Mg^{+2}	0.801	1.027
Mn^{+2}	0.039	0.063
Fe^{+2}	3.841	3.614
Fe^{+3}	0.104	0.108
Al^{+3}	1.215	1.188
Si^{+4}	2.681	2.704
Al^{+3}	1.319	1.296
Total	10.000	10.000
0	10.000	10.000
OH	8.000	8.000
Mg/(Mg+Fe)	0.169	0.216
Fe^{+3}/Fe^{+2}	0.014	0.014
	Mole Fraction	
$Mg_6Si_4O_{10}(OH)_8$	- 0.326	- 0.572
$Mg_5Al_2Si_3O_{10}(OH)_8$	0.551	0.913
$Fe^{+2}_5Al_2Si_3O_{10}(OH)_8$	0.716	0.484
$Fe^{+2}_5Fe^{+3}_2Si_3O_{10}(OH)_8$	0.052	0.109

12.7. Formation of Scheelite

Scheelite is concentrated in the mica skarn zone(average over 6 wt % WO_3) with lower average values in the amphibole(1.5 wt % WO_3) and pyroxene-garnet skarn(0.3 wt % WO_3). Scheelite is observed as inclusions in garnet in some specimens(e.g. 103118, Fig. 10.17a), showing that deposition occurred during silicate formation. Fluid inclusion data indicate scheelite precipitation took place from 500°C down to about 300°C.

Hsu and Galli(1973) and Hsu(1977) have shown the effects of f_{O_2} and f_{S_2} on the stability of scheelite, molybdenite, powellite and tungstenite at temperatures of 527°C and 577°C.

Scheelite stability is limited by the stability of tungstenite(WS_2):

$$Ca^{++} + WS_2 + 2O_2 = CaWO_4 + S_2 \qquad (28)$$

Thermochemical calculation extrapolating the data of Helgeson(1969) to 350°C allow construction of the equilibrium boundary between WS_2 and $CaWO_4$ for given $^{a}Ca^{++}$ at total pressure = 1 kb(Fig. 12.9).

Similar calculations for the $MoS_2/CaMoO_4$ boundary involve this reaction:

$$Ca^{++} + MoS_2 + 2O_2 = CaMoO_4 + S_2 \qquad (29)$$

Adding this equation:

$$H_2O = 2H^+ + \tfrac{1}{2}O_2 \qquad (30)$$

The effect of pH can be included(Fig. 12.10) as in:

$$Ca^{++} + WS_2 + 3/2\ O_2 + H_2O = CaWO_4 + S_2 + 2H^+ \qquad (31)$$

$$Ca^{++} + MoS_2 + 3/2\ O_2 + H_2O = CaMoO_4 + S_2 + 2H^+ \qquad (32)$$

These diagrams indicate that the stability field of molybdenite + scheelite is compatible with f_{O_2}- f_{S_2} conditions determined by other constraints, assuming that $^{a}H_2O = 1$. The temperature of 350°C only covers part of the range of scheelite precipitation but extrapolation of some of the thermochemical data to higher temperature is unreliable.

The Mo content of scheelite is higher in the mica skarn zone than the outer zones. This may reflect the rather higher f_{O_2} conditions deduced for

the mica skarn zone, the assumption being that the Mo content of scheelite is likely to increase towards the powellite field(Hsu and Galli, 1973). Alternatively the activity of molybdenum species may have varied. Molybdenite is rare in the skarns and only found in the quartz-mica skarn (specimen 103215); it is more common, occurring with scheelite(Mo-poor), in quartz veins(Fig. 12.9). Outer rims of scheelite relatively depleted in molybdenum(e.g. Fig. 6.29) may reflect a decline in molybdenum activity in the fluids with time.

Calculated solubility products of scheelite at reasonable temperature indicate that WO_4^{2-} ions alone cannot account for ore transport(Khodakovskiy and Mishin,1971). Experimental studies indicate that scheelite solubility in water or NaCl-KCl-H_2O solutions is dependent on temperature, salinity and pH(Yastrebova et al.,1963; Foster, 1977; Krumhansl, 1977). The results can be largely accounted for assuming the presence of tungstate ions in solution(Halley, 1982; Wesolowski et al.,1982). Experiments also indicate that heteropolytungstic acid, $H_8Si(W_2O_7)_6$ and fluorine complexes are not important transporting agents(Barabanov, 1971; Krumhansl, 1977). The very low carbonate ion concentrations that occur even in solutions having fairly high CO_2 content suggest that carbonate complexes are not likely to be important(Halley, 1982).

Recent experimental work by Wesolowski et al.(1982) has determined tungsten solubility in NaCl-H_2O solutions at varying pH and salinity from 95° to 290°C. The solubility product and the ionization constants at various salinities are given below, with other data:

$K_1 = (Ca^{++})(WO_4^{2-})$ — Khodakovskiy and Mishin(1971)

$K_2 = (H^+)(WO_4^{2-})/(HWO_4^-)$

$K_3 = (H^+)(HWO_4^-)/(H_2WO_4)$ — Ivanova and Khodakovskiy(1968) at zero salinity, remainder from Wesolowski et al.(1982).

$K_4 = (H^+)^2(WO_4^{2-})/(H_2WO_4)$

T(°C)	Ionic strength	log K_1	log K_2	log K_3	log K_4
150	0	-9.02	-5.28	-3.61	-8.89
	0.104		-4.09		
	1.01		-3.80		
	5.12		-3.90	-4.48	-8.48
200	0	-9.80	-6.04	-4.40	-10.44
	0.104		-4.68		
	1.01		-4.17		
	5.12		-4.06	-3.58	-7.64
250	0	-10.80	-6.85	-5.28	
	0.104		-5.21		
	1.01		-4.56		
	5.12		-4.31	-3.11	-7.42
290	0.104		-5.64		
	1.01		-4.78		
300	0	-11.95	-7.68	-6.19	
350	0	-13.21	-8.55	-7.15	

Fig. 12.11 displays the dependence of K_2 on ionic strength.

For Sangdong conditions, pH = 4 to 6, I = 1.0(approximately) and, for convenience, T = 350°C, the dominant species are clearly WO_4^{2-} and HWO_4^-. H_2WO_4 is only stable at low pH, high temperature and high ionic strength.

The extrapolated experimental value of K_2 at 350°C is taken as -5.15 (Fig. 12.11). The activity coefficient of WO_4^{2-} is not known so is assumed to be 1; this clearly introduces a source of error perhaps as great as an order of magnitude.

Total tungsten(W_t) in solution in equilibrium with scheelite can be written as:

$$a_{W_t} = a_{WO_4^{2-}} + a_{HWO_4^-}$$

$$\text{then } a_{W_t} = K_1/a_{Ca^{++}}(1 + a_{H^+}/K_2)$$

Clearly the a_{W_t} at fixed salinity is an inverse function of pH and $a_{Ca^{++}}$, and increases with falling temperature(Figs. 12.12 & 12.13). For pH = 4, I = 1.0, $a_{Ca^{++}}$ must equal 10^{-7} to achieve 1-2 ppm W in Sangdong solutions

at 350°C(1-2 ppm W seems a reasonable minimum content to form the deposit).

The calculated solubility of tungsten increasing with falling temperatures is at variance with the experimental results of Foster(1977) and Wesolowski et al.(1982) and probably means the solubility products of scheelite are in error. The experimental results of Foster(1977) and Wesolowski et al.(1982) show that K^+ and Na^+ are significant in controlling solubility. Decreases of K^+ and Na^+ in Sangdong fluids by crystallization of amphibole or mica minerals may have assisted in precipitating scheelite in these amphibole-mica skarns.

Reaction involving growth of the Sangdong skarn both consume and release H^+ and/or HCl. The growth of muscovite increases pH but the change from amphibole to biotite lowers it. Determination of pH variation probably requires detailed mass transfer calculation, which are beyond the scope of this study. There is also no strong indication of temperature gradient except that in the later stages of quartz growth there is an outward temperature decrease, which would bring about scheelite precipitation. Decrease in temperature and increase in pH may both be important in causing scheelite precipitation but change in the $^aCa^{++}$ seems likely to be the dominant mechanism. The growth of all but the muscovite skarn involves increase of Ca^{++}(other Ca species such as $CaCl_2$) in the fluid, and increase of $^aCa^{++}$ leads to a proportional reduction in ^aW_t under Sangdong conditions. Thus a change from $10^{-7.09}$ to $10^{-6.1}$ in $^aCa^{++}$ at 350°C, I = 1.0 and pH = 4 results in an order of magnitude reduction in tungsten in solution from 2 ppm to 0.2 ppm(Fig. 12.12).

The virtual absence of wolframite in the skarns testifies to a high $^aCa^{++}$ or high $^aCa^{++}/^aFe^{++}$ in the ore fluid. It is noted that quartz veins derived from solutions that have not penetrated calcareous rocks bear wolframite and that this is locally converted scheelite at a later stage.

At 350°C, pH = 4 and I = 1.0, tin solubility would be about 0.1 ppm in the presence of cassiterite(Patterson et al.,1981). The solutions would approach saturation with increasing pH, and decreasing f_{O_2} and T°C, all factors that could lead to cassiterite saturation in the outer skarn zones(where cassiterite has been detected).

Fig. 12.9. Log fO_2- log fS_2 diagram indicating the stability field of scheelite

(free energy for Ca^{++} is based on data of Helgeson, 1969, Appendix 11.1).

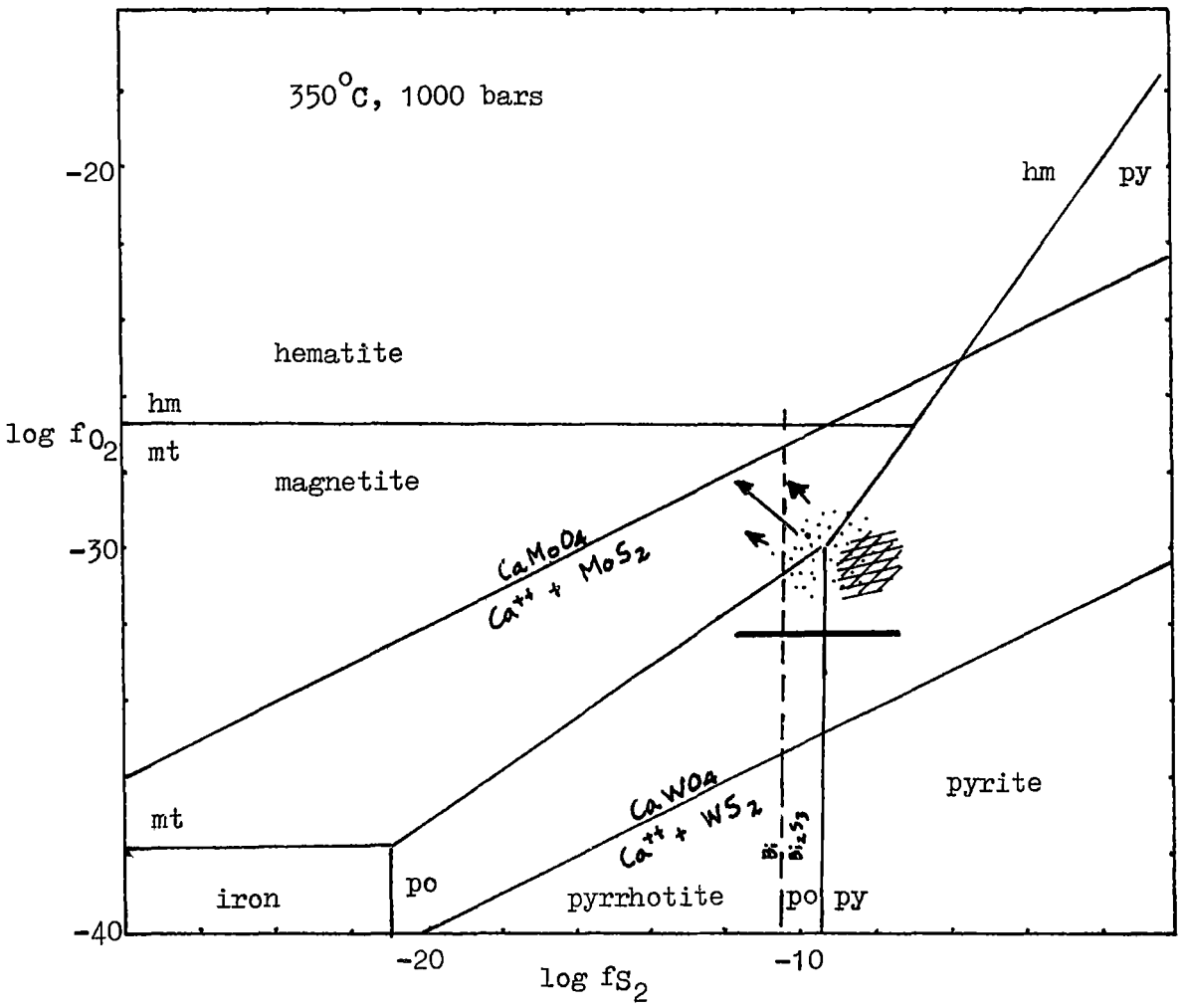

oxygen fugacity of chlorite formation

Mo-poor(blue fluorescent) scheelite

indicates increasing Mo-content of scheelite

Mo-poor scheelite - molybdenite - pyrite in molybdenite-quartz veins.

Fig.12.10. Scheelite stability field dependent on $^{a}Ca^{++}$, pH, fS_2 and fO_2 at 350°C.

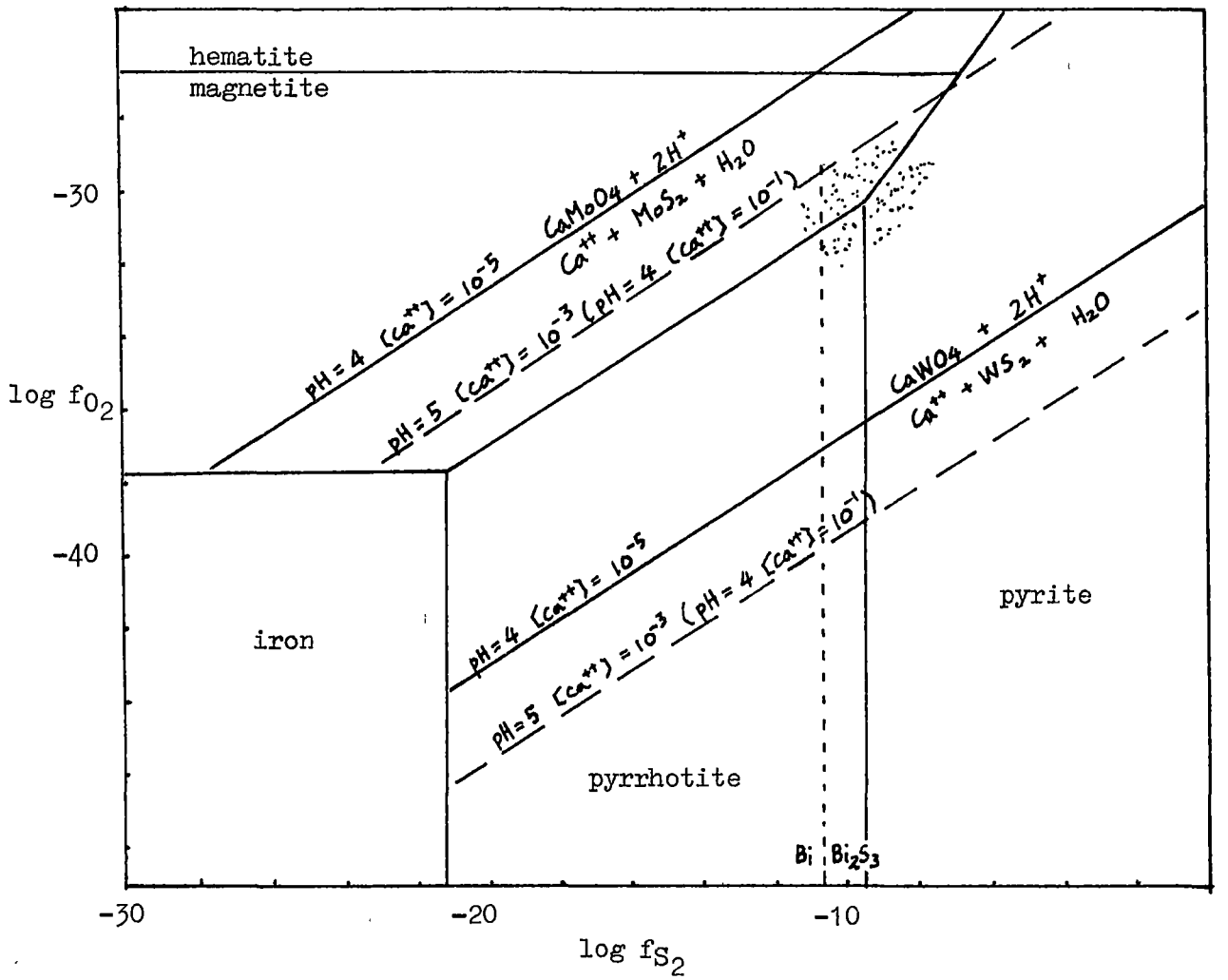

field of mica skarn

Fig. 12.11. Dependence of K_2 on ionic strength.

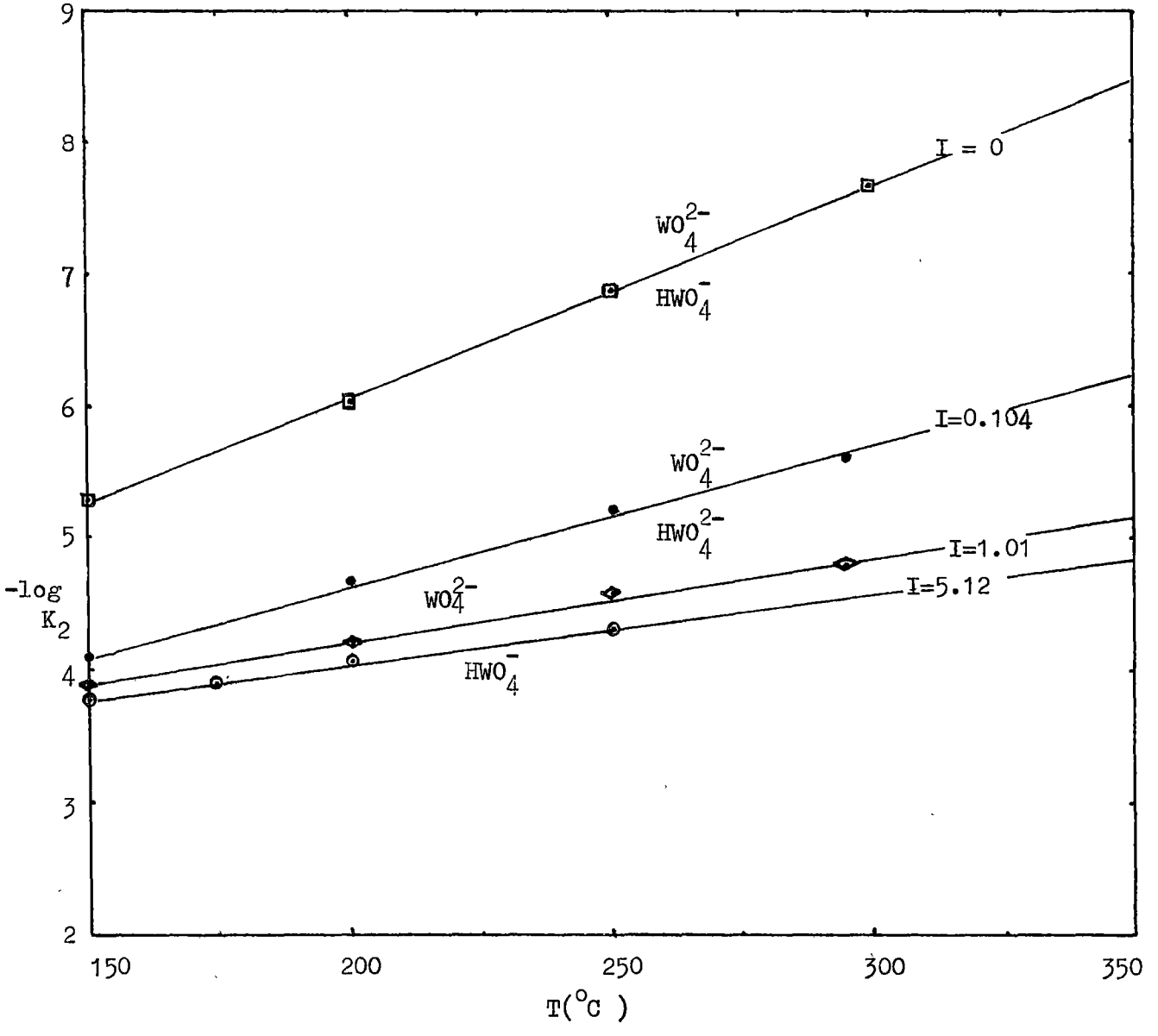

I = 0, from Ivanova and Khodakovskii(1968)

I = 0.104, 1.01, 5.12, from Wesolowskii et al.(1982)

Fig. 12.12. Control of pH and $^{a}Ca^{++}$ at 350°C, I = 1.0, on the solubility of W_t in equilibrium with scheelite.

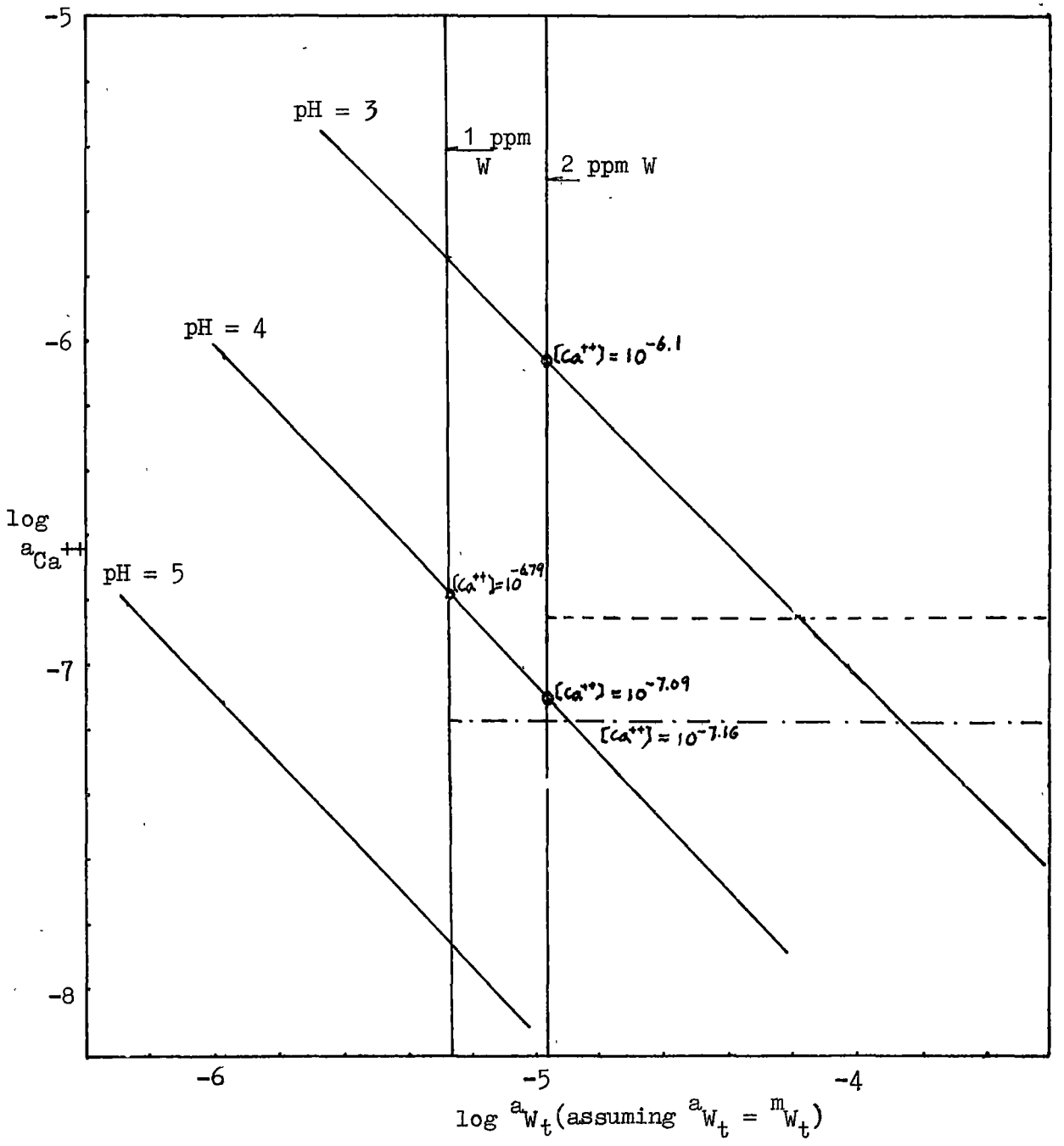

- - 2 ppm - indicates $^{a}Ca^{++}$ and pH required to maintain 1-2 ppm W
— 1 ppm — solution in equilibrium with scheelite.

Fig. 12.13. Solubility of W_t(as HWO_4^- + $WO_4^=$) in equilibrium with scheelite at I = 1.0 for $^aCa^{++}$ = 10^{-7}, 10^{-6}, & 10^{-5} .

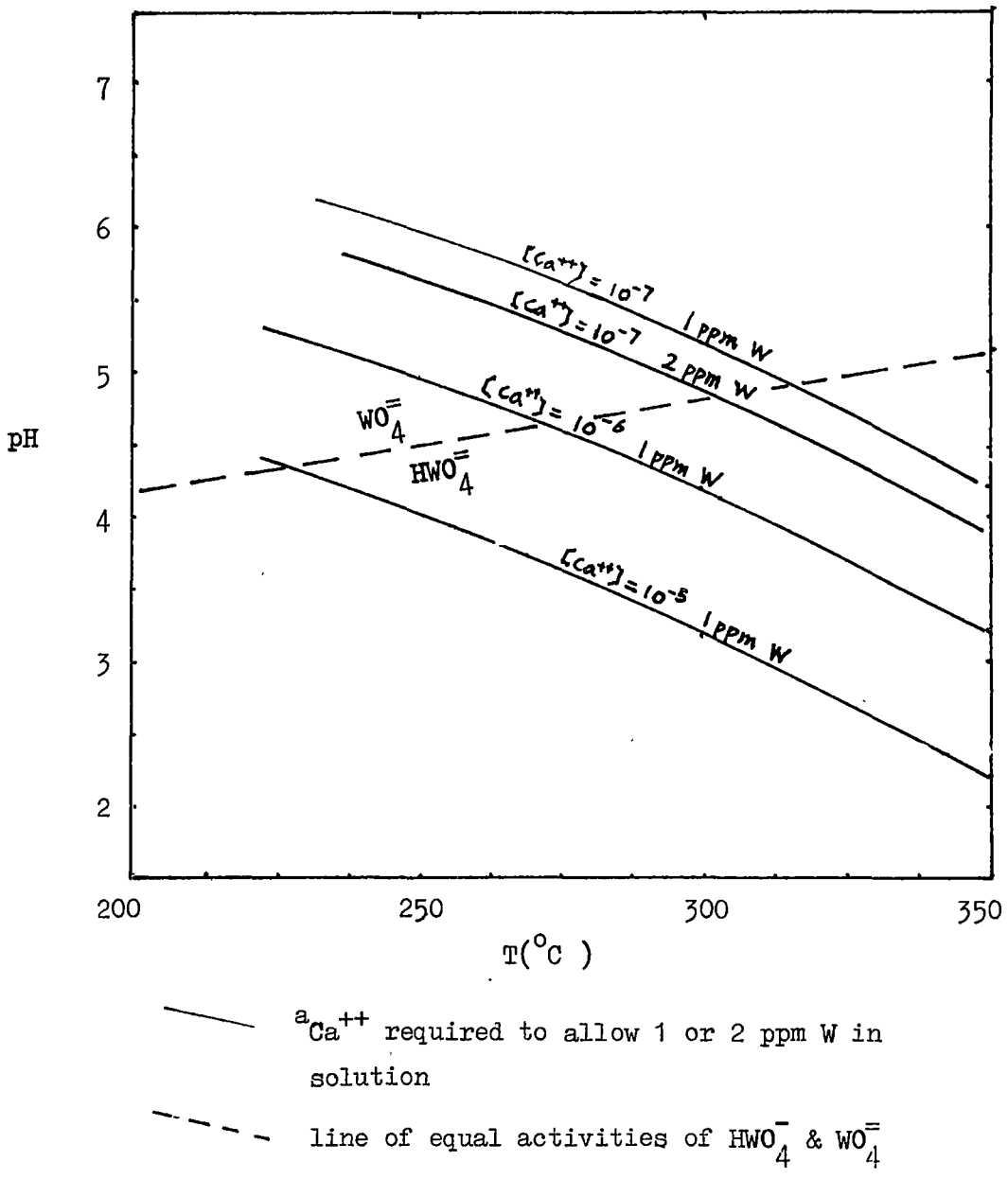

12.8. Formation of the Quartz Veins

Wolframite-rich quartz veins occur mainly along faults obliquely intersecting the M1 orebody, molybdenite veins occur along the bedding plane between the M1 skarn and the footwall slate, and chalcopyrite-rich veins occur mainly filling joints or faults within the M1 orebody. Small scheelite-bearing quartz veins swarm along fractures in the footwall side of the Myobong slate below the central part of the M1 orebody. Some of the quartz veins are dispersed into the quartz-muscovite skarn without showing a sharp boundary, however, most of quartz veins cut the skarn orebodies with a sharp boundary between them. This features indicate that quartz vein mineralization took place following formation of the amphibole-biotite skarns, synchroneously with formation of the quartz-muscovite skarn.

A possible circulation path for the ore fluids may be represented by the scheelite-bearing quartz veins that are concentrated in the footwall slate and the molybdenite-bearing quartz veinlets(containing no scheelite at all) which are confined within the Jangsan Quartzite directly below the central zone of the M1 orebody(Fig. 13.1).

A distinctive feature is the almost complete separation of wolframite and molybdenite in the vein system, indicating the existence of fluids of different composition. The two vein types formed at similar, and relatively high, temperatures(300°- 400°C). However, the abundance of sericite on the walls of the molybdenite veins and general lack of sericite in the wolframite veins may indicate differences in a_{K^+} or pH. The molybdenite veins contain no scheelite and few other sulphides reinforcing the thesis that they represent a distinctive phase of fluid activity. The $a_{Ca^{++}}$ in the wolframite veins must initially have been very low but it probably increased later to allow deposition of calcite and scheelite under conditions of relatively high f_{CO_2}.

Pyrrhotite occurs in a few wolframite-bearing samples but nowhere else, indicating rather higher f_{O_2}/f_{S_2} conditions in the veins than in the skarn orebody. The lack of magnetite may reflect low f_{O_2} or higher ΣS and the lack of bismuth indicates relatively high f_{S_2}(Table 4.1 ; Fig. 12.9).

The chalcopyrite-rich veins formed at lower temperatures than the molybdenite and wolframite veins, and the presence of sphalerite and galena indicates temperatures of deposition down to 250°C or so. A possible evolutionary path of the copper-bearing veins is indicated in Fig. 12.8a.

13. THE EVOLUTION OF THE SANGDONG SKARNS

Despite drilling into the Jangsan Quartzite and the Precambrian schist about 500 m below the 3rd level(Fig. 4.17b), no intrusive pluton has been encountered at Sangdong(H.J. Lee, personal communication, 1983). The age of the deposit(Farrar et al.,1978) appears to be about 81-84 Ma, a period in which magmatism took place nearby and magmatic tungsten mineralization formed in other parts of Korea(e.g. 80 to 96 Ma at the Sannae Mine, Ishihara et al.,1981). Magmatic tungsten mineralization also developed at about this time in Japan(64 to 96 Ma, Shibata and Ishihara, 1974), at the Yukon(80 to 92 Ma, Dick and Hodgson, 1982), at Pine Creek(74 to 87 Ma, Gray et al.,1968), and at Vostok in Russia(84 Ma, Levarshev, 1972). Most tungsten deposits(e.g. Pine Creek, MacTung, King Island, Salau) are clearly related to granitoid plutons and a similar situation is inferred from mineralogy and fluid inclusions, and the oxygen- and sulphur-isotope ratios inferred for the fluids, all point to the presence of a substantial pluton beneath the mine. There is no evidence of an earlier enrichment of tungsten in the rocks, as suggested by Kim(1976), and the mineralization is regarded as epigenetic. The closure of the outer skarns when drawn in the plane of the M1 orebody and distribution of the quartz veins indicates the location of a rising plume of hot fluid(Fig. 13.1).

The fluid appears to have moved up a NE fracture zone(Fig. 4.3) that controls the orientation of the skarn zones and the distribution of T_h values in the mica-amphibole skarn zones. Analysis of groundwater circulation during cooling of plutons by Norton and Knight(1977) indicates that it is difficult to raise ground temperatures sufficiently high to form wollastonite-bearing skarns at a distance of 0.5 km from a pluton boundary in a uniformly permeable medium. To achieve the required temperature distribution and maintain temperatures 400°C during growth of the hydrous skarn appears to require fluid transfer in faults or zones of highly permeable strata.

It is also clear that the rocks beneath the ore horizon must have been chemically inert in tne sense that solution acidity was not affected, and a fairly reduced condition was maintained.

The skarn zones are believed to evolve as follows(see Figs. 13.1 & 13.2).

1) During, or immediately preceding emplacement of the inferred pluton, the rocks of the mine area are warmed by groundwater circulating as a result of magmatic heating. This short-lived phase seems inevitable though there is no specific evidence for it. At King Island, Kwak(1978b) found relatively low temperature, low salinity fluids in the cores of garnet crystals that preceded the development of saline, high temperature fluids.

2) With increased temperature a zone of wollastonite-bearing garnet-pyroxene skarn developed, about 1.5 km x 1.2 km x 0.5 km in extent. The temperature probably ranged from 510° to 560°C and reaction involving fluid, limestone and slate occurred with increasing chemical mobility of elements such as Mg, Fe, Ca and CO_2.

3) Development of the early pyroxene-garnet skarn merged to a phase involving solutions of essentially magmatic origin.

Reaction with the early skarn resulted in the development of the mica, amphibole, and late pyroxene-garnet skarns by diffusion + infiltration metasomatism. The resulting mineralogical zones grew outward from the central area of the hot plume, widening with time, leaving relics of earlier skarn throughout the deposit. Small scale zonation along fractures shows a similar evolutionary pattern.

The later pyroxene-garnet skarns have fluid inclusions showing evidence of boiling and T_h values range from 313° to 580°C(average 418°C). Likely pressures for a NaCl-H_2O system are 400 bars at 400-500°C but there is insufficient data for the more complex natural system(NaCl-KCl-$CaCl_2$ $MgCl_2$-H_2O) to determine quantitative pressures. A hydrostatic regime is inferred for this stage, possibly brought about by tectonic fracturing of the overburden. No evidence of boiling is seen in the lower temperature

members of this assemblage, indicating a sealing of the system and a reversion to lithostatic pressure, tentatively estimated at 800 bars from sphalerite compositions. Lack of gas-dominated inclusions in the mica- and amphibole-rich skarns and the veins indicates similar lithostatic conditions in these rocks. It is concluded that the skarns formed from boiling solutions are slightly earlier(and higher temperature) than the others. The inferred hydrostatic conditions may have given way to lithostatic possibly by sealing of fractures due to mineral precipitation.

The data are inadequate to identify temperature gradients within the skarn but a decline is seen close to the country rock contacts. To maintain a sharp boundary with steep temperature and chemical gradients probably requires double-diffusive mechanisms, such as advocated by Eastoe(1979) for porphyry copper systems. In this model the mass of hot, magmatic fluid is contained within an envelope of hot groundwater of contrasting salinity during the life of individual surges of ore fluid. Similar(see Fig. 13.1) conditions could prevail in the Sangdong aureole with a hot, low salinity groundwater that gradually or occasionally mixes and becomes incorporated into the ore system. The incoming ore fluid during this period has the following general characteristics:

T	$313^{\circ}\sim 600^{\circ}C(?)$	$\overset{m}{\Sigma}S$	$\approx 2.5 \times 10^{-3}$
pH	$\approx$ 4.0 at $350^{\circ}C$	f_{O_2}	$\approx 10^{-23}\sim 10^{-31}$
XCO_2	0.1 mole (?)	f_{S_2}	$\approx 10^{-9}\sim 10^{-12}$
		$\delta^{34}S_{H_2S}$	$4.5\sim 5.3$ permil
$m_{Ca^{++}}$	$<10^{-6}$ mole (inferred)	$\delta^{18}O_{H_2O}$	$6.6\sim 8.5$ permil
mK^{+}	$\approx 10^{-1}$ mole (by analogy)	$\delta^{13}O_{CO_2}$	$-5.3\sim 0.9$ permil

There is a clear trend of declining temperature with time, from $T>500^{\circ}C$ for the early skarns to $300^{\circ}C$ or so for the final muscovite skarn in the core of the deposit.

The $^{a}Ca^{++}$ may increase during the life of an individual packet of fluid moving through the skarn zones by reactions with amphibole and pyroxene skarns, and possibly by localized recirculation of fluids that have reacted with carbonates. These factors may account for a change from wolframite-rich veins to scheelite-bearing skarns.

The major overall changes involved in developing the skarns are addition of FeO, MnO, K_2O, SiO_2, Al_2O_3, WO_3 and H_2O to the rocks and loss of CaO.

Equilibrium with the incoming ore fluid was approached in the development muscovite-rich assemblage in the core of the deposit, at temperatures of about 350° or 400°C. Chloritization of biotite and amphibole probably took place in these later stages of skarn growth.

Quartz-molybdenite and quartz-wolframite veins formed in footwall rocks and around the skarn during skarn growth. T_h values of vein and skarn are similar, and overall P-T-X conditions for the vein appear similar to the skarns. The relationships between molybdenite and wolframite veins are not clear.

4) Quartz precipitation continued to relatively low temperatures(290° to 350°C) throughout the skarn and in the late veins. These veins cut the skarn, are sulphide-rich, particularly in chalcopyrite, and carry sphalerite and galena. The solutions generally are of similar composition to earlier solutions and appear be still largely of magmatic origin. Some recycling of scheelite and precipitation of low Mo-scheelite occurred at this time. occurred at this time.

5) Later stages of fluid circulation involved formation of quartz and calcite, and locally hematite, at temperature $\ll$250°C. $\delta^{13}C$ data of calcite from a molybdenite-bearing calcite vein indicate the involvement of non-magmatic fluid.

Fig. 13.1. Diagrammatic vertical section of Sangdong skarns showing fluid circulation.

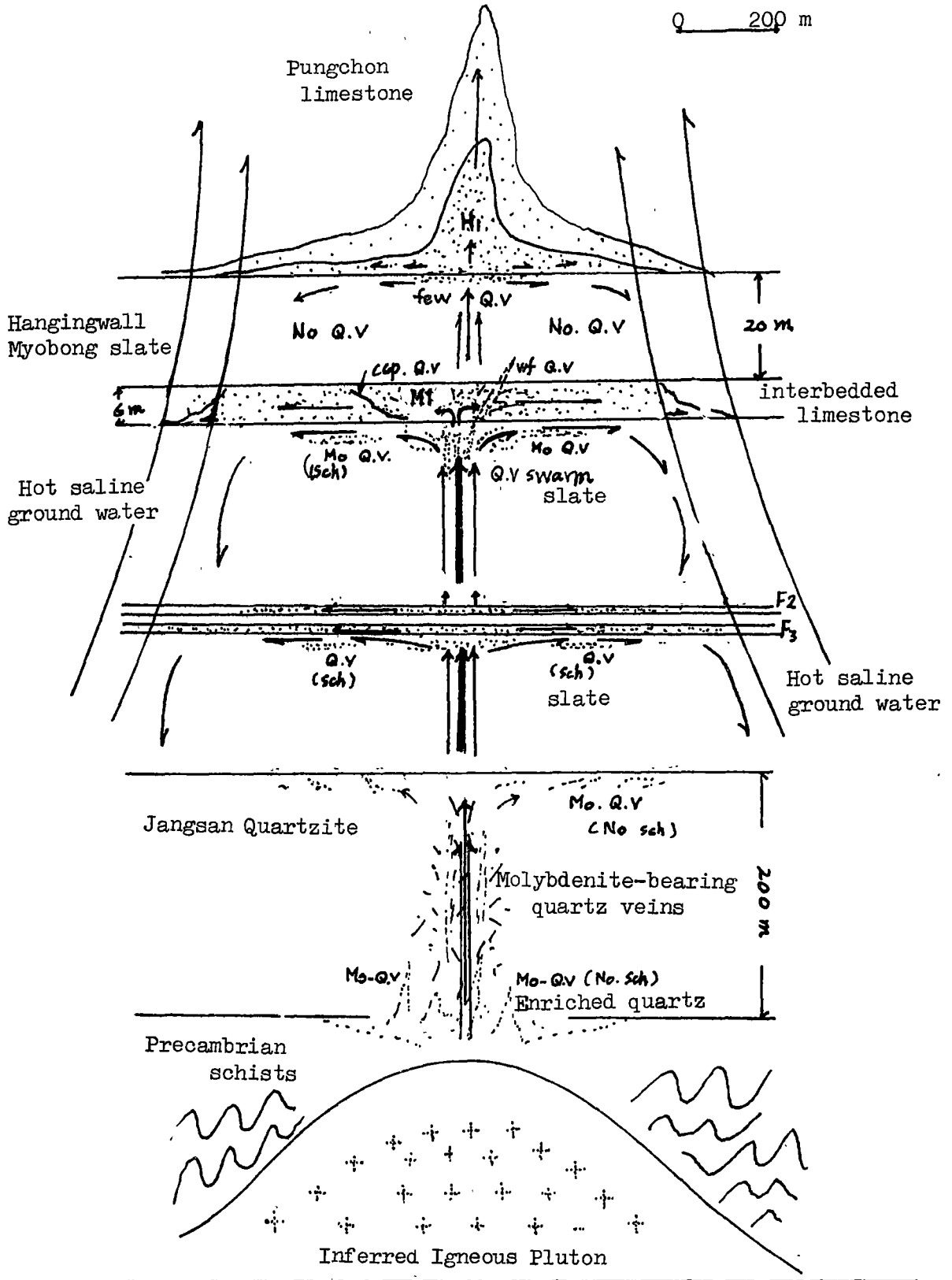

No Q.V = No quartz veins are developed in hangingwall slate
Q.V = quartz vein; wf = wolframite; ccp = chalcopyrite; Mo = molybdenite

Enriched Quartz = strong silicification at the bottom of the Jangsan quartzite may be responsible for increasing the thickness of the quartzite.
(sch) = quartz veins contains scheelite.

Fig. 13.1. Generalized Conditions of Evolution of the Sangdong Deposit.

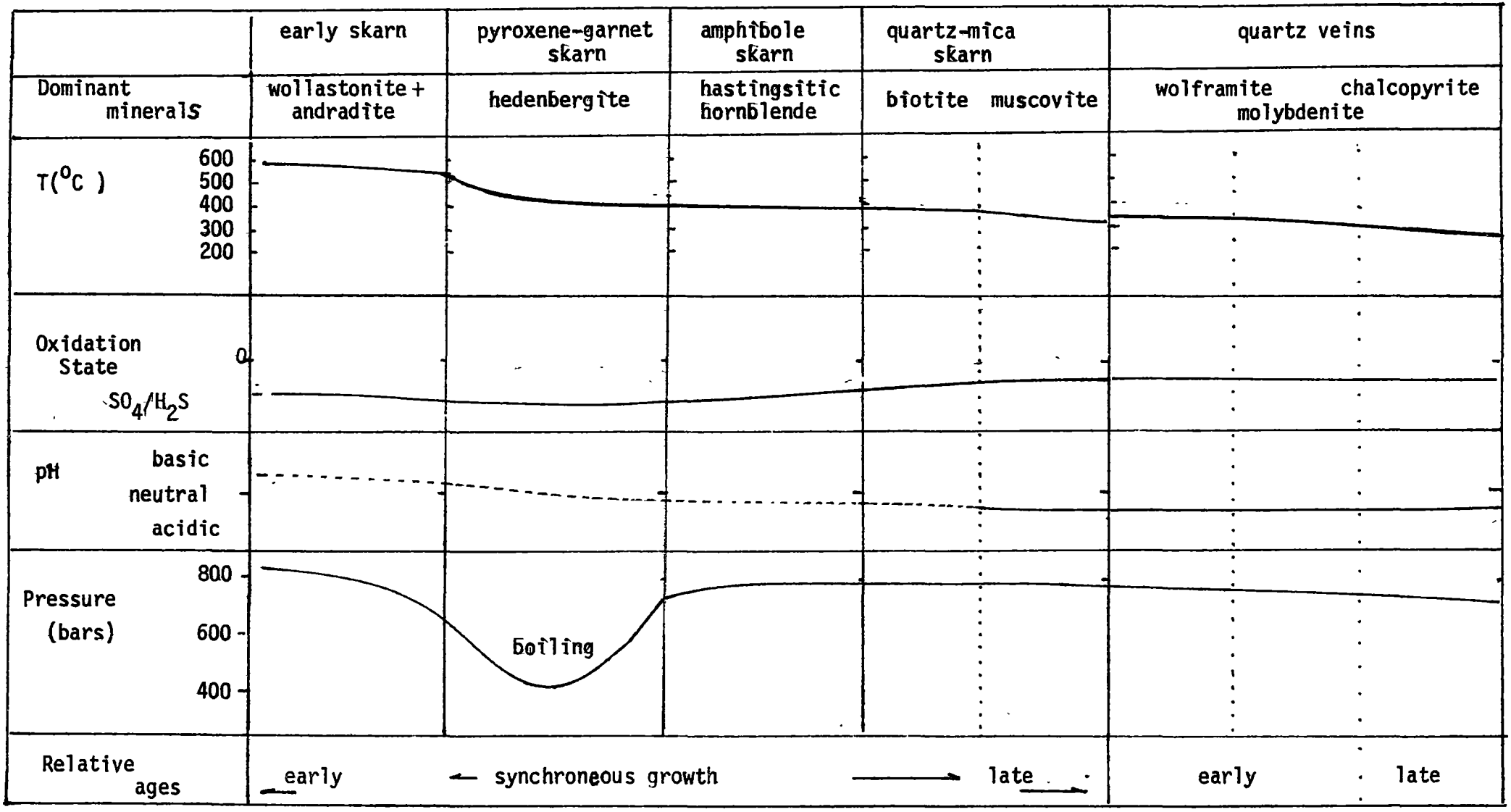

REFERENCES

Bachinski, D.J., 1969. Bond strength and sulfur isotope fractionation in coexisting sulfides. Econ. Geol. 64, 56-65.

Barabanov, V.F., 1971. Geochemistry of tungsten. Int. Geol. Rev. 13, 332-344.

Barin, I., Knacke, O., and Kubaschewski, O., 1977. Thermochemical properties of inorganic substances. v.1 & 2. Springer-Verlag.

Bird, D.K., and Helgeson, H.C., 1981. Chemical interaction of aqueous solutions with epidote-feldspar mineral assemblages in geologic systems. II: equilibrium constraints in metamorphic/geothermal processes. Am. J. Sci. 281, 576-614.

Blattner, P., 1975. Oxygen isotopic composition of fissure-grown quartz, adularia, and calcite from Broadlands geothermal field, New Zealand, with an appendix on quartz-K feldspar-calcite-muscovite oxygen isotope geothermometers. Am. J. Sci. 275, 785-800.

Bottinga, Y., 1968. Calculation of fractionation factors for carbon and oxygen isotopic exchange in the system calcite-carbon dioxide-water. J. Phys. Chem. 72, 800-808.

Burruss, R.C., 1981. Analysis of phase equilibria in C-O-H-S fluid inclusions. in L.S. Hollister et al.(ed), Short Course In Fluid Inclusions: Application to Petrology. 39-73.

Burt, D.M., 1974. Metasomatic zoning in Ca-Fe-Si exoskarns. in A.W. Hofmann et al.(ed), Geochemical Transport and Kinetics. Washington, D.C. Carnegie Institution Wash., Pub. 634, 287-293.

Burton, J.C., 1978. Experimental and mineralogical studies of skarn silicates. Unpub. Ph.D. thesis, University of Tennessee, Knoxville, 155p.

Burton, J.C., Taylor, L.A., and Chou, I.M., 1979. Skarn mineralogy: stability of hedenbergite and hedenbergite-johannsenite solid solutions (abs.): Geol. Soc. Am. 11, 396. (Abstract with Programs)

Burton, J.C., Taylor, L.A, and Chou, I.M., 1982. Determination of the f_{O_2}- T stability relations of hedenbergite and hedenbergite-johannsenite solid solutions by the hydrogen fugacity sensor technique. Econ. Geol. 77, 764-783.

Charoy, B., 1979. Greisenisation et fluides associés a Cligga Head, Cornwall(sud-ouest de l' Agleterre). Bull. Mineral, 102, 633-641.

Clark, A.H., 1981. Personal communication on age dating results of tin-bearing pegmatite at Sunkyeong tin mine near Sangdong Mine.

Clayton, R.N., O'Neil, J.R. and Mayeda, T., 1972. Oxygen isotope exchange between quartz and water. J. Geophys. Res., 77, 3057-3067.

Cloke, P.L., and Kesler, S.E., 1979. The halite trend in hydrothermal solutions. Econ. Geol. 74, 1823-1831.

Collins, P.L., 1979. Gas hydrates in CO_2-bearing fluid inclusions and the use of freezing data for estimation of salinity. Econ. Geol. 74, 1435-1444.

Collins, P L., 1981. The geology and genesis of the Cleveland tin deposit, Western Tasmania: Fluid Inclusion and Stable Isotope Studies. Econ. Geol. 76, 365-392.

Crawford, M.L., 1981. Phase equilibria in aqueous fluid inclusions. in L.S. Hollister et al.(ed), Short Course In Fluid inclusions. Mineral assoc. Canada, p. 75-100.

Deer, W.A., Howie, R.A., and Zussman J., 1963, 1972. Rock Forming Minerals. v. 1 - 5. Longmans.

Dick, L.A., and Hodgson, C.J., 1982. The MacTung W-Cu(Zn) contact metasomatic and related deposits of the Northeastern Canadian Cordillera. Econ. Geol. 77, 845-867

Eastoe, C.J., 1979. The formation of the Panguna porphyry copper deposit, Bougainville, Papua New Guinea. Unpub. Ph.D. thesis, University of Tasmania, Australia. 255p.

Einaudi, M.T., 1977. Petrogenesis of the copper-bearing skarn at the Mason Valley Mine, Yerington District, Nevada. Econ. Geol. 72, 769-795.

Farrar, E., Clark, A.H., and Kim, O.J., 1978. Age of the Sangdong tungsten deposit, Republic of Korea, and its bearing on metallogeny of the soutnern Korean peninsula. Econ. Geol. 73, 547-566.

Foster, R.P., 1977. Solubility of scheelite in hydrothermal chloride solutions. Chem. Geol. 20, 27-43.

French, B.M., 1966. Some geological implications of equilibrium between graphite and a C-H-O gas phase at high temperatures and pressures. Rev. Geophys. 4, 223-253.

Gabert, G., and Vinken, R., 1962. Report on geological research work on mineral deposits in the Taebaek area(Republic of Korea), The scheelite deposit of Sangdong. Unpub. submitted to the Government of Republic of Korea, p. 116-156.

Gallagher, D., 1947. Mineral resources of southern Korea. Geol. Surv. Korea.

Gamble, R.P., 1982. An experimental study of sulfidation reactions involving andradite and hedenbergite. Econ. Geol. 77, 784-797.

Gehrig, M., Lentz, H., and Franck, E.U., 1979. Thermodynamic properties of water-carbon dioxide-sodium chloride mixtures at high temperatures and pressures. in K.D. Timmerhaus et al.(ed), High-Pressure Science and Technology, 1, Physical Properties and Material Synthesis. p. 539-542.

Gilbert, M.C., 1966. Synthesis and stability relations of the hornblende, ferropargasite. Am. J. Sci. 264, 698-742.

Gray, R.F., Hoffman, V.J., Bagan, R.J., and McKinley, H.L., 1968. Bishop tungsten district, California. in J.D. Ridge (ed), Ore Deposits of United States 1933-1967. v.2, 1532-1554.

Greenwood, H.J., 1967. Wollastonite: stability in H_2O-CO_2 mixtures and occurrence in a contact-metamorphic aureole near Salmo, British Columbia, Canada. Am. Mineral., 52, 1669-1680.

Gustafson, W., 1974. The stability of andradite, hedenbergite and related minerals in the system Ca-Fe-Si-O-H. J. Petrol. 15, 455-496.

Guy, B., 1979. Petrologie et geochemie isotopique (S,C,O) des skarns a scheelite de Costabonne, Pyrenees - Orientales, France (English abstract, 11p). Unpub. Ph.D. thesis, 238p.

Halley, S.W., 1982. Solubility of tungstate mineral. Unpub. hon. reading essay, University of Tasmania, 91p.

Han, T.W., 1978. Description of the geology of the Sangdong tungsten deposit with suggestions for further exploration using geochemical techniques. J. Korean Inst. Mining Geol., 11, 143-167(in English).

Helgeson, H.C., 1969. Thermodynamics of hydrothermal systems at elevated temperatures and pressures. Am. J. Sci. 267, 729-804.

Helgeson, H.C., Delany, J.M., Nesbitt, H.W., and Bird, D.K., 1978. Summary and critique of the thermodynamic properties of rock-forming minerals. Am. J. Sci. 278 (A), 1-229.

Hong, M.S., Kim, Y.J., and Yun. S., 1970. Geology and ore deposits of western vicinity of Sangdong scheelite mine. J. Korean Inst. Mining Geol. 3, 35-47.

Hsu, L.C., 1977. Effects of oxygen and sulfur fugacities on the scheelite-tungstenite and powellite-molybdenite stability relations. Econ. Geol. 72, 664-670.

Hsu, L.C., and Galli, P.E., 1973. Origin of the scheelite-powellite series of minerals. Econ. Geol. 68, 681-696.

Hwang, J.W., 1970. Study on properties of Sangdong scheelite. J. K.T.M.C. Research and Development. v.5, no.4, 10-13.

Hwang, K.Y., 1962. Study on properties of Sangdong powellite. Metal and Fuel (reports of lab. K.T.M.C).

Ishihara, S., Lee, D.S., and Kim, S.Y., 1981. Comparative study of Mesozoic granitoids and related W-Mo mineralization in southern Korea and southwestern Japan. Mining Geol. Japan. 31, 311-314.

Ivanova, G.F., and Khodakovskiy, I.L., 1968. Transport of tungsten in hydrothermal solutions. Geochem. Int. 5, 779-780.

Jeong, C.K., 1963. Study on zonal distribution in the main orebody of the Sangdong ore deposits. Unpub. mine report.

John, Y.W., 1963. Geology and origin of Sangdong tungsten mine, Republic of Korea. Econ. Geol. 58, 1285-1300.

John, Y.W., 1978. Sangdong Mine, Korea. in H. Imai (ed), Geological Studies of the Mineral Deposits in Japan and East Asia. University of Tokyo press.

Kerrick, D.M., and Slaughter, J., 1976. Comparison of methods for calculating and extrapolating equilibria in P-T-Xco_2 space. Am. J. Sci. 276, 883-916.

Khodakovskiy, I.L., and Mishin, I.V., 1971. Solubility products of calcium molybdate and calcium tungstate; ratio of powellite to scheelite mineralization under hydrothermal conditions. Int. Geol. Rev. v.13, no.5, 760-768.

Kim, K.H., 1980. Carbon and oxygen isotope studies of the Paleozoic limestones from the Taebaegsan region, South Korea. J. Korean Inst. Mining Geol. 13, 21-27.

Kim, O.J., 1971. Metallogenic epochs and provinces of South Korea. J. Geol. Soc. Korea. 7, 37-59.

Kim, O.J., 1975. Granites and tectonics of South Korea. J. Korean Inst. Mining Geol. 8, 222-230.

Kim, O.J., and Kim, K.H., 1978. On the genesis of the ore deposits of Yemi district in the Taebaegsan metallogenic province. J. Natural Sci. Res. Inst. Yonsei University, 2, 71-94.

Kim, O.J., and Park, H.I., 1970. Preliminary report on the geology of Sangdong scheelite mine. J. Korean Inst. Mining Geol. 3, 25-34.

Kim, S.Y., 1976. Geology, mineralogy and geochemistry of tungsten deposits of the Sangdong-Ogbang area, South Korea. Unpub. Ph.D. thesis, University of Leed, U.K., 346 p.

Klepper, M.P., 1947. The Sangdong tungsten deposits, southern Korea. Econ. Geol. 42, 465-477.

Kobayashi, T., 1966. The Cambro-Ordovician formations and faunas of South Korea, Part 10, Sect. A. The Chosen Group of South Korea; University of Tokyo Fac. Sci., J., Sect. 2, v.16, pt1, 1-84.

Korzhinskii, D.S., 1968. The theory of metasomatic zoning. Mineral Deposita, 3, 222-231.

Korzhinskii, D.S., 1970. Theory of metasomatic zoning. London. Oxford University Press.

Krauskopf, K.B., 1970. Tungsten(Wolfram). in K.H. Wedpohl(ed), Handbook Geochemistry, Vol. 11/2, Springer-Verlag, 74-B to 70-O.

Kretschmar, U., and Scott, S.D., 1976. Phase relations involving arsenopyrite in the system Fe-As-S and their application. Can. Miner. 14, 364-386.

Krumhansl, J., 1977. Geochemistry of tungsten. Unpub. Ph.D. thesis, Stanford University, U.S.A.

Kwak, T.A.P., 1978a. Mass balance relationships and skarn forming processes at the King Island scheelite deposit, King Island, Tasmania, Australia. Am. J. Sci. 278, 943-968.

Kwak, T.A.P., 1978b. The conditions of formation of the King Island scheelite contact skarn, King Island, Tasmania, Australia. Am. J. Sci., 278, 969-999.

Kwak, T.A.P., and Tan, H.T., 1981. The geochemistry of zoning in skarn minerals at the King Island (Dolphin) mine. Econ. Geol. 76, 468-497.

Kwak, T.A.P., and Tan, H.T., 1981b. The importance of $CaCl_2$ in fluid composition trends - evidence from the King Island (Dolphin) skarn deposit. Econ. Geol. 76, 955-960.

Leake, B.E., 1978. Nomenclature of amphiboles. Am. Miner. 63, 1023-1052.

Lee, D.S., and Kim, S.W., 1969. Microscope study of Sangdong tungsten ore deposits, Korea. 1, 1-12.

Lee, H.Y., and Lee, J.D., 1971. Conodont fauna from the Great Limestone Series in Dongjeom district, Samcheoggun, Gangwondo, and its stratigraphical significance. Geo. Soc. Koreas. 2, 89-107.

Levashev, G.B., Govorov, I.N., Strizhkova, A A. and Grechischeva, A.P., 1972. The regional geochemistry of tungsten in Primorye. Geochem. Inst. 9, 279-293.

Linke, W.F., 1965. Solubility of inorganic and metal-organic compounds. (4th ed.), 2, Am. Chem. Soc. 1914p.

Liou, J.G., 1974. Stability relations of andradite-quartz in the system Ca-Fe-Si-O-H. Am. Miner. 59, 1016-1025.

Maucher, A., 1976. The strata bound cinnibar-stibnite-scheelite deposits. in Wolf, K.H. (ed), Handbook of Strata-bound and Stratiform Ore Deposits, v.7, 477-503.

Moon, K.J., 1972. The distribution of Bi-minerals in the Sangdong mine. J. Geol. Soc. Korea, 8, 217-221.

Moon, K.J., 1974. Study on mineral paragenesis in the Sangdong scheelite deposits. Unpub. M.Sc. thesis, University of Yonsei, Korea.

Moon, K.J., and Lee, H.J., 1980. A study on the molybdenum in scheelite of Sangdong tungsten orebodies. J. Korean Inst. Mining Geol. 13, 117-127.

Newberry, R.J., 1982. Tungsten-bearing skarns of the Sierra Nevada.1. The Pine Creek Mine, California. Econ. Geol. 77, 823-844.

Norton, D., and Knight, J., 1977. Transport phenomena in hydrothermal systems, cooling plutons. Am. J. Sci. 277, 937-981.

Ohmoto, H., and Rye, R.O., 1979. Isotope of sulfur and carbon. in Barnes, H.L.,(ed), Geochemistry of hydrothermal ore deposits, 2nd ed. New York, John Wiley and Sons, p. 509-567.

O'Neil, J.R., Clayton, R.N., and Mayeda, T.K., 1969. Oxygen isotope fractionation in divalent metal carbonates. J. Chem. Phys. 51, 5547-5558.

Patterson, D.J., 1979. Geology and mineralization at Renison Bell, western Tasmania. Unpub. Ph.D. thesis, University of Tasmania.

Patterson, D.J., Ohmoto, H., and Solomon, M., 1981. Geologic setting and genesis of cassiterite-sulfide mineralization at Renison Bell, western Tasmania. Econ. Geol. 76, 393-438.

Potter, R.W., 1977. Pressure corrections for fluid-inclusion homogenization temperatures based on the volumetric properties of the system NaCl-H_2O. J. Res. U.S. Geol. Suv. v.5, no.5, 603-607.

Potter, R.W., Clynne M.A and Brown, D.L., 1978. Freezing point depression of aqueous sodium chloride solutions. Econ. Geol. 73, 284-285.

Purtscheller, F., and Rammlmair, D., 1982. Alpine metamorphism of diabase dikes in the Oetztal-stubai metamorphic complex. TMPM Tsch. Min. Petr. Mitt. 29, 205-221.

Ravich, M.I., and Borovaya, F.E., 1949. Phase equilibria in ternary water-salt systems at elevated temperatures. Akad. Nauk. U.S.S.R. Izvyestiya Syktora Fiz. -Khim. Analiza, 19, 69-81.

Reedman, A.J., and Um, S.H., 1976. Geology of Korea. Geol. Min. Inst. Korea.

Reynolds, R.C., 1972. Rubidium: element and geochemistry. in Fairbridge, R.W (ed), the Encyclopedia of Geochemistry and Environmental Science, Van Nostrand Reinhold Company. p. 1050-1052.

Ripley, E.M., and Ohmoto, H., 1980. A FORTRAN program for plotting mineral stabilities in the Fe-Cu-S-O system in terms of log (SO_4/H_2S) or log f_{O_2} vs pH or T: Computers Geosci. 5, 289-300.

Robie, R.A., Hemingway, B.S., and Fisher, J.R., 1978. Thermodynamic properties of minerals and related substances at 298.15 K and 1 bar(10^5pascals) pressure and at higher temperatures. Geol. Surv. Bull. 1452, 458p.

Roedder, E., 1963. Studies of fluid inclusions II; Freezing data and their interpretation: Econ. Geol. 58, 167-211.

Roedder, E., 1967., 1967. Metastable superheated ice in liquid-water inclusions under high negative pressure. Science, 155, 1413-1417.

Roedder, E., 1971. Fluid inclusion studies on the porphyry-type ore deposits at Bingham, Utah; Butte, Montana; and Climax Colorado. Econ. Geol. 66, 98-120.

Roedder, E., 1972. Composition of fluid inclusions. U.S. Geol. Surv., Prof. Paper 440 JJ.

Rose, A.W., and Burt, D.M., 1979. Hydrothermal alteration. in Barnes, H.L. (ed), Geochemistry of Hydrothermal Ore Deposits. New York, Wiley Interscience, 173-235.

Sato, K., Shibata, K., Uchimi, S., and Shimazaki, H., 1981. Mineralization age of Shinyemi Zn-Pb-Mo deposits in the Taebaegsan area, southern Korea. Mining Geol. Japan. 31(4), 335-336.

Scott, S.D., and Barnes, H.L., 1971. Sphalerite geothermometry and geobarometry. Econ. Geol. 66, 653-669.

Shibata, K., and Ishihara, S., 1974. K-Ar ages of major tungsten and molybdenum deposits in Japan. Econ. Geol. 69, 1207-1214.

Shimazaki, H., and Yamanaka, T., 1973. Iron wollastonite from skarns and its stability relation in the $CaSiO_3$-$CaFeSi_2O_6$ join. Geochem. J. 7, 67-79.

Shimizu, M., and Shimazaki, H., 1981. Application of the sphalerite geobarometer to some skarn-type ore deposits. Mineral Deposita, 16, 45-50.

So, C.S., 1968. Die scheelit-lagersätte Sangdong. Unpub. Dissertation. Munchen University, West Germany.

Sourirajan, S., and Kennedy, G.C., 1962. The system H_2O-NaCl at elevated temperatures and pressures. Am. J. Sci. 260, 115-141.

Takenouchi, S., and Kennedy, G.C., 1964. The binary system H_2O-CO_2 at high temperatures and pressures. Am. J. Sci. 262, 1055-1074.

Tan, T.H., and Kwak, T.A.P., 1979. The measurement of the thermal history around the Grassy Granodiorite, King Island, Tasmania, by use of fluid inclusion data. J. Geol. 87, 43-54.

Taylor, B.E., and Liou, J.G., 1978. The low temperature stability of andradite in C-O-H fluids. Am. Mineral. 63, 378-393.

Taylor, H.P. Jr., 1979. Oxygen and hydrogen isotiope relationships in hydrothermal deposits. in H.L. Barnes(ed), Geochemistry of Hydrothermal Ore Deposits, 2nd ed. John Wiley & Sons. 236-277.

Uchida, E., and Iiyama, J.T., 1982. Physicochemical study of skarn formation in the Shinyama iron-copper ore deposit of the Kamaishi mine, northeastern Japan. Econ. Geol. 77, 809-820.

Ueda, N., 1969. Evolution of the continent in north-eastern Asia (Reconnaissance survey of geochronology of the Korean peninsula). J. Korean Inst. Mining Geol. 2, 96-97.

Walshe, J.L., and Solomon, M., 1981. An investigation into environment of formation of the vol anic-hosted Mt. Lyell copper deposits using geology, mineralogy, stable isotopes, and a six-component chlorite solid solution model. Econ. Geol. 76, 246-284.

Wesolowski, D., Drummond, S.E., Mesmer, R.E., and Ohmoto, H., 1982. Tungsten speciation in NaCl solutions to 300°C. Abstracts with programs, 75th annual meeting. Geol. Soc. Am. Oct. 18-21, p 645.

Wones, D., 1981. Mafic silicates as indicators of intrusive variables in granitic magmas. J. Soc. Mining Geol. Japan. 31(4), 191-212.

Yastrebova, L.F., Borina, A.F., and Ravich, M.I., 1963. Solubility of $CaMoO_4$ and $CaWO_4$ in aqueous KCl and NaCl at high temperatures. Russ. J. Inorg. Chem., 8, 105-110.

Ypma, P., 1979. Workshop manual as fluid inclusions. Latrobe University, Melbourne. 27p.

Yun, S.K., 1966. Relations of structural pattern and tungsten deposition in the Sangdong mine and its vicinity. J. Geol. Soc. Korea, 2, 1-16.

Yun, S.K., and Einaudi, M.T., 1982. Zinc-lead skarns of the Yeonhwa-Ulchin district, South Korea. Econ. Geol. 77, 1013-1032.

Zharikov, V.A., 1970. Skarns. Int. Geol. Rev. 12, 541-559, 619-647, 760-775.

Yun, S.K., and Silberman, M.L., 1979. K-Ar geochronology of igneous rocks in Yeonhwa-Ulchin zinc-lead district and southern margin of Taebaegsan basin, Korea. Geol. Soc. Korea Journ, v.15, 1, 89-99.

Appendix 1

LIST OF SPECIMENS FROM SANGDONG, KOREA

Abbreviations

Mineral

ad = andradite
amp = amphibole
ap = apatite
Bi = native bismuth
bi = bismuthinite
bt = biotite
ca = calcite
ccp = chalcopyrite
dp = diopside
ep = epidote
fl = fluorite
gn = garnet
hb = hornblende
hd = hedenbergite
ms = muscovite
mc = mica
mo = molybdenite
mt = magnetite
pl = plagioclase
po = pyrrhotite
py = pyrite
px = pyroxene
qz = quartz
sch = scheelite
sph = sphene
vs = vesuvianite
wlf = wolframite
wol = wollastonite
sp = sphalerite

Rock

sk = skarn
amp-sk = amphibole-rich skarn
qz-mc sk = quartz-mica skarn
px-gn sk = pyroxene-garnet skarn
ch. Rk = cherty rock
P-Ls = Pungchon limestone
M-sl = Myobong slate
M1 Ls = interbedded limestone stratigraphically equivalent to M1 orebody
F. Ls = interbedded limestone stratigraphically equivalent to F. orebody
H.W = hangingwall
F.W = footwall
Ls = limestone
sl = slate
J. Qtz = Jangsan quartzite
Qtz = quartzite.

dyk = dyke

Location

+3 = Jangsan level
+2 = Baegun level
+1 = Taebaeg level
+0 = Sangdong level
-1 = the 1st level
-3 = the 3rd level
. . .
-17 = the 17th level

bl = block

H.W = hanging-wall
F.W = footwall

Type of Specimen

R = hand specimen
T = thin section
PT = polished T.
PS = polished section

D = X-ray disc
P = X-ray pill
PD = powdered specimen

F = chips for fluid inclusion study

103050	0201	Ls	Eopyeong area, M1 Ls.		D. P.
103051	0202	Ls	Eopyeong area, M1 Ls.		D. P.
103052	0196	Ls	-15, 30bl. relic of M1 Ls.		D. P.
103053	0197	Ls	-16, 36bl. relic of M1 Ls.		D. P.
103054	0188	sk	-5, 19bl. relict wol sk in qz-mc sk.		D. P.
103055	0188	sk	-5, 19bl. px sk replacing wol sk	PT.	D. P.
103056	px-1L	sk	-1, px-gn sk in M1		D. P.
103057	px-5L	sk	-5, px-gn sk in M1		D. P.
103058	px-10L	sk	-10, px-gn sk in M1		D. P.
103059	0161	sk	+2, 21bl. gn dominant sk.		D. P.
103060	0161	sk	+2, 21bl. px sk replacing 103059		D. P.
103061	0163	sk	-7, 24bl. amp sk repalcing gn sk		D. P.
103062	0083a	sk	+0, 14bl. minor amp sk in px-gn sk.	PT.	D. P.
103063	0083b	sk	+0, minor qz-mc sk.		D. P.
103064	0125	sk	-6, M1, mt-bearing amp sk.		D. P.
103065	0116	sk	-5, 24bl. M1, Mo-poor sch bearing qz-mc sk.		D. P.

103066	0218	sk	+1, M1 qz-mc sk	D. P.
103067	0228	sk	+0, M1 qz-mc sk, bt-rich	D. P.
103068	0229	sk	+0, M1 qz-mc sk, ms-rich	D. P.
103069		ch	-7, typical ch.Rk.	D. P.
103070	0203	sl	Eopyeong area, M-sl about 15m below M1 Ls	PT.D. P.
103071	0204	sl	same as 103070	D. P.
103072	0205a	sl	M-sl, drill core, 17 m below -3 M1	D. P.
103073	0205b	sl	M-sl, drill core, 36 m below -3 M1	D. P.
103074	0205c	sl	M-sl, drill core, 62 m below -3 M1	D. P.
103075	0200a	ch	-16, 36bl. ch.Rk between M1 Ls and H.W sl	D. P.
103076	0200b	sl	-16, 36bl. M-sl contacted with 103075	D. P.
103077	0144	dyk	-6, 17bl. Mo-bearing felsitic dyk, in H1	D. P.
103078	0186	dyk	-13, surrounded by minor qz-mc sk in px-gn sk(M1)	PT.D. P.
103079	0187	dyk	+1, black, mafic dyk cutting M-sl	D. P.
103080	0105	dyk	+2, dyk altered to sk	F.D. P.
103081	0106	dyk	+2, dyk altered to sk, bt-rich	D. P.
103082	0107	dyk	+2, dyk altered to sk	D. P.
103083	0162a	sk	+2, 21bl. gn dominant sk	D. P.
103084	0162b	sk	+2, 21bl. amp-px sk replacing 103083	D. P.
103085	0162c	Q.V	+2, 21bl. 2 cm thick intruding 103083	D. P.
103086	7-1	sk	-7, western end of -7, M1 px-gn sk replaced by amp & po	R.PT.
103087	7-2	sk	-7, M1 px-gn sk	F.R.PT.
103088	7-3	sk	-7, M1 px-gn sk, locally replaced by amp	R.PT.
103089	7-6	sk	-7, M1 px-gn sk, hd & gn replaced by qz & fl	R.
103090	7-8	sk	-7, M1 hd dominant px sk with fine Q.V-let	R.PT.
103091	7-10	sk	-7, M1 gn sk replaced by amp	R.PT.
103092	7-11	sk	-7, M1 amp-mc sk, mainly composed of hb, bt & chlorite	R.PT.
103093	7-12	sk	-7, M1 qz-mc sk, bt rich	F.R.PT.
103094	7-13	sk	-7, M1 amp-sk	F.R.PT.
103095	7-14	sk	-7, M1 amp-sk	R.PT.
103096	7-15	sk	-7, M1 amp-sk	R.PT.
103097	7-16	sk	-7, M1 qz-mc sk, bt rich	F.R.PT.
103098	7-17	sk	-7, M1 amp-sk having relict px-gn sk	R.PT.
103099	7-18	sk	-7, M1 amp-px sk	R.PT.
103100	7-21	sk	-7, M1 px-qz sk	R.PT.
103101	7-22	sk	-7, M1 px-gn sk, px dominant, fragile	R.PT.
103102	7-24	sk	-7, M1 px-gn sk(near 1st incline)	R.PT.
103103	0219	sk	+0, M1 amp-px sk, hd replaced by amp	R.PT.
103104	001	sk	-1, M1 late px sk, hd dominant	R.
103105	007		-15, in F.W sl, ca-vein containing fl, euhedral qz with sericite at walls	R. F.
103106	0048	Q.V	-5, 12bl. fl, euhedral qz, Mo-free sch	R. F.
103107	0060a	sk	-7, minor scale zoning, ms-rich qz-mc sk	D.P.R.PT.
103108	0060b	sk	-7, " bt-rich qz-mc sk	D.P.R.PT.
103109	0060c	sk	-7, " mc-amp sk	D.P.R.PT.
103110	0060d	sk	-7, " amp sk	D.P.R.PT.
103111	0060e	sk	-7, " px-gn sk	D.P.R.PT.
103112	0060f	sk	-7, " gn-px sk	D.P.R.
103113	0050a	sk	-15, M1 px-pl sk, mo occurs with Mo-free sch along amp veinlet	R.PT.
	0050b	sk	-15, M1 px-pl sk, Mo-rich sch occurs along amp veinlet	R.PT.
103114	s-23	sl	-7, F.W sl	PT.
103115	s-24	ch	-1, near 3rd incline, contacted with sl	PT.
103116	0037	sk	-3, M1 qz-mc sk ms & chlorite	R.PT.
103117	0228	sk	+0, M1 qz-mc sk, ms-rich	R. PT.

103118	0158	sk	gn sk replaced by hd in band(M1, -1)	R.PT.
103119	0155	sk	-3, 2bl. coarse bt sk replacing px sk	R.PT.
103120	0212	sk	-7, M1 coarse amp enriched with sch	R.PT.
103121	BT-6	sk	-3, M1 qz-mc sk, containing mo	PS.
103122	M5-17	sk	-5, M1 amp -px sk boundary (mt & po)	PT.
103123	0224	dyk	+2, dyke rock altered to cherty phase	PT.
103124	0121	sk	-3, M1 qz-mc sk, ms-rich with illite, Mo-poor sch	PT.
103125	0217	sk	-3, M1 bt-rich qz-mc sk, same as 103121	R.
103126	0216	sk	+0, wlf & sch Q.V	R.PT.
103127	BT-5	sk	-15, M1, ms-fl-ca-qz-sch sk in px-gn sk	R.
103128	002	Ls	-6, cross to H1, brecciated P-Ls	R.D.P.
103129		ch	+2, near adit, ch-Rk in H.W. M-sl	R.D.P.
103130	0022a	dyk	+0, near no.2 Sangdong adit	R.D.P.
103131	0022b	dyk	+0, near 103130, felsic dyk	R.D.P.
103132	0063	dyk	in outside of mineralization	R.D.P.
103133	0066	dyk	in outside of mineralization	R.D.P.
103134	s-18	sk	-7, M1 qz-mc sk, bt-rich	R.PT.
103135	s-5	sk	H1, wol-gn sk	R.PT.
103136	0192	sk	-6, cross to H1, ad-wol vein along a joint	R.PT.
103137	0236	ch	ch.Rk, +0, garnets occur in the ch.Rk	R.PT.
103138	s-7	sk	wol-ad sk, sch occurs in qz veinlet	R.PT.
103139	s-12	sk	-14, px-pl-vs-sch	R.PT.
103140	s-17	sk	-7, M1 amp sk	R.PT.
103141	0136	sk	-7, 24bl. px-gn sk	R.
103142	0232	Q.V	+0, Mo-free sch bearing Q.V in F.W. sl	R.
103143				
103144	14-3	sk	-14, M1 px-pl sk	T.
103145	Ls-7	Ls	see Appendix 1.1	D.P.T.
103146	Ls-10	Ls	see Appendix 1.1	D.P.T.
103147	0220	sk	+1, M1 px-gn sk replaced by amp	R.
103148		sk	px-gn sk replaced by amp (-1, M1)	R.
103149	0117	sk	typical amphibole sk(-1,M1)	R. T.
103150	BT-1	sk	-7, 26bl. bt-rich qz-mc sk	R.
103151	0185	Q.V	-5, mo-bearing qz vein. used for S isotope	R.
103152	0208	Q.V	drilling core, mo-bearing J. Qtz. "	R.
103153	0168	sk	+2, near 3rd incline, po-rich px sk. "	R.
103154	008b	Q.V	-5, 15bl. clear qz in milky white qz vein	R. F.
103155	008a	Q.V	-5, 15bl. milky white qz	R. F.
103156	0138	ca.V	-3, mo-bearing ca vein, qz in ca vein	R. F.
103157	0237	sch	+0, large grains of sch in amp sk	R. F.
103158	0159	Q.V	-5, 19bl. abundant fl occur in qz vein	R. F.
103159	0207a	Qtz	drilled core, J.Qtz with mo-bearing qz veinlets, 94 m below -3	R. F.
103160	0207b	Qtz	same as above, 153 m below -3	R. F.
103161	0207c	Qtz	same as above, 373 m below -3	R. F.
103162	10-5	sk	-10, px-gn sk	T.
103163	102b	sk	+0, 14bl. minor scale zoning, Fig. 4.6.	
103164	14-pl	sk	-14, px-pl sk	T.
103165	BT-4	sk	-3, ms-rich qz-mc sk	
103166	3-4	sk	-3, M1 px-gn sk	T.
103167	7M27	sk	-7, 27bl. bt-rich qz-mc sk	T.
103168	s-dp	sk	-1, typical px-sk	PT.
103169	0126	sk	+1, px sk with diagenic qz veinlets	PT.
103170	0214	sch	+0, 15bl. enriched qz-rich part in qz-mc sk, sch show zonal distribution of Mo content	R.F.
103171	a-1-7	Q.V	+0, sphalerite-wlf-sch-ccp qz vein	PS
103172	k-1-5	Q.V	-7 sphalerite bearing wlf rich Q.V.	PS
103173	q-1-7	Q.V	-14, spnalerite bearing ccp rich Q.V.	PS

103174				
103175				
103176		Q.V	-3, mo-bearing quartz vein with sericite. Fig.4.14	
103177	10-26	sk	-10, 26bl. px-gn sk	R.
103178	0194	sk	-5, mt & amp replacing px, po vein in mt	R.
103179	7-4	sk	-7, po & amp replacing px	R.
103180	10-2	sk	-10, ep-px sk	R.
103181	0151	sk	H1, px-gn sk	R. PT.
103182	j-1-3	ca.V	+3, mo bearing ca vein	F.
103183	j-3-3	Q.V	+3, py-ccp-bi-ca-sericite vein	F.
103184	j-4-1	Q.V	+3, ccp-rich qz vein	F.
103185	b-2-1	Q.V	+2, barren qz vein	F.
103186	b-5-3	Q.V	+2, bismuthinite-bearing qz vein	F.
103187	b-3-3	Q.V	+2, wlf-sp-ccp-sch-fl-qz vein	F.
103188	b-6-5	Q.V	+2, ccp-mo-sch qtz vein	F.
103189	b-2-4	Q.V	+2, bi-ccp-py-ca-sericite qz vein	F.
103190	b-2-3	Q.V	+2, mo-py qz vein	F.
103191	b-3-1	Q.V	+2, bi-mo-sch qz vein	F.
103192	a-2-1	Q.V	+0, mo-py qz vein	R.
103193	a-2-3	Q.V	+0, mo-py-ccp-bi-sch qz vein	F.
103194	a-2-4	Q.V	+0, mo-ccp-bi-fl qz vein	F.
103195	e-5-4	Q.V	-3, mo-sericite qz vein	R.
103196	e-4-2	Q.V	-3, barren quartz vein	F.
103197	e-2-5	Q.V	-3, mo-fl-ca-sericite qz vein	F.
103198	e-1-2	Q.V	-3, barren quartz	F.
103199	e-5-2	Q.V	-3, barren quartz	F.
103200	f-2-2	Q.V	-4, mo-ccp qz vein	F.
103201	f-2-1a	Q.V	-4, barren	F.
103202	f-2-1	Q.V	-4, mo-ca-fl-galena qz vein	F.
103203	f-3-4	Q.V	-4, mo-sch-sericite qz vein	F.
103204	f-3-5	Q.V	-4, mo-sch-py qz vein	F.
103205	f-2-3	Q.V	-4, mo-fl-ca-galena qz vein	F.
103206	f-2-4	Q.V	-4, ccp-arsenopy-sp-py-wfl-sch qz vein	F.
103207	g-1-1	Q.V	-6, ccp-arsenopy-py-sch-wfl qz vein	F.
103208	g-1-4	Q.V	-6, ccp-sp-sch-wfl qz vein	F.
103209	k-2-4	Q.V	-7 mo-py-sch qz vein	F.
103210	k-1-5	Q.V	-7 barren	F.
103211	m-2-6	Q.V	-9 barren	F.
103212	m-1-2	Q.V	-9 barren	R.
103213	m-1-8	Q.V	-9 ccp-sp-sch-wlf qz vein	F.
103214	m-2-4	Q.V	-9 ccp-sp-py-arsenopy qz vein	F.
103215	n-2-1	Q.V	-10 wfl-sch-po-ms qz vein	F.
103216	n-1-6	Q.V	-10 ccp-sch-sericite-fl-ca qz vein	F.
103217	n-1-7	Q.V	-10 ccp-py-galena-sp-sericite qz vein	F.
103218	n-1-8	Q.V	-10 barren	F.
103219	p-1-3	Q.V	-12 barren	R.
103220	p-1-2	Q.V	-12 bi-arsenopy-galena-sp	F.
103221	p-2-1	Q.V	-12 ccp-py-wfl-sch-sericite qz vein	F.
103222	p-2-5	Q.V	-12 ccp-py-galena-sp-sericite qz vein	R.
103223	p-2-3	Q.V	-12 ccp-sp-py-arsenopy qz vein	F.
103224	q-2-2	Q.V	-14 ccp-sp-sch-wfl-sericite qz vein	F.
103225	q-1-2	Q.V	-14 barren	F.
103226	q-1-7	Q.V	-14 ccp-sp-sericite qz vein	F.
103227	q-3-1	Q.V	-14 Wfl-sch-ccp-sp qz vein	R.
103228	0034		+2 wol sk in H1(expanded into P-Ls), Fig. 4.4	

103229	0036	sk	-3, 17bl. qz-mc sk, ms-rich	R.PT.
103230	0211	Q.V	-3, mo bearin qz-ca vein	R.
103231	0126	sk	+2, barren qz veinlets in px sk,& qz-mc sk	R.
103232	0120	dyk	+2, dyk altered to sk	R. PT.
103233	0119	Q.V	+1, 5bl. bi-qz vein	R. F.
103234	0092	sk	-7, 27bl, amp sk showing Mo-free sch and Mo-rich sch,(Mo-rich sch occur in qz veinlet)	R.
103235	0182	sk	-6, mt occurring in 'front' of amp sk in px sk	R.
103236				
103237	0112	sch	+0, 14bl. sch concentrated in qz-bt sk	R. F.
103238	0232	Q.V	+0, 19bl sch qz vein, silicified sl	R. F.
103239	0237	sch	+0, large grains of sch in amp sk	R. F.
103240	7-20	sk	-7, amp sk replacing gn sk	R.
105982	J-1	sk	+3, px sk, hd,fl,qz	R. F.
105983	B-2	sk	+2 px sk, hd & qz	R.
105984	T-1	qz	+2 qz in px sk	R. F.
105985	T-2	qz	+2 qz in px sk	R. F.
105986	T-3	qz	+2 qz associated with sch in px sk	R. F.
105987	T-4	qz	+2 qz associated with sch in px sk	R. F.
105988	T-5	qz	+2 qz in px sk	R. F.
105989	T-6	qz	+2 qz in px sk	R. F.
105990	T-7	qz	+2 qz in qz-mc sk	R. F.
105991	T-8	qz	+2 qz in qz-mc sk	R. F.
105992	T-9	qz	+2 qz in qz-amp sk	R. F.
105993	T-10	qz	+2 qz in qz-amp sk	R. F.
105994	T-11	qz	+2 qz in qz-amp sk	R. F.
105995	0-1	qz	+0 qz and fl in px sk	R. F.
105996	East1	qz	+0 qz in px sk	R. F.
105997	0112	qz	+0 qz in qz-mc sk	R. F.
105998	0214	qz	+0 same as 103170	R. F.
105999	0217	qz	+0 same as 103125	F.
106000	1-1	qz	-1 qz in px sk	R.
106001	1st-1	qz	-1 qz in px sk	R. F.
106002	D-1	qz	-1 qz in px sk replaced by qz-mc sk	R. F.
106003	D-2	qz	-1 qz in px zone	R. F.
106004	D-3	qz	-1 qz in amp sk	R. F.
106005	D-4	qz	-1 qz in amp sk	R. F.
106006	D-5	qz	-1 qz in qz-mc sk	R. F.
106007	D-6	qz	-1 qz in qz-mc sk	R. F.
106008	D-7	qz	-1 qz in qz-mc sk	R. F.
106009	D-8	qz	-1 qz in qz-mc sk	R. F.
106010	3-1	qz	-3 qz in px sk	R. F.
106011	E-1	qz	-3 qz in px zone	R. F.
106012	E-2	qz	-3 qz in qz-mc sk	R. F.
106013	E-3	qz	-3 qz in qz-mc sk	R. F.
106014	E-5	qz	-3 qz in qz-mc sk, with large grains of sch.	R. F.
106015	0121	qz	-3 qz in qz-mc sk, same as 103124	F.
106016	E-6	qz	-3 qz in qz-mc sk	R. F.
106017	E-7	qz	-3 qz in qz-mc sk	R. F.
106018	E-8	qz	-3 qz in amp sk	R. F.
106019	E-9	qz	-3 qz in amp sk	R. F.
106020	E-10	qz	-3 qz in amp sk	R. F.
106021	E-12	qz	-3 qz in amp-px sk	R. F.
106022	F-1	qz	-4 qz in amp sk	R. F.
106023	F-3	qz	-4 qz in qz-mc sk	R. F.
106024	F-4	qz	-4 qz in qz-mc sk	R. F.
106025	F-5	qz	-4 qz in qz-mc sk	R. F.

106026	F-6	qz	-4, qz in qz-mc sk	R. F.
106027	F-7	qz	-4, qz in qz-mc sk	R. F.
106028	F-8	qz	-4, qz in amp sk, abundant ap	R. F.
106029	0118	qz	-4, qz in qz-mc sk	R. F.
106030	0114	qz	-4, qz in amp sk	R. F.
106031	K-1	qz	-7, qz in px-gn sk zone	R. F.
106032	K-2	qz	-7, qz in px-gn sk zone	R. F.
106033	K-3	qz	-7, qz in amp sk	R. F.
106034	K-4	qz	-7, qz in amp sk	R. F.
106035	K-5	qz	-7, qz in qz-mc sk	R. F.
106036	K-6	qz	-7, qz in amp sk	R. F.
106037	K-8	qz	-7, qz in amp sk	R. F.
106038	K-9	qz	-7, qz in qz-mc sk	R. F.
106039	K-10	px	-7, hd in px sk	R. F.
106040	K-14	qz	-7, qz in qz-mc sk	R. F.
106041	K-19	qz	-7, qz in qz-mc sk	R. F.
106042	K-23	qz	-7, qz in qz-mc sk	R. F.
106043	K-24	qz	-7, qz in amp sk	R. F.
106044	7-13a	qz	-7, qz in qz-mc sk	R. F.
106045	7-15	qz	-7, qz in qz-mc sk	R. F.
106046	7-23	qz	-7, qz in qz-mc sk	R. F.
106047a	7-24a	qz	-7, qz in px sk	R.
b	7-24b	qz	-7, qz in qz-mc sk	R. F.
106048	7-27	qz	-7, qz in amp sk	R. F.
106049	9-11	qz	-9, qz in amp sk	R. F.
106050	M-6	qz	-9, qz in amp sk	R. F.
106051	M-7	qz	-9, qz in amp sk	R. F.
106052	N-21	qz	-10 qz in px zone	R. F.
106053	N-23	qz	-10 qz in px-gn zone	R. F.
106054	N-24	qz	-10 qz in px-qz sk, abundant sch	R. F.
106055	N-25	qz	-10 qz in px-gn sk zone	R. F.
106056	N-26	qz	-10 qz in px-gn sk zone	R. F.
106057	N-27	qz	-10 qz in px-gn zone	R. F.
106058	N-22-1	qz	-10 qz in px-gn sk	R. F.
106059	N-29	qz	-10 qz in amp sk	R. F.
106060	N-30	qz	-10 qz in amp sk	R. F.
106061	N-32	qz	-10 qz in amp sk	R. F.
106062	N-33	qz	-10 qz in px sk	R.
106063	N-34	qz	-10 qz in px sk	R. F.
106064	N-36	qz	-10 qz in amph sk	R. F.
106065	12-33	qz	-12 qz in amp sk	R. F.
106066	12-27	qz	-12 qz in px-gn sk	R.
106067	p-2	qz	-12 qz in px-gn sk	R. F.
106068	p-3	qz	-12 qz in px-gn sk	R. F.
106069	p-4	qz	-12 qz in amp sk	R. F.
106070	p-5	qz	-12 qz in amp sk	R. F.
106071	0089	qz	-12 sch dominant part with barren qz veins	F.
106072	Q-1	qz	-14 qz in px-gn sk	R. F.
106073	Q-2	qz	-14 qz in px-gn sk	R. F.
106074	Q-3	qz	-14 qz in px-gn sk	R. F.
106075	Q-5	qz	-14 qz in px-gn sk	R. F.
106076	Q-6	qz	-14 qz in px-gn sk	R. F.
106077	Q-7	qz	-14 qz in px-gn sk	R. F.
106078	Q-8	qz	-14 qz in px-gn sk	R. F.
106079	Q-33	qz	-14 qz in px-gn sk	R.

106080	J-1	sk	+3	px-gn sk	hd dominant	R. F.
106081	J-2	sk	+3	px-gn sk	"	R. F.
106082	B-2	sk	+2	px-gn sk	"	R. F.
106083	B-3	sk	+2	px-gn sk	"	R. F.
106084	B-4	sk	+2	px-gn sk	"	R. F.
106085	T-1	sk	+1	px-gn sk	"	R. F.
106086	T-2	sk	+1	px-gn sk	"	R. F.
106087	T-3	sk	+1	px-gn sk	"	R. F.
106088	T-4	sk	+1	px-gn sk	"	R. F.
106089	T-5	sk	+1	px-gn sk	"	R. F.
106090	A	sk	+0	px-gn sk	"	R.
106091	B	sk	+0	px-gn sk	"	R.
106092	C	sk	+0	px-gn sk	"	R.
106093	0-1	sk	+0	px-gn sk	"	R.
106094	east1	sk	on the surface of the mine, gn-px sk			R.
106095	eastA	sk		"	gn dominant	R. F.
106096	eastB	sk		"	"	R. F.
106097	eastF	sk		"	"	R. F.
106098	eastG	sk		"	"	R. F.
106099	1-1	sk	-1	px-gn sk	hd dominant	R. F.
106100	1-2	sk	-1	px-gn sk	"	R. F.
106101	1-inc	sk	-1	px-gn sk	"	R.
106102	3-1	sk	-3	px-gn sk	"	R. F.
106103	3-2	sk	-3	px-gn sk	"	R.
106104	4-0	sk	-4	px-gn sk	"	R.
106105	4-1	sk	-4	px-gn sk	"	R. F.
106106	5-0a	sk	-5	px-gn sk	"	R. F.
106107	5-0b	sk	-5	px-gn sk	"	R.
106108	7-2	sk	-7	px-gn sk	gn dominant	R.
106109	7-6	sk	-7	px-gn sk	hd dominant	R.
106110	7-10	sk	-7	px-gn sk	"	R. F.
106111	7-12	sk	-7	px-gn sk	"	R. F.
106112	7-16	sk	-7	px-gn sk	"	R. F.
106113	7-24	sk	-7	px-gn sk	"	R.
106114a	7-24a	sk	-7	px-gn sk	"	R. F.
106114b	7-24b	sk	-7	px-gn sk	gn dominant	R. F.
106115	7-34-1	sk	-7	px-gn sk	hd dominant	R.
106116	9-1	sk	-9	px-gn sk	"	R. F.
106117	9-2	sk	-9	px-gn sk	"	R. F.
106118	9-3	sk	-9	px-gn sk	"	R. F.
106119	9-5	sk	-9	px-gn sk	"	R. F.
106120	9-7	sk	-9	px-gn sk	"	R. F.
106121	9-9	sk	-9	px-gn sk	"	R. F.
106122	9-10	sk	-9	px-gn sk	"	R. F.
106123	9-11	sk	-9	px-gn sk	"	R. F.
106124	9-13	sk	-9	px-gn sk	"	R. F.
106125	N-11-1	sk	-10	px-gn sk	gn dominant	R. F.
106126	N-12-1	sk	-10	px-gn sk	hd dominant	R. F.
106127	N-13-2	sk	-10	px-gn sk	"	R. F.
106128	N-14-1	sk	-10	px-gn sk	"	R. F.
106129	N-15-1	sk	-10	px-gn sk	"	R. F.
106130	N-23-2	sk	-10	px-gn sk	"	R. F.
106131	N-25-2	sk	-10	px-gn sk	"	R. F.
106132	N-26-2	sk	-10	px-gn sk	"	R. F.
106133	N-29-2	sk	-10	px-gn sk	"	R. F.
106134	N-32-1	sk	-10	px-gn sk	"	R. F.
106135	N-34-1	sk	-10	px-gn sk	"	R. F.
106136	N-35-2	sk	-10	px-gn sk	"	R. F.

106137	12-23	sk	-12	px-gn sk, hd dominant	R.
106138	12-25	sk	-12	px-gn sk, hd dominant	R. F.
106139	12-27	sk	-12	px-gn sk, hd dominant	R.
106140	12-29	sk	-12	px-gn sk, "	R. F.
106141	12-31	sk	-12	px-gn sk, "	R. F.
106142	12-A	sk	-12	px-gn sk, "	R.
106143	12-32	sk	-12	px-gn sk, "	R. F.
106144	12-33	sk	-12	px-gn sk, "	R. F.
106145	12-37	sk	-12	px-gn sk, "	R.
106146	Q-33	sk	-14	px-gn sk, hd dominant	R.
106147	16-28	sk	-16	px-gn sk, hd dominant	R. F.
106148	16-32	sk	-16	px-gn sk, "	R.
106149	16-35	sk	-16	px-gn sk, "	R. F.
106150	16-36	sk	-16	px-gn sk, "	R.
106151	E-11	sch	-3	sch in qz-mc sk	R. F.
106152	K-21	sch	-7	sch in qz-mc sk	R. F.
106153	K-13	sch	-7	sch in qz-mc sk	R. F.
106154	B-1-2	py	+2	ccp-rich qz vein	R.
106155	B-1-6	py	+2	ccp-rich qz vein	R.
106157	sang	py	+0	ccp-rich qz vein	R.
106158	3-21	py	-3	ccp-rich qz vein	R.
106159	0128	po	+1	po-rich(with minor ccp) Q.V	R.
106160	po-o	po	+0	po-rich px sk(sk replaced by po)	R.
106161	po-5	po	-5	po-rich px sk "	R.
106162	po-7	po	-7	po-rich px sk "	R.
106163	po-15	po	-15	po-rich px sk "	R.
106164	po-17	po	-17	po-rich px sk "	R.
106165	005	ccp	-1	ccp occur closely associated with wlf and sch in qz vein	R. F.
106166	0056	ccp	-7	ccp-rich qz vein with no sch	R.
106167	0035	ccp	+2	ccp-rich qz vein with sericite	R.
106168	0119	bi	+1, 5bl.	bi bearing qz vein	R.
106169	sk	bi		bi recovered from milling process in the mine	PD.
106170	0089	sch	-12, 24bl.	very fine sch occur in silicified rock	R. F.
106171	0088	dyk	+2	dyke altered to skarn	R. F.
106172	0044	Q.V	-3	sch bearing qz vein with little sulphides	R. F.
106173	0093	sk	+0	bt-rich qz-mc sk enclosing Mo-rich Mo-poor sch	R. F.
106174	wfl-sk	sk	-3	wfl, hm. mt, arsenopy, sch & ca occur in qz-mc(ms) sk	R. PT.
106175	Ls-5	Ls	near Eopyeong area, M1 Ls		P. D.
106176	Ls-11	Ls	near Sesong, M1 Ls		P. D.
106177	Ls-12	Ls	near Yeonnaegol, M1 Ls		P. D.
106178	Ls-13	Ls	near Sangdong mine, M1 Ls		P. D.
106179	Ls-14	Ls	near skarn orebody on the surface, +0 level.		P. D.
106180	Ls-17	Ls	-17	M1 Ls, outside of mineralization	P. D.
106181	K-38-1	Ls	-7	relics of M1 Ls in the skarn	P. D.
106182	K-38-2	Ls	-7	relics of M1 Ls in the skarn	P. D.

Appendix 2. Location of samples from the interbedded limestone stratigraphically equivalent to the M1 skarn orebody.

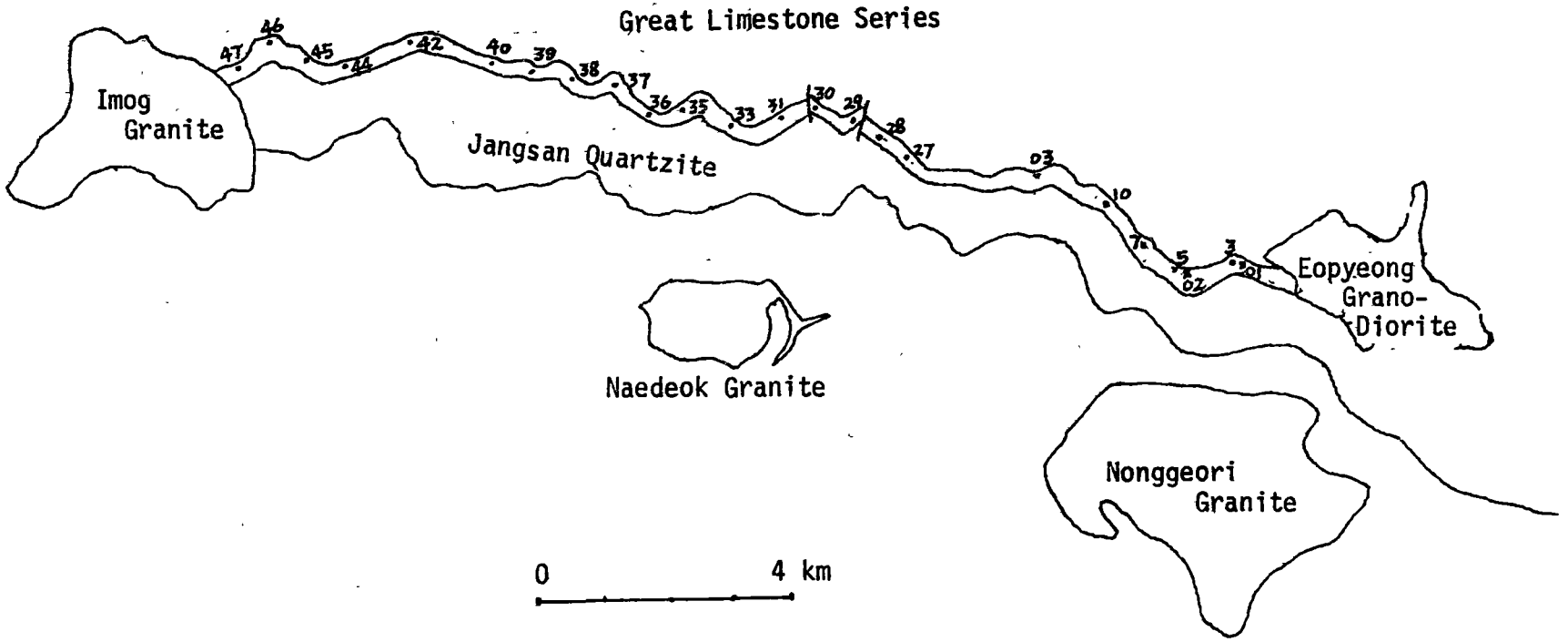

Appendix 3. Chemical Compositions of the Interbedded Limestone Corresponding to the M1 Skarn Orebody(analysed by XRF).

Sample	SiO_2	TiO_2	Al_2O_3	Fe_2O_3	MnO	MgO	CaO	K_2O	Na_2O	P_2O_5	LOI	Total
ls-3	5.71	0.06	1.49	0.98	0.17	11.50	41.59	0.0	n.d	n.d	37.32	98.82
ls-5	3.90	0.03	0.62	2.04	0.14	1.98	49.79	0.24	n.d	0.06	40.83	99.65
ls-7	6.70	0.06	1.60	1.09	0.09	0.84	39.49	0.68	n.d	0.03	39.49	99.33
ls-10	2.45	0.02	0.54	0.76	0.06	3.24	49.73	0.22	n.d	0.03	42.56	99.59
xf-01	2.67	n.d	0.89	0.83	0.20	17.36	32.81	0.03	n.d	n.d	43.55	98.34
xf-02	3.81	n.d	2.60	0.71	0.34	0.84	49.34	0.25	n.d	0.06	40.96	98.94
xf-03	1.43	n.d	1.85	0.38	0.20	0.09	52.58	0.10	n.d	0.05	42.43	99.72
xf-04	4.38	n.d	1.14	1.01	0.28	0.96	52.25	0.05	n.d	0.06	39.45	99.59
ls-27	1.78	n.d	0.26	0.60	0.22	2.09	52.03	0.04	n.d	0.07	41.92	99.01
ls-29	24.35	0.30	4.71	4.55	1.03	1.39	39.59	0.11	n.d	0.49	23.84	100.38
ls-30	15.94	0.17	1.35	1.71	0.68	1.04	43.15	0.58	n.d	0.07	33.99	98.08
ls-31	1.71	n.d	0.43	0.49	0.26	0.85	52.98	0.09	0.01	0.03	42.19	99.05
ls-33	3.67	0.04	0.73	1.15	0.35	0.96	52.77	0.25	n.d	0.03	41.14	101.08
ls-35	0.92	0.02	0.61	0.59	0.07	1.12	52.14	0.19	n.d	0.01	42.86	98.53
ls-36	4.35	0.05	1.27	0.60	0.05	1.05	53.51	0.51	n.d	0.02	40.42	101.82
ls-37	3.98	0.04	1.00	0.43	0.15	1.35	50.47	0.38	n.d	0.12	40.69	98.60
ls-38	10.27	0.35	1.78	2.68	0.69	1.77	45.26	0.19	n.d	0.13	35.85	98.98
ls-39	4.02	0.04	0.96	0.37	0.10	1.92	50.58	0.37	n.d	0.02	41.01	99.41
ls-40	3.61	0.04	0.88	0.33	0.11	2.11	50.94	0.38	n.d	0.02	41.18	99.59
ls-42	2.44	0.03	0.95	0.29	0.09	0.93	55.04	0.48	n.d	0.03	41.39	101.68
ls-44	3.16	0.02	0.86	0.93	0.20	0.57	51.93	0.34	n.d	0.14	40.70	98.85
ls-45	1.45	0.02	0.47	0.26	0.11	0.89	54.37	0.30	n.d	0.07	42.00	99.93
ls-46	18.92	0.22	2.91	4.02	1.48	1.56	37.95	0.64	1.07	0.18	30.24	99.20
ls-47	2.06	0.02	0.44	0.83	0.08	4.66	51.19	0.07	n.d	0.03	41.17	100.54

* Trace elements(ppm)

Sample	Zn	Cu	Ni	Sr	Rb	Bi	Mo	W
ls-3	6.2	0	5.3	151.4	1.9	0	12.1	0
ls-5	15.8	16.2	5.7	466.9	6.9	0.7	0	2.3
ls-7	8.5	1.4	7.3	297.9	20.0	3.6	4.5	0
ls-10	3.8	0.4	3.9	308.7	4.9	4.1	6.2	1.9
xf-01	6.6	5.9	4.0	92	1.3	0	0	2.5
xf-02	4.5	14.7	3.1	325.9	9.6	0	0	2.1
xf-03	13.2	24.8	3.8	318.4	3.8	0	0	3.2
xf-04	45.3	18.9	6.3	314.9	0	0	0	9.4
ls-27	525.4	21.2	4.2	238.8	0.2	3.6	5.9	0
ls-29	117.9	58.3	15.0	475.3	5.0	17.9	8.7	2.5
ls-30	7.9	20.8	4.8	419.5	22.2	3.2	5.4	1.0
ls-31	14.2	8.4	2.2	362.8	4.3	2.8	6.9	2.8
ls-33	5.3	4.7	4.5	612.0	4.0	3.6	5.4	0
ls-35	19.4	3.6	3.0	567.9	7.2	0.3	5.9	0
ls-36	5.5	2.7	5.5	329.4	12.9	0	16.0	0.2
ls-37	8.7	26.9	6.1	527.7	9.1	4.0	10.1	3.5
ls-38	20.1	25.7	10.1	470.2	7.7	0.4	15.7	3.4
ls-39	3.2	0.1	5.5	423.3	7.7	2.8	13.3	0.2
ls-40	3.9	0.6	7.0	433.2	6.6	1.5	14.1	2.0
ls-42	8.9	1.8	6.0	321.5	8.3	0.8	12.9	0.7
ls-44	8.7	0	6.7	47.1	9.2	0.1	7.0	2.1
ls-45	4.0	1.0	4.1	259.2	5.1	2.5	6.6	0
ls-46	18.1	6.2	9.4	381.3	19.3	3.2	4.4	2.4
ls-47	19.2	1.9	2.5	443.1	1.2	3.0	11.2	0.2

Appendix 4. Chemical Compositions of Granitic Rocks near Sangdong mine, analysed by XRF.

	Naedeok Granite	Gakhi Granite	Eopyeong Granodiorite (A)	Granodiorite (B)	Imog(Yemi) Granite (a)	Granite (b)
SiO_2	72.54	71.04	64.89	63.75	67.82	67.72
TiO_2	0.01	0.14	0.65	0.62	0.33	0.42
Al_2O_3	14.11	14.40	14.54	14.80	13.33	15.41
Fe_2O_3	0.55	1.94	4.26	1.78	2.84	3.75
FeO	0.51			2.47		
MnO	0.01	0.02	0.07	0.07	0.04	0.08
MgO	0.02	0.30	3.10	2.97	0.96	1.42
CaO	0.49	0.61	4.91	4.94	2.55	3.32
K_2O	5.06	5.11	3.17	3.21	5.52	3.65
Na_2O	4.11	3.16	4.05	3.76	2.56	3.50
P_2O_5	0.45	0.28	0.21	0.23	0.08	0.14
L.O.I.	0.57	0.96	0.63	0.62	0.98	1.09
Total	98.43	97.96	100.48	99.22	97.01	100.50
Trace elements(ppm)						
Sn	13.5	46.3	*	n.d	*	*
Zn	21.4	53.9	36.5	31.2	17.8	40.6
Cu	1.5	2.3	42.8	78.3	61.6	n.d
Ni	6.9	10.0	37.6	984.1	7	8.4
Sr	106.2	64.4	605.1	539.9	269.1	401.7
Rb	270.2	330.6	76.9	88.9	217.9	106.8
Pb	16.8	34.6	*	8.3	*	*
Bi	3.0	2.9	1.1	6.3	13.9	2.0
Mo	n.d	n.d	4.0	4.8	4.0	1.2
W	17.8	37.7	n.d	n.d	2.6	m.d

* not analysed.

n.d analysed but not detected.

Appendix 5. Chemical Compositions of Dykes in the Mineralized Zone and Unmineralized Zone(analysed by XRF).

	Unmineralized Zone				Mineralized Zone			
	XF-36	XF-37	XF-38	XF-39	XF-26	XF-27	XF-28	XF-25
SiO_2	57.74	55.32	55.32	72.02	46.29	48.79	48.32	56.22
TiO_2	0.90	0.78	0.88	0.60	1.04	0.48	0.55	0.83
Al_2O_3	16.19	15.75	14.85	5.79	20.01	5.57	7.01	19.22
Fe_2O_3	7.27	3.53	7.09	13.03	4.0	3.88	1.31	5.61
FeO						5.99	5.54	1.09
MnO	0.12	0.08	0.08	0.04	0.23	0.48	0.33	0.10
MgO	4.1	3.7	6.58	2.08	5.19	16.48	17.26	3.26
CaO	3.37	10.19	6.13	1.90	21.81	11.02	13.45	3.31
Na_2O	2.76	n.d	3.22	n.d	0.06	n.d	n.d	3.24
K_2O	2.27	7.51	2.33	2.17	0.04	1.71	3.88	4.57
P_2O_5	0.21	0.17	0.22	0.11	0.23	0.41	0.36	0.27
LOI	3.16	1.49	2.53	2.77	0.60	5.34	1.62	2.17
Total	98.08	98.51	99.24	100.51	99.49	100.15	99.63	99.87
Trace elements(ppm)								
Sn	0	0	0	0	13.8	0	70.1	3.2
Zn	81.1	36.4	55.7	27.7	191.5	97	146.9	64.8
Cu	13.5	35.1	11.8	10.4	4.6	27.9	8.8	5.2
Ni	15.4	93.6	125.2	38.8	689.1	52.7	577.4	10.9
Sr	507.7	435.8	413.1	23.8	40.2	323.8	53.7	222.8
Rb	61.8	350.7	89.0	59.0	214.6	64.0	386.9	2.2
Th	3.0	3.7	3.4	3.8	7.4	21.5	0	8.7
Pb	12.5	18.9	10.9	5.7	4.9	5.6	6.0	2.8
Bi	0.7	0.7	1.2	0	0	0	0	0
Mo	0	0	0	2.9	0	2.9	3	133.0
W	3.2	5.8	3.9	12.7	0	99.6	7.9	4.2

*Sample List

XF-25(0144):-6th level, felsitic, MoS_2 and chalcopyrite are observed.

XF-26(0186):-13th level, quartz-mica skarn surrounds this dike in Px zone

XF-27(0187):+1st level, dark mafic.

XF-28(0105):+3rd level, altered,coarse grained biotite, sericite and quartz

XF-36(0063), XF-37(0066), XF-38(0073), XF-39(7052)

Appendix 6.1 Chemical Compositions of Different Zones in Garnet Crystals Between Different Coloured Crystals From the 7th level.

Key;

@ = Brown part of a garnet crystal B = A brown garnet

* = Colourless part of a garnet crystal G = A greenish garnet

Iso(Ani) = Isotropic(Anisotropic) part of a garnet crystal

	103102		103098		103101			103101	
	@	*	@	*	B	B	G	Iso	Ani
SiO_2	38.66	39.64	36.99	37.26	37.55	37.80	37.42	38.13	38.75
TiO_2	0.82	1.15	0.45	n.d	n.d	0.26	0.39	0.33	0.46
Al_2O_3	14.83	18.19	4.70	4.69	11.50	18.83	10.07	9.57	17.25
Cr_2O_3	n.d	n.d	0.23	n.d	0.24	n.d	0.21	n.d	n.d
Fe_2O_3	10.56	4.28	22.72	22.81	16.31	12.27	16.52	16.71	7.22
MnO	0.61	n.d	0.28	0.26	1.44	6.71	0.63	0.40	0.68
MgO	n.d	n.d	0.48	0.53	0.17	n.d	n.d	n.d	0.23
CaO	34.52	36.65	34.15	34.45	32.39	24.21	34.76	34.85	35.41
*Total	100	99.86	100.1	100.12	99.97	100.47	100.24	100.51	101.47
	Numbers of ions on the basis of 12 oxygens								
Si	3.008	3.023	3.036	3.051	3.083	3.004	3.096	3.148	3.028
Ti	0.048	0.066	0.028	0.000	0.035	0.016	0.024	0.021	0.027
Al	1.362	1.637	0.455	0.454	1.113	1.756	0.982	0.932	1.588
Fe	0.618	0.246	1.502	1.406	1.12	0.816	1.142	1.154	0.472
Cr	0.000	0.000	0.003	0.000	0.016	0.000	0.017	0.000	0.000
Mn	0.04	0.000	0.019	0.018	0.100	0.452	0.022	0.028	0.045
Mg	0.000	0.000	0.059	0.065	0.000	0.000	0.000	0.000	0.026
Ca	2.878	2.995	3.002	3.024	2.850	2.062	3.080	3.083	2.964
Total	7.954	7.967	8.104	8.018	8.317	8.106	8.363	8.366	8.150
X_{ad}	0.308	0.131	0.747	0.736	0.481	0.260	0.530	0.548	0.224
X_{gr}	0.678	0.869	0.226	0.238	0.478	0.560	0.455	0.443	0.753
X_{other}	0.014	0.000	0.027	0.026	0.041	0.180	0.015	0.009	0.023

* Total before normalized

Appendix 6.2. Variation in Chemical Compositions of Three Garnets from the 7th level.

Specimen 103089

	rim					core		rim
	-5	-4	-3	-2	-1	0	3	5
SiO_2	36.20	37.23	37.56	36.98	38.32	38.22	37.77	35.26
TiO_2	0.71	0.48	0.58	0.41	0.45	0.37	0.47	0.68
Al_2O_3	11.47	7.77	9.70	10.92	14.16	11.31	15.73	14.56
Cr_2O_3	0.30	0.28	0.29	n.d	n.d	n.d	0.21	0.29
Fe_2O_3	16.19	20.29	18.03	17.09	13.27	16.62	9.41	9.63
MnO	1.92	1.35	1.51	1.74	1.88	1.65	1.81	2.04
MgO	n.d	0.22	n.d	n.d	n.d	0.23	n.d	n.d
CaO	33.21	32.38	32.33	32.67	31.92	31.61	34.59	37.53
Si	2.910	3.012	3.009	2.964	3.002	3.030	2.951	2.812
Ti	0.043	0.029	0.035	0.025	0.027	0.022	0.028	0.041
Al	1.088	0.742	0.917	1.033	1.309	1.058	1.451	1.371
Cr	0.018	0.018	0.018	0.000	0.000	0.000	0.013	0.019
Fe	0.980	1.235	1.087	1.031	0.782	0.991	0.553	0.578
Mn	0.130	0.092	0.103	0.118	0.125	0.111	0.120	0.140
Mg	0.000	0.027	0.000	0.000	0.000	0.027	0.000	0.000
Ca	2.861	2.807	2.776	2.807	2.680	2.685	2.896	3.207
Total	8.030	7.962	7.945	7.978	7.925	7.924	8.012	8.168

	Specimen 103087			Specimen 103101					
	core	middle	rim	core(0)	1	2	3	4	rim(5)
SiO_2	37.12	36.30	36.71	37.80	37.58	37.76	37.55	38.20	38.17
TiO_2	n.d	n.d	n.d	0.26	0.43	0.45	0.57	n.d	n.d
Al_2O_3	3.99	1.89	2.32	18.83	18.83	12.16	11.50	12.33	11.84
Cr_2O_3	n.d	n.d	n.d	n.d	n.d	n.d	0.24	0.21	n.d
Fe_2O_3	23.57	26.13	26.49	12.27	12.29	16.78	16.31	14.63	15.01
MnO	0.35	0.28	0.65	6.71	6.38	2.27	1.44	1.12	1.10
MgO	n.d	0.53	n.d	n.d	n.d	n.d	n.d	n.d	n.d
CaO	34.99	34.60	33.83	24.21	24.49	30.58	32.39	33.52	33.88
K_2O	n.d	0.27	n.d	n.d	n.d	n.d	n.d	n.d	n.d
Si	3.080	3.031	3.054	3.004	2.986	3.094	3.083	3.107	3.115
Ti	0.000	0.000	0.000	0.016	0.026	0.028	0.035	0.000	0.000
Al	0.391	0.187	0.228	1.756	1.763	1.175	1.113	1.182	1.139
Cr	0.000	0.000	0.000	0.000	0.000	0.000	0.016	0.013	0.000
Fe	1.472	1.641	1.659	0.816	0.817	1.150	1.120	0.995	1.025
Mn	0.024	0.020	0.046	0.452	0.429	0.157	0.100	0.077	0.076
Mg	0.000	0.066	0.000	0.000	0.000	0.000	0.000	0.000	0.000
Ca	3.088	3.095	3.016	2.062	2.085	2.686	2.850	2.921	2.962
K	0.000	0.029	0.000	0.000	0.000	0.000	0.000	0.000	0.000
Total	8.055	8.069	8.003	8.106	8.106	8.290	8.317	8.295	8.317

Appendix 6.3. Variation in Chemical Compositions of Garnets.

Specimen 103084

Crystal A

	core				rim
SiO_2	37.08	37.18	37.03	37.12	36.93
Al_2O_3	3.13	3.59	1.37	3.47	1.2
TiO_2	n.d	n.d	n.d	0.23	n.d
Cr_2O_3	0.25	n.d	n.d	n.d	n.d
Fe_2O_3	24.98	24.69	27.23	24.73	27.9
MnO	0.42	0.82	0.67	0.53	0.67
MgO	n.d	n.d	n.d	n.d	0.25
CaO	34.14	33.72	33.7	33.92	33.05

Total : 100

Crystal B

	core				rim
SiO_2	36.65	37.47	37.13	37.09	40.02
Al_2O_3	0.36	3.22	2.39	2.02	0.65
Fe_2O_3	28.5	24.81	25.98	26.32	26.69
MnO	0.59	0.35	0.68	0.34	1.16
MgO	n.d	n.d	n.d	n.d	0.4
CaO	33.68	34.15	33.81	34.22	31.09
Total	99.78	100.00	99.99	99.99	100.01

Crystal C

	core			rim	Mean
SiO_2	37.0	37.14	37.1	37.39	37.16
Al_2O_3	0.57	1.45	1.74	0.87	1.16
Fe_2O_3	28.06	26.95	26.55	28.78	27.59
MnO	0.35	0.33	0.59	0.77	0.61
MgO	0	0	0	0.31	0.08
CaO	34.02	34.13	34.02	31.88	33.51

Crystal D

	core			rim
SiO_2	37.10	37.39	36.93	39.32
Al_2O_3	1.74	0.87	1.20	1.36
Fe_2O_3	26.55	28.78	27.90	24.83
MnO	0.59	0.77	0.67	0.72
MgO	0	0.31	0.25	1.44
CaO	34.02	31.88	33.05	32.33

Appendix 6.4. Comparison of Chemical Compositions of Pyroxenes Between Early and Late Ones in Specimen 103148. (See Fig. 5.17a)

SiO_2	49.20	49.14	49.01	48.77	48.9	48.54
Al_2O_3	0.22	0.23	0.25	n.d	n.d	n.d
FeO	25.1	25.91	25.72	25.67	24.84	25.38
MnO	2.5	1.91	2.36	1.45	2.43	2.64
MgO	0.71	0.37	0.67	1.26	1.32	0.74
CaO	22.27	22.45	21.99	22.85	22.52	22.7
Total	100	100	100	100	100	100
			Numbers of ions			
Si	2.011	2.012	2.007	1.996	2.000	1.995
Al	0.01	0.011	0.012	0.000	0.000	0.000
Fe	0.858	0.887	0.881	0.879	0.85	0.872
Mn	0.087	0.066	0.082	0.05	0.084	0.092
Mg	0.043	0.023	0.041	0.077	0.08	0.045
Ca	0.975	0.985	0.965	1.002	0.987	1.000
X_{hd}	0.868	0.909	0.877	0.873	0.838	0.864
X_{jh}	0.088	0.068	0.082	0.050	0.083	0.091
X_{dp}	0.044	0.023	0.041	0.077	0.079	0.045

Appendix 6.5. Chemical Compositions of Coexisting Pyroxene and Garnet Rims.
Specimen 103104

	A		B		C		D	
	Px	Gn	Px	Gn	Px	Gn	Px	Gn
SiO_2	49.27	37.2	48.74	37.41	49.52	37.57	48.84	39.37
Al_2O_3	n.d	4.07	0.25	1.58	0.33	4.48	0.38	4.34
FeO	25.41	24.39	25.69	26.99	24.92	23.48	25.36	19.98
MnO	1.57	0.65	1.44	0.46	1.72	n.d	1.66	0.43
MgO	0.91	n.d	1.15	n.d	1.07	n.d	1.08	n.d
CaO	22.84	33.69	22.72	33.65	22.44	34.47	22.69	35.57
Total	(100.41)	(99.65)	(99.80)	(99.96)	(99.74)	(100.1)	(101.2)	(99.99)
			Numbers of ions					
Si	2.012	3.22	1.993	3.281	2.014	3.229.	1.995	3.329
Al	0.00	0.414	0.012	0.164	0.016	0.454	0.018	0.427
Fe^{+3}		1.586		1.836		1.546		
Fe^{+2}	0.868	0.18	0.879	0.149	0.848	0.142	0.866	1.42
Mn	0.054	0.048	0.05	0.035	0.059	0.00	0.057	0.043
Mg	0.056	0.00	0.07	0.00	0.065	0.00	0.066	0.00
Ca	0.995	3.124	0.996	3.171	0.978	3.17	0.993	3.249
X_{hd}	0.888		0.880		0.872		0.876	
X_{ad}		0.793		0.918		0.773		0.769
$X_{hd/1-X_{hd}}$	7.05		7.33		6.81		7.06	
$X_{ad/1-X_{ad}}$		3.831		11.2		3.405		3.33

Appendix 6.6. Microprobe Analyses of Amphiboles in specimen 103084(mainly replacing garnet) and in specimen 103122(mainly replacing pyroxene).

	Amphibole replacing garnet			Amphibole replacing pyroxene		
	1	2	3	a	b	c
SiO_2	45.15	44.61	47.93	46.45	48.41	47.23
Al_2O_3	6.13	5.5	3.9	3.79	2.35	4.07
FeO	30.64	29.93	30.19	35.14	34.75	34.3
MnO	0.92	1.13	1.39	1.25	1.26	1.2
MgO	3.24	3.18	3.44	1.96	2.06	1.78
CaO	11.32	11.19	11.34	10.02	10.06	10.34
Na_2O	0.53	0.58	0.41	1.1	1.12	0.75
K_2O	0.48	0.45	0.28	0.29	0	0.34
Total	98.41	96.57	98.88	96.76	97.91	96.9
	Numbers of ions					
Si	7.145	7.199	7.498	7.372	7.625	7.441
Al	0.855	0.801	0.502	0.628	0.375	0.559
Al	0.289	0.246	0.217	0.081	0.062	0.196
Fe	4.056	4.04	3.949	4.661	4.577	4.520
Mn	0.123	0.154	0.185	0.169	0.169	0.167
Mg	0.765	0.764	0.801	0.464	0.483	0.418
Ca	1.919	1.935	1.901	1.702	1.698	1.744
Na	0.162	0.182	0.125	0.337	0.341	0.226
K	0.097	0.093	0.056	0.058	0.00	0.069
$\frac{100Mg}{Fe+Mg+Mn}$	15.47	15.41	16.23	9.05	9.55	8.46
Mg/Mg+Fe	0.159	0.159	0.169	0.091	0.095	0.085

Appendix 6.7. Classification of Calcic Amphiboles.
(Leake, 1978)

Calcic Amphibole: $(Ca+Na)_B \geq 1.34$, $Na_B < 0.67$

A. $(Na+K)_A < 0.50$, $Ti < 0.50$

$\frac{Mg}{(Mg+Fe^{++})}$

8.00 7.75	7.5 7.25	7.0 6.75	6.5 6.25	6.0 5.15
tremolite	tr-Hb	magnesio-hornblende	tsch-Hb	tschermakite (alumino-tschermakite) 0.90
actinolite	act-Hb			
Fe-actinolite	Fe-act Hb	ferro-hornblende (Fe-Hb)	Fe-tsch-Hb	Fe-tschermakite 0.50 0.0

B. $(Na+K)_A \geq 0.50$, $Ti < 0.50$, $Fe^{3+} \leq Al^{VI}$ 1.0

silicic edenite	edenite	eden-Hb.	par-Hb	pargasite 0.7
			ferroan par-Hb	ferroan pargasite
silicic Fe-edenite	ferro-edenite	Fe-eden-Hb.	Fe-par-Hb	Fe-pargasite 0.5

C. $(Na+K)_A \geq 0.50$, $Ti < 0.50$ $Fe^{3+} > Al^{VI}$ 0.0

silicic edenite	edenite	eden-Hb	magnesio-hast-Hb	magnesio-hastingsite 1.0
			magnesian hast-Hb	magnesian hastingsite 0.7
silicic Fe-edenite	ferro-edenite	Fe-eden-Hb.	hast-Hb	hastingsite 0.3

0.0

D. $Ti \geq 0.50$

kaersutite 1.0
ferro-kaersutite 0.5 0.0

* Key for abbreviation;

tr = tremolitic	tsch = tschermakitic
act = actinolitic	par = pargasitic
Fe = ferro	Hb = hornbelende
eden = edenitic	hast = hastingsitic

Appendix 6.8. Comparison of Chemical Compositions of Biotites Occurring in Different Host Rocks(Zones).

	103120 (greenish) (replacing amphibole)					103119 (brown) (replacing pyroxene)				
	g-3	h-1	h-2	f-1	g-1	j-2	j-3	j-4	d-1	d-7
SiO_2	34.88	34.67	35.10	35.00	35.92	35.37	34.93	35.22	35.42	35.33
TiO_2	0.35	0.25	0.46	n.d	0.51	1.71	1.53	1.63	1.46	1.44
Al_2O_3	14.78	15.42	15.12	14.2	15.17	14.23	14.96	14.31	15.13	14.57
FeO	31.65	32.0	31.01	32.34	29.92	28.89	30.24	29.49	29.05	29.21
MnO	0.38	n.d	0.38	0.68	0.44	0.33	0.30	0.35	0.36	0.41
MgO	4.82	4.75	4.93	4.46	4.44	6.39	5.96	5.95	5.77	6.24
CaO	n.d	n.d	n.d	0.68	0.27	n.d	n.d	n.d	n.d	n.d
Na_2O	0.45	0.57	0.61	0.40	0.87	0.56	0.52	0.47	0.30	0.45
K_2O	8.01	8.35	8.36	8.49	8.46	8.52	7.55	8.59	8.50	8.35
Total	95.32	96.01	95.97	96.25	96.0	96.0	95.99	96.01	95.99	96.0
	Numbers of ions on the basis of 22 oxygens									
Si	5.627	5.580	5.626	5.674	5.728	5.621	5.554	5.617	5.616	5.615
Al	2.373	2.420	2.374	2.326	2.272	2.379	2.446	2.383	2.384	2.385
Al	0.436	0.505	0.487	0.387	0.579	0.288	0.357	0.308	0.445	0.343
Ti	0.040	0.03	0.056	0.000	0.061	0.204	0.183	0.195	0.175	0.173
Fe	4.269	4.308	4.158	4.386	3.989	3.839	4.021	3.933	3.854	3.883
Mn	0.052	0.000	0.052	0.057	0.060	0.044	0.040	0.047	0.048	0.054
Mg	1.163	1.140	1.180	1.079	1.056	1.515	1.413	1.415	1.365	1.478
Ca	0.000	0.000	0.000	0.119	0.045	0.000	0.000	0.000	0.000	0.000
Na	0.152	0.178	0.190	0.128	0.270	0.173	0.163	0.142	0.094	0.141
K	1.783	1.714	1.710	1.757	1.720	1.727	1.532	1.748	1.719	1.693
Total	15.895	15.875	15.833	15.913	15.780	15.79	15.709	15.788	15.710	15.765
Mg/(Mg+Fe)	0.214	0.209	0.221	0.197	0.209	0.283	0.260	0.265	0.262	0.276

Appendix 6.9. Comparison of chemical compositions of biotites in the quartz-mica skarn at the 7th level.

	103092 (green)			103093 (green)					103097 (brown)				
	c-1	a-2	a-1	c-1	b-2	h-1	h-2	i-2	a-1	b-1	c-1	c-2	d-1
SiO_2	36.56	36.20	35.61	34.85	34.65	35.86	36.09	35.64	35.80	36.56	36.20	36.86	35.96
TiO_2	0.48	0.50	0.38	0.45	0.26	n.d	n.d	n.d	1.01	0.72	0.46	0.69	0.48
Al_2O_3	13.68	13.80	14.09	15.27	15.11	14.86	14.42	14.84	16.31	13.56	14.31	14.19	14.56
FeO	27.97	28.17	29.50	29.66	30.66	29.63	29.44	29.78	25.91	28.83	27.59	26.27	28.53
MnO	0.48	0.73	0.63	0.77	0.53	0.59	0.62	0.74	0.76	0.41	0.80	0.71	0.81
MgO	7.94	7.61	8.59	5.49	6.25	5.68	6.05	5.68	6.94	6.65	7.04	7.84	6.34
CaO	0.71	0.48	0.40	0.61	0.48	0.60	0.57	0.47	0.55	0.48	0.55	0.51	0.44
Na_2O	n.d	n.d	n.d	n.d	n.d	n.d	n.d	n.d	n.d	n.d	n.d	n.d	n.d
K_2O	7.84	8.50	6.78	8.91	8.04	8.80	8.80	8.86	8.75	8.80	9.02	8.93	8.88
Total	95.66	95.99	95.98	96.01	95.98	96.02	95.99	96.01	96.03	96.01	95.97	96.0	96.0
	Numbers of ions on the basis of 22 oxygens												
Si	5.755	5.729	5.616	5.582	5.554	5.717	5.749	5.694	5.559	5.799	5.728	5.777	5.711
Al	2.245	2.271	2.384	2.418	2.446	2.283	2.252	2.306	2.405	2.201	2.272	2.223	2.289
Al	0.293	0.303	0.236	0.465	0.404	0.509	0.541	0.489	0.599	0.336	0.397	0.397	0.437
Ti	0.056	0.059	0.045	0.053	0.03	0.000	0.000	0.000	0.118	0.085	0.055	0.081	0.057
Fe	3.683	3.728	3.891	3.974	4.104	3.951	3.923	3.980	3.387	3.824	3.650	3.443	3.789
Mn	0.107	0.097	0.084	0.104	0.072	0.078	0.083	0.100	0.100	0.054	0.106	0.093	0.108
Mg	1.864	1.794	2.020	1.311	1.492	1.350	1.436	1.353	1.617	1.573	1.659	1.833	1.500
Ca	0.120	0.081	0.068	0.106	0.082	0.103	0.096	0.080	0.092	0.082	0.093	0.085	0.075
K	1.574	1.715	1.363	1.819	1.643	1.790	1.788	1.806	1.743	1.781	1.82	1.833	1.799
Total	15.70	15.78	15.80	15.83	15.83	15.78	15.87	15.81	15.62	15.74	15.78	15.77	15.77
Mg /(Mg+Fe)	0.336	0.325	0.342	0.248	0.267	0.255	0.268	0.254	0.323	0.292	0.313	0.348	0.284

Appendix 6.10.
Chemical Compositions of Chlorites closely associated with
**Biotite, *Amphibole, Muscovite® and Illite®®

	** 103120				** 103119		** 103192			* 103090	* 103096	® 103116			® 103127			®® 103124	
SiO_2	23.30	22.94	23.81	23.77	24.19	23.12	25.64	26.84	25.28	23.28	34.19	23.66	28.90	24.55	25.30	24.12	24.50	25.77	28.08
TiO_2	n.d	n.d	n.d	n.d	n.d	n.d	n.d	0.25	n.d	n.d	n.d	n.d	n.d	n.d	n.d	n.d	n.d	n.d	n.d
Al_2O_3	18.66	19.04	18.80	18.55	18.87	17.99	18.22	16.63	18.02	19.37	10.92	21.65	21.88	20.55	22.17	22.18	21.05	20.37	21.39
FeO	40.98	40.57	39.16	40.18	35.95	38.05	34.22	33.47	35.90	43.45	30.50	34.78	34.30	36.85	25.33	25.72	26.25	35.26	30.81
MnO	0.40	0.62	0.41	n.d	0.73	0.63	0.62	0.54	0.66	0.81	1.34	0.98	0.31	0.48	2.43	2.69	1.43	0.90	0.66
MgO	4.67	4.42	5.31	5.23	6.28	5.89	9.29	9.09	7.92	1.20	10.16	6.97	9.55	8.65	12.56	11.49	11.54	6.16	5.19
CaO	n.d	n.d	n.d	n.d	n.d	n.d	n.d	n.d	n.d	n.d	0.90	n.d	n.d	n.d	n.d	n.d	n.d	n.d	n.d
Na_2O	n.d	0.42	0.11	0.14	0.36	n.d	n.d	n.d	n.d	n.d	n.d	n.d	n.d	n.d	n.d	0.31	n.d	n.d	0.26
K_2O	n.d	n.d	0.41	n.d	n.d	n.d	n.d	n.d	0.22	n.d	n.d	n.d	1.08	n.d	n.d	n.d	n.d	n.d	n.d
Total	87.51	88.01	88.01	87.87	86.38	85.68	87.99	86.82	88.00	88.11	88.01	88.04	96.02	91.08	87.79	86.51	84.77	88.47	86.39
	Numbers of ions on the basis of 28 oxygens																		
Si	5.382	5.307	5.451	5.459	5.544	5.429	5.675	5.955	5.666	5.449	7.338	5.677	5.764	5.413	5.376	5.248	5.419	5.682	6.129
Al	2.618	2.693	2.549	2.541	2.456	2.571	2.325	2.045	2.334	2.551	0.662	2.323	2.236	2.587	2.624	2.752	2.581	2.318	1.871
Al	2.47	2.505	2.531	2.487	2.647	2.416	2.430	2.630	2.427	2.796	2.102	3.354	2.908	2.754	2.929	2.936	2.907	2.976	3.631
Ti	-	-	-	-	-	-	-	0.042	-	-	-	-	-	-	-	-	-	-	-
Fe	7.919	7.849	7.500	7.718	6.891	7.473	6.335	6.696	6.728	8.508	5.475	6.469	5.722	6.228	4.502	4.681	4.855	6.502	5.624
Mn	0.078	0.121	0.080	-	0.142	0.126	0.116	0.127	0.124	0.160	0.243	0.184	0.052	0.089	0.438	0.496	0.268	0.168	0.122
Mg	1.609	1.525	1.812	1.790	2.145	2.061	3.067	2.982	2.647	0.418	3.250	2.308	2.840	2.844	3.978	3.728	3.806	2.025	1.689
Ca	-	-	-	-	-	-	-	-	-	-	0.206	-	-	-	-	-	-	-	-
Na	-	0.190	0.050	0.063	0.160	-	-	-	-	-	-	-	-	-	-	-	-	-	0.109
K	-	-	0.121	-	-	-	-	-	0.063	-	-	-	0.273	-	-	-	-	-	-
Total	20.08	20.19	20.09	20.06	19.99	20.08	19.95	20.48	19.99	19.88	19.28	20.31	19.80	19.92	19.85	19.84	19.84	19.67	19.18

Appendix 6.11: Microprobe Analyses of Amphiboles from the Minor Zonal Structure(see mean values in Table 8.4).

	Part C				Part D						Part E			Part F			
SiO_2	40.79	42.53	41.34	45.29	42.81	42.49	41.71	41.88	40.64	42.50	37.44	37.01	36.20	37.67	37.68	38.40	39.75
TiO_2	n.d	n.d	n.d	n.d	n.d	n.d	n.d	n.d	n.d	n.d	n.d	n.d	n.d	n.d	0.24	n.d	n.d
Al_2O_3	10.81	9.66	10.43	6.89	6.76	7.13	8.51	7.48	8.39	7.15	11.29	11.22	11.75	11.05	10.68	10.56	9.57
FeO	27.15	26.07	27.03	23.86	31.89	31.73	32.31	32.12	32.00	31.61	33.6	32.88	33.95	33.66	33.83	33.51	33.48
MnO	0.80	0.88	0.73	0.85	0.91	0.97	1.01	0.95	0.82	1.26	0.47	0.45	0.47	0.84	0.70	0.92	0.98
MgO	3.74	5.03	4.08	6.89	2.00	1.94	2.15	1.92	1.88	2.30	0.60	0.38	n.d	n.d	n.d	n.d	0.22
CaO	11.13	10.70	11.00	10.78	10.57	10.60	9.09	10.43	10.81	10.47	10.96	10.88	11.11	11.28	11.48	11.32	11.09
Na_2O	1.63	1.43	1.53	1.30	1.38	1.50	1.17	1.51	1.52	1.44	1.45	1.09	1.06	0.78	0.65	0.88	0.88
K_2O	0.95	0.72	0.87	0.60	0.68	0.68	1.15	0.71	0.92	0.65	1.93	2.00	2.44	1.73	1.74	1.52	1.03
Total	97.0	97.0	97.0	97.0	97.0	97.0	97.0	97.0	96.98	97.38	97.94	95.91	97.0	97.0	97.01	97.11	97.0
					Numbers of ions												
Si	6.526	6.724	6.592	7.052	6.979	6.927	6.801	6.851	6.675	6.919	6.213	6.246	6.101	6.294	6.302	6.302	6.579
Al	1.474	1.276	1.408	0.948	1.021	1.073	1.199	1.149	1.325	1.081	1.787	1.754	1.899	1.706	1.698	1.607	1.421
Al	0.565	0.524	0.552	0.316	0.278	0.305	0.435	0.293	0.299	0.291	0.42	0.478	0.436	0.47	0.408	0.465	0.445
Fe	3.632	3.447	3.605	3.108	4.348	4.326	4.392	4.395	4.396	4.302	4.662	4.64	4.785	4.702	4.732	4.665	4.635
Mn	0.109	0.118	0.097	0.112	0.126	0.135	0.14	0.132	0.114	0.122	0.066	0.064	0.068	0.119	0.1	0.129	0.137
Mg	0.892	1.812	0.97	1.600	0.485	0.473	0.522	0.467	0.462	0.557	0.149	0.095	0.000	0.000	0.000	0.000	0.054
Ca	1.979	1.812	1.88	1.799	1.846	1.836	1.587	1.828	1.902	1.827	1.948	1.967	2.007	2.019	2.056	2.019	1.967
Na	0.506	0.438	0.471	0.394	0.436	0.476	0.372	0.480	0.484	0.455	0.468	0.357	0.348	0.25	0.21	0.285	0.282
K	0.192	0.144	0.177	0.12	0.141	0.141	0.238	0.148	0.194	0.135	0.408	0.43	0.523	0.369	0.371	0.302	0.218
100Mg/Fe+Mg	21.0	25.6	21.2	34.0	10.0	9.9	10.6	9.6	9.5	11.4	3.1	2.0	0	0	0	0	1.2

Appendix 6.12. Analytic Results of Amphibole-Pyroxene(secondary) Skarn(B) Occurring Along a Quartz Vein(C) in the Garnet-dominant (See Fig. 5.17b, specimen 103084) Skarn(A).

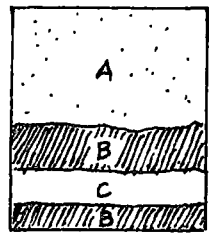

	Garnet skarn (A)	Amphibole-Pyroxene skarn (B)	Quartz Vein (C)
SiO_2	39.81	43.47	72.48
TiO_2	0.02	0.03	0.02
Al_2O_3	1.99	2.55	2.16
Fe_2O_3	19.40	4.75	2.59
FeO	6.29	21.06	5.04
MnO	1.12	1.39	0.25
MgO	1.11	1.34	0.41
CaO	29.53	21.37	8.02
Na_2O	n.d	n.d	5.2
K_2O	0.03	0.27	0.04
P_2O_5	0.08	0.11	n.d
LOI	1.18	3.25	4.12
Total	100.56	99.59	100.33
Trace elements(ppm)			
Sn	855.3	435.2	241
Zn	144.7	266.2	832.2
Cu	30.4	52.7	347.6
Ni	12.4	11.2	8.8
Sr	5.6	6.2	39
Rb	0	6.4	9.2
Pb	16.8	16.5	230.4
Bi	4.2	161.7	1452.8
Th	26.7	11.6	0
Mo	11.8	373.8	697.8
W	268.9	1637.2	2318.5

Appendix 6.13. Comparison of Chemical Compositions of Pyroxenes in Part A(associated with the primary garnet) and in Part B(associated with amphiboles) from 103084.

	Secondary Pyroxene				Primary Pyroxene			
SiO_2	49.55	48.84	49.16	49.16	49.29	49.36	49.71	49.49
Al_2O_3	0.23	0.68	0.45	0.46	n.d	n.d	n.d	n.d
FeO	20.62	23.45	21.92	22.19	21.91	22.25	21.26	22.39
MnO	3.18	1.55	2.19	2.26	4.22	3.98	3.98	3.67
MgO	3.56	2.90	3.44	3.25	1.67	1.62	2.09	1.6
CaO	22.87	22.58	22.84	22.68	22.9	22.78	22.96	22.85
(Total)	100.43	100.41	100.53	99.75	100.12	100.24	102.5	102.6
	Numbers of ions							
Si	1.992	1.976	1.981	1.983	2.005	2.008	2.011	2.011
Al	0.008	0.024	0.018	0.017	0.00	0.00	0.00	0.00
Al	0.003	0.008	0.003	0.005	0.00	0.00	0.00	0.00
Fe	0.693	0.793	0.739	0.749	0.745	0.757	0.719	0.761
Mn	0.108	0.053	0.075	0.077	0.146	0.137	0.136	0.126
Mg	0.213	0.175	0.207	0.196	0.101	0.098	0.126	0.097
Ca	0.985	0.979	0.986	0.98	0.998	0.993	0.996	0.995

Mean Values

	Secondary	Primary
SiO_2	49.18	49.46
Al_2O_3	0.46	0
FeO	22.01	21.95
MnO	2.30	3.96
MgO	3.29	1.75
CaO	22.74	22.87

Appendix 6.14 Chemical Composition of chlorite occurring in a quartz veinlet(Specimen 103084).

SiO_2	23.38	23.33	22.79
Al_2O_3	19.54	19.44	20.24
FeO	42.19	39.51	41.73
MnO	1.18	1.48	1.46
MgO	2.67	4.17	2.37
Total	88.96	87.94	88.59
		Numbers of ions	
Si	5.385	5.374	5.272
Al	2.615	2.626	2.728
Al	2.690	2.653	2.791
Fe	8.126	7.611	8.073
Mn	0.229	0.289	0.287
Mg	0.917	1.432	0.818
100Mg/Mg+Fe	10.14	15.84	9.2

Appendix 7. A spectrophotometric method for the determination of FeO in rocks(Modified Shapiro).

* Reagents and Equipment

Orthophenanthroline:	Crush to a powder
Sulphuric acid:	50 ml of conc. acid to 450 ml of water
Hydrofluoric acid:	48%
Boric acid:	5 % solution
Sodium citrate:	10 % solution
A metal dipper:	A scoop with a 3/16" diameter hole to hold 20 mg of orthophenanthroline powder
Teflon vessels:	Special decomposition vessels with screw caps

A rock sample having a known FeO content between 5 and 10 %, to be used as a standard (e.g. Tas-Dol-1 7.86 %, ZGI-BM 7.28 %, BCR-1 9.05 %).

* Procedure

1. Weigh 10.0 mg rock powder(200 mesh essential) into a teflon decomposition vessel. Two standards and one blank are needed for each run(Only 5 specimens are recommendable).
2. Add one dipper (approx. 20 mg) of powdered orthophenanthroline to each teflon vessel.
3. Add 3 ml of 10 % H_2SO_4 solution.
4. Add ½ ml of HF with a plastic safety pipette. Swirl to ensure complete wetting of the sample. Screw on teflon lids tightly.
5. Place teflon vessels in 110°C oven for 1½ hours.
6. Meanwhile transfer 5 ml of boric acid solution to a series of 100 ml beakers in a fume cupboard.
7. Remove teflon vessels from oven as quickly as possible (ideally all at the same time) and stand in cold water for 10-15 minutes.
8. Transfer to fume cupboard. Wearing gloves and safety spectacles, wash each sample with 20 ml sodium citrate into the beakers. One standard is done first and the other at the end.
9. Wash contents into 100 ml volumetric flasks and make up to mark.
10. Determine absorbances in a spectrophotometer at a wavelength of 555 millimicron using the blank as a reference.
11. If samples are 'cloudy' read all absorbance at 640 millimicron against the blank as a reference.
12. Calculate as follows; For each solution subtract the absorbance at 640 mμ to obtain absorbance due to colour. Divide the known FeO value for the standard rock by the absorbance of its colour to obtain a factor. Multiply the factor by the colour absorbance for each sample to obtain % FeO.

Appendix 7.1.

Semi-quantitative analyses of the pyroxene-garnet skarn to show variation in the chemical composition with depth (analysed by mine laboratory).

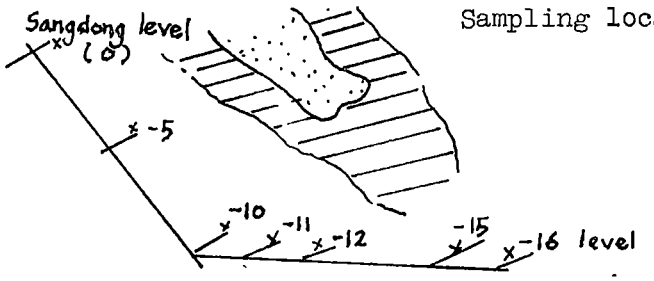

Level	(0)	- 5	-10	-11	-12	-15	-16
SiO_2	48.6	48.3	44.4	50.7	43.2	46.8	46.7
Al_2O_3	2.6	2.8	2.7	2.0	3.0	2.9	2.4
Fe_2O_3	26.5	25.6	28.2	25.9	25.7	28.6	26.8
MnO	1.4	1.6	1.3	1.2	1.5	1.3	1.3
MgO	2.2	1.8	1.5	1.7	1.7	1.7	1.7
CaO	18.3	19.4	20.3	16.9	25.7	19.4	22.7
Na_2O	.005	.004	.001	.003	.004	.007	.010
K_2O	0.2	0.1	0.2	0.1	0.2	0.1	0.1
P_2O_5	0.5	0.2	0.1	0.2	0.2	0.1	0.2
WO_3	0.1	0.1	0.1	0.1	0.1	0.1	0.1
Total	100.4	99.8	98.8	98.7	101.3	101.2	101.9

Appendix 7.2.

Average Chemical Compositions of Different Skarns and Original Limestone.

	limestone	wollastonite skarn	pyroxene-garnet skarn	amphibole skarn	quartz-mica skarn
SiO_2	4.22	42.98	46.0	52.49	59.65
TiO_2	0.03	n.d	0.2	0.25	0.22
Al_2O_3	1.34	1.3	2.48	5.46	8.17
Fe_2O_3	0.14	6.75	4.54	6.03	3.48
FeO	0.59	1.70	14.47	14.52	5.78
MnO	0.16	0.56	1.59	0.74	0.23
MgO	1.73	0.93	0.85	1.63	2.01
CaO	49.33	32.24	25.46	11.55	3.73
Na_2O	n.d	n.d	n.d	0.46	0.04
K_2O	0.35	(1.68)	0.31	0.83	2.92
P_2O_5	0.03	0.05	0.06	0.17	0.40
WO_3	n.d	0.01	0.1	2.50	8.0
LOI	41.96	11.62	3.53	3.94	5.54
Total	99.89	99.81	99.31	100.57	100.17
Trace elements(ppm)					
Sn	0	1338.7	533	200	104
Zn	5	49	232	202	192
Cu	8	12	28	45	155
Ni	5	6	12	30	23
Sr	350	22	11	22	21
Rb	10	103	19	109	530
Th	0	2	9	281	0
Pb	9	10	8	23	121
Bi	0	207	131	1185	2939
Mo	3	0	7	310	498

Appendix 8.1. Petrography of The Small Scale Zoning

Part A(103107) is similar to ore of the quartz-mica skarn of the M1 orebody. It is mainly composed of quartz, muscovite, chlorite, scheelite, fluorite, calcite, epidote, apatite, pyrrhotite, bismuthinite and chalcopyrite. Quartz and brownish chlorite grains show granoblastic inequigranular amoeboid fabric with a decussate texture. Sulphide minerals and scheelite commonly occur in chlorite. Large grains of quartz appear to be porphyroblastic pushing aside mafic minerals.

Part B(103108) is similar to Part A, but a little more brownish in colour. It is composed of quartz, biotite, scheelite, chlorite, apatite, fluorite, calcite, pyrrhotite, chalcopyrite and sphalerite. Relict pyroxene grains are often observed. Sample 103108 has an equigranular polygonal fabric with smaller quartz grains compared to Part A. Locally, inequigranular quartz grains replace smaller grains of equigranular quartz. Euhedral or subhedral biotite crystals with greenish form a decussate fabric.

Part C(103109) is that part of the quartz-amphibole skarn close to the quartz-mica zone. It is a transitional between the quartz-mica zone and the amphibole zone. It is mainly composed of quartz, biotite, amphibole, scheelite, with minor apatite and pyrrhotite. It shows a similar fabric to Part A. Fresh and clear biotites are ringed by altered biotite or muscovite and this biotite-dominant part is sharply bounded by the amphibole-dominant part.

Part D(103110) is essentially an amphibole skarn. It is mainly composed of amphibole, quartz, magnetite, pyrite, pyrrhotite, calcite, fluorite, native bismuth, bismuthinite, galena and sphalerite. Magnetite occurs only close to Part E(the pyroxene skarn), and it occurs commonly in pyrrhotite. Scheelite commonly shows rings of inclusions, which are native bismuth, pyrite and amphibole.

Part E(103111) is pyroxene skarn, in which garnet is largely replaced by dark green late pyroxene(hedenbergite), numbers of large pyroxene crystals and brown garnet crystals commonly appear parallel, lining up in fine grains of pyroxenes. This textual pattern seems to have been formed due to recrystallization which may be coeval with the amphibole formation. Rounded grains of scheelite are common within the hedenbergite. Amphibole occurs with quartz and calcite in veinlets. Sulphide minerals are rare except for a few grains of bismuthinite filling interstices of pyroxenes.

Part F(103112) is typical pyroxene-garnet skarn, locally replaced by amphibole veinlets and dark green pyroxene. A few grains of pyrrhotite were observed, but scheelite is rare.

Part F represents the pyroxene-garnet skarn of the M1 orebody at the 7th level. Part E corresponds to that part of the pyroxene-garnet skarn which is partly replaced by late pyroxene during formation of the quartz-mica and the amphibole skarns. The boundary between the pyroxene-garnet skarn(Parts E and F) and Part D is irregular. A number of fine amphibole veinlets cut Part E as well as Part F and occur along fractures.

Appendix 8.2. Chemical Compositions of Pyroxenes in Parts F and E.

Part F

SiO_2	48.70	49.33	48.65	48.96	47.75	48.92	47.80	47.85	49.52	47.89	48.54
Al_2O_3	n.d	n.d	n.d	n.d	0.31	n.d	0.83	0.39	n.d	n.d	0.15
FeO	27.23	21.98	25.24	25.06	27.70	24.53	27.30	28.35	23.28	28.48	25.92
MnO	1.31	1.49	1.62	1.79	1.70	1.55	1.05	1.73	1.70	1.44	1.54
MgO	0.32	3.94	1.58	1.53	0.42	2.22	0.57	n.d	3.32	0.21	1.41
CaO	22.39	23.27	22.91	22.66	22.13	22.78	22.45	21.68	22.17	21.99	22.44
Na_2O	n.d	n.d	n.d	n.d	n.d	n.d	n.d	n.d	n.d	n.d	n.d
Total	99.95	100	100	100	100	100	100	100	99.99	100	100

Part E

SiO_2	48.63	47.96	47.51	48.01	47.89	48.03	48.10	48.24	46.46	47.57	47.84
Al_2O_3	n.d	0.33	n.d	0.43	0.33	0.44	n.d	0.27	0.28	0.51	0.21
FeO	26.20	27.29	26.79	27.43	26.48	25.69	27.19	26.95	25.16	27.48	26.67
MnO	1.19	1.26	1.42	1.1	1.24	1.0	1.18	1.12	1.48	1.13	1.21
MgO	1.69	0.84	1.34	0.83	1.62	1.78	0.99	1.22	1.51	1.03	1.29
CaO	22.29	21.86	22.94	21.75	21.93	23.36	21.82	21.74	24.57	21.80	22.41
Na_2O	n.d	0.45	n.d	0.45	0.51	0.6	0.71	0.45	0.54	0.48	0.42
Total	100	99.99	100	100	100	100	99.99	100	100	100	100

Appendix 8.3.
Chemical Compositions of Garnet from Part F and Part E

	Part F								Part E			
	E-1	D-1	D-4	H-4	D-5	C-1	C-2	Mean	A	B1	G1	Mean
SiO_2	37.31	36.60	37.05	37.42	38.83	37.90	38.20	37.62	37.94	37.22	37.48	37.55
TiO_2	n.d	0.32	0.43	0.34	0.38	0.42	0.44	0.39	n.d	n.d	n.d	n.d
Al_2O_3	8.55	9.38	8.15	6.41	11.77	14.77	15.03	10.58	12.03	11.09	11.94	11.69
Fe_2O_3	18.75	18.85	20.07	22.70	15.13	9.92	10.04	16.49	16.14	17.65	17.42	17.07
MnO	1.2	1.35	0.68	0.56	1.27	2.02	1.77	1.26	0.94	1.19	1.22	1.17
CaO	34.19	33.50	33.63	32.56	32.62	34.96	34.53	33.71	32.95	32.85	31.54	32.45
Total	100	100	100	100	100	100	100	100	100	100	99.6	99.93
Numbers of ions on the basis of 12 oxygens												
Si	3.219	3.07	3.119	3.184	3.154	3.031	3.045		2.102	3.08	3.086	
Al	0.845	0.928	0.809	0.643	1.127	1.393	1.412		1.16	1.082	1.159	
Fe^{+3}	1.155	1.052	1.164	1.335	0.85	0.581	0.561		0.84	0.918	0.841	
Ti	0.000	0.02	0.027	0.022	0.023	0.026	0.027		0.000	0.000	0.000	
Fe^{+2}	0.16	0.27	0.249	0.28	0.178	0.082	0.108		0.264	0.304	0.358	
Mn	0.085	0.096	0.049	0.041	0.087	0.132	0.119		0.065	0.083	0.085	
Ca	3.073	3.01	3.034	2.968	2.839	2.997	2.949		2.887	2.913	2.783	

Appendix 8.4. K' values of Garnet and Pyroxene in Parts E and F

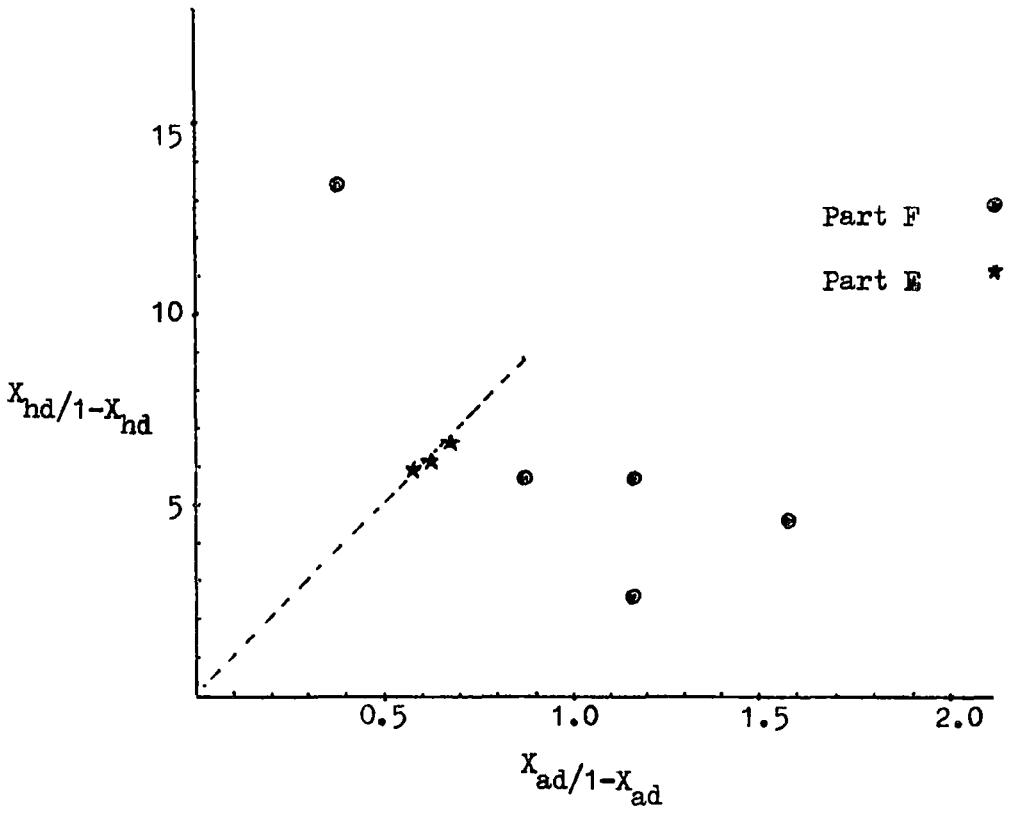

Part F	X_{hd}	$X_{hd}/1-X_{hd}$	X_{ad}	$X_{ad}/1-X_{ad}$	K'
e1	0.72	2.57	0.54	1.17	2.19
d2	0.85	5.67	0.47	0.89	6.37
d3	0.85	5.67	0.54	1.17	4.85
h2	0.82	4.56	0.61	1.56	2.92
c3	0.93	13.29	0.27	0.37	35.91
Part E					
a1	0.86	6.14	0.38	0.61	10.07
b2	0.87	6.69	0.4	0.67	9.98
gf	0.857	5.99	0.36	0.56	10.70

Appendix 8.5. Variation in Chemical Compositions of Pyroxenes and Amphiboles.

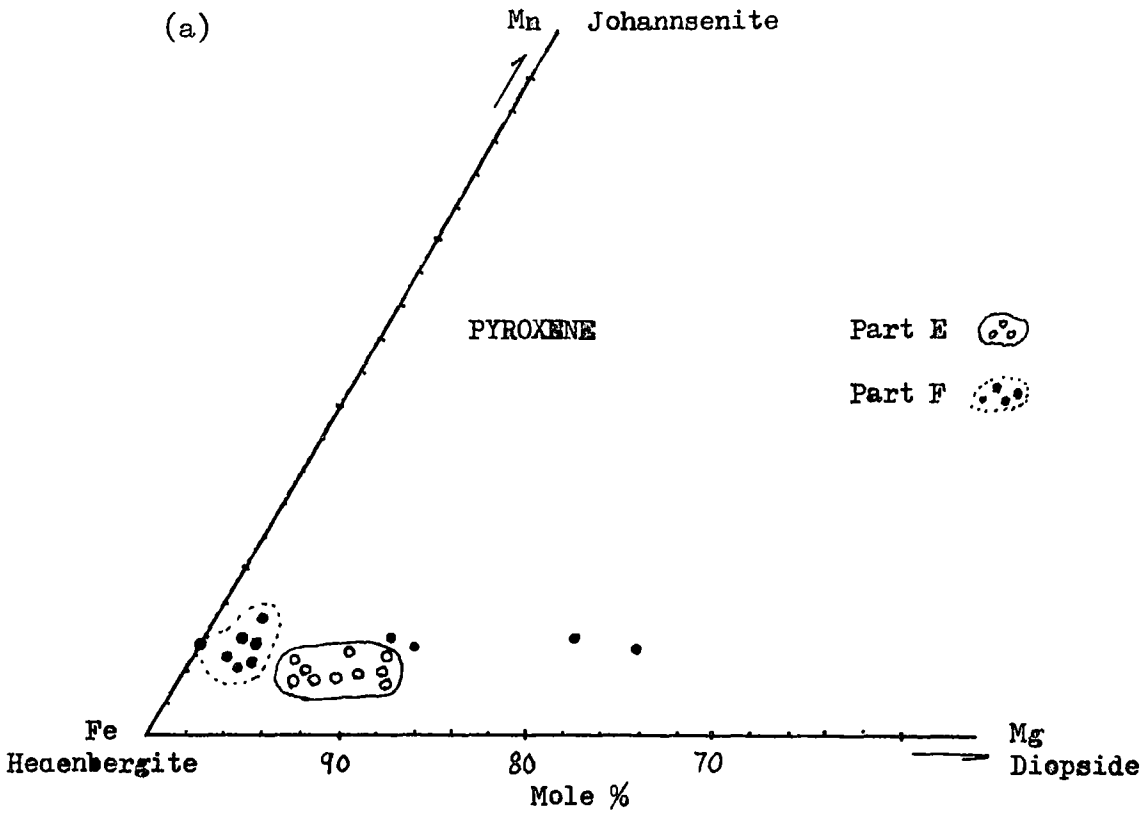

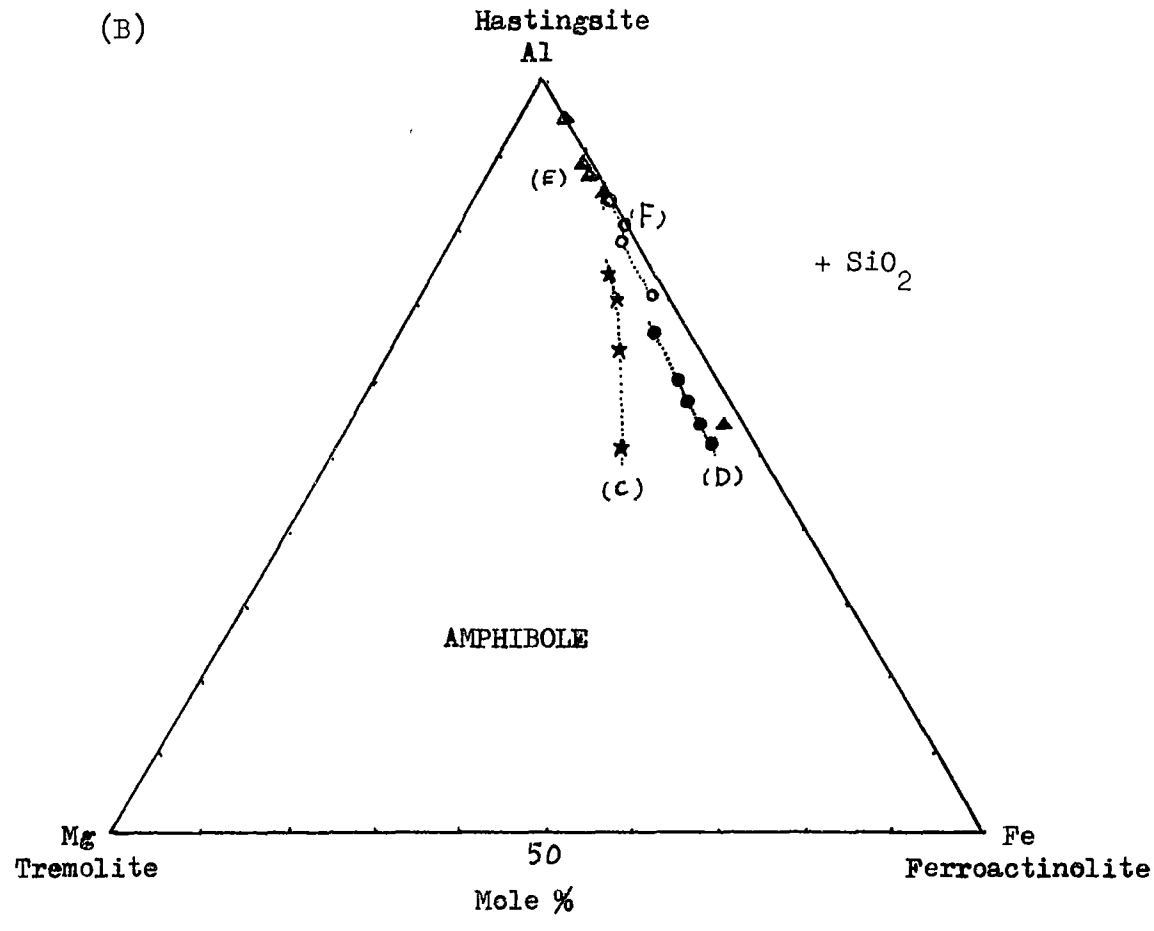

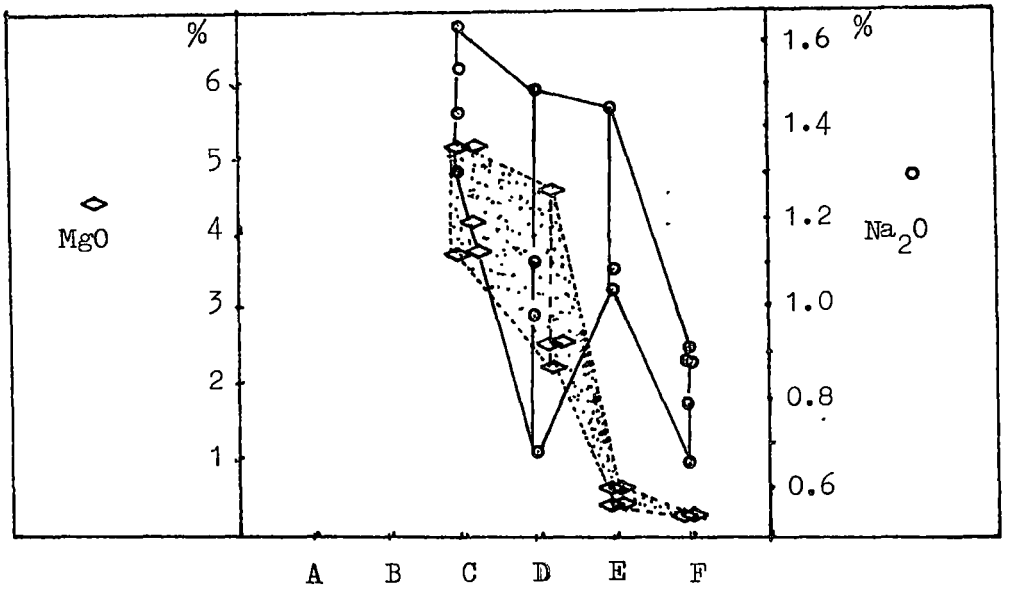
%
6
5
4
3
2
1
MgO
1.6 %
1.4
1.2
1.0
0.8
0.6
Na_2O
A B C D E F

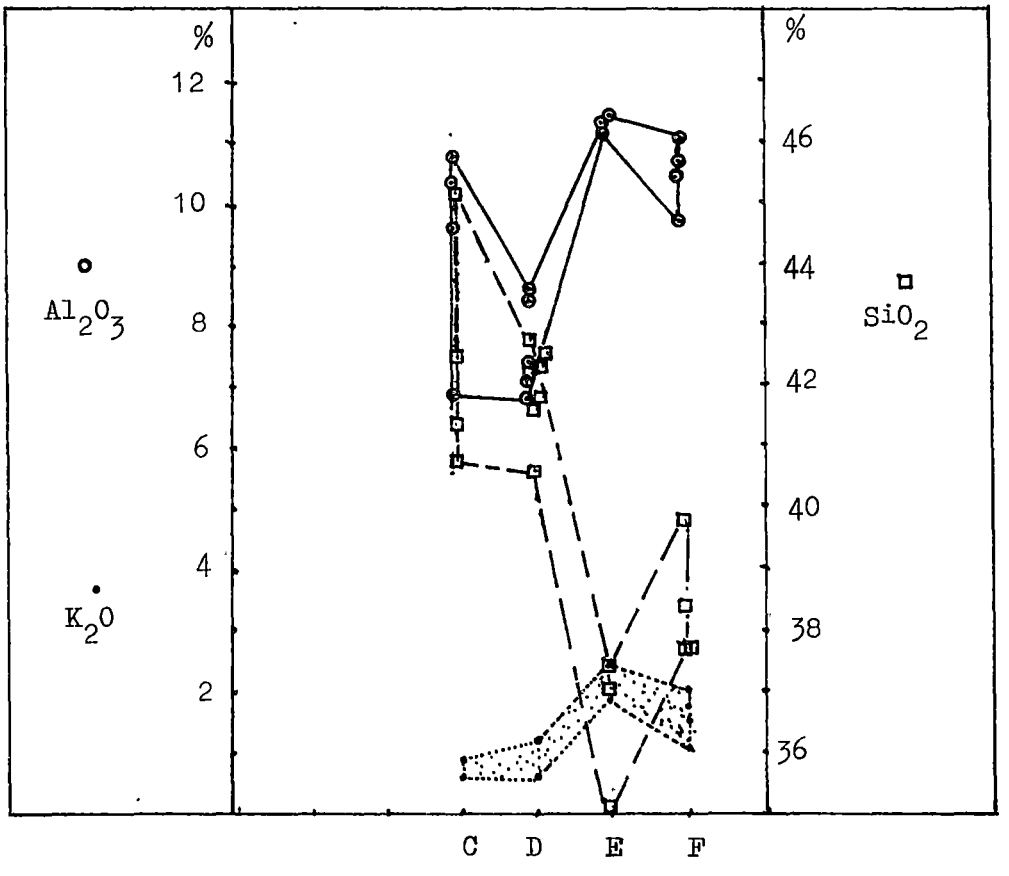
%
12
10
8
6
4
2
Al_2O_3
K_2O
%
46
44
42
40
38
36
SiO_2
C D E F

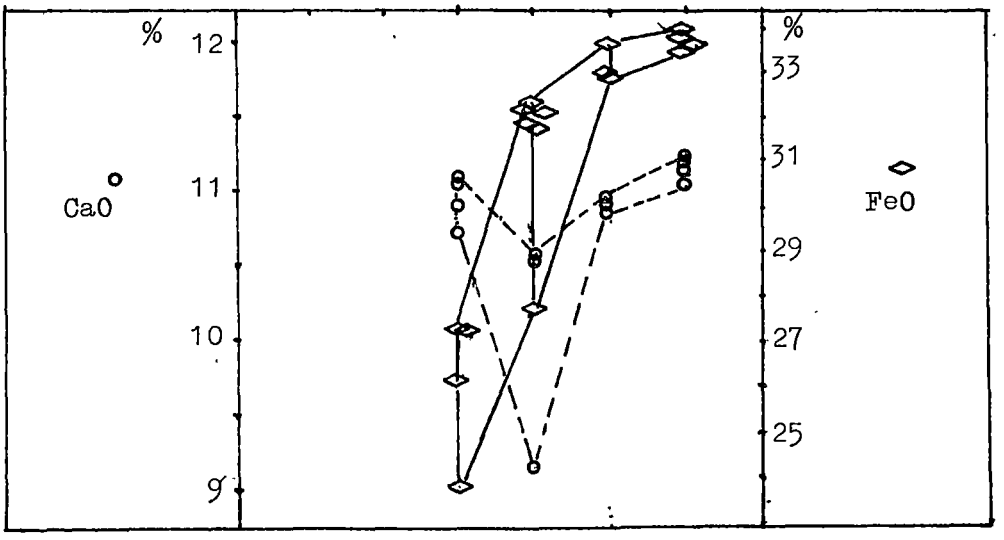
%
12
11
10
9
CaO
%
33
31
29
27
25
FeO

Appendix 8.7. Variation in chemical composition of amphibole from Part C to Part F

	*103109 C	103110 D	103111 E	103112 F
SiO_2	42.49	42.01	36.88	38.38
Al_2O_3	9.45	7.57	11.42	10.47
FeO	26.03	31.94	33.48	33.62
MnO	0.82	0.99	0.46	0.86
MgO	4.94	2.03	0.33	0.06
CaO	10.9	10.33	10.98	11.29
Na_2O	1.47	1.42	1.2	0.79
K_2O	0.78	0.79	2.12	1.51
Total	96.88	97.08	96.87	96.98
100MgO/FeO	18	6	0.9	0.1

Part C & D = amphibole zone

Part E & F = pyroxene zone

*103109 amphibole coexisting with biotite

Appendix 8.8. Variation in chemical composition of a single crystal of amphibole from Part F.

	core	middle	rim
SiO_2	37.67	39.75	47.79
TiO_2	n.d	n.d	n.d
Al_2O_3	11.05	9.57	1.45
FeO	33.66	33.48	34.32
MnO	0.84	0.98	1.22
MgO	n.d	0.22	n.d
CaO	11.28	11.09	11.28
Na_2O	0.78	0.88	0.91
K_2O	1.73	1.03	n.d
Total	97.01	97.0	96.97
$\frac{K_2O + Al_2O_3}{SiO_2+FeO+MnO}$	0.177	0.143	0.017

Appendix 8.9 . Comparison of Chemical Compositions of Biotites Between Part C and Part B.

	Part B					Part C			
	A3	A1	D1	B1	Mean	G1	G2	I	Mean
SiO_2	38.49	36.71	36.36	36.31	36.97	35.76	36.40	35.51	35.89
TiO_2	0.94	0.74	0.5	0.34	0.63	0.29	0.24	0.36	0.30
Al_2O_3	15.64	17.3	15.23	14.19	15.59	14.08	13.87	14.22	14.06
FeO	21.80	23.78	25.45	27.41	24.61	27.33	26.12	30.37	27.94
MnO	0.57	0.66	0.88	0.78	0.72	0.46	0.72	n.d	0.40
MgO	8.68	7.79	8.06	8.18	8.18	7.40	7.98	7.19	7.52
CaO	n.d	n.d	n.d	n.d	n.d	0.82	0.76	0.64	0.74
Na_2O	0.27	0.51	0.37	n.d	0.29	0.58	0.44	0.93	0.65
K_2O	9.39	8.88	8.91	8.81	9.0	9.24	9.47	6.76	8.49
Total	95.78	96.38	95.76	96.02	95.99	95.96	96.0	95.98	95.99
Numbers of ions on the basis of 22 oxygens									
Si	5.882	5.634	5.694	5.723		5.680	5.748	5.630	
Al	2.118	2.366	2.306	2.277		2.320	2.252	2.370	
Al	0.699	0.763	0.506	0.358		0.319	0.330	0.288	
Ti	0.108	0.086	0.059	0.039		0.035	0.028	0.044	
Fe	2.786	3.052	3.333	3.613		3.631	3.450	4.028	
Mn	0.073	0.086	0.117	0.103		0.062	0.096	0.000	
Mg	1.978	1.783	1.881	1.921		1.752	1.878	1.700	
Ca	0.000	0.000	0.000	0.000		0.139	0.118	0.110	
Na	0.081	0.152	0.113	0.000		0.179	0.136	0.284	
K	1.830	1.739	1.780	1.770		1.873	1.908	1.368	
$\frac{Mg}{Mg+Fe}$	0.415	0.369	0.361	0.347		0.326	0.353	0.297	

Appendix 8.10. Comparative chemical compositions of biotites in different localities.

	Small scale quartz-mica skarn in the pyroxene-rich zone and the amphibole-rich zone				M1 quartz-mica skarn (on the 7th level)	
	Part B	Part C	*103119	**103120	103093	103097
SiO_2	36.97	35.89	35.17	35.11	34.89	36.25
TiO_2	0.63	0.30	1.46	0.14	0.18	0.72
Al_2O_3	15.59	14.06	15.04	14.94	14.81	14.66
FeO	24.61	27.94	29.68	31.38	30.67	27.33
MnO	0.72	0.40	0.28	0.34	0.57	0.72
MgO	8.18	7.52	5.96	4.68	6.02	6.99
CaO	n.d	0.74	n.d	0.26	0.70	0.51
Na_2O	0.29	0.65	0.42	0.58	n.d	n.d
K_2O	9.00	8.49	8.0	8.46	8.13	8.91
@Total	95.99	95.99	96.01	95.89	95.97	96.09

*103119 = replacing the pyroxene-garnet skarn

**103120 = replacing the amphibole skarn

n.d = not detected

@Total are not normalized.

Appendix 8.11.. Composition of muscovite in part A(105107).

	a-1	a-2	g-1	g-3	Average M1
SiO_2	47.62	47.43	47.65	47.62	48.78
TiO_2	0.42	0.82	0.31	0.21	0.04
Al_2O_3	30.26	30.73	27.82	31.10	30.6
FeO	3.03	2.66	3.43	3.65	3.01
MnO	n.d	n.d	n.d	n.d	n.d
MgO	1.85	1.69	3.83	1.12	2.36
CaO	1.07	1.07	2.03	1.09	0.31
Na_2O	0.49	0.49	0.30	0.50	0.26
K_2O	11.27	11.11	10.65	11.12	10.63
Total	96.01	96.0	96.02	96.41	95.99

Numbers of ions on the basis of 22 oxygens

Si	6.405	6.365	6.437	6.385
Al	1.595	1.635	1.563	1.615
Al	3.209	3.232	2.873	3.306
Ti	0.042	0.083	0.032	0.021
Fe	0.341	0.298	0.387	0.409
Mn	0	0	0	0
Mg	0.371	0.338	0.771	0.224
Ca	0.154	0.154	0.294	0.156
Na	0.129	0.127	0.078	0.131
K	1.933	1.901	1.836	1.901

Appendix 8.12. Comparison of Chemical Compositions of Chlorites in Part A and Part B.

	Part A				Part B			
	a-3	c-1	e-1	g-2	g-2	g-4	g-5	f-1
SiO_2	26.98	26.08	26.52	27.76	23.84	28.52	24.29	27.27
Al_2O_3	18.35	18.29	19.93	19.06	20.06	17.36	19.86	15.79
FeO	32.37	34.19	29.91	28.22	36.93	32.45	35.18	36.47
MnO	n.d	n.d	1.2	1.23	0.73	0.71	1.61	0.40
MgO	9.87	9.03	10.24	10.91	6.06	6.32	6.76	7.49
CaO	n.d	n.d	n.d	n.d	n.d	2.31	n.d	0.29
Na_2O	0.44	0.41	0.58	n.d	0.40	0.52	0.3	0.29
K_2O	n.d	n.d	n.d	n.d	n.d	n.d	n.d	n.d
Total	88.01	88.0	88.38	87.56	88.02	88.19	88.0	88.0
Si	5.876		5.706		5.378	6.245		
Al	2.214		2.294		2.622	1.755		
Al	2.578		2.761		2.718	2.725		
Fe	5.897		5.383		6.969	5.942		
Mn	0		0.219		0.140	0.132		
Mg	3.205		3.283		2.037	2.064		
Ca	0		0		0	0.543		
Na	0.186		0.24		0.176	0.22		
K	0		0		0	0		
Mg/Mg+Fe x100	35.2	32	37.88	40.8	22.62	25.78	25.52	26.79

Appendix 9.1. Difference in FeO/Fe_2O_3 in mineralized and unmineralized Myobong slates.
(analysed by Geological Survey of Korea)

	$FeO_{wt\%}$	Fe_2O_3	FeO/Fe_2O_3
Mineralized zone(at Taebag level)			
slate close to M1(block 13)	6.20	1.47	4.2
slate close to M1(block 20)	7.50	1.08	6.9
slate close to F1(block 3)	7.86	1.43	5.5
slate close to F2(block 13)	7.22	1.65	4.4
Unmineralized zone(to east the mine)			
slate 1(about 100 m east)	4.62	2.67	1.7
slate 2(about 200 m east)	11.0	2.97	3.7
slate 4(about 500 m east)	3.25	3.81	0.9
slate 5(about 800 m east)	4.11	2.93	1.4
slate 6(about 2 km east)	5.19	2.10	2.5

Appendix 9.2. Difference in Mineralogical Compositions Between Mineralized and Unmineralized Slates

Unmineralized slate	Mineralized slate
Hematite, Chlorite, Rutile, Apatite, Muscovite, Ilmenite, Biotite, Quartz, Plagioclase(albite)	Chlorite, Apatite, Ilmenite, Biotite, Quartz, Tourmaline, Zircone, Calcite, Orthoclase, Pyrite, Plagioclase(anorthite anorthite-bytownite oligoclase-andesine)

All minerals were identified by microprobe

Appendix 10. Fluid Inclusion Studies

Appendix 10.1. Microthermometry Apparatus

Maker: Chaixmeca
patent 74-10227(France)
built under CNRS-ANVAR license

Range: minimum temperature = -180°C
maximum temperature = +600°C

Calibration: showing almost constant difference as shown by Eastoe (1979).
its differences are as follows;

(°C)							
Measured temperatures	-56.1	0.0	100	200	300	400	500
Corrected temperature	-56.6	0.0	99	196	293	399	(487)

The melting points of substances used for calibration(Eastoe, 1979);

n-hexane	-95°C
n-octane	-56.8°C
CO_2(in fluid inclusions supplied by the Chaixmeca Co.)	-56.6°C
CCl_4	-23.0°C
Merck Schmelzkoerper 9670	70°C
" 9735	135°C
" 9800	200°C
" 9847	247°C
$NaNO_3$	306.8°C
$K_2Cr_2O_7$	398°C

Methodology : The inclusions were frozen and T_f measurement taken before measurement of T_h. Many inclusions did not nucleate ice on cooling because of small size. Warming of frozen samples was equilibration with atmosphere although the heating rate was also controlled by application of N_2. For heating observations, samples were generally heated at a rate of 6 to 10°C per minute upto 200°C. After reaching this temperature heating rate reduced to 0.2 - 0.3°C per minute close to homohenization temperature. After homogenization, the inclusion was allowed to cool and if bubble did not reappear the results were excluded. Inclusions developed along fractures in quartz with $T < 120$°C were excluded.

Appendix 10.2 Data from Fluid Inclusions of Quartz in the Quartz Veins.

Sample No.	Types of Q.V.	Types of Inclusion	T_h(°C)	T_f(°C)	T_m(°C)	Salinity (NaCl wt %)	Remarks
Jangsan level(+3rd level)							
103182	Mo	A	281	-2.1		3.8	1st T_m=-20
			375				
			385				rare,small
103183	Py	A	207				sericite
			247				
			260				rare,small
103184	Cpy	A	306				
Baegun level(+2nd level)							
103185	Barren	A	216				
			292				
			298				
103190	Mo	A	266				
			333				
			346				
103189	Bi	A	320				
103191	Mo,Bi		250	-2.1		3.8	sericite
			332	-3.1		5.3	1st T_m=-20
			397				
103186	Bi	A	248				
			264				sericite
103188	Cpy	A	231				
			266				
			319				
103187	Wf	A	298				
Sangdong level(0 level)							
103192	Mo	A	274				
			314				
			317				
			335				
103193	Mo	A	208				
			242				
			272				
103194	Mo	A	238				
			336				
			357				

-3rd level

103156	Mo	A	230	-3.6		6.3	Quartz in
			243	-4.5		7.2	calcite vein
		B	223				$L\text{-}CO_2$ T_h= 25.1
103198	Barren	A	151	-3.6		6.3	1st T_m= -23.7
			176	-4.7		7.8	
		B	199				$L\text{-}CO_2$ T_h= 28.9
		A	241	-6.1		9.4	
103197	Mo	A	190, 226				
103196	Barren	A	194				very rare
103199	Barren	A	181	-6.7		10	
103195	Mo	A	169, 236				

-4th level

103202	Barren	A	275	-3.6		6.3	
			300				
	Mo	C	252-293		263-267	34	see Table 10.10
		A	344	-2.2		4	
			362	-2.6		4.6	
			323	-2.7		4.7	1st T_m = -30.2
103200	Mo		302				
			378				
			405				critical point
103205	Mo	A	295				
103206	Cpy	A	246				no scheelite
103203a	Mo	A	158				margin of quartz vein
			178				
			215				no scheelite
b	Mo	A	262				middle of quartz vein
			335				
			344				
c	Mo	A	282				between a and b
			333				closer to b
d	Mo	A	229				between a and b
			270				closer to a
e			252				later fine vein
f		C	222		321		$T_m(NaCl) > T_h$
103204	Mo	A	264	-9.9		13	
			278	-12.5		16.9	
103154	Mo	C	128-277		165-235	30-32	halite only
		C	238-275		289-422	28-49	halite + sylvite
	Mo	A	267				see Table 10.10
			313				
			348	-2.6		4.6	
103155	Mo	A	239				milky white quartz
		B	243				$L\text{-}CO_2$ T_h= 29.1

-6th level						
103207	Cpy	A	293			Bubble moves actively
103208	Cpy	A	170	-4.7	7.3	1st T_m=-20
			217	-3.5	6	
				-4.1	6.4	
-7th level						
103209	Mo	A	259			
			292			
			380			
103210	Barren	A	200			
			235			no scheelite
			298	-7.1	11.2	1st T_m=-21
-9th level						
103212	Barren	A	162			very rare
			282			
103213	Cpy	A	204			
			314			
103214	Cpy	A	214			fluorite(160-171)
			223			no scheelite
		A	280			
		B	265			L-CO_2 T_h=30.5
-10th level						
103216	Cpy	A	212			
			220			no scheelite
			233			
103217	Cpy	A	169			
			176	-0.7	1.3	1st melting T=-21
103215	Wf	A	348	-4.7	7.3	
			395			
		B	394			L-CO_2 T_h=30.7 C.P.
		A	272	-4.1	6.4	1st T_m= -21
103218	Barren	A	221			
-12 level						
103220	Bi	A	134			secondary
			172			
103219	Barren	A	295			
			303			
			346			
103221	Cpy	A	283	-6.8	10.3	fluorite(262)
			301			
			317			

103222	Cpy	A	138 199	sericite
103223	Cpy	A	206	rare
-14th level				
103225	Barren	A	209 230 240 265 320	no scheelite
103224	Cpy	A	204 230 240 265 320	sericite
103224	Cpy	A	204	sericite
103226	Cpy	A	143 191	
103227	Wf	A	246	

---

* sericite=it indicates the quartz vein which gives alteration(sericite at margins of quartz vein) to slate.

* no scheelite=it indicates no scheelite is observed in the quartz vein.

* Barren = it indicates the quartz vein showing no sulphide or wolframite.

Appendix 10.3 Data from fluid inclusions of quartz in the M1 skarn orebody.

Sample No.	Zone	Types of Inclusions	Temperatures(°C) T_h	T_f	T_m	Salinity NaCl wt %	Remarks (associated minerals, T_h)
Jangsan(+3) level							
105982	Px	C	194		451	51	Pyroxene(405-444) Fluorite(195-236)
Baegun(+2) level							
105983	Px	A	254				Pyroxene(374-490)
Taebag(+1) level							
105984	Px	A	175 186				Bubble moves at room temperature
105985	Px	A	174 176				
105986	Px	A	136 190 196				Pseudosecondary Scheelite(207)
105987	Px	A	130				Few inclusions Abundant scheelite
105988	Px	A	132 140				
105989	Px	A	179				Quartz-mica ore Abundant scheelite
105990	Qm	A	339				
105991	Qm	A	215 244	-1.2 -3		1.8 5.0	
105992	Hb	A	168 207 220				Scheelite(226-265)
105993	Hb	A	245 297 307	-1.9		3.1	
105994	Hb	A	225 297	-2.9		5	
		C	343		327		
Sangdong(0) level							
105995	Px	A	257				Pyroxene(390) fluorite(208)
105996	Px	A	242				Pyroxene(313)
105997	Qm	A	248				Scheelite(348)

103125	Qm	A	177 283	-1.5 -5.3		2.3 8.7	1st T_m = -20.1 1st T_m^m = -23.5
		C	126		119		
103170	Qm	A	291 336				Scheelite(345)
-1st level							
106000	Px	A	226				Pyroxene(403)
106001	Px	A	281				Pyroxene(385)
106002	Px(qm)	A	188				Abundant scheelite (256-305)
106003	Px	A	199				
106004	Hb	A	243 259 273	-4.3		7	dark bubble clear bubble
		C	168		185	30	
106005	Hb	A	200				
106006	Qm	A	202				Abundant scheelite (305-306)
106007	Qm	A	245				
106008	Qm	A	213	-5.2		8.3	
106009	Qm	A	198 206				very tiny & rare
-3rd level							
106010	Px	A	215				Pyroxene(344-548)
106011	Px	A	190 238 259				rim of quartz core of quartz
103121	Qm	C	152		182	30	
106012	Qm	A	356				
106013	Qm	A	275 300 305	-3.9		6.8	
106014	Qm	A	198				Scheelite(229)
106015	Qm	A	318				
106016	Qm	A	225				
106017	Qm	A	232 264 306				

106018	Hb	A	208			
106019	Hb	A	192 209			
106020	Hb	A	208	-3.1	5.2	1st T_m= -50.5
		B	308			L-CO_2 T_h=28.9
106021	Hb(px)	A	236 303	-3.0	5	
-4th level						
106022	Hb	A	216			
106023	Qm	A	172 260 303			
106024	Qm	A	222 279	-2.7	4.7	Scheelite(368)
106025	Qm	A	265 311 355			
106026	Qm	A	189 198	-3.8 -4	6.6 6.9	Scheelite(279) (285)
106027	Qm	A	313	-2.1	3.8	
106028	Hb	A	213 245 299			Apatite(285)
106029	Qm	A	222			
106030	Hb	A	213 220 235	-5.6	9.0	
-7th level						
106031	Px	A	177			
106032	Px	A	241			
106033	Hb	A	235			
106034	Hb	A	150 178 197 220 270	- 0	0	Secondary
106035	Qm	A	267 272 292	-6.7	10	Opaque daughter mineral

106036	Hb	A	223 226 256			
106037	Hb	A	206			
106038	Qm	A	338 365 374	-2.7	4.7	
106040	Qm	A	201			Scheelite(276)
106041	Qm	A	190	0	0	Apatite(253)
106042	Qm	A	219	-0.7	1.3	1st melting T =-21
106043	Hb	A	172 192 207	-1.0 -3.5	1.6 5.9	
106044	Qm	A	276 397			Amphibole(287-293) C.P
106045	Qm	A	293			
106046	Qm	A	183			Amphibole-rich
106047a	Px	A	239 265			Pyroxene(381)
106047b	Qm	A	205 208			Pyroxene(381)
106048	Hb	A	194			Biotite(286)
-9th level						
106049	Hb	A	315			Pyroxene(388-399)
106050	Hb	A	298 321 325			
106051	Hb	A	222 238 299	-2.1 -2.8	3.8 4.7	
-10th level						
106052	Px	A	214			
106053	Px	A	176			Bubble actively moves at R.T*
106054	Px	A	297			Abundant scheelite very rare F.I.**
106055	Px	A	210			

*R.T = room temperature
**F.I = fluid inclusion

106056	Px	C	156		132	29	NaCl daughter
106057a	Px	A	180				intruded by
106057b	Px	A	176				
106058	Px	A	227				
106059	Hb	A	218				
106060	Hb	A	310				
106061a	Hb	A	260 293 295				Clearly transparent Apatite(307)
106061b	Px	A	177				Milky white, bubble moves at room temperature
106062	Px	A	218				
106063	Px	A	256				
106063	Hb	A	245 304				Scheelite(318)
-12th level							
106065	Hb	A	221				Pyroxene(432-456)
106066	Px	A	188 196				Pyroxene(398-399)
106067	Px	A	169 186				
106068	Px	A	196 206				Scheelite(316)
106069	Hb	A	355				
106070	Hb	A	209				
106133	Px	A	231	0		0	Scheelite(297)
-14th level							
106072	Px	A	199 208, 211	-5.7		9	Pyroxene(399)
106073	Px	A	178 200				Scheelite(287)
106074	Px	A	183,195				Apatite(272-290)
106075	Px	A	171,177				
106076	Px	A	212				
106077	Px	A	239				
106078	Px	A	254 274	-2		3.7	
106079	Px	A	262				

Appendix 10.4

Data of Fluid Inclusions from Pyroxene.

Level & Specimen No.	Type of Inclusion	Temperature(^{o}C) T_h	T_f	Salinity NaCl wt %	Remarks
Jangsan lv.					
106081 (J-2)	A(g,l)	386, 397			
Baegun lv.					
106082 (B-2)	A(g-l)	374, 388, 413 490,>580			
106083 (B-3)	A(g,l)	399, 413			Homogenized to vapour phase
106084 (B-4)	A(g,l)	359, 369, 425			C.P. Gn(387)
Taebag lv					
106085 (T-1)	A(g-l)	411, 424			
106086 (T-2)	A(g-l)	404 380			vapour phase liquid phase
106087 (T-3)	A(g,l)	468, 491			
106088 (T-4)	A(g,l)	361, 478			
106089 (T-5)	A(l,g)	$397^{(V)}$, $413^{(L)}$			vapour & liquid
Sangdong lv.					
106090 (A)	A(g)	429			
106091 (B)	A(g)	424, 505, 508, 573			
106092 (C)	A(l)	381, 430			
106093 (O-1)	A(l)	390			
106094 (East1)	A(l)	373, 394, 412, 420, 474	-2.3	4.1	1st T_m = -50.2
	C(NaCl)	448		31	T_m = 230(NaCl)
106095 (EastA)	A(g)	396, 481			
106096 (EastB)	A(g)	469			
106097 (EastF)	A(g)	368			
106098 (EastG)	A(l,g)	313			
-1st lv.					
106099 (1-1)	A(l,g)	401			vapour phase
106100 (1-2)	A(l)	396			

106101 (1-inc)	A(l-g)	332, 374, 378 385 401, 448			qtz(281) fl(257)
-3rd lv.					
106102 (3-1)	A(g-l)	458,*474, 548			*qtz(215)
106103 (3-2)	A(g)	380$^{(V)}$, 422$^{(L)}$	-14.7	18.2	1st Tm = -57
	C(NaCl)	580		47.5	T_m= 414(NaCl)
-4th lv.					
106104 (4-0)	A(l,g)	455			
106105 (4-1)	A(l,g)	380, 422, 499			fl(266)
	C(NaCl)	301		32	T_m= 235(NaCl)
-5th lv.					
106106 (5-0a)	A(g-l)	354, 375, 378 401, 469			
	(g)	396 403			C.P
106107 (5-0b)	A(l)	382			qtz(304)
-7th level					
106109 (7-6)	A(g,l)	383, 386 390, 392 407			
106110 (7-10)	A(l)	376, 384			
106111 (7-12)	A(g,l)	368, 376 483	-11	16	
106112 (7-16)	A(g-l)	401			
106113 (7-24)	A(g,l)	418			Homogenized to vapour & liquid
106114a(7-24a)	A(g,l)	381	-0.5	0.6	qtz(239-265)
	(l)	379			
	(g,l)	439, > 580			no qtz. associated
106114b(7-24b)	A(l)	395			gn(489-491)
106039 (K-10)	A(l)	416			C.P
106115(7-34-1)	A(g,l)	512, 526 415			close to gn. close to qtz(215)
-9th lv.					
106116 (9-1)	A(g-l)	359, 371, 384$^{(V.L)}$			
106117 (9-2)	A(l,g)	360, 376, 404			Homogenized to vapour phase

106118 (9-3)	A(g)	402, 411 > 580	Homogenized to vapour phase
106119 (9-5)	A(g,l)	405 418	vapour phase liquid phase
106120 (9-7)	A(g,l)	408, 411, 424	
106121 (9-9)	A(g-l)	$366^{(V-L)}$, $371^{(L)}$, $383^{(V)}$	vapour & liquid
106122 (9-10)	A(g-l)	372, 390, 405 449, 503, 508	
106123 (9-11)	A(l)	388, 399	qtz(315)
106124 (9-1.:	A(l)	418, 446	

-10th lv.

106126 (N-12-1)	A(g,l)	408, 420, 463	
106127(N-13-2)	C(NaCl)	493	T_m= 398(NaCl)
106128(N-14-1)	A(g) (l,g) (g)	444 392 394, 389, 413	
106129(N-15-1)	A(g,l)	375, 461	
106130(N-23-2)	A(g,l)	376, 422, 444	C.P(422)
106131(N-25-2)	A(g)	424 462	liquid phase hm. vapour phase hm.
106132(N-26-2)	A(g,l)	361, 363 434, 437	
106134(N-32-1)	A(g) (g,l)	435 406, 408	
106133(N-29-2)	A(l,g)	411 439	vapour phase hm. liquid phase hm.
106135(N-34-1)	A(g,l)	409	vapour phase hm. gn(411)
106136(N-35-2)	A(g,l)	447	

-12th lv.

106137 (12-23)	A(g,l)	414 462 476	liquid phase hm. vapour phase hm. liquid phase hm.
106138 (12-25)	A(g,l)	425, 435, 532	
106139 (12-27)	A(l)	398, 399	qtz(188-196)

106140 (12-29)	A(g,l)	374			Homogenized to liquid phase
		420, 465			vapour phase
	C(NaCl)	504		30 %	T_m= 224(NaCl)
106141 (12-31)	A(l)	367, 373	-3.7	6.3	
106142 (12-A)	A(g)	406			
	(l)	343			
106143 (12-32)	A(g,l)	332, 430, 456 471, 490 580			
106144 (12-33)	A(g,l)	432			liquid phase hm.
		456			vapour phase hm.
106145 (12-37)	A(l,g)	388, 408, 435			
-14th lv.					
106146 (Q-33)	A(g,l)	399			qtz(208)
-16th lv.					
106147 (16-28)	A(g)	445,>580			
106148 (16-32)	A(l)	415			
106149 (16-35)	A(g,l)	455, 556			
106150 (16-36)	A(g,l)	426, 431, 445			
	C(NaCl)	503		31 %	T_m= 230(NaCl)

* Key of abbreviation;

g = type A inclusion showing a big vapour bubble(over 50 % area) at the room temperature

l = type A inclusion showing a small bubble(less 50 % area) at the room temperature

g,l more g observed than l at room temperature
g-l more or less same amounts of g and l are observed at room temperature
l,g more l observed than g at room temperature

hm. homogenized

qtz = quartz gn = garnet fl = fluorite

(v) T_h homogenizing in the vapour phase

(L) T_h homogenizing in the liquid phase

Appendix 1.0.5. Data from fluid inclusions in fluorite.

In quartz veins

Sample No.	Appearance	T_h(°C)	T_f(°C)	Salinity NaCl wt %	Reference Associated minerals(T_h)
103214 (m-2-4)	violet	195, 201			
	blue	173	-1.6	2.6	qtz(214-280)
103158 (0159)	pale violet	220	-2.0	3.8	qtz(226-239)
					Bubble moving at room temperature
103142 (0232)		162, 191, 208 266 342, 361	-0.2	0.2	qtz & sch (233-280)
103221 (p-2-1)		127, 262			qtz(283-317)
103157 (0048)		220	-1.7	2.8	calcite vein
M1 skarn orebody					
106080 (j-1)		195 236, (T_m)=451			px(405-444) & qtz(132-194)
106089 (t-5)		196, 208 312	-0.1	0.1	px(399),qtz(257) 1st T_m=-52.7
106105 (4-1)		223, 225, 266			gn(580)
106149 (16-35)		236			px(420)
106099 (1st-1)	green solid	257	-7.6	10.8	px(448)
106089 (t-5')		220	-7.9	11.0	qtz(212)&px(406)
106102 (3-1)		202, 245	0.0		px(458-548)
106123 (9-11)		198 165	0.0 -1.2	1.8	px(399)
103120 (0212)		161, 213, 376(C.P)®	-2.2, -5.1	4-8.7	sch(342) Calcite vein
106144 (12-33)	green solid *	166 188 197	-5.4 *-0.8 -8.5	8.9 1.3 12.5	px(432-456) gn(439-442)
106141 (12-31)	* green solid	177 394	-4.9 *-0.5 -7.9	4.4 1.0 11.0	pseudosecondary

® C.P = critical temperature

Appendix 10.6. Data from type A inclusions in scheelite classified by their occurrence in different zones

Specimen No.	Type of Inclusion	Appearance	T_h (C°)	T_f	Salinity (NaCl wt %)		Associated Mineral(T_h)
In the pyroxene-garnet zone							
(T-3) 105986	A		207				Qtz(196)
(D-1) 106002	A		256, 293, 305				Qtz(188)
(K-10) 106039	A		246, 498			**	Px(416)
(P-3) 106068	A		287				Qtz(178-200)
(Q-2) 106073	A		316				Qtz(196-206)
(001) 103104	A		255				
(0089) 106170	A		297	-2.1	3.8	**	
In the amphibole zone							
(T-9) 105992	A		226-239 247-265	-0.9	1.4		
(E-11) 106151	A		284				
(K-21) 106152	A		251, 271				
(K-23) 106042	A		225				Qtz(226) @@
(7-13A) 106044	A		375, over 600			@@	Qtz(397=C.P)
(N-36) 106064	A		318				Qtz(304)
(0093) 106173	A		334			**	homogenized to vapour phase
(0237) 103239	A		302, 314 323-324			@*	Qtz(201-255)
In the quartz-mica zone							
(0212) 103120	A		326	-0.9	1.4	@@	
			342	-0.8	1.3		
(0112) 103237	A		348			**	Qtz(282)
(0214) 103170	C		376	NaCl T_m= 173 KCl T_m= 81		@@	
	A		345				
	A		307-310				Pseudosecondary
	C		310	NaCl T_m= 272		@@	

(0214)103170	A	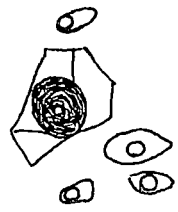	330			@@	
	A		290			**	
			278	-5.3	8.8		
			268				
(K-13) 106153	A		433			*@	No fluid inclusions in quartz at all
(K-14) 106040	A		276	- 2.0	3.7	@@	Qtz(201)
(044) 106172	A		381	-22.0	23	@@	1st T_m = -50

*Key; @@ indicates Mo-rich scheelite showing yellow fluorescent colour

** indicates Mo-poor scheelite showing blue fluorescent colour

Appendix 10.7. Comparison of T_h values between Mo-rich part and Mo-poor part in the zonation of a scheelite, and between two different single crystals

Sample No.	Types of Zone or Crystal	Appearance of Inclusions	Temperatures (°C) T_h	T_m	T_f	Reference (salinity)
103170 (chip A)	Mo-rich core	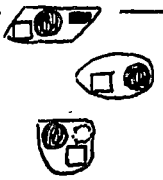		246		decrepitated at 354°C
				191		
				189		
			345			
			307-310			pseudo-secondary
*103170 (chip B)	Mo-rich core	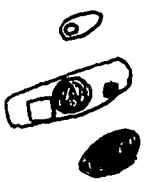	330			
			310	272		35 wt % NaCl
						hardly see inside
	Mo-poor rim	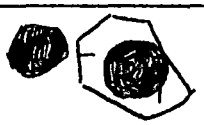	290		-5.3	8.7 wt % NaCl
			278			
		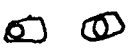	268			pseudo-secondary
103142	Mo-poor scheelite (quartz vein)	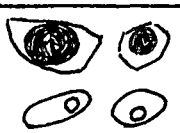	335		-2.8	4.7 wt % NaCl
					-1.1	1.7 wt % NaCl
103120	Mo-rich scheelite (QM skarn)		326		-0.9	1.4 wt % NaCl
			342		-0.8	1.3 wt % NaCl
106040	Mo-rich scheelite (QM skarn)		276		-2.0	3.7 wt % NaCl
106170	Mo-poor scheelite (PG skarn)		297		-2.1	3.8 wt % NaCl

*103170 (see Fig. 6.29)

QM = quartz-mica PG = pyroxene-garnet

Appendix 10.8. T_h of fluid inclusions in Apatites, Amphibole, and Biotites from the M1 ore body.

Specimen No.	Appearance	T_h(C°)	T_f(C°)	Salinity (NaCl wt %)	Associated Minerals(T_h)
Apatite					
(N-32) 106061		308			Qtz(293-295)
(K-19) 106041		253			Qtz(190)
(E-1) 106011		257	-2.9	5	Qtz(190-238)
		319			
(F-8) 106028		285			Qtz(213-245)
(K-4) 106034		279			Qtz(220-270)
		287-298			
(Q-3) 106074		272-292			Qtz(195)
(0112) 103237		299			Qtz(228-232)
		301			
Amphibole					
(N-13-1) 106127		292			
		307			
(7-13) 106044		287			
		293			Qtz(207)
Biotite					
(7-12) 106111		381			
(0091) 106173		286			Qtz(194)

Appendix 10.9. Data for fluid inclusions in garnets of the M1 orebody.

Sample No.	Appearance.	T_h(°C)	T_f(°C)	Salinity wt % NaCl	Associated Mineral(T_h)	Reference
106084		365 374			Px(359-369) Px(423-425)	
103118		364			Px(400)	A fine scheelite is enclosed
106100		>585	-21.8	17.5 % CaCl		1st T_m=-50
106094		387	- 8.2	11.9		
106096		412-420				Homogenized to vapour phase
106105		>585	-4.3	7	Px(>585)	
106108		383-392 407				Homogenized to vapour phase
106115		585				
106113		349-375 489-491 433			Px(395)	C.P.
106119	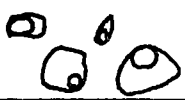	405(V) 418(L)				Homogenized to vapour phase
106125		480				Bubble was moving on heating
106131		462			Px(424)	
106137	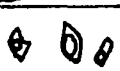	411			Px(409)	
106136		>585				Brown garnet
106144	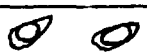	439-442			Px(432-456)	
106149		420				Homogenized to vapour phase

Appendix 10.10. Data for type B(liquid CO_2 bearing) inclusions.

Sample No. (Host Mineral)	Rock Types	Appearance	CO_2 T_h (°C)	T_h (°C)	NaCl wt %	Density of CO_2 (g/cc)	Remarks
103160 (quartz)	Jangsan Quartzite	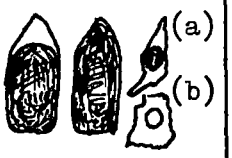 (a) (b)	23.7	293		0.19	CO_2-rich
				137	7.9		
103161 (quartz)	Jangsan Quartzite	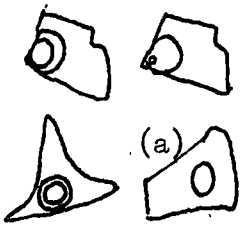 (a)	28.8	254		0.70	
				178			type A
			23.7	236		0.78	
103155 (quartz)	Quartz Vein		29.1	243	5	0.55	
				239			type A
103156 (quartz)	Calcite Vein		25.1	223		0.6	
				230	6.3		type A
				243	7.2		type A
103160 (fluorite)	Quartz Vein	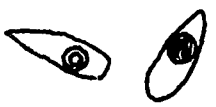	28.1	220	2.8	0.67	
				220	5		type A
103158 (fluorite)	Quartz Vein		28.2	220		0.67	
103214 (quartz)	Quartz Vein		30.5	265		0.25	Homogenized to vapour
106020 (quartz)	M1 QM skarn		28.9	308		0.65	
			28.1	308		0.67	
103198 (quartz)	Quartz Vein		28.9	199		0.65	
				151	6.3		type A
				170	7.8		type A
103215 (quartz)	Quartz Vein		30.7	394(C.P)			
				347			type A

Appendix 10.11. Data from Type C inclusions.

Sample No. (Zone)	Host Mineral	Appearance	T_h(°C)	T_m(°C)	Salinity wt % NaCl (KCl) @ K/Na
106056 (px)	quartz		132	156	29 %
106080 (px)	quartz		194	451	51
	fluorite		236	451	51
106105 (px)	pyroxene		301	235	32
106140 (px)	pyroxene		504	224	30
106094 (px)	pyroxene		448	230	31
106103 (px)	pyroxene		580	414	47.5
106066 (px)	quartz		190	227	33
106004 (amp)	quartz		168	185	30
103125 (q.m)	quartz		126	119	29
103121 (q.v)	quartz		152	182	30
103202 (q.v)	quartz		256	263	34
			252	264	34
			293	267	34
103203 (q.v)	quartz		222	321	39
103154 (q.v)	quartz	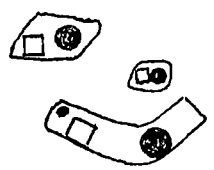	229	235	32
			277	232	32
			233	172	30
			128	170	30
			233	165	30
103237 (q.m)	scheelite		324		solid did not melt
106150	pyroxene		503	230	31

			T_h(°C)	T_m(°C)	
103170(a) (q.m)	quartz		310	272	35
	scheelite		291	246	32
103215 (q.v)	quartz		394(C.P)		solid = hematite
103170(b) (q.m)	scheelite		376	81(KCl) 173(NaCl)	20(KCl) 22(NaCl) @ 0.71
		Decripitated at	357(T_d)	189 191 246	
103154 (q.v)	quartz		275	405	47
			238	422	49
			251	90(KCl) 404(NaCl)	14.5(KCl) 38.6(NaCl) 0.29
			275	237(KCl) 405(NaCl)	29(KCl) 31(NaCl) 0.73
			239	89(KCl) 289(NaCl)	16.6(KCl) 28.3(NaCl) 0.45
* 103160	quartz		133	90	27.5

---

px = the pyroxene-garnet skarn zone

amp = the amphibole-rich zone

q.m = the quartz-mica rich zone

q.v = quartz veins

* = Jangsan Quartzite

Appendix 10.12. Examples of Significant Differences in T_h.

(Ex.1) Between transparent bubble and dark coloured bubble.

Specimen(0217) showing unusual occurrence of molybdenite

103125

	T_h(°C)	T_f(°C)	Salinity(NaCl wt %)
	177	-1.5	2.5
	283	-5.3	8.1

(Ex.2) Garnet enclosing a scheelite inclusion and Pyroxene close to it.

Specimen(0158) 103118

Homogenized		Garnet	Pyroxene		Homogenized
in liquid		364°C	400°C		in vapour

(Ex.3) Specimen(0159) 103158

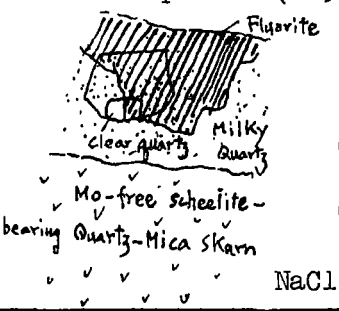

	Fluorite	Quartz		
	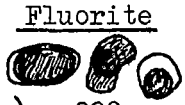			
T_h(°C)	220	236	226	239
T_f(°C)	-2.0	-1.9	-2.9	-3.2
NaCl wt %	3.8	3.1	5.0	5.4

(Ex.4) From core to rim in a scheelite crystal, and a quartz crystal.

Specimen(0214) 103170

In scheelite

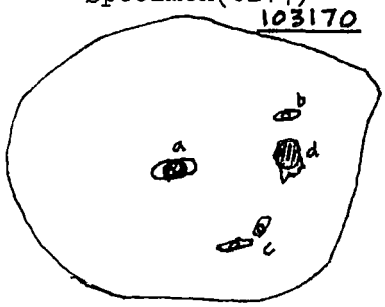

	T_h(°C)	T_m(°C)
(a)	345	
(b)	338	
(c)	307-310	
(d)	leaking	

In quartz

(e)	291	
(f)	336	
(g)	246	291

Specimen(T-9) 105992

In scheelite

(h)	247	
(i)	239	
(j)	226	
(k)	265	

In quartz

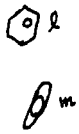

(l)	207	
(m)	220	

Appendix 10.13. Description of Phase Changes in Fluid Inclusions on Cooling and Heating Runs.

Ex. 1. Sample No. 103182. molybdenite-quartz vein, host mineral is quartz,

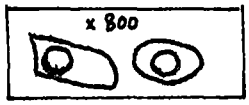

type A inclusion, Jangsan level.

1. Frozen to $-110^{\circ}C$.
2. Solid phase(dark spots) disappeared at $-51^{\circ}C(T_e)$.
3. Round gas bubble changed from its original form to a irregular shape at $-32^{\circ}C$.
4. A solid phase observed near the bubble disappeared at $-22.4^{\circ}C$.
5. Final ice melted out at $-4.3^{\circ}C(T_f)$.
6. Recovered the original round form of the bubble at $-2.1^{\circ}C$.

Interpretation

$NaCl-CaCl_2-H_2O$ system (see Appendix 10.14)

Ratio of NaCl : $CaCl_2$: H_2O = 7 : 5 : 88

Salinity = 7 wt % NaCl equivalent

Ex. 2. Sample No. 103202. molybdenite-quartz vein, host mineral is quartz,

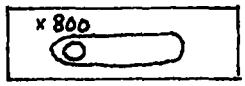

type A inclusion, -4th level.

1. Frozen to $-130^{\circ}C$.
2. Observed ice only in the area of vapour phase at $-80^{\circ}C$
3. Colour of the liquid phase changed at $-20.1^{\circ}C$.
4. Observed ice appearing as dots in the liquid phase
5. Ice melted out at $-2.6^{\circ}C(T_f)$.

$NaCl-H_2O$ system

Salinity = 4.6 wt % NaCl

Ex. 3. Sample No. 103154(chip a), molybdenite-quartz vein, host mineral is quartz, type C inclusion, 4th level.

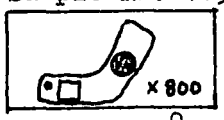

1. Frozen to $-110^{\circ}C$, but no changes of shape of vapour bubble and halite.
2. Solid (ice and $CaCl_2 \cdot 6H_2O$) melted from $-56^{\circ}C(T_e)$.
3. New solid particles($MgCl_2 \cdot 12H_2O$?) appeared at about $-50^{\circ}C$.
4. The solid melted actively from $-40.9^{\circ}C$.
5. All solids disappeared at $-29.6^{\circ}C$ while the halite crystal maintained its original shape.
6. Repeated cooling runs made the halite crystal dissolve at about $-15^{\circ}C$ and the halite changed its shape from the cubic to a round form and several tiny round solids(i.e. hydrohalite, $NaCl \cdot 2H_2O$) appeared in the liquid phase.
7. The hydrohalite crystals dissolved actively from $-6^{\circ}C$ and finally disappeared at $-0.6^{\circ}C$.
8. A solid(NaCl) appeared near the round halite at $0.5^{\circ}C$.
9. The halite grew, changing shape from round to square, and a smaller halite grew a little and eventually made one halite crystal like the original one at about $40^{\circ}C$.
10. The halite melted out at $165^{\circ}C$ and the vapour bubble disappeared at $233^{\circ}C$.

$NaCl-CaCl_2-MgCl_2-H_2O$ system

$CaCl_2$: $MgCl_2$ = 1 : 1.7 (see Appendix 10.15)

H_2O : ($CaCl_2$+ $MgCl_2$) = 53 : 48 (Appendix 10.15)

Salinity = 29.8 wt % NaCl equivalent

(NaCl : ($MgCl_2$ + $CaCl_2$) difficult to determine).

Ex. 4. Sample No. 103154(chip b). molybdenite-quartz vein, host mineral is 

quartz, type C(halite-sylvite bearing) inclusion, 4th level.

1. Frozen to -170°C, sylvite dissolved and disappeared, but halite showed no change on cooling runs(three times repeated).
2. Solidified liquid phase showed cracks at -110°C
3. Observed cracks in the solidified liquid phase showing the shape of a tortoise-shell at -79° ± 0.6°C and disappearing at -67°C.
4. Observed tiny dark spots occurring in the liquid phase following disappearance of cracks. The solidified liquid phase started to melt at -61.4°C(T_e)
5. Observed many round solid grains in the liquid at -59.1°C.
6. Solids except halite melted actively, but suspended melting when cooling temperature was maintained -51° ± 1°C for 20 minutes.
7. Solids except halite melted out at -41.3° ± 0.6°C.
8. The sylvite crystal melted out at 237°C(T_mKCl).
9. The vapour bubble disappeared at 275°C(T_h ; vapour homogenization)
10. The halite crystal melted out at 405°C (T_mNaCl)

NaCl-KCl-$CaCl_2$-$MgCl_2$-H_2O system

NaCl : KCl : H_2O = 31 : 29 : 40 (see Fig. 10.21)

Ex. 5. Sample No. 103161. Jangsan Quartzite, host mineral is quartz, 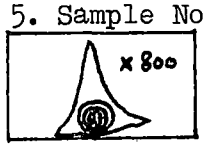

type B(liquid CO_2-bearing) inclusion, 192 m above sea l.

1. Frozen to -110°C.
2. Observed solid phase in the dark gas bubble and solids(ice) disappeared at -56°C(CO_2 melted). (solid phase in the bubble : see Ex.6)
3. Tiny round solids appeared on the bubble and they started to melt at -26.8°C and melted out at -20.3°C(hydrohalite).
4. Ice finally melted out at -5.2°C ; giving 8 % wt NaCl salinity.
5. The liquid CO_2 homogenized into the liquid phase at 23.7°C($T_h CO_2$)
6. Inclusion homogenized into the liquid phase at 236°C.(T_h)

$NaCl-CO_2-H_2O$ system

Density of liquid CO_2 phase at $40^{\circ}C$ = 0.78 g/cc

Mole % H_2O = 88 % Salinity = 8 wt % NaCl equivalent

Ex. 6. Sample No. 103158. quartz vein, host mineral is fluorite, type A inclusion, in skarn, Sangdong level.

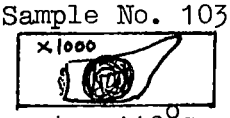

1. Frozen to $-110^{\circ}C$.
2. The liquid(solidified) phase showed a change from $-53^{\circ}C(T_e)$ and solid in the liquid phase disappeared at $-50.3^{\circ}C$
3. Observed nucleation of solids in the vapour phase at $-44^{\circ}C$.
4. Outline of the dark bubble changed, and a change of texture inside the liquid phase took place from $-32.2^{\circ}C$
5. The shrunk bubble showed solid phase and a circular form in the core of vapour phase, and solids started to melt at $-26.2^{\circ}C$.
6. *The solid phase in the bubble disappeared at $-8.9^{\circ}C$.
7. The bubble recovered its original shape at -5.9°.

* Solid phase in the bubble = Ice adhered to surface of bubble as following figures.

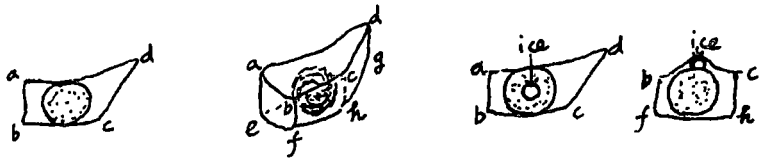

$NaCl-CaCl_2-H_2O$ system (see Appendix 10.14)

Salinity = 12.7 wt % NaCl equivalent

Ex. 7. Sample No. 103202. Barren quartz vein, host mineral is quartz, type A inclusion, -4th level.

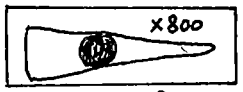

1. Frozen to $-110^{\circ}C$.
2. Bubble shrunk at $-34^{\circ}C$ on cooling.
3. Solids appeared suddenly at $-35^{\circ}C$ on warming(T_n ice)
4. Colour of the liquid phase changed at $-27.9^{\circ}C(T_e)$.
5. Two solids melted out at $-25.7^{\circ}C$ and others melted out at $-19.6^{\circ}C$

6. Bubble getting smaller from $-12^{\circ}C$ and recovered the original shape at $-0.4^{\circ}C$.

$NaCl-H_2O$ system

Metastable

Ex. 8. Sample No. 103214. a chalcopyrite-quartz vein, host mineral is 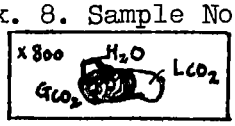

quartz, type B inclusion, 9th level.

1. Frozen to $-105^{\circ}C$, the vapour bubble(CO_2) nucleated suddenly, as if it exploded, at $-105^{\circ}C(T_{nCO_2})$
2. Solid in the bubble melted suddenly and the gas bubble returned to the original shape at $-55.1^{\circ}C(T_mCO_2)$
3. The liquid CO_2 homogenized into vapour phase at $30.5^{\circ}C$.
4. Inclusion homogenized at $263^{\circ}C(T_h)$

CO_2-H_2O system

Ratio of CO_2: H_2O = 10 : 1 Density of CO_2 phase = 0.25 g/cc

Bulk density of inclusion = 14.28 moles/litre(Burruss, 1981)

Ex. 9. Sample No. 106039. M1 quartz-mica skarn ore, host mineral is 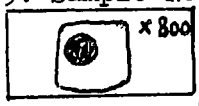

scheelite, type A inclusion, 7th level.

1. Frozen to $-90^{\circ}C$, the vapour bubble shrank, and several solids observed.
2. Solids started to change their shapes at $-53.5^{\circ}C(T_e)$ and formed round shapes at $-47^{\circ}C$.
3. Only three solids left at $-19^{\circ}C$.
4. The solids reacted to form one(ice) at $-10^{\circ}C$.
5. The ice melted out at $-1.0^{\circ}C$, recovering the original form of bubble(T_f).
6. Homogenized into the liquid phase at $246^{\circ}C(T_h)$

$NaCl-CaCl_2-H_2O$ system

Difficult to distinguish ice from hydrohalite or $CaCl_2 \cdot 6H_2O$, so ratio uncertain.

Salinity = 1.6 wt % NaCl equivalent

Ex. 10. Sample No. 106041. M1 quartz-amphibole skarn ore, host mineral is quartz, type A inclusion(secondary), 7th level.

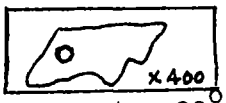

1. Frozen to -90°C, the vapour bubble disappeared at -32°C.
2. Ice started to melt at -20°C.
3. Ice finally disappeared with appearance of the vapour bubble, at 0.3°C.

* * * *

Metastable. Final melting point might be raised by negative pressure due to stretching.

Ex. 11. Sample No. 106111. M1 pyroxene-garnet skarn ore, host mineral is pyroxene(hedenbergite), type A inclusion, 7th level.

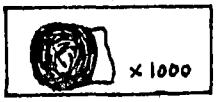

1. Frozen to -90°C.
2. Observed solids in the liquid phase to start to change at -53.7°C(T_e).
3. Yellow spotty solids recrystallized at -43.7°C.
4. Solids melted actively from -38.4°C and all solid phase disappeared at -33°C.
5. The liquid phase change its colour and showed spotty solids at -26°C.
6. The spotty solids disappeared at about -22°C and then new ice phase started to melt at -20°C.
7. All ice melted out and vapour bubble recovered its original round shape at -11°C(T_f).
8. Inclusion homogenized into the liquid phase at 483°C (T_h).

$NaCl-CaCl_2-H_2O$ system

$NaCl : CaCl_2 = 1 : 4$ (see Appendix 10.14)

Salinity = 16 wt % NaCl equivalent.

Ex. 12. Sample No. 106004. M1 quartz-amphibole skarn ore, host mineral is quartz, type A inclusion, 1st level.

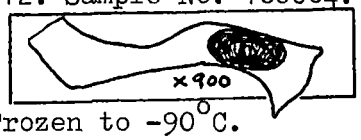

1. Frozen to -90°C.
2. Liquid phase changed due to crystallization of ice from -65°C.
3. Spotty dark solids surround by clear round ring (it looks like frog's spawn) appeared in the liquid phase at -59°C.
4. Solids started to melt at -35°C, and all melted out at -20°C(T_f).
5. Inclusion homogenized into the liquid phase at 259°C(T_h).

If solid observed at -35°C was ice, the system would be $CaCl_2$-H_2O, salinity = 13.8 wt % $CaCl_2$.

If $NaCl \cdot 2H_2O$, then it is a NaCl-$CaCl_2$-H_2O system and salinity = 22.4 wt % NaCl equivalent, with

NaCl : $CaCl_2$ = 1 : 4.5.

Ex. 13. Sample No. 106172. M1 quartz-mica skarn ore, host mineral is scheelite, type A inclusion, 3rd level.

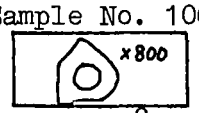

1. Frozen to -110°C.
2. All solids melted out before -50°C on heating.
3. Observed appearance of a large angular solid phase at -39°C.
4. The solid became smaller and round at -32°C.
5. Liquid phase in the inclusion became clear about -22°C.

NaCl-$CaCl_2$-H_2O system

Salinity = about 23 wt % NaCl equivalent , with

NaCl : $CaCl_2$ = 1.2 : 3.8.

Appendix 10.14. $NaCl-CaCl_2-H_2O$ system, compositions in weight percent. Data from Yanatieva(Crawford, 1981).

● Ex. 1. sample 103182

◉ Ex.11. sample 106111

○ Ex.13. sample 106004

□ Ex. 6. sample 103158

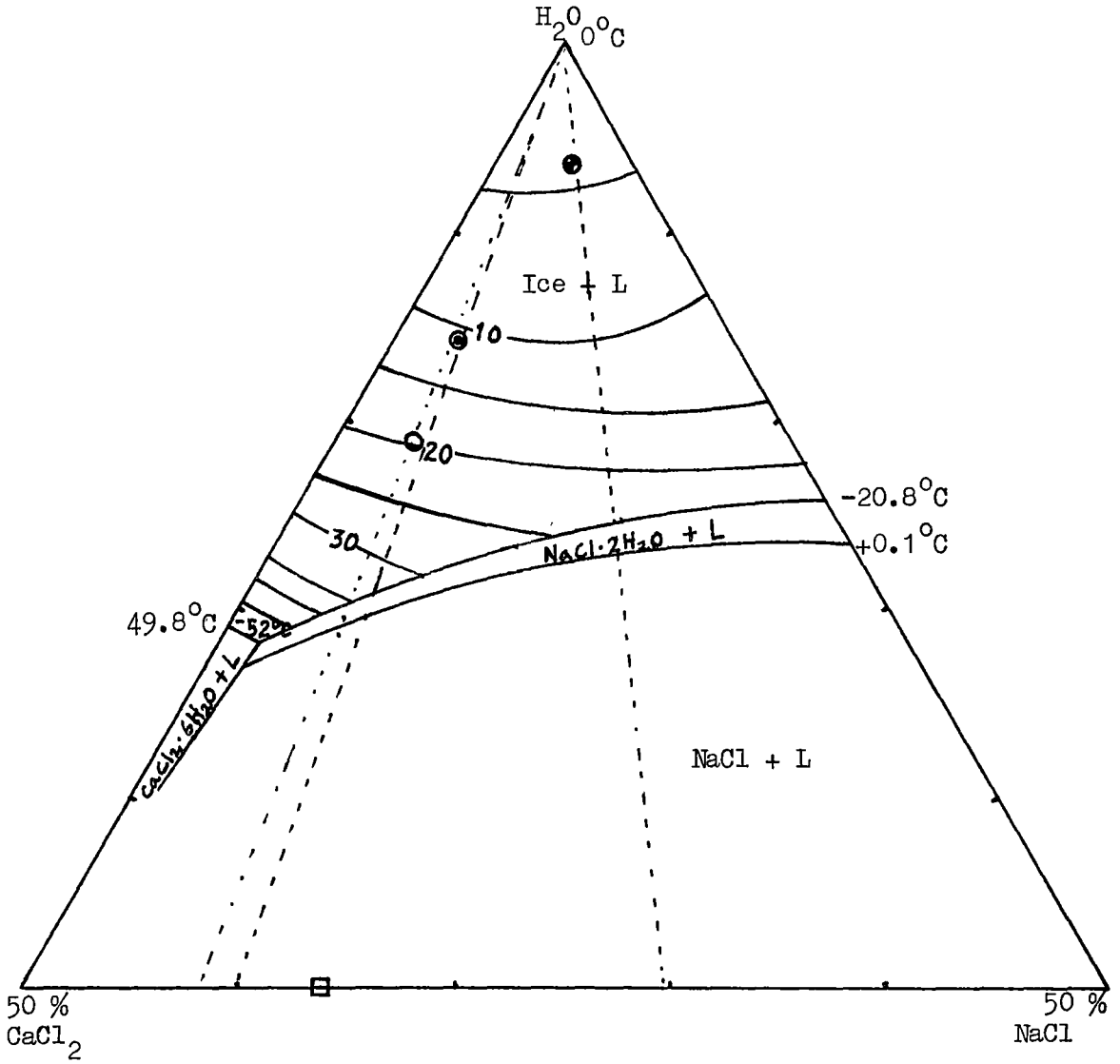

Appendix 10.15. $NaCl-CaCl_2-MgCl_2-H_2O$ system

Data from Luzhnaya and Vereshtchetina(Crawford, 1981).

(A)

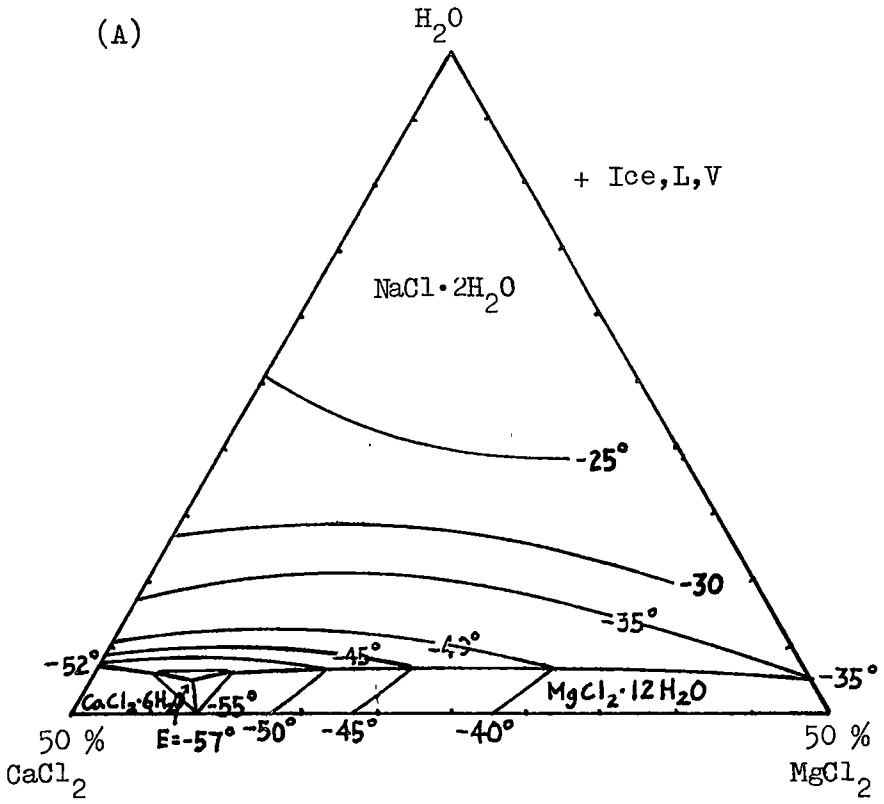

(B) Section through the system at a $CaCl_2/MgCl_2$ ratio of 3 : 1

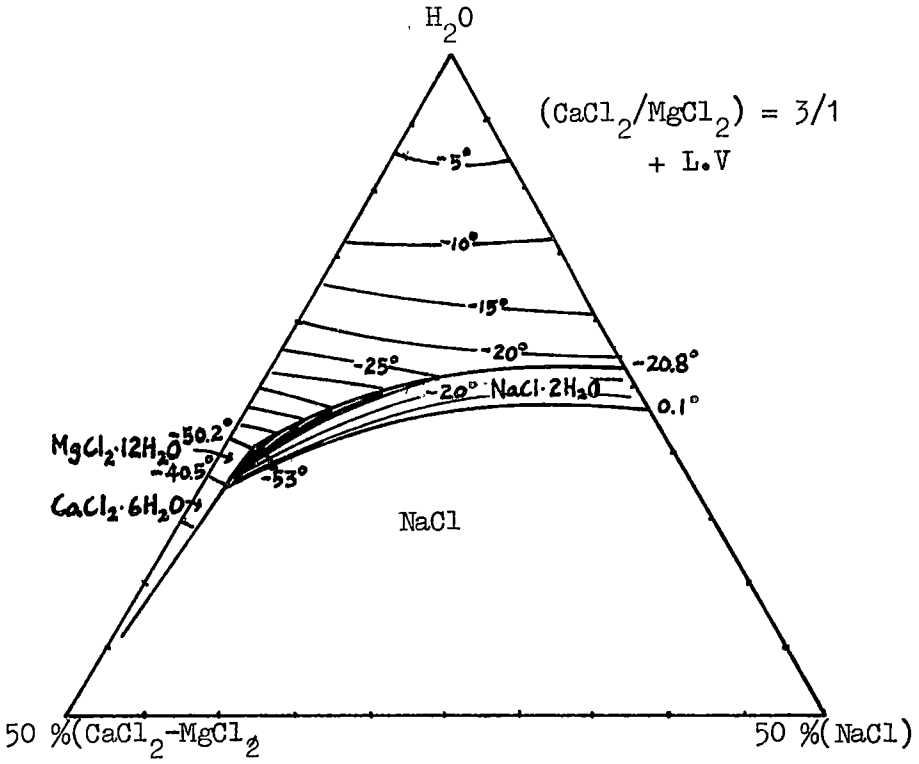

Appendix 11. SO_2 Extraction For Sulphur Isotope Analyses.

* Weight of sulphides (using 0.15 g Cu_2O)

Pyrite	12.0 mg
Chalcopyrite	16.0 mg
Galena	50.0 mg
Sphalerite	20.0 mg
Molybdenite	17.0 mg
Bismuthinite	34.0 mg

* Principles

Weighed sulphide samples are roasted at 950°C with Cu_2O. The resulting gas invariably contains CO_2 and H_2O in addition to SO_2, and the impurities must be extracted before the SO_2 can be put in the mass spectrometer. A little CO_2 is tolerable, but water must be removed entirely.

The separation of the gases is brought about using difference in their freezing properties. Water is frozen out with an acetone-dry ice freezing mixture. CO_2 has a vapour pressure more than 400X that of SO_2 at the freezing point of n-pentane(-131°C). This enables a separation by pumping away the CO_2. Reference: Oana, S. and Ishikawa, H.(1966), Geochem. J., v.1, p.45.

* Preparation of Cu_2O

Commercial and reagent grade Cu_2O are contaminated with organic compounds and unsuitable for use. Pure Cu_2O is made from reagent grade CuO by heating to 800°C in the combustion tube under rough vacuum for 20-30 minutes. The dark red crystals are crushed in an agate mortar to give a bright orange-red powder which is stored in a stoppered bottle in a dessicator. Cu_2O may oxidise and absorb H_2O and CO_2 with time so only a limited quantity is made and kept for 2-3 weeks.

Ref. Robinson, B.W. and Kasakabe, M., 1975. Quantitative preparation of SO_2, for $^{34}S/^{32}S$ analyses, from sulphides by combustion with cuprous oxide: Anal. Chem. 47, 7, 1179-1181.

* Figure. Sulphur Isotope Line

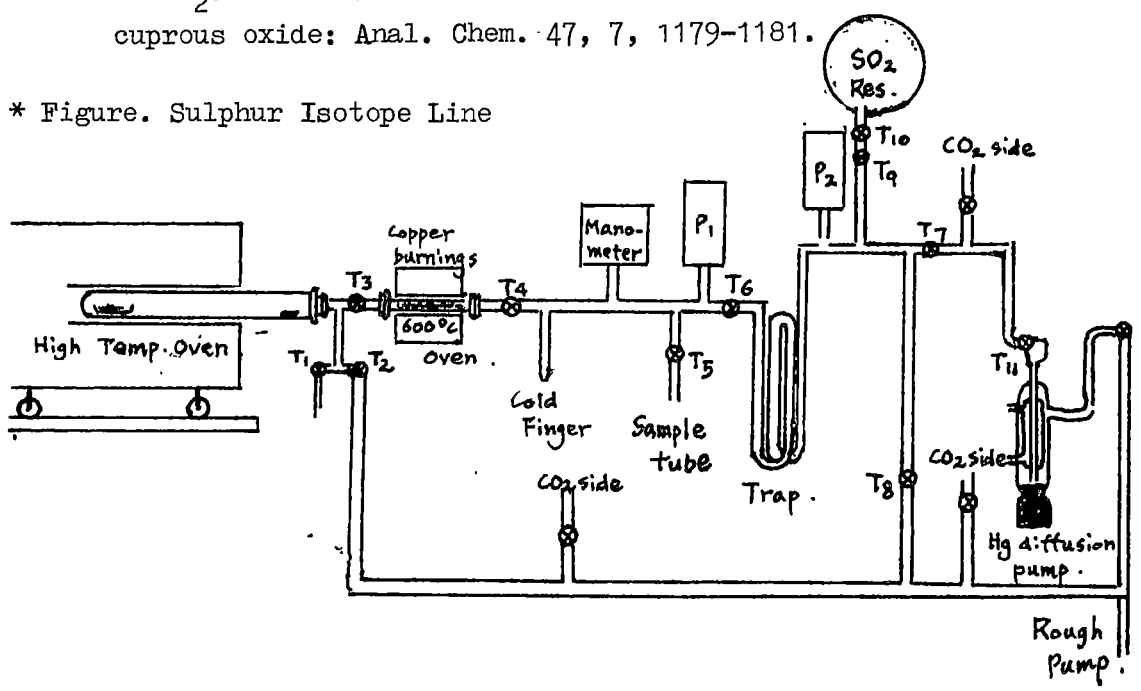

Appendix 11.1. CO_2 Extraction For Carbon & Oxygen Isotope Analyses.

Loading

1. Close line of at tap(2) and pump the line out (low vacuum, then high vacuum)
2. Load 30 mg(approximate) of calcite into reaction tube, if samples are impure, we need samples more than 30 mg.
3. Put Phosphoric acid into large section of reaction tube(6-7 ml).
4. Put tube on to the line, place nitrogen on the "trap" and vacuum out to 10^{-3}kpa(approximately) and close tap on the reaction tube. Leave a couple of minutes and check for leaks, close tap again and place in water bath ($25^{o}C$) for 12 hours.
5. Tip phosphoric acid into the calcite.

Collecting CO_2

1. Place "collection bulb" on the end of the line and the reaction tube on the beginning of the line. Pump the system out to 10^{-3}kpa with the aid of nitrogen on "trap". Close off taps(2),(3) & (4). Take nitrogen off, warm up with the hair drier. Close off vacuum taps when completely pumped out.
2. Open reaction tube tap and freeze down in the "trap". When pressure stops decreasing, pump the non-condensable away and close off tap(1).
3. Close off vacuum taps, open tap(2), take away nitrogen and freeze water trap with nitrogen, then put acetone-dry ice mixture on it. Open tap(3) and once the CO_2 has thawed out, freeze down in cold finger.
4. Take away nitrogen, thaw the CO_2 out and freeze down in the "trap" and repeat the same procedure as before.
5. Close off tap(3), thaw out the cold finger contents, open tap(4) and freeze down in "collection bulb".
6. Close off tap and take bulb off the line.

Figure. Carbon Isotope Line

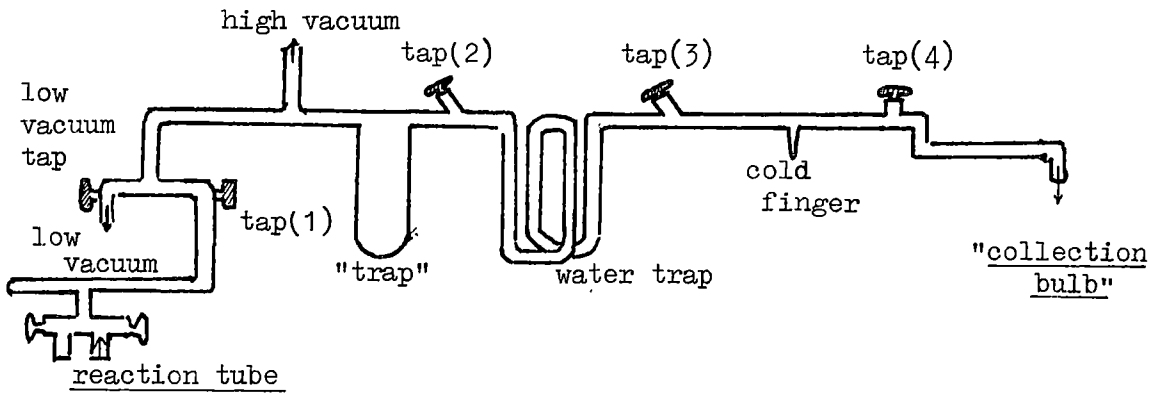

Appendix 11.2. Carbon and Oxygen Isotope Values.

$$\delta(‰) = (R_{sample} - R_{standard} / R\ std) \times 1000 \qquad (R = C^{13}/C^{12}\ ,\ O^{18}/O^{16})$$

$$\delta C^{13}_{PDB} = 1.0676\ C^{13}_{measured} - 0.0338\ O^{18}_{measured}$$

$$\delta O^{18}_{PDB} = 1.0014\ O^{18}_{measured} + 0.009\ C^{13}_{correct}$$

$$\delta O^{18}_{SMOW} = 1.03086\ O^{18}_{PDB} + 30.86$$

Standard;

δO^{18} = -19.4 ‰

δC^{13} = -28.7 ‰

Appendix 11.3. Detection limits of trace elements analysed by XRF(Philip).

Sn	4 ppm	Ni	2 ppm
W	5	Rb	2
Mo	3	Sr	2
Bi	5	Th	6
Pb	3		
Zn	2		

Appendix 12.1. Calculated Free Energy Data($\Delta G_{formation}$, KJ/mol).

Temp.(^{o}K)	Hedenbergite	Andradite	Scheelite
298	-2674.34	-5428.29	-1516.17
400	-2618.16	-5308.92	-1479.84
500	-2563.35	-5192.62	-1444.55
600	-2508.99	-5077.43	-1409.64
700	-2455.06	-4963.23	-1375.08
800	-2401.49	-4849.83	-1340.80
900	-2348.19	-4737.05	-1306.76
1000	-2295.10	-4624.69	-1272.90

Temp.(^{o}K)	Powellite	Ferberite	Tungsten disulphide
298	-1439.67	-1089.11	-200.97
400	-1403.42	-1054.99	-181.14
500	-1368.31	-1022.05	-161.93
600	-1333.66	- 989.54	-142.96
700	-1299.43	- 957.39	-124.22
800	-1265.56	- 925.53	-105.70
900	-1231.99	- 893.90	- 87.39
1000	-1198.67	- 862.47	- 69.27

Appendix 12.2.

Activity Coefficient of Aqueous Species(data from Tas. Uni. computer programme).

(ionic strength = 1.122)

	250°C	350°C
K^+	-0.43	-0.76
Ca^{++}	-1.16	-1.89
H^+	-0.19	-0.41

Thermodynamic data for Ca^{++} in aqueous solution at 25°C, 1 atm.

	ΔH^o (cal $mole^{-1}$)	S^o (cal $mole^{-1}deg^{-1}$)	Average heat capacity 200°C	250°C	300°C
Ca^{++}	-12770	-13.2	105	109	118

(Helgeson, 1969)

Equilibrium Constants for Reactions(Ohmoto, 1972).

	250°C	300°C	350°C
$CaCO_3 = Ca^{++} + CO_3$	-12.72	-14.10	-15.5
$H_2O = H^+ + OH^-$	-11.04	-11.03	-11.42
$3KAlSi_3O_8 + 2H^+ = KAl_3Si_3O_{10}(OH)_2 + 6SiO_2 + 2K^+$	9.2	8.6	8.2
$2KAl_3Si_3O_{10}(OH)_2 + 2H^+ + 3H_2O = 3Al_2Si_2O_5(OH)_4 + 2K^+$	6.2	5.44	4.9

Appendix. 12.3. Calculation of Gibbs Free Energy of Formation($\Delta G^{\ominus}_{f,T}$) Values from Heat Capacity($C^{\ominus}_p$) Data, Entropy($S^{\ominus}_{298}$) and Enthalpy of Formation($\Delta H^{\ominus}_{f;298}$) Data.

Basic Equation(Robie et al.,1978 ; Helgeson et al., 1978)

$$\Delta G^{\ominus}_{f,T} = \Delta H^{\ominus}_{f,298K} + T \cdot \Delta\left[\frac{G^{\ominus}_T - H^{\ominus}_{298K}}{T}\right]_{reac.} = \Delta H^{\ominus}_{f,298K} + T\cdot\Delta F^{\ominus}_{298}(T)$$

where $\Delta F^{\ominus}_{298}(T)$ is the change in the Gibbs Free Energy Function for the formation reaction from the elements in their standard states(1 bar, 298K).

$$S^{\ominus}_T = \int_{298}^{T} C^{\ominus}_p \cdot d \ln T + S^{\ominus}_{298}$$

$$(H^{\ominus}_T - H^{\ominus}_{298}) = \int_{298}^{T} C^{\ominus}_p \cdot d T$$

$$F^{\ominus}_{298}(T) = \left(\frac{G^{\ominus}_T - H^{\ominus}_{298}}{T}\right) = \frac{(H^{\ominus}_T - H^{\ominus}_{298})}{T} - S^{\ominus}_T$$

For each element in formation reaction

$$\left[\frac{G^{\ominus}_T - H^{\ominus}_{298}}{T}\right] = \frac{\int_{298}^{T} C^{\ominus}_p \cdot dT}{T} - \left[\int_{298}^{T} \frac{C_p}{T} \cdot dT + S^{\ominus}_{298}\right]$$

Eg. $FeWO_4$

$$\Delta C_p = \Delta a + \Delta b\cdot T + \Delta c\cdot T^{-2} \; (+ \Delta d\cdot T^{-1/2} + \Delta e\cdot T^2)$$

C_p eqn. (Fe) $28.175 - 7.3178 \times 10^{-3}T - 2.8953 \times 10^{5}T^{-2} + 2.5041 \times 10^{-5}T^2$

(W) $24.843 + 2.2255 \times 10^{-3}T + 3.5044 \times 10^{-7}T^2 - 1.1153 \times 10^{5}T^{-2}$

(O_2) $48.318 - 6.9132 \times 10^{-4}T - 4.2066 \times 10^{-0.5} + 4.9923 \times 10^{5}T^{-2}$

Formation reaction from the elements : $F^{\ominus}_{298}(T)$ needs to be calculated from C_p eqn & $S^{\ominus}_{298}$ data for each element + $FeWO_4$.

$Fe + W + 2O_2 = FeWO_4$

$\Delta a = 121.922 - (2 \times 48.318) - 24.843 - 28.175 = -27.732$

$\Delta b = 3.677 \times 10^{-2} + (2 \times 6.9132) \times 10^{-4} - 2.2255 \times 10^{-3} + 7.3178 \times 10^{-3}$
$= 4.3245 \times 10^{-2}$

$\Delta c = -2.8033 \times 10^{5} - (2 \times 4.9923 \times 10^{5}) + (1.1153 \times 10^{5}) + 2.8953 \times 10^{5}$
$= -8.7773 \times 10^{5}$

$\Delta d = + (2 \times 4.2066 \times 10^{2}) = 8.4132 \times 10^{2}$

$\Delta e = - 3.5044 \times 10^{-7} - 2.5041 \times 10^{-5} = -2.5391 \times 10^{-5}$

$\Delta S^{298}_f = 131.796 - 2 \times 205.15 - 27.28 - 32.64 = -338.424$

$\Delta H^{298}_f = -1,190,013 \text{ (J.)} - 2 \times 0 - 0 - 0 = -1,190,013 \text{ J}$

$$\Delta\left[\frac{G^{\ominus}_T - H^{\ominus}_{298}}{T}\right] = \left[\quad\right]_{FeWO_4} - 2\left[\quad\right]_{O_2} - \left[\quad\right]_{Fe} - \left[\quad\right]_{W}$$